ISSN 0975 2595

PRAJÑĀ

Volume 24-25, December 2017

Journal of Pure and Applied Sciences

SARDAR PATEL UNIVERSITY
VALLABH VIDYANAGAR
Gujarat - 388 120, INDIA
www.spuvvn.edu

PRAJÑĀ - Journal of Pure and Applied Sciences

(Abbreviation: *PRAJÑĀ - J. Pure & Appl. Sci.*)

Since 1991 Sardar Patel University has been regularly publishing the ***PRAJÑĀ* - Journal of Pure and Applied Sciences** with an aim of providing a platform to Academicians, Researchers and Scientists for the rapid dissemination of original scientific work carried out in the Universities and Research Laboratories. All articles published in *PRAJÑĀ* are deemed to reflect the individual views of the authors and not the official points of view of the Sardar Patel University.

A Peer Reviewed Journal

Indexed in Indian Science Abstracts

Published by the Registrar, Sardar Patel University, Vallabh Vidyanagar, Gujarat - 388 120

Printed at Sardar Patel University Press, Vallabh Vidyanagar, Gujarat-388 120

PRAJÑĀ - Journal of Pure and Applied Sciences

Volume 24-25, December 2017

UGC APPROVED JOURNAL (No. 48135)

ISSN 0975 – 2595

An Official Publication of

Sardar Patel University

Vallabh Vidyanagar, Gujarat - 388 120, India

www.spuvvn.edu E-mail: spu.prajna@gmail.com

Sardar Patel University

is grateful to

Prof. Vithalbhai A. Patel

Humboldt State University, Arcata, Califonia, USA,
whose generous donation to organize academic activities
in the name of Shri Ishwarbhai Ambalal Patel (Shertha) helped
to meet a part of the publication cost of *PRAJÑĀ* Journal.

****

The Editorial Board of *PRAJÑĀ* is grateful to all those experts who rendered their valuable services as referees for reviewing the papers received for this volume of the Journal.

****

The computational assistance received from
Miss. Darshana Kanthecha,
Research Student of Chemistry Department
for making of this volume of
PRAJÑĀ Journal is also gratefully acknowledged.

****

PRAJÑĀ - Journal of Pure and Applied Sciences

Volume 24-25 **December 2017**

CONTENTS

MATHEMATICS

PHYSICS

Sardar Patel University Press, Vallabh Vidyanagar, Gujarat - 388 120, INDIA

CHEMISTRY

HOMESCIENCE

ELECTRONICS

COMPUTER SCIENCE

MATERIAL SCIENCE

PRAJÑĀ - **Journal of Pure and Applied Sciences Vol. 24 – 25 : 1 – 6 (2017)**
ISSN 0975 - 2595

INFLUENCE OF TRANSVERSE SURFACE ROUGHNESS THROUGH A SERIES OF FLOW FACTORS ON THE PERFORMANCE OF A ROUGH FINITE PLANE SLIDER BEARING

GIRISH C. PANCHAL[1], HIMANSHU C. PATEL[2] AND G. M. DEHERI[3]

[1]Assistant Professor, Department of Mathematics, Government Engineering College, Modasa-383315, Gujarat-India.
E-mail. girish.maths@gecg28.ac.in, Telephone. +91-9825145377.
[2]Professor, Department of Mathematics, L. D. College of Engineering, Ahmedabad-380009, Gujarat-India.
E-mail. dr.prof.hcpatel@ldce.ac.in . Telephone. +91-9978440975.
[3]Former Associate Professor, Department of Mathematics, S.P. University, Vallabh Vidyanagar-388120, Gujarat-India. E-mail. gmdeheri@rediffmail.com . Telephone.02692233289.

ABSTRACT

An analysis of the influence of roughness parameters on the pressure and load carrying capacity for a rough finite inclined plane slider bearing with transversely rough surfaces has been conducted through a series of empirical pressure and shear flow factors. The associated stochastically averaged Reynolds' type equation is solved with suitable boundary conditions. Expressions are obtained for pressure and load carrying capacity. The numerical results are presented graphically. It can be seen that the load carrying capacity increases with the decrease in the surface roughness pattern parameter.

Keywords: Reynolds' equation, Finite inclined plane slider bearing, Pressure flow factor, Shear flow factor, Transverse Roughness, Load carrying capacity.

INTRODUCTION

It is assumed in many theoretical studies on lubricating films that the bearing surfaces are smooth. In reality this assumption is valid until the ratio of the nominal film thickness to the standard deviation of the roughness becomes large enough. The study of roughness effect is very important from the bearing's life period point of view. It is well known that the bearing surfaces after having some run-in and wear develop roughness. Sometimes even the contamination of lubricants and chemical degradation of the surfaces contribute to the roughness.

Due to an enormous use of slider bearings in various fields, like clutch plates, automobile transmission etc., there are many studies dealing with the investigations of slider bearings. The effect of surface roughness was dealt with many investigations viz. Tonder [1], Liao-Liang Ke et al. [2] and Thomas et al. [3]. The stochastic concept and Stochastic Reynolds' equation governing the mean pressure in bearings having transverse and longitudinal roughness were introduced by Christensen and Tonder [4-7]. This stochastic approach formed the basis of the analysis to study the effect of surface roughness in a number of investigations [8-10]. The thermal and roughness effects on different characteristics of finite rough tilted pad slider bearings were analyzed by Deresse and Sinha [11]. It was observed that for nonparallel slider bearing the load carrying capacity due to the combined effect is less than the load capacity due to the roughness effect for both longitudinal and transverse roughness models. Panchal et al. [12-13] analyzed the influence of roughness parameters on the pressure and load carrying capacity in a rough finite plane slider bearing for longitudinally rough surfaces by taking account of the influence of surface roughness through a series of flow factors, in which it was seen that the load carrying capacity decreases with the increase in the surface roughness pattern parameter.

The surface roughness effects on the dynamic characteristics of slider bearings with finite width were theoretically studied by Chiang, Hsiu-Lu et al. [9] and observed that the steady load-carrying capacity, dynamic stiffness and damping coefficient were increased as the effects of transverse roughness increased while the influences of the isotropic and longitudinal roughness had a reverse tendency. The effect of surface roughness on hydrodynamic lubrication of slider bearings of various film shapes such as plane, exponential, secant and hyperbolic slider

was analyzed by Andharia et al. [10]. Patir and Cheng [14-15] modified the averaged Reynolds' equation for rough surfaces. They defined pressure and shear flow factors which were obtained independently by numerical flow simulation using randomly generated roughness profiles. Etsion and Izhak [16] analyzed that theoretical modelling of surface texturing in hydrodynamic lubrication is a necessary first step to obtain favorable effect of the texturing. The effects of surface roughness characteristics on the load carrying capacity of tilt pad thrust bearings with water lubrication were studied though the average flow model by Wang, Yuechang et al. [18].

In this paper, an analysis has been conducted to evaluate the influence of surface roughness parameters and flow factors which are strongly dependent on the surface pattern parameter on a transversely rough plane inclined slider bearing.

ANALYSIS

Patir and Cheng [14-15] developed "Averaged Reynolds' equation" which took an account of the surface topography [17] (Fig. 1).

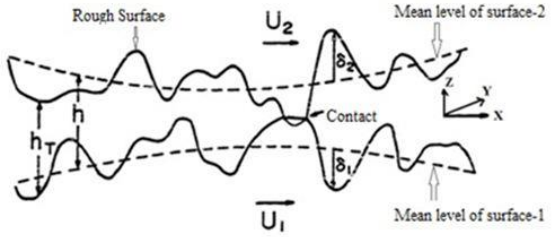

Fig. 1 Surface roughness and film geometry

The mean pressure in a rough slider bearing is governed by the averaged Reynolds' equation:

$$\frac{\partial}{\partial x}\left[\varphi_x \frac{h^3}{12\mu}\frac{\partial \bar{p}}{\partial x}\right]+\frac{\partial}{\partial y}\left[\varphi_y \frac{h^3}{12\mu}\frac{\partial \bar{p}}{\partial y}\right] = \frac{U}{2}\frac{\partial \bar{h}_T}{\partial x}+\frac{U\sigma}{2}\frac{\partial \varphi_s}{\partial x} \quad (1)$$

where φ_x and φ_y are pressure flow factors, φ_s is shear flow factor, $h_T=h+\delta$ is local film thickness, h is nominal film thickness (compliance), $\bar{h}_T$ is expected value of mean gap between two surfaces (separation), U is velocity of slider, μ is viscosity of lubricant, $\sigma=\sqrt{\sigma_1^2+\sigma_2^2}$ is composite r.m.s. roughness and $\bar{p}$ is mean pressure level.

The investigation assumes that the flow of lubricant is steady and in X-direction only. Moreover, for transversely rough surface *(γ < 1)*, the variations in roughness heights in *X*-direction are significant [17] (Fig. 2) so far as the performance is concerned. Hence, the effect of shear flow factor-φ_s is significant, which of course is negligible in the case of longitudinal rough surface *(γ > 1)*. Here γ is ratio of *x* and *y* correlation lengths of roughness.

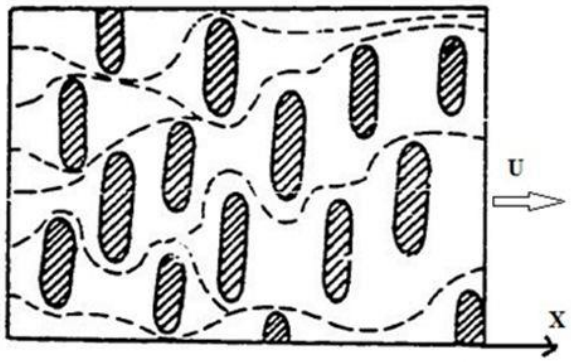

Fig. 2 Transverse rough surface (γ<1)

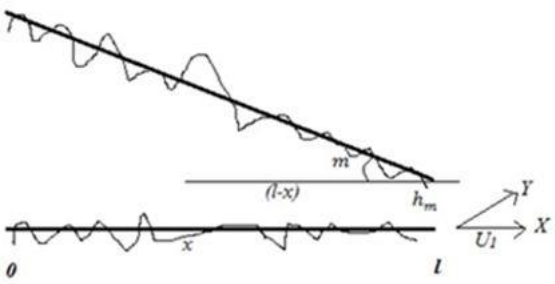

Fig. 3 Inclined plane slider bearing geometry

In view of above assumptions, Eq. (1) results in,

$$\frac{\partial}{\partial x}\left[\varphi_x \frac{h^3}{12\mu}\frac{\partial \bar{p}}{\partial x}\right]=\frac{U}{2}\frac{\partial \bar{h}_T}{\partial x}+\frac{U\sigma}{2}\frac{\partial \varphi_s}{\partial x} \quad (2)$$

For a rough plane slider bearing having the configuration as shown in Fig. 3, one considers

$$h = h_m + m(l - x) \tag{3}$$

where, h_m is minimum film thickness at the trailing edge of the slider bearing, l is the length of the slider bearing, m is the inclination of the slider bearing(Fig. 3).

Since δ is assumed to be stochastic in nature and is governed by the probability density function $f(\delta)$, $-c < \delta < c$, the mean α, the standard deviation σ and the skewness parameter ε are described as in Christensen – Tonder [4-7] and Deheri et al. [8] as:

$$E(R) = \int_{-c}^{c} R\, f(\delta)\, d\delta \tag{4}$$

$$E(\delta) = \alpha \tag{5}$$

$$E\left[(\delta - \alpha)^2\right] = \sigma^2 \tag{6}$$

And

$$E\left[(\delta - \alpha)^3\right] = \varepsilon \tag{7}$$

Where, c is maximum deviation from the mean film thickness. It is noteworthy that while α and ε can assume both positive and negative values, σ is always positive.

Following the discussion of in Christensen - Tonder [4-7], an approximation to $f(\delta)$ is,

$$f(\delta) = \begin{cases} \dfrac{32}{35c}\left(1 - \dfrac{\delta^2}{c^2}\right) & -c \le \delta \le c \\ 0 & \textit{elsewhere} \end{cases} \tag{8}$$

Thus $\bar{h}_T$ can be approximated as,

$$\bar{h}_T = \frac{13h}{8} \approx h \tag{9}$$

Now as per the averaging process discussed by Deheri et al. [8], Eq. (2) reduces to,

$$\frac{d}{dx}\left[\varphi_x \frac{g(h)}{12\mu}\frac{d(\bar{p})}{dx}\right] = \frac{U}{2}\frac{dh}{dx} + \frac{U\sigma}{2}\frac{d\varphi_s}{dx} \tag{10}$$

Where $(\bar{p})$ is expected value of the mean pressure level $\bar{p}$ and

$$g(h) = h^3 + 3h^2\alpha + 3h(\sigma^2 + \alpha^2) + (\varepsilon + 3\sigma^2\alpha + \alpha^3) \tag{11}$$

The empirical relations for φ_x and φ_s provided by Patir [17] are as under:

$$\varphi_x = 1 - C e^{-rH} \quad (\gamma \pi 1) \tag{12}$$

And

$$\varphi_s = A_1 H^{\alpha_1} e^{-\alpha_2 H + \alpha_3 H^2} \quad (\gamma \pi 1) \tag{13}$$

The dimensionless forms of these flow factors are

$$\varphi_x = 1 - C e^{-rh^* H_m} \quad (\gamma \pi 1) \tag{14}$$

And

$$\varphi_S = A_1 (h^* H_m)^{\alpha_1} e^{-\alpha_2 (h^* H_m) + \alpha_3 (h^* H_m)^2} \quad (\gamma \pi 1) \tag{15}$$

Where

$$H = \frac{h}{\sigma},\ h^* = \frac{h}{h_m},\ H_m = \frac{h_m}{\sigma} \tag{16}$$

While the constants C, r, A_1, α_1, α_2 and α_3 are given as functions of γ in the Table 1 and Table 2 (Patir [17]).

Making use of the following dimensionless quantities

$$h^* = \frac{h}{h_m},\ X = \frac{x}{l},\ m^* = \frac{ml}{h_m},\ \bar{P} = \frac{h_m^{\,2}(\bar{p})}{\mu U l},$$
$$\alpha^* = \frac{\alpha}{h_m},\ \sigma^* = \frac{\sigma}{h_m},\ \varepsilon^* = \frac{\varepsilon}{h_m^{\,3}} \tag{17}$$

And

$$G(h^*) = h^{*3} + 3h^{*2}\alpha^* + 3h^*(\sigma^{*2} + \alpha^{*2}) + (\varepsilon^* + 3\sigma^{*2}\alpha^* + \alpha^{*3}) \tag{18}$$

Eq. (10) turns to the dimensionless form

$$\frac{d}{dx}\left[\varphi_X\, G(h^*)\frac{d\bar{P}}{dX}\right] = 6\frac{d}{dX}\left[h^* + \sigma^* \varphi_S\right] \tag{19}$$

With the aid of the following boundary conditions:

$$\bar{P} = 0, \text{ at } X = 0 \text{ and } 1 \tag{20}$$

$$\frac{d\bar{P}}{dX} = 0, \text{at which the mean gap is maximum}$$

Eq. (19) leads to,

$$\bar{P}(X) = \int_0^X \frac{6\left(h^* + \sigma^* \varphi_X\right) - Q^*}{\varphi_X \, G(h^*)} dX \qquad (21)$$

Where,

$$Q^* = \frac{\int_0^1 \frac{6\left(h^* + \sigma^* \varphi_X\right)}{\varphi_X \, G(h^*)} dX}{\int_0^1 \frac{1}{\varphi_X \, G(h^*)} dX} \qquad (22)$$

The dimensionless load carrying capacity per unit width is given by,

$$W^* = \frac{w h_m^{\,2}}{\mu U l} = \int_0^1 \bar{P} \, dX$$

$$\therefore W^* = \int_0^1 \left[\int_0^X \frac{6\left(h^* + \sigma^* \varphi_X\right) - Q^*}{\varphi_X \, G(h^*)} dX \right] dX \qquad (23)$$

RESULTS AND DISCUSSION

In Fig. 4-6, we have the variations in load carrying capacity of the bearing with respect to α, which establish that the load carrying capacity increases with the increasing values of α (-ve) while α (+ve) causes decrease in the load carrying capacity, a property similar to the case of longitudinal roughness pattern [12,13]. We can observe that the increasing values of standard deviation σ, skewness ε (+ve) and roughness pattern parameter γ decrease the load carrying capacity.

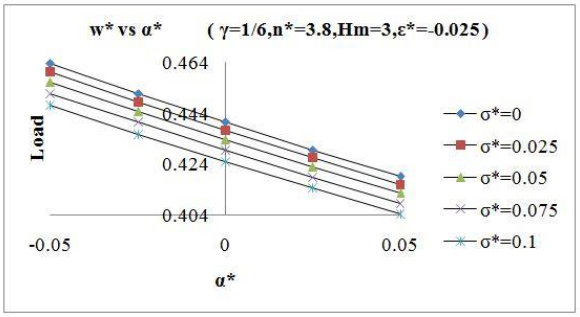

Fig. 4 Variation of load carrying capacity with respect to **α***

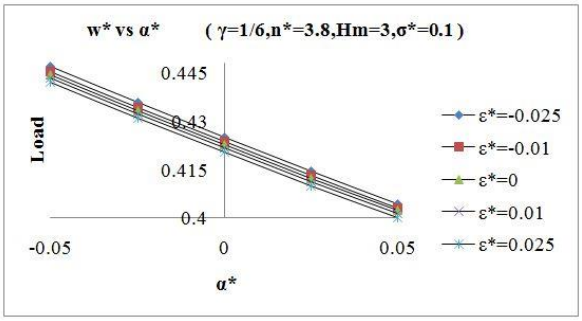

Fig. 5 Variation of load carrying capacity with respect to **α***

The variations in load carrying capacity of the bearing with respect to the standard deviation σ can be seen from Fig. 7-9, for various values of ε, α and γ. These reveal that the load carrying capacity enhances due to the decreasing values of standard deviation, increasing values of negatively skewed roughness, increasing values of variance (-ve) and decreasing values of roughness pattern parameter γ of the surfaces.

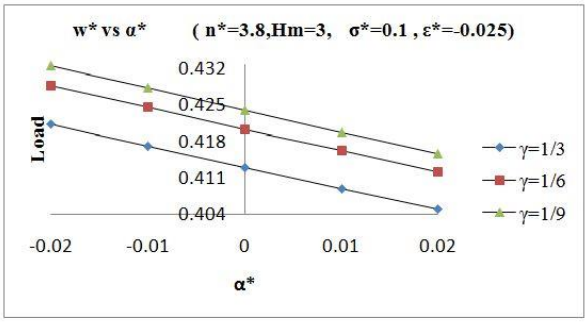

Fig. 6 Variation of load carrying capacity with respect to **α***

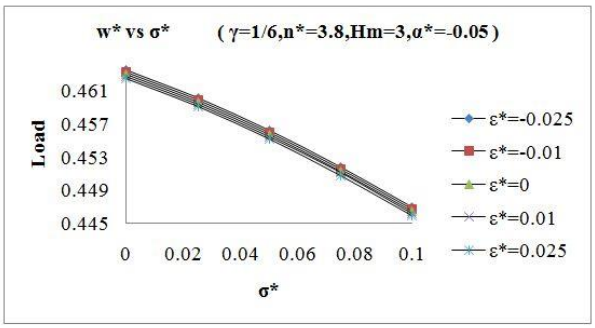

Fig. 7 Variation of load carrying capacity with respect to **σ***

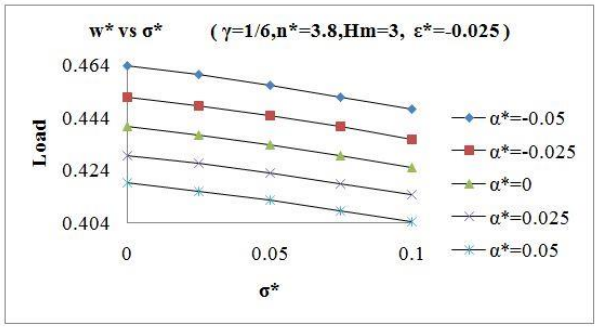

Fig. 8 Variation of load carrying capacity with respect to **σ***

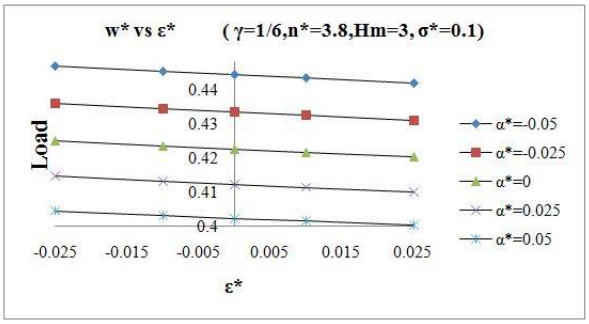

Fig. 11 Variation of load carrying capacity with respect to **ε***

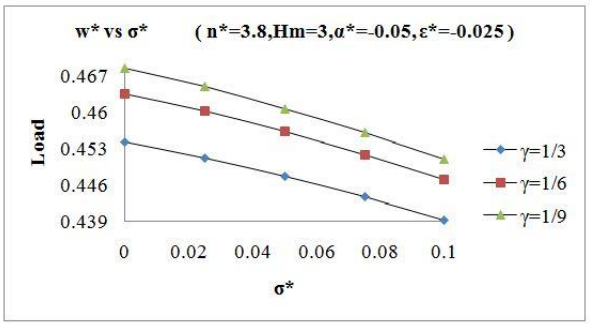

Fig. 9 Variation of load carrying capacity with respect to **σ***

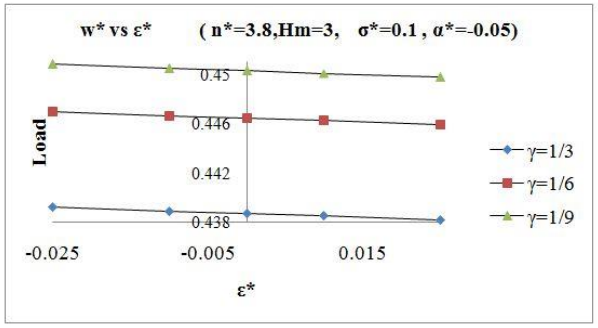

Fig. 12 Variation of load carrying capacity with respect to **ε***

Fig. 10-12 dealing with the effect of skewness on the load carrying capacity establishes that the load carrying capacity increases with the negatively skewed roughness, similar to the case of longitudinal roughness pattern [12-13] but the rate at which it goes up is very small.

The trend of load carrying capacity with respect to the roughness pattern parameter γ amplifies as the surface is more transverse while in the case of longitudinal roughness [12] the load carrying capacity reduces as the surface roughness is more longitudinal.

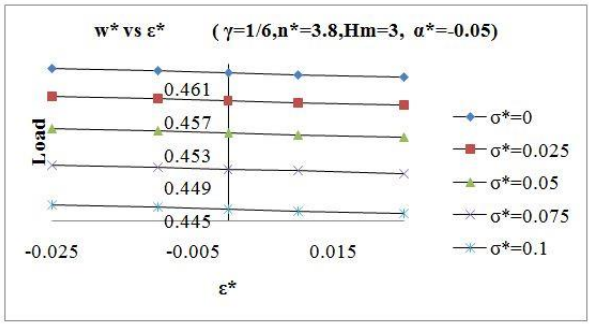

Fig. 10 Variation of load carrying capacity with respect to **ε***

CONCLUSION

In this paper, the effect of roughness parameters on the pressure and load carrying capacity for a rough finite inclined plane slider bearing with transversely rough surface has been analyzed. The results obtained here are compared with those of [8, 12-13]. It is observed that the load carrying capacity can be increased by decreasing the value of the roughness pattern parameter. This investigation suggests that the adverse effect of transverse surface roughness can be overcome to a great extent in the case of negatively skewed roughness under the presence of variance (-ve). However, from longevity point of view, the roughness aspect needs to be evaluated while designing the bearing system.

REFERENCES

[1] Tonder, K. C. (1972): Surface distributed waviness and roughness. First world conference in Industrial Tribology. Vol. 3.

[2] Ke, Liao-Liang, et al. (2010): Sliding frictional contact analysis of functionally graded piezoelectric layered half-plane. Acta mechanica 209.3-4: 249-268.

[3] Thomas, Evan, Mircea D. Pascovici, and Romeo P. Glovnea (2015): Load carrying capacity of a heterogeneous surface bearing. Friction 3.4: 287-293.

[4] Christensen H. (1969): Stochastic Models for Hydrodynamic Lubrication of Rough Surfaces. Proceedings of the Institution of Mechanical Engineers, vol. 184 no. 1 1013-1026.

[5] Christensen H., Tonder K. (1971): The Hydrodynamic Lubrication of Rough Bearing Surfaces of Finite Width. Journal of Lubrication Tech 93(3), 324-329.

[6] Christensen H., Tonder K. (1972): Waviness and Roughness in Hydrodynamic Lubrication. Proceedings of the Institution of Mechanical Engineers, vol. 186 no. 1, 807-812.

[7] Christensen H. (1972): A Theory of Mixed Lubrication. Proceedings of the Institution of Mechanical Engineers, vol. 186 no. 1 421-430.

[8] Deheri, G. M., P. I. Andharia, and R. M. Patel. (2005): Transversely rough slider bearings with squeeze film formed by a magnetic fluid. International Journal of Applied Mechanics and Engineering 10.1: 53-76.

[9] Chiang, Hsiu-Lu, et al. (2005): Surface roughness effects on the dynamic characteristics of finite slider bearings. Journal of CCIT 34.1: 1-11.

[10] P. I. Andharia, J. L. Gupta and G. M. Deheri. (2001): Effect of Surface Roughness on Hydrodynamic Lubrication of Slider Bearings. Tribology Transactions, Volume 44, Issue 2, pages 291-297.

[11] Deresse, Getachew A., and Prawal Sinha. (2011): THD analysis for finite slider bearing with roughness: special reference to load generation in parallel sliders. Acta mechanica 222.1-2: 1-15.

[12] Panchal Girishkumar C., Himanshu C. Patel and G. M. Deheri. (2016): Influence of surface roughness through a series of flow factors on the performance of a longitudinally rough finite slider bearing. Annals of the Faculty of Engineering Hunedoara-International Journal of Engineering 14.2.

[13] Panchal, G. C., H. C. Patel, and G. M. Deheri. (2016): Influence of magnetic fluid through a series of flow factors on the performance of a longitudinally rough finite slider bearing. Global Journal of Pure and Applied Mathematics 12.1: 783-796.

[14] Patir, Nadir, and H. S. Cheng. (1978): An average flow model for determining effects of three-dimensional roughness on partial hydrodynamic lubrication. Journal of Tribology 100.1: 12-17.

[15] Patir, Nadir and H. S. Cheng. (1979): Application of average flow model to lubrication between rough sliding surfaces. Journal of Tribology 101.2: 220-229.

[16] Etsion, Izhak. (2013): Modeling of surface texturing in hydrodynamic lubrication. Friction 1.3: 195-209.

[17] Patir N (1978): Effects of surface roughness on Partial film lubrication using an average flow model based on numerical simulation. Northwestern University, Ph.D. Chapter-2.

[18] Wang, Yuechang, et al. (2017): Surface roughness characteristics effects on fluid load capability of tilt pad thrust bearings with water lubrication. Friction: 1-10.

Table-1: Relation between γ, C, r and H

γ	**C**	**r**	***H***
1/3	1.16	0.42	H >0.75> 0.5
1/6	1.38	0.42	H > 1>0.5
1/9	1.48	0.42	H >1>0.5

Table-2: Relation between γ, A_1, α_1, α_2, α_3 and H

γ	A_1	α_1	α_2	α_3	$H=h/\sigma$
1/3	1.858	1.01	0.76	0.03	H > 0.5
1/6	1.962	1.08	0.77	0.03	H > 0.5
1/9	2.046	1.12	0.78	0.03	H > 0.5

PRAJÑĀ - **Journal of Pure and Applied Sciences Vol. 24 – 25 : 7–10 (2017)**
ISSN 0975 - 2595

INVENTORY MODEL FOR THE RAYLEIGH DISTRIBUTED DETERIORATION UNDER DEMAND INCLINING MARKET CONDITION

N. D. RAYKUNDALIYA

Department of Mathematics, Gujarat Arts and Science College, Ahmadabad, Gujarat
Email: nidhiray@gmail.com

ABSTRACT

In this paper, we introduce a deterministic inventory model under replenishment policy over a fixed planning period for the deteriorating items. Demand functionfollows positive linear trend. The holding cost is considered to be constant and shortages are allowed and moderately backlogged. Further, we assume that the deterioration rate follows the Rayleigh distribution. The model is explained analytically by diminishing the total inventory cost and obtained optimum period.

KEY WORDS: Inventory Model, Deterioration, Rayleigh Distribution, Partial Backlogging, Inclining Demand

INTRODUCTION

In last few years many researchers have developed inventory models for perishable items such as medicines, electronic components, food items, drugs and fashion goods. As we know, in reality the inventory is continuously reducing due to its demand and deterioration. Moreover the demand is changes consistently over the time period, most of the research is carried out related to inventory models, with linearly changing demand. Furhter, researchers extended these inventory models by considering the time and price sensitivity. Silver and Meal [19] gave modified EOQ models for time varying demand pattern. Inventory replenishment policy for the linear trend in demand over a finite time horizon was analytically solved by Donaldson [3]. However, this model is much complex as computationally point of view. For more clarity Ritchie ([15], [16] and [17]) derived simple procedure to find exact solution of that model. Mitra etal. [12] formulated a simple procedure for adjusting the economic order quantity model for the case of both increasing / decreasing linear trend in demand.

Deterioration takes place in many real life situations such as an expire date of medicines, failure of the batteries as they age and spoilages of an items .Deterioration is either constant over time or the Weibull distributed (i.e. time dependent). Dave and Patel [2] derived an inventory model for deteriorating items with time dependent demand which is linearly propostional. Hollier and Mak [6] formulated ordering policies for deteriorating items where demand function deplates exponentially over time. Several authors Raafat [14], Shah and Shah [18] and Goyal and Giri [4] have narrated idea of deteriorating demand and developed the inventory models.

All the above discussed inventory models were formulated in a static environment where the demand is assumed to be constant and steady over a finite planning horizon. However, in the realistic product lifecycle, demand is increasing with time during the growth phase. Mandal [9] studied an EOQ model for the Weibull distributed deteriorating items under ramp-type demand and shortages. Mishraand Singh ([10], [11]) constructed an inventory model for ramp-type demand, time dependent deteriorating items with salvage value and shortages and deteriorating inventory model for time dependent demand and holding cost and with partial backlogging. Hung [7] investigated an inventory model with generalized type demand, deterioration and back order rates. Mishra et al. [13] considered time dependent demand and developed an inventory model for deteriorating items where deterioration rate and holding cost are constants shortages are allowed and partially backlogged.

Lord Rayleigh (1880) introduced the Rayleigh distribution in connection with problem in the field of acoustics. It has some relation with the Weibull, chi-square or extreme value distributions. The important characteristic of the Rayleigh distribution is that its hazard function is increase function of time. For more details, one can refer the Johnson, Kotz and Balakrishnant [8].

Recently, Acharya and Debata [1] introduced an inventory model for constant deteriorating with time increasing demand under partial backlogging.On the line of Acharya and Debata [1] we generalize the inventory models. Here, we consider linearly time dependent demand and develop an inventory model for deteriorating items have one parameter the Rayleigh distribution, in which shortages is allowed and partially backlogged. This paper is organized as follow: In Section 2, we give notation and assumptions. The probability density function, cumulative distribution function and hazard rate function are discussed in Section 3. The mathematical model for inventory is developed in Section 4 and concluding remarks are given in Section 5.

NOTATION AND ASSUMPTION

Fundamental notation and assumption used in this paper is as follows

Assumption:

- Demand is time dependent linear function
- The replenishment rate is infinite
- Deterioration rate follow one parameter Rayleigh distribution
- Shortages are allowed and are partially backlogged
- Lead time is zero

Notations:

- Demand rate $D(t) = a + bt;\ \ a, b > 0$ are constants
- $I(t)$ level of inventory at time $t,\ 0 \leq t \leq T$
- T length of the cycle
- Deterioration rate $\theta(t) = \frac{t}{\sigma^2};\ \sigma > 0$ is scale parameter
- t_1 time when the inventory level reaches zero
- t_1^* optimal time
- A static ordering cost per order
- C_θ cost of deterioration per item
- C_h inventory holding cost per unit per unit time
- C_s shortage cost per unit per unit time
- I_m maximum inventory level for the ordering cycle, such that $I_m = I(0)$
- $C_T(t_1)$ average total cost per unit time under the condition $t_1 \leq T$

PROBABILITY DENSITY FUNCTION, CUMULATIVE DISTRIBUTION FUNCTION AND HAZARD RATE FUNCTION OF THE RAYLEIGH DISTRIBUTION

The random variable t is said to have one parameter Rayleigh distribution if its probability density function is given by

$$f(t;\sigma^2) = \frac{t}{\sigma^2} e^{-\frac{t^2}{2\sigma^2}}\ ;\ t > 0\ ;\ \sigma > 0\ ,$$

where σ is scale parameter

and the corresponding cumulative distribution function is given by

$$F(t;\sigma^2) = \left(1 - e^{-\frac{t^2}{2\sigma^2}}\right);\ t > 0\ ;\ \sigma > 0\ ,$$

and its hazard (Deterioration) rate function is

$$\theta(t;\sigma^2) = \frac{\mathrm{f(t)}}{1-\mathrm{F(t)}} = \frac{t}{\sigma^2};\ \ t > 0\ ;\ \sigma > 0$$

MATHEMATICAL MODEL

The behavior of the inventory system can be defined by the following differential equations:

$$\frac{dI(t)}{dt} = -D(t) - \theta(t)I(t)\ ;\quad 0 \leq t \leq t_1 \quad (1)$$

$$\frac{dI(t)}{dt} = -D(t) t_1 \leq t \leq T \qquad (2)$$

With initial condition $I_m = I(0), I(t_1) = 0$

The solution of equation (1) and (2) using series expansion and neglecting the higher terms of σ^2 by considering $\sigma > 0.7$with boundary conditions is as follows

$$I(t) = a(t_1 - t) + \frac{b}{2}(t_1^2 - t^2) + \frac{a}{6\sigma^2}(t_1^3 - t^3) +$$

$$\frac{b}{8\sigma^2}(t_1^4 - t^4) - \frac{a}{2\sigma^2}(t_1 - t)t^2 -$$

$$\frac{b}{2\sigma^2}(t_1^2 - t^2)t^2 \; ; 0 \le t \le t_1 \qquad (3)$$

$$I(t) = a(t_1 - T) + \frac{b}{2}(t_1^2 - T^2); \quad t_1 \le t \le T \qquad (4)$$

Maximum inventory level can be computed as

$$I_m = I(0) = at_1 + \frac{bt_1^2}{2} + \frac{a}{6\sigma^2}t_1^3 + \frac{b}{8\sigma^2}t_1^4 \qquad (5)$$

Now, total number of deteriorating items, sayD_T during time interval $[0, t_1]$ is

$$D_T = I_m - \int_0^{t_1} D(t)dt = \frac{a}{6\sigma^2}t_1^3 + \frac{b}{8\sigma^2}t_1^4 \qquad (6)$$

Total number of inventory holding, sayH_T during the interval $[0, t_1]$is

$$H_T = \int_0^{t_1} I(t)dt = \frac{at_1^2}{2} + \frac{b}{3}t_1^3 + \frac{a}{12\sigma^2}t_1^4 + \frac{b}{30\sigma^2}t_1^5 \qquad (7)$$

Total shortage quantity, say B_T during the interval $[t_1, T]$ is

$$B_T = -\int_{t_1}^{T} I(t)dt = \frac{a}{2}\left(T^2 + \frac{3}{2}t_1^2 - 2t_1T\right) + \frac{b}{6}(T^3 + 2t_1^3 - 3t_1^2T) \qquad (8)$$

Hence, average cost per unit time under the condition $t_1 \le T$ is

$$C_T(t_1) = \frac{1}{T}[A + C_\theta D_T + C_h H_T + C_s B_T] \qquad (9)$$

To minimized the total average cost $C_T(t_1)$ the necessary condition is $\frac{dC_T(t_1)}{dt_1} = 0$.

Which gives

$$\frac{1}{T}\left[C_\theta\left(\frac{a}{2\sigma^2}t_1^2 + \frac{b}{2\sigma^2}t_1^3\right) + C_h\left(at_1 + bt_1^2 + \frac{a}{3\sigma^2}t_1^3 + \frac{b}{6\sigma^2}t_1^4\right) + C_s\left(\frac{3at_1}{2} - aT + bt_1^2 - bt_1T\right)\right]$$

$$= g(t_1) \text{ (say)} \qquad (10)$$

Now, $g(0) = -aC_s < 0$ and

$$g(T) = \frac{1}{T}\left[C_\theta\left(\frac{a}{2\sigma^2}T^2 + \frac{b}{2\sigma^2}T^3\right) + C_s\left(\frac{aT}{2}\right) + C_h\left(aT + bT^2 + \frac{a}{3\sigma^2}T^3 + \frac{b}{6\sigma^2}T^4\right)\right] > 0$$

and

$$g'(t) = \frac{1}{T}\left[C_\theta\left(\frac{at_1}{2\sigma^2} + \frac{3b}{2\sigma^2}t_1^3\right) + C_h\left(a + 2bt_1 + \frac{a}{\sigma^2}t_1^2 + \frac{2b}{3\sigma^2}t_1^3\right) + C_s\left(\frac{3a}{2} + 2bt_1 - bT\right)\right] > 0$$

Which indicates that the function is strictly monotonically increasing function and equation (10) has unique solution (say) t_1^* where$t_1^* \epsilon [0, T]$ which gives the minmum answer.
Therefore, we have

Property:
Inventory model for the rayleigh distributed deterioration under the condition $0 < t_1 < T$, $C_T(t_1)$ obtains its minimumat $t_1 = t_1^*$ where $g(t_1^*) = 0$ if t_1^*<*T*.

CONCLUDING REMARKS

In this paper, we studied replenishment policy over a fixed planning period for a deteriorating items having deterministic demand with positive linear trend and shortages. The holding cost was considered to be constant over a planning period and the deteriorating items follow the Rayleigh distribution. The model was solved analytically by minimizing the total inventory cost and obtained optimal period. In future, one can generalized the model by applying time varying holding cost and by considering time varying demand having Weibull distribution. Numerical analysis can be performed to validate solution obtained for inventory policy.

REFERENCES

[1] Acharya and Debata (2014). An inventory model for deteriorating items with time dependent demand under partial backlogging. International Journal of Research

in Advent Technology, Volume 2, issue 1,pp. 86-90

[2] Dave, U. and Patel, L. K. (1981). (T, Si) – policy inventory model for deteriorating items with time proportional demand. Journal of the Operational Research Society,32, pp. 137 – 142.

[3] Donaldson, W. A. (1977). Inventory replenishment policy for a linear trend in demand – an analytical solution. Operational Research Quarterly, 28,pp. 663 – 670.

[4] Goyal, S. K. and Giri, B. C. (2001). Recent trends in modeling of deteriorating inventory. European Journal of Operational Research, 134, pp. 1 – 16.

[1] Hollier, R. H. and Mak, K.L. (1983).Inventory replenishment policies for deteriorating items in declining market. International Journal of Production research, 21, pp. 813-826.

[2] Hung, K. C. (2011). An Inventory model with generalized type demand, deterioration and backorder rates. Eur. J. Oper.Res., 208, pp. 239-242.

[3] Johnson, N.L., Kotz,S. and Balakrishnan, N.(1994). Continuous Univariate Distribution-Volume 1. John Wiley & Sons, New York.

[4] Mandal, B. (2010). An EOQ model for Weibull distributed deteriorating items under ramp type demand and shortages.Opsearch, 47, pp.158-165.

[5] Mishra, V. K., Singh, L. S. (2011a). Inventory model for ramp type demand, time dependent deteriorating items withsalvage value and shortages. Int. J. Appl. Math. Stat., 23, pp.84-91.

[6] Mishra, V. K., Singh, L. S. (2011b). Deteriorating inventory model for time dependent demand and holding cost with partial backlogging. Int. J. Manage. Sci. Eng. Manage, 6, pp.267-271.

[7] Mitra, A., Cox, J. F. and Jesse, R. R. (1984). A note on determining order quantities with a linear trend in demand. Journal of the Operational Research Society, 39, pp.687 – 692.

[8] Mishra, V. K., Singh, L. and Kumar, R. (2013): An inventory model for deteriorating items with time dependent demand and time varying holding cost under partial backlogging. J. Indst. Eng. Int., 9, pp.4-8.

[9] Raafat, F.(1991). Survey of literature on continuously deteriorating inventorymodels. Journal of the Operational Research Society, 40, pp.27 – 37.

[10] Ritchie, E. (1980). Practical inventory replenishment policies for a linear trend in demand followed by a period of steady demand. Journal of the Operational Research Society, 31, pp. 605 – 613.

[11] Ritchie, E. (1984). The EOQ for linear increasing demand: A simple optimal solution. Journal of the Operational Research Society, 35, pp.949 – 952.

[12] Ritchie, E. (1985). Stock replenishment quantities for unbounded linear increasing demand: An interesting consequence of the optimal policy. Journal of the Operational Research Society, 36, pp.737 – 739.

[13] Shah, Nita H. and Shah, Y. K. (2000). Literature survey on inventory models for deteriorating items. Economic Annals, 44, pp. 221 – 237.

[14] Silver, E. A. and Meal, H. C. (1969). A simple modification of the EOQ for the case of varying demand rate. Production of Inventory Management, 10 (4), pp.52 – 65.

PRAJÑĀ - **Journal of Pure and Applied Sciences Vol. 24 – 25 : 11–14 (2017)**
ISSN 0975 - 2595

Lanczos Potential for Weyl Metric

A.H. HASMANI[1], A.C. PATEL[2] AND RAVI PANCHAL[3]

[1]*Department of Mathematics, Sardar Patel University, Vallabh Vidyanagar-388120.*
[2]*Department of Applied Sciences and Humenities, Hasmukh Goswami College of Engineering, Vahelal-382330.*
[3]*Mathematics and Humanities Department, Gandhinagar Institute of Technology, Moti Bhoyan-382721.*

ABSTRACT

The Weyl metric represents a static spacetime which is non-vacuum in nature and does not fall in any of the Petrov types. In this paper, we have obtained Lanczos potential for the Weyl metric.

Keywords: Lanczos Potential, Newman-Penrose Formalism, Weyl Metric.

INTRODUCTION

It is known that the Weyl curvature tensor C_{hijk} (gravitational field) can be generated by the covariant differentiation of a rank three tensor L_{ijk} through the equation ([10], [11], [17])

$$\begin{aligned} C_{hijk} &= L_{hij;k} - L_{hik;j} + L_{jkh;i} - L_{jki;h} \\ &+ L_{(hk)}g_{ij} + L_{(ij)}g_{hk} - L_{(hj)}g_{ik} - L_{(ik)}g_{hj} \\ &+ \frac{2}{3}L^{pq}_{p;q}\left(g_{hj}g_{ik} - g_{hk}g_{ij}\right), \end{aligned} \tag{1}$$

where

$$L_{ij} = L^{k}_{i\ j;k} - L^{k}_{i\ k;j}. \tag{2}$$

Equation (1) is known as Weyl-Lanczos relation and the tensor L_{ijk} is known as Lanczos potential. It satisfies the following properties

$$\begin{aligned} &L_{ijk} = -L_{jik,} \\ &L^{t}_{it} = 0,\ (or\ g^{kl}L_{kil} = 0), \\ &L_{ijk} + L_{jki} + L_{kij} = 0, \\ &L_{ij}^{\ k} = 0. \end{aligned} \tag{3}$$

Due to the properties (3), the non-trivial components of the Lanczos potential tensor reduces to ten out of sixty four. For arbitrary spacetimes, it is difficult to solve Weyl-Lanczos relation (1), as they are non-linear in nature. However, Novello and Velloso have obtained Lanczos potential for perfect fluid spacetimes by considering different conditions on general observer quantities. Newman-Penrose (NP) form of Weyl-Lanczos relation has proved useful for finding Lanczos potential for vacuum spacetimes of particular Petrov types [6]. Due to involvement of tetrad components of Ricci tensors in the NP field equations, Lanczos potential for non-vacuum spacetimes becomes difficult. Thus, it will become helpful to find Lanczos potential for particular non-vacuum spacetimes and it will lead us to Lanczos potential for arbitrary spacetimes. Recently, Hasmani and Panchal [16] have obtained Lanczos potential for Vaidya metric and Van-Stockum metric. Many solutions of Weyl-Lanczos relations have been obtained [1]-[12],[18],[20],[21]. But, a large class of solutions is still uncovered especially for non-vacuum spacetimes. Thus, it is fruitful to find Lanczos potentials for unknown situations.

The Weyl metric is non-vacuum and none of the Petrov types. The Lanczos potential for this metric has been obtained and the Lanczos scalars have been expressed in term of spin coefficients. The necessary computations are carried out using Mathematica programs developed by Hasmani and co-workers [13]-[15].

WEYL METRIC

The Weyl metric [15], in cylindrical coordinates, is given by

$$ds^2 = \frac{1}{f}[e^{2\gamma}\left(dr^2 + dz^2\right) + r^2 d\varphi^2] - f dt^2, \tag{4}$$

where f and γ are real function of r and z.

The following is chosen null tetrad,

$$l^k = \frac{1}{\sqrt{2}}\left(e^{-\gamma}\sqrt{f}\,\delta_1^k + \frac{1}{\sqrt{f}}\,\delta_4^k \right),$$
$$n^k = \frac{1}{\sqrt{2}}\left(-e^{-\gamma}\sqrt{f}\,\delta_1^k + \frac{1}{\sqrt{f}}\,\delta_4^k \right),$$
$$m^k = \frac{1}{\sqrt{2}}\left(e^{-\gamma}\sqrt{f}\,\delta_2^k + i\frac{\sqrt{f}}{r}\,\delta_3^k \right), \qquad (5)$$
$$\overline{m}^k = \frac{1}{\sqrt{2}}\left(e^{-\gamma}\sqrt{f}\,\delta_2^k - i\frac{\sqrt{f}}{r}\,\delta_3^k \right).$$

General Observer Quantities

For the Weyl metric (4), we choose a unit time like velocity vector as,

$$u^k = \frac{1}{\sqrt{2}}\left(l^k + n^k\right) = \left(0,0,0,\frac{1}{\sqrt{f}}\right). \qquad (6)$$

A field of observers with this velocity is expansion-free, shear-free and rotation-free. Also, the non-zero components of acceleration vector are,

$$a_1 = -\frac{f'}{2f}, \quad a_2 = -\frac{f_z}{2f}, \qquad (7)$$

where prime (') denotes partial derivative with respect to r, and partial derivative with respect to z is denoted by suffix. The non-zero independent components of electric part of the Weyl tensor are,

$$E_{11} = \frac{1}{6rf}\left(-3rf_z\gamma_z + rf_{zz} + rf\gamma_{zz} + f' - 3f\gamma' + 3rf'\gamma' - 2rf'' + rf\gamma''\right),$$
$$E_{12} = E_{21} = \frac{1}{2rf}\left(-f\gamma_z + r\gamma_z f' + rf_z\gamma' + rf_z'\right),$$
$$E_{22} = \frac{1}{6rf}\left(3rf_z\gamma_z - 2rf_{zz} + rf\gamma_{zz} + f' + 3f\gamma' - 3rf'\gamma' + rf'' + rf\gamma''\right),$$
$$E_{33} = \frac{re^{-2\gamma}}{6f}\left(-2f'' + rf_{zz} + rf'' - 2rf\gamma_{zz} - 2rf\gamma''\right) \qquad (8)$$

and all components of magnetic parts of the Weyl tensor vanish. Thus, the Weyl metric is purely electric.

Newman-Penrose Quantities

The following are non-vanishing spin coefficients,

$$\kappa = -\nu = \frac{e^{-\gamma}}{2\sqrt{2f}}\left(f\gamma_z - f_z\right),$$
$$\tau = -\pi = -\frac{\sqrt{f}e^{-\gamma}}{2\sqrt{2}}\gamma_z,$$
$$\sigma = \lambda = \frac{\sqrt{f}e^{-\gamma}}{2\sqrt{2}\,r}\left(1 - r\gamma'\right), \qquad (9)$$
$$\rho = \mu = \frac{e^{-\gamma}}{2\sqrt{2f}\,r}\left(rf' - f - rf\gamma'\right),$$
$$\varepsilon = \gamma = \frac{e^{-\gamma}}{4\sqrt{2f}}\,f',$$
$$\alpha = -\beta = \frac{e^{-\gamma}}{4\sqrt{2f}}\,f_z$$

and NP Weyl scalars are as follows,

$$\Psi_0 = \Psi_4 = -\frac{e^{-2\gamma}}{4r}\left(rf_z\gamma_z - rf_{zz} + rf\gamma_{zz} + f' + f\gamma' - rf'\gamma' + rf\gamma''\right),$$
$$\Psi_1 = \Psi_3 = \frac{e^{-2\gamma}}{4r}\left(-f\gamma_z + rf'\gamma_z + rf_z\gamma' - rf_z'\right),$$
$$\Psi_2 = -\frac{e^{-2\gamma}}{12r}\left(-3rf_z\gamma_z + rf_{zz} + rf\gamma_{zz} + f' - 3f\gamma' + 3rf'\gamma' - 2rf'' + rf\gamma''\right). \qquad (10)$$

The following are non-vanishing Newman-Penrose complex scalars for Weyl metric,

$$\Phi_{00} = \Phi_{22} = \frac{e^{-2\gamma}}{8rf}\left(-2rf_z^{\,2} - 3rf'^2 + 2ff' + 2ff_{zz} + 2rff'' + 2f^2\gamma' - 2rf^2\gamma_{zz} - 2rf^2\gamma''\right),$$
$$\Phi_{01} = \Phi_{10} = \frac{e^{-2\gamma}}{8rf}\left(2f^2\gamma_z - rf_z f'\right),$$
$$\Phi_{02} = \Phi_{20} = \frac{e^{-2\gamma}}{8rf}\left(-rf_z^{\,2} - 2f^2\gamma' - 2rf^2\gamma'' - 2rf^2\gamma_{zz}\right),$$

$$\Phi_{11} = \frac{e^{-2\gamma}}{16rf}\left(-3rf_z^{\,2} - rf'^2 - 4f^2\gamma' + 2ff' + 2rff_{zz} + 2rff''\right),$$
$$\Phi_{12} = \Phi_{21} = \frac{e^{-2\gamma}}{8rf}\left(-2f^2\gamma_z + rf_z f'\right). \quad (11)$$

Thus, the metric (4) is non-vacuum and none of the Petrov types.

LANCZOS POTENTIAL

For Weyl metric (4) with tetrad (6), the field of observer u^k is shear-free and irrotational. Thus, the Lanczos potential [20] is given by,

$$L_{ijk} = a_i u_j u_k - a_j u_i u_k, \quad (12)$$

up to a gauge. To exhibit L_{ijk} in the Lanczos gauge, we have considered,

$$L_{ijk} = a_i u_j u_k - a_j u_i u_k - \frac{1}{3}\left(a_i g_{jk} - a_j g_{ik}\right). \quad (13)$$

The non-zero independent components of the Lanczos potential tensor for Weyl metric are as follow,

$$L_{121} = \frac{e^{2\gamma} f_z}{6f^2}, \qquad L_{122} = -\frac{e^{2\gamma} f'}{6f^2},$$
$$L_{133} = -\frac{r^2 f'}{6f^2}, \qquad L_{144} = -\frac{f'}{3},$$
$$L_{233} = -\frac{r^2 f_z}{6f^2}, \qquad L_{244} = -\frac{f_z}{3} \quad (14)$$

and non-zero Lanczos potential scalars [16] as follows

$$L_0 = -3L_2 = 3L_5 = -L_7 = \frac{e^{-\gamma} f_z}{4\sqrt{2f}},$$
$$L_1 = L_6 = -\frac{e^{-\gamma} f'}{6\sqrt{2f}}. \quad (15)$$

RESULTS AND DISCUSSION

Using Lanczos scalars (15) and spin coefficients (9), it is possible to establish a linear relationship between them for the Weyl metric as,

$$L_0 = -3L_2 = 3L_5 = -L_7 = \alpha,$$
$$L_0 = L_6 = -\frac{2}{3}\varepsilon. \quad (16)$$

CONCLUSION

The Weyl metric is non-vacuum spacetime which is none of the Petrov types. Lanczos potential for the Weyl metric has been obtained. The Lanczos potential scalars depend on only two spin coefficients α and ε. Also, it supports the conjecture that there is linear relationship between Lanczos scalars and spin coefficients. It is hoped that the results obtained here will help researchers for finding the Lanczos potential for other non-vacuum spacetimes.

ACKNOWLEDGEMENT

The authors are thankful to the learned anonymous referee for his valuable comments which enhanced the content of the manuscript.

REFERENCES

[1] Ahsan, Z., and Bilal, M. (2010): A Solution of Weyl-Lanczos Equations for Arbitrary Petrov Type D Vacuum Spacetimes. *International Journal of Theoretical Physics*, **49:** 2713-2722.

[2] Ahsan, Z., and Bilal, M. (2010): On the Lanczos Potential for Petrov Type N Spacetimes. *Journal of Vectorial Relativity*, **5:** 1-8.

[3] Ahsan, Z., and Bilal, M. (2011): Lanczos Potential and Perfect Fluid Spacetimes. *International Journal of Theoretical Physics*, **50:** 1752–1768.

[4] Ahsan, Z., and Bilal, M. (2012): On the Lanczos Potential for Petrov Type III Spacetimes. *Journal of Tensor Society*, **6:** 127-134.

[5] Ahsan, Z., and Bilal, M. (2013): Lanczos Potential for Arbitrary Petrov Type II Spacetimes. *International Journal of Theoretical Physics*, **52:** 4275-4282.

[6] Ares de Parga, G., Chayoya A., A., O., And Lopez Bonilla, J. L. (1989): Lanczos Potential. *Journal of Mathematical Physics*, **30:** 1294-1295.

[7] Caltenco, J., López-Bonilla, J., and Zúñiga-Segundo, A. (2002): Lanczos Spin tensor and GHP Formalism. *Czechoslovak Journal of Physics*, **52:** 901-909.

[8] Dolan, P., and Kim, C. W. (1994): Some Solutions of the Lanczos Vacuum Wave Equation. *Proceedings of the Royal Society*

of London A: Mathematical, Physical and Engineering Sciences, **447:** 577–585.

[9] Dolan, P., and Muratori, B. D. (1998): The Lanczos Potential for Vacuum Space-Times with an Ernst Potential. *Journal of Mathematical Physics,* **39:** 5406-5420.

[10] Dolan, P., and Kim, C. W. (1994): Some Solutions of the Lanczos Vacuum Wave Equation. *Proceedings of the Royal Society of London A: Mathematical, Physical and Engineering Sciences*, 447, **1931:** 577-585.

[11] Dolan, P., and Kim, C. W. (1994) The Wave Equation for the Lanczos Potential I. *Proceedings of the Royal Society of London A: Mathematical, Physical and Engineering Sciences,* **447:** 557-575.

[12] Edgar, S. B., and Höglund, A. (2000): The Lanczos Potential for Weyl-Candidate Tensors Exists Only in Four Dimensions. *General Relativity and Gravitation,* **32:** 2307–2318.

[13] Hasmani, A. (2010): Algebraic Computation of Newman-Penrose Scalars in General Relativity using Mathematica. *Journal of Science,* **1:** 82–83.

[14] Hasmani, A., and Andharia, P. (2011): Algebraic Computation of Spin Coefficients in Newman-Penrose Formalism using Mathematica. *Journal of Dynamical Systems and Geometric, Theories* **9:** 27–36.

[15] Hasmani, A. H., and Panchal, R. (2015): Algebraic Computations of General Observer Quantities using Mathematica. *Astrophysics and Space Science,* **359:** 1–5.

[16] Hasmani, A. H., and Panchal, R. (2016): Lanczos Potential for Some Non-Vacuum Spacetimes. *The European Physical Journal Plus,* **131:** 1–6.

[17] Lanczos, C. (1962): The Splitting of the Riemann Tensor. *Rev. Mod. Phys.*, **34:** 379-389.

[18] Maher, W. F., and Zund, J. D. (1968): A Spinor Approach to the Lanczos Spin Tensor. *Il Nuovo Cimento A* (1965-1970), **57:** 638–648.

[19] Newman, E., and Penrose, R. (1962): An Approach to Gravitational Radiation by a Method of Spin Coefficients. *Journal of Mathematical Physics,* **3:** 566-578.

[20] Novello, M., and Velloso, A. L. (1987): The Connection between General Observers and Lanczos Potential. *General Relativity and Gravitation,* **19:** 1251–1265.

[21] O'Donnell, P. (2004): Letter: A Solution of the Weyl-Lanczos Equations for the Schwarzschild Space-Time. *General Relativity and Gravitation,* **36:** 1415-1422.

[22] Roberts, M. D. (1995): The Physical Interpretation of the Lanczos Tensor. *Il Nuovo Cimento B,* (1971-1996), **110:** 1165–1176.

[23] Weyl, H. (1917): The theory of gravitation. *Annalen Phys,* **54:** 1-14.

PRAJÑĀ - **Journal of Pure and Applied Sciences Vol. 24 – 25 : 15–22 (2017)**
ISSN 0975 - 2595

MATHEMATICAL MODELLING OF FINGERO-IMBIBITION PHENOMENON IN HETEROGENEOUS POROUS MEDIUM WITH MAGNETIC FIELD EFFECT

MAHENDRA A. PATEL[1] AND N. B. DESAI[2*]

[1]Government Engineering College, Gandhinagar-382028, Gujarat (India),
E-mail: mahendraapatel@yahoo.co.in. Telephone. +91-9737730526
[2] A. D. Patel Institute of Technology, New V. V. Nagar-388121, Gujarat (India),
E-mail: drnbdesai@yahoo.co.in. Telephone. +91-9327158932

ABSTRACT

The present paper discusses the mathematical model for fingero-imbibition phenomenon arising in fluid flow through the heterogeneous porous medium with magnetic field effect during secondary oil recovery process. The mathematical formulation leads to a nonlinear partial differential equation and its solution has been obtained with appropriate boundary conditions by homotopy analysis method. The solution represents the saturation of injected water for fingero-imbibition phenomenon which increases when distance increases for given time. The graphical and numerical representations of the solution are discussed.

Keywords: Fluid flow, Heterogeneous porous medium, Fingero-imbibition phenomenon, Homotopy analysis method.

AMS subject classification: 76S05, 76Txx, 65Nxx, 35Q35.

INTRODUCTION

If a porous medium filled with some phase (oil) is brought into contact with another phase (water) which preferentially wets the medium, there is a spontaneous flow of the wetting phase (water) into the medium and a counter flow of the native phase (oil) from the medium. This phenomenon occurring due to the difference of wetting abilities of the phases is called imbibition phenomenon. Besides this if a porous medium filled with one phase (oil) is displaced by another phase (water) of lesser viscosity, then instead of regular displacement of the whole front, protuberances may occur which shoot through the porous medium at relatively very high speed giving rise to the fingering phenomenon. This simultaneous occurrence of both phenomena fingering and imbibition is known as fingero-imbibition phenomenon (see fig. 1).

The imbibition phenomenon have been investigated by many researches with different aspects. Mishra and Verma [3] have discussed imbibition in the flow of two immiscible fluids (oil and water) with magnetic field. Shah and Verma [5] have obtained the numerical solution of fingero-imbibition phenomenon through homogeneous porous media with magnetic field using finite difference method. Desai [21] has discussed the imbibition phenomenon by similarity transform. Patel, Mehta and Patel [9] have discussed mathematical model of imbibition phenomenon in heterogeneous porous media. Parikh, Mehta and Pradhan [10] have discussed mathematical modeling of fingero-imbibition phenomenon in homogeneous porous medium with magnetic field effect in vertical downward direction. Patel, Rabari and Bhathawala [11] have obtained numerical solution of imbibition phenomenon in a homogeneous medium with magnetic fluid.

In the present work, we have developed the mathematical model for fingero-imbibition phenomenon in heterogeneous porous medium with magnetic field effect. The mathematical formulation leads to the governing nonlinear partial differential equation. The solution of the problem have been obtained using homotopy analysis method [20]. The main aim of this work is to find the solution (the saturation of injected water) of the fingero-imbibition phenomenon in

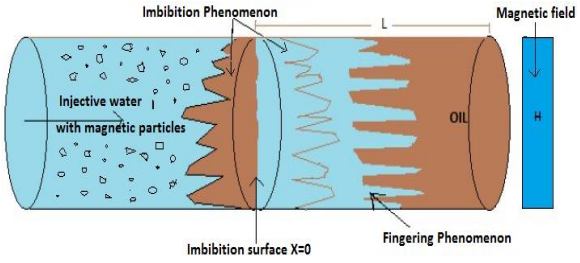

Figure 1: Fingero-imbibition phenomenon.

the heterogeneous porous medium with magnetic field effect.

AIM AND SCOPE OF THE WORK

The aim with this work is to discuss the mathematical model for fingero-imbibition phenomenon arising in fluid flow through the heterogeneous porous medium with magnetic field effect during secondary oil recovery process. The solution of problem is obtain by using homotopy analysis method. This solution represents the saturation of injected water which helps us to predict the amount of water required to inject for recovering oil. This type of mathematical model is useful for predicting oil recovery from petroleum reservoir.

STATEMENT OF THE PROBLEM

Here we consider the cylindrical piece of heterogeneous porous matrix of length *L* which is filled with oil. During the secondary oil recovery process, the imbibition phenomenon will occur simultaneously with fingering which describes the fingero-imbibition phenomenon. It is considered that the flow of water with magnetic particles and oil in the heterogeneous porous medium under the variable magnetic field effect. In this work assumed that the injected water is conductive while the oil is non-conductive and the effect of a variable magnetic field is to increase the velocity of injected water by gradient of $\frac{\omega H^2}{8\pi}$ where ω is permeability of magnetic field H. It is assumed that the Darcy's law is valid for the investigated flow system for the mathematical model of the fingero-imbibition phenomenon and the average cross sectional area occupied by the fingers was observed.

The saturation of the injected water $S_w(x,t)$ is then defined as the average cross-sectional area occupied by injected water at distance x and time t. The porosity and permeability of heterogeneous porous medium may vary from one place to another place. Considered that the porosity and permeability of heterogeneous porous medium are the functions of variable x only.

MATHEMATICAL MODEL

The velocity of injected water V_w and velocity of oil V_o can be represented due to Darcy's law as [14, 15]:

$$V_w = -\frac{k_w}{\delta_w} K \left[\frac{\partial P_w}{\partial x} + \frac{\omega H}{4\pi}\frac{\partial H}{\partial x}\right] \quad (1)$$

$$V_o = -\frac{k_o}{\delta_o} K \frac{\partial P_o}{\partial x} \quad (2)$$

where V_w and V_o are the velocities of water and oil respectively, k_w and k_o are the relative permeabilities of water and oil respectively, δ_w and δ_o are the constant viscosities of water and oil respectively, K is the variable permeability of the heterogeneous porous medium, P_w and P_o are the pressures of water and oil respectively, ω is permeability of magnetic field H.

The equation of continuity of injected water is

$$P\frac{\partial S_w}{\partial t} + \frac{\partial V_w}{\partial x} = 0 \quad (3)$$

where $P = P(x)$ is the variable porosity of the heterogeneous porous medium.

The pressure difference is given by the capillary pressure P_c:

$$P_c = P_o - P_w\,. \quad (4)$$

The imbibition condition for countercurrent imbibition phenomenon can be expressed as [14]

$$V_w = -V_o\,. \quad (5)$$

Using equations (1), (2) and (4) in (5), we get

$$\frac{\partial P_w}{\partial x} = -\left(\frac{k_w}{\delta_w} + \frac{k_o}{\delta_o}\right)^{-1}\left(\frac{k_o}{\delta_o}\frac{\partial P_c}{\partial x} + \frac{k_w}{\delta_w}\frac{\omega H}{4\pi}\frac{\partial H}{\partial x}\right). \quad (6)$$

According to Scheidegger [14], we have

$$\frac{k_w}{\delta_w}\frac{k_o}{\delta_o}\left(\frac{k_w}{\delta_w} + \frac{k_o}{\delta_o}\right)^{-1} \approx \frac{k_o}{\delta_o}. \quad (7)$$

On substituting the value of $\frac{\partial P_w}{\partial x}$ with (7) in equation (1), we get

$$V_w = K\frac{k_o}{\delta_o}\left[\frac{\partial P_c}{\partial x} - \frac{\omega H}{4\pi}\frac{\partial H}{\partial x}\right]. \quad (8)$$

Substituting equation (8) into (3), we get

$$P\frac{\partial S_w}{\partial t} + \frac{\partial}{\partial x}\left[K\frac{k_o}{\delta_o}\frac{\partial P_c}{\partial x} - K\frac{k_o}{\delta_o}\frac{\omega H}{4\pi}\frac{\partial H}{\partial x}\right] = 0. \quad (9)$$

We assume that the capillary pressure P_c is a continuous linear function of the form [19]

$$P_c = -\beta S_w \tag{10}$$

where β is a constant.

Due to Scheidegger and Johnson [1], we assume the standard relationship between phase saturation and relative permeability as

$$k_w = S_w \text{ and } k_o = 1 - \alpha S_w \tag{11}$$

where α is a constant.

For the heterogeneous porous medium, we assume the porosity and permeability as functions of x only [2],

$$P(x) = \frac{1}{a_1 - a_2 x} \text{ and } K(x) = K_0(1 + bx) \tag{12}$$

where a_1, a_2, K_0 and b are positive constants. Since $P(x)$ can't exceed unity, we assume that $a_1 - a_2 x \geq 1$.

For simplicity, we consider $K \propto P$ [17],

$$K = K_c P \tag{13}$$

where K_c is a constant.

Considering the magnetic field in the x- direction only, we write H as [4, 22]

$$H = \lambda x^n \tag{14}$$

where λ is a constant parameter and n is an integer.

Using the value of H for $n = 1$ in equation (9) with equations (13), (11) and (10), we get

$$\frac{\partial S_w}{\partial t} = \frac{\beta K_c}{\delta_o P}\frac{\partial}{\partial x}\left[P(1 - \alpha S_w)\frac{\partial S_w}{\partial x}\right] + \frac{K_c \omega \lambda^2}{4\pi \delta_o P}\frac{\partial}{\partial x}[P(1 - \alpha S_w)x]. \tag{15}$$

Using dimensionless variables

$$X = \frac{x}{L}, \qquad T = \frac{\beta K_c t}{\delta_o L^2},$$

equation (15) becomes,

$$\frac{\partial S_w}{\partial T} = \frac{1}{P}\frac{\partial}{\partial X}\left[P(1 - \alpha S_w)\frac{\partial S_w}{\partial X}\right] + \frac{\omega \lambda^2 L^2}{4\pi \beta P}\frac{\partial}{\partial X}[P(1 - \alpha S_w)X]. \tag{16}$$

Now,

$$\frac{1}{P}\frac{\partial P}{\partial X} = \frac{\partial(\log P)}{\partial X}$$

$$= \frac{\partial}{\partial X}\left(\frac{a_2 L X}{a_1} - \log a_1\right)$$

$$(neglecting\ higher\ order\ terms\ of\ X)$$

$$= \frac{a_2 L}{a_1}.$$

Equation (16) reduces to

$$\frac{\partial S_w}{\partial T} = \frac{\partial}{\partial X}\left[(1 - \alpha S_w)\frac{\partial S_w}{\partial X}\right] + A(1 - \alpha S_w)\frac{\partial S_w}{\partial X} + B\frac{\partial}{\partial X}[(1 - \alpha S_w)X] + AB(1 - \alpha S_w)X \tag{17}$$

where $A = \frac{a_2 L}{a_1}$, $B = \frac{\omega \lambda^2 L^2}{4\pi\beta}$ and $S_w(x,t) = S_w(X,T)$.

A set of suitable boundary conditions for fingero-imbibition phenomenon are considered as

$$S_w(0,T) = \frac{T}{5} \text{ and } S_w(1,T) = \frac{1 + 3T}{5} \tag{18}$$

The equation (17) is the desired governing nonlinear partial differential equation for the fingero-imbibition phenomenon in the heterogeneous porous medium with magnetic field effect. The solution $S_w(X,T)$ of equation (17) represents the saturation of injected water at distance X and time T.

APPLICATION OF HOMOTOPY ANALYSIS METHOD

In 1992, Liao [20] proposed a new technique homotopy analysis method (HAM) to obtain solutions of nonlinear differential equations. Many authors have applied the HAM for solving ordinary differential equations and partial differential equations. For example, Liao [16] has discussed solution of various ODEs by HAM. Liao [6] has obtained solution for an unsteady boundary-layer flow due to an impulsively stretched sheet by HAM. Ali and Mehmood [7] have discussed the solution of the unsteady boundary layer flow equations by HAM. Darvishi and Khani [8] have applied the HAM to solve the foam drainage equation. Patel and Desai [12, 13, 23] have applied the HAM to one dimensional

partial differential equation arising in fluid flow through porous medium.

Let us consider the nonlinear partial differential equation according to equation (17) as

$$\mathcal{N}[\varphi(X,T;q)] = 0 \tag{19}$$

where $q \in [0,1]$ is the embedding parameter, $\varphi(X,T;q)$ is an unknown function and a nonlinear operator $\mathcal{N}$ is defined as

$$\begin{aligned}\mathcal{N}[\varphi(X,T;q)] = &\frac{\partial^2\varphi(X,T;q)}{\partial X^2} \\ &- \alpha\varphi(X,T;q)\frac{\partial^2\varphi(X,T;q)}{\partial X^2} \\ &- \alpha\left\{\frac{\partial\varphi(X,T;q)}{\partial X}\right\}^2 \\ &+ (A - B\alpha X)\frac{\partial\varphi(X,T;q)}{\partial X} \\ &- A\alpha\varphi(X,T;q)\frac{\partial\varphi(X,T;q)}{\partial X} \\ &- (B\alpha + AB\alpha X)\varphi(X,T;q) \\ &+ ABX + B - \frac{\partial\varphi(X,T;q)}{\partial T}\end{aligned} \tag{20}$$

According to boundary conditions (18), it is straightforward to choose initial approximation as

$$S_{w_0}(X,T) = \frac{T + X^2 + T(X + X^2)}{5} \tag{21}$$

Now we choose the linear operator as

$$\mathcal{L}[\varphi(X,T;q)] = \frac{\partial^2\varphi(X,T;q)}{\partial X^2} \tag{22}$$

which has the property $\mathcal{L}(f) = 0$ when $f = 0$.

Let $c_0 \neq 0$ be the convergence control parameter and $H(X,T)$ be a non-zero auxiliary function. Liao [20] constructed, the so-called zeroth-order deformation equation

$$\begin{aligned}(1-q)\mathcal{L}\big[\varphi(X,T;q) - S_{w_0}(X,T)\big] \\ = qc_0H(X,T)\mathcal{N}[\varphi(X,T;q)]\end{aligned} \tag{23}$$

where $S_{w_0}(X,T)$ is an initial approximation of $S_w(X,T)$. When $q = 0$ and $q = 1$, we have

$$\varphi(X,T;0) = S_{w_0}(X,T) \text{ and } \varphi(X,T;1) = S_w(X,T) \tag{24}$$

respectively. Therefore, when q increases from 0 to 1, the solution $\varphi(X,T;q)$ deforms (varies) from the initial approximation $S_{w_0}(X,T)$ to the solution $S_w(X,T)$. By Taylor's theorem, we expand $\varphi(X,T;q)$ in powers of q as

$$\varphi(X,T;q) = S_{w_0}(X,T) + \sum_{m=1}^{\infty} S_{w_m}(X,T)q^m \tag{25}$$

where

$$S_{w_m}(X,T) = \frac{1}{m!}\frac{\partial^m\varphi(X,T;q)}{\partial q^m}\bigg|_{q=0}. \tag{26}$$

Assume that the linear operator, the initial approximation, the convergence control parameter and the auxiliary function are selected such that the series (25) is convergent at $q = 1$. Then at $q = 1$, the series (25) becomes

$$S_w(X,T) = S_{w_0}(X,T) + \sum_{m=1}^{\infty} S_{w_m}(X,T) \tag{27}$$

Define the vector $\overrightarrow{S_{w_n}} = \{S_{w_0}(X,T), S_{w_1}(X,T), \dots, S_{w_n}(X,T)\}$. Differentiating (23) m times with respect to q and then putting $q = 0$ and finally dividing them by $m!$, we have the so-called high-order deformation equation

$$\begin{aligned}\mathcal{L}\big[S_{w_m}(X,T) - \chi_m S_{w_{m-1}}(X,T)\big] \\ = c_0H(X,T)\mathcal{R}_m\big(\overrightarrow{S_{w_{m-1}}}\big)\end{aligned} \tag{28}$$

where

$$\begin{aligned}\mathcal{R}_m\big(\overrightarrow{S_{w_{m-1}}}\big) = &\frac{\partial^2 S_{w_{m-1}}}{\partial X^2} - \alpha\sum_{j=0}^{m-1} S_{w_j}\frac{\partial^2 S_{w_{m-1-j}}}{\partial X^2} \\ &- \alpha\sum_{j=0}^{m-1}\frac{\partial S_{w_j}}{\partial X}\frac{\partial S_{w_{m-1-j}}}{\partial X} \\ &+ A\frac{\partial S_{w_{m-1}}}{\partial X} - B\alpha X\frac{\partial S_{w_{m-1}}}{\partial X} \\ &- A\alpha\sum_{j=0}^{m-1} S_{w_j}\frac{\partial S_{w_{m-1-j}}}{\partial X} \\ &- B\alpha S_{w_{m-1}} - AB\alpha X S_{w_{m-1}} \\ &+ (B + ABX)(1 - \chi_m) \\ &- \frac{\partial S_{w_{m-1}}}{\partial T}, m \geq 1\end{aligned} \tag{29}$$

and

$$\chi_m = \begin{cases} 0\ , & when \quad m \leq 1 \\ 1\ , & when \quad m > 1. \end{cases} \tag{30}$$

Here we consider the auxiliary function as $H(X,T) = 1$. Then the equation (28) becomes

$$S_{w_m}(X,T) = \chi_m S_{w_{m-1}}(X,T) + c_0\mathcal{L}^{-1}\left[\mathcal{R}_m\left(\overrightarrow{S_{w_{m-1}}}\right)\right] + C_1X + C_2 \quad (31)$$

where C_1 and C_2 are determined by the boundary conditions $S_{w_m}(0,T) = 0$ and $S_{w_m}(1,T) = 0$, $m \geq 1$. Solution of (31) gives $S_{w_1}(X,T), S_{w_2}(X,T)$ and so on. Hence the homotopy series solution of (17) is as

$$\begin{aligned} S_w(X,T) = {} & \frac{T + X^2 + T(X + X^2)}{5} + c_0\left[-\frac{X}{20} + \frac{X^2}{10}\right. \\ & - \frac{X^3}{30} - \frac{X^4}{60} - \frac{TX}{5} + \frac{TX^2}{5} - \frac{BX}{2} \\ & + \frac{BX^2}{2} - \frac{ABX}{6} + \frac{ABX^3}{6} \\ & + \frac{A}{5}\left(-\frac{X}{3} + \frac{X^3}{3} - \frac{5TX}{6} + \frac{TX^2}{2}\right. \\ & \left. + \frac{TX^3}{3}\right) - \frac{\alpha}{25}\left(-\frac{X}{2} + \frac{X^4}{2} - 3TX\right. \\ & + TX^2 + TX^3 + TX^4 - 3T^2X \\ & \left. + \frac{3T^2X^2}{2} + T^2X^3 + \frac{T^2X^4}{2}\right) \\ & - \frac{A\alpha}{25}\left(-\frac{X}{10} + \frac{X^5}{10} - \frac{47TX}{60} + \frac{TX^3}{3}\right. \\ & + \frac{TX^4}{4} + \frac{TX^5}{5} - \frac{27T^2X}{20} + \frac{T^2X^2}{2} \\ & \left. + \frac{T^2X^3}{2} + \frac{T^2X^4}{4} + \frac{T^2X^5}{10}\right) \\ & - \frac{B\alpha}{5}\left(-\frac{X}{4} + \frac{X^4}{4} - \frac{13TX}{12} + \frac{TX^2}{2}\right. \\ & + \frac{TX^3}{3} + \frac{TX^4}{4}\Big) - \frac{AB\alpha}{5}\Big(-\frac{X}{20} \\ & + \frac{X^5}{20} - \frac{3TX}{10} + \frac{TX^3}{6} + \frac{TX^4}{12} \\ & \left. + \frac{TX^5}{20}\right)\Big] + \cdots \quad (32) \end{aligned}$$

The solution (32) represents the saturation of injected water at distance X and time T for the fingero-imbibition phenomenon arising in fluid flow through the heterogeneous porous medium with magnetic field effect.

As pointed out by Liao, the convergence of the homotopy series solution depends upon the value of convergence control parameter c_0. The proper value of c_0 has been obtained using c_0-curves. Many authors have discussed the convergence of the homotopy series solution. For example, Liao [6, 16], Ali and Mehmood [7], Darvishi and Khani [8], Patel and Desai [12, 13, 23] have chosen a proper value of c_0 providing us the convergent homotopy series solution of nonlinear ODEs and PDEs. With the help of Mathematica package for nonlinear BVPs [18], the so-called c_0-curves are plotted for 20th order approximation. This helps us to discover the range for the admissible values of c_0, which corresponds to the horizontal line segment. It is obvious that the valid domain of c_0 is $-1.2 \leq c_0 \leq -0.4$ from the c_0-curves (see figures 2-4). This means that the series (32) converges for these values of c_0.

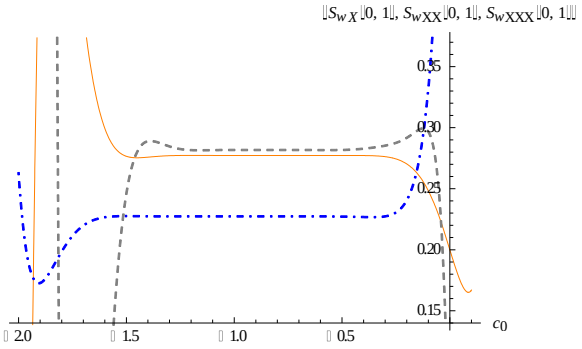

Figure 2: The c_0-curves of $S_{wX}(0,1)$ (Solid line), $S_{wXX}(0,1)$ (DotDashed line) and $S_{wXXX}(0,1)$ (Dashed line).

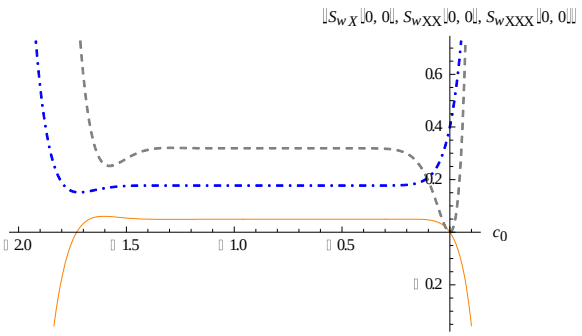

Figure 3: The c_0-curves of $S_{wX}(0,0)$ (Solid line), $S_{wXX}(0,0)$ (DotDashed line) and $S_{wXXX}(0,0)$ (Dashed line).

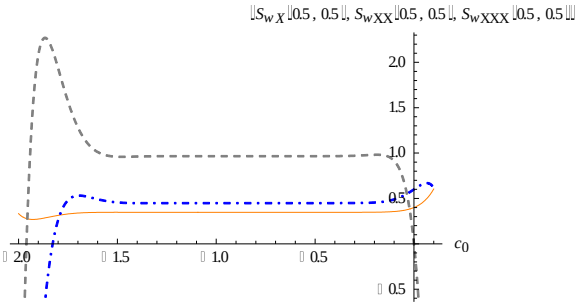

Figure 4: The c_0-curves of $S_{wX}(0.5, 0.5)$ (Solid line), $S_{wXX}(0.5, 0.5)$ (DotDashed line) and $S_{wXXX}(0.5, 0.5)$ (Dashed line).

RESULTS AND DISCUSSION

The following values of constants are considered as: $L = 1, \alpha = 1.11, a_1 = 2, a_2 = 1, \beta = 0.1, \omega = 0.1, \lambda = 0.1$ and we choose the proper value of the convergence control parameter $c_0 = -0.8$ to obtain convergent series solution. We have considered first 20 terms of series solution. Hence it gives an approximate solution of fingero-imbibition phenomenon in heterogeneous porous media with magnetic field effect. Table 1 indicates the numerical values of saturation of injected water for fingero-imbibition phenomenon at distance X for time T. Graphical presentation of the saturation of injected water is obtained by using Mathematica software. The graph of saturation of injected water versus distance X for fixed time $T = 0.1, 0.2, \ldots, 1$ is given in fig. 5 and fig. 6 represents the graph of saturation of injected water versus time T for fixed distance $X = 0.1, 0.2, \ldots, 1$

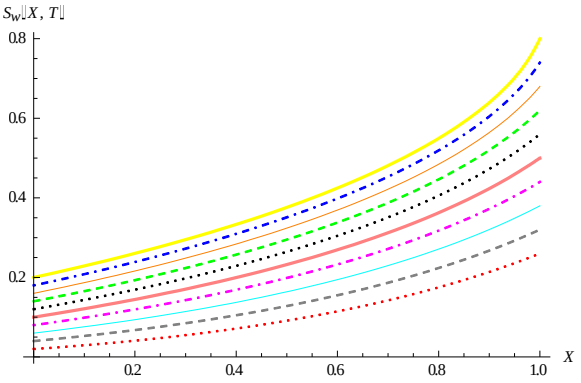

Figure 5: Saturation of water v/s distance X for fixed time $T = 0.1(\textbf{lower most graph}), 0.2, \ldots, 1(\textbf{upper most graph})$.

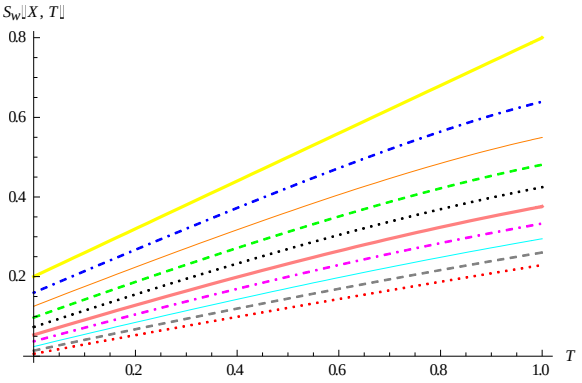

Figure 6: Saturation of water v/s time T for fixed distance $X = 0.1(\textbf{lower most graph}), 0.2, \ldots, 1(\textbf{upper most graph})$.

COMPARATIVE STUDY WITH FINGERO-IMBIBITION PHENOMENON IN HETEROGENEOUS POROUS MEDIUM WITHOUT MAGNETIC FIELD EFFECT

Patel and Desai [13] have discussed homotopy series solution for fingero-imbibition phenomenon in heterogeneous porous medium without magnetic field effect. Table 2 shows the comparative numerical values of the saturation of injected water of fingero-imbibition phenomenon without magnetic field effect [13] and with magnetic field effect.

CONCLUSION

We have discussed the fingero-imbibition phenomenon in heterogeneous porous medium with magnetic field effect under certain assumptions. The homotopy series solution (32) represents the saturation of injected water. The solution (32) satisfies the boundary conditions (18). Numerical and graphical representations are obtained using Mathematica software. Table 1 indicates the numerical values of the saturation of injected water. Figures 5 and 6 give graphical representation. It is concluded that the saturation of injected water of fingero-imbibition phenomenon increases when the distance increases for given time T. Due to additional magnetic field effect the saturation of injected water is more increasing than the saturation of injected water without magnetic field effect. We can conclude that the magnetic field effect plays an important role in the fingero-imbibition

phenomenon in the heterogeneous porous medium.

REFERENCES

[1] Scheidegger, A. E. and Johnson, E. F., (1961), The statistically behavior of instabilities in displacement process in porous media, Canadian J. Physics, 39 (2), pp. 326-334.

[2] Verma, A. P., (1969), Statistical behavior of fingering in a displacement process in heterogeneous porous medium with capillary pressure, Canadian J. Physics, 47 (3), pp. 319-324.

[3] Mishra, S. K. and Verma, A. P., (1974), Imbibition in the flow of two immiscible fluids with magnetic field, The Physics of fluids, American Institute of Physics, 17 (6), pp. 1338-1340.

[4] Verma, A. P., (1980), Instabilities in two phase flow through porous media with magnetic field, Multiphase transport: Fundamentals, Reactor Safety, Applications (Ed. T. N. Veziroglu), Hemisphere Publication Corporation, Washington, 3, pp. 1323-1335.

[5] Shah, R. C. and Verma, A. P., (1998), Fingero-imbibition phenomenon through porous media with magnetic field, Indian J. of Engg. and Materials Sciences, 5, pp. 411-415.

[6] Liao, S. J., (2006), An analytic solution of unsteady boundary-layer flows caused by an impulsively stretching plate, Commun. Nonlinear Sci. Numer. Simul., 11 (3), pp. 326-339.

[7] Ali, A., Mehmood, A., (2008), Homotopy analysis of unsteady boundary layer flow adjacent to permeable stretching surface in a porous medium, Commun. Nonlinear Sci. Numer. Simul., 13, pp. 340-349.

[8] Darvishi, M. T. and Khani, F., (2009), A series solution of the foam drainage equation, Computers and Mathematics with Applications, 58, pp. 360-368.

[9] Patel, K. R., Mehta, M. N. and Patel, T. R., (2013), A mathematical model of imbibition phenomenon in heterogeneous porous media during secondary oil recovery process, Applied Mathematical Modelling, 37, pp. 2933-2942.

[10] Parikh, A. K., Mehta, M. N. and Pradhan, V. H., (2014), Mathematical modeling and analysis of fingero-imbibition phenomenon in homogeneous porous medium with magnetic field effect in vertical downward direction, I. J. of Latest Tech. in Engg., Management & Appl. Sci., 3 (10), pp. 17-23.

[11] Patel, A. V., Rabari, N. S. and Bhathawala, P. H., (2015), Numerical solution of imbibition phenomenon in a homogeneous medium with magnetic fluid, IOSR J. of Mathematics, 11(4), pp. 11-19.

[12] Patel, M. A. and Desai, N. B., (2016), Homotopy analysis solution of countercurrent imbibition phenomenon in inclined homogeneous porous medium, Global J. Pure and Appl. Math., 12 (1), pp. 1035-1052.

[13] Patel, M. A. and Desai, N. B., (2017), Homotopy analysis method for fingero-imbibition phenomenon in heterogeneous porous medium, Nonlinear Science Letters A: Math., Phy. and Mech., 8 (1), pp. 90-100.

[14] Scheidegger, A. E., (1960), The Physics of flow through porous media, Revised edition, University of Toronto Press, Toronto.

[15] Bear, J., (1972), Dynamics of fluids in porous media, American Elsevier Publishing Company, Inc., New York.

[16] Liao, S. J., (2003), Beyond perturbation: Introduction to the homotopy analysis method, Chapman and Hall/CRC Press, Boca Raton.

[17] Cheng, Z., (2007), Reservoir simulation: Mathematical techniques in oil recovery, Society for Industrial and Applied Mathematics, Philadelphia.

[18] Liao, S. J., (2012), Homotopy analysis method in nonlinear differential equations, Higher Education Press, Beijing and Springer-Verlag Berlin Heidelberg.

[19] Mehta, M. N., (1977), Asymptotic expansions of fluid flow through porous media, Ph.D. Thesis, South Gujarat University, Surat, India.

[20] Liao, S. J., (1992), The proposed homotopy analysis technique for the solution of nonlinear problems, Ph.D. Thesis, Shanghai Jiao Tong University, Shanghai, China.

[21] Desai, N. B., (2002), The study of problems arises in single phase and multiphase flow through porous media, Ph.D. Thesis, South Gujarat University, Surat, India.

[22] Banerji, A. C. and Srivastava, K. M., (1963), Radial oscillations of variable magnetic star and the origin of the planetary system, Proceedings of the National Academy of Sciences, India, 33 (A), pp. 125-148.

[23] Patel, M. A. and Desai, N. B., (2017), A mathematical model of cocurrent imbibition phenomenon in inclined homogeneous porous medium, Kalpa Publications in Computing, ICRISET2017, Selected Papers in Computing, 2, pp. 51-61.

Table-1: Numerical values of the saturation of injected water with magnetic field effect.

T	$X=0.1$	$X=0.2$	$X=0.3$	$X=0.4$	$X=0.5$	$X=0.6$	$X=0.7$	$X=0.8$	$X=0.9$	$X=1.0$
0.1	0.0294702	0.0409648	0.0548286	0.0714324	0.0911921	0.1145950	0.1422402	0.1749026	0.2136411	0.2600000
0.2	0.0528328	0.0676626	0.0848556	0.1048177	0.1280162	0.1550146	0.1865255	0.2235014	0.2672979	0.3200000
0.3	0.0759336	0.0938712	0.1141989	0.1373570	0.1638673	0.1943772	0.2297319	0.2711031	0.3202373	0.3800000
0.4	0.0987564	0.1195543	0.1427983	0.1689628	0.1986268	0.2325306	0.2716734	0.3174967	0.3722661	0.4400000
0.5	0.1212845	0.1446740	0.1705897	0.1995398	0.2321627	0.2692999	0.3121271	0.3624155	0.4231194	0.5000000
0.6	0.1435009	0.1691909	0.1975056	0.2289855	0.2643291	0.3044852	0.3508272	0.4055203	0.4724262	0.5600000
0.7	0.1653884	0.1930648	0.2234759	0.2571912	0.2949670	0.3378610	0.3874590	0.4463816	0.5196575	0.6200000
0.8	0.1869300	0.2162553	0.2484289	0.2840434	0.3239060	0.3691771	0.4216559	0.4844582	0.5640480	0.6800000
0.9	0.2081090	0.2387224	0.2722926	0.3094260	0.3509672	0.3981617	0.4529997	0.5190818	0.6044820	0.7400000
1.0	0.2289092	0.2604273	0.2949965	0.3332228	0.3759679	0.4245282	0.4810286	0.5494552	0.6393414	0.8000000

Table-2: Comparative numerical values of the saturation of injected water without magnetic field effect and with magnetic field effect.

T	$X=0.1$	$X=0.2$	$X=0.3$	$X=0.4$	$X=0.5$	$X=0.6$	$X=0.7$	$X=0.8$	$X=0.9$	$X=1.0$
0.1	0.0294301	0.0408938	0.0547358	0.0713267	0.0910823	0.1144897	0.1421481	0.1748322	0.2136012	0.2600000
0.1	0.0294702	0.0409648	0.0548286	0.0714324	0.0911921	0.1145950	0.1422402	0.1749026	0.2136411	0.2600000
0.2	0.0527940	0.0675937	0.0847656	0.1047151	0.1279096	0.1549123	0.1864359	0.2234330	0.2672591	0.3200000
0.2	0.0528328	0.0676626	0.0848556	0.1048177	0.1280162	0.1550146	0.1865255	0.2235014	0.2672979	0.3200000
0.3	0.0758961	0.0938046	0.1141118	0.1372578	0.1637642	0.1942783	0.2296453	0.2710369	0.3201998	0.3800000
0.3	0.0759336	0.0938712	0.1141989	0.1373570	0.1638673	0.1943772	0.2297319	0.2711031	0.3202373	0.3800000
0.4	0.0987202	0.1194901	0.1427143	0.1688671	0.1985275	0.2324355	0.2715902	0.3174333	0.3722302	0.4400000
0.4	0.0987564	0.1195543	0.1427983	0.1689628	0.1986268	0.2325306	0.2716734	0.3174967	0.3722661	0.4400000
0.5	0.1212496	0.1446122	0.1705089	0.1994478	0.2320674	0.2692088	0.3120477	0.3623551	0.4230855	0.5000000
0.5	0.1212845	0.1446740	0.1705897	0.1995398	0.2321627	0.2692999	0.3121271	0.3624155	0.4231194	0.5000000
0.6	0.1434674	0.1691316	0.1974281	0.2288975	0.2642381	0.3043985	0.3507520	0.4054637	0.4723946	0.5600000
0.6	0.1435009	0.1691909	0.1975056	0.2289855	0.2643291	0.3044852	0.3508272	0.4055203	0.4724262	0.5600000
0.7	0.1653563	0.1930080	0.2234018	0.2571073	0.2948806	0.3377792	0.3873886	0.4463291	0.5196290	0.6200000
0.7	0.1653884	0.1930648	0.2234759	0.2571912	0.2949670	0.3378610	0.3874590	0.4463816	0.5196575	0.6200000
0.8	0.1868992	0.2162010	0.2483583	0.2839637	0.3238244	0.3691004	0.4215907	0.4844107	0.5640233	0.6800000
0.8	0.1869300	0.2162553	0.2484289	0.2840434	0.3239060	0.3691771	0.4216559	0.4844582	0.5640480	0.6800000
0.9	0.2080794	0.2386705	0.2722254	0.3093505	0.3508905	0.3980903	0.4529401	0.5190399	0.6044621	0.7400000
0.9	0.2081090	0.2387224	0.2722926	0.3094260	0.3509672	0.3981617	0.4529997	0.5190818	0.6044820	0.7400000
1.0	0.2288809	0.2603777	0.2949326	0.3331515	0.3758960	0.4244623	0.4809749	0.5494194	0.6393273	0.8000000
1.0	0.2289092	0.2604273	0.2949965	0.3332228	0.3759679	0.4245282	0.4810286	0.5494552	0.6393414	0.8000000

PRAJÑĀ - **Journal of Pure and Applied Sciences Vol. 24 – 25 : 23–29 (2017)**
ISSN 0975 - 2595

SHLIOMIS MODEL BASED FERROFLUID LUBRICATION OF A ROUGH ANNULAR SQUEEZE FILM UNDER COUPLE STRESS EFFECT

HIMESH A. PATEL[1], HIMANSHU C. PATEL[2] AND G.M. DEHERI[3]

[1]Assistant Professor, Science & Humanities Department, Gujarat Power Engineering & Research Institute, Mewad, Mehsana-383315, Gujarat State, India.
E-mail.himesh.patel4@gmail.com . Telephone.+91-9428389902
[2]Professor, Department of Mathematics, L. D. College of Engineering, Ahmedabad-380009, Gujarat State, India. E-mail. dr.prof.hcpatel@ldce.ac.in . Telephone.+91-9978440975
[3]Associate Professor, Department of Mathematics, Saradar Patel University, Vallabh Vidyanagar-388120, Gujarat State, India. E-mail. gmdeheri@rediffmail.com . Telephone.02692233289

ABSTRACT

This paper aims to analyze the combined effect of magnetism and couple stress effect on the performance of the squeeze film in rough annular bearings. Shliomis model has been adopted to describe the magnetic flow. The pressure distribution is obtained after solving the associated stochastically averaged Reynolds type equation. Then the load carrying capacity is calculated. The results presented in graphical forms indicate that the combined effect of magnetism and couple stress may be nearly sufficient to counter the adverse effect of transverse roughness by suitably choosing the aspect ratio.

Keywords: Squeeze film, Annular plates, magnetism, Couple stress, roughness, load carrying capacity.

INTRODUCTION

For centuries, many interesting materials have been attracting the investigators and scientists due to their extraordinary properties and industrial usage. Magnetic fluid is one of such smart materials, which are not obtainable free state in nature, but are to be synthesized. These fluids have a good number of applications in the field of science and engineering etc.

Due to the wide application of the magnetic fluid, many researchers have used magnetic fluids as a lubricant in various geometry of bearing systems. Tipei (1982) investigated the theory of lubrication using ferrofluid and applied it in short bearings. Sinha et al. (1993) studied the effect of ferrofluid lubrication on cylindrical rollers. Osman et al. (2001) worked on the static and dynamic characteristics of magnetized journal bearings lubricated with ferrofluid. Shah and Bhat (2005) examined the effect of magnetic fluid lubrication on a squeeze film between curved annular plates considering rotation of magnetic particles. Deheri et al. (2006) discussed the effect of circular step bearings under the presence of a ferrofluid. Ahmed and Singh (2007) analyzed the effect of porous-pivoted slider bearing with slip velocity using ferrofluid. Urreta et al. (2009) studied the performance of hydrodynamic journal bearing lubricated with magnetic fluids. Patel et al. (2010) investigated the effect of a short hydrodynamic slider bearing in the presence of a ferrofluid. Patel et al. (2012) studied the performance of hydrodynamic short journal bearings lubricated with magnetic fluid. All the above studies have found that the effect of the bearing system gets enhanced owing to magnetization.

The squeeze film performance is commonly applied in gears, aircraft engines, automotive engines, gyroscopes and the mechanics of synovial joints in human being and animals. A good number of researches with reference to squeeze films have been discussed for the parallel surfaces by Gould (1967), in curved annular plates by Gupta and Vora (1980), in annular disks by Lin (2001) and a sphere and plane surface by Chou et al. (2003).

Many methods were proposed to improve the performance of the bearing system, One such method was the use of couple stress fluid. Bujurke and Jayaraman (1982) analyzed the influence of couple stresses in squeeze films. Bujurke and Naduvinamani (1991) investigated the performance of narrow porous journal bearing lubricated with couple stress fluid. Lin (1997) dealt with the effect of squeeze film characteristics of long partial journal bearing lubricated with couple stress fluid. Lin (2000)

studied the performance of squeeze film characteristics between a sphere and a flat plate using couple stress fluid model. These studies have predicted about higher load carrying capacity, lower coefficient of friction, and delayed time of approach in comparison with the Newtonian case.

The bearing surfaces are assumed smooth in all the above discussions. But it is not realistic because, after having some run-in and wear or through the manufacturing process and the impulsive damage, the bearing surfaces could be roughed. Various techniques have been proposed to deal with the effect of surface roughness on the performance characteristics of squeeze film bearings, Christensen and Tonder (1969a, 1969b, 1970) modified the stochastic theory of Tzeng and Saibel (1967) to study the effect of surface roughness in general. Many research papers are abound dealing with the hydrodynamic lubrication of rough surfaces using stochastic method of Christensen and Tonder (1969a, 1969b, 1970) such as the works on the porous annular disks by Ting(1975), the journal bearing by Guha (1993), Chiang et al. (2004), the spherical bearing by Gupta and Deheri (1996), Hydrodynamic slider bearing by Nanduvinamani et al. (2003), the curved annular plates by Bujurke et al. (2007), Deheri and Abhangi (2011) and Shimpi and Deheri (2012), the circular plates by Patel et al. (2009), Shimpi and Deheri (2010). All the above investigations make it clear that roughness affects the performance significantly. Patel and Deheri (2013) investigated the performance of various porous structures on the performance of a Shliomis model based magnetic fluid lubrication of a squeeze film in rotating rough porous curved circular plates. It was established that the adverse effect of transverse roughness could be overcome by the positive effect of ferrofluid lubrication in the case of negatively skewed roughness by suitably choosing curvature parameters and rotational inertia when Kozeny- Carman's model was used for porous structure.

ANALYSIS

Figure 1 presents the configuration of the bearing system. It consist of two parallel annular disks, each of inner radius $r_i$and outer radius r_0. The upper disk approaches the lower one with a squeezing velocity $-\frac{dh}{dt}$.

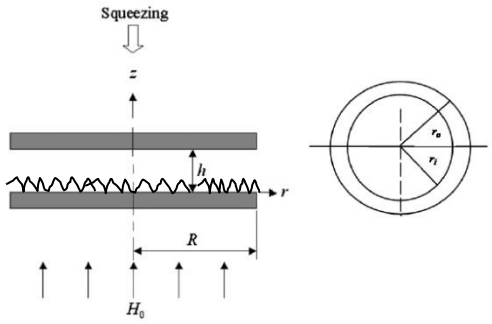

Fig.1 Cross section of Annular Disk

The bearing surfaces are considered to be transversely rough. The film thickness h(x) of the lubricant film for present study is assumed to be

$$h = \bar{h} + h_s$$

where $\bar{h}$ is the mean film thickness characterizing the random roughness of the bearing surfaces, h_s is assumed to be stochastic in nature and governed by probability distribution function as discussed and derived by Christensen and Tonder (1969a, 1969b 1970). Also the mean $\bar{\alpha}$, the standard deviation $\bar{\sigma}$ and the parameter $\bar{\varepsilon}$ which is the measure of symmetry of the random variable h_s, are defined as in Christensen and Tonder (1969a, 1969b 1970). The details regarding the roughness aspects can be obtained from Christensen and Tonder (1969a, 1969b 1970).

Here the flow model of Shliomis (1972,1974) is considered to study the effect of magnetic fluid.Making use of discussion of Lin et al. (2013) the modified Reynolds equation governing the pressure distribution for the performance of a ferrofluid lubricated squeeze film in annular disks with non Newtonian couple stress effect is obtained as

$$f(h, l_c, \emptyset, \tau)\frac{1}{r}\frac{d}{dr}\left\{r\frac{dp}{dr}\right\} = 12\eta_0(1+\tau)(1+2.5\emptyset)\frac{dh}{dt} \qquad (1)$$

Where,

$$g(h, lc, \emptyset, \tau) = h^3 - 12\frac{l_c^2}{(1+\tau)(1+2.5\emptyset)}h(3\bar{\alpha}^2 + 3\bar{\sigma}^2) + 24\frac{l_c^3}{(1+\tau)^{3/2}(1+2.5\emptyset)^{3/2}}\tanh\left[\frac{\sqrt{(1+\tau)(1+2.5\emptyset)}}{2l_c}h(3\bar{\alpha}^2 + 3\bar{\sigma}^2)\right] + 3\bar{\sigma}^2\bar{\alpha} + \bar{\alpha}^3 + \bar{\varepsilon} + 3h^2\bar{\alpha} \quad (2)$$

Introducing the non- dimensional quantities,

$$r^* = \frac{r}{r_0},\quad P^* = \frac{ph_0^3}{\eta_0 r_0^2\left(\frac{dh}{dt}\right)}, h^* = \frac{h}{h_0},$$

$$g^*(h^*, C, \emptyset, \tau) = \frac{g}{h_0^3} \quad (3)$$

and solving equation (1) with the boundary condition

$$p = 0 \text{ at } r = r_{i,}\ r = r_0 \quad (4)$$

The expression for non dimensional pressure distribution is found to be

$$P^* = \frac{3(1+\tau)(1+2.5\phi)}{g^*(h^*, C, \emptyset, \tau)}\left\{r^{*^2} + \frac{1}{logK}[(1-K^2)logr^*] - 1\right\} \quad (5)$$

where,

$$g^*(h^*, C, \emptyset, \tau) = h^{*3} - 12\frac{C^2}{(1+\tau)(1+2.5\emptyset)}h^*(3\bar{\alpha}^{*2} + 3\bar{\sigma}^{*2}) + 24\frac{C^3}{(1+\tau)^{3/2}(1+2.5\emptyset)^{3/2}}\tanh\left[\frac{\sqrt{(1+\tau)(1+2.5\emptyset)}}{2C}h^*(3\bar{\alpha}^{*2} + 3\bar{\sigma}^{*2})\right] + 3\bar{\sigma}^{*2}\bar{\alpha}^* + \bar{\alpha}^{*3} + \bar{\varepsilon}^* + 3h^{*2}\bar{\alpha}^* \quad (6)$$

where, α^* is non dimensional variance, σ^* is dimensionless standard deviation, ε^* is non dimensional skewness and K = aspect ratio $\frac{r_i}{r_0}$.

Integrating the film pressure over the film region yields the load carrying capacity in dimensionless form as

$$W^* = \frac{3(1+\tau)(1+2.5\phi)}{2g^*}(K^2-1)\left[1 - \frac{1}{logK}(K^2-1)\right] \quad (7)$$

Observe that in the limiting case $r_i \to 0$ the results of Lin et al. (2013) can be derived from the present analysis.

RESULTS AND DISCUSSION

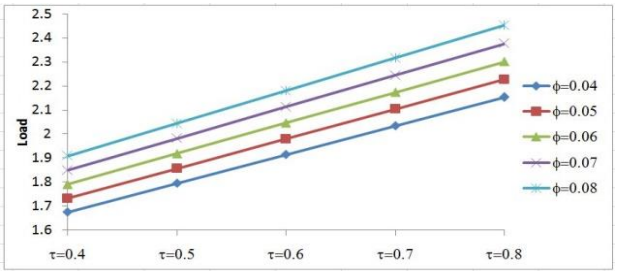

Figure- 2 Variation of Load carrying capacity with respect to ϕ and τ.

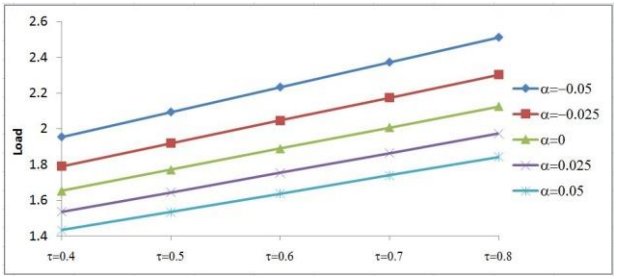

Figure- 3 Variation of Load carrying capacity with respect to α and τ.

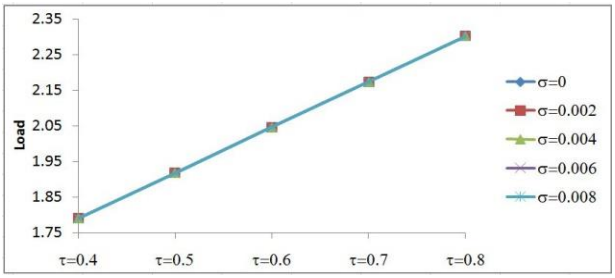

Figure- 4 Variation of Load carrying capacity with respect to σ and τ.

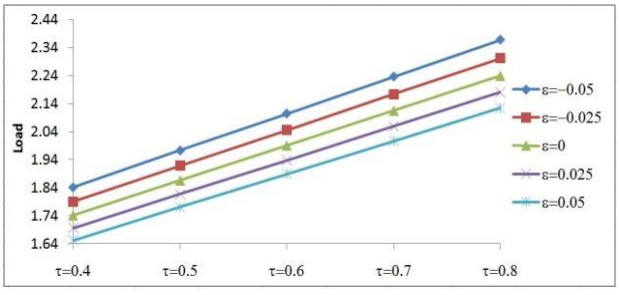

Figure- 5 Variation of Load carrying capacity with respect to ε and τ.

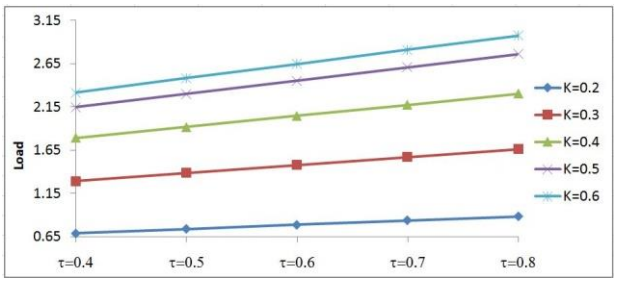

Figure- 6 Variation of Load carrying capacity with respect to ε and τ.

Figures 2 to 6 indicate that the load carrying capacity increases sharply due to the magnetization parameter. Further, from Figure 4 it is seen that the effect of standard deviation on the load carrying capacity with respect to magnetization is negligible.

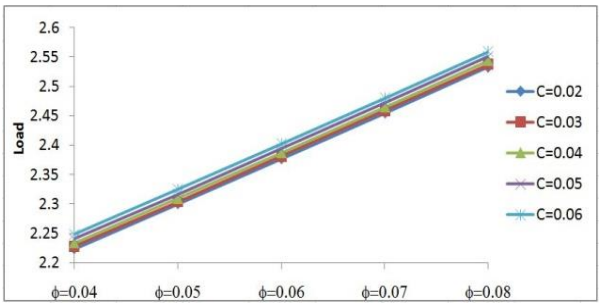

Figure- 7 Variation of Load carrying capacity with respect to C and ϕ.

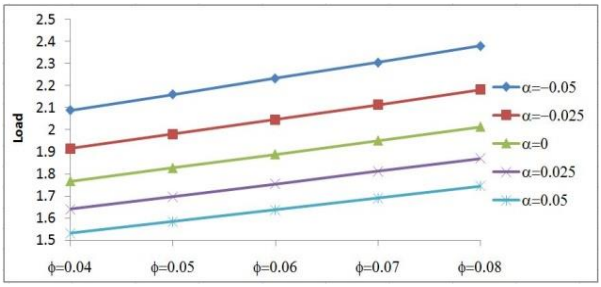

Figure- 8 Variation of Load carrying capacity with respect to α and ϕ.

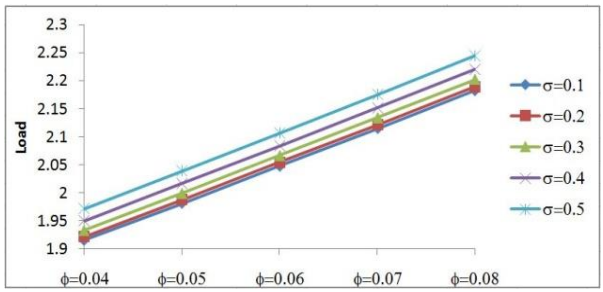

Figure- 9 Variation of Load carrying capacity with respect to σ and ϕ.

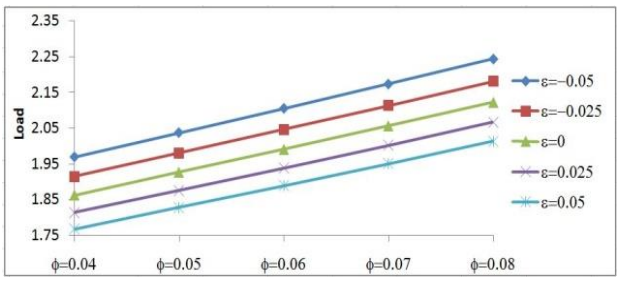

Figure- 10 Variation of Load carrying capacity with respect to $\boldsymbol{\varepsilon}$ and $\boldsymbol{\phi}$.

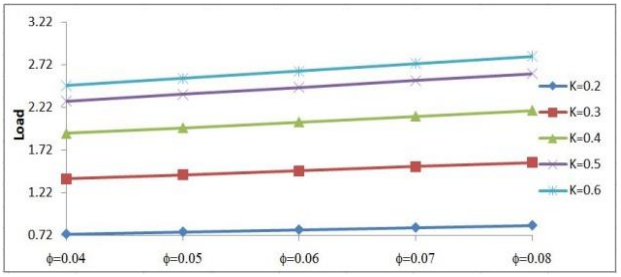

Figure- 11 Variation of Load carrying capacity with respect to K and ϕ.

Figures 7 - 11 dealing with the load profile with respect to volume concentration parameter suggest that the load carrying capacity increases considerably with the increase in volume concentration parameter.

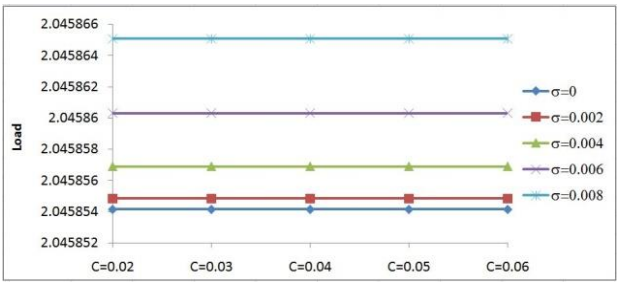

Figure- 12 Variation of Load carrying capacity with respect to σ and C.

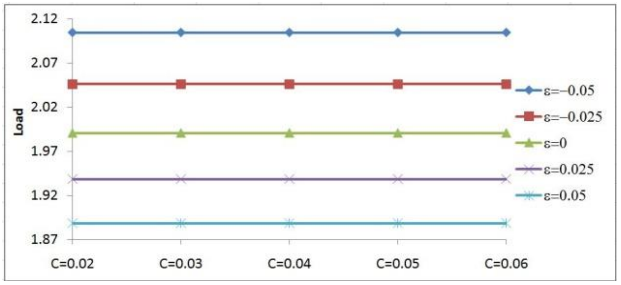

Figure- 13 Variation of Load carrying capacity with respect to ε and C.

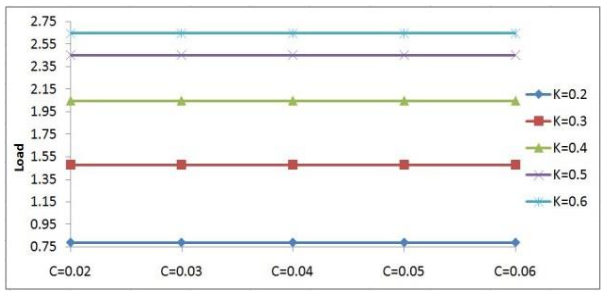

Figure- 14 Variation of Load carrying capacity with respect to $\boldsymbol{K}$ and $\boldsymbol{C}$.

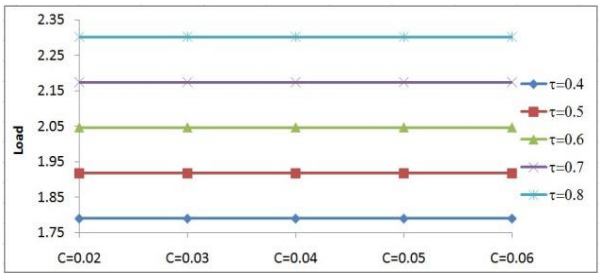

Figure- 15 Variation of Load carrying capacity with respect to τ and C.

The couple stress effect shown in Figures 12 - 15 establishes that it has just only nominal effect on the performance characteristics.

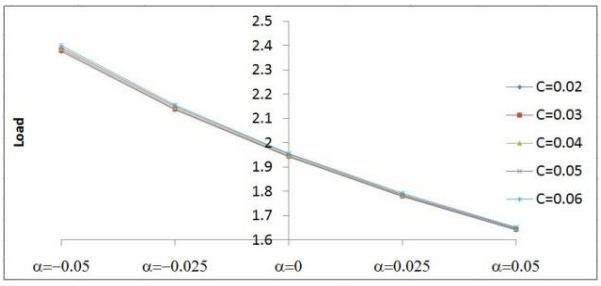

Figure- 16 Variation of Load carrying capacity with respect to C and α.

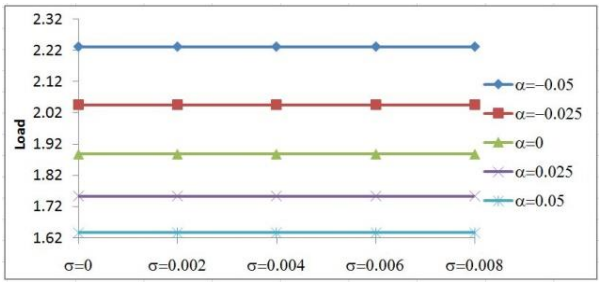

Figure- 17 Variation of Load carrying capacity with respect to α and σ .

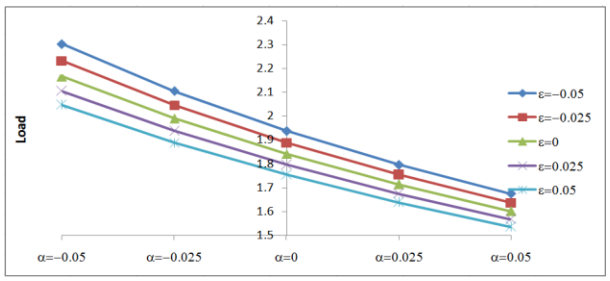

Figure- 18 Variation of Load carrying capacity with respect to ε and α.

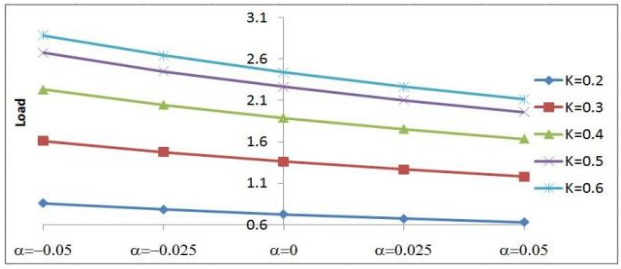

Figure- 19 Variation of Load carrying capacity with respect to K and α.

Figures 16 - 19 describing the load profile with respect to the variance suggest that the variance (+ve) decreases the load carrying capacity while it is opposite for variance (-ve).

Further, the effect of standard deviation on the distribution of load carrying capacity with respect to variance remains negligible. [Figure 17].

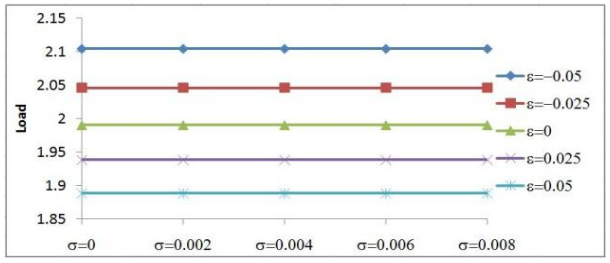

Figure- 20 Variation of Load carrying capacity with respect to ε and σ.

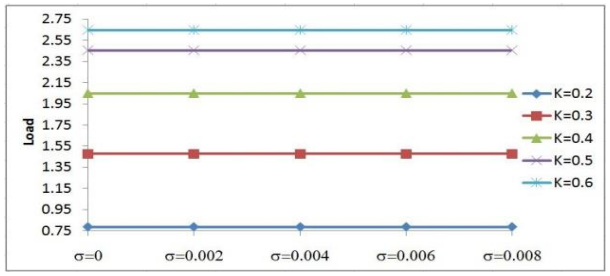

Figure- 21 Variation of Load carrying capacity with respect to K and σ.

From Figures 20 and 21 it is observed that the adverse effect of standard deviation is at the best nominal.

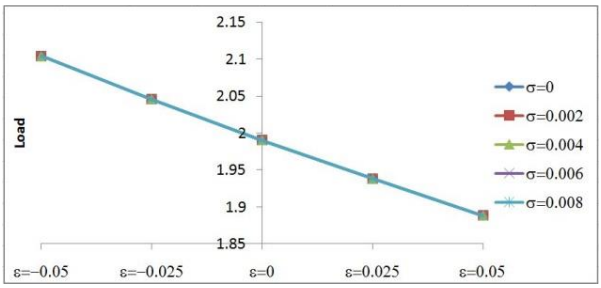

Figure- 22 Variation of Load carrying capacity with respect to σ and ε.

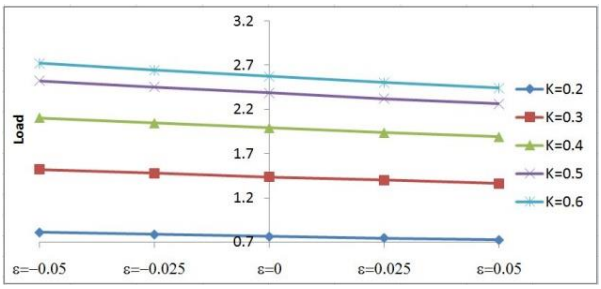

Figure- 23 Variation of Load carrying capacity with respect to K and ε.

CONCLUSION

The magnetic fluid lubrication may go a long way in reducing the adverse effect of roughness for moderate to higher values of couple stress parameter However this paper establishes that the roughness must be given due consideration while designing the bearing system even if a suitable magnetic strength is in force.

REFERRENCES

[1] Tipei, N. (1982). Theory of lubrication with ferrofluids- Application to short bearings. *ASME, Transactions, Journal of Lubrication Technology*, 104, 510-515.

[2] Agrawal, V. K. (1986). Magnetic-fluid-based porous inclined slider bearing. *Wear*, 107(2), 133-139.

[3] Sinha, P., Chandra, P., & Kumar, D. (1993). Ferrofluid lubrication of cylindrical rollers with cavitation. *Acta Mechanica*, 98(1), 27-38.

[4] Ram, P., & Verma, P. D. (1999). Ferrofluid lubrication in porous inclined slider bearing. *Indian Journal of Pure and Applied Mathematics*, 30(12), 1273-1282.

[5] Osman, T. A., Nada, G. S., & Safar, Z. S. (2001). Static and dynamic characteristics of magnetized journal bearings lubricated with ferrofluid. *Tribology International*, 34(6), 369-380.

[6] Shah, R. C., & Bhat, M. V. (2005). Ferrofluid squeeze film between curved annular plates including rotation of magnetic particles. *Journal of Engineering Mathematics*, 51(4), 317-324.

[7] Deheri, G. M., Patel, H. C., & Patel, R. M. (2006). Performance of magnetic fluid based circular step bearings. *Mechanics*, 57(1), 22-27.

[8] Ahmad, N., & Singh, J. P. (2007). Magnetic fluid lubrication of porous-pivoted slider bearings with slip velocity. *Proceedings of the Institution of Mechanical Engineers, Part J: Journal of Engineering Tribology*, 221(5), 609-613.

[9] Urreta, H., Leicht, Z., Sanchez, A., Agirre, A., Kuzhir, P., & Magnac, G. (2010). Hydrodynamic bearing lubricated with magnetic fluids. *Journal of intelligent material systems and structures*, 21(15), 1491-1499.

[10] Patel, R. M., Deheri, G. M., & Vadher, P. A. (2010). Performance of a magnetic fluid-based short bearing. *Acta Polytechnica Hungarica*, 7(3), 63-78.

[11] Patel, N. S., Vakharia, D. P., & Deheri, G. M. (2012). A study on the performance of a magnetic-fluid-based hydrodynamic short journal bearing. *ISRN Mechanical Engineering*, 2012.

[12] Gould, P. (1967). Parallel surface squeeze films: the effect of the variation of viscosity with temperature and pressure. *Journal of lubrication Technology*, 89(3), 375-380.

[13] Gupta, J. L., & Vora, K. H. (1980). Analysis of squeeze films between curved annular plates. *Journal of lubrication technology*, 102(1), 48-50.

[14] Lin, J. R. (2001). Magneto-hydrodynamic squeeze film characteristics between annular disks. *Industrial Lubrication and Tribology*, 53(2), 66-71.

[15] Chou, T. L., Lai, J. W., & Lin, J. R. (2003). Magneto-hydrodynamic squeeze film characteristics between a sphere and a plane surface. *Journal of Marine Science and Technology*, 11(3), 174-178.

[16] Naduvinamani, N. B., Hiremath, P. S., & Gurubasavaraj, G. (2002). Effect of surface roughness on the static characteristics of rotor bearings with couple stress fluids. *Computers & structures*, 80(14), 1243-1253.

[17] Lin, J. R. (1997). Squeeze film characteristics of long partial journal bearings lubricated with couple stress fluids. *Tribology International*, 30(1), 53-58.

[18] Lin, J. R. (2000). Squeeze film characteristics

between a sphere and a flat plate: couple stress fluid model. *Computers & Structures*, 75(1), 73-80.

[19] Bujurke, N. M., & Jayaraman, G. (1982). The influence of couple stresses in squeeze films. *International Journal of Mechanical Sciences*, 24(6), 369-376.

[20] Bujurke, N. M., & Naduvinamani, N. B. (1991). On the performance of narrow porous journal bearing lubricated with couple stress fluid. *Acta mechanica*, 86(1), 179-191.

[21] Christensen, H., & Tonder, K. C. (1969). *Tribology of rough surfaces: stochastic models of hydrodynamic lubrication* (Vol. 10, pp. 69-18). SINTEF report.

[22] Christensen, H., & Tonder, K. (1973). The hydrodynamic lubrication of rough journal bearings. *Journal of Lubrication Technology*, 95(2), 166-172.

[23] Christensen, H., & Tonder, K. (1971). The hydrodynamic lubrication of rough bearing surfaces of finite width. *Journal of Lubrication Technology*, 93(3), 324-329.

[24] Tzeng, S. T., & Saibel, E. (1967). Surface roughness effect on slider bearing lubrication. *Asle Transactions*, 10(3), 334-348.

[25] Ting, L. L. (1975). Engagement behavior of lubricated porous annular disks. Part I: squeeze film phase—surface roughness and elastic deformation effects. *Wear*, 34(2), 159-172.

[26] Guha, S. K. (1993). Analysis of dynamic characteristics of hydrodynamic journal bearings with isotropic roughness effects. *Wear*, 167(2), 173-179.

[27] Chiang, H. L., Hsu, C. H., & Lin, J. R. (2004). Lubrication performance of finite journal bearings considering effects of couple stresses and surface roughness. *Tribology International*, 37(4), 297-307.

[28] Gupta, J. L., & Deheri, G. M. (1996). Effect of roughness on the behavior of squeeze film in a spherical bearing. *Tribology Transactions*, 39(1), 99-102.

[29] Naduvinamani, N. B., Fathima, S. T., & Hiremath, P. S. (2003). Hydrodynamic lubrication of rough slider bearings with couple stress fluids. *Tribology International*, 36(12), 949-959.

[30] Bujurke, N. M., Naduvinamani, N. B., & Basti, D. P. (2007). Effect of surface roughness on the squeeze film lubrication between curved annular plates. *Industrial Lubrication and Tribology*, 59(4), 178-185.

[31] Deheri, G. M., Patel, R. M., & Abhangi, N. D. (2011). Magnetic fluid-based squeeze film behavior between transversely rough curved annular plates: a comparative study. *Industrial Lubrication and Tribology*, 63(4), 254-270.

[32] Shimpi, M. E., & Deheri, G. M. (2012). Magnetic fluid-based squeeze film behaviour in curved porous-rotating rough annular plates and elastic deformation effect. *Advances in Tribology*, 2012.

[33] Patel, H., Deheri, G. M., & Patel, R. M. (2009). Magnetic fluid-based squeeze film between porous rotating rough circular plates. *Industrial Lubrication and Tribology*, 61(3), 140-145.

[34] Shimpi, M. E., & Deheri, G. M. (2010). Surface roughness and elastic deformation effects on the behaviour of the magnetic fluid based squeeze film between rotating porous circular plates with concentric circular pockets. *Tribology in Industry*, 32(2), 21-30.

[35] Patel, J. R., & Deheri, G. (2013). Shliomis model based ferrofluid lubrication of squeeze film in rotating rough curved circular disks with assorted porous structures. *American Journal of Industrial Engineering*, 1(3), 51-61.

[36] Bhat, M. V. (2003). Lubrication with a magnetic fluid. *Team Spirit (India) Pvt. Ltd.*

[37] Abhangi, N. D., & Deheri, G. M. (2012). Numerical modelling of squeeze film performance between rotating transversely rough curved circular plates under the presence of a magnetic fluid lubricant. *ISRN Mechanical Engineering*, 2012.

[38] Patel, H. A., Patel, M. P., Patel, H. C., & Deheri, G. M. (2014). Squeeze Film Performance in Parallel Rough Circular Disks Lubricated by Ferrofluid with Non-newtonian Couple Stress Effect. In Proceedings of International Conference on Advances in Tribology and Engineering Systems (pp. 111-115). *Springer*, New Delhi.

[39] Patel, H. A., Patel, H. C., & Deheri, G. M. (2015). FERROFLUID BASED SQUEEZE FILM PERFORMANCE IN ANNULAR DISKS WITH NON NEWTONIAN COUPLE STRESSES. *Annals of the Faculty of Engineering Hunedoara*, 13(4), 255.

[40] Patel, N. S., Vakharia, D. P., Deheri, G. M., & Patel, H. C. (2017). Experimental performance analysis of ferrofluid based hydrodynamic journal bearing with different combination of materials. Wear, 376, 1877-1884.

PRAJÑĀ - **Journal of Pure and Applied Sciences Vol. 24 - 25 : 30 - 37 (2017)**
ISSN 0975 - 2595

SOLUTION OF Nth ORDER FUZZY INITIAL VALUE PROBLEM

KOMAL R.PATEL[1] AND NARENDRASINH B.DESAI[2*]

[1]Assistant Professor, Applied Sciences and Humanities Department, ITM Universe, Vadodara-390510, Gujarat, India. Email: komalpatel2121982@gmail.com
[2]Associate Professor, Head of Applied Sciences and Humanities Department, ADIT, V.V.Nagar-388121, Gujarat, India. Email: drnbdesai@yahoo.co.in

ABSTRACT

In this paper we consider higher order linear differential equations with fuzzy initial values that occurs in almost all engineering branches. Here, We find solution for constant coefficient and variable coefficient third order linear differential equation by using method based on properties of linear transformation We show that fuzzy problem has unique solution if corresponding crisp Problem has unique solution. We will also prove that if the initial values are triangular fuzzy numbers, then the values of the solution at a given time are also triangular fuzzy numbers. We are going to propose a method to find fuzzy solution. We present three examples, one is homogeneous and another is non-homogeneous linear differential equation with constant coefficient and third is non-homogeneous linear differential equation with variable coefficient (Cauchy-Euler equation) to illustrate applicability of proposed method. We also plot graphs to show difference between exact and fuzzy solutions. This shows that our method is practical and applicable to solve nth order fuzzy initial value problems.

AMS Subject Classification code: 34A07: Fuzzy differential equations.
Keywords: Fuzzy initial value problem, Fuzzy set, Fuzzy number and linear transformation.

INTRODUCTION

Fuzzy initial value problem occurs in almost all Engineering branches. The term "Fuzzy differential equation" was put forward for the first time by Kandel and Byatt [1],The fuzzy initial value problem was studied by Seikkala [26].The fuzzy initial problem has been investigated by many authors so far Buckley and Feuring [7,8]; Buckley, Feuring, and Hayashi [9]; Lakshmikantham and Nieto [18]; Bede and Gal [5]; Bede, Rudas, and Bencsik [3]; Perfilieva et al.[25]; Chalco-Cano and Román-Flores[10,11]; Khastan, Bahrami, and Ivaz [14]; Gasilov, Amrahov, and Fatullayev [17]; Khastan,Nieto,Rodríguez-López [16]; Patel, Desai [22].Gasilo et al.[13],Gomes and Barros [4,28] proposed concepts of fuzzy calculus, analogically to classical calculus, and studied fuzzy differential equations in terms of this calculus. Under certain conditions, they established the existence of a solution for the first order fuzzy initial value problem and suggested a solution method. Gasilov et al. [17] benefitted from properties of linear transformations and proposed a method to find fuzzy bunch of Solution functions for linear equation. The method is applicable to higher order linear differential equations with constant coefficients.

Most of the researchers assume that derivative in the differential equation as a derivative of a fuzzy function in some sense. In earlier researches the derivative was considered as derivative. A study in this direction was made by Kaleva [19,20,21]. When Hukuhara derivative is used, then uncertainty of the solution may increase infinitely with time.

Furthermore, Bede and Gal [5] showed that a simple fuzzy function, generated by multiplication of differentiable crisp function and a fuzzy number, may not have Hukuhara derivative. In order to overcome this difficulty Bede and Gal [5] developed the generalized derivative concept and after that the studies about this subject were accelerated (Bede[2]); Bede et al [6]; Khastan and Nieto[15]; Chalco-Cano,Román-Flores[10,11,29]. But in case of generalized Hukuhara derivatives there are four different cases for second order fuzzy differential equation. Khastan A.,Gasilov.N.A., Fatullayev.A.G, Amrahov.S.E.[27], found solution of constant coefficient FBVP. Patel, Desai [23,24] solve fuzzy initial value problems by fuzzy Laplace transform.

In this paper we consider the fuzzy initial value problem as a set of crisp problem using properties of linear transformations. We solve higher order Cauchy-Euler's equation. For clarity we explain the proposed method for third order fuzzy linear differential equations, but the results are true for higher-order equations too. The fuzzy solution proposed by our method coincides with extension principle's results.

PRELIMINARIES

Definition: Membership function:

A fuzzy set $\tilde{A}$ can be defined as a pair of the universal set U and the membership function $\mu: U \rightarrow [0,1]$ for each $x \in U$, the number $\mu_{\tilde{A}}$ is called the membership degree of x in $\tilde{A}$.

Definition: $\alpha - cut\ set$:

$For\ each\ \alpha \in (0,1]$ the crisp set
$A_\alpha = \{x \in U | \mu_{\tilde{A}}(x) \geq \alpha\}$ is called
$\alpha - cut\ set$ of $\tilde{A}$.We use the notation
$\tilde{u} = \left(u_{L,}(\alpha), u_R(\alpha)\right)$ $0 \leq \alpha \leq 1$ to indicate a fuzzy number in parametric form. We denote $\underline{u}$ = $u_L(0)$ and $\bar{u}$ = $u_R(0)$ to indicate the left and the right end-points of $\tilde{u}$ respectively. an α-cut of $\tilde{u}$ is an interval $[u_{L,}(\alpha), u_R(\alpha)]$, which we denote as $u_\alpha = [\underline{u}\alpha, \bar{u}\alpha]$.

Definition:Fuzzy Number

A fuzzy number is a fuzzy set like $U: R \rightarrow I = [0,1]$ which satisfies:

(a) u is upper semi-continuous.

(b) u is fuzzy convex i.e.$(\lambda x + (1-\lambda)y) \geq \min\{u(x), u(y)\}\ \forall x, y \in R, \lambda \in [0,1]$

(c) u is normal i.e $\exists x_0 \in R$ for which $u(x_0) = 1$

(d)$For\ each\ \alpha \in (0,1], supp\ u = \{x \in R | u_\alpha(x) > 0\}$ is support of u,and its $cl(supp\ u)$ is compact.

Definition: Triangular Fuzzy Number:

The Triangular fuzzy number as $\tilde{u}$= (a, b, c) for which $u_{L,}(\alpha)$ = a + α (b − a), $u_R(\alpha)$ = b - α (c − b) and $\underline{u}$ = a, $\bar{u}$= c. In geometric interpretations, we refer to the point b as a vertex.

Let us consider a triangular fuzzy number $\tilde{u}$ = (p, 0, q) the vertex of which is 0 (Note that p < 0 and q > 0 in this case).Then $u_L(\alpha)$ = (1−α) p and $u_R(\alpha)$ = (1−α) q and consequently, α-cuts are intervals

$$[(1-\alpha)\, p, (1-\alpha)\, q] = (1-\alpha)[p, q]$$

From the last representation one can see that an α-cut is similar to the interval [p, q] (i.e. to the 0-cut) with similarity coefficient (1−α).
We often express a fuzzy number $\tilde{u}$ as $\tilde{u} = u_{cr} + \tilde{u}_{un}$(crisp part + uncertainty). Here u_{cr} is a number with membership degree 1 and represents the crisp part (the vertex) of $\tilde{u}$,while $\tilde{u}_{un}$ represents the uncertain part with vertex at the origin.

For a triangular fuzzy number $\tilde{u}$= (a, b, c) we have $u_{cr} = b$ and $\tilde{u}_{un} = (a-b, 0, c-b)$.

Properties of Fuzzy Valued Number

For arbitrary $u = (\underline{u}(r), \bar{u}(r))$ $v = (\underline{v}(r), \bar{v}(r))$,

$0 \leq r \leq 1$ and arbitrary $k \in R$.

We define addition, subtraction, multiplication, scalar multiplication by k.

$$u + v = (\underline{u}(r) + \underline{v}(r), \bar{u}(r) + \bar{v}(r))$$
$$u - v = (\underline{u}(r) - \bar{v}(r), \bar{u}(r) - \underline{v}(r))$$
$$u \cdot v = (\min\{\underline{u}(r)\bar{v}(r), \underline{u}(r)\underline{v}(r), \bar{u}(r)\bar{v}(r), \bar{u}(r)\underline{v}(r)\}, \max\{u(r)\bar{v}(r), \underline{u}(r)\underline{v}(r), \bar{u}(r)\bar{v}(r), \bar{u}(r)\underline{v}(r)\})$$
$$ku = \begin{cases} (k\underline{u}(r), k\bar{u}(r)) & if\ \ k \geq 0 \\ (k\bar{u}(r), k\underline{u}(r)) & if\ \ k < 0 \end{cases}$$

Definition:Hukuhara difference

Let $x, y \in E$.If there exists $z \in E$ such that $x = y + z$, then z is called the Hukuhara difference of fuzzy numbers x and y, and it is denoted by $z = x\ \Theta\ y$. The Θ sign stands for Hukuhara-difference and $x\ \Theta\ y \neq x + (-1)\ y$.

Definition:Hukuhara differential

Let $f: (a, b) \rightarrow E$ and $t_0 \in (a, b)$ if there exists an element $f'(t_0) \in$ E such that for all $h > 0$ sufficiently small, exists $f(t_0 + h)\ \Theta\ f(t_0)$, $f(t_0)\ \Theta f(t_0 - h)$ and the limits holds(in the metric D)

$$\lim_{h \to 0} \frac{f(t_0+h)\ \Theta\ f(t_0)}{h} = \lim_{h \to 0} \frac{f(t_0)\ \Theta\ f(t_0-h)}{h} = f'(t_0)$$

Here derivative is considered as Hukuhara derivative.

FUZZY INITIAL VALUE PROBLEMS (FIVPS)

In this section, we have described a fuzzy initial value problem (FIVP) and concept of solution**.** We investigate a fuzzy Initial value problem with crisp linear differential equation and fuzzy initial values. FIVP can arise in modeling of a process the dynamics of which is crisp but there are uncertainties in initial values.

Consider the nth order fuzzy initial value problem where $b_n(x) \neq 0$.

$$\left\{\begin{array}{c} b_n(x)y^n + b_{n-1}(x)y^{n-1} + \cdots + b_1(x)y' + b_0(x)y = f(x) \\ y(l) = \widetilde{A_1} \\ y'(l) = \widetilde{A_2} \\ y''(l) = \widetilde{A_3} \\ \cdots \\ \cdots \\ y^{n-1}(l) = \widetilde{A_n} \end{array}\right\} \quad (1)$$

Where $\widetilde{A_1}, \widetilde{A_2}, \widetilde{A_3}, \ldots, \widetilde{A_n}$ are fuzzy numbers and $b_0(x), b_1(x), \ldots, b_n(x)$ and $f(x)$ are continuous crisp functions or constants and l is any integer.Let us represent the initial values as $\widetilde{A_1} = a_1 + \widetilde{a_1}$, $\widetilde{A_2} = a_2 + \widetilde{a_2}, \ldots, \widetilde{A_n} = a_n + \widetilde{a_n}$ where $a_1, a_2, \ldots, a_n$ are crisp numbers while $\widetilde{a_1}$ $\widetilde{a_2}, \ldots, \widetilde{a_n}$ are fuzzy numbers. We split the FIVP in Eq.(1) to the following problems:

Associated crisp problem (which is non-homogeneous)

$$\left\{\begin{array}{c} b_n(x)y^n + b_{n-1}(x)y^{n-1} + \cdots + b_1(x)y' + b_0(x)y = f(x) \\ y(l) = a_1 \\ y'(l) = a_2 \\ y''(l) = a_3 \\ \cdots \\ \cdots \\ y^{n-1}(l) = a_n \end{array}\right\} \quad (2)$$

Homogeneous problem with fuzzy initial values

$$\left\{\begin{array}{c} b_n(x)y^n + b_{n-1}(x)y^{n-1} + \cdots + b_1(x)y' + b_0(x)y = 0 \\ y(l) = \widetilde{a_1} \\ y'(l) = \widetilde{a_2} \\ y''(l) = \widetilde{a_3} \\ \cdots \\ \cdots \\ y^{n-1}(l) = \widetilde{a_n} \end{array}\right\} \quad (3)$$

It is easy to see if $y_{cr}(x)$ and $\tilde{y}_{un}(x)$ are solutions of Eq.(2) and Eq.(3) respectively then $\tilde{y}(x) = y_{cr}(x) + \tilde{y}_{un}(x)$ is a solution of the given problem in Eq.(1). Hence, Eq.(1) is reduced to solving a non-homogeneous equation with crisp conditions in Eq.(2) and homogeneous equation with fuzzy initial conditions in Eq.(3). Therefore, we will investigate how to solve Eq.(1).To determine $\tilde{y}(x)$ we consider Linear transformation $T: R^n \to R$, $T(u) = v\,u$, where v is fixed $n\,x\,n$ determinant and $u = [a_1, a_2, \ldots a_n]^T$.

THE SOLUTION ALGORITHM

The solution algorithm consists of four steps:

- Represent the initial values as $\widetilde{A_1} = a_1 + \widetilde{a_1}$, $\widetilde{A_2} = a_2 + \widetilde{a_2}, \ldots, \widetilde{A_n} = a_n + \widetilde{a_n}$
- Find linear independent solutions $y_1(x)$, $y_2(x), \ldots, y_n(x)$ of the crisp differential equation $b_n(x)y^n + b_{n-1}(x)y^{n-1} + \cdots b_1(x)y' + b_0(x)y = f(x)$.Constitute the vector-function $s(x) = (y_1(x), y_2(x), \ldots, y_n(x))$, the determinant W and calculate the vector-function $t(x) = s(x)W^{-1} = (t_1(x), t_2(x), \ldots, t_n(x))$ by formula at $x = l$.

  The Wronskain

$$W = \begin{vmatrix} y_1(l) & y_2(l) & \ldots & y_n(l) \\ \vdots & \vdots & \ddots & \vdots \\ {y_1}^{n-1}(l) & {y_2}^{n-1}(l) & \ldots & {y_n}^{n-1}(l) \end{vmatrix}$$

  and $\det(W) \neq 0 \;\; \therefore W^{-1}\, exist.$
- Find the solution $y_{cr}(x)$ of the non-homogeneous crisp problem.
- The solution of the given problems
  For homogeneous FIVP
  $\tilde{y}(x) = t_1(x)\,\widetilde{a_1} + t_2(x)\,\widetilde{a_2} + \ldots + (x)\,\widetilde{a_n}$.
  For non-homogeneous FIVP
  $\tilde{y}(x) = y_{cr}(x) + t_1(x)\,\widetilde{a_1} + t_2(x)\,\widetilde{a_2} + \ldots + t_n(x)\,\widetilde{a_n}$.

EXAMPLES

Example:5.1 Solve the 3rd order FIVP with constant coefficient homogeneous equation.

$$\left\{\begin{array}{c} y''' + 3y'' + 3y' + y = 0 \\ y(0) = (-0.5, 0, 1) \\ y'(0) = (-1, 0, 1) \\ y''(0) = (-1, 0, 0.5) \end{array}\right\} \quad (4)$$

The problem is homogeneous and initial values are fuzzy numbers with vertices at 0.therefore solution by solution algorithm.$y(x) = e^{-x}$, $y_2(x) = xe^{-x}$and $y_3(x) = x^2e^{-x}$are linearly independent solution for the equation $y''' + 3y'' + 3y' + y = 0$.

Hence $s(x) = (e^{-x}, xe^{-x}, x^2e^{-x})$ and

$$W = \begin{vmatrix} 1 & 0 & 0 \\ -1 & 1 & 0 \\ 1 & -2 & 2 \end{vmatrix} \quad \text{and}$$

$$t(x) = s(x)W^{-1} = (t_1(x), t_2(x), t_3(x)),$$
$$t(x) = (e^{-x} + xe^{-x} + \frac{x^2}{2}e^{-x}, xe^{-x} + x^2e^{-x}, \frac{x^2}{2}e^{-x})$$

$$\tilde{y}_{un}(x) = (e^{-x} + xe^{-x} + x^2e^{-x})(-0.5,0,1) + (xe^{-x} + x^2e^{-x})(-1,0,1) + \frac{x^2}{2}e^{-x}(-1,0,0.5)$$

Where the arithmetic operations are considered to be fuzzy operations.

The fuzzy solution $\tilde{y}(x)$ form band in the xy-coordinate space (Fig.1)

Since the initial values are triangular fuzzy numbers, an α-cut of the solution can be determined by similarity coefficient $(1-\alpha)$, i.e.

$y_\alpha(x) = (1-\alpha)[\underline{y}(x), \bar{y}(x)]$

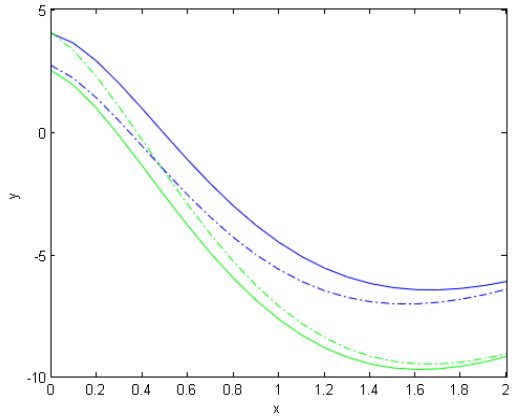

Fig.1 The fuzzy solution, obtained by the proposed method, for Example 5.1

Example:5.2 Consider the 3rd order FIVP with constant coefficient non-homogeneous equation.

$$\left\{\begin{matrix} y''' + 3y'' + 3y' + y = 30e^{-x} \\ y(0) = (2.5,3,4) \\ y'(0) = (-4,-3,-2) \\ y''(0) = (-48,-47,-46.5) \end{matrix}\right\} \qquad (5)$$

We represent the initial values as

$\tilde{A}$= (2.5,3,4) = 3 + (-0.5,0,1),
$\tilde{B}$= (-4,-3,-2) = -3 + (-1,0,1),
$\tilde{C}$=(-48,-47,-46.5) = - 47 + (-1,0,0.5).

we solve crisp non-homogeneous crisp problem

$$\left\{\begin{matrix} y''' + 3y'' + 3y' + y = 30e^{-x} \\ y(0) = 3 \\ y'(0) = -3 \\ y''(0) = -47 \end{matrix}\right\} \qquad (6)$$

And the crisp solution

$$y_{cr}(x) = (3 - 25x^2)e^{-x} + 5x^3e^{-x}$$

$$y_{cr}(x) = 3(e^{-x} + xe^{-x} + x^2e^{-x}) - 3(xe^{-x} + x^2e^{-x}) - \frac{47x^2}{2}e^{-x} + 5x^3e^{-x}$$

Fuzzy homogeneous problem to find the uncertainty of the solution is as follows:

$$\left\{\begin{matrix} y''' + 3y'' + 3y' + y = 0 \\ y(0) = (0.5,0,1) \\ y'(0) = (-1,0,1) \\ y''(0) = (-1,0,0.5) \end{matrix}\right\} \qquad (7)$$

This problem is the same as Example 1. Hence, the solution is

$$\tilde{y}_{un}(x) = (e^{-x} + xe^{-x} + x^2e^{-x})(-0.5,0,1) + (xe^{-x} + x^2e^{-x})(-1,0,1) + \frac{x^2}{2}e^{-x}(-1,0,0.5)$$

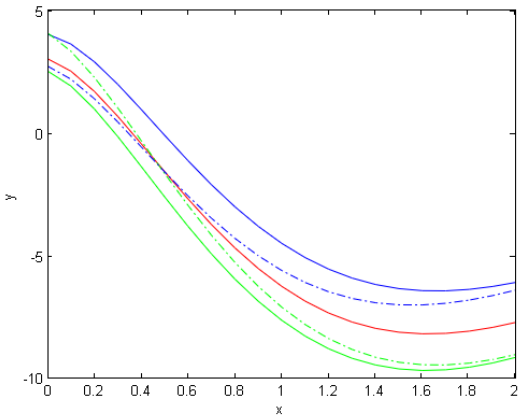

Fig. 2 The fuzzy solution $\tilde{y}(x)$, obtained by the proposed method, for Example 5.2.Red line represents the crisp solution.

PRAJÑĀ - **Journal of Pure and Applied Sciences Vol. 24 - 25 : 30 - 37 (2017)**
ISSN 0975 - 2595

We add this uncertainty to the crisp solution and get the fuzzy solution of the given FIVP

$$\tilde{y}(x) = y_{cr}(x) + \tilde{y}_{un}(x)$$

$$= (e^{-x} + xe^{-x} + x^2e^{-x})(2.5,3,4)$$
$$+ \ (xe^{-x} + x^2e^{-x})(-4,-3,-2)$$
$$+\frac{x^2}{2}e^{-x}(-48,-47,-46.5) + 5x^3e^{-x}$$

In above example if we take $x \to \infty$ then fuzziness in solution is disappeared. So the solution goes nearer to zero if we increase x.(see Fig.3)

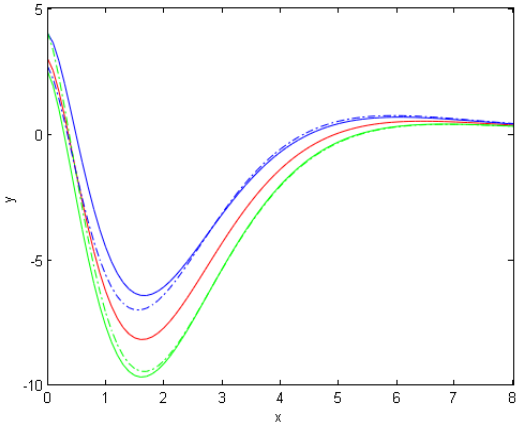

Fig. 3 If x increases fuzziness disappears

Example:5.3 Consider 3rd order FIVP with variable coefficient.

$$\left\{\begin{array}{c}(x^3D^3 - 3x^2D^2 + 6xD - 6)y = \frac{12}{x} \\ y(1) = (4,5,6) \\ y'(1) = (12,13,14.5) \\ y''(1) = (9.5,10,11)\end{array}\right\} \quad (8)$$

$$\left\{\begin{array}{c}(x^3D^3 - 3x^2D^2 + 6xD - 6)y = \frac{12}{x} \\ y(1) = 5 \\ y'(1) = 13 \\ y''(1) = 10\end{array}\right\} \quad (9)$$

Associated non-homogeneous problem has the solution i.e. exact solution of non-homogeneous problem

$$y_{cr}(x) = \frac{-138}{24}x + \frac{328}{24}x^2 + \frac{-69}{24}x^3 - \frac{1}{24x}$$

Consider homogeneous equation

$$\left\{\begin{array}{c}(x^3D^3 - 3x^2D^2 + 6xD - 6)y = 0 \\ y(1) = (-1,0,1) \\ y'(1) = (-1,0,0.5) \\ y''(1) = (-0.5,0,1)\end{array}\right\} \quad (10)$$

The problem is homogeneous and initial values are fuzzy numbers with vertices at 0.therefore solution by solution algorithm.$y_1(x) = x$, $y_2(x) = x^2$ and $y_2(x) = x^3$ are linearly independent solution of equation

$$(x^3D^3 - 3x^2D^2 + 6xD - 6)y = 0$$

Hence $s(x) = (x, x^2, x^3)$ and

$$W = \begin{vmatrix}1 & 1 & 1\\ 1 & 2 & 3\\ 0 & 2 & 6\end{vmatrix}$$

And

$t(x) = s(x)W^{-1} = (t_1(x), t_2(x), t_3(x))$

$$t(x) = \left(3x - 3x^2 + x^3, -2x + 3x^2 - x^3, \frac{x}{2} - x^2 + \frac{x^3}{2}\right)$$

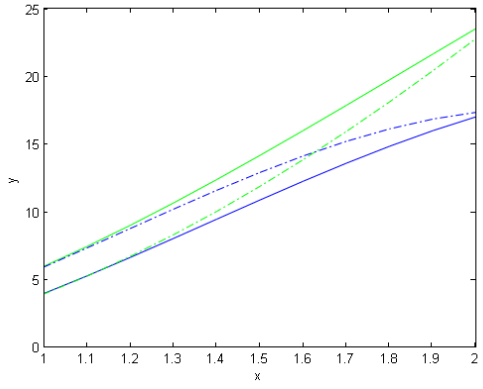

Fig.4 The fuzzy solution, obtained by the proposed method, for Example 5.3

The fuzzy solution is

$$\tilde{y}_{un}(x) = (3x - 3x^2 + x^3)(-1,0,1)$$
$$+(-2x + 3x^2 - x^3)(-1,0,0.5)$$
$$+ \ (\frac{x}{2} - x^2 + \frac{x^3}{2})(-0.5,0,1)$$

PRAJÑĀ - **Journal of Pure and Applied Sciences Vol. 24 - 25 : 30 - 37 (2017)**
ISSN 0975 - 2595

We add this uncertainty to the crisp solution and get the fuzzy solution of the given FIVP

$$\tilde{y}(x) = y_{cr}(x) + \tilde{y}_{un}(x)$$
$$= (3x - 3x^2 + x^3)(4,5,6)$$
$$+(-2x + 3x^2 - x^3) \quad (12, 13, 14.5)$$
$$+(\frac{x}{2} - x^2 + \frac{x^3}{2}(9.5,10,11) - \frac{1}{24x}$$

$$\tilde{y}(x) = -6x + 14x^2 - 3x^3 - \frac{1}{24x}$$

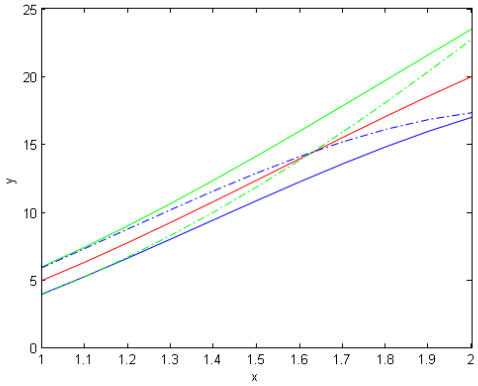

Fig.5 The fuzzy solution, obtained by the proposed method, for Example 5.3.Red line represents the crisp solution.

In above example if we increase x and as we take $x \to \infty$ then fuzziness in solution increases and goes to infinite.

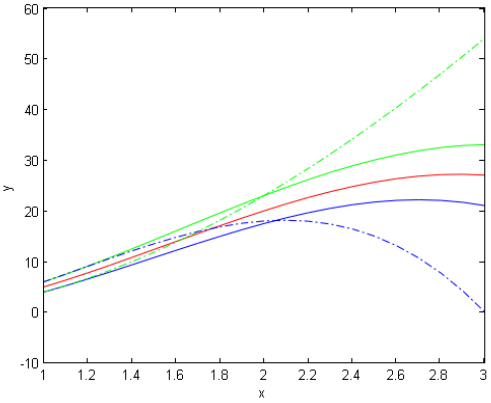

Fig. 6 If we increase x fuzziness increases

Example:5.4 Consider a unit mass sliding on a frictionless table attached to a spring, with spring constant k =16. Suppose the mass is lightly tapped by a hammer every T seconds. Suppose that the first tap occurs at time t = 0 and before that time the mass is at rest. Describe what happens to the motion of the mass for the tapping period T =1.

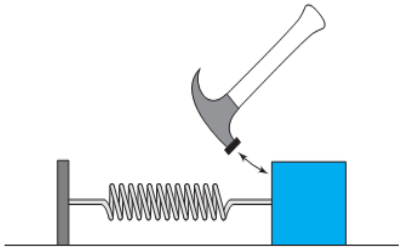

Mass tapped periodically with a hammer.

Fig. 7

$$\left\{\begin{matrix} x''(t) + 16\,x(t) = sint \\ x(0) = 0 \\ x'(0) = 1 \end{matrix}\right\} \qquad (11)$$

Consider the homogeneous equation with fuzzy parameters.

$$\left\{\begin{matrix} x''(t) + 16\,x(t) = 0 \\ x(0) = (-1,0,1) \\ x'(0) = (-0.5,0,1) \end{matrix}\right\} \qquad (12)$$

The problem is homogeneous and initial values are fuzzy numbers with vertex 0 therefore solution by solution algorithm. $x_1(t) = cos4t\,, x_2(t) = sin4t$ are linearly independent solution for the equation $x''(t) + 16x(t) = 0$

Hence $s(t) = (cos4t, sin4t)$ and

$$W = \begin{vmatrix} 1 & 0 \\ 0 & 4 \end{vmatrix}$$

and $y(t) = (y_1(t), y_2(t))$
Here $y(t) = (cos4t, (1/4)\,sin4t)$
$\tilde{x}_{un}(t)$ = (cos4t)(−1,0,1) + (1/ 4)sin4t(−0.5,0,1)
Crisp solution of given non-homogeneous problem $x_{cr}(t)$ = (7/ 30)$sin4t$ + (1/15)$sint$.

$$\tilde{x}(t) = x_{cr}(t) + \tilde{x}_{un}(t)$$

$=cos4t(-1,0,1)+(7/30)sin4t(0.5,1,2)$
+ (1/15)$sint$ = (7/ 30)$sin4t$ + (1/ 15)$sint$

where arithmetic operations are considered to be fuzzy operations. the fuzzy solution $\tilde{x}(t)$form band in the tx-coordinate space.(Fig.8)

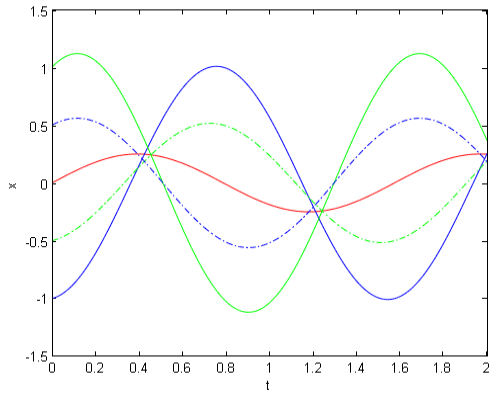

Fig.8:The periodic fuzzy solution by properties of Linear transformation

If we apply periodic force to block, it will move in given open interval that we denote by triangular fuzzy number, Here the damping force is negligible. The spring mass system occurs in all most all engineering branches as well as in the many real life situations.

CONCLUSIONS

In this paper we have represented the fuzzy initial value problems as a set of crisp problems. We have proposed a solution method based on the properties of linear transformations. For clarity we have explained the proposed method for third order linear differential equation but it is applicable for nth order also. Here we have solved third order Cauchy-Euler equation i.e. we solved variable coefficient initial value problems based on the properties of linear transformations. We also solved one application level problem.

AIM AND SCOPE OF THE WORK

The aim of paper is to find solution of any Fuzzy differential equation having uncertain initial conditions. In future we are going to solve Fuzzy differential equations having the applications in different branches of engineering. we will solve higher order FBVP based on the properties of linear transformations.

REFERENCES

[1] Kandel A., Byatt W. J. , “Fuzzy differential equations,.” in Proceedings of the International Conference on Cybernetics and Society, (1978.): pp. 1213–1216, Tokyo, Japan, .
[2] B, Bede. “A note on “two-point boundary value problems associated with non-linear fuzzy differential equations”.” Fuzzy Sets Syst (2006): 157:986–989.
[3] Bade, B, I,J. Rudas and A.L. Bencsil. “First order linear fuzzy differential equations under generalized differentiability.” Information Sciences, (2007):177:1648-1662.
[4] Barros L C, Gomes L T, Tonelli P A. “ Fuzzy differential equations: an approach via fuzzification of the derivative operator.” Fuzzy Sets Syst. (doi:10.1016/j.fss.2013.03.004).
[5] Bede B, Gal S G. “Generalizations of the differentiability of fuzzy number valued functions with applications to fuzzy differentia lequation.” Fuzzy Sets Syst (2005): 151:581–599.
[6] Bede B, Stefanini L. “Generalized differentiability of fuzzy-valued functions.” Fuzzy Sets Syst. (2012): doi:10.1016/j.fss.2012.10.003.
[7] Buckley JJ, Feuring T. “ Fuzzy differential equations.” Fuzzy Sets Syst (2000): 110:43–54.
[8] —. “Fuzzy initial value problem for Nth-order linear differential equation.” Fuzzy Sets Syst (2001): 121:247–255.
[9] Buckley JJ, Feuring T, Hayashi Y. “ Linear systems of first order ordinary differentia lequations:fuzzy initial conditions.” Soft Comput (2002): 6:415–421.
[10] Chalco-Cano Y, Román-Flores H. “ On the new solution of fuzzy differential equations.” Chaos Solitons Fractals (2008): 38:112–119.
[11] —. “Comparation between some approaches to solve fuzzy differential equations.” Fuzzy Sets Syst (2009): 160(11):1517–1527 .
[12] Desai, N. B. “Fuzzy modeling and its application.” M.Phil Dessertation (1997).
[13] Gasilov N A, Amrahov ¸SE, Fatullayev AG. “ A geometric approach to solve fuzzy linear systems of differential equations.” Appl Math Inf Sci (2011a): 5:484–495 .
[14] Khastan A, Bahrami F, Ivaz K. “New results on multiple solutions for Nth-order fuzzy differential equations under generalized differentiability.” Bound Value Probl. (2009): doi:10.1155/2009/395714.
[15] Khastan A, Nieto JJ. “A boundary value problem for second order fuzzy differential equations.” Nonlinear Anal (2010): 72:3583–3593 .

[16] Khastan A, Nieto JJ, Rodríguez-López R. "Variation of constant formula for first order fuzzy differential equations. " Fuzzy Sets Syst (2011): 177:20–33.
[17] Gasilov N. A., Fatullayev A. G. ¸ Amrahov S. E., Khastan A "A new approach to fuzzy initial value problem." Soft Comput (2013): DOI 10.1007/s00500-013-1081-z.
[18] Lakshmikantham, V. and J.J. Nieto. "Differential equations in metric spaces:an introduction and an application to fuzzy differential equations." Dynamics of (2003): A, vol. 10, no. 6, pp. 991–1000.
[19] Kaleva O., "A note on fuzzy differentia lequations." Non linear Anal (2006): 64:895–900 .
[20] —. "Fuzzy differential equations." Fuzzy Sets Syst. (1987): 24:301– 317 .
[21] —. "The Cauchy problem for fuzzy differential equations. ." Fuzzy Sets Syst (1990): 35:389–396.
[22] Patel K. R, Desai N.B. "Solution of fuzzy initial value problems." ADIT Journal of Engineering (December 2015): Vol.12,No.1,53-57.
[23] Patel K. R., Desai N. B. "Solution of variable coefficient fuzzy differential equations by fuzzy Laplace transform." IJRITCC Vol.5,Issue:6 (June 2017): 927-942.
[24] Patel K.R, Desai N.B. "Solution Of Fuzzy Initial Value Problems By Fuzzy Laplace Transform." Kalpa Publications in Computing,ICRISET2017 (Vol.2,June 12, 2017): 25-37.
[25] Perfilieva I, Meyer H,Baets B,Plšková D. "Cauchyproblemwith fuzzy initial condition and its approximate solution with the help of fuzzy transform. ." In: IEEE world congress on computational intelligence (WCCI 2008), (2008): p 6.
[26] Seikkala, S. "On the fuzzy initial value problem." Fuzzy Sets and Systems, (1987): vol. 24, no. 3, pp. 319–330.
[27] Gasilov N, Amrahov ¸SE, Fatullayev AG. "Linear differential equations with fuzzy boundary values." In: Proceedings of the 5th international conference"Application of Information and Communication Technologies" (2011b): (AICT2011) (ISBN: 978-1-61284-830-3), pp 696–700.Baku, Azerbaijan, October 12–14.
[28] Gomes L T, BarrosL C. "Fuzzy calculus via extension of the derivative and integral operators and fuzzy differential equations." In:Proceedings of annual meeting of the NAFIPS (North American Fuzzy Information Processing Society) (2012): pp 1–5 .
[29] Chalco-Cano Y, Román-Flores H,Rojas-Medar MA. "Fuzzy differential equations with generalized derivative." In:Proceedings of 27th NAFIPS international conference IEEE (n.d.).

PRAJÑĀ - **Journal of Pure and Applied Sciences Vol. 24 – 25 : 38 – 46 (2017)**
ISSN 0975 - 2595

MATHEMATICAL INVESTIGATION OF COUNTER-CURRENT IMBIBITION PHENOMENON IN HETEROGENEOUS POROUS MEDIUM

DIPAK J. PRAJAPATI[1] AND N. B. DESAI[2]*

[1]*Assistant Professor, Department of Mathematics, Government Engineering College, Modasa.-383315, Gujarat State, India. E-mail. djganit@gmail.com* . Telephone. +91-9727176963
[2]*Head , Department of Mathematics, A. D. Patel Institute of Technology, New V. V. Nagar-388121, Gujarat State, India. E-mail. drnbdesai@yahoo.co.in* . Telephone. +91-9327158932

ABSTRACT

The counter-current imbibition phenomenon in heterogeneous porous medium which arises during secondary oil recovery process in petroleum reservoirs is discussed. An optimal homotopy analysis method is applied to obtain the approximate analytical solution of the governing nonlinear partial differential equation with appropriate boundary conditions. Also the counter-current imbibition phenomenon is derived if the porous medium is homogeneous. The convergence of the approximate analytical solution is decided by using averaged squared residual of governing equation. The numerical values are obtained for the saturation of injected water and saturation profiles are plotted using Mathematica in heterogeneous as well as homogeneous porous medium.

Keywords: Counter-current imbibition, Darcy law, Conservation of mass, Squared residual.

AMS subject classification: 76T99, 76S05, 76A02, 78M50.

INTRODUCTION

Fractured reservoirs are important petroleum resources. They are composed of two continua: the fracture network and matrix. The fractures are highly permeable as compared to the matrix whose permeability may be several orders of lower magnitude. But majority of the recoverable oil is contained in the matrix network. Fracure network has very less amount of oil in it. Waterflooding is frequently implemented to increase recovery in fractured reservoirs.

The performance of waterflooding depends crucially on the wettability of the reservoir. If the reservoir is oil-wet, water will not readily displace oil in the matrix and only the oil in the fractures will be displaced, resulting in poor recoveries. In water-wet fractured reservoirs, imbibition can lead to significant recoveries. Imbibition is the mechanism of displacement of non-wetting phase by wetting phase. Strong capillary forces lead to the imbibition of water as the wetting phase into the matrix and the discharged oil is displaced into the fractures.

Imbibition can take place by co-current and/or counter-current flow. In co-current flow the water and oil flow in the same direction, and water pushes oil out of the matrix. In counter-current flow, the oil and water flow in opposite directions, and oil escapes by flowing back along the same direction along which water has imbibed. Co-current imbibition is faster and can be more efficient than counter-current imbibition but counter-current imbibition is often the only possible displacement mechanism for cases where a region of the matrix is completely surrounded by water in the fractures.

Counter-current imbibition phenomenon is discussed by many researchers. Cocurrent and countercurrent imbibition in a water-wet matrix block is discussed by Pooladi-Darvish and Firoozabadi [1]. Through a detailed study of the governing equations and boundary conditions they have provided significant insight into the mathematical and physical differences between co- and counter-current imbibition. Experimental study of co-current and counter-current flows in natural porous media is done by Bourbiaux and Kalaydjian [2]. Behbahani et al. [3] have performed the fine grid, one- and two-dimensional simulations of counter-current imbibition and have compared the results with experimental measurements in the literature. Reis and Cil [4] have developed a model for oil expulsion by counter-current water imbibition in rocks. Patel et al. [5] has obtained a homotopy series solution to a nonlinear partial differential equation arising from a mathematical model of the counter–current imbibition phenomenon in a heterogeneous porous medium. Patel and Meher [6] have discussed the counter-current imbibition phenomenon in heterogeneous porous media with gravitational and inclination effect and have calculated the saturation rate of

wetting phase by using Adomian decomposition method. Patel and Desai [7] have obtained approximate analytical solution for countercurrent imbibition phenomenon in inclined homogeneous porous medium.

In this work we have discussed one dimensional counter-current imbibition in heterogeneous porous medium and the approximate analytical expression for the solution of the governing nonlinear partial differential equation with appropriate boundary conditions is obtained by optimal homotopy analysis method. Also we derive the approximate analytical solution in the case if the porous medium is homogeneous. Fluids (water and oil) are assumed immiscible and incompressible, and the porous solid matrix is assumed to be rigid.

AIM AND SCOPE

The aim of this work is to obtain the convergent approximate analytical solution for the saturation of injected water as a function of position and time by optimal homotopy analysis method. This type of solution can help to predict the amount of water required to inject for recovering oil from the petroleum reservoir during secondary oil recovery process. Hence this type of mathematical investigation is useful for predicting oil recovery from petroleum reservoir.

PROBLEM FORMULATION

We have considered a fully oil saturated sample of rectangular porous matrix of length l with only one permeable side which is exposed to an adjacent formation of the injected fluid (i) as water as shown in Fig.1. The open side of the matrix is labeled as imbibition face.

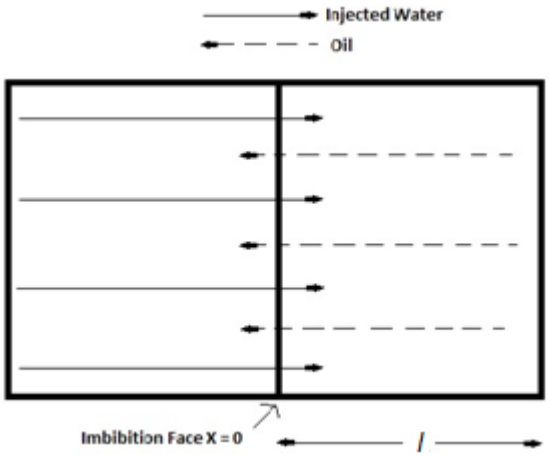

Fig.1. Schematic of 1D counter-current imbibition

This arrangement gives rise to the phenomenon of linear counter-current imbibition that is a spontaneous flow of water into the porous matrix and a counter flow of oil from the matrix.

Assuming the validity of Darcy's law, the volumetric flow rates (Darcy velocities) V_i and V_n of water and oil can be written as [19]

$$V_i = -K(x)\frac{k_i}{\mu_i}\frac{\partial p_i}{\partial x} \tag{1}$$

$$V_n = -K(x)\frac{k_n}{\mu_n}\frac{\partial p_n}{\partial x} \tag{2}$$

where $K(x)$ is the permeability of the heterogeneous medium which is nonconstant function of position, k_i and k_n are the relative permeabilities of water and oil respectively, μ_i and μ_n are the constant viscosities of water and oil respectively, p_i and p_n are the pressures of water and oil respectively.

Assuming the absence of any source and/or sink term, conservation mass equation for water volume can be written as [19,21]

$$P(x)\frac{\partial S_i}{\partial t} + \frac{\partial V_i}{\partial x} = 0 \tag{3}$$

where $P(x)$ is the porosity of the heterogeneous porous matrix which is nonconstant function of position.

In counter-current imbibition phenomenon, oil and water are flowing in

opposite direction. We assume that the sum of their velocities is zero.[26] i.e.

$$V_i + V_n = 0 \tag{4}$$

The capillary pressure p_c generally is expressed as the pressure in the nonwetting phase minus the pressure in the wetting phase, and so commonly a positive value. We define the water-oil capillary pressure as [21]

$$p_c(S_i) = p_n - p_i \tag{5}$$

Since the capillary pressure is a function of the phase saturation, we consider [27]

$$p_c = -\beta S_i \tag{6}$$

where β is a positive capillary pressure parameter.

For definiteness of the mathematical analysis, the relationship between phase saturation and relative permeability as given by Scheidegger and Johnson (1961) is used here [11].

$$k_i = S_i \tag{7}$$

According to Oroveanu [10], the porosity and permeability of the heterogeneous porous medium are:

$$P(x) = \frac{1}{a - bx} \tag{8}$$

and

$$K(x) = K_c P(x) \tag{9}$$

where $a - bx \geq 1 \quad for \quad all \quad x \in [0, l]$ and a, b and K_c are constants.

Using (1) and (2) in (4), we have

$$\frac{k_i}{\mu_i} K(x) \frac{\partial p_i}{\partial x} + \frac{k_n}{\mu_n} K(x) \frac{\partial p_n}{\partial x} = 0 \tag{10}$$

Using (5), this becomes

$$\left(\frac{k_i}{\mu_i} + \frac{k_n}{\mu_n} \right) \frac{\partial p_i}{\partial x} + \frac{k_n}{\mu_n} \frac{\partial p_c}{\partial x} = 0 \tag{11}$$

Simplyfying, we obtain

$$\frac{\partial p_i}{\partial x} = -\frac{k_n}{\mu_n} \left(\frac{k_i}{\mu_i} + \frac{k_n}{\mu_n} \right)^{-1} \frac{\partial p_c}{\partial x} \tag{12}$$

On substituting the value of $\frac{\partial p_i}{\partial x}$ in (1), we get

$$V_i = K(x) \frac{k_i}{\mu_i} \frac{k_n}{\mu_n} \left(\frac{k_i}{\mu_i} + \frac{k_n}{\mu_n} \right)^{-1} \frac{\partial p_c}{\partial x} \tag{13}$$

Using (13) in (3), we get

$$P \frac{\partial S_i}{\partial t} + \frac{\partial}{\partial x} \left[K(x) \frac{k_i}{\mu_i} \frac{k_n}{\mu_n} \left(\frac{k_i}{\mu_i} + \frac{k_n}{\mu_n} \right)^{-1} \frac{\partial p_c}{\partial x} \right] = 0 \tag{14}$$

According to Scheidegger [21], it is assumed that

$$\frac{k_i}{\mu_i} \frac{k_n}{\mu_n} \left(\frac{k_i}{\mu_i} + \frac{k_n}{\mu_n} \right)^{-1} \approx \frac{k_i}{\mu_i}$$

Hence (14) reduces to

$$P \frac{\partial S_i}{\partial t} + \frac{\partial}{\partial x} \left[K(x) \frac{k_i}{\mu_i} \frac{\partial p_c}{\partial S_i} \frac{\partial S_i}{\partial x} \right] = 0 \tag{15}$$

Using (6), (7) and (9) into (15), we get

$$P(x) \frac{\partial S_i}{\partial t} - \frac{\beta K_c}{\mu_i} \frac{\partial}{\partial x} \left[S_i P(x) \frac{\partial S_i}{\partial x} \right] = 0$$

which reduces to

$$\frac{\partial S_i}{\partial t} - \frac{\beta K_c}{\mu_i} \left[S_i \frac{\partial^2 S_i}{\partial x^2} + S_i \frac{\partial S_i}{\partial x} \frac{1}{P} \frac{\partial P}{\partial x} + \left(\frac{\partial S_i}{\partial x} \right)^2 \right] = 0 \tag{16}$$

Using dimensionless variables

$$X = \frac{x}{l}, \quad T = \frac{\beta K_c}{\mu_i l^2} t$$

(16) reduces to

$$\frac{\partial S_i}{\partial T} - S_i \frac{\partial^2 S_i}{\partial X^2} - S_i \frac{\partial S_i}{\partial X} \frac{1}{P} \frac{\partial P}{\partial X} - \left(\frac{\partial S_i}{\partial X} \right)^2 = 0 \tag{17}$$

Using binomial theorem, we can simplify $\frac{1}{P} \frac{\partial P}{\partial X}$ as follows

$$\frac{1}{P}\frac{\partial P}{\partial X} = \frac{\partial}{\partial X}\left[\ln P\right] = \frac{\partial}{\partial X}\left[\frac{blX}{a} - \ln a\right] = \frac{bl}{a}$$

Using this (17) reduces to

$$\frac{\partial S_i}{\partial T} - S_i\frac{\partial^2 S_i}{\partial X^2} - \frac{bl}{a}S_i\frac{\partial S_i}{\partial X} - \left(\frac{\partial S_i}{\partial X}\right)^2 = 0 \tag{18}$$

Eq. (18) is nonlinear partial differential equation governing the counter-current imbibition in heterogeneous porous medium. The solution of this equation represents the saturation of injected water.

Let at the imbibition face, the saturation of injected water be linear function of time, that is

$$S_i(0,T) = \alpha T \quad for \quad T > 0 \tag{19}$$

where α is constant.

Since, it is assumed that the porous matrix is completely surrounded by an impermeable surface except for one end, we consider

$$\frac{\partial S_i}{\partial X}(1,T) = 0 \quad for \quad T > 0 \tag{20}$$

We solve equation (18) together with boundary conditions (19) and (20) using optimal homotopy analysis method [12-18,22-25].

SOLUTION OF THE PROBLEM USING OPTIMAL HOMOTOPY ANALYSIS METHOD

We choose

$$S_{i_0}(X,T) = \alpha T\left[e^{-X} + Xe^{-1}\right] \tag{21}$$

as the initial approximation of $S_i(X,T)$ which satisfies boundary conditions (19) and (20). We select the linear operator as

$$\mathrm{L}[\phi(X,T;q)] = \frac{\partial^2\phi(X,T;q)}{\partial X^2} \tag{22}$$

with the property

$$\mathrm{L}[f] = 0 \quad when \quad f = 0. \tag{23}$$

where $q \in [0,1]$ is the embedding parameter. Furthermore, based on governing equation (18), a nonlinear operator is defined as

$$\begin{aligned}\mathrm{N}[\phi(X,T;q)] = {} & \frac{\partial\phi(X,T;q)}{\partial T} \\ & - \phi(X,T;q)\frac{\partial^2\phi(X,T;q)}{\partial X^2} \\ & - \frac{bl}{a}\phi(X,T;q)\frac{\partial\phi(X,T;q)}{\partial X} \\ & - \left\{\frac{\partial\phi(X,T;q)}{\partial X}\right\}^2\end{aligned} \tag{24}$$

Let c_0 denote a nonzero auxiliary parameter. The zeroth order deformation equation is [25]

$$\begin{aligned}&(1-q)\mathrm{L}[\phi(X,T;q) - S_{i_0}(X,T)] \\ &= c_0 qH(X,T)\mathrm{N}[\phi(X,T;q)]\end{aligned} \tag{25}$$

In (25), $H(X,T)$ is nonzero auxiliary function and $\phi(X,T;q)$ is an unknown function.

Obviously, when $q = 0$ and $q = 1$, we have from (23) and (25),

$$\phi(X,T;0) = S_{i_0}(X,T) \tag{26}$$

and $$\phi(X,T;1) = S_i(X,T) \tag{27}$$

Therefore, the solution $\phi(X,T;q)$ varies from the initial approximation $S_{i_0}(X,T)$ to the exact solution $S_i(X,T)$ of (18) as q increases from 0 to 1.

Obviously, $\phi(X,T;q)$ is determined by the auxiliary linear operator L, the initial guess $S_{i_0}(X,T)$ and the auxiliary parameter c_0. They can be selected with great freedom..

Assuming that all of them are so properly selected such that the Maclaurin series

$$\phi(X,T;q) = S_{i_0}(X,T) + \sum_{m=1}^{\infty} S_{i_m}(X,T)q^m \tag{28}$$

exists and besides converges at $q = 1$, we have the homotopy-series solution

$$S_i(X,T) = S_{i_0}(X,T) + \sum_{m=1}^{\infty} S_{i_m}(X,T) \tag{29}$$

where $S_{i_m}(X,T) = \frac{1}{m!}\frac{\partial^m \phi(X,T;q)}{\partial q^m}|_{q=0}$ (30)

Differentiating the zeroth order deformation equations (25) m times with respect to the embedding parameter q and then dividing them by $m!$ and finally setting $q=0$ i.e. in case of no embedding, we have the so called high order deformation equations

$$\begin{aligned} &\mathrm{L}[S_{i_m}(X,T) - \chi_m S_{i_{m-1}}(X,T)] \\ &\quad = c_0 H(X,T) R_m(X,T) \end{aligned} \quad (31)$$

subject to the boundary conditions

$$S_{i_m}(0,T) = 0, \quad \frac{\partial S_{i_m}}{\partial X}(1,T) = 0, \quad m \geq 1 \quad (32)$$

where

$$\begin{aligned} R_m(X,T) &= \frac{1}{(m-1)!}\frac{\partial^{m-1} \mathrm{N}[\phi(X,T;q)]}{\partial q^{m-1}}|_{q=0} \\ &= \frac{\partial S_{i_{m-1}}}{\partial T} - \frac{bl}{a}\sum_{k=0}^{m-1} S_{i_k}\frac{\partial S_{i_{m-1-k}}}{\partial X} \\ &\quad - \sum_{k=0}^{m-1} S_{i_k}\frac{\partial^2 S_{i_{m-1-k}}}{\partial X^2} - \sum_{k=0}^{m-1}\frac{\partial S_{i_k}}{\partial X}\frac{\partial S_{i_{m-1-k}}}{\partial X} \end{aligned}$$

and $\chi_m = \begin{cases} 0 & \text{if } m \leq 1, \\ 1 & \text{if } m > 1. \end{cases}$

For the sake of simplicity, we take $H(X,T) = 1$.

The equations (31) are second order nonhomogeneous ordinary linear differential equations with constant cofficients for all $m \geq 1$ and can be solved by symbolic computation software such as Mathematica. Thus we have converted the original nonlinear problem (18)-(19)-(20) into an infinite sequence of linear subproblems (31)-(32). Hence the approximate analytical solution to the governing nonlinear problem takes the form:

$$\begin{aligned} S_i(X,T) &= \alpha T\left[e^{-X} + Xe^{-1}\right] \\ &+ c_0[\alpha e^{-X} + \frac{\alpha e^{-1}}{6}X^3 - \frac{bl\alpha^2 e^{-2}}{6a}T^2X^3 \\ &+ \left(\frac{bl}{a} - 2\right)\frac{\alpha^2}{4}T^2 e^{-2X} + \frac{bl\alpha^2 e^{-1}}{a}T^2 e^{-X} \\ &+ \left(\frac{bl}{a} - 1\right)\alpha^2 e^{-1}T^2 Xe^{-X} + \frac{\alpha e^{-1}}{2}X \\ &+ \frac{2bl\alpha^2 e^{-2}}{a}T^2 X - \frac{\alpha^2 e^{-2}}{2}T^2 X^2 \\ &- \left(\frac{bl}{a} - 2\right)\frac{\alpha^2}{4}T^2 - \alpha - 2\left(\frac{bl}{a} - 1\right)\alpha^2 e^{-1}T^2 \\ &+ \left(\frac{bl}{a} - 2\right)\alpha^2 e^{-1}T^2] + \Lambda \end{aligned} \quad (33)$$

The optimal value of c_0 can be obtained by minimizing averaged squared residual E_m.

As given by Liao [23,24], the averaged squared residual at the m th order of approximation is

$$\begin{aligned} E_m &= \frac{1}{(M+1)(N+1)}\sum_{i=0}^{M}\sum_{j=0}^{N}\left\{\mathrm{N}\left[\sum_{n=0}^{m} S_{i_n}\left(\frac{i}{M},\frac{j}{N}\right)\right]\right\}^2 \end{aligned} \quad (34)$$

Since the squared residual E_m is a function of c_0, we can find the optimal value of c_0 from

$$\frac{dE_m(c_0)}{dc_0} = 0 \quad (35)$$

This optimization method for obtaining the optimal value of c_0 has been applied recently to a number of problems for nonlinear ordinary and partial differential equations by many researchers [12-18,22-24].

The optimal value of c_0 is found by the minimum of E_{15} using Mathematica. We find that E_{15} attains its minimum value

1.4341×10^{-6} at $c_0 = -0.09$ which we can notice in Fig.2 which shows the curve of averaged squared residual E_{15} versus c_0.

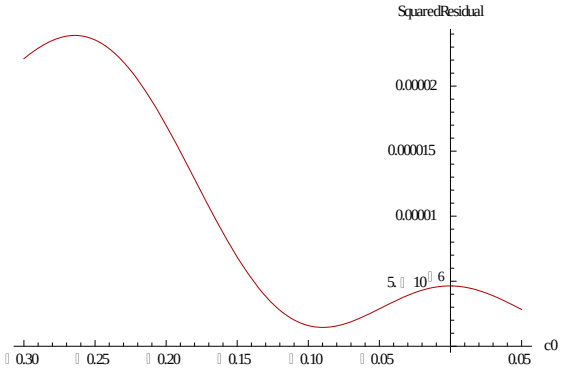

Fig.2. Averaged Squared Residual at fifteenth order of approximation versus convergence-control parameter

RESULTS AND DISCUSSION

The BVPh, a Mathematica package, is used to obtain numerical representation. Table 1 indicates the numerical values of saturation of injected water for different distance X and time T upto 15th order approximation using $c_0 = -0.09$. We have considered the unit length l of porous matrix, $a = 2$ and $b = 1$. Fig.3 represents the graph of $S_i(X,T)$ versus time T for fixed values of distance $X == 0.1,0.2,\Lambda\ ,1$ .The lowermost graph corresponds to $X == 0.1$ and the uppermost corresponds to $X == 1$. Numerical values of Table 1 are used for Fig.3.

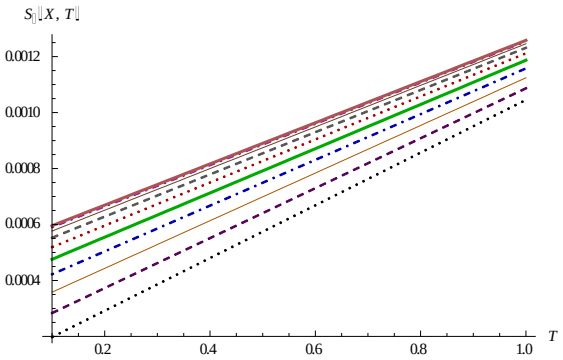

Fig 3. Saturation of injected water versus time for fixed values of distance

Derivation of Counter-current imbibition in homogeneous porous medium

If the porous medium is homogeneous, then its porosity is constant. Taking $b = 0$ in (8), the porosity P = constant and (18) reduces to

$$\frac{\partial S_i}{\partial T} - S_i \frac{\partial^2 S_i}{\partial X^2} - \left(\frac{\partial S_i}{\partial X}\right)^2 = 0 \qquad (36)$$

which is the governing equation for counter-current imbibition phenomenon in homogeneous porous medium. The solution of (36) can be obtained from (33) by taking $b = 0$ which is as follows.

$$\begin{aligned} S_i(X,T) &= \alpha T\left[e^{-X} + Xe^{-1}\right] \\ &+ c_0[\alpha e^{-X} + \frac{\alpha e^{-1}}{6}X^3 - \frac{\alpha^2}{2}T^2 e^{-2X} \\ &- \alpha^2 e^{-1}T^2 Xe^{-X} + \frac{\alpha e^{-1}}{2}X - \frac{\alpha^2 e^{-2}}{2}T^2X^2 \\ &+ \frac{\alpha^2}{2}T^2 - \alpha] + \Lambda \end{aligned} \qquad (37)$$

This represents the approximate analytical expression for the saturation of injected water in homogeneous porous medium. The value of c_0 is obtained by minimizing averaged squared residual.

Fig.4 shows the curve of averaged squared residual E_{15} versus c_0 for homogeneous porous medium. The optimal value of c_0 is -0.21 corresponding to the minimum value 1.11576×10^{-6} of E_{15}.

The numerical values of saturation of water in the case of homogeneous porous medium are obtained upto 15^{th} order approximation using using $c_0 = -0.21$ which are as shown in Table 2. Fig.5 shows the saturation profile of injected water versus time for fixed values of distance $X == 0.1,0.2,\Lambda\ ,1$ upto 15^{th} order approximation. The lowermost graph corresponds to $X == 0.1$ and the uppermost corresponds to $X == 1$.

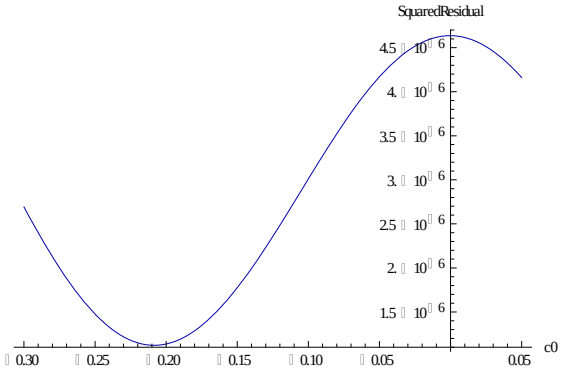

Fig.4. Averaged Squared Residual at fifteenth order of approximation versus convergence-control parameter for homogeneous porous medium

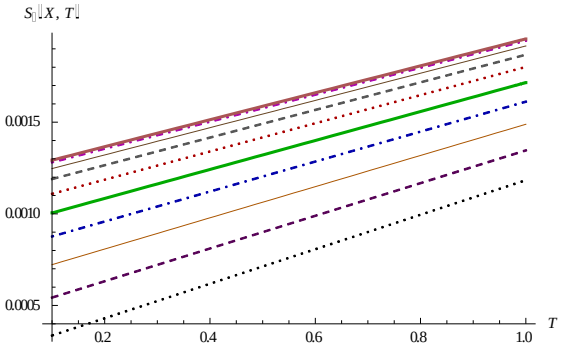

Fig.5. Saturation of injected water versus time for fixed values of distance in homogeneous porous medium

CONCLUSION

One-dimensional counter-current imbibition has been investigated, in which a non-wetting phase (oil) is displaced by a wetting phase (water). The optimal homotopy analysis method has been used to develop an approximate analytical expressions for the saturation of wetting phase (water) in heterogeneous and homogeneous porous medium.

At fixed location, the saturation of water increases as time increases which indicates that the oil will be displaced from the reservoir.

It has been found that the saturation of water increases fast in homogeneous porous medium as compared to the heterogeneous porous medium. So the oil recovery from homogeneous porous medium is fast than the oil recovery from heterogeneous medium.

REFERENCES

[1] Pooladi-Darvish, M. and Firoozabadi, A. Cocurrent and countercurrent imbibition in a water-wet matrix block, SPE Journal, 5 (2000).

[2] Bourbiaux, B.J., Kalaydjian, F.J. Experimental study of cocurrent and countercurrent flows in natural porous media, SPE Reserv. Eng., 5 (1990), 361-368.

[3] Behbahani, H.S., Donato G.D. and Blunt, M.J. Simulation of counter-current imbibition in water-wet fractured reservoirs, Journal of Petroleum Science and Engineering, 50 (2006), 21-39.

[4] Reis, J.C. and Cil, M. A model for oil expulsion by counter-current water imbibition in rocks: One dimensional geometry, Journal of Petroleum Science and Engineering, 16 (1996), 61-69.

[5] Patel, K. K.;Mehta, M. N.; Singh, T. R. A homotopy series solution to a nonlinear partial differential equation arising from a mathematical model of the counter–current imbibition phenomenon in a heterogeneous porous medium, European Journal of Mechanics-B/Fluids, 60(2016), 119-126.

[6] Patel, H. S.; Meher, R. Approximate analytical study of Counter-current imbibition phenomenon in a heterogeneous porous media, Applied Mathematical Sciences, 10(14) (2016), 673-681.

[7] Patel, M. A.; Desai, N. B. Homotopy analysis solution of countercurrent imbibition phenomenon in inclined homogeneous porous medium, Global Journal of Pure and Applied Mathematics, 12(1) (2016), 1035-1052.

[8] Brownscmobe, E.R. and Dyes, A.B. Water-imbibition displacement-a possibility for the Spraberry, Drilling and Production Practice of API, 16 (1952), 383-390.

[9] Verma, A. P. Statistical behaviour of fingering in a displacement process in heterogeneous porous medium with capillary pressure, Canadian Journal of Physics, 47(3) (1969), 319-324.

[10] Oroveanu, T. Scurgerea Fluiidelor Prin Medii Poroase Neomogene, Editura Academiei Republicii Populare Romine, 92 (1963).

[11] Scheidegger, A. E.; Johnson, E. F. The statistically behaviour of instabilities in displacement process in porous media, Canadian Journal of Physics, 39(2) (1961), 326-334.

[12] Liao, S. J. An optimal homotopy analysis approach for strongly nonlinear differential equations, Commun. Nonlinear Sci. Numer. Simul., 15 (2010), 2003-2016.

[13] Baxter, M.; Robert, A.; Gorder, V.; Vajravelu, K. On the choice of auxiliary linear operator in the optimal homotopy

analysis of the Cahn-Hilliard initial value problem, Numer Algor, 66(2) (2014), 269-298.

[14] Prajapati, D. J.; Desai, N. B. The solution of immiscible fluid flow by means of optimal homotopy analysis method, International Journal of Computer and Mathematical Sciences, 4(8) (2015).

[15] Prajapati, D. J.; Desai, N. B. Application of the basic optimal homotopy analysis method to fingering phenomenon, Global Journal of Pure and Applied Mathematics, 12(3) (2016), 2011-2022.

[16] Prajapati, D. J.; Desai, N. B. Optimal homotopy analysis solution of fingero-imbibition phenomenon in homogeneous porous medium with magnetic fluid effect, Kalpa Publications in Computing, 2(2017), 85-94.

[17] Prajapati, D. J.; Desai, N. B. Approximate analytical solution for the fingero-imbibition phenomenon by optimal homotopy analysis method, International Journal of Computational and Applied Mathematics, 12(3)(2017), 751-761.

[18] Prajapati, D. J.; Desai, N. B. Analytic analysis for oil Recovery during cocurrent imbibition in inclined homogeneous porous medium, International Journal on Recent and Innovation Trends in Computing and Communication, 5(7)(2017), 189-194.

[19] Bear, J. Dynamics of fluids in porous media, American Elsevier Publishing Company, Inc., New York, 1972.

[20] Muskat, M. The flow of homogeneous fluids through porous media, First edition, McGraw-Hill Book Company, Inc., New York and London, 1937.

[21] Scheidegger, A. E. The Physics of flow through porous media, revised edition, University of Toronto Press, Toronto, 1960.

[22] Vajravelu, K.; Van Gorder, R. A. Nonlinear flow phenomena and homotopy analysis: Fluid flow and Heat transfer, Higher Education Press, Beijing and Springer-Verlag Berlin Heidelberg, 2012.

[23] Liao, S. J. Homotopy analysis method in nonlinear differential equations, Higher Education Press, Beijing and Springer-Verlag Berlin Heidelberg, 2012.

[24] Liao, S. J. Advances in the homotopy analysis method, World Scientific, (2013)

[25] Liao, S. J. Beyond perturbation: Introduction to the homotopy analysis method, Chapman and Hall/CRC Press, Boca Raton, 2003.

[26] Chen, Z. Reservoir simulation: Mathematical techniques in oil recovery, SIAM, Philadelphia,2007.

[27] Mehta, M. N. Asymptotic expansions of fluid flow through porous media, Ph.D. Thesis, South Gujarat University, Surat, India, 1977.

TABLES

Table 1: Numerical values of saturation of injected water in heterogeneous porous medium

X	T=0.1	T =0.2	T =0.3	T =0.4	T =0.5	T=0.6	T =0.7	T =0.8	T =0.9	T=1
0.1	1.97715E-4	2.91878E-4	3.8604E-4	4.80202E-4	5.74363E-4	6.68524E-4	7.62685E-4	8.56845E-4	9.51004E-4	1.04516E-3
0.2	2.83615E-4	3.72846E-4	4.62076E-4	5.51305E-4	6.40533E-4	7.29761E-4	8.18987E-4	9.08213E-4	9.97438E-4	1.08666E-3
0.3	3.58281E-4	4.43399E-4	5.28516E-4	6.13632E-4	6.98746E-4	7.8386E-4	8.68972E-4	9.54082E-4	1.03919E-3	1.1243E-3
0.4	4.22189E-4	5.03936E-4	5.85682E-4	6.67426E-4	7.49168E-4	8.30909E-4	9.12648E-4	9.94385E-4	1.07612E-3	1.15786E-3
0.5	4.75726E-4	5.54773E-4	6.33817E-4	7.12861E-4	7.91902E-4	8.70941E-4	9.49978E-4	1.02901E-3	1.10805E-3	1.18708E-3
0.6	5.19192E-4	5.96145E-4	6.73097E-4	7.50046E-4	8.26993E-4	9.03938E-4	9.80881E-4	1.05782E-3	1.13476E-3	1.2117E-3
0.7	5.52812E-4	6.28221E-4	7.03629E-4	7.79034E-4	8.54436E-4	9.29837E-4	1.00523E-3	1.08063E-3	1.15602E-3	1.23141E-3
0.8	5.76743E-4	6.51105E-4	7.25466E-4	7.99824E-4	8.74179E-4	9.48532E-4	1.02288E-3	1.09723E-3	1.17157E-3	1.24592E-3
0.9	5.91078E-4	6.64844E-4	7.38607E-4	8.12368E-4	8.86126E-4	9.59881E-4	1.03363E-3	1.10738E-3	1.18113E-3	1.25488E-3
1	5.95857E-4	6.69433E-4	7.43006E-4	8.16576E-4	8.90143E-4	9.63708E-4	1.03727E-3	1.11083E-3	1.18439E-3	1.25794E-3

Table 2: Numerical values of saturation of injected water in homogeneous porous medium

X	T=0.1	T =0.2	T =0.3	T =0.4	T =0.5	T=0.6	T =0.7	T =0.8	T =0.9	T=1
0.1	3.35851E-3	4.30026E-4	5.24198E-4	6.18367E-4	7.12531E-4	8.06693E-4	9.0085E-4	9.95004E-4	1.08915E-3	1.1833E-3
0.2	5.42933E-4	6.32184E-4	7.21428E-4	8.10666E-4	8.99898E-4	9.89123E-4	1.07834E-3	1.16755E-3	1.25676E-3	1.34596E-3
0.3	7.2271E-4	8.07851E-4	8.92984E-4	9.78108E-4	1.06322E-3	1.14833E-3	1.23343E-3	1.31852E-4	1.40360E-3	1.48867E-3
0.4	8.76395E-4	9.58166E-4	1.03993E-3	1.12168E-3	1.20342E-3	1.28515E-3	1.36686E-3	1.44857E-3	1.53027E-3	1.16116
0.5	1.00498E-3	1.08405E-3	1.16311E-3	1.24215E-3	1.32119E-3	1.40021E-3	1.47922E-3	1.55822E-3	1.63721E-3	1.71618E-3
0.6	1.10924E-3	1.18622E-3	1.26318E-3	1.34013E-3	1.41707E-3	1.49399E-3	1.5709E-3	1.6478E-3	1.72469E-3	1.80156E-3
0.7	1.18979E-3	1.26522E-3	1.34064E-3	1.41604E-3	1.49143E-3	1.56681E-3	1.64217E-3	1.71752E-3	1.79285E-3	1.86817E-3
0.8	1.24706E-3	1.32144E-4	1.39581E-3	1.47016E-3	1.5445E-3	1.61883E-3	1.69314E-3	1.76744E-3	1.84172E-3	1.91599E-3
0.9	1.28132E-3	1.35511E-3	1.42888E-3	1.50263E-3	1.57637E-3	1.6501E-3	1.72381E-3	1.79751E-3	1.87119E-3	1.94486E-3
1	1.29273E-3	1.36633E-3	1.43991E-3	1.51347E-3	1.58702E-3	1.66056E-3	1.73408E-3	1.80758E-3	1.88108E-3	1.95455E-3

PRAJÑĀ - **Journal of Pure and Applied Sciences Vol. 24 – 25 : 47 – 54 (2017)**
ISSN 0975 - 2595

EFFECT OF EXOTIC PREDATOR ON A NATIVE PREY-PREDATOR SYSTEM WITH SPECIAL REFERENCE TO KUNO WILDLIFE SANCTUARY IN INDIA: A MODEL

O.P.MISRA[1], PRAMOD KUSHWAH[2] AND CHHATRAPAL SINGH SIKARWAR[1]

[1,2] School of Mathematics and Allied Sciences, Jiwaji University, Gwalior (M.P.) – 474011, INDIA
[3] Govt. M.J.S.P.G. College, Bhind (M.P.) – 477001, INDIA Email: pramod.kushwah.mjs@gmail.com

ABSTRACT

In this paper, a mathematical model is proposed to study the effect of exotic lion population on prey-predator system consisting of native herbivore population and native leopard population with special reference to Kuno Wildlife Sanctuary in India. The model includes three state variables viz; density of herbivore population, density of leopard population and density of exotic lion population. Stability analysis of all the feasible equilibrium points of the models is carried out. We concluded that interior equilibrium point becomes more stable if inter specific interference coefficient due to exotic lion species as well as constant recruitment rate of lion population decreased. It is also pointed out that the recruitment rate of Asiatic lion plays as a critical role in the dynamical behaviour of the system. Finally numerical simulation is carried out to support the analytical results of the models.

KEYWORDS:- Native species; Exotic species; Equilibia; Biological invasion; Stability

INTRODUCTION

The dynamic relationship between predators and their prey has long been and will continue to be one of the dominant themes in both ecology and mathematical ecology due to its universal existence and importance [1-7]. Many authors have studied effect of exotic predator on native prey species using mathematical models [8-10]. The interesting study of realistic mathematical models in theoretical ecology is a very good reflection of their use in helping to understand the dynamic process involved and in making practical prediction.

It has been noticed in the Gir National Park located in Gujrat in India that the population of lions and have attained an equilibrium level and the expansion limits have been reached. There are large scale deaths in the lion population annually because of overcrowding increasing and intraspecific competition. Asiatic lion prides require large territories but there is limited space at Gir wildlife sanctuary, which is boxed in on all sides by heavy human habitation.

Kuno Wildlife Sanctuary or Palpur-Kuno Wildlife Sanctuary (between latitudes of 25°30'-25°53'N & longitude of 77°07'-77°26'E) lies in the Sheopur district of north western Madhya Pradesh, a state in central India [11]. An area of 344.686 square kilometers was set aside as a Wildlife Sanctuary in 1981. This park is home to many species of wild animals including wolves, monkeys, leopards, nilgai and possibly a few remaining Bengal Tigers.

Government of India planned to shift the Asiatic lion from Gir National Park to other places. The Kuno Wildlife Sanctuary was selected as the reintroduction site for the endangered Asiatic lion because it is the former range of the lions before it was hunted into extinction in about 1873. Currently the Asiatic lion reintroduction project is underway. The lions are to be reintroduced from Gir Wildlife Sanctuary in the neighboring Indian state of Gujarat where they are currently overpopulated. The reintroduction project of Asiatic lion to other wildlife sanctuary such as Kuno National Park, requires quantitative investigation to predict the future scenario of the Kuno National Park with respect to survival or extinction of both native and exotic populations.

In view of this the main purpose of this paper is to construct a model to study the effect of exotic species (Asiatic lion) on the growth dynamics of native prey (herbivore) and native predator leopard species.

BASIC ASSUMPTIONS AND MATHEMATICAL MODEL

Let $x(t)$ denotes the density of herbivore population, $y(t)$ denotes the density of leopard population and $z(t)$ denotes the density of exotic lion (Asiatic) population. It is assumed that at present the Asiatic lion is exotic to the habitat

(Kuno National Park). It is also assumed that the herbivore population has a logistic growth rate, linear interaction with leopard population on account of exotic lion interference and type of interaction considered in the model with exotic lion population is taken from [12-13]. It is a well-known fact that a lion does not kill the prey if it is not hungry. It will primarily kill feed, therefore, the predation term in the equation describing lion dynamics will depend on the prey and predator densities, as well as Type II functional response. We assume that r and k are the growth rate and the carrying capacity of herbivore population respectively. d_1 is death rate of leopard population. d_2 is the death rate of exotic lion population. m is the constant recruitment rate of Asiatic lion (exotic) under the reintroduction project. a is the predation rate of herbivore population by lion population. b is the predation rate of herbivore population by leopard population. e_1 and e_2 are conversion efficiencies of native leopard species and exotic lion species. f is the decay rate of leopard species due to predation by lion species. c is the interspecific interference coefficient due to exotic lion species. h is the intraspecific interference coefficient due to exotic lion species, which is determined by the population size of the exotic lion. In view of the above, the resultant system dynamics is governed by the following system of differential equations:

Model 1 (With exotic species)

$$\frac{dx}{dt} = rx\left(1-\frac{x}{k}\right) - axz - \frac{bxy}{1+cz}, \qquad (2.1)$$

$$\frac{dy}{dt} = \frac{be_1xy}{1+cz} - d_1y - fyz, \qquad (2.2)$$

$$\frac{dz}{dt} = m + \frac{ae_2xz}{1+hz} - d_2z, \qquad (2.3)$$

with initial condition as $x(0) \geq 0, y(0) \geq 0$ and $z(0) \geq 0$.

Where $r, k, a, b, c, f, h, m, d_1, d_2, e_1, e_2$ are positive constants.

In the absence of exotic lion species the above system (2.1)-(2.3) is governed by the following system of differential equations:

Model 2 (Without exotic species)

$$\frac{dx}{dt} = rx\left(1-\frac{x}{k}\right) - bxy, \qquad (2.4)$$

$$\frac{dy}{dt} = be_1xy - d_1y, \qquad (2.5)$$

with non-negative initial condition as $x(0) \geq 0$ and $y(0) \geq 0$.

EQUILLIBRIA OF THE MODELS 1 AND 2

In this section, we analyze the system of equations (2.4)-(2.5) under the initial conditions. We find all the possible feasible equillibria of the system of equations (2.4)-(2.5). The system has three feasible equillibria, namely

(i) Trivial equilibrium point $E_T \equiv (0,0)$.

(ii) Axial equilibrium point $E_A \equiv (k, 0)$.

(iii) Interior Equilibrium point $E_P \equiv \left(x^{\#}, y^{\#}\right)$.

Where,

$$x^{\#} = \frac{d_1}{be_1}, y^{\#} = \frac{r(be_1k - d_1)}{b^2e_1k}.$$

Equilibrium point E_P exists if $be_1k > d_1$.

We now analyze the system of equations (2.1)-(2.3) under the initial conditions. We find all the possible feasible equillibria of the system of equations (2.1)-(2.3). The system has two feasible equillibria, namely

(i) Boundary equilibrium point $E_{B_e} \equiv (\tilde{x}, 0, \tilde{z})$.

Where,

$$\tilde{x} = \frac{(1+h\tilde{z})(d_2\tilde{z} - m)}{ae_2\tilde{z}},$$

$$\tilde{z} = \frac{r(\beta_1 + mh) + \sqrt{r^2(\beta_1 + mh)^2 + 4mr\beta_2}}{2\beta_2},$$

$$\beta_1 = ae_2k - d_2, \beta_2 = a^2e_2k + hrd_2.$$

Equilibrium point E_{B_e} exist if $d_2\tilde{z} > m$ i.e. $m < m_1^*$.

Where,

$$m_1^* = \frac{rd_2}{a}$$

(ii) Interior Equilibrium point $E_{P_e} \equiv (x^*, y^*, z^*)$.

Where,

$$z^* = \frac{\beta_3x^* - \beta_4}{\beta_5 + \beta_6x^*} = g(x^*),$$

$$y^* = \frac{[r\beta_7 - \beta_8g(x^*) - \beta_9g^2(x^*)]\left(1 + cg(x^*)\right)}{b^2e_1k},$$

$$\beta_3 = bhd_2e_1, \beta_4 = hd_1d_2 + cfm,$$

$$\beta_5 = chd_1d_2 + cfhm + f(h-c)d_2$$

$$\beta_6 = acfe_2, \beta_7 = be_1k - d_1,$$

$$\beta_8 = fr + cd_1r + abe_1k, \beta_9 = cfr$$

x^* is the root of the equation

$$G_1x^{*3} + G_2x^{*2} + G_3x^* + G_4 = 0.$$

Where,

$G_1 = be_1\beta_6^2,$

$G_2 = 2be_1\beta_5\beta_6 - d_1\beta_6^2 - \beta_3\beta_6\beta_{10} - cf\beta_3^2,$

$G_3 = be_1\beta_5^2 - 2d_1\beta_5\beta_6 - \beta_3\beta_5\beta_{10} + \beta_4\beta_6\beta_{10} + 2cf\beta_3\beta_4,$

$G_4 = \beta_4\beta_5\beta_{10} - cf\beta_4^2 - d_1\beta_5^2, \beta_{10} = f + cd_1.$

Hence unique root x^* is positive if $G_2 > 0$ and $G_4 < 0$.

Therefore equilibrium point $E_{P_e} \equiv (x^*, y^*, z^*)$ exists if

$\beta_3 x^* > \beta_4, h > c, r\beta_7 > \beta_8 g(x^*) + \beta_9 g^2(x^*),$

$2be_1\beta_5\beta_6 > d_1\beta_6^2 + \beta_3\beta_6\beta_{10} + cf\beta_3^2,$

$cf\beta_4^2 + d_1\beta_5^2 > \beta_4\beta_5\beta_{10}.$

BOUNDEDNESS OF THE SOLUTIONS OF THE MODELS 1 AND 2

Lemma 4.1 All the solutions of system of equations (2.4)-(2.5) with the positive initial condition are uniformly bounded within the region $\boldsymbol{\Omega_1}$.

Where,

$$\boldsymbol{\Omega_1} = \left\{(x,y) : 0 \le x \le k, 0 \le e_1 x + y \le \frac{2e_1 kr}{\theta}, \theta = min(r, d_1)\right\}$$

for any $\theta > 0$ is a region of attraction.

Lemma 4.2 All the solutions of system (2.1)-(2.3) with the positive initial condition are uniformly bounded within the region $\boldsymbol{\Omega_2}$.

Where,

$$\boldsymbol{\Omega_2} = \left\{(x,y,z) : 0 \le x \le k, 0 \le e_1 x + y \le \frac{2e_1 kr}{\theta}, 0 \le z \le \frac{m}{d_2 - ake_2}, \theta = min(r, d_1), d_2 > ake_2\right\}$$

for any $\theta > 0$ is a region of attraction.

DYNAMICAL BEHAVIOUR OF THE MODELS 1 AND 2

In the previous section, we observed that the system of equations (2.4)-(2.5) have three feasible equilibria E_T, E_A and E_P. We will now study the dynamical behaviour of the system about all the three feasible equilibria.

(i) The variational matrix for the system of equations (2.4)-(2.5) evaluated at E_T is

$$J_{E_T} \equiv J(0,0) = \begin{bmatrix} r & 0 \\ 0 & -d_1 \end{bmatrix}.$$

The eigen values of the characteristic equation of J_{E_T} are $\lambda_1 = r$ and $\lambda_2 = -d_1$. It is seen from these eigen values that equilibrium point E_T is unstable.

(ii) The variational matrix for the system of equations (2.4)-(2.5) evaluated at E_A is

$$J_{E_A} \equiv J(k,0) = \begin{bmatrix} -r & -bk \\ 0 & bke_1 - d_1 \end{bmatrix}.$$

The eigen values of the characteristic equation of J_{E_A} are $\lambda_1 = -r$ and $\lambda_2 = bke_1 - d_1$. It is seen from these eigen values that equilibrium point E_A is stable provided $bke_1 < d_1$.

Remark 5.1 :- It may be observed from the stability condition of E_A that herbivore species will survive and leopard species will tend to extinction if the product of predation rate of leopard population due to predation of herbivore population by leopard population, conversion efficiency of leopard species and carrying capacity of herbivore population is less than death rate of leopard species.

(iii) The variational matrix for the system of equations (2.4)-(2.5) evaluated at E_P is

$$J_{E_P} \equiv J(x^\#, y^\#) = \begin{bmatrix} \frac{-rx^\#}{k} & -bx^\# \\ be_1 y^\# & 0 \end{bmatrix}.$$

The characteristic equation for variational matrix J_{E_P} is given by

$$\lambda^2 + B_1\lambda + B_2 = 0. \qquad (5.1)$$

Where,

$$B_1 = \frac{rx^\#}{k}, B_2 = b^2 e_1 x^\# y^\#.$$

Since $B_1 > 0$ and $B_2 > 0$. Therefore using Routh-Hurwitz criteria all the roots of equation (5.1) are negative or have negative real parts. Hence equilibrium point E_P is locally asymptotically stable.

Remark 5.2:- It may be observed from the stability condition of E_P that herbivore species and leopard species will survive if the product of predation rate of leopard population due to predation of herbivore population by leopard population, conversion efficiency of leopard species and carrying capacity of herbivore population is greater than death rate of leopard species. We also concluded that if equilibrium point E_P exists then equilibrium point E_A is unstable.

In the previous section, we observed that the system of equations (2.1)-(2.3) have two feasible

equilibria E_{B_e} and E_{P_e} . We will now study the dynamical behaviour of the system about all the three feasible equilibria.

(i) The variational matrix for the system of equations (2.1)-(2.3) evaluated at E_{B_e} is

$$J_{E_{B_e}} \equiv J(\tilde{x}, 0, \tilde{z})$$

$$= \begin{bmatrix} \frac{-r\tilde{x}}{k} & \frac{-b\tilde{x}}{1+c\tilde{z}} & -a\tilde{x} \\ 0 & \frac{be_1\tilde{x}}{1+c\tilde{z}} - d_1 - f\tilde{z} & 0 \\ \frac{ae_2\tilde{z}}{1+h\tilde{z}} & 0 & -\frac{m}{\tilde{z}} - \frac{ahe_2\tilde{x}\tilde{z}}{(1+h\tilde{z})^2} \end{bmatrix}.$$

The one eigen value of characteristic equation of $J_{E_{B_e}}$ is

$$\lambda_1 = \frac{be_1\tilde{x}}{1+c\tilde{z}} - d_1 - f\tilde{z}\,.$$

The rest eigen values of characteristic equation of $J_{E_{B_e}}$ will obtain from following equation

$$\lambda^2 + C_1\lambda + C_2 = 0. \qquad (5.2)$$

Where,

$$C_1 = \frac{r\tilde{x}}{k} + \frac{m}{\tilde{z}} + \frac{ahe_2\tilde{x}\tilde{z}}{(1+h\tilde{z})^2},$$

$$C_2 = \frac{r\tilde{x}}{k}\left(\frac{m}{\tilde{z}} + \frac{ahe_2\tilde{x}\tilde{z}}{(1+h\tilde{z})^2}\right) + \frac{a^2e_2\tilde{x}\tilde{z}}{1+h\tilde{z}}.$$

Since $C_1 > 0$ and $C_2 > 0$. Therefore using Routh-Hurwitz criteria all the roots of equation (5.2) are negative or have negative real parts. Hence equilibrium point E_{B_e} is locally asymptotically stable provided

$$d_1 + f\tilde{z} > \frac{be_1\tilde{x}}{1+c\tilde{z}}\,.$$

Again on simple calculation, we observed that E_{B_e} is locally asymptotically stable provided $m_2^* < m$.

Where,

$$m_2^* = \frac{-H_2 + \sqrt{H_2^2 - 4H_1H_3}}{2H_1},$$

$$H_1 = \beta_9 r^2(h\beta_8 - \beta_9 + rh^2\beta_7),$$

$$H_2 = r\beta_8(\beta_2\beta_8 + r\beta_1\beta_9) + r^2\beta_7(h\beta_2\beta_8 + 2\beta_2\beta_9 + 2hr\beta_1\beta_9),$$

$$H_3 = r\beta_7(r\beta_1\beta_2\beta_8 + r^2\beta_1^2\beta_9 - r\beta_2^2\beta_7).$$

Remark 5.3:- It may be observed from the stability condition of E_{B_e} that herbivore species and exotic lion species will survive and leopard species will tend to extinction if constant recruitment rate of exotic lion population exists between two critical values m_1^* and m_2^*.

(ii) The variational matrix for the system of equations (2.1)-(2.3) evaluated at E_{P_e} is

$$J_{E_{P_e}} \equiv J(x^*, y^*, z^*)$$

$$= \begin{bmatrix} \frac{-rx^*}{k} & \frac{-bx^*}{1+cz^*} & -ax^* + \frac{bcx^*y^*}{(1+cz^*)^2} \\ \frac{be_1y^*}{1+cz^*} & 0 & -fy^* - \frac{bce_1x^*y^*}{(1+cz^*)^2} \\ \frac{ae_2z^*}{1+hz^*} & 0 & -\frac{m}{z^*} - \frac{ahe_2x^*z^*}{(1+hz^*)^2} \end{bmatrix}.$$

The characteristic equation for variational matrix $J_{E_{P_e}}$ is given by

$$\lambda^3 + A_1\lambda^2 + A_2\lambda + A_3 = 0. \qquad (5.3)$$

Where,

$$A_1 = \frac{rx^*}{k} + \frac{m}{z^*} + \frac{ahe_2x^*z^*}{(1+hz^*)^2},$$

$$A_2 = \frac{rx^*}{k}\left(\frac{m}{z^*} + \frac{ahe_2x^*z^*}{(1+hz^*)^2}\right) + \frac{a^2e_2x^*z^*}{1+hz^*} + \frac{bx^*y^*}{(1+cz^*)^2}\left(be_1 - \frac{ace_2z^*}{1+hz^*}\right),$$

$$A_3 = y^*\left(\frac{b^2e_1mx^*}{z^*(1+cz^*)^2} - \frac{afe_2z^*}{1+hz^*}\right) + \frac{abe_1e_2x^*y^*z^*}{(1+hz^*)(1+cz^*)^2}\left(\frac{bhx^*}{(1+hz^*)} - c\right).$$

Again on simple calculation, we observed that $A_1 > 0, A_2 > 0, A_3 > 0$ and $A_1A_2 - A_3 > 0$ if (i) $be_1 > ae_2$ (ii) $bm > ae_2z^*$ (iii) $hd_1 > ce_1$ (iv) $h > c$ are being satisfied.

Using the Routh-Hurwitz criteria, we derive that the equilibrium point E_{P_e} is locally asymptotically stable, if (i) $be_1 > ae_2$ (ii) $bm > ae_2z^*$ (iii) $hd_1 > ce_1$ (iv) $h > c$ are being satisfied.

Remark 5.4:- It may be observed from the stability condition of E_{P_e} that all the three species that is herbivore species, leopard species and exotic lion species would coexist if (i) ratio of predation rates of leopard to lion is greater than the ratio of conversion efficiencies of lion to leopard, (ii) product of constant recruitment rate of exotic lion population and predation rate of herbivore population by leopard population is greater than product of predation rate of herbivore population by exotic lion population, conversion efficiency and equilibrium level of exotic lion population, (iii) ratio of intra specific interference coefficient within exotic lion species to inter specific interference coefficient due to

exotic lion species is greater than ratio of conversion efficiency of leopard population to death rate of leopard population, and (iv) the intra specific interference coefficient within exotic lion species is greater than the inter specific interference coefficient due to exotic lion species.

NUMERICAL EXAMPLE

In this section, we present a simulation analysis to explain the applicability of results in model 1 and model 2. Now we choose the following values of parameters in model 2

$r = 1.5; k = 100; ; b = 0.15; e_1 = 0.1; d_1 = 0.5$. Using above set of parameters, the stability region Ω_1 and interior equilibrium point E_P is given by

$$\Omega_1 = \{(x, y) \in R_+^2 : 0 \le x \le 100, 0 \le y \le 60\}.$$

$E_P \equiv (x^{\#}, y^{\#}) = (33.3803,\ 6.6658)$. The Fig. 6.1(a) illustrates the system stability behaviour of the interior equilibrium point of the model 2. Fig. 6.1(b) shows phase plane graph between herbivore species and leopard species in the model 2.

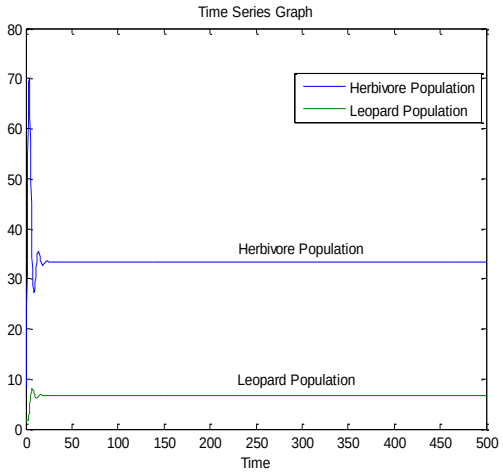

Fig. 6.1(a): Time series graph of the asymptotically stable interior equilibrium point $E_P(33.3803,\ 6.6658)$ of the model 2 with initial value $(8, 2)$.

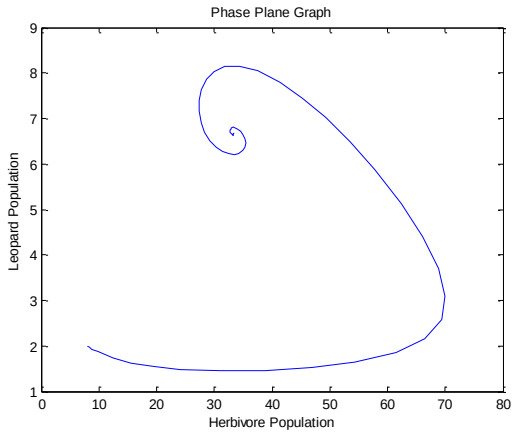

Fig. 6.1(b): Phase plane graph of the asymptotically stable interior equilibrium point $E_P(33.3803,\ 6.6658)$ of the model 2 with initial value $(8, 2)$.

Now we choose the following values of parameters in model 1

$$r = 1.5; k = 100; a = 0.2; b = 0.15; e_1 = 0.1; e_2 = 0.008; f = 0.05; d_1 = 0.2;\ d_2 = 0.2; c = 0.01; m = 0.5; h = 0.1. \quad (7.1)$$

Using above set of parameters given in (7.1), the stability region Ω_2 and interior equilibrium point E_{P_e} is given by

$$\Omega_2 = \{(x, y, z) \in R_+^3 : 0 \le x \le 100, 0 \le y \le 150, 0 \le z \le 12.5\}.$$

$E_{P_e} \equiv (x^*, y^*, z^*) = (23.7817,\ 3.8227,\ 2.9313)$. The Fig. 6.2(a) illustrates the system stability behaviour of the interior equilibrium point of the model 1. Fig. 6.2(b) shows phase plane graph between herbivore species, leopard species and exotic lion species in the model 1.

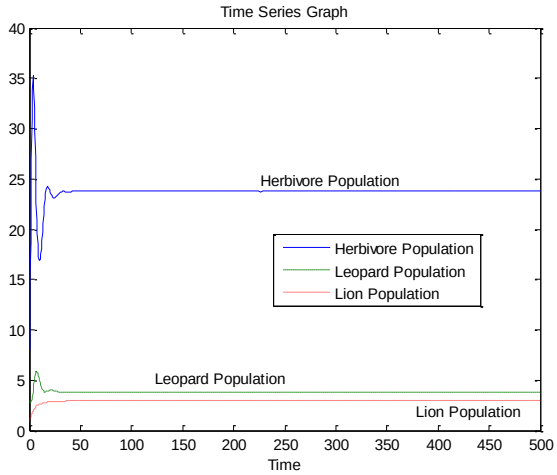

Fig. 6.2(a): Time series graph of the asymptotically stable interior equilibrium

point$E_{P_e}(23.7817,\ 3.8227,\ 2.9313)$ of the model 1 with initial value $(8, 3, 1)$.

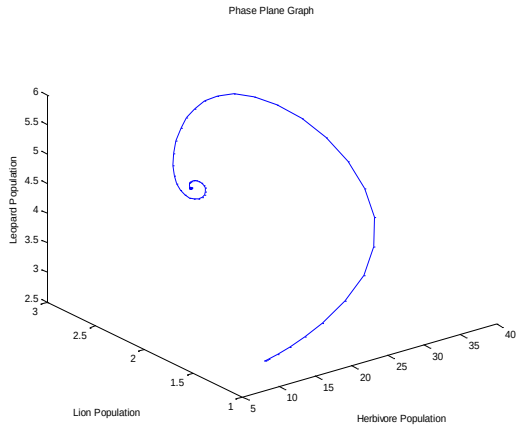

Fig. 6.2(b): Phase plane graph of the asymptotically stable interior equilibrium point $E_{P_e}(23.7817,\ 3.8227,\ 2.9313)$ of the model 1 with initial value $(8, 3, 1)$.

Now we explain the effect of changing of constant recruitment rate on account of Asiatic lion (exotic) on the model 1. Using distinct values of m as well as remaining parameters are same as given in table 6.1 of model 1, then behaviour of stable equilibrium points are given in following table 6.1.

Table 6.1: Behaviour of equilibrium point for distinct values of m.

m	**Behaviour of equilibrium point**
$0 < m < m_2^* = 0.888$	E_{B_e} is unstable E_{P_e} is stable
$m_2^* = 0.888 \leq m < m_1^* = 1.5$	E_{B_e} is stable E_{P_e} is unstable
$m \geq m_1^* = 1.5$	E_{B_e} is unstable E_{P_e} is unstable

(i) From Fig. 6.3, it may be noted that herbivore population and exotic lion species will survives and leopard population become extinct for $m = 1$

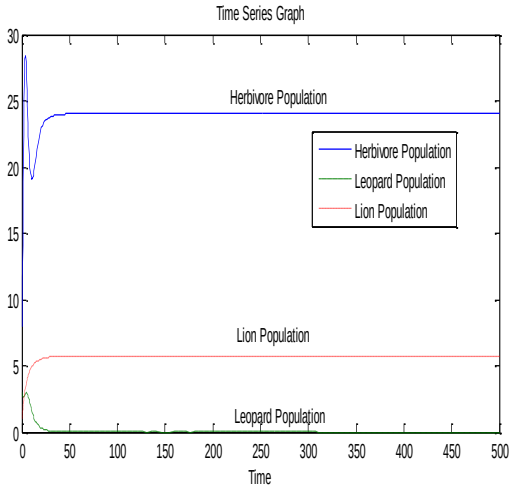

Fig. 6.3: Time series graph of the asymptotically stable boundary equilibrium point $E_{B_e}(24.0312,\ 0,\ 5.6987)$ of the model 1 with initial value $(8, 3, 1)$.

The Fig. 6.4(a), Fig. 6.4(b), and Fig. 6.4(c), illustrate the stable equilibrium level of herbivore population, Leopard population and Asiatic lion (Exotic species) population respectively for distinct values of m.

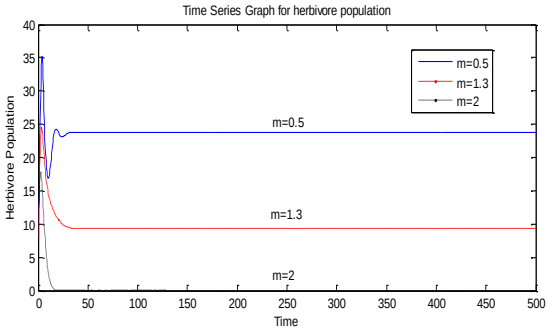

Fig. 6.4(a) Stable equilibrium level of herbivore population of the model 1 for distinct values of m.

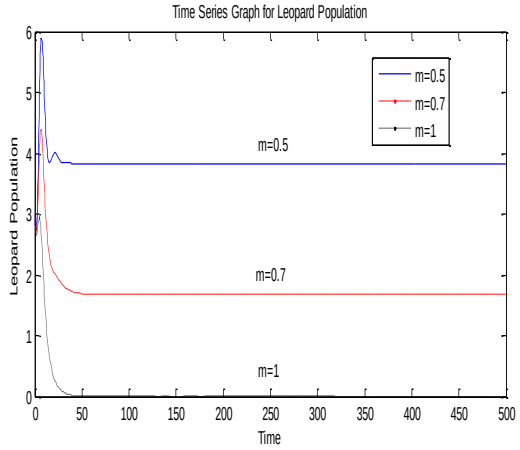

Fig. 6.4(b) Stable equilibrium level of leopard population of the model 1 for distinct values of m.

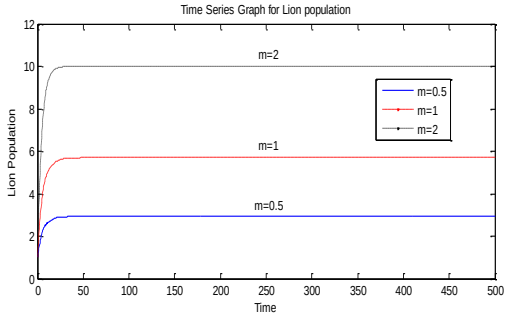

Fig. 6.4(c) Stable equilibrium level of lion population of the model 1 for distinct values of m.

CONCLUSION

In this paper, we have proposed a mathematical model to study the effect of Asiatic lion population on prey-predator system consisting native herbivore population and leopard population. From the stability of boundary equilibrium point E_{Be} [See Fig. 6.3], it is observed that the leopard population will not survive and consequently herbivore population will survive and exotic lion population will also survive. It may be observed from the stability conditions of interior equilibrium E_{P_e} that all the three species that is herbivore species, leopard species and exotic lion species would coexist if (i) ratio of predation rates of leopard to lion is greater than the ratio of conversion efficiencies of lion to leopard, (ii) product of constant recruitment rate of exotic lion population and predation rate of herbivore population by leopard population is greater than product of predation rate of herbivore population by exotic lion population, conversion efficiency and equilibrium level of exotic lion population, (iii) ratio of intra specific interference coefficient within exotic lion species to inter specific interference coefficient due to exotic lion species is greater than ratio of conversion efficiency of leopard population to death rate of leopard population, and (iv) the intra specific interference coefficient within exotic lion species is greater than the inter specific interference coefficient due to exotic lion species. From the global stability analysis of equilibrium point E_{P_e} we derived that E_{P_e} is more stable if interspecific interference coefficient due to exotic lion species as well as constant recruitment rate of lion population decreased. We observed that the positive interior equilibrium point E_{P_e} is stable for $0 < m < m_2^*$ (See Fig. 6.2(a), 6.2(b)). Boundary equilibrium point E_{P_e} is stable for $m_2^* \leq m < m_1^*$ (see Fig. 6.3). The switching in stability behaviour based on constant recruitment rate of lion population □ is also observed (See Fig. 6.2(a), 6.2(b), 6.3). Finally we conclude that if constant recruitment rate of exotic lion population is greater than some critical value m_1^* then it is harmful to native prey-predator system. The constant recruitment rate of lion population creates complex phenomena in the system.

REFERENCE

[1] Sinha, S., Misra, O.P. and Dhar, J. (2010) : Modelling a predator–prey system with infected prey in polluted environment. Applied Mathematical Modelling, 34 : 1861–1872.

[2] Bairagi, N. and Jana, D. (2011) : On the stability and Hopf bifurcation of a delay-induced predator–prey system with habitat complexity. Applied Mathematical Modelling, 35: 3255–3267.

[3] Misra, O.P., Sinha, P. and Singh, C. (2013) : Stability and bifurcation analysis of a prey–predator model with age based predation. Applied Mathematical Modelling, 37 : 6519–6529.

[4] Terry, A. J. (2013) : Prey resurgence from mortality events in predator–prey models. Nonlinear Analysis: Real World Applications, 14 : 2180–2203.

[5] Ddumba, H., Mugisha, J.Y.T., Gonsalves, J.W. and Kerley, G.I.H. (2013) : Periodicity and limit cycle perturbation analysis of a predator–prey model with interspecific species' interference, predator additional food and dispersal. Applied Mathematics and Computation, 219 : 8338–8357.

[6] Nandi, S. K., Mondal, P. K., Jana, S., Haldar, P. and Kar, T.K., (2015) : Prey-Predator Model with Two-Stage Infection in Prey: Concerning Pest

Control. Journal of Nonlinear Dynamics, doi.org/10.1155/2015/948728
[7] Diop, O., Moussaoui, A. and Sene, A., (2016) : Positive periodic solution of an augmented predator-prey model with seasonal harvest of prey and migration of predator. Journal of Applied Mathematics and Computing, 52 : 417-437.
[8] Zhang, J., Fan, M. and Kuang, Y. (2006) : Rabbits killing birds revisited. Mathematical Biosciences, 207 : 100–127.
[9] Fan, M., Kuang, Y. and Feng, Z. (2005) : Cats protecting birds revisited. Bulletin of mathematical biology, 67 : 1081-1106.
[10] Fay, T. H. and Greeff, J. C., (2006) : Lion, wildebeest and zebra: A predator–prey model. Ecological Modeling, 196 : 277-288.
[11] Website: https://en.wikipedia.org/wiki/ Kuno_Wildlife_Sanctuary
[12] Fay, T. H., Greeff, J. C., Eisenbergc, B. E. and Groeneveld, H. T. (2006) : Testing the model for one predator and two mutualistic prey species. Ecological Modeling, 196 : 288-255.
[13] Zhang, Z. (2008) : Qualitative Analysis for a Prey-Mesopredator - Superpredator Model. Applied Mathematical Sciences, 02 : 2067 – 2080.

PRAJÑĀ - **Journal of Pure and Applied Sciences Vol. 24 – 25 : 55 – 58 (2017)**
ISSN 0975 - 2595

TRANSPORT PROPERTY MEASUREMENTS IN WSe_{2-X} CRYSTALS

K. R. CHAUDHARI[1], RAVI JOSHI[2], AJAY M. AGARWAL[*1] AND G. K. SOLANKI[3]

[1]Department of Electronics / Physics, Shree Jayendrapuri Arts & Science College,Bharuch-392 001, Gujarat, India.
[2]Department of Electronics, M. B. Patel Science College, Anand -388 001, Gujarat, India.
[3]Department of Physics, Sardar Patel University, Vallabh Vidyanagr -388 120, Gujarat, India.
Email: kc.ele11@gmail.com

ABSTRACT

Electrical resistivity and Hall effect measurements have been carried out on crystals of WSe_{2-x} grown by Direct Vapour Transport technique. The effect of changing the selenium content on the electrical properties of the grown crystals has been thoroughly investigated and its implications have been discussed.

Keywords: WSe_{2-x}, Hall effect, Activation Energy.

INTRODUCTION

The dichalcogenides of tungsten (WSe_2) possess C7 type crystal structure. In this structure each W atom is in 6- fold co-ordination with the chalcogen (Se) atoms lying in a hexagonally packed plane.

The atoms in sandwich layers are bonded partly by ionic and partly by covalent bonding and the interlayer interaction is due to the van der Waal's bonding. Because of this strong anisotropy in the bonding, the layered transition metal dichalcogenides show marked anisotropy in their physical properties.

The effective use of solar energy in photovoltaic or photoelectrochemical applications depends in part on the development of materials that can show high conversion efficiency and longterm stability under operation. In addition, the desirable material should have a band gap that closely matches the solar spectrum and be made of readily available and inexpensive materials. Single crystals of transition metal dichalcogenides have band gaps (1.1 – 1.6 eV) that closely match the solar spectrum and exhibit high conversion efficiencies. In addition, they can achieve long term stability due to the fact that the transitions are localized in the non-bonding d-orbitals of the metal. Among TMDC's WSe_2 occupies a favorable position with suitable band gap of 1.57 eV and is one of the most promising material in PEC solar cell applications [1]. Since changing the content of Se in WSe_2 single crystals alter its electrical properties, which in turn has an effect on its photoelectrochemical behavior, it was thought worthwhile to carry out electrical resistivity and Hall effect measurements on single crystals of WSe_{2-x} grown by direct vapour transport method.

In order to see the effect of defects such as stacking faults etc., it is desirable to measure the resistance in the direction normal to the basal plane, hence resistance measurements normal to the basal plane were carried out on WSe_{2-x} single crystals in the temperature range 298K to 853K.

EXPERIMENTAL

The single crystals of WSe_{2-x} used in the present investigations were grown by direct vapour transport technique [2]. The room temperature electrical resistivity, Hall mobility, Hall coefficient and carrier concentration were determined using the standard method of Van der Pauw.

The electrical resistivity measurements in the temperature range 77-300K were carried out using the conventional four probe technique with the help of a low temperature resistivity set up (Figure1) manufactured by Scientific Solutions Bombay. The system is designed to fit directly into any of the standard liquid nitrogen containers. The system is supplied with a standard ½ inch valve for evacuating and a ¼ inch valve for introducing the exchange gas, monitoring vacuum etc.

[*1]*Corresponding Author: draagl@yahoo.com*

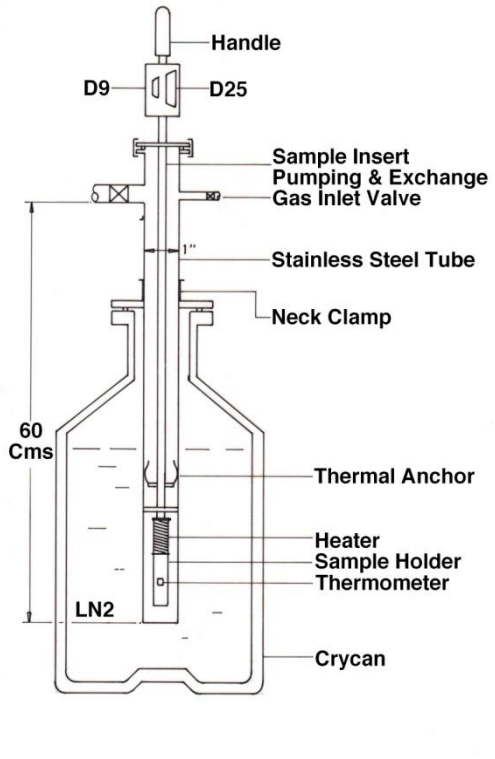

Fig.1. Experimental Set – up for Low – Temperature Resistivity Measurements.

Four copper wires were attached with the conducting silver paste on each specimen. Samples whose ohmic contacts were checked before measurements were fixed on a sample holder. The sample holder consists of a gold-plated copper assembly mounted with a standard platinum thermometer and a heater in close thermal contact with the sample holder. The temperature was varied with the use of a heater.

The experimental set up for the measurement of resistance normal to the basal plane was fabricated in University Science and Instrumentation Centre (USIC).

The experimental set up is shown in figure 2. The crystal was mounted on the sample holder , which was then inserted into the sample chamber , and then closed from the top. The temperature of the sample could be raised by introducing the sample chamber assembly into a furnace. The temperature of the sample was measured with the help of a Cr-Al thermocouple kept in the vicinity of the sample. Starting from room temperature, the temperature of the sample was increased slowly in steps of 10^{o} C till the final temperature was reached, and at each step the corresponding value of the resistance of the sample was noted. To avoid excessive heating of the sample chamber, it was cooled by circulating water around it with the help of tubing wound around it.

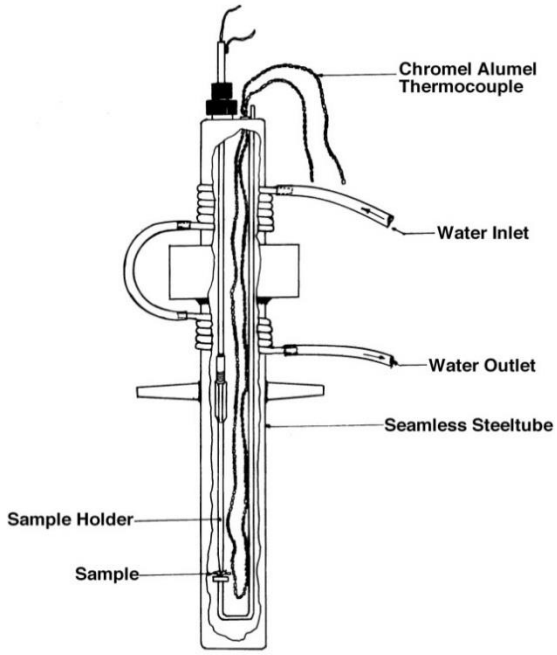

Fig.2. Cross – section of the Two Probe set – up for Resistivity Measurements parallel to c – axis.

RESULTS AND DISCUSSION

The Hall effect measurements on the grown crystals are reported in Table 1. The Hall coefficient R_H and the carrier concentration 'n' have been calculated, assuming the single carrier conduction model and using the relation,

$$\mu_H = \frac{R_H}{\rho} \quad \text{and} \quad n = \frac{-1}{eR_H}$$

where 'e' is the electronic charge. The Hall coefficient has a positive value.

A study of Table 1 reveals the following facts: The room temperature resistivity decreases with the decrease in selenium content. All the crystals are essentially p-type. The Hall coefficient decreases with the decrease in selenium content.

Crystal	ρ (Ωcm)	R_H (cm^3/ C)	μ_H (cm^2/ V.sec)	n (cm^{-3}) x10^{17}	Ea (eV)
WSe_2	0.81	146	178	0.43	0.06
$WSe_{1.98}$	0.59	143	242	0.44	0.06
$WSe_{1.97}$	0.40	133	345	0.47	0.05
$WSe_{1.93}$	0.35	125	357	0.50	0.04
$WSe_{1.90}$	0.32	100	312	0.62	0.04

The Hall mobility increases as the selenium content is decreased. The carrier concentration of all the crystals is more or less of the same order, but still there is a definite increase in the value of carrier concentration with the increase in the value of x.

Table 1 : Data of WSe_{2-x} Crystals

The plots of log ρ vs 1/T are shown in Fig.3 for all the off-stoichiometric crystals used in this study. All the plots exhibit a classical semiconducting nature. The values of the activation energies calculated from the above plots show a decreasing trend with the decrease in selenium content.

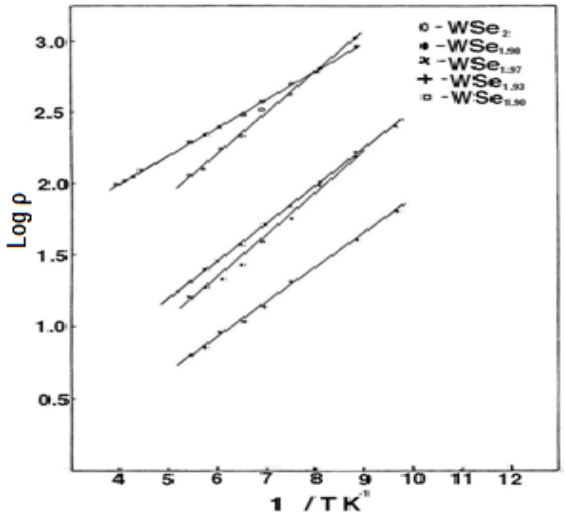

Fig.3 Low Temperature (77K – 303K) electrical resistivity plots (log ρ vs 1/T) for all p-type off – stoichiometric WSe_{2-x} single crystals

The p-type nature of the WSe_{2-x} crystals can be explained by considering a proper electronic sharing between $5d^46s^2$ electrons from tungsten and $4s^24p^4$ electrons from selenium. From the chemistry of these two elements we know that there exist two valence states (+4 and +6) for tungsten and three valence states (+2, +4 and +6) for selenium.

In WSe_{2-x} crystals, two selenium atoms are effectively associated with one tungsten atom. Therefore it is possible for the eight electrons from the incomplete p sub shells of selenium to go for a covalent bonding with the six $5d^46s^2$ electrons. This would ultimately give rise to vacancies for two more electrons to perform the complete covalent bonding. This vacancy would obviously be at the heavy metallic sites provided by tungsten atom. These vacancies will provide a positive hole like character to the material thus making them behave like p-type semiconductors.

An EDAX analysis of the specimens of WSe_{2-x} carried out [3] clearly points out that crystals of WSe_{2-x} grown by direct vapour transport method grow with hybridized valence states due to the presence of higher valence states of selenium.

Since the higher valence states in selenium are formed by the electronic transition from p-level to d-level in the N-shell, the generation of holes will take place a little bit deeper in the valence band and will affect the semiconducting properties of the materials.

Now a change in stoichiometry in WSe_{2-x} gives rise to a "local strain field" which pumps the selenium into higher valence states. Accordingly, the development of higher valence states will be related to the composition of $WSe_{2-x.}$ The greater the value of x in WSe_{2-x} more will be the off-stoichiometry and greater will be the number of positive charge carriers leading to a reduction in resistivity as experimentally observed. This increase in the number of charge carriers is confirmed from the Hall effect measurements.

The systematic decrease in the value of activation energy of the samples with the decreasing selenium content in the low temperature resistivity measurements can only be

explained in terms of off-stoichiometry introduced in the samples with the change in the selenium content. Since all these crystals are grown by direct vapour transport method there is no transporting agent to account for this change in activation energy.

As a representative example of WSe_{2-x} the resistance of WSe_2 and $WSe_{1.97}$ parallel to c-axis was measured as a function of temperature. Figures 4 and 5 show the plot of resistance versus temperature.

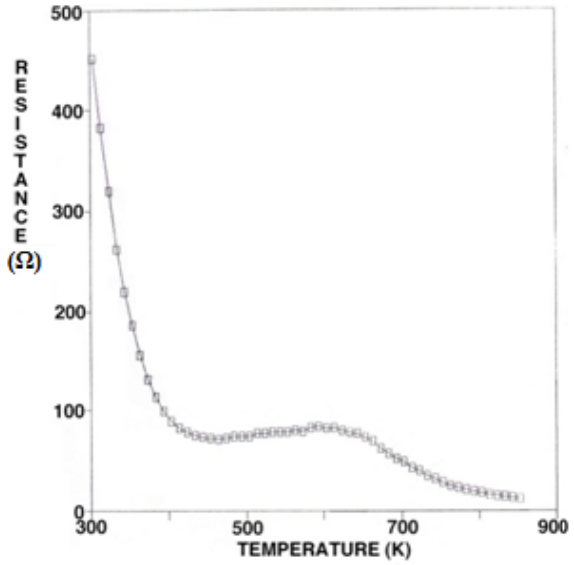

Fig.4. Plot of resistance versus temperature for WSe_2.

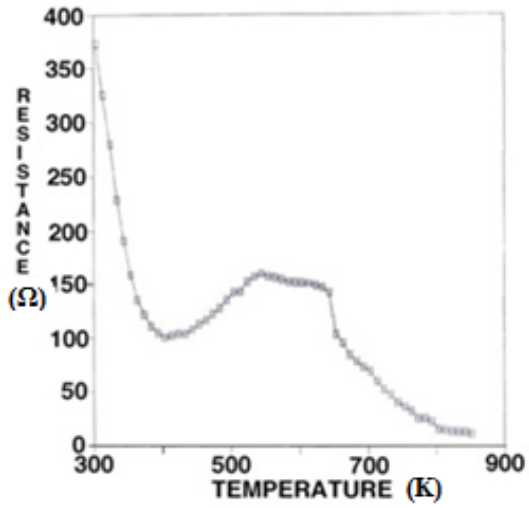

Fig.5. Plot of resistance versus temperature for $WSe_{1.97}$.

A comparison of the values of resistance at room temperature with the similar values along the basal plane clearly brings out the anisotropic character of our specimen. The anisotropic ratio for WSe_2 and $WSe_{1.97}$ is found to be 9.95 and 9.38 respectively.

A close inspection of the curves brings out the following facts:

In the case of WSe_2 the resistance goes on decreasing with an increase in temperature as is seen in the case of any normal semiconductor.

However in case of $WSe_{1.97}$ the resistance at first decreases up to the temperature of 403 K, thereafter there is an increase in resistance from 403K to 543 K. Once again the resistance remains constant from 583 K to 643 K and thereafter decreases in the same manner as seen for WSe_2. The apparent change in behavior of the two samples has to do with the stoichiometry of the two samples. More experiments are needed for understanding the exact mechanism involved in the process of conduction along the c-axis.

ACKNOWLEDGEMENTS

The alumnus of SPU Dr Ajay M Agarwal and Shri K R Chaudhari are heartily grateful to Dr N M Patel (Principal) Shree J P Arts & Science College, Bharuch-392001, Gujarat, India for his motivation towards the sanction of Research Project funded by University Grants Commission, Pune. Also, Dr. R.M. Joshi is thankful to Management, M.B. Patel Science College, Anand. In addition, the Authors are thankful to Prof. U.H. Patel for providing us the necessary Research Facilities.

REFERENCES

[1] M.P. Deshpande, S.K.Gupta, Ajay Agarwal, M.K.Agarwal (2001) Transport and optical property measurements in indium intercalated molybdenum diselenide single crystals grown by DVT technique. Synth.Metals **123**, 73

[2] M.K.Agarwal, J.D.Kshatriya, P.D.Patel, P.K.Garg (1982) Growth condition and crystal structure parameters of layer compounds in the series WSe_{2-x}. J.Cryst.Growth **60** , 9**.**

[3] Pankaj R Patel,H S Patel, J R Rathod,K D Patel & V M Pathak (2013) Growth, Structural and Electrical Characterization of Tungsten Diselenide Crystals Grown by DVT Technique. Amer. J. Cond. Matt. Phys. **3,** 13.

PRAJÑĀ - **Journal of Pure and Applied Sciences Vol. 24 – 25 : 59 – 77 (2017)**
ISSN 0975 - 2595

EFFICIENT COUPLING OF A LASER DIODE TO A QUADRIC INTERFACE MICROLENS TIPPED CIRCULAR CORE PHOTONIC CRYSTAL FIBER WITH OPTIMIZATION OF STRUCTURE PARAMETER USING ABCD MATRIX FORMALISM

SUMANTA MUKHOPADHYAY
St. Paul's Cathedral Mission College, Department of Physics, 33/1 Raja Rammohan Roy Sarani, Kolkata-700009, West Bengal, India. E-mail: sumukherjee_74@yahoo.com

ABSTRACT

We theoretically investigate the coupling optics involving a laser diode emitting two wavelengths either 1.3 μm or 1.5 μm and a series of circular core photonic crystal fibers with different air filling ratio and hole-pitch via quadric interface microlens of six different focal lengths on the tip of such fibers. Instead of considering special ABCD matrix for individual microlens like hyperbolic, parabolic and elliptical (hemispherical included) one, a simple and accurate unified transfer ABCD matrix for refraction of quadric microlens under paraxial approximation is utilized to analyze the theoretical coupling efficiency, based on Gaussian beam approximation. Further, it is observed that, for a fit structure parameter of quadric interfaced microlens, photonic crystal fiber with air filling ratio of 0.35 and hole-pitch of 5.0 μm comes out to be the most suitable one to couple laser diode for both wavelengths of practical interest, specially that of light emitting wavelength $\lambda = 1.5\mu m$. ***Moreover, the coupling efficiency can reach to nearly 100 % with simultaneous optimization of structure parameter and focal length of specific lensed fiber. The analysis should find use in ongoing investigations for optimum launch optics for the design of quadric interface microlens on the tip of photonic crystal fiber.***

Keywords: ABCD matrix, Quadric interface-lensed fiber, Structure parameter, Circular core photonic crystal fiber.

INTRODUCTION

Photonic crystal fiber (PCF), also known as microstructured optical fiber, has proved to be one of the most promising member for present-day fiber optic communication system and thereby becoming a subject of growing interest in Research and Development (R&D) for scientists, technologists and researchers. PCF is actually a unique type of pure silica optical fiber [1-3] with an array of air holes running along the total length of the fiber, reminiscent of a crystal lattice, which gives to this type of fiber, its name. The core is created by omitting the central air hole of the structure (Figure 1). Depending upon the light-guiding mechanism, PCFs can be categorized into two main classes. The first one, air-guided hollow core PCF in which light is guided by the photonic band-gap (PBG) effect, a mechanism that does not require a higher refractive index in the core to confine and guide light. The PBG guidance effect relies on coherent backscattering of light into the core. If the frequency of the light is in the bandgap of two-dimensional photonic crystal formed by the periodic cladding, light is guided by the PBG effect. A PBG fiber has air holes in the core region surrounded by a solid silica cladding with microscopic air holes running along its total length. Different kinds of band gap PCFs such as low loss air core, all solid have been also designed which find important applications that include CO_2 laser beam transmission, gas sensing, etc.[4].

On the other hand, the second one, index-guided solid core PCF for which the lower effective refractive index of the surrounding holes creates the cladding and the light is confined to the central solid core as in conventional optical fibers (COFs) and guided by modified total internal reflection (MTIR) mechanism. The index-guiding fiber, has a solid core region surrounded by a solid silica cladding, with regularly distributed air holes in a periodic arrangement, whose effective refractive index depends on the ratio of air to glass, also known as the air-fill ratio that comprises the structure. Due to the holes in the cladding region, the effective refractive index of the cladding region is reduced, which will provide the refractive index variation necessary to support total internal reflection at core cladding interface. Therefore, the light is confined to the

solid silica core, which has a relatively higher index than the effective cladding refractive index [4, 5]. Due to high design flexibility of PCFs compared to COFs, important optical properties can be tailored in PCFs [4, 5]. For index guiding solid core PCFs, these properties include endlessly single modeness, large mode area, high numerical aperture, high birefringence, high nonlinear coefficient and tailorable large dispersion [4]. Moreover, PCFs can transport light with very low loss in certain wavelength where COFs possess very large loss [5].

In some applications, preserving the state of polarization in fiber is important, particularly, this is essential in coherent optical communications and some specific fiber-optic sensors. The polarization state of the optical field can be maintained by introducing modal birefringence. Contrary to small achievable birefringence in COFs, high birefringence can be easily achieved in PCFs due to the large index contrast between core and cladding. The key technique is to destroy the symmetry of the structures of core and cladding. The structural symmetry of the core and cladding can be destroyed either by changing the shape or the size of the air holes near the core region or by changing both [4, 5]. Though the band gap PCF promises very large birefringence ($\sim 5.45\times10^{-2}$) at 1.55 μm [4], the birefringence of the index guided PCF yields also a very large value ($\sim 2.22 \times 10^{-2}$) [5] at same wavelength of light**.** Both types of fibers could be useful in designing fiber optic sensors which rely on fiber birefringence. The high value of birefringence will be useful in maintaining the polarization of electric fields, thus, making these fibers attractive in the fabrication of different fiber optic sensors such as temperature, humidity, pressure, strain, acoustic wave etc. These fibers may be also useful in the fabrication of polarization controllers [4, 5]. Moreover, band gap PCFs may be also useful in optical communications [4]. Bhattacharya and Konar have proposed a new type of index-guided PCF with triangular lattice of air holes which can be utilized for spectroscopy, biomedical application and supercontinuum generation [6]. Sharma et al. [7] have investigated a PCF which provides a moderate dispersion and large optical nonlinearity simultaneously, thereby their proposed PCF can act as a very efficient nonlinear medium for supercontinuum generation. The interest in supercontinuum generation is driven by several important applications such as optical metrology, optical coherence tomography, spectroscopy, wavelength division multiplexing and frequency comb generation [7]. Thus, in view of a wide range of optoelectronic applications of PCF in different sectors, the study of this special kind of optical fiber is of immense importance [8].

Now, one of the most recent and exciting developments in the field of photonics has been undoubtedly the fabrication of microlenses on the tip of optical fiber as far as coupling of a semiconductor laser diode (LD) to single mode fiber (SMF) is concerned. Actually, a wide range of photonic integrated semiconductor devices needs highly efficient, low-loss coupling which requires a gradual spot size transformation of the laser mode for the better compatibility of the wavefront and spot size of the laser beam to those of the guided mode in the fiber. Thus, optical packaging of semiconductor LD needs high coupling efficiencies and large misalignment tolerances from the viewpoint of its application based orientation for making the devices more rugged, more reliable and easier to handle. Moreover, the advantage of miniature and alignment free optical design between the microlens and the fiber, demands the fabrication of microlens on the tip of the fiber. The advantage of the design of more-compact optical components and modules also makes the design and fabrication of fiber microlens extremely attractive. Benefit of fiber sensing and optical recording also demands the use of fiber microlenses [9]. These microlenses, whether conical or hemispherical, possess the advantage of being self-centred. Such microlenses may have hyperbolic, hemispherical, parabolic, elliptic surfaces to modulate the spot size of LD light incident on them and transmit it into the SMF [10-22].

Now, it may be relevant to mention in this connection that the coupling optics involving hyperbolic microlens on the tip of the circular core step index single mode fiber (CCSISMF) [14, 15] as well as on the tip of circular core graded index single mode fiber (CCGISMF) [16] have been previously reported based on concerned ABCD matrix formalism [14, 15]. Moreover, the coupling optics

involving hemispherical microlens on the tip of CCSISMF [17] as well as on the tip of CCGISMF [18] in absence of transverse and angular misalignments have also been already reported based on concerned theoretical ABCD matrix model [17]. The coupling optics involving parabolic microlens on the tip of CCSISMF [19, 20] as well as on the tip of CCGISMF [21] have been recently reported based on very popular and relevant ABCD matrix formalism [19, 20].

Generally, fiber with hyperbolic, hemispherical, parabolic, elliptic microlens on its tip is nomenclatured as quadric interface lensed fiber of which structure parameter is an important generalized parameter for optimizing the coupling efficiency. The coupling optics involving quadric interface microlens (QIML) on the tip of CCSISMF [23, 24] as well as on the tip of CCGISMF [25] have been reported very recently based on concerned unified ABCD matrix formalism [23]. Moreover, in designing optimum launch optics involving such above mentioned microlenses like hyperbolic, hemispherical, parabolic, theoretical computations of such coupling efficiencies require cumbersome and lengthy numerical integrations [10-13]. The application of the ABCD system matrix formalism [14-25] for prediction of the excitation efficiency for coupling of a LD via different type of above-mentioned microlenses on the tip of different kinds of COFs has simplified calculations, nevertheless, yielding extremely accurate results [14-25]. Furthermore, calculations by this formalism are simple and executable with very little computation as well.

Thus, in the context of coupling optics there are considerable amount of research works on microlenses like hyperbolic, hemispherical, parabolic microlenses etc. on the tip different kinds of circular core COFs which have enriched the literature [10-25]. However, as per as R&Ds related with microlensing coupling schemes on the tip of circular core photonic crystal fibers (CCPCFs) are concerned, only a research paper investigating coupling of LD to solid core PCF via hyperbolic microlens has been reported very recently [26]. Though there are some research papers in literature related with quadric interfaced microlensing on the tip of different types of circular core COFs like CCSISMF [23, 24], CCGISMF [25], no such information is available regarding a study of coupling optics involving LD and CCPCF via QIML on the tip of the fiber. Moreover, the simplicity and effectiveness of method of computation of coupling optics of QIML involving ABCD matrix formalism [23-25] motivates us to concentrate on the present work, which aims the study of the coupling optics involving a LD via a QIML on the tip of CCPCF using relevant ABCD matrix [23-25]. Actually, it had been shown that prediction of the coupling optics in the case of a QIML on the tip of CCSISMF [23, 24] as well as on the tip of CCGISMF [25] have produced excellent results if we employ simple ABCD matrix formalism. Concerned calculations are executable with very little computations. It may be relevant to mention in this connection that in the case of a semiconductor LD emitting $1.3\mu m$ wavelength of light, uncoated QIMLs on the tip of a CCSISMF produce 99.87% coupling efficiency [23] i.e., an ideal LD having a symmetrical modal output and a QIML with an anti-reflection coating, has a theoretical coupling efficiency of nearly 100% [23]. Therefore, the effect of Fresnel backward reflection can be neglected in our requisite study of coupling optics. Such a study, which as per our knowledge, reported for the first time, should deserve the immediate attention of experimentalists.

In the first part of this paper, using simple, accurate and unified ABCD matrix formalism for refraction by a quadric interface [23, 24] we theoretically investigate the coupling efficiencies between a semiconductor LD emitting light of wavelength $\lambda = 1.3\ \mu m$ [12] and a series of CCPCFs with different air filling ratio d/Λ and hole pitch or lattice constant Λ [26] via QIML of six different focal parameters [23, 24] on the tip of these fibers in absence of possible transverse and angular mismatches. In the second part, we carry out the similar investigation for a LD emitting light of wavelength $\lambda = 1.5\ \mu m$ [12]. A comparison between these two cases is performed.

Further, we employ Gaussian field distributions for both the LD and the fiber. Experimentalists, system engineers and packagers would find these results appealing in designing CCPCFs with appropriate calibration, in the context of its simplicity compared to other

deeply involved rigorous methods like finite difference method (FDM) and finite element method (FEM). The present analysis, reported for the first time, contains significant new results in connection with the prediction of the suitable optogeometry of the QIML as well as that for the appropriate design of fiber geometry, i.e., core size, air hole pitch, size and the distribution of air holes, at a suitable wavelength emitted from the LD. The result will be extremely important for the designers and packagers who can, accordingly, mould and shape the desired QIML at the fiber end to achieve optimum coupling optics involving CCPCF in which air hole pitch, size, and distribution are additional degrees of freedom in comparison with the COFs.

THEORY AND ANALYSIS

Preview of fiber spot sizes of CCPCF

In our study, we consider an all-silica CCPCF having a triangular lattice of uniform structure for the air-hole of diameter d and glass matrix elongated along the entire length of the propagation direction of the fiber, as shown in Figure 1. The air-holes are distributed symmetrically around a central silica defect, which is actually an omitted air-hole, acting as the core of the said CCPCF. The infinite air-hole matrix with lattice-constant or hole-pitch Λ and air filling ratio d/Λ has been considered to act as the cladding of the CCPCF. Since the core-index n_{CO} is greater than that of the effective cladding index n_{FSM}, the fiber can guide light by the mechanism of MTIR as in case of a conventional step index fiber (CSF) [26, 27].

Now, the fundamental modal field in a CCPCF is approximated as a Gaussian function [26, 28] in the single mode region where air filling fraction of the PCF is smaller than 0.45 [29]

$$\psi_f = \exp\left[-\frac{x^2+y^2}{w_{eff}^2}\right] \tag{1}$$

where w_{eff} corresponds to the spot size of the CCPCF.

The upper and lower limits of the propagation constants β of the guided modes through the core of the CCPCF satisfy [8, 27]

$$k n_{CO} > \beta > \beta_{FSM} \tag{2}$$

where, $k=2\pi/\lambda$ being the wave number associated with the operating wavelength λ, n_{CO} is the refractive index of silica or the core material and β_{FSM} is the propagation constant of the fundamental space-filling mode (FSM), which is the fundamental mode in the infinite photonic crystal cladding without any defect or core.

The index corresponding to the FSM or the effective cladding index is [8, 27]

$$n_{FSM} = \frac{\beta_{FSM}}{k} \tag{3}$$

The procedure for obtaining the value of n_{FSM} for given parameters of the CCPCF at operating wavelength of light is detailed in Appendix A [26, 27]. Here all the coefficients are determined by applying the least square fitting method for the operating wavelengths $\lambda = 1.3\mu m$ and $\lambda = 1.5\mu m$, presented in Tables 1 and 2, respectively. These coefficients are utilized to determine the values of n_{FSM} of the CCPCF for various values of hole-pitch and the air filling ratio at any particular wavelength of interest [26].

The effective cladding index n_{FSM} can be used to find the effective *V*-parameter of the CCPCF, treating the CCPCF like a CSF, with its cladding and core indices same as those of infinite photonic crystal structure and silica, respectively. Now the effective *V* value of the CCPCF is given by [26, 27, 30, 31]

$$V_{eff} = \frac{2\pi}{\lambda} a_{eff} \left[n_{CO}^2 - n_{FSM}^2 \right]^{1/2} \tag{4}$$

where a_{eff} is the effective core radius which is assumed [26, 27, 30, 31] to be $\Lambda/\sqrt{3}$ and λ is the operating wavelength.

Then using Marcuse formula [28], the modal spot size w_{eff}, half of the mode field diameter (MFD) can be written as [26-28, 32]

$$\frac{w_{eff}}{a_{eff}} = 0.65 + \frac{1.619}{V_{eff}^{3/2}} + \frac{2.879}{V_{eff}^{6}} \tag{5}$$

The spot size of the CCPCF, w_{eff} is obtained by using Eq. (5), where V_{eff} being the effective *V*-parameter, calculated from Eq. (4). The method of such calculation has been detailed in Appendix A [26, 27].

Formulation of microlens coupling scheme

The coupling scheme to be studied is shown in Figure 1. Here, *L* is the separation distance in between the laser source and the nearest point of the QIML end of the fiber [23-25]. Our analysis is based on some usual approximations [10, 14-18, 20, 21, 23-26] like Gaussian field distributions for both the source and the fiber, no transmission loss, perfect matching of the polarisation mode of the fiber field, and that on the microlens surface, sufficient angular width of the microlens for ensuring the interception of entire power radiated by the source for typical values of the microlens parameters employed. However, since the spherical aberration is really determined by the properties of the microlens itself, its elimination is difficult by the said adjustment [33].

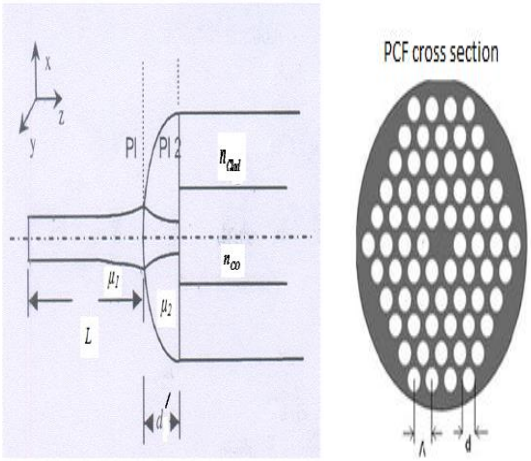

Figure 1. Geometry of LD to single mode CCPCF coupling via QIML on the tip of the fiber; μ_1 and μ_2 stand for refractive indices of incident and microlens media respectively.

The field Ψ_u representing the output of the LD at a distance *u* from the QIML surface is expressed by [23-25, 34-36]

$$\Psi_u = \exp\left[-\left(\frac{x^2}{w_{1x}^2}+\frac{y^2}{w_{1y}^2}\right)\right]\exp\left[-\frac{ik_1}{2}.\frac{x^2+y^2}{R_1}\right] \quad (6)$$

Here, elliptical intensity profiles of the laser beams are approximated by Gaussian spot sizes w_{1x} and w_{1y} along two mutually perpendicular directions, one perpendicular (X) and the other parallel (Y) to the junction planes, k_1 is the wave number in the incident medium and R_1 is the radius of curvature of the wavefronts from the LD. Our analysis is restricted to single frequency laser emitting only one spatial mode with a Gaussian intensity profile.

Moreover, it is already established that Gaussian approximations for the fundamental mode in circular core SMF [14-18, 20, 21, 23-26] sufficiently represent accurate results in the context of coupling losses for different types of microlensing schemes.

The QIML transformed laser field Ψ_v on the fiber plane 2 can be represented by [23-25, 34-36]

$$\Psi_v = \exp\left[-\left(\frac{x^2}{w_{2x}^2}+\frac{y^2}{w_{2y}^2}\right)\right]\exp\left[-\frac{ik_2}{2}\left(\frac{x^2}{R_{2x}}+\frac{y^2}{R_{2y}}\right)\right] \quad (7)$$

where w_{2x}, w_{2y} are, respectively, microlens transformed spot sizes, R_{2x}, R_{2y} being the respective transformed radii of curvature of the refracted wavefronts in the X and Y directions and k_2 is the wave number in the microlens medium. The method of finding w_{2x}, w_{2y}, R_{2x} and R_{2y} in terms of w_{1x}, w_{1y} and R_1 with the relevant ABCD matrix for QIML on the tip of the fiber is available in literature [23-25] and once again discussed in the Appendix B for ready reference. However, the different values of structure parameter *P* describe different structures of QIML like elliptical, hyperbolic, spherical and parabolic microlenses which are introduced in Table 3 [23-25].

The source to fiber coupling efficiency via QIML on the tip of the fiber is expressed in terms of well known overlap integral by [14-18, 20, 21, 23-26, 34-37]

$$\eta = \frac{\left|\iint \Psi_v \Psi_f^* dxdy\right|^2}{\iint |\Psi_v|^2 dxdy \iint |\Psi_f|^2 dxdy} \qquad (8)$$

Therefore η_0, the coupling efficiency in absence of misalignment, for CCPCF is given by [26]

$$\eta_0 = \frac{4w_{2x}w_{2y}w_{eff}^2}{\left[\left(w_{eff}^2 + w_{2x}^2\right)^2 + \frac{k_2^2 w_{2x}^4 w_{eff}^4}{4R_{2x}^2}\right]^{1/2}\left[\left(w_{2y}^2 + w_{eff}^2\right)^2 + \frac{k_2^2 w_{2y}^4 w_{eff}^4}{4R_{2y}^2}\right]^{1/2}} \qquad (9)$$

However, Eq. (9) can be obtained by employing Eqs. (1) and (7) in Eq. (8).

RESULTS AND DISCUSSION

Optogeometrical parameters under consideration

Our formalism employs the unified ABCD matrix under the paraxial approximation in order to predict the relevant coupling optics involving a LD and CCPCF via QIML on the tip of the fiber. For the estimation of coupling efficiencies in absence of any possible transverse and angular misalignments for a QIML of specific focal length on the tip of CCPCF, we firstly use a LD emitting light of wavelength $\lambda = 1.3\mu m$ with $w_{1x} = 1.081\mu m, w_{1y} = 1.161\mu m$ [12] and then LD emitting light of wavelength $\lambda = 1.5\mu m$ with $w_{1x} = 0.843\mu m$, $w_{1y} = 0.857\mu m$ [12]. The LD parameters used in this investigation are mentioned in Table 4. For the LD emitting light of abovementioned first wavelength, we study the coupling efficiencies for a series of CCPCFs having different air filling ratio d/Λ and hole-pitch or lattice-constant Λ [26] as mentioned in Tables 5(a) and 5(b). We choose three typical values of d/Λ, in the single moded region ($d/\Lambda \le 0.45$) corresponding to each arbitrary Λ value (Λ = 2.3, 3.0, 3.5, 4.0, 4.5, 5.0 μm), as 0.35, 0.40, 0.45 [26]. Different fiber spot sizes w_{eff} for these three d/Λ values corresponding to each Λ value (Λ = 2.3, 3.0, 3.5, 4.0, 4.5, 5.0 μm) [26] are then calculated [26, 27] and shown in Tables 5(a) and 5(b) where we also present the relevant structure parameters with corresponding maximum coupling efficiencies for $\lambda = 1.3\mu m$.

Following [14-18, 20, 21, 23-26] once again, the maximum depth of the microlens d' is taken as $6.0\,\mu m$ while the refractive index $\mu (= \mu_2 / \mu_1)$ of the material of the microlens with respect to surrounding medium is once again taken as 1.55. Further, since estimation of coupling efficiency on the basis of planar wave model for the input beam from the LD facet departs slightly from that on the basis of spherical wave model [14-18, 20, 21, 23-26], we consider planar wave model for the input beam from the LD facet for the sake of simplicity.

For the values of focal length (L) 7.6, 12.6, 17.6 [23] and 8.19, 12.1875, 16.19 [24] μm, respectively, we calculated the coupling efficiency varying with the structure parameter (P), and the results are shown in respective Tables 5(a) and 5(b). Then we use a LD emitting light of wavelength $\lambda = 1.5\mu m$ with $w_{1x} = 0.843\mu m, w_{1y} = 0.857\mu m$ [12]. We compute again relevant structure parameters with resulting maximum coupling efficiencies for the above same set used in the first part of this investigation and present them in Tables 6(a) and 6(b), respectively. The comparative optimized results of coupling efficiencies and coupling losses are shown in Table 7.

Results for coupling scheme without misalignment consideration

From Tables 5(a)-6(b), it is generally observed that the coupling efficiency can be improved through optimizing the structure parameter or in other words the structure parameter of the QIML is a key parameter that affects directly the coupling efficiency.

Now, it is observed from Tables 5(a) and 5(b) that the coupling efficiency can reach to 99.8334 % (i.e. coupling loss of 0.0072 dB) for a fit structure parameter (*P*) of 4.9 μm and a focal length (*L*) of 8.19 μm for the CCPCF with air filling ratio $d/\Lambda = 0.45$ and hole-pitch or lattice-constant $\Lambda = 4.5\mu m$ having spot size w_{eff} of 3.236339 μm, in case of excitation by a LD emitting light of abovementioned first wavelength. Moreover, from Tables 6(a) and 6(b), it is once again observed that for the fit structure parameter (*P*) of 4.3 μm, the maximum coupling efficiency can reach to 99.8423 % (i.e. coupling loss of 0.0068 dB) when L = 7.6 μm for the CCPCF with $d/\Lambda = 0.35$, $\Lambda = 5.0\mu m$ having corresponding spot size w_{eff} of 4.490145 μm, for excitation by a LD emitting light of abovementioned second wavelength.

It is seen from these Tables that for excitation by LDs emitting light of wavelengths $\lambda = 1.3\mu m$ and $\lambda = 1.5\mu m$, respectively, the maximum coupling efficiencies are nearly equal (99.8334% for CCPCF with $d/\Lambda = 0.45$, $\Lambda = 4.5\mu m$ having w_{eff} of 3.236339 μm for excitation by LD #1 and 99.8355 %, for CCPCF with $d/\Lambda = 0.35$, $\Lambda = 5.0\mu m$ having w_{eff} of 4.490145 μm for excitation by LD #2, respectively) for coupling by LDs via a QIML of identical focal length L = 8.19 μm on the tip of these respective fibers. Moreover, the structure parameters have a very little difference in case of such excitation by LDs emitting light of two wavelengths of practical interest (i.e. P = 4.9 μm for $\lambda = 1.3\mu m$ and P = 4.6 μm for $\lambda = 1.5\mu m$). It is also observed that, for excitation by a LD # 2 emitting light of wavelength $\lambda = 1.5\mu m$, the maximum coupling efficiency corresponds with CCPCFs with $d/\Lambda = 0.35$, $\Lambda = 5.0\mu m$ with w_{eff} of 4.490145 μm using QIML of all focal lengths proposed in our study. However, for excitation by LD # 1 emitting light of wavelength $\lambda = 1.3\mu m$, the coupling efficiency is once again maximum for CCPCFs with $d/\Lambda = 0.35$, $\Lambda = 5.0\mu m$ having w_{eff} of 4.433909 μm using QIML with all focal lengths used in our study except only two focal lengths L = 7.6 μm and 8.19 μm. Thus for identical values of fiber parameters of CCPCF with air filling ratio $d/\Lambda = 0.35$ and hole-pitch $\Lambda = 5.0\mu m$, the coupling efficiency can reach to nearly 100 % (99.6879 % for structure parameter P = 7.0 μm using QIML with focal length L= 12.1875 μm in case of excitation by LD # 1 emitting λ= 1.3 μm and 99.8423 % for structure parameter P = 4.3 μm using QIML with focal length L= 7.6 μm in case of excitation by LD # 2 emitting λ= 1.5 μm). Now, it may be relevant to mention in this connection that the wavelength at and around 1.5 μm is the region where the erbium doped fiber amplifier and Raman gain fiber amplifier operate efficiently and elegantly [16, 21]. Thus, the comparison between these results of maximum coupling efficiencies for the requisite CCPCF excited with two wavelengths predicts that CCPCFs with air filling ratio $d/\Lambda = 0.35$ and hole-pitch $\Lambda = 5.0\mu m$ are generally most suitable in the context of the aforesaid coupling optics involving CCPCFs for both wavelengths of practical interest and this excitement is uniquely excellent for excitation by a LD emitting specially light of wavelength $\lambda = 1.5\mu m$. Also it is revealed in our study that so far as the demand of achieving the merit of appreciable working distance to have maximum coupling efficiency on the tip of CCPCFs are concerned, this merit is acquired by CCPCF with $d/\Lambda = 0.35$ and $\Lambda = 5.0\mu m$. These values of V_{eff} for light of wavelengths $\lambda = 1.3\mu m$ and $\lambda = 1.5\mu m$, respectively, correspond to low V region which is very well known for evanescent wave coupling in optical fiber directional coupler.

For a typical estimation of knowledge of excitation via QIML with focal length (*L*) of 8.19 μm and 7.6 μm, respectively excited with LD # 1, 2 emitting light of wavelength $\lambda = 1.3\mu m$ and $\lambda = 1.5\mu m$, respectively we present the variation of coupling efficiencies versus the structure parameter for fibers

corresponding to $d/\Lambda = 0.45$, $\Lambda = 4.5\mu m$ with w_{eff} of 3.236339 μm and $d/\Lambda = 0.35$, $\Lambda = 5.0\mu m$ with w_{eff} of 4.490145 μm as shown in Figure 2. Figure 3 represents the variation of coupling efficiencies versus the structure parameter for fibers corresponding to $d/\Lambda = 0.45$, $\Lambda = 4.5\mu m$ with w_{eff} of 3.236339 μm and $d/\Lambda = 0.35$, $\Lambda = 5.0\mu m$ with w_{eff} of 4.490145 μm for excitation via QIML with identical focal length (L) of 8.19 μm, respectively excited with LD # 1, 2 emitting light of wavelength $\lambda = 1.3\mu m$ and $\lambda = 1.5\mu m$, respectively. However, in Figure 4, we have plotted the variation of coupling efficiencies versus the structure parameter for fibers corresponding to identical $d/\Lambda = 0.35$, $\Lambda = 5.0\mu m$ with w_{eff} of 4.433909 μm and 4.490145 μm, respectively for excitation via QIML with corresponding focal length (L) of 12.1875 μm and 7.6 μm, respectively excited with LD # 1, 2 emitting light of wavelength $\lambda = 1.3\mu m$ and $\lambda = 1.5\mu m$, respectively. In all of these figures, solid line (_____ denoting EFF0) corresponds to $\lambda = 1.3\mu m$, dashed line (---------- denoting EFF0DS) to $\lambda = 1.5\mu m$. We see that although the values of the typical structure parameters relevant with the maximum coupling efficiencies corresponding to curves are more or less the same, the optimum coupling efficiency is relatively better observed when the corresponding most suitable CCPCF is excited with LD #2 emitting light of wavelength $\lambda = 1.5\mu m$, in addition to the achievement of the appreciable working distance.

In CSFs, the single-mode optical bandwidth is typically limited by a higher-order mode cutoff at short wavelengths and macro-bend loss at long wavelengths [38]. On the other hand, the PCF can be designed to be endlessly single-mode (ESM), a term first coined by Birks et al. [8] referring to the fact that no higher-order modes are supported regardless of the wavelength. The ESM property has the specious consequence that the waveguide can be scaled to

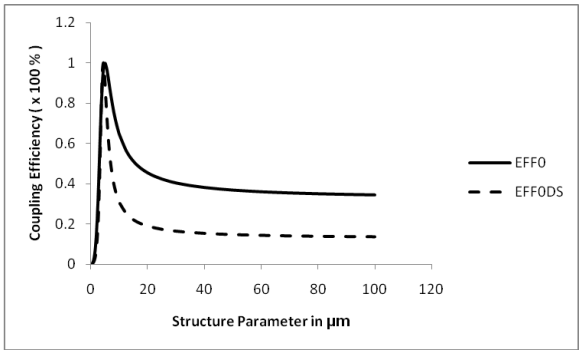

Figure 2. Variation of coupling efficiencies versus the structure parameter for fibers corresponding to $d/\Lambda = 0.45$, $\Lambda = 4.5\mu m$ with w_{eff} of 3.236339 μm and $d/\Lambda = 0.35$, $\Lambda = 5.0\mu m$ with w_{eff} of 4.490145 μm for excitation via QIML with focal length (L) of 8.19 and 7.6 μm, respectively excited with LD # 1, 2, emitting light of wavelength $\lambda = 1.3\mu m$ and $\lambda = 1.5\mu m$, respectively. Solid line (_____ denoting EFF0) corresponds to $\lambda = 1.3\mu m$, dashed line (---------- denoting EFF0DS) to $\lambda = 1.5\mu m$.

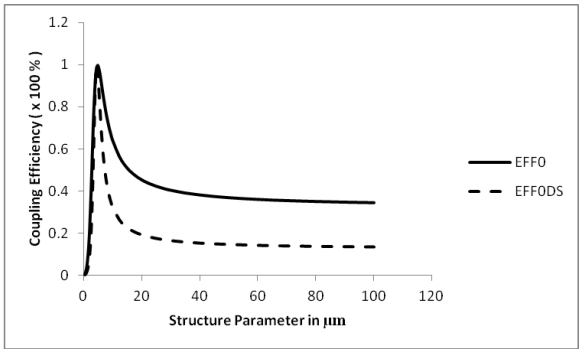

Figure 3. Variation of coupling efficiencies versus the structure parameter for fibers corresponding to $d/\Lambda = 0.45$, $\Lambda = 4.5\mu m$ with w_{eff} of 3.236339 μm and $d/\Lambda = 0.35$, $\Lambda = 5.0\mu m$ with w_{eff} of 4.490145 μm for excitation via QIML with identical focal length (L) of 8.19 μm, respectively excited with LD # 1, 2, emitting light of wavelength $\lambda = 1.3\mu m$ and $\lambda = 1.5\mu m$, respectively. Solid line (_____ denoting EFF0) corresponds to $\lambda = 1.3\mu m$, dashed line (---------- denoting EFF0DS) to $\lambda = 1.5\mu m$.

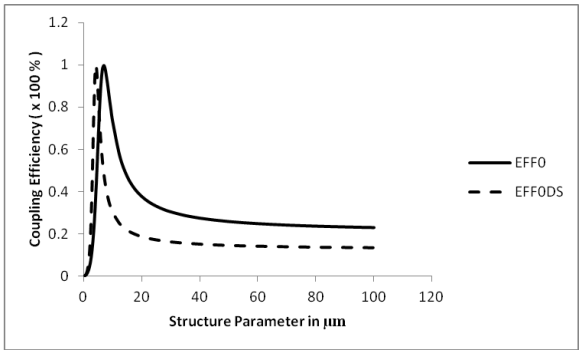

Figure 4. Variation of coupling efficiencies versus the structure parameter for fibers corresponding to identical $d/\Lambda = 0.35$, $\Lambda = 5.0\mu m$ with w_{eff} of 4.433909 μm and 4.490145 μm, respectively for excitation via QIML with corresponding focal length (L) of 12.1875 and 7.6 μm, respectively excited with LD # 1, 2, emitting light of wavelength $\lambda = 1.3\mu m$ and $\lambda = 1.5\mu m$, respectively. Solid line (_____ denoting EFF0) corresponds to $\lambda = 1.3\mu m$, dashed line (---------- denoting EFF0DS) to $\lambda = 1.5\mu m$.

an arbitrary dimension while remaining single mode [38]. Moreover, the PCF is found to have a significantly larger bandwidth than the CSF of an identical MFD as per as the measurements of the single-turn bend loss, spectral attenuation, etc. are concerned [38]. Recently PCFs with zero dispersion wavelengths around the 1.5 μm communications window have also been demonstrated [39]. This communication window provides efficient and elegant operation of erbium doped fiber amplifier and Raman gain fiber amplifier [16, 21]. However, it is observed in our present analysis that, for fit focal length of 8.19 μm of QIML on the tip CCPCF with air filling ratio of 0.45 and hole-pitch of 4.5 μm, the maximum coupling efficiency can reach to 99.8334 % for the structure parameter P = 4.9 μm in case of excitement by a LD emitting light of wavelength $\lambda = 1.3\mu m$. The corresponding value of coupling efficiency comes out to be 99.6879% for the structure parameter P = 7.0 μm using QIML of focal length L = 12.1875 μm on the tip of CCPCF with air filling ratio of 0.35 and hole-pitch of 5.0 μm in case of excitement by the same LD emitting light of wavelength $\lambda = 1.3\mu m$. It is observed generally that the respective value of the maximum coupling efficiency is 99.8423 % for fit focal length of 7.6 μm of QIML on the tip most efficient CCPCF with air filling ratio of 0.35 and hole-pitch of 5.0 μm, for the working distance P = 4.3 μm in case of excitement by a LD emitting light of wavelength $\lambda = 1.5\mu m$. Consequently the coupling losses, in absence of possible misalignments, have been reduced for excitement by a LD emitting light of wavelength $\lambda = 1.5\mu m$ in comparison with that obtained for excitement by a LD emitting light of wavelength $\lambda = 1.3\mu m$. Moreover, it is mentioned in Reference [40] that the additional design parameters of hole diameter d and hole-to-hole spacing Λ in CCPCF, enable much greater flexibility in the design of dispersion to suit the required application while in CSFs, group velocity dispersion is usually dominated by the dispersion of the bulk silica. Thus, our present analysis and results point out the merit of CCPCFs with specific air filling ratio of 0.35 and hole-pitch or lattice-constant of 5.0 μm in coupling by a LD emitting specially light of wavelength $\lambda = 1.5\mu m$ via hyperbolic microlens [26] as a special case of QIML of specific focal parameter on its tip. Although there is only a research paper involving experimental demonstration of efficient laser coupling through a hollow core PCF [41] in literature, there is limitation of availability of experimental research papers in the field of microlens coupling involving solid core PCFs. However, we are fortunate enough to compare our proposed results with those mentioned in the available literature [42] for the paraboloidal-shaped microlens etched from an SMF and fused on PCF having MFD of 11.1 μm excited by a LD of wavelength 1.31 μm. It is observed that our presented coupling scheme as a special case of QIML is in excellent agreement with those results mentioned in Reference [42]. Moreover, the excellent agreement of our results as special cases of QIML like hyperbolic microlens for CCPCF coupling in comparison with the available earlier theoretical results for coupling of CCPCF via such hyperbolic [26] microlens certifies the correctness of our simple formalism which is executable with little computations. We also conclude that structure parameter is not only the main factor to affect the maximum coupling efficiency. To acquire the maximum coupling efficiency, simultaneous optimization

of focal length and structure parameter is important**.**

Thus, it shows that once the structure parameters of QIML are optimized, the system designer will design appropriate microlens of suitable optogeometry according to their convenience. Hence, the method and results should find wide applications in prediction of optimal launch optics involving QIML, which has emerged as a potential candidate. Moreover, with the advent of new progress in nanotechnology, we are optimistic that the future technologist, will involve any breakthrough to reduce the dispersion values, associated with the wavelength 1.3 and 1.5 μm, by further optimization of the structure and better control of the fluctuations in fiber diameter and, ultimately realize and test our results of the above proposed theoretical formalism experimentally in near future.

CONCLUSION

The coupling optics involving LD to CCPCF excitation for different fiber parameters via QIML with different focal lengths on the tip of such fibers is theoretically formulated and investigated for the first time, to the best of our knowledge, in absence of possible transverse and angular mismatches. For a series of CCPCFs with different air filling ratio d/Λ and lattice-constant Λ, appropriate structure parameters are optimized so as to give maximum coupling efficiency for those respective fibers. Analytical expressions for the relevant quantities of practical interest are prescribed. Instead of considering special ABCD matrix for individual microlens like hyperbolic, hemispherical, elliptic and parabolic one, a unified expression for transfer ABCD matrix for refraction of QIML under paraxial approximation has been considered to simplify and execute the relevant calculations easily. The analysis will be extremely important and useful for the design of optimum launch optics in order to obtain maximum light coupling efficiency. The best maximum coupling is achieved for a CCPCF with air filling ratio of 0.35 and hole-pitch or lattice- constant of 5.0 μm when excited with LD emitting light of wavelength $\lambda = 1.3 \mu m$ and specially that of $\lambda = 1.5 \mu m$. Further, the importance of achieving appreciable structure parameter to have maximum coupling efficiency also stands in favour of the said CCPCF. For simplicity, we consider the two sources have same intensity profiles. It is observed from the standpoint of relevant coupling optics that LD emitting light of wavelength λ= 1.5 μm may be taken as a better alternative to source of wavelength λ= 1.3 μm as the lowest loss of window of glass corresponds with λ= 1.5 μm. But our data for λ= 1.3 μm is equally useful for such microlens coupling scheme. Moreover, simultaneous optimization of structure parameter and focal length is of immense importance in both the cases. In comparison with the other deeply involved rigorous methods like FEM and FDM, the application of novel unified ABCD matrix has simplified the analysis as the concerned calculations need very little computations. This methodology will be beneficial for the system engineers and packagers working in the field of optimum launch optics involving QIML on the tip of the CCPCF. Our study has the potential merit that once the structure parameters of QIML are optimized, the system designer will design appropriate microlens of suitable optogeometry in accordance with their convenience.

Appendix A

The usual normalized parameters u and v for the infinite cladding region of the chosen CCPCF are given by [2, 26, 27]

$$u = k\Lambda\left(n_{CO}^2 - \frac{\beta^2}{k^2}\right)^{1/2} \quad \text{(A1)}$$

and

$$v = k\Lambda\left(n_{CO}^2 - 1\right)^{1/2} \quad \text{(A2)}$$

with

$$u^2 + w^2 = v^2. \quad \text{(A3)}$$

In order to obtain the effective cladding index n_{FSM}, a basic air-hole at the centre of a hexagonal unit cell is approximated to a circle in a regular photonic crystal [8, 26, 27]. Then from relevant boundary conditions for the fields and their derivatives in terms of appropriate special functions, corresponding to a fixed value of v, obtained from Eq. (A2) for fixed Λ and λ - values, the concerned u values are computed for

different d / Λ values at a particular λ from the following Eq., taking n_{CO} = 1.45 [2, 26, 27]

$$wI_1(a_n w)\left[J_1(bu)Y_0(a_n u)-J_0(a_n u)Y_1(bu)\right] +uI_0(a_n w)\left[J_1(bu)Y_1(a_n u)-J_1(a_n u)Y_1(bu)\right]=0 \quad \text{(A4)}$$

where $a_n=\frac{d}{2\Lambda}$, $b=\left(\frac{\sqrt{3}}{2\pi}\right)^{1/2}$.

Using Eq. (A4), Russell has provided a polynomial fit to u, only for d/Λ = 0.4 and n_{CO} = 1.444. Further, for all d/Λ values of practical interest in the endlessly single mode region of a CCPCF, where d/Λ is less than 0.45, one should have a more general equation for wide applications [27].

The values of n_{FSM} are determined by replacing β/k in Eq. (A1) with n_{FSM} and this will lead to a modified simpler formulation of n_{FSM} as [26, 27]

$$n_{FSM}=A+B\left(\frac{d}{\Lambda}\right)+C\left(\frac{d}{\Lambda}\right)^2 \quad \text{(A5)}$$

where A, B and C are the three different optimization parameters, dependent on both the relative hole-diameter or hole-size d/Λ and the hole-pitch Λ.

Since optical communication window corresponds with two operating wavelengths of 1.3 μm and 1.5 μm, this study finds the coefficients for these two wavelengths of practical interest for different possible hole-pitches and hole-sizes of the CCPCF. Such modification in such a fitting is advantageous in the sense that it will help to reduce computation time since only nine coefficients are required in calculation instead of twenty seven coefficients [26, 27].

Now, for each value of Λ with the variations of d/Λ, the n_{FSM} values corresponding to respective u values obtained from Eq. (A4) are determined. Applying least square fitting of n_{FSM} in terms of d/Λ to Eq. (A5) for a particular Λ, the values of A, B and C can be then estimated. The various values of A, B and C are then simulated for different Λ in the endlessly single mode region of the CCPCF, resulting in the empirical relations of A, B and C in Eq. (A5), in terms of Λ, as given in the following [26, 27]

$$A=A_0+A_1\Lambda+A_2\Lambda^2 \quad \text{(A6)}$$

$$B=B_0+B_1\Lambda+B_2\Lambda^2 \quad \text{(A7)}$$

$$C=C_0+C_1\Lambda+C_2\Lambda^2 \quad \text{(A8)}$$

where A_i, B_i and C_i ($i=0,1$ and 2) are the optimization parameters for A, B and C, respectively. Computing A, B and C from Eqs. (A6-A8), one can find n_{FSM} directly for any d/Λ and Λ value at any particular λ using Eq. (A5) in the endlessly single mode region of the CCPCFs.

Appendix B

The relation between input and output parameters (q_1,q_2) of the light beam is given by

$$q_2=\frac{Aq_1+B}{Cq_1+D} \quad \text{(B1)}$$

where

$$\frac{1}{q_{1,2}}=\frac{1}{R_{1,2}}-\frac{i\lambda_0}{\pi w_{1,2}^2\mu_{1,2}} \quad \text{(B2)}$$

with symbols having their usual meanings as already described.

The ray matrix *M* for the QIML on the tip of the fiber is given by [23-25]

$$M=\begin{pmatrix}A & B\\ C & D\end{pmatrix}$$

$$M=\begin{pmatrix}1 & d'\\ 0 & 1\end{pmatrix}\begin{pmatrix}1 & 0\\ \frac{1-\mu}{\mu P} & \frac{1}{\mu}\end{pmatrix}\begin{pmatrix}1 & L\\ 0 & 1\end{pmatrix} \quad \text{(B3)}$$

where $A=1+\frac{d'(1-\mu)}{\mu P}$

$$B = L + \frac{(1-\mu)Ld'}{\mu P} + \frac{d'}{\mu}$$

$$C = \frac{1-\mu}{\mu P}$$

$$D = \frac{1}{\mu} + \frac{(1-\mu)L}{\mu P} \qquad \text{(B4)}$$

where d' is the maximum depth of the microlens, P is the structure parameter of the quadric interface lensed fiber, and L is the working distance which is also the distance of the LD from the microlens.

Again, the refractive index of the material of the microlens with respect to the surrounding medium is represented by $\mu(=\mu_2/\mu_1)$. The transformed beam spot sizes and radii of curvature in the X and Y directions are found by using expressions in Eq. (B4) in Eqs. (B1) and (B2) and can be expressed as

$$w_{2x,2y}^2 = \frac{A_1^2 w_{1x,1y}^2 + \dfrac{\left(\lambda_1^2 B^2\right)}{w_{1x,1y}^2}}{\mu(A_1 D - BC_1)} \qquad \text{(B5)}$$

$$\frac{1}{R_{2x,2y}} = \frac{A_1 C_1 w_{1x,1y}^2 + \dfrac{\left(\lambda_1^2 BD\right)}{w_{1x,1y}^2}}{A_1^2 w_{1x,1y}^2 + \dfrac{\left(\lambda_1^2 B^2\right)}{w_{1x,1y}^2}} \qquad \text{(B6)}$$

where

$$\lambda_1 = \frac{\lambda}{\pi}, \quad \lambda = \frac{\lambda_0}{\mu_1}, \quad A_1 = A + \frac{B}{R_1} \quad \text{and}$$

$$C_1 = C + \frac{D}{R_1}. \qquad \text{(B7)}$$

In plane wavefront model, the radius of curvature R_1 of the wavefront from the laser facet $\rightarrow\infty$. This leads to $A_1 = A$ and $C_1 = C$.

REFERENCES

[1] Russell, P. St. J. (2003) Photonic crystal fibers. *Science*, **299**: 358-362.

[2] Russell, P. St. J. (2006) Photonic-crystal fibers. *J. Lightwave Technol.*, **24**: 4729–4749.

[3] Bjarklev, A., Broeng, J. and Bjarklev, A. S. (2003) *Photonic Crystal Fibres*, Springer Science & Business Media Inc, NewYork.

[4] Bhattacharya, R. and Konar, S. (2012) Extremely large birefringence and shifting of zero dispersion wavelength of photonic crystal fibers. *Opt. & Laser Technol.*, **44**: 2210–2216.

[5] Sharma, M., Borogohain, N. and Konar, S. (2013) Index Guiding Photonic Crystal Fibers With Large Birefringence and Walk-Off. *J. Lightwave Technol.*, **31**: 3339-3344.

[6] Bhattacharya, R. and Konar, S. (2008) Design of a Photonic Crystal Fiber with Zero Dispersion Wavelength Near 0.65 µm. *Fiber and Integrated Opt.*, **27**: 89–98.

[7] Sharma, M., Konar, S. and Khan, K. R. (2015) Supercontinuum generation in highly nonlinear hexagonal photonic crystal fiber at very low power. *J. Nanophotonics*, **9**: 093073(1-8).

[8] Birks, T. A., Knight, J. C. and Russell, P. St. J. (1997) Endlessly single-mode photonic crystal fiber. *Opt. Lett.*, **22**: 961-963.

[9] Li, E. (2006) Characterization of fiber lens. *Opt. Lett.*, **31**: 169-171.

[10] Presby, H. M. and Edwards, C. A. (1992) Near 100% efficient fibre microlenses. *Electron. Lett.*, **28**: 582-584.

[11] Edwards, C. A., Presby, H. M. and Dragone, C. (1993) Ideal microlenses for laser to fiber coupling. *J. Lightwave Technol.*, **11**: 252-257.

[12] John, J., Maclean, T. S. M., Ghafouri-Shiraz, H. and Niblett, J. (1994) Matching of single-mode fibre to laser diode by microlenses at 1.5 μm wavelength. *IEE Proc. Optoelectron.*, **141**: 178-184.

[13] Presby, H. M. and Edwards, C. A. (1992) Efficient coupling of polarization maintaining fiber to laser diodes. *IEEE Photon. Technol. Lett.*, **4**: 897-899.

[14] Gangopadhyay, S. and Sarkar, S. N. (1996) Laser diode to single-mode fibre excitation via hyperbolic lens on the fibre tip: Formulation of ABCD matrix and efficiency computation. *Opt. Commun.*, **132**: 55-60.

[15] Gangopadhyay, S. and Sarkar, S. N. (1997) ABCD matrix for reflection and refraction of Gaussian light beams at surfaces of hyperboloid of revolution and efficiency computation for laser diode to single-mode fiber coupling by way of a hyperbolic lens on the fiber tip. *Appl. Opt.*, **36**: 8582-8586.

[16] Mukhopadhyay, S. and Sarkar, S. N. (2011) Coupling of a laser diode to single mode circular core graded index fiber via hyperbolic microlens on the fiber tip and identification of the suitable refractive index profile with consideration for possible misalignments. *Opt. Eng.*, **50**: 045004(1-9).

[17] Gangopadhyay, S. and Sarkar, S. N. (1998) Laser diode to single-mode fiber excitation via hemispherical lens on the fiber tip: Efficiency computation by ABCD matrix with consideration for allowable aperture. *J. Opt. Commun.*, **19**: 42-44.

[18] Bose, A., Gangopadhyay, S. and Saha, S. C. (2012) Laser diode to single mode circular core graded index fiber excitation via hemispherical microlens on the fiber tip: Identification of suitable refractive index profile for maximum efficiency with consideration for allowable aperture. *J. Opt. Commun.*, **33**: 15-19.

[19] Liu, H., Liu, L., Xu, R. and Luan, Z. (2005) ABCD matrix for reflection and refraction of Gaussian beams at the surface of a parabola of revolution. *Appl. Opt.*, **44**: 4809-4813.

[20] Liu, H. (2008) The approximate ABCD matrix for a parabolic lens of revolution and its application in calculating the coupling efficiency. *Optik*, **119**: 666-670.

[21] Mukhopadhyay, S. (2016) Coupling of a laser diode to single mode circular core graded index fiber via parabolic microlens on the fiber tip and identification of the suitable refractive index profile with consideration for possible misalignments. *J. Opt.*, **45**: 312–323.

[22] Massey, G. A. and Siegman, A. E. (1969) Reflection and refraction of Gaussian light beams at tilted ellipsoidal surfaces. *Appl. Opt.*, **8**: 975-978.

[23] Huang, J. and Yang, H. J. (2010) ABCD matrix model of quadric interface-lensed fiber and its application in coupling efficiency calculation. *Optik*, **121**: 531-534.

[24] Keshavarz, A. and Kazempour, M. (2012) Numerical calculation of coupling efficiency for an elegant Hermite-Cosh-Gaussian beams. *International J. of optics and Photonics*, **6**: 75-82.

[25] Mukhopadhyay, S. (2017) Laser diode to circular core graded index single mode fiber excitation via quadric interface microlens on the fiber tip and identification of the suitable refractive index profile for maximum coupling efficiency with optimization of structure parameter. *J Opt.*, **46**:359–367.

[26] Karak, A., Kundu, D., Mukhopadhyay, S. and Sarkar, S. N. (2015) Investigation of coupling of a laser diode to photonic crystal fiber via hyperbolic microlens on the fiber tip by ABCD matrix formalism. *Opt. Eng.*, **54**: 086102(1-7).

[27] Kundu, D. and Sarkar, S. (2014) Prediction of propagation characteristics of photonic crystal fibers by a simpler, more complete and versatile formulation of their effective cladding indices. *Opt. Eng.*, **53**: 056111(1-6).

[28] Marcuse, D. (1977) Loss analysis of single-mode fiber splices. *J. Bell Syst. Tech.*, **56**: 703–718.

[29] Hirooka, T., Hori, Y. and Nakazawa, M. (2004) Gaussian and sech approximations of mode field profiles in photonic crystal fibers. *IEEE Photon. Technol. Lett.*, **16**: 1071-1073.

[30] Koshiba, M. and Saitoh, K. (2004) Applicability of classical optical fiber theories to holey fibers. *Opt. Lett.*, **29**: 1739–1741.

[31] Saitoh, K. and Koshiba, M. (2005) Empirical relations for simple design of photonic crystal fibers. *Opt. Express*, **13**: 267-274.

[32] Ghatak, A. K. and Thyagarajan, K. (1998) *Introduction to Fiber Optics*, Cambridge University Press, United Kingdom.

[33] Bass, M. and Mahajan, V. N. (2010) *Handbook of Optics, in Geometrical and Physical Optics, Polarised Light, Components and Instruments*, McGraw-Hill, NewYork, Vol**.** 1, Edn. 3, Chapter 22 and Chapter 29.

[34] Sarkar, S. N., Thyagarajan, K. and Kumar, A. (1984) Gaussian approximation of the fundamental mode in single mode elliptic core fibers. *Opt. Commun.*, **49**: 178-183.

[35] Sarkar, S. N., Pal, B. P. and Thyagarajan, K. (1986) Lens coupling of laser diodes to monomode elliptic core fibers. *J. Opt. Commun.*, **7**: 92-96.

[36] Ghatak, A. K. and Thyagarajan, K. (1998) *Optical Electronics*, Cambridge University Press, United Kingdom, Chapter 13, pp 411-415.

[37] Sakai, J. and Kimura, T. (1980) Design of miniature lens for semiconductor laser to single mode fiber coupling. *IEEE J. Quantum Electron.*, **QE-16**: 1059–1066.

[38] Nielsen, M. D. , Folkenberg, J. R., Mortensen, N. A. and Bjarklev, A. (2004) Bandwidth comparison of photonic crystal fibers and conventional single mode fibers. *Opt. Express*, **12**: 430-435.

[39] Hansen, K. P., Jensen, J. R., Jacobsen, C., Simonsen, H. R., Broeng, J., Skovgaard, P. M. W., Peterson, A. and Bjarklev, A. (2002) Highly Nonlinear Photonic Crystal Fiber with Zero-Dispersion at 1.55μm. paper FA9 in *Optical Fiber Communication Conference 2002, Vol. **70** of OSA Trends in Optics and Photonics Series*, Optical Society of America, Washington, D.C..

[40] Reeves, W. H., Knight, J. C., Russell, P. St. .J. and Roberts, P. J. (2002) Demonstration of ultra-flattened dispersion in photonic crystal fibers. *Opt. Express***, 10**: 609- 613.

[41] Al-Janabi, A. H., Taher, H. J. and Laftah, S. M. (2011) Efficient transportation of Nd laser beam through photonic crystal fiber. *Indian J. Phys.*, **85**: 1299-1307.

[42] Peng, Z. S. and Wang, L. (2006) Optical coupling between a lensed photonic crystal fiber and a laser diode in *Int. Conf. on Communications, Circuits and Systems*, IEEE, Guilin.

Table 1: Values of all coefficients required for the formulation of effective cladding index n_{FSM} at $\lambda = 1.3\mu m$.

$\lambda = 1.3\mu m$			
	$i = 0$	$i = 1$	$i = 2$
A_i	1.430434	0.003803	-0.000214
B_i	0.069387	-0.012541	0.000650
C_i	-0.375746	0.107635	-0.008799

Table 2: Values of all coefficients required for the formulation of effective cladding index n_{FSM} at $\lambda = 1.5\mu m$.

$\lambda = 1.5\mu m$			
	$i = 0$	$i = 1$	$i = 2$
A_i	1.432783	0.002170	-0.000036
B_i	0.063468	-0.007890	0.000147
C_i	-0.415418	0.114257	-0.009127

Table 3: Structure parameters for different kinds of surface

Kinds of Surface	Mathematical Relation	Amount of Structure Parameter
Elliptical	$\frac{x^2}{a^2} + \frac{y^2}{b^2} = 1$	$P = \frac{b^2}{a}$
Hyperbolic	$\frac{x^2}{a^2} - \frac{y^2}{b^2} = 1$	$P = \frac{b^2}{a}$
Spherical	$x^2 + y^2 = r^2$	$P = r$
Parabolic	$x^2 = 2tz$	$P = t$

Table 4: Laser diode parameters

LD	Wavelength λ (μm)	Spot size w_{1x} (μm)	Spot size w_{1y} (μm)	λ_1 (μm)	k_2 (μm^{-1})
#1	1.3	1.081	1.161	0.4138	7.4915
#2	1.5	0.843	0.857	0.4775	6.4926

Table 5 (a):Results for optimum coupling efficiency for a series of CCPCFs with different air filling ratio d/Λ and hole-pitch or lattice-constant Λ via QIML with different focal lengths *L*, following Reference [23], at operating wavelength $\lambda = 1.3\mu m$. (*P* indicates structure parameter, w_{eff} indicates fiber spot size and η_0 indicates coupling coefficient without misalignment)

$d' = 6.0\ \mu m$, $\mu = 1.55$

d/Λ	Λ (μm)	w_{eff} (μm)	L = 7.6 μm		L = 12.6 μm		L = 17.6 μm	
			P(μm)	η_0	P(μm)	η_0	P(μm)	η_0
0.35	2.3	2.475538	4.2	0.971445	6.0	0.690619	7.7	0.454344
	3.0	2.744393	4.4	0.993208	6.4	0.760424	8.3	0.518478
	3.5	3.071572	4.6	0.997630	6.7	0.835083	8.8	0.595929
	4.0	3.482297	4.7	0.976379	6.9	0.908854	9.2	0.687721
	4.5	3.957274	4.7	0.926894	7.1	0.965260	9.5	0.781383
	5.0	4.433909	4.8	0.863142	7.2	0.993311	9.7	0.858528
0.40	2.3	2.106083	3.8	0.913878	5.2	0.588561	6.5	0.370322
	3.0	2.422810	4.2	0.965212	5.9	0.676283	7.5	0.441929
	3.5	2.740655	4.4	0.993026	6.4	0.759495	8.3	0.517582
	4.0	3.121711	4.6	0.996578	6.7	0.845315	8.9	0.607539
	4.5	3.553313	4.7	0.970427	7.0	0.919161	9.3	0.702685
	5.0	3.985642	4.7	0.923359	7.1	0.967701	9.5	0.786460
0.45	2.3	1.859907	3.5	0.861853	4.6	0.523169	5.5	0.320938
	3.0	2.191350	3.9	0.929727	5.5	0.612178	6.8	0.388939
	3.5	2.493922	4.2	0.973391	6.0	0.695539	7.7	0.458695
	4.0	2.845339	4.5	0.996920	6.5	0.784828	8.5	0.542585
	4.5	3.236339	4.6	0.992372	6.8	0.867485	9.0	0.633722
	5.0	3.627302	4.7	0.963599	7.0	0.929320	9.3	0.717923

Table 5 (b):Results for optimum coupling efficiency for a series of CCPCFs with different air filling ratio d/Λ and hole-pitch or lattice-constant Λ via QIML with different focal lengths *L*, following Reference [24], at operating wavelength $\lambda = 1.3\mu m$. (*P* indicates structure parameter, w_{eff} indicates fiber spot size and η_0 indicates coupling coefficient without misalignment)

$d' = 6.0\ \mu m, \mu = 1.55$

d/Λ	Λ (μm)	w_{eff} (μm)	$L = 8.19\mu m$		$L = 12.1875\mu m$		$L = 16.19\mu m$	
			P(μm)	η_0	P(μm)	η_0	P(μm)	η_0
0.35	2.3	2.475538	4.4	0.946862	5.9	0.714602	7.2	0.510379
	3.0	2.744393	4.6	0.979414	6.2	0.783506	7.8	0.577949
	3.5	3.071572	4.8	0.997517	6.5	0.855865	8.2	0.657715
	4.0	3.482297	4.9	0.991492	6.7	0.925266	8.6	0.749187
	4.5	3.957274	5.0	0.956133	6.9	0.975480	8.8	0.838185
	5.0	4.433909	5.0	0.902107	7.0	0.996879	9.0	0.906903
0.40	2.3	2.106083	4.0	0.876610	5.1	0.612378	6.1	0.419925
	3.0	2.422810	4.4	0.938650	5.8	0.700368	7.1	0.497149
	3.5	2.740655	4.6	0.979088	6.2	0.782605	7.8	0.577010
	4.0	3.121711	4.8	0.998321	6.6	0.865542	8.3	0.669481
	4.5	3.553313	4.9	0.987759	6.8	0.934756	8.6	0.763719
	5.0	3.985642	5.0	0.953331	6.9	0.977530	8.8	0.842846
0.45	2.3	1.859907	3.6	0.818513	4.5	0.546070	5.2	0.365880
	3.0	2.191350	4.1	0.895095	5.3	0.636190	6.4	0.440147
	3.5	2.493922	4.5	0.949598	5.9	0.719555	7.3	0.514993
	4.0	2.845339	4.7	0.987520	6.3	0.807316	7.9	0.603014
	4.5	3.236339	4.9	0.998334	6.6	0.886680	8.4	0.695812
	5.0	3.627302	4.9	0.983145	6.8	0.943965	8.7	0.778419

Table 6(a):Results for optimum coupling efficiency for a series of CCPCFs with different air filling ratio d/Λ and hole-pitch or lattice-constant Λ via QIML with different focal lengths *L*, following Reference [23], at operating wavelength $\lambda = 1.5\mu m$. (*P* indicates structure parameter, w_{eff} indicates fiber spot size and η_0 indicates coupling coefficient without misalignment)

$d^{/}$ = 6.0 μm, μ = 1.55

d/Λ	Λ (μm)	w_{eff} (μm)	L = 7.6 μm		L = 12.6 μm		L = 17.6 μm	
			P(μm)	η_0	P(μm)	η_0	P(μm)	η_0
0.35	2.3	2.805033	3.9	0.847159	6.0	0.482761	7.9	0. 286801
	3.0	2.969228	4.0	0.880081	6.2	0.519201	8.2	0.312642
	3.5	3.256532	4.1	0.927812	6.4	0.582515	8.6	0.359583
	4.0	3.628935	4.2	0.970748	6.6	0.661208	9.0	0.422344
	4.5	4.058139	4.2	0.995378	6.8	0.743838	9.2	0.495324
	5.0	4.490145	4.3	0.998423	6.8	0.816096	9.4	0.567315
0.40	2.3	2.310718	3.6	0.729077	5.2	0.376696	6.5	0.215833
	3.0	2.573870	3.8	0.795021	5.7	0.432000	7.3	0.252122
	3.5	2.869064	4.0	0.860238	6.1	0.496944	8.0	0.296780
	4.0	3.225618	4.1	0.923267	6.4	0.575772	8.6	0.354433
	4.5	3.625593	4.2	0.970448	6.6	0.660528	9.0	0.421773
	5.0	4.026105	4.2	0.994422	6.7	0.738035	9.2	0.489914
0.45	2.3	1.999448	3.2	0.649134	4.4	0.318155	5.4	0.179004
	3.0	2.301137	3.6	0.726516	5.2	0.374748	6.5	0.214600
	3.5	2.589569	3.8	0.798786	5.7	0.435414	7.4	0.254402
	4.0	2.924104	4.0	0.871401	6.1	0.509179	8.1	0.305460
	4.5	3.292278	4.1	0.932844	6.4	0.590240	8.6	0.365529
	5.0	3.660019	4.2	0.973449	6.6	0.667503	9.0	0.427649

Table 6 (b): Results for optimum coupling efficiency for a series of CCPCFs with different air filling ratio d/Λ and hole-pitch or lattice-constant Λ via QIML with different focal lengths *L*, following Reference [24], at operating wavelength $\lambda = 1.5\mu m$. (*P* indicates structure parameter, w_{eff} indicates fiber spot size and η_0 indicates coupling coefficient without misalignment)

$d' = 6.0\ \mu m$, $\mu = 1.55$

d/Λ	Λ (μm)	w_{eff} (μm)	$L = 8.19\mu m$		$L = 12.1875\mu m$		$L = 16.19\mu m$	
			P(μm)	η_0	P(μm)	η_0	P(μm)	η_0
0.35	2.3	2.805033	4.2	0.797345	5.8	0.505784	7.4	0.329184
	3.0	2.969228	4.3	0.833296	6.0	0.543075	7.6	0.357866
	3.5	3.256532	4.4	0.888228	6.2	0.607330	8.0	0.409503
	4.0	3.628935	4.5	0.942324	6.4	0.686441	8.3	0.477593
	4.5	4.058139	4.5	0.981306	6.5	0.768302	8.5	0.555204
	5.0	4.490145	4.6	0.998355	6.6	0.838702	8.7	0.630064
0.40	2.3	2.310718	3.8	0.673935	5.1	0.396536	6.2	0.249560
	3.0	2.573870	4.0	0.741737	5.5	0.453667	6.9	0.290436
	3.5	2.869064	4.2	0.811804	5.9	0.520353	7.5	0.340278
	4.0	3.225618	4.4	0.882767	6.2	0.600533	8.0	0.403865
	4.5	3.625593	4.5	0.941915	6.4	0.685762	8.3	0.476982
	5.0	4.026105	4.5	0.979275	6.5	0.762638	8.5	0.549516
0.45	2.3	1.999448	3.4	0.593903	4.4	0.335743	5.2	0.207711
	3.0	2.301137	3.8	0.671365	5.1	0.394499	6.2	0.248144
	3.5	2.589569	4.0	0.745581	5.6	0.457139	6.9	0.292993
	4.0	2.924104	4.2	0.823603	6.0	0.532787	7.6	0.349901
	4.5	3.292278	4.4	0.894339	6.2	0.615107	8.0	0.416003
	5.0	3.660019	4.5	0.946045	6.4	0.692720	8.3	0.483264

Table 7: Comparative results for optimum coupling coefficient η_0 and coupling loss CL_0 for CCPCFs with different air filling ratio d/Λ and hole-pitch or lattice-constant Λ excited with LD #1 and LD #2 for different focal lengths *L*. (*P* indicates structure parameter, and w_{eff} indicates fiber spot size)

$d' = 6.0\ \mu m$, $\mu = 1.55$

$\lambda = 1.3\ \mu m$						$\lambda = 1.5\ \mu m$				
L (μm)	d/Λ	Λ (μm)	w_{eff} (μm)	P (μm)	η_0 and CL_0 (dB)	d/Λ	Λ (μm)	w_{eff} (μm)	P (μm)	η_0 and CL_0 (dB)
7.6	0.35	3.5	3.071572	4.6	0.997630 0.0115	0.35	5.0	4.490145	4.3	0.998423 0.0068
8.19	0.45	4.5	3.236339	4.9	0.998334 0.0072	0.35	5.0	4.490145	4.6	0.998355 0.0071
12.1875	0.35	5.0	4.433909	7.0	0.996879 0.0136	0.35	5.0	4.490145	6.6	0.838702 0.7639
12.6	0.35	5.0	4.433909	7.2	0.993311 0.0291	0.35	5.0	4.490145	6.8	0.816096 0.8826
16.19	0.35	5.0	4.433909	9.0	0.906903 0.4244	0.35	5.0	4.490145	8.7	0.630064 2.0061
17.6	0.35	5.0	4.433909	9.7	0.858528 0.6624	0.35	5.0	4.490145	9.4	0.567315 2.4617

PRAJÑĀ - **Journal of Pure and Applied Sciences Vol. 24 – 25 : 78 – 83 (2017)**
ISSN 0975 - 2595

STRUCTURAL, OPTICAL, ELECTRICAL AND THERMAL PROPERTIES OF InP CRYSTALS

M. P. DESHPANDE[1], HITESHKUMAR R. BHOI[2], KIRAN N. PATEL, PIYUSH RAJPUT, KRISHNABEN CHAUHAN,

S. H. CHAKI AND ANKUR J. KHIMANI

Department of Physics, Sardar Patel University, Vallabh Vidyanagar, Anand, 38120 Gujarat, India.

Email: vishwadeshpande@yahoo.co.in[1], bhoihitesh92@live.com[2]

ABSTRACT

The structural, optical, electrical and thermal properties of as grown Indium Phosphide crystals (InP) are investigated in this present work. The crystals provided to us were grown by Liquid Encapsulated Czochralski (LEC) method. We have used this crystal to characterize and study the various properties of it. The EDAX spectra showed the purity of given crystals. The structural parameters are calculated from the Powder X-ray Diffractogram (XRD). The band gap of crystal was determined from UV-VIS-NIR spectra. Raman spectra was obtained in the temperature range 80K to 300K from which Gruneisen parameter and isobaric Raman shift were calculated. Resistivity showed the semiconducting nature of InP crystals and we measured thermal conductivity at 80°C temperature. Hall-effect measurement and Thermoelectric power measurements showed the n-type nature of this crystal.

Keywords: InP Crystal, Raman spectroscopy, isobaric Raman shift

1. INTRODUCTION

InP is an important material due to its excellent optical properties. Therefore, the study of InP crystals is very significant. InP is III-V compound semiconductor with n-type behavior. InP has a face centered cubic "Zinc blende" structure. InP has been extensively investigated recently for various scientific and technological aspects and to excess new class of fundamental material for high speed semiconductor technology. InP is a key material for opto-electronics and finds application in different optical and microwave devices. InP as a substrate material provides good thermal stability and crystal perfection in semiconductor technology **[1]**.

In the present article, we report the structural, optical, electrical and thermal properties of InP crystals by various characterization techniques.

2. METHODOLOGY

We have used here InP crystals grown by Liquid Encapsulated Czochralski (LEC) method provided to us by other worker.

3. OBSERVATIONS

The elemental composition of given InP samples was determined by energy dispersive analysis of X-rays (EDAX) attached with Philips EM400 electron microscope. X-ray diffraction pattern of powdered InP crystal was recorded on Rigaku X-ray diffractometer with CuK_α radiation (λ=1.5418 Å). Energy gap of InP crystal was measured by UV-VIS-NIR Perkin Elmer Lambda 19 (Range: 180-3200 nm) spectrometer. Room temperature Raman spectra is obtained with the help of Jobin Yvon Horibra LABRAM-HR visible (400 – 1100 nm) with diode laser (473nm, 25mW) as an excitation source. Low temperature Raman spectra of InP crystals was also obtained with the same instrument in the temperature range (80 K – 260 K). For variable temperature measurement there is a LINKAM THMS 600 heating and cooling microscope stage, which allows for the micro-Raman measurement to be performed within 77K to 900K temperature range.

Temperature dependent resistivity of sample is measured with increasing temperature. The sample is sandwiched between two holders having resistance measuring probe. The sample thickness and surface area are measured in prior to the experiment performed then the value of resistivity is determined. The resistance of the sample is measured directly with RISH multi 12S unit, the sample assembly is inserted into the

furnace and measurements are recorded at a difference of 5°C.

The thermal conductivity of the crystal was measured by the simplest method known as divided bar method **[2]**. The temperature of the furnace is controlled with dimmerstat. In this method a thin crystal plate whose thermal conductivity is to be measured is sandwiched between two metal rods. The cross section of crystal was of same size of that metal sample holder. The heat is provided from the one end of metal rod passing through the crystal and finally out from the second metal rod. Conditions are controlled so that a steady state is reached.

For Hall-effect measurement the experiment was performed using Hall-effect setup, electrical contacts are taken by silver paste and connected to Hall probe. The results were measured keeping constant magnetic field of 1000 gauss and 1500 gauss, then varying the probe current, Hall voltages are measured.

The Seebeck coefficient, also known as the thermoelectric power or thermo-power, is usually measured by a dc or ac technique **[3]**. Here, we have discussed dc technique which is one of the simplest transport measurements. It requires a thermal gradient to be established along a sample and measuring both the thermoelectric voltage and the temperature difference between two points along the length of the sample. The Seebeck coefficient is then simply obtained by simple relation.

4. RESULTS AND DISCUSSION

4.1 Elemental analysis

EDAX analysis: It is evident from EDAX spectra that no elemental peaks other than In and P were observed indicating purity of grown crystals as shown in **figure 4.1**

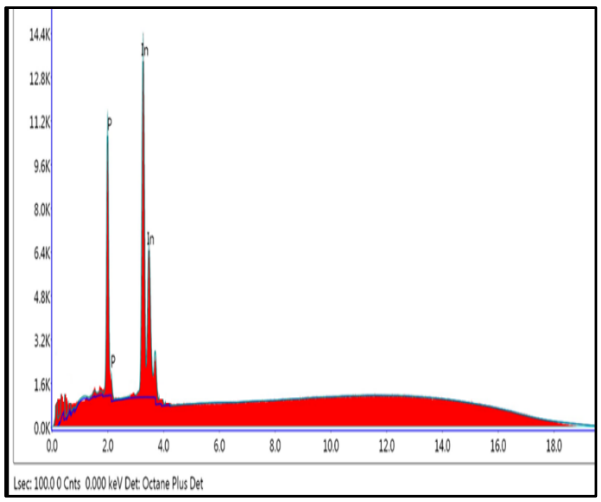

Figure 4.1 EDAX spectra of InP crystal

The weight percentage of In and P comes out as 48.30 and 51.70 respectively which matches with reported value [4].

4.2 Structural property

X-ray diffraction (XRD) study: The X-ray diffractogram is shown in **figure 4 .2.**

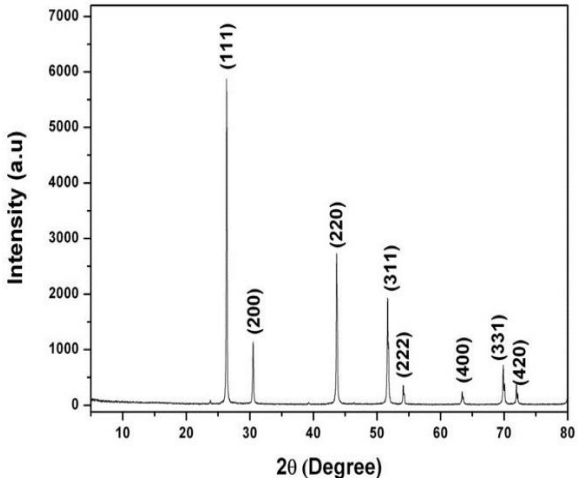

Figure 4.2 X-ray Diffractogram

The peak appearing at 2θ = 26.36°, 30.52°, 43.66°, 51.69°, 54.16°, 63.40°, 69.86° and 71.93° are indexed as (111), (200), (220), (311), (222), (400), (331) and (420)respectively based ona Zinc blend structure of InP with B3 phase (JCPDS file no. 10-0216) [4]. The lattice parameter comes out to be 5.860Å which is very

close to reported value.Also the crystalite size of InP crystals varies from 62.45nm to 94.67nm.

4.3 Optical studies

4.3.1UV-VIS-NIR spectroscopy: The UV-VIS-NIR absorption spectra of InP crystal appears at around 840 nm. We have determined the energy band gap of InP crystals using well known Tauc relation **[5]**.

$$(\alpha h\nu)^n = \text{A } (h\nu - E_g) \qquad (1)$$

where, α is the absorption coefficient, hν is photon energy, A is absorbance, E_g is optical band gap, n is the number characterising the nature of the transition process, n=2 for the direct transition and n=1/2 for indirect transition. Hence, the optical band gap for the absorption edge can be obtained by extrapolating the linear portion of the $(\alpha h\nu)^n$Vs. hν curve to the energy axis as shown in **figure 4.3**.

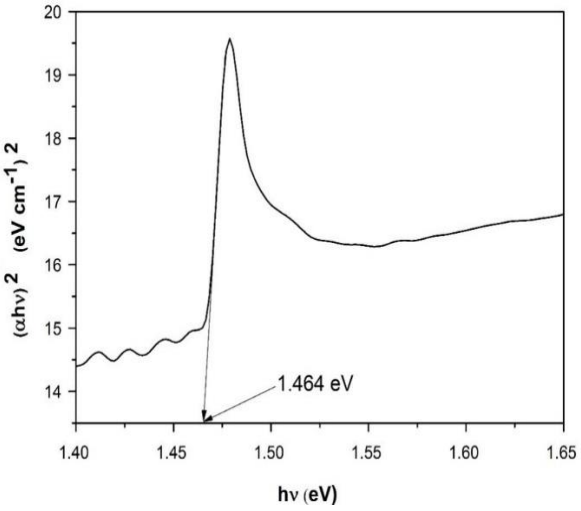

Figuer 4.3 Tauc plot of InP crystal

The band gap energy estimated from Tauc plot comes out to be 1.46 eV and matches well with the reported value 1.41 eV **[6].**

4.3.2 Raman Spectroscopy: Results from Raman spectroscopy shows presence of TO mode at 300.2$cm^{-1}$and LO mode at 339.1 cm^{-1}at room temperature **[7]**. Further, the measurement at liquid nitrogen (80 K) temperature shows TO at 306.81 cm^{-1} and LO at 344.87 cm^{-1}**[8,9]**.

Low temperature Raman spectra of InP was also studied in the temperature range (80 K – 260 K). Raman peak are found to increase with decrease in temperature. Furthermore, in these temperature range line width are continuous and gradual down to 80 K. The plot of intensity Vs Raman shift is displayed in the **figure 4.4** at different temperatures. It can be seen that as temperature decreases the Raman peak for both TO and LO mode becomes sharper and shifts towards right hand side. The change in Raman spectra in this temperature range are related to change in strength of bond due to the temperature induced lattice volume expansion. The temperature dependent Raman shift in peaks shows thermal expansion and anharmonic interaction between the phonon modes.

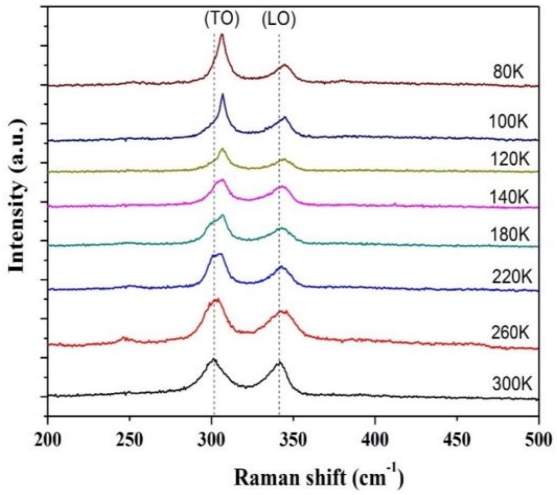

Figure 4.4 Stack plot for Raman shift

From above low temperature study of Raman shift we can determine the isobaric mode Grüneisen parameter. The Grüneisen parameter describes the effect on vibrational property of material on changing the volume, these volume changes may be a consequence of pressure or temperature change. The relation is given below for constant pressure.

$$\gamma_{i\,P} = -\frac{1}{\alpha\,\omega_i}\left(\frac{d\omega_i}{dT}\right)_P \qquad (2)$$

where, α is thermal expansion coefficient,
P for constant pressure. $\omega_i$is room temperature Raman shift.

From these results the Grüneisen parameter comes out to be 1.05 for TO mode and 1.15 for LO mode as shown in **figure 4.5**

This temperature dependence can be understood in terms of anharmonic character of lattice. Literature shows that Grüneisen parameter closely follows the behavior of thermal expansion coefficient α. From the value of slope and linear thermal expansion coefficient α taken from the reported value 5×10^{-6}/deg. and results are in good agreement with the reported value 1.44 ± 0.2 for TO mode and 1.24±0.2 for LO mode [**10]**.

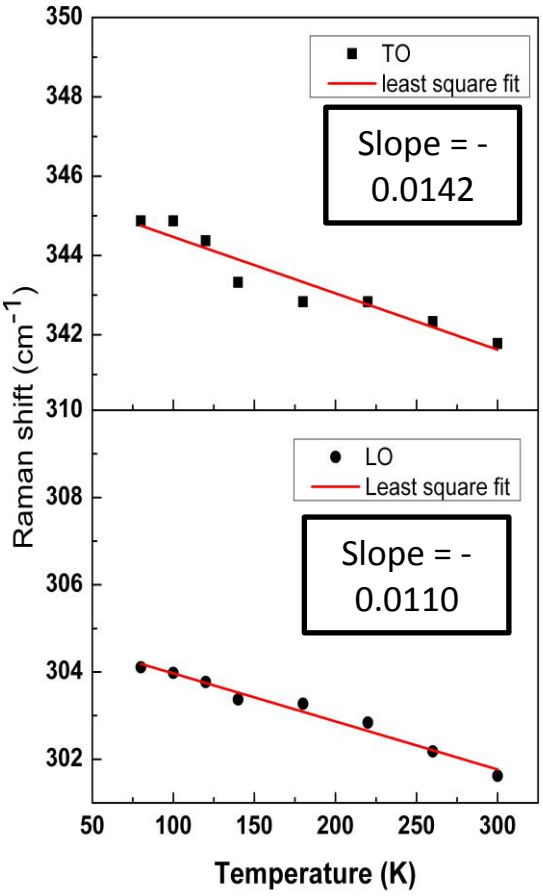

Figure 4.5 Raman shift Vs. temperature

4.4 Electrical properties

4.4.1 Resistivity: The resistivity of InP crystal was measured with increasing temperature from room temperature to 500 C°. From the measured value of resistance R, thickness of the sample L and area A, we determined the resistivity ρ given as **[11]**.

$$\rho = R\frac{A}{L} \qquad (3)$$

The area of the sample is measured approximately as 0.4 cm^2.

From the plot of resistivity vs. temperature as given in **figure 4.6**, it can be seen that resistivity decreases as the temperature increases showing semiconducting behavior of the crystal.

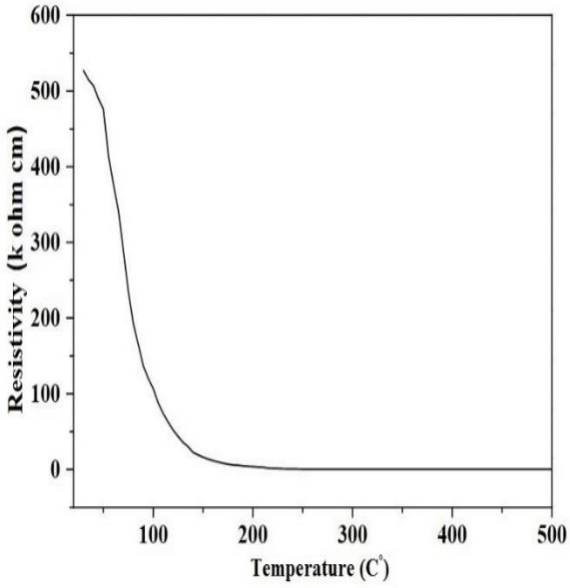

Figure 4.6 Plot of Resistivity vs. Temperature

We measure the room temperature resistivity as 5.2× 10^5 Ω cm which is found little less

compared to the reported value 1.0× $10^7\Omega$ cm **[12]**.

4.4.2 Hall-effect measurement: The results were measured keeping constant magnetic field 1000 gauss and 1500 gauss, then varying the probe current, Hall voltages are measured. The value of carrier concentration comes out to be $3.2\times10^{14}cm^{-3}$ and InP crystals shows n-type behavior **[13]**.

4.4.3 Seebeck Coefficient: The Seebeck coefficient measured with increasing temperature is shown in **figure 4.**7. From the slope of the ΔV vs. ΔT the Seebeck coefficient obtained and comes out to be
S = -232 μV/°C.

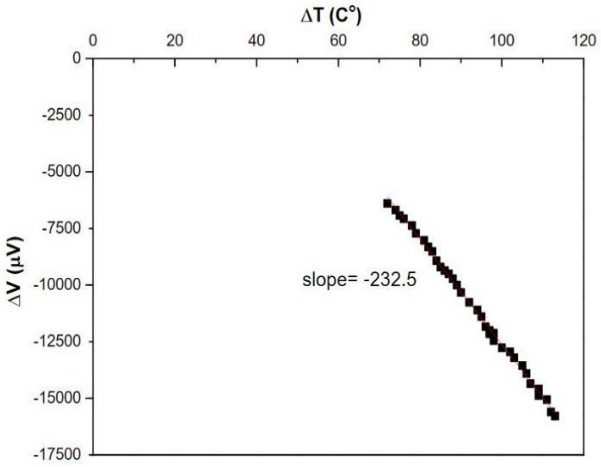

Figure 4.7 Plot of ΔV vs. ΔT

This value is almost half from the reported value of -594 μV/°C **[14]**.

4.5 Thermal Property

4.5.1 Thermal conductivity: Thermal conductivity of InP crystal was measured by divided bar method**.** It is better to choose the voltage such that the ambient temperature is about 80°C.Temperatures of four thermocouples are read of periodically until two or three successive readings do not show any change indicating steady state conditions. The crystal thickness and the distances of the thermocouples from the lower end and the gradient are calculated. The coefficient of thermal conductivity for the crystal is then calculated as 0.63 W/cm °C and matches well with the reported results at 300K **[15]**.

4.6 CONCLUSION

Grown single crystal of InP by LEC method was used in present work. EDAX analysis confirms the purity of grown InP crystal.
The X-ray diffraction confirmed that the InP crystal has Zinc blende face centered cubic structure. The XRD pattern was well indexed and the calculated lattice parameter comes out to be 5.860 Å, which is in good agreement with the reported literature and JCPDS card. The absorption spectra show significant absorption peak at 840 nm with band gap equal to 1.46 eV. The Raman spectra shows presence of TO mode at 300.2 $cm^{-1}$and LO mode at 339.1cm^{-1}at room temperature. Further, the measurement at liquid nitrogen (80 K) temperature shows TO at 306.81 cm^{-1} and LO at 344.87 cm^{-1}.The room temperature resistivity comes out to be 5.2×10^5 Ω cm and as the temperature increases resistivity decreases.

The calculated thermal conductivity of InP crystals comes out to be K_c = 0.63 W/cm °C at 353K.Hall Effect measurement shows carrier concentration in InP crystal as n = $3.2\times10^{14}cm^{-3}$. Seebeck coefficient determined is S = -232.5 μV/°C. Both these results show n-type nature of the InP crystal.

ACKNOWLEDGEMENTS

We are thankful to SICART (Sophisticated Instrumentation Centre for Applied Research and Technology) for EDAX and UV-VIS-NIR characterization of our sample. We are also Thankful to Dr. Vasant Sathe from IUC- DAE, Indore for helping in characterizing my samples by Raman spectroscopy at low temperature.

REFERENCES

[1] Fang, D., Wang, X., Xu, Y. and Tan, L. (2006) Growth and properties of InP single crystals. J. of crystal growth, **66:** 327-332.

[2] D Srideshmukhand, D. and Subhadra, K. Thermal conductivity of solids. Experiments in solid state physics. pp. 74-80.

[3] Chen, F.,Cooley, J., Hults, W. and Smith, J. (2001) Low frequency AC measurement of the Seebeck coefficient. Review of scientific instruments, **72:** 4201-4206.

[4] Ramamoorthy, K., Sanjeevirajaa, C., Jayachandran, M., Sankaranarayanan, K., Bhattacharya, P., Kukreja, L. (2001) Preparation and characterization of ZnO thin films on InP by laser-molecular beam epitaxy technique for solar cells. J. of crystal growth **226:** 281-286.

[5] Deshpande, M., Patel, K. N., Gujarati, V., Patel, K., Chaki, S. Structural, thermal and optical properties of Nickel Oxide (NiO) Nanoparticles Synthesized by Chemical Precipitation Method (2016) Advanced Materials Research 1141: 65-71.

[6] Helm, U., Roder, O., Queisser H. and Pilkuhn, M. **(**1970) Photoluminescence of InP. J. of Luminescence **1-2:** 542-551.

[7] Mooradian, A. and Wright, G., (1966) First order Raman effect in III-V compound. Solid State Communi. **4:** 4-434.

[8] Pinczuk, A., Ballman, A., Nahory, R., M. A. Pollack, M., and Worlock., J., (1979) Raman scattering studies of surface charge layers and Schottky barrier formulation in InP. J. of Vacuum Science & Technology **16:** 1168.

[9] Hinrichs, K., Schierhorn, A., Haier, P., Esser, N., Richter, W., and Sahm, J. (1997) Phys. Rev. Lett. **79:**961.

[10] Soma, T., Satoh, J. and Matsuo, H., (1982) Thermal expansion coefficient of GaAs and InP. Solid State Communi. **12:** 889-892.

[11] Zhenhua, Z. and Ctirad, U. (2005) Apparatus for Seebeck coefficient and electrical resistivity measurements of bulk thermoelectric materials at high temperature. Rev. of scientific instruments **76:** 023901.

[12] Kainosho, K., Shimakura, H., Yamamoto, H. And Oda, O. (1991) Undoped semi insulating InP by high pressure annealing. Appl. Phys. Lett. **59:** 932.

[13] Leloup, J., Djerassi, H. and Albany J. Jordan, (1978) Hall effect in n-type InP crystals: Thermal activation. Energy and influence of compensation. J. Appl. Phys **49:** 3359-3362

[14] Kudman, I. and Steigmeier, E. (1964) Thermal conductivity and Seebeck coefficient of InP. Phys. Rev. Lett. **133**: A1666.

[15] Jordan A. (1985) Some thermal and mechanical properties of InP essential to crystal modeling. J. of crystal growth **71:** 559-565.

PRAJÑĀ - **Journal of Pure and Applied Sciences Vol. 24 – 25 : 84 – 86 (2017)**
ISSN 0975 - 2595

PHONONS IN TERNARY METALLIC GLASS Cu-Ti-Zr

S.G. KHAMBHOLJA[1]* AND B.Y. THAKORE[2]
[1]Department of Science & Humanities, B & B Institute of Technology, Vallabh Vidyanagar, 388120, Gujarat, India
[2]Department of Physics, Sardar Patel University, Vallabh Vidyanagar, 388120, Gujarat, India
* Corresponding author: physik.shyam@gmail.com

ABSTRACT

In the present paper, results of our theoretical calculations of phonon frequencies and elastic constants for ternary metallic glass Cu-Ti-Zr are reported. Model potential formalism is used to compute the inter-ionic interactions. Phonon frequencies are calculated using the phenomenological approach of Hubbard and Beeby. The results are discussed in the light of experimental findings. Further, elastic constants are also estimated.

Keywords: Phonons, Ternary metallic glass, Elastic Constants.

INTRODUCTION

Synthesis of metallic glasses is challenging as metals easily crystallize upon solidification [1]. Further, bulk metallic glasses (BMGs) could also be synthesized [2]. Due to such advancement in synthesis, large amount of experimental and theoretical work on structural and elastic properties of metallic glasses is carried out by various researchers [3-12]. Copper based binary and bulk metallic glasses have shown exceptional physical properties like low mass, high strength, extraordinary plasticity etc [13]. Recently, various researchers have reported results of different physical properties of Cu-Zr based BMGs [14-16]. It is reported that the interionic interactions within hard sphere model system can be well described in terms of various forms of potentials like LJ potential, Morse potential, Dzugotov potential etc [1]. The most common feature in such potentials is that they show a first minimum at a nearest neighbor distances. Since such simple forms are insufficient to describe the interatomic interactions in metals [1], we need to use some realistic form of potential. In our recent work [5-7] we have adopted model potential formalism to describe the interatomic interactions in binary metallic glasses. Similar formulations have been used by other researchers also [15, 16]. Use of such a model potential within Wills-Harisson form is proved as reliable tool to describe the interatomic interactions in non-crystalline phase like metallic glasses, liquid metals and their alloys [5-7, 17, 18]. Recently, Han et al [10] have reported the liquid to glass transition in Cu Ti Zr glass forming system using molecular dynamics simulation. They have reported structural properties of this ternary system using Stillinger-Weber potential. However, the study of vibrational dynamics of this metallic glass is still missing and we thought it worthwhile to explore the vibrational properties of this system using a reliable theoretical tool. Thus, in the present work, we have calculated the phonon frequencies in ternary system Cu-Ti-Zr for its specific composition $Cu_{60}Ti_{20}Zr_{20}$ using model potential formalism in conjunction with phenomenological approach of Hubbard and Beeby [19]. The results are compared with experimental and other theoretical results, wherever available. The paper is organized as following. The next section deals with the theoretical formulation used to compute the interatomic interactions and phonon frequencies in ternary system. The results are discussed in section 3 and the findings are concluded in section 4.

METHODOLOGY

The effective ion-ion interaction in s-p bonded system is given as

$$V(r) = \frac{Z^2 e^2}{r} + \frac{2}{\pi}\int dq F(q)\exp(-iq\cdot r) \qquad (1)$$

In addition to above equation (1), while dealing with the transition metals, the *d band* correction is also important one [5-7]. In the present work, we have corrected the equation (1) by adding the *d band* correction terms as mentioned in [5-7]. $F(q)$ in (1) is an energy wave number characteristic. In the present study, we have considered the concept of "effective atom" to compute the dispersion curves. We have used Ashcroft's empty core model potential [20]. This model potential contains only one

parameter, the core radius. This parameter can be obtained through fitting specific quantities with the experimental ones. Instead of fitting procedure, we have calculated the core radius from the known Wigner-Seitz radius [5-7]. The exchange-correlation effects are incorporated through the forms of Ichimaru and Utsumi (IU) [21], as this form satisfy the compressibility sum rule in the long wavelength limit and can be applied to large range of densities. Along with effective pair potential, another important quantity is the pair correlation function of metallic glass. This function can be obtained through any experimental techniques or computer experiments like molecular dynamics simulation. Han et al [10] have obtained the pair correlation function of system of our interest using molecular dynamics simulation. In the present work, at this stage, we have adopted these values of Han et al [10] to compute the phonon frequencies.

Within the phenomenological approach of Hubbard and Beeby [19], the phonon frequencies are calculated using following set of equations (2) and (3);

$$\omega_l^2(q) = \omega_E^2\left[1 - \frac{3\sin(q\sigma)}{(q\sigma)} - \frac{6\cos(q\sigma)}{(q\sigma)^2} + \frac{6\sin(q\sigma)}{(q\sigma)^3}\right] \quad (2)$$

$$\omega_t^2(q) = \omega_E^2\left[1 + \frac{3\cos(q\sigma)}{(q\sigma)^2} - \frac{3\sin(q\sigma)}{(q\sigma)^3}\right] \quad (3)$$

Here, ω_E is the maximum phonon frequency and is given by following expression

$$\omega_E^2 = \frac{4\pi . n_{eff}}{3M_{eff}} \int_0^\infty g(r) r^2 V^{"}(r) dr \quad (4)$$

The $V_{eff}^{"}(r)$ in above expression (4) denotes the second order derivative of the effective pair potential and the upper limit in the integration is decided by the length of the $g(r)$ in the computation.

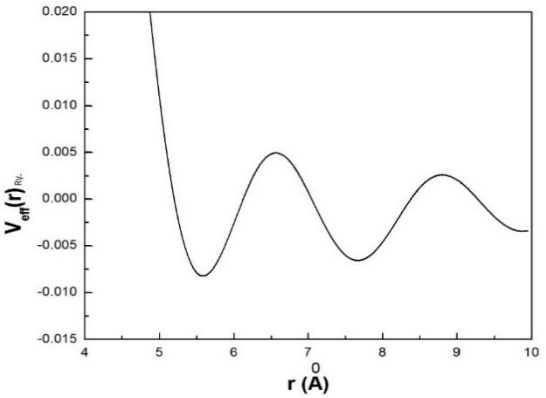

Figure 1. Effective pair potential in ternary metallic glass $Cu_{60}Ti_{20}Zr_{20}$.

The M_{eff} and n_{eff} are the effective atomic mass, effective number density respectively, and are calculated for present ternary system by weighted average over their concentration [5-6].

The M_A, M_B, n_A, n_B represents the atomic masses and number densities of the pure A and B components of the alloy respectively. Since in the long wavelength limit the phonon dispersion curves shows an elastic behavior which permit us to compute longitudinal and transverse sound velocities and other elastic constants [5-7].

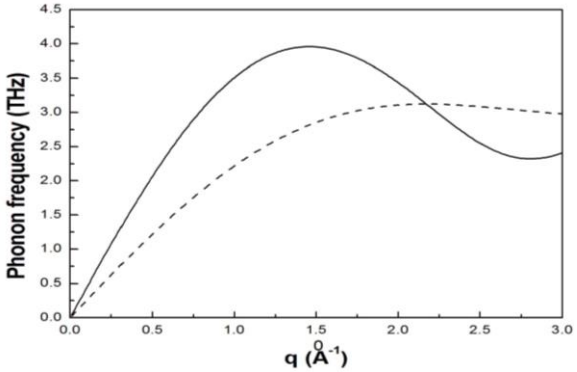

Figure 2. Longitudinal and Transverse Phonon Frequencies in $Cu_{60}Ti_{20}Zr_{20}$.

RESULTS AND DISCUSSION

In the present work, we have computed the effective pair potential using second order perturbation theory within Wills Harrison form along with *d band* correction terms. The computed pair potential is shown in Fig. 1. The existence of Friedel oscillations is clearly observed in the pair potential. The computed longitudinal and transverse phonon frequencies are shown in Fig. 2. It is seen that at large q values, momentum transfer is due to longitudinal phonons only. Transverse modes have very small role in momentum transfer as they undergo large thermal modulation. The first minimum in the longitudinal branch occurs at 2.8 $Å^{-1}$, near which the static structure factor should show principal peak. Hubbard-Beeby model considers each system as isotropic and hence it assumes the fix value of ratio of longitudinal to transverse sound velocity and hence fix value of Poisson's ratio i.e. 0.25. This is observed in our previous work [5-7]. Poisson's ratio is an important parameter in determining "*intrinsic plasticity*" of a material [1]. An et al [22] have noted that if the value of Poisson's ratio is less than 0.31, the material is brittle and its higher value is related to ductility of a material. Since, the presently used approach of Hubbard and Beeby avoids "*intrinsic plasticity*" of non-crystalline material, we can not put any concrete remark about brittleness or ductility of

Cu-Ti-Zr system. However, we can certainly say that the calculated longitudinal phonon frequency show all broad features of collective excitation in a metallic glass. From the long wavelength limit, we have calculated sound velocities of longitudinal and transverse branch and the results are 4.35 x 10^5 m/s and 2.51 x 10^5 m/s, respectively. Further, we have estimated bulk modulus of this system and the calculated value is 75.55 GPa. This value is in accordance with the hardness of metallic glass. In the study of Cu-Zr binary metallic glass also [5-7], a higher value of bulk modulus is observed, which indicates high hardness of Cu-Zr based metallic glasses.

CONCLUSION

In the present work, we have estimated the phonon frequencies and elastic constants of $Cu_{60}Ti_{20}Zr_{20}$ ternary metallic glass. This system has high hardness as observed through its bulk modulus. Modification in HB approach is required to correctly estimate the ductility and/or brittleness of a metallic glass.

ACKNOWLEDGEMENT

SGK is grateful to DAE-BRNS for Research Grant under a Major Research Project F. No. 39/14/29/2016-BRNS.

REFERENCES

[1] Cheng, Y Q., Ma, E., (2011) Atomic level structure and structure-property relationship in metallic glasses. Progress in Material Science, **56:** 379-473.

[2] Luzgin, D., Antonowicz, J., Georgarakis, K., Vaughan, G., Yavari. A., and Inoue, A., (2008) Real space structural studies of Cu-Ti-Zr glassy alloys. J. Alloys and Compounds, **466**: 106-110.

[3] Tian, L., Cheng, Y., Shan, Z., Li, J., Wang, C., Han, X., Sun, J., and Ma, E., (2012) Approaching ideal elastic limit of metallic glasses. Nature Communications, DOI: 10.1038/ncomms1619.

[4] Inoue, A., Zhang, W., Zhang, T., and Kurosaka, K., (2001) High- strength Cu-based bulk glassy alloys in Cu–Zr–Ti and Cu–Hf–Ti ternary systems. Acta Mater., **49:** 2645-2652.

[5] Khambholja, S.G., Thakore, B.Y., Gajjar, P.N., Bhatt, N.K., Jani, A.R., (2014) Theoretical study of collective dynamics in Cu50Zr50 metallic glass, Narosa, New Delhi, Vol. 01, pp 83-85.

[6] Khambholja, S.G., Thakore, B.Y., Jani, A.R., (2016) Phonons in binary metallic glass Cu-Zr. Advanced Material Research, **1141:** 162-165.

[7] Khambholja, S.G., Ladva, A.L., and Thakore, B.Y., (2016) Phonons in binary glass Cu65Zr35. AIP Conf. Proc. **1728:** 020202(1)-020202(7).

[8] Patel, A.T., and Pratap, A., (2012) Study of kinetics of glass transitions of metallic glasses. J. Thermal Analysis and Calorimetry, **110:** 8-12.

[9] Agrawal, P.C., (2005) Phonon dispersion in ternary metallic glass Pd-Si-Cu. Mat. Sci. & Engg. A, **404:** 301-304.

[10] Han, X., and Teichler, H., (2007) Liquid-to-Glass transition in bulk-glass forming $Cu_{60}Ti_{20}Zr_{20}$ alloy by molecular dynamics simulation. Phys. Rev. E, **75**: 061561-061567.

[11] Nakashima, S., Kawatika, T., Otomo, T., Suenaga, R., Baron, A., Tusutsui, S., Kohara, S., Takeda, S., Itoh, K., Kato, H., Fukunaga T., and Hasegawa, M., (2007) Phonon dispersion in metallic glass $CuZr_2$ J. Phys. C **92:** 012136-012139.

[12] Ward, L., Agrawal, A., Flores, K., and Windi, W., Rapid production of accurate embedded atom method potentials for metal alloys arxiv preprint 1209.0619.

[13] Mattern, N., Schops, A., Kuhn, U., Acker, J., Khvostikova, O., and Eckert, (2008) J., Structural behavior of Cu_xZr_{100-x} metallic glass J. Non Cryst. Solids, **354:** 1054-1060.

[14] Mei Bo, T., Qian, Z., Xiang, P., Hua, W., (2004) Bulk metallic glass formation near a quaternary Cu-Zr-Ti-Al eutectic point. Chins. Phys. Lett., **21:** 901-903.

[15] Saxena, N.S., Bhandari, D., Pratap, A., and Saxena, M.P., (1990) Structure and dynamics of to component metallic glass. J. Phys. C **2** 9475.

[16] Thakore, B.Y., Gajjar, P.N., and Jani, A.R., (2000) Collective modes in $Ca_{70}Mg_{30}$ metallic glass. Bull. Mat. Science, **23:** 5-8.

[17] Thakore, B.Y., Khambholja, S.G., Suthar, P.H., Bhatt, N.K., and Jani, A.R., (2010) Collective modes and elastic constants of liquid $Al_{83}Cu_{17}$ binary alloys. Chin. Phys. Lett. **27:** 096203-096206.

[18] Thakore, B.Y., Khambholja, S.G.., Joshi, M., and Jani, A.R., (2011) Phonon modes in non-crystalline Lithium, Sodium and their binary alloys. J. Opto. Elec. Adv. Mater. **13:** 400-407.

[19] Hubbard, J., and Beeby, J.L., (1968) Collective motion in liquids. J. Phys. C **2**: 556-570.

[20]Ashcroft, N.W., (1966) Electron-ion pseudopotentials in metals. Phys. Lett **23**: 48-56.

[21] Ichimaru, S., and Utsumi, K., (1981) Analytical expression for dielectric screening function of strongly coupled electron liquids at metallic and lower densities. Phys. Rev. B. **24:** 3220-3225.

[22] An, J., Yim, H., and Haein, C., (2010) Compositional dependence of thermal and elastic properties of Cu-Ti-Zr-Ni bulk metallic glass Int. J. Minerals, Metallurgy and Materials, **17**: 318-322.

PRAJÑĀ - **Journal of Pure and Applied Sciences Vol. 24 – 25 : 87 – 92 (2017)**
ISSN 0975 - 2595

INTERMOLECULAR INTERACTIONS IN MOLECULAR STRUCTURE OF 7-(4-METHOXY-PHENYL)-2,5-DIPHENYL-7H-PYRROLO[2,3-d] PYRIMIDINE-4-YL-AMINE, MONOHYDRATE: X-RAY DIFFRACTION TECHNIQUE

B. D. PATEL[1], U. H. PATEL[2] AND HARDIK JOSHIPURA[3]

[1]M. B. Patel Science College, Anand

[2]Department of Physics, Sardar Patel University, Vallabh Vidyanagar Email: u_h_patel@yahoo.com

[3]Organic Synthesis Laboratory, M. G. Science Institute, Ahmedabad

ABSTRACT

The title molecule, 7-(4-methoxy-phenyl)-2,5-diphenyl-7h-pyrrolo[2,3-d]pyrimidine-4-yl-amine monohydrate ($C_{25}H_{20}N_4O$ H_2O), a novel pyrrolo-pyrimidine derivative crystallizes in a triclinic crystal system in space group $P\bar{1}$ with two molecules per asymmetric unit with two solvent water molecules. Molecular structure is solved with good accuracy with final residual index R converged to 0.097 and goodness of fit S = 1.053. Significant number of intermolecular interactions like N-H…N, C-H…O, C-H…N, π…π and C-H…π interactions involving all possible donor and acceptor groups contribute to the molecular packing.

Keywords: Pyrrolo-pyrimidine derivative, asymmetric unit, Molecular structure, Residual index.

INTRODUCTION

Pyrrolo-pyrimidine derivatives belong to an important class of N-heterocyclic compounds possessing large biological spectrum like-Antitumor, antiallergic, antiviral, insulin releasing, carbonic anhydrase inhibitory and anti-inflammatory activities [1-6]. In continuation of our interest to work out the three dimensional structures of significant N-heterocyclic derivatives, we report here the molecular structure of 7-(4-methoxy-phenyl)-2,5-diphenyl-7h-pyrrolo[2,3-d]pyrimidine-4-yl-amine, monohydrate (HX3) and the intermolecular interactions involved therein [7-9]. The chemical structure of it, is shown in Figure: 1.

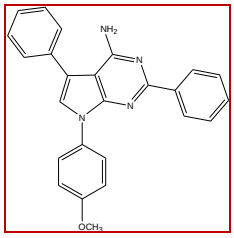

Figure: 1 The chemical structure of the title molecule

METHODOLOGY

The title compound (HX3) has been synthesized by nucleophilic displacement reaction method. Tiny brown diamond like single crystals of it have been grown by slow evaporation method in toluene. Good diffraction quality single crystals, have been picked up for intensity data collection on single crystal CAD-4 diffractometer using ω-2θ scan mode with graphite monochromated MoKα radiation (λ=0.71073 Å) at CSMCRI, Bhavnagar. . The preliminary crystallographic data along with data collection details are summarized in Table 1.

Table-1: Preliminary crystallographic data with data collection details

Chemical name	7-(4-methoxy-phenyl)-2,5-diphenyl-7h-pyrrolo[2,3-d] Pyrimidine-4-yl amine, monohydrate
Chemical formula	$C_{25}H_{20}N_4O, H_2O$
Molecular weight	408.45 amu
Crystal system	Triclinic
Space group	$P\bar{1}$
a	9.8892(23) Å
b	14.4153(34) Å
c	16.4569(38) Å
α	78.361(4)°
β	74.082(4)°
γ	78.049(5)°
Volume (V)	2180.81 $Å^3$
Z	4 (two molecules per asymmetric unit)
$\rho_{c,}$	1.244 gm/cm^3
μ	0.081 mm^{-1}
F(000)	856

The structure has been solved using Direct methods and refined by SHELX program [10] built-in within WINGX software program [11]. The final residual index R is 0.097 for 9502 reflections and 561 parameters with goodness of fit S= 1.053. The ORTEP view of the molecule drawn using PLATON software [12], indicating atomic numbering scheme with thermal ellipsoids drawn at 50% probability level is depicted in Figure: 2.

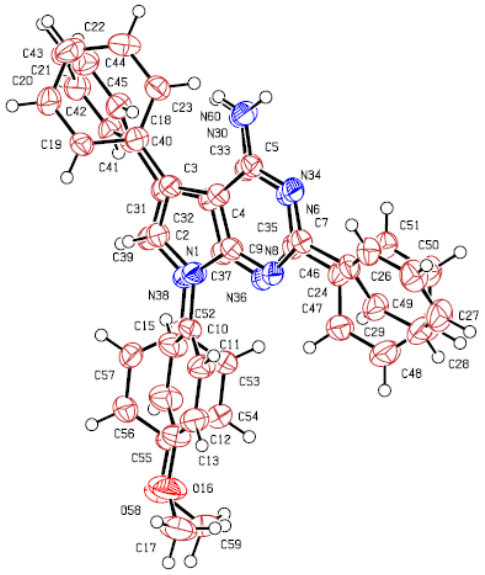

Figure: 2 The ORTEP view of the molecule with two molecules per asymmetric unit

OBSERVATIONS

The title molecule crystallizes in triclinic system with space group $P\bar{1}$ with two molecules in the asymmetric unit alongwith two molecules of solvent water. The fused ring of both the molecules in the asymmetric unit is almost superimposed to each other in the lattice with an angle between two nine membered rings is 2.92 (10)° in molecule A and 1.45(17)° in molecule B.

The selected bond lengths and bond angles involving non-hydrogen atoms are presented in Table 2. The weighted average intra ring torsional angles of the pyrrole and pyridimine rings confirmed a planar configuration of the nine membered ring system for both the molecules. The C-N bond lengths in the fused pyrimidine ring vary from 1.331(4) to 1.429(4) Å, the range of variation agrees reasonably well with literature values for similar structures [13]. The two Nsp2-C bonds: N1-C9 = 1.380(4) Å and N1-C2 = 1.381 (4) Å of the pyrrole ring (Molecule A) and those bonds N38-C37 = 1.374 (4) Å and N38-C39 = 1.376 (4) Å in molecule B, are consistent with the reported average value [14].

As normally observed in similar fused derivatives, fusion of the two rings results in significant strain leading to the opening up of the endocyclic angle C4-C9-N8 = 127.2 (3)° and N6-C7-N8 = 127.2(3)° in molecule A and C32-C37-N36 = 127.0 (3)° and N34-C35-N36 = 126.9(3)° in molecule B respectively [15]. The effect is also observed in the exocyclic angles C3-C4-C5 = 138.1(3)° and N1-C9-N8 = 124.4(3)° of molecule A and C31-C32-C33 = 138.1(3)° and N38-C37-N36 = 125.0(3)° in molecule B of the fused ring system. Molecular dimensions of benzyl phenyl and the methoxy phenyl ring of both the molecules A and B are normal.

Table-2: Bond lengths (Å) and Bond Angles ( )° involving non-hydrogen atoms with estimated standard deviation in parentheses

Molecule A		Molecule B	
N1 - C2	1.381(4)	N34 - C35	1.344(4)
N1 - C9	1.380(4)	N34 - C33	1.349(4)
N1 - C10	1.429(4)	N36 - C37	1.334(4)
N6 - C5	1.349(4)	N36 - C35	1.331(4)
N6 - C7	1.334(4)	N38 - C39	1.376(4)
N8 - C7	1.333(4)	N38 - C37	1.374(4)
N8 - C9	1.331(4)	N38 - C52	1.427(4)
O16 - C13	1.379(4)	O58 - C59	1.403(5)
O16 - C17	1.422(6)	O58 - C55	1.361(4)
N30 - C5	1.342(4)	N60 - C33	1.340(4)

C2-N1- C9	107.6(2)	N60-C33-C32	122.2(3)
C2-N1-C10	124.9(3)	N34-C35-N36	126.9(3)
C9-N1-C10	127.3(3)	C35-N36-C37	113.3(3)
C5-N6-C7	118.6(3)	C37-N38-C39	107.7(3)
C7-N8-C9	112.8(3)	C37-N38-C52	126.9(3)
		C39-N38-C52	125.1(3)

RESULTS AND DISCUSSION

Table: 3. Dihedral angles between various least-square planes

Plane	Plane	Angle ( )˚
1.(N_1 - C_2 - C_3 - C_4 - C_9)	2.(C_4 - C_5 - N_6 - C_7 - N_8 - C_9)	3.0(1)
6 (N_1- C_2 - C_3 - C_4 – C_5 - N_6 – C_7 - N_8 – N_9)	5 (C_{24} - C_{25} - C_{26} - C_{27} - C_{28} - C_{29})	33.8(1)
6 (N_1- C_2 - C_3 - C_4 – C_5 - N_6 – C_7 - N_8 – N_9)	4 (C_{18} - C_{19} - C_{20} – C_{21} - C_{22} - C_{23})	42.9(1)
6 (N_1- C_2 - C_3 - C_4 – C_5 - N_6 – C_7 - N_8 – N_9)	3 (C_{10} - C_{11} - C_{12} - C_{13} - C_{14} - C_{15})	38.7(1)
7 (C_{31} - C_{32} - C_{37} - N_{38} - C_{39})	8 (C_{32} - C_{33} - N_{34} - C_{35} - N_{36} - C_{37})	1.5(1)
12 (C_{31} - C_{32} - C_{33} - N_{34} - C_{35} - N_{36} - C_{37} - N_{38} - C_{39})	11 (C_{52} - C_{53} - C_{54} - C_{55} - C_{56} - C_{57})	41.3(1)
12 (C_{31} - C_{32} - C_{33} - N_{34} - C_{35} - N_{36} - C_{37} - N_{38} - C_{39})	10 (C_{46} - C_{47} - C_{48} - C_{49} - C_{50} - C_{51})	23.27(11)
12 (C_{31} - C_{32} - C_{33} - N_{34} - C_{35} - N_{36} - C_{37} - N_{38} - C_{39})	9 (C_{40} - C_{41} - C_{42} - C_{43} - C_{44} - C_{45})	42.35(08)

All the three phenyl rings of respective molecules are coplanar within themselves (the maximum deviation of the atoms from the respective least-square planes is 0.019(3) Å for benzyl ring 0.008(3) Å for (C10...C15) ring and -0.011(3) Å for (C18-C23) ring). The fused ring system of pyrrole and pyrimidine ring of molecule A is almost planar with dihedral angle of 2.92(17)° and that in molecule B is 1.45(17)°, further confirming the planarity of the fused ring system. The benzyl ring plane (C18….C23) of molecule A and the phenyl ring (C40….C45) of molecule B are almost perpendicular to each other, with dihedral angle of 83.44(11)˚,

The methyl phenyl ring plane of molecule A is oriented at 78.77(17)˚ to that of molecule B whereas the phenyl ring plane C_{24} - C_{25} - C_{26} - C_{27} - C_{28} - C_{29} of molecule A lies almost parallel to C_{46} - C_{47} - C_{48} - C_{49} - C_{50} - C_{51} of molecule B with dihedral angle 20.69(18)˚. The torsional angles defining molecular conformation are:

C_9-N_1-C_{10}-C_{15}	-145.4(3)	N_{36}-C_{35}-C_{46}-C_{47}	-21.7(4)
C_2-N_1-C_{10}-C_{11}	-137.2(3)	C_{39}-C_{31}-C_{40}-C_{45}	135.4(3)
C_{37}-C_{32}-C_{33}-N_{34}	-2.6(4)	C_4-C_3-C_{18}-C_{23}	45.5(5)

Crystal Packing

The supramolecular structure is mainly stabilized by N-H…N, C-H…N and C-H…O interactions (Figure: 3) along with direction specific π…π (Figure: 4) and C-H…π interactions (Figure: 5). About half a dozen significant C-H…π interactions involving different moieties contributing to the crystal packing. All these C-H…π interactions are of type III as per the Malone et al, [16] which is the most favourable type of interaction for organic molecule except the C_{22}-H_{22}…Cg_5 interaction which is of type II. The details of these interactions are tabulated in Table 4.

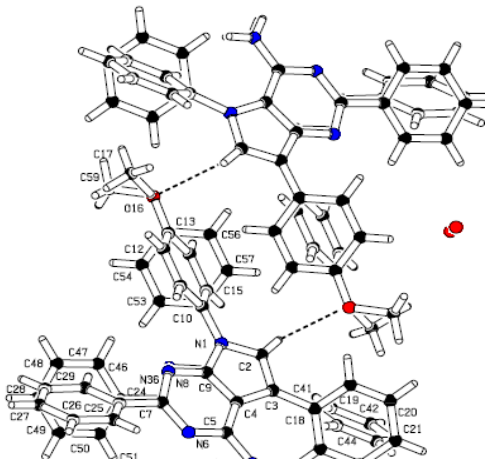

Figure-3: C-H…O interactions in the molecules

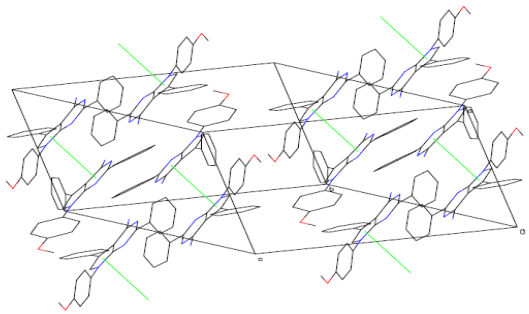

Figure-4: π-π interactions shown with green lines in the packing diagram of molecules

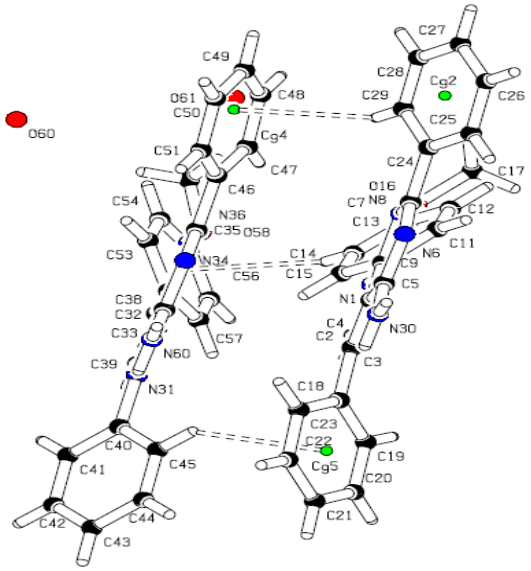

Figure-5: C-H…π interactions shown with double dash lines in the diagram of molecules

Symmetry related molecules are oriented in such a manner that it facilitates intermolecular π…π interactions and C-H….π interactions. The rare face-to-face π…π interactions with a dihedral angle of 1.72(17)°, the distance 3.916 Å between the ring centroids, the slippage distance 1.056 Å, are observed and details of it are given in Table 5. The strong conventional N-H…N interactions add its contributions in the molecular packing. Each amine nitrogen N30 and N60 acts as bifurcated donors via H31 and H601 in two strong hydrogen bond interactions with N34 and N6 respectively and also both these amine nitrogen work as accepter in other two strong interactions with N30 and N60 of symmetry related molecules respectively. There are few more C-H…O and C-H…N interactions, though weak but significant, contributing to the stability of the supramolecular structure, are tabulated in Table 6.

Supplementary Data

The .cif file of this structure has been deposited with Cambridge Crystallographic Data Center as supplementary publication no: CCDC 1572247. Copy of the data may be obtained, free of charge, on application to CCDC, 12 Union Road, Cambridge CB2 1EZ, UK.

Table-4: X-H…Cg Interactions

X-H … Cg	H…Cg (Å)	X…Cg (Å)	X-H…Cg ( )°	H⊥	Type
C_{14} – H_{14}...C g_{11}	2.95	3.706	139	2.829	III
C_{22} – H_{22}...C g_5	2.69	3.544	152	2.686	II
C_{25} – H_{25}...C g_8	2.95	3.678	136	2.845	III
C_{29} – H_{29}...C g_{10}	2.95	3.694	138	2.804	III
C_{42} – H_{42}...C g_4	2.91	3.680	141	2.824	III
C_{45} – H_{45}...C g_4	2.98	3.739	140	2.879	III
$Cg_4 = C_{18} - C_{19} - C_{20} – C_{21} - C_{22} - C_{23}$			$Cg_5 = C_{24} - C_{25} - C_{26} - C_{27} - C_{28} - C_{29}$		
$Cg_8 = C_{32} - C_{33} - N_{34} - C_{35} - N_{36} - C_{37}$			$Cg_{10} = C_{46} - C_{47} - C_{48} - C_{49} - C_{50} - C_{51}$		
$Cg_{11} = C_{52} - C_{53} - C_{54} - C_{55} - C_{56} - C_{57}$					

Table-5: π…π interactions

Cg(I) Cg (J)	Cg(I)…Cg (J) Å	Cg… P (Å)	α	γ	Δ (Å)
1 8	3.916	3.771	1.72	15.69	1.056

Table-6: Hydrogen bonding interactions

D-H…A	D-H Å	H…A (Å)	D…A (Å)	∠D-H…A ( )°
N_{30}-H_{31}-N_{34} i	0.860(2)	2.268(2)	3.113(3)	168.05(20)
N_{30}-H_{31}-N_{60} i	0.860(2)	2.933(3)	3.642(4)	141.04(20)
N_{60}-H_{601}-N_{6} i	0.860(2)	2.290(2)	3.123(3)	163.05(20)
N_{60}-H_{601}-N_{30} i	0.860(2)	2.945(3)	3.642(4)	139.86(20)
C_{51}-H_{51}-N_{30} i	0.930(3)	2.668(3)	3.430(4)	139.62(22)
C_{25}-H_{25}-N_{60} i	0.930(4)	2.700(3)	3.406(4)	133.39(22)
C_{39}-H_{39}-O_{58} ii	0.930(3)	2.949(2)	3.857(4)	165.73(22)
C_{19}-H_{19}-O_{58} ii	0.930(3)	2.889(3)	3.601(5)	134.39(20)
C_{23}-H_{23}-N_{6} iii	0.930(3)	2.990(3)	3.895(5)	164.48(21)

Equivalent points

0. x,y,z	i. -x+1,-y+1,-z	ii. -x,-y+1,-z+1
iii. -x,-y+1,-z	iv. x-1,+y,+z	v. -x-1,-y+1,-z+1

CONCLUSION

Molecular orientation of both the molecules A and B in the lattice is such that it facilitates more than dozens of modest to strong varied kind of intermolecular interactions- N-H…N, C-H…O, C-H…N, π…π and C-H…π interactions resulting in strong molecular stability.

ACKNOWLEDGEMENT

Authors are thankful to Department of Physics, Sardar Patel University, Vallabh Vidyanagar for providing lab facilities and to CSMCRI, Bhavnagar for intensity data collection of the title single crystal. BDP is also thankful to M. B. Patel Science College for giving necessary permission to carry out the research work.

REFERENCES

[1] Hutzenlaub, W., Tolman, R. L. & Robins, R. K. (1972): Azapurine nucleosides. 1. Synthesis and antitumor activity of certain 3-.beta.-D-ribofuranosyl- and 2'-deoxy-D-ribofuranosyl-v-triazolo[4,5-d]pyrimidines, *J. MED. CHEM.* **15:** 879–883.

[2] Smith, C. W., Sidwell, R. W., Robins, R. K. & Tolman, R. L. (1972): Azapurine Nucleosides.

.

2. Synthesis and Antiviral Activity of 7-Amino-3-D-Arabinofuranosyl-V-Triazolo(4,5-D) pyrimidine and Related Nucleosides, *J. Med. Chem.* **15**: 883–887.

[3] T.H. Maren, (1976): Reactions between structure and biological activity of sulfonamides, *Annu. Rev. Pharmacol. Toxicol.* **16:** 309–327.

[4] C.T. Supuran, A. Scozzafava, B.C. Jurca, M.A. Iiies, (1998): Carbonic anhydrase inhibitors-part 49: Synthesis of substituted ureido and thioureido derivatives of aromatic herterocyclic sulphonamides with increased affinities of isozyme I, *Eur. J. Med. Chem.* **33:** 83–93.

[5] J.J. Li, D. Anderson, E.G. Burton, J.N. Cogburn, J.T. Collins, D.J. Garland, S.A. Gregory, H.C. Huang, P.C. Isakson, C.M. Koboldt, E.W. Logusch, M.B. Morton, W.E. Perkins, E.J. Reinhard, K. Seibert, A.W. Veenhuizem, Y. Zang, D.B. Reitz, (1995): 1,2-Diarylcyclopentens as selective cyclooxygenase-2 inhibitors and orally active anti-inflammatory agents, *J. Med. Chem.* **38:** 4570–4578.

[6] H. Yoshino, N. Veda, J. Niijima, H. Sugumi, Y. Kotake, N. Koyanagi, K. Yoshimatsu, M. Asada, T. Watanabe, T. Nagasu, K. Tsukahara, A. Lijima, K. Kitoh, (1992) Novel sulfonamides as potentially systemically active antitumor agents, *J. Med. Chem*. **35:** 2496–2497.

[7] Urmila H. Patel, Bharat D. Patel, Rajesh D. Modh and Pinal D. Patel, (2007) 1,1' Sulfonyl diimidazole, Acta Cryst. *E* **63**, o3598–o3599.

[8] Urmila H. Patel, Rajesh D. Modh and Dhaval A. Shah, (2013), *Acta Cryst. C* **69**: o1286-o1287.

[9] U. H. Patel, C. G. Dave, M. M. Jotani and H. C. Shah (2002), 1,3-Dimethyl-2-oxo-4,6-diphenyl-1,2,3,4-tetrahydropyridine-3-carbonitrile**,** *Acta Cryst. C* **58**: o191-o192.

[10] G. M. Sheldrick (2008): A short history of SHELX, *Acta Cryst. A* **64:** 112-122.

[11] L. J. Farrugia (2012): WinGX and ORTEP for windows: an update. *J. Appl. Cryst.* **45**: 849-854.

[12] Spek, A. L. (2009): Structure validation in chemical crystallography, *Acta Cryst. D* **65**: 148-155

. **[13]** B.D. Patel, U.H. Patel and D.A. Shah, (2015): A Novel Crystal and Molecular Structure of 7-(4-Chloro-Phenyl)-5-Phenyl-4- Pyrrolidin-1-yl-7H-Pyrrolo[2,3-d]Pyrimidine, *Elixir Appl. Chem.* **84**: 33530-33535.

[14] Allen, F. H., Kennard, O., Watson, D. G., Brammer, L., Orphen, A. G., & Taylor, R. (1987), J. Chem. Soc. Perkin Trans. **2**: S1-S19.

[15] R. D. Modh (2009). *Crystal molecular structure, supramolecular aggregation of pyrrolo[2,3-d]pyrimidine derivatives-X-ray crystallographic analysis*, Ph. D Thesis, Sardar Patel University, Vallabh Vidyanagar, India.

[16] John F. Malone, Catherine M. Murray, Michael H. Charlton, Robert Docherty and Aidan J. Lavery (1997): X-H…π (phenyl) interactions Theoretical and crystallographic observations, J. *Chem. Soc., Faraday T rans.,* **93(19)**: 3429-3436.

PRAJÑĀ - **Journal of Pure and Applied Sciences Vol. 24 – 25 : 93 – 96 (2017)**
ISSN 0975 - 2595

EFFECT OF MULTIPOLARITY-SIX DEFORMATION PARAMETER IN SUPER HEAVY NUCLEI

J.UMAI PARVATHIY

Department of Physics, Sri Sarada College for Women, Trunelveli-627 011, Tamil Nadu India.

ABSTRACT

The progress towards the exploration of Island of stability is the active research area in the Nuclear Physics field. Alpha Decay is an important tool to identify the super heavy nuclei and its properties. Analyzation of half life time values of Alpha Decay chain predicts information about long-lived super heavy elements. Many nuclear models have been so far estimated to determine the half life time values. More than ninety Trans-Actinide isotopes of fifteen super heavy elements have already been observed. Here in this work using Cubic plus Yukawa plus Exponential (CYE) model the alpha decay half life time values of super heavy nuclei in the Trans-Actinide region by incorporating higher order multi-polarity six deformation parameter is calculated and its stability is analyzed. The results obtained are compared with the theoretical and also with the available experimental values. The comparison of the calculated half lives follow the same trend as the reference values.

Keywords: Alpha decay,Deformation, Half Life, Super heavy nuclei,Trans-Actinides .

INTRODUCTION

The existence of the "Island of Stability"(IoS) in super heavy nuclei is predicted by a number of theoretical methods. Stability of super heavy elements depends on various factors such as nuclear shapes, deformations, energy, angular momentum etc. Also it is analyzed by the accurate measurement of half-life time values of alpha decay. In the present work half life time measurement is done based on Cubic plus Yukawa plus Exponential (CYE) model by two sphere approximation [1,2]. This model uses a Cubic potential in the pre-scission region connected by Coulomb plus Yukawa plus exponential potential in the post-scission region with zero point vibration energy. The calculation of alpha decay half-life without deformation [3] for the super heavy elements in the Trans-Actinide region is calculated initially and the model is enhanced further with the incorporation of higher multi-polarity hexacontratetrapole (β_6) deformation parameter.

METHODOLOGY

The properties of Trans-actinide elements are studied by a realistic model called as the Cubic plus Yukawa plus Exponential (CYE) model. It has a cubic potential for the overlapping region which is smoothly connected Yukawa plus exponential potential for the region after separation. Then the potential as a function of r for the post-scission region is given by

$$V(r) = \frac{Z_1 Z_2 e^2}{r} + V_n(r) - Q, \quad r \geq r_t \quad \text{--- (1)}$$

Where

$V_n(r)$ is the nuclear interaction energy and written in the form

$$V_n(r) = -D\left[F + \frac{r - r_t}{a}\right]\frac{r_t}{r}\exp\left[\frac{(r_t - r)}{a}\right]$$

$r_t = R_1+R_2$ is the sum of their equivalent sharp surface radii. As long as the distance of their center of mass is greater than $r_t = R_1+R_2$ (R_1 and R_2 are the radii of the daughter and the alpha particle) the only source of potential energy is the electrostatic repulsion and hence denotes the first term of equation.

The depth constant D is given by

$$D = 4a^3 g \frac{\left(\frac{R1}{a}\right) g\left(\frac{R_2}{a}\right)\exp(-r_{12}/a) Cs'}{r_0^2 r_{12}}$$

where g(x) = xcoshx – sinhx, and for the case of two separated nuclei,

$C_{S'} = [C_S(1)\, C_S(2)]^{1/2}$

The constant F is given by

$$F = 4 + \frac{r_{12}}{a} - \frac{f\left(\frac{R_1}{a}\right)}{\left(\frac{R_1}{a}\right)} - \frac{f\left(\frac{R_2}{a}\right)}{g\left(\frac{R_2}{a}\right)}$$

Where $F_{(x)} = x^2 \sin hx, R_i = r_0 A_i^{1/3}$

$C_s(i) = a_s(1 - K_s I_i^2)$ *and* $I_i = (N_i - Z_i / A_i,)(i = 1,2)$

Half-life time of the system [4] is calculated using the formula

$$T = \frac{1.433\ x\ 10^{-21}\ (1+exp\ K)}{E_v} \quad \text{--- (2)}$$

Where k is a constant and given by

$$K = \frac{2}{\eta} - \left\{ \int_{r_a}^{r_t} [2B(r)V(r)]^{1/2}.dr + \frac{2}{\eta}\int_{r_t}^{r_b} [2B(r)V(r)]^{1/2} \right\}.dr$$

r_a and r_b being the two appropriate zeros of the integrand.

E_v is the zero point vibration energy. Super heavy nuclei (SHN) are axially symmetric [5]. Therefore, SHN are described by the deformation parameter expression for the radius vector describing the nucleus surface (in the intrinsic frame of reference) in terms of spherical harmonics and is written in the form,

$$R(\theta, ¢) = R_0 + [1 + \sum_{l=1}^{\alpha} \sum_{m=-l}^{l} \beta_{lm}\ Y_l^m\ ] \quad \ldots(3)$$

R_0 - is the nuclear radius for a spherical one also called as an equilibrium radius.

Y_l^m - are the spherical harmonics representing the surface disturbances

β_{lm} - deformed parameters

θ&¢ - polar angles with respect to arbitrary axis.

Since Y_l^m are the orthogonal, β_6 parameter corresponding to a specific shape is determined from the formula [6] as

$$\beta_{lm} = \frac{\sqrt{4\pi}\ \int R(\theta,\emptyset)\ y_2^m\ (\theta,\emptyset)\ d\alpha}{\int R(\theta,\emptyset)\ y_0^0\ (\theta,\emptyset)\ d\alpha} \quad \text{---(4)}$$

Where R is the radius vector.

The properties of a nucleus are very sensitive functions of its deformationparameters such as (Quadrupoleβ_2,hexadecapoleβ_4, hexacontatetrapole β_6,,Octupole-β_8). The analysis on nuclear deformation parameters has proved [7] that it is sufficient to consider the multi-polarities up to eight (i.e. up to β_8). The odd multi-polarities β_3, $\beta5$, $\beta7$ contribute only to light nuclei. Thus the deformation parameters β_2, $\beta4$, $\beta6$, $\beta8$ are sufficient enough for the study of properties in all super heavy nuclei [8].The contribution of higher order hexadecapole (β_4) deformation parameter in the calculation of half-life time values is predicted in the earlier work [9]. The predicted higher order hexacontatetrapole deformation parameter [10, 11] in super heavy nuclei is included in this work with its deformation parameter values taken from [13] and the half-life time values are calculated for the Trans-Actinide region in the range with atomic number Z= 104 to 121.

RESULTS AND DISCUSSION

The calculated half-life time values using CYE model with higher order multipolarity deformation parameter (β_6)are recorded in Table 1.

Table-1: Comparison of half-lives calculated using CYE model by incorporating higher order multi-polarity deformation parameter (β_6) with the theoretical and also with the available experimental values.

Nucleus	Q(MeV)	$\text{Log}_{10} T_{\frac{1}{2}}(s)$			
		CYE Model		Theory [12]	Expt. [14-24]
		WoD	With (β_6)		
$^{255}Rf_{104}$	8.95	0.76	0.55	1.038	0.204
$^{256}D_{105}$	9.19	0.37	0.20	0.699	0.230
$^{259}Sg_{106}$	9.815	-1.13	-1.19	-0.773	-0.319
$^{262}Bh_{107}$	10.576	-2.87	-3.05	-3.498	-2.097
$^{266}Ha_{108}$	10.381	-2.07	-2.02	-3.868	-2.638
$^{270}Mt_{109}$	10.227	-1.36	-1.26	-2.089	-2.301
$^{267}Da_{110}$	11.823	-4.89	-4.94	-4.405	-5.523
$^{272}Ro_{111}$	11.029	-2.77	-2.70	-2.265	-2.824
$^{277}Co_{112}$	11.666	-4.04	-3.90	-3.495	3.1155
$^{285}Ni_{113}$	9.927	-1.28	0.70	-0.619	0..643
$^{286}Fl_{114}$	10.373	-0.20	-0.01	-0.790	-0.886
$^{289}Ms_{115}$	10.504	-0.26	-0.32	-1.431	-1.319
$^{290}Li_{116}$	11.042	-1.36	-1.46	-3.254	-2.167
$^{293}Ts_{117}$	11.233	-1.56	-1.31	-1.331	-1.824
$^{294}Og_{118}$	11.862	-2.78	-2.00	-3.313	-2.149
$^{292}X_{119}$	13.17	-5.30	-4.89	-4.71[13]	-
$^{287}X_{120}$	13.98	-6.49	-6.00	-6.07[13]	-
$^{293}X_{121}$	14.14	-6.70	-6.27	-6.39[13]	-

PRAJÑĀ - **Journal of Pure and Applied Sciences Vol. 24 – 25 : 93 – 96 (2017)**
ISSN 0975 - 2595

The results are compared with the theoretical Formalism [12, 13] and also with the available experimental results [14-24]. Figure 1 shows the contour map of half-life time values without the inclusion of β_6 parameter. The large inner closed circles in the plot represent the region of in-stability in the Trans-Actinide nuclei.

This has been shown in Figure 2 which predicts the contour map of half-life time values with the inclusion of β_6 parameter. The closed circles in the plot represent the region of in-stability in the Trans-Actinide nuclei and the decrement in the area represents increase in the stability of the super heavy nuclei.

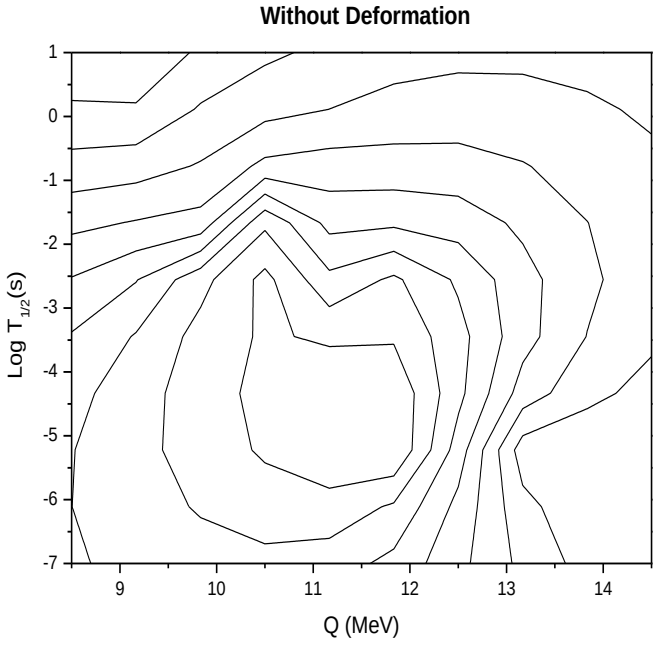

Figure1,showsthe contour map of half life time values without the inco deformation.

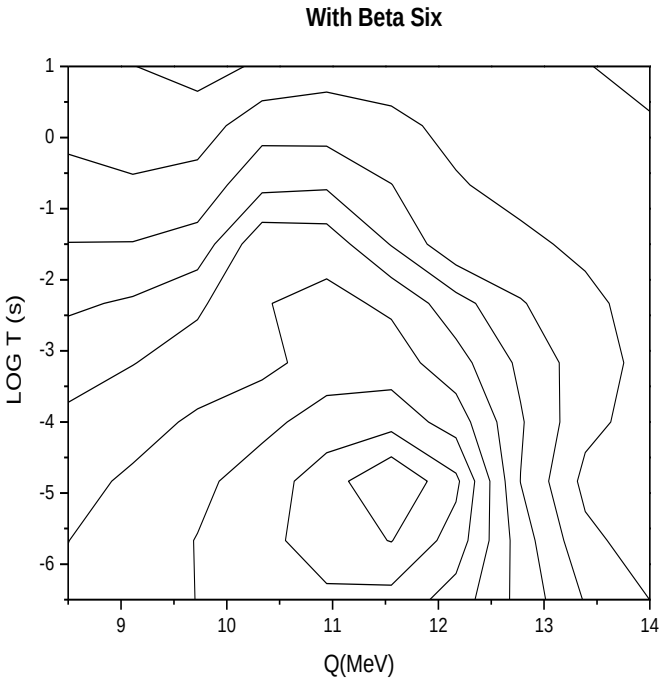

Figure 2, shows the contour map of half- life time values with incorporation of multi-polarity six deformation.

The inclusion of β_6 deformation parameter influences collective rotation of the nucleus leading to enlarged shell gap [25, 26] thereby increasing the binding energy to more than 1MeV and henceforth this increment correspondingly increases the half-life time values. Also comparison predicts that the calculated half life time values mostly increases with the inclusion of β_6 parameter [27] and reaches closer to the experimental value. Therefore, the contribution of higher order multi-polarity deformation-six parameter increases the stabilization of the nucleus. This had been proved for the nucleus ^{254}No[28]whose stability increases by increasing its binding energy to about 1.5MeV.

CONCLUSION

For a super heavy nuclei a decisive role after quadrupole deformation (β_2) which is the largest, dominant and positive in almost all the region of deformed nuclei is played by the starring hexadecapole deformation (β_4) parameter. The role of higher multi-polarity component (β_6) has been disregarded in the calculations for a long time in the study about the properties of super heavy nuclei. But even though these higher multi-polarity component (β_6) are smaller and since it changes through the region, the deformation – six (β_6) parameters becomes the main responsible parameter to increase the half-life time values. Therefore stabilization in the Trans-Actinide

region due to the incorporation of higher order multi-polarity six deformation parameter will provide a new guide for future experiments to study about the properties of the heavy and super heavy nuclei.

REFERENCES

[1] Shanmugam, G., and Kamalakaran, B. (1988): *Physical Review **C*** **38** 1377.

[2] Shanmugam, G., Carmel vigila Bai, G. M. and Kamalaharan, B. (1995): *Physical Review **C*** **51** 2616.

[3] Carmel Vigila Bai, G. M. and Umai Parvathiy, J. (2015): *Pramana - Journal of Physics* **Vol. 84**, No.1, 113-116.

[4] Cwiok, S. and Sobiczewski, A. (1992): *Z. Phys.A* 342:203.

[5] Poenaru, D.N. and Ivascu, M. (1984): *J. Phys.* **45**,1099.

[6] Tayal, D.C. (2012): *Nuclear Physics*, Himalaya P ublishing House.

[7] Sobiczewski, A., Patyk, Z., Cwiok, C., Rozmej, P., (1998): *Nuclear Phys. A* 485:16.

[8] Smolanczuk, R., Sobiczewski, A., Oganessian, Yu.Ts., Oertzen, W Von, Kalpakchieva, R(Eds.*)*, (1995): *Proc. XV Nucl.Phys. Conf*, Russia.

[9] Umai Parvathiy, J. (2017): *International Journal of Scientific Research in Physics and Applied Sciences*, Vol.**5,** Issue 4, pp 13-16.

[10] Patyk, Z., Sobiczewski, A., (1991): *Nucl. Phy. A* **533**, 132.

[11] Patyk, Z., Sobiczewski, A. (1991): *Phys.Lett. B **256**, 307.*

[12] Viola, V.E. and Seaborg, G.T. (1996): J. Inorganic Nucl.Chem.**28**, 741.

[13] Moller, P., Nix, J.R. and Kratz, K.L. (1997): At. Data Nucl. Data Tables **66**, 131.

[14] Budaca, A.L., Sili Steanu, I. (2011): Romanian Reports in Physics **Vol**. **63** (Supplement) 1147–1166.

[15] Oganessian,Yu.TS.,Utyonkov, V.K.and Dimitriev, D.N. (2005): Physical Review **C72** 034611.

[16] Oganessian,Yu. Ts. (2006): Pure Applied Chemistry **78** 889.

[17] Oganessian, Yu. TS., Abdulin, F.Sh. and Bailey, P.D. (2010): Physical Review Letter **104** 0142502.

[18] Oganessian, Yu. Ts. *et al.* (2013): Phys. Rev. C **87** 014302.

[19] Hofmann, S. *et al.* (2002): European Physics Journal **A14** 147 (2002)

[20] Hofmann, S. and Munzenberg, G. (2000): Rev. Modern Physics **72** 733.

[21] Hofmann, S. *et al*. (1996): Zeit. Physics A **354** 229.

[22] Morita, K. (2004): Japanese Physical Society **J 73** 2593.

[23]Dvorak, J. *et al*. (2006): Physical Review Letter **97** 242501.

[24] Dullmann, Ch. E., Schadel, M., Yakershev, A., Turler, A., Eberhardt, K., and Kratz, J.V., (2010): Physical Review Letters **104** 252701.

[25] Liu, H.L., Xu, F.R., Walkers, P.M., (2011): Bertulani, C.A, *Phys. Rev. C**83***, 011303.

[26] Liu, H.L., Xu, F.R., and walker, P.M. (2012): *Phys. Rev. C **86** ,011301R.*

[27] Umai Parvathiy, J. and Carmel Vigila Bai, G.M. (2014): RAC Multidisciplinary Journal of Research with ISBN No. 2230-7362, Volume **1,** No.8.

[28] Sobiczewski, A., Pomorski, K.(2007): Progress in Particle and Nuclear Physics, 58, 292-349.

PRAJÑĀ - **Journal of Pure and Applied Sciences Vol. 24 – 25 : 97 – 100 (2017)**
ISSN 0975 - 2595

OPTICAL AND MAGNETIC PROPERTIES OF SCHIFF BASED TRANSITION METAL COMPLEXES OF (Z)-5-(METHOXYMETHOXY)-2-(1-(PHENYLIMINO)ETHYL)PHENOL) AND (Z)-2-BROMO-4-CHLORO-6-(1-((4-NITROPHENYL)IMINO)ETHYL)PHENOL DERIVATIVES

JATIN G. JAYSWAL[2], SAHAJ A. GANDHI[3], U. H. PATEL[1], VIJAY M. BAROT[2], MAHESH K. PATEL[1], KHUSHBU K. LALVANI[1], SACHIN B. PANDYA[1], KAUSHIK P. CHAUDHARY[1] AND BHAVESH N. SOCHA[1]
[1]Department of Physics, Sardar Patel University, Vallabh Vidyanagar, Anand, Gujarat – 388120. Email: u_h_patel@yahoo.com
[2]P.G.Center in Chemistry, Smt. S.M.Panchal Science Collage, Talod, Gujarat - 383305
[3]Bhavan's Shri I.L. Pandya Arts-Science and Smt. J.M. Shah Commerce Collage, Dakor, Gujarat- 388225

ABSTRACT

Acetophenol and aromatic amine derivatives are antibacterial agents. The biological activities of metal complexes differ from those of either ligand or the metal ions. An increase or decreases in biological activities have been reported for several transition metal complexes. Novel metal Copper (II) (B1) and Nickel (II) (M4) complexes of Acetophenol and aromatic derivatives have been synthesized by Schiff based method. Optical properties investigated by UV-VIS spectroscopy in the range 200-800 nm and the photoluminescence study of these chelates has been carried out for the emission properties. Moreover, the Magnetic Susceptibility study is also performed to explore the magnetic response of these chelate against magnetic field.

Keywords: Antibacterial agents, Metal complexes, Optical and magnetic properties.

INTRODUCTION

Compounds with the structure of –C=N– (azomethine group) are known as Schiff bases, which are usually synthesized by condensation of primary amines and active carbonyl groups. Schiff bases are an important class of compounds in the medicinal and the pharmaceutical field, including antibacterial **[1, 2]**, antifungal **[3, 4]**, and antitumor activity **[5, 6]**.Acetophenol and aromatic amine derivatives have been found wider use as antibacterial agents. Biological activity of metal complexes differs from those of either ligands or the metal ions and increased and or decreased biological activities have been reported for several transition metallic complexes **[7].** The individual Schiff bases are considered to be promising antifungal, anticonvulsant activity for treatment of HIV. As a part of our ongoing research work novel compounds to investigate the structure function relationship, we report here the magnetic and optical properties of the novel metal complexes of (Z)-5-(methoxymethoxy)-2-(1-(phenylimino)ethyl)phenol) [B1]and (Z)-2-bromo-4-chloro-6-(1-((4-nitrophenyl)imino)ethyl)phenol[M4]derivatives.

METHODOLOGY

SYNTHESIS

The methanolic solution of transition metals copper (II) and nickel (II) (0.01mol, 10ml) and Schiff bases ligand (Z)-5-(methoxymethoxy)-2-(1-(phenylimino)ethyl)phenol) and (Z)-2-bromo-4-chloro-6-(1-((4nitrophenyl)imino)ethyl)phenol derivatives have been taken in 1:2 (metal /ligand) ratio. The pH solution has been maintained during the course of the reaction by adding few drops of liq.NH3/glacial acetic acid. The reaction mass was refluxed for 2-3 hours on a water bath. After the end of reaction, it was cooled to room temperature and solvent was allowed to evaporate. Precipitated colored complexes was filtered and washed with methanol: water (1:1) mixture, recrystallized from methanol and dried over anhydrous CaCl2 in desiccators. It was further dried in an electric oven at 50-70°C. The chemical structure of synthesized metal chelates [Cu (II), Ni (II)] of Schiff base ligand(Z)-5-(methoxymethoxy)-2-(1-(phenylimino)ethyl)phenol) and (Z)-2-bromo-4-chloro-6-(1-((4-nitrophenyl)imino)ethyl)phenol derivatives are as shown in **Figure 1(a)**&**Figure1(b).**

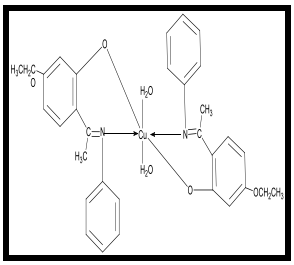

Figure: 1(a) The chemical diagram of compound B1.

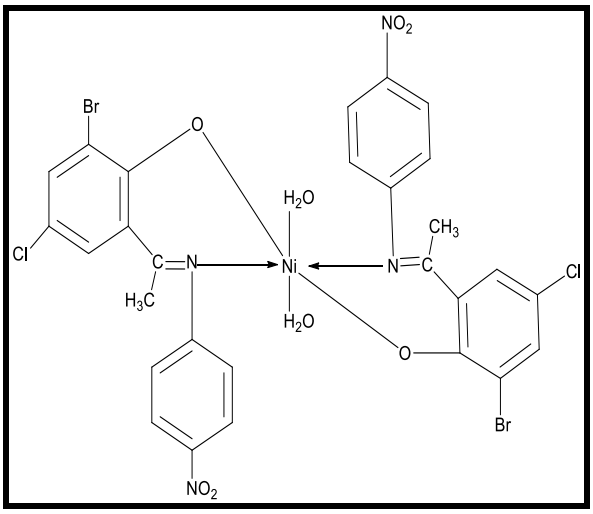

Figure: 1(b) The chemical diagram of compound M4.

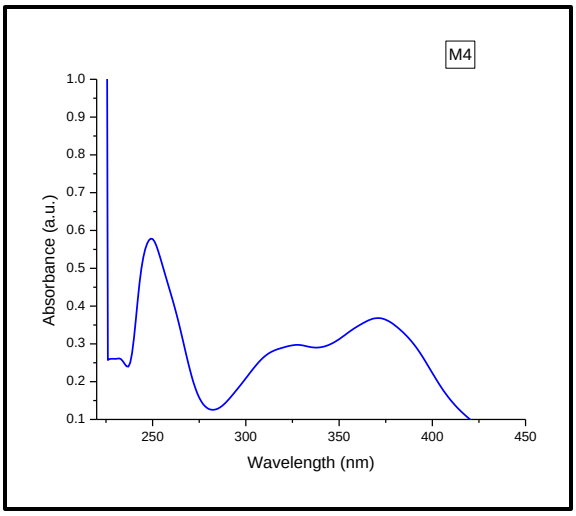

Figure: 2(b) Absorption spectra of compound M4.

RESULTS AND DISCUSSION

Optical Investigations

1. UV-VIS Spectroscopy

The solution of the title compounds are prepared by dissolving powdered compound in DMSO solvent to record the absorption spectra of compounds and are presented in **Figure 2(a)** and in **Figure2(b)**. In UV-VIS absorption spectrum of B1 compound, the two maximum absorption peaks at 258nm , 277 nm and in the spectrum of M1 compound, the three maximum absorption peaks observed about 249.31, 327.61, 370.86 nm respectively which reveal $\pi \rightarrow \pi^*$ transition. **[8-10]**

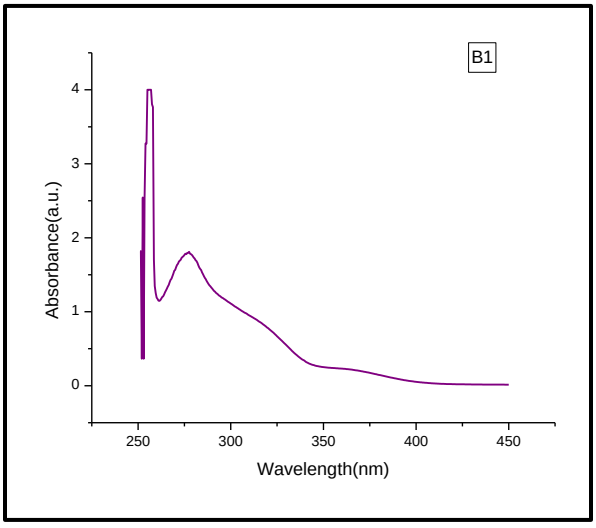

Figure: 2(a) Absorption spectra of compound B1.

2. Photoluminescence Spectroscopy

Photoluminescence (PL) spectra of ligand-metal complexes are recorded in liquid state at room temperature and are depicted in **Figure 3(a)** and in **Figure 3(b)**. An excitation state applied to B1 and M4 compounds is 300 nm. The maximum emissions found in B1 are 485 nm, 530 nm, 601 nm and that of for M4 are 486 nm, 528 nm, 600 nm respectively. The strong emission for metal complex can be assigned as ligand-to-metal charge transfer.

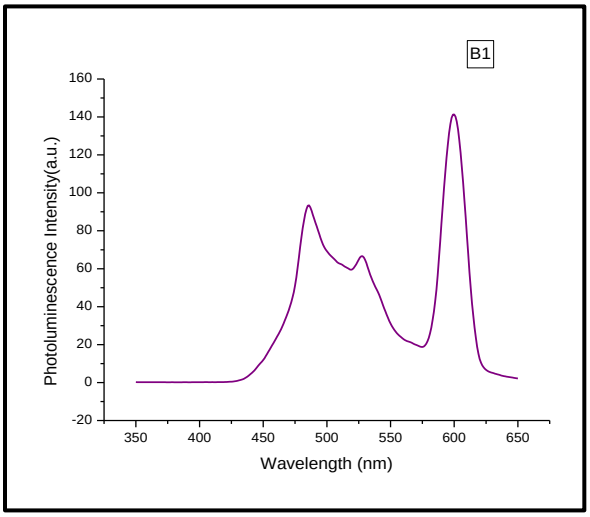

Figure: 3(a) Emission spectra of compound B1.

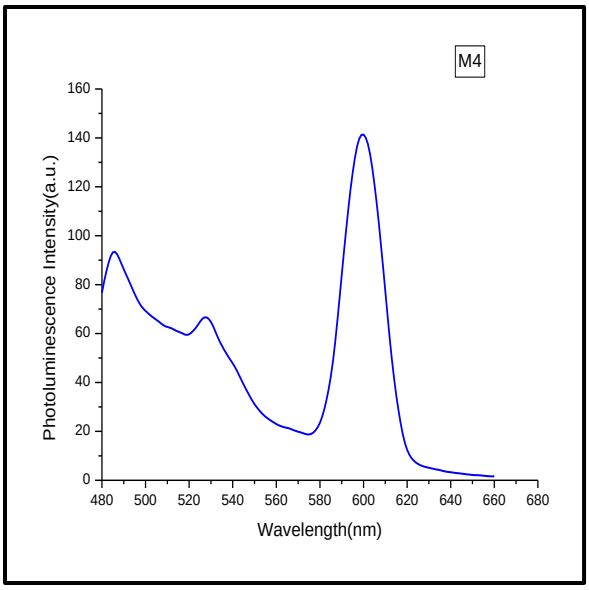

Figure: 3(b) Emission spectra of compoundM4.

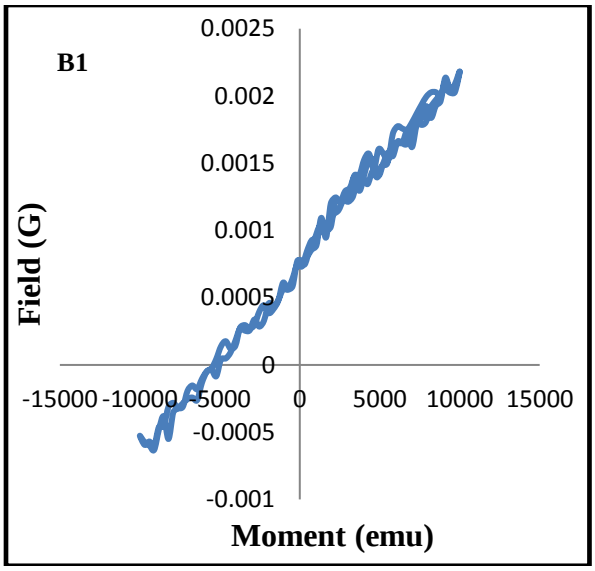

Figure: 4(a) Magnetic measurement of compound B1.

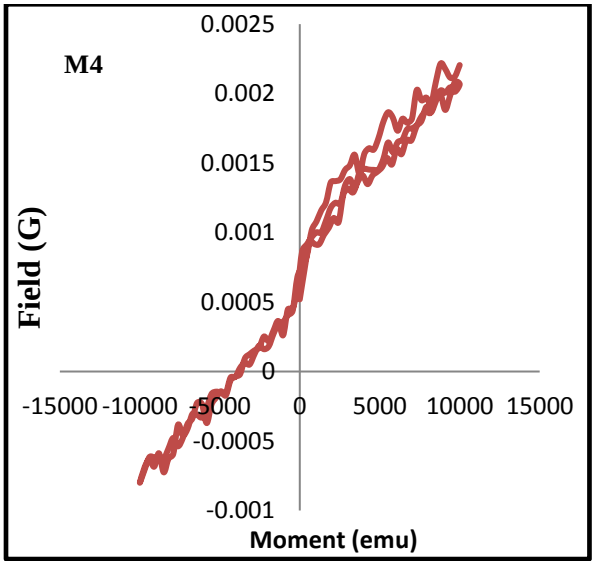

Figure: 4(b) Magnetic measurement of compound M4.

3. Magnetic Susceptibility

The Magnetic measurement of compounds B1 and M4 are shown in **Figure 4(a)** and in **Figure 4(b)** respectively**.** The magnetic behavior of the title compounds B1 and M4 are studied at room temperature (293K). The graphs have been plotted for Magnetic field (G) vs. Magnetic moment for compound B1 and M4. The slope of the graph gives magnetic susceptibility: χ = M/H. For B1 complex, slope = 1.43837×10^{-7} emu/G. The slope is positive, which reveals that the title compound B1 possesses paramagnetic property. In the metal complex B1,Cu (II) ion ($3d^9$) has one unpaired electron in the 3d shell, therefore compound is considered to have magnetic moment close to the spin-only value $1.73\mu_B$. For M4 complex, slope = 1.57404×10^{-7}emu/G. The slope is positive, which reveals that the title compound M4 possesses paramagnetic property. In the metal complex M4, Ni (II) ion ($3d^8$) has two unpaired electron in the 3d shell, therefore compound is considered to have magnetic moment close to $2.83\mu_B$.

CONCLUSION

Schiff bases are considered as a very important class of organic compounds because of their ability to form complexes with transition metal ions. The Cu (II) and Ni (II) metal complexes of (Z)-5-(methoxymethoxy)-2-(1-(phenylimino) ethyl)phenol) and (Z)-2-bromo-4-chloro-6-(1-((4-nitrophenyl)imino)ethyl)phenol derivatives are successfully synthesized. Both the metal complexes form a distorted octahedral coordination geometry connecting metal ion via oxygen and nitrogen atoms. The optical property supported by PL, reveals that both the chelates exhibit luminescence property. The value of magnetic succeptibility [χ for B1, M4 is 1.43837×10^{-7} emu/G, 1.57404×10^{-7}emu/G respectively] indicates paramagnetic behaviour

of both the metal complexes. Further study to investigate 3-D structure of both these compounds is in progress.

ACKNOWLEDGEMENT

Authors are thankful to UGC, New Delhi, for providing Fluorescence Spectrometer facility sanctioned under DSA-1 grant to Department of Physics, Sardar Patel University, Vallabh Vidyanagar, Anand, Gujarat, India. We acknowledge the help received from Department of Chemistry, Sardar Patel University, Vallabh Vidyanagar, and Gujarat, India for UV-VIS data and we also acknowledge the help received from CHARUSAT, Changa, Anand, Gujarat, India for Magnetic susceptibility characterization.

REFERENCES

1. P. Panneerselvam, B. A. Rather, D. R. S. Reddy, and N. R. Kumar, (2009), Synthesis and anti-microbial screening of some Schiff bases of 3-amino-6,8-dibromo-2-phenylquinazolin-4(3H)-ones, *European Journal of Medicinal Chemistry*,**44(5)**, 2328–2333.
2. X. Jin, J. Wang, and J. Bai, (2009) Synthesis and antimicrobial activity of the Schiff base from chitosan and citral, *Carbohydrate Research*, **344(6)**, 825–829.
3. S. K. Bharti, G. Nath, R. Tilak, and S. K. Singh, (2010) Synthesis, anti-bacterial and anti-fungal activities of some novel Schiff bases containing 2,4-disubstituted thiazole ring, *European Journal of Medicinal Chemistry*,**45(2)**, 651–660.
4. G. B. Bagihalli, P. G. Avaji, S. A. Patil, and P. S. Badami, (2008) Synthesis, spectral characterization, in vitro antibacterial, antifungal and cytotoxic activities of Co(II), Ni(II) and Cu(II) complexes with 1,2,4-triazole Schiff bases, *European Journal of Medicinal Chemistry*, **43(12)**, 2639–2649.
5. Y. C. Liu and Z. Y. Yang, (2009) Crystal structures, antioxidation and DNA binding properties of Eu(III) complexes with Schiff-base ligands derived from 8-hydroxyquinoline-2-carboxyaldehyde and three aroylhydrazines, *Journal of Inorganic Biochemistry*, **103(7)**, 1014–1022.
6. H. Nawaz, Z. Akhter, S. Yameen, H. M. Siddiqi, B. Mirza, and A. Rifat, (2009) Synthesis and biological evaluations of some Schiff-base esters of ferrocenyl aniline and simple aniline, *Journal of Organometallic Chemistry*, **694(14)**, 2198–2203.
7. Satyanarayan, M, Tiwari P, Tripathi B K, Srivastava A k and Pratap R., (2004) Synthesis and antihyperglycemic activity of chalcone based aryloxypropanolamines, *BioorgMedChem*, **12(5),**883-889.
8. K. K. Narang, J. K. Gupta, (1977), Sulfadrug complexes of zinc(II), cadmium(II) and mercury(II), *Transition Metal Chemistry*, **2,** 181-183.
9. A. D. Tella, J. A. Obaleye, (2011) Divalent metal complexes of 4-amino-N-pyrimidin-2-ylbenzene sulphonamide and their antimalarial activities against Plasmodium berghei, *Bull. Chem. Soc. Ethio*, **25,** 371.
10. Sanjay M. Tailor, Urmila H. Patel, (2017) Nickel (II) complex of 4-amino-N-(2-pyrimidinyl) benzenesulfonamide: Synthesis, spectroscopic characterization, antimicrobial activity, crystal structure, and Hirshfeld surface analysis, *Inorganic and nanometal chemistry*, 47**(2),** 234-243.

PRAJÑĀ - **Journal of Pure and Applied Sciences Vol. 24 – 25 : 101 – 105 (2017)**
ISSN 0975 - 2595

SYNTHESIS AND X-RAY POWDER DIFFRACTION STUDIES: METAL COMPLEXES (Co(II), Ni(II) AND Cu(II)) OF SCHIFF BASE LIGAND 4-BROMO-2-CHLORO-6-[(1Z)-N-(PHENYL) ETHANIMIDOYL] PHENOL

J. G. JAISWAL[1], SAHAJ A. GANDHI[2], TARUNABEN J. PADARIYA[3], V.M. BAROT[1] AND URMILA H. PATEL[3]

[1]P. G. Center in Chemistry, Smt. S. M. Panchal Science College, Talod
[2]Bhavan's Shri I. L. Pandya Arts –Science and Smt. J. M. Shah Commerce College, Dakor, Gujarat, India
[3]Department of Physics, Sardar Patel University, Vallabh Vidyanagar, Gujarat 388120, India. u_h_patel@yahoo.com

ABSTRACT

Schiff bases are an important class of organic compounds, which play an important role in medicinal and pharmaceutical applications. Co(II), Ni(II) and Cu(II) complexes with bidentate Schiff base ligand, 4-bromo-2-chloro-6-[(1Z)-N-(phenyl) ethanimidoyl] phenol (BCEP) have been successfully synthesized. The structural characterization of the synthesized metal complexes have been estimated by analyzing powder X-ray diffraction technique. It reveals that Co and Cu metal complexes crystallize in monoclinic system with P 1 2_1 1 and P 1 2_1/a space group respectively, whereas Ni metal complex crystallizes in triclinic system with P$\bar{1}$space group.

Keywords: Schiff bases, metal complexes, powder X- ray diffraction study

INTRODUCTION

Schiff bases are condensation products of primary amines and carbonyl compounds and they discovered by a German chemist, Nobel Prize winner, Hugo Schiff in 1864. Structurally, Schiff base (also known as imine or azomethine) is an analogue of a ketone or aldehyde in which the carbonyl group (C=O) has been replaced by an imine or azomethine group. Schiff base ligands are essential in the field of coordination chemistry, especially in the development of complexes of Schiff bases because these compounds are potentially capable of forming stable complexes with metal ions[1]. The individual Schiff bases are considered to be promising antifungal medicines[2]. Isatin Schiff base ligands are marked by antiviral activity, and this fact is very useful in the treatment of HIV[3]. In addition, it is also found that these compounds have anticonvulsant activity and may be included in the anti-epileptic drugs[4]. Due to the presence of the imine group, the electron cloud of the aromatic ring and electronegative nitrogen, oxygen and sulfur atoms in the Schiff bases molecules, these compounds effectively prevent corrosion of mild steel, copper, aluminum and zinc in acidic medium[5]. Schiff bases and Mannich bases of isatin are known to possess a wide range of pharmacological properties including antibacterial, anticonvulsant, antifungal and antiviral activities[6-9]. Schiff's bases are also important compounds owing to their wide range of industrial applications[10]. As a part of our ongoing research on synthesis of novel compounds and characterization by X-ray diffraction studies[11-13], here we report the synthesis and characterizations of metal complexes (Co, Ni and Cu) of schiff base ligand 4-bromo-2-chloro-6-[(1Z)-N-(phenyl) ethanimidoyl] phenol.

EXPERIMENTAL

Synthesis: General Preparation of Metal chelates (Co(II), Ni(II) and Cu(II)) of Schiff base ligand 4-bromo-2-chloro-6-[(1Z)-N(phenyl) ethan imid oyl] phenol (BCEP)

The appropriate methanolic solution of transition metals (Co, Ni and Cu) (0.01mol, 10 ml) and schiff base ligand (BCEP) (0.02mol, 20 ml.) are taken in a 1:2 (metal/ligand) ratio. PH is maintained during the course of the reaction by adding few drops of liquid N_2. The reaction mass is refluxed for 3-4 hours on a water bath. After completion of the reaction, it is cooled to room temperature and solvent is evaporated naturally. Precipitated colored complex is filtered and washed with methanol: water (1:1) mixture, recrystallized from methanol and dried over anhydrous $CaCl_2$ in desiccators. It is further dried in an electric oven at 50-70 ℃. The chemical diagram of synthesized metal chelates (Co(II), Ni(II) and Cu(II)) of Schiff base ligand 4-bromo-2-chloro-6-[(1Z)-N-

(phenyl)ethanimidoyl] phenol (BCEP) are as shown in Figure 1a, 1b and 1c respectively.

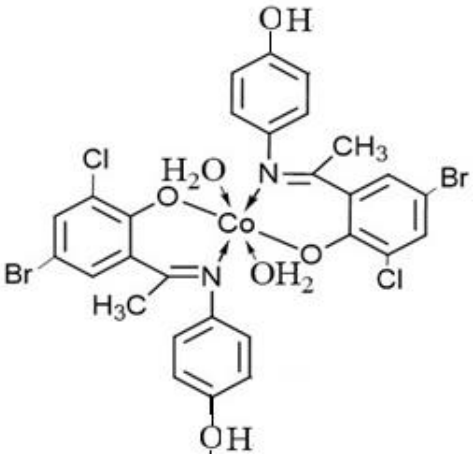

Fig. 1(a)

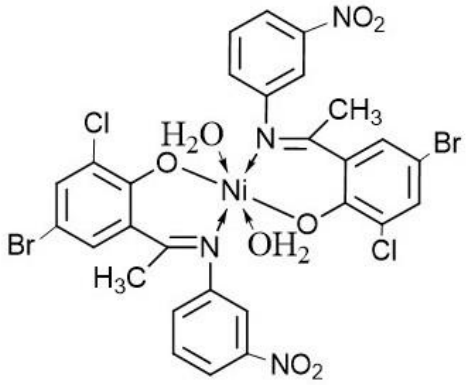

Fig. 1(b)

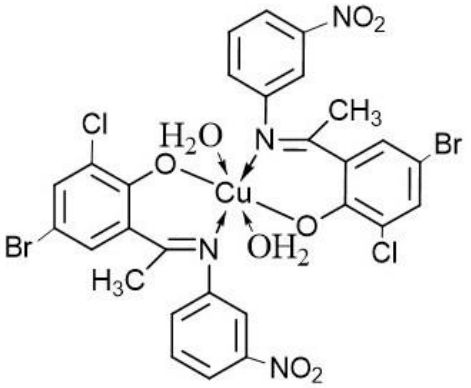

Fig. 1(c)

Figure 1 The chemical diagram of metal chelates (Co(II), Ni(II) and Cu(II)) of Schiff base ligand 4-bromo-2-chloro-6-[(1Z)-N-(phenyl)ethanimidoyl] phenol (BCEP).

RESULTS AND DISCUSSION

Powder X- ray diffraction pattern are recorded for metal chelates (Co(II), Ni(II) and Cu(II)) of schiff base ligand 4-bromo-2-chloro-6-[(1Z)-N-(phenyl) ethanimidoyl] phenol (BCEP). All the diffraction data are collected on Rigaku Ultima IV diffractometer using CuKα1 radiation (λ = 1.5406 Å) and the powder diffraction patterns for all the metal complexes of Co, Ni and Cu are presented in the Figure 1a, 1b and 1c respectively. The Figure 1d shows the overlay diagram of powder XRD pattern of all three Co, Ni and Cu metal complexes. The experimental 2θ range is 05–60° with a step size of 0.01° and a counting time of 30 second per step. The program WinPLOTR package[14] are used for the graphics and all the experimental raw data are indexed by McMaille version 4.00 [15] method using DASH software package[16]. The figures of merit are achieved for Co metal complex are F_{20} = 88.60 (0.0034, 68) and M_{20} = 34.00. Pawley refinement results confirmed that Co metal complex is crystallizes in monoclinic system with space group P 1 2_1 1 and unit-cell parameters: a = 19.9706 (0.0121) Å, b = 11.6535 (0.0080) Å, c = 10.9452 (0.0053) Å, α = 90°, β = 97.727 (0.031)°, γ = 90°, unit-cell volume V = 2524.125Å^3. In the metal complex of Ni, the figures of merit are as: F_{20} = 84.76 (0.0074, 32) and M_{20} = 27.84. The Ni complex crystallizes in triclinic system with space group $P\bar{1}$ and unit-cell parameters are, a = 11.0617 (0.0298) Å, b = 11.6582 (0.0269) Å, c = 14.4534 (0.0257) Å, α = 105.370 (0.127)°, β = 110.545 (0.113)°, γ = 109.779 (0.153)°, unit-cell volume V = 1478.394 Å^3. Indexing results of the third metal complex of Cu confirmed that it crystalizes in monoclinic with space group $P12_1/a$ and unit-cell parameters after the Pawley refinement are [a = 19.5983 (0.0120) Å, b = 14.4228 (0.0083) Å, c = 8.3842 (0.0041) Å, β = 92.106 (0.030)° and unit-cell volume V = 2368.306 Å^3]. The figures of merit obtained from the X-Ray data F_{20} = 97.54 (0.0026, 80) and M_{20} = 40.21.Table 1 summarized the significant peaks of 2θ, d-spacing, FWHM and corresponding (h k l) for all three metal complexes of Co, Ni and Cu. The practical size of the synthesized compounds varies from 50 Å to 1000 Å for Co metal complex, 20 Å to 2000 Å for Ni metal complex and for Cu metal complex 100Å to 500Å respectively.

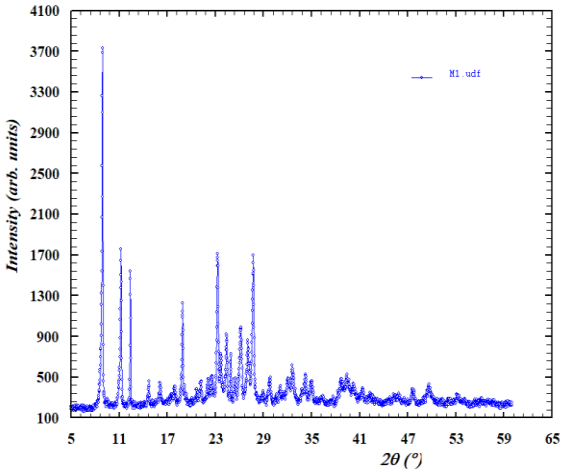

Fig. 2 (a)

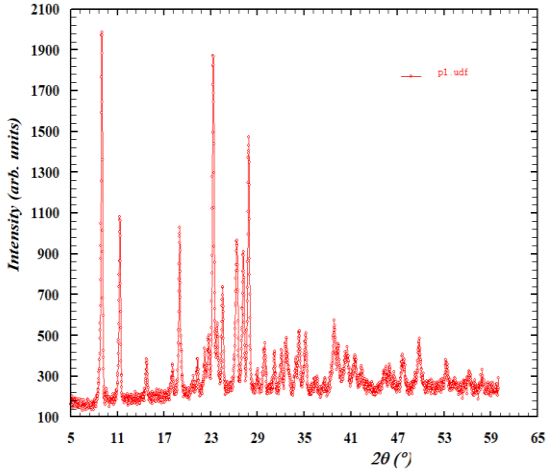

Fig. 2 (b)

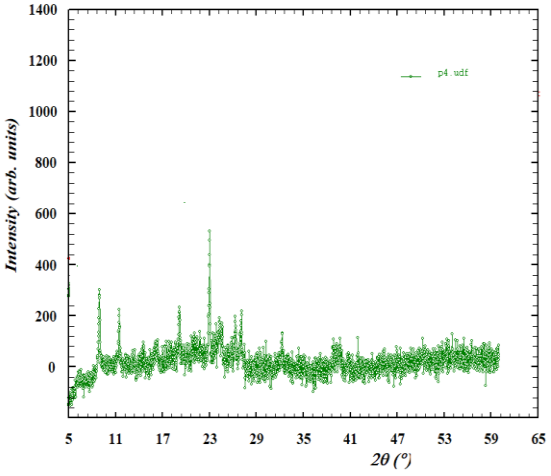

Fig. 2 (c)

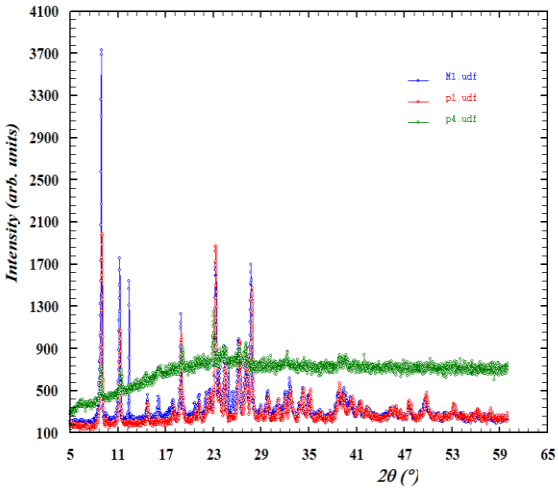

Fig. 2 (d)

Figure 2 (a) XRD pattern of Co metal with ligand BCEP (b) XRD pattern of Ni metal with ligand BCEP and (c) XRD pattern of Cu metal with ligand BCEP (d) overlap diagram of XRD pattern of all three Co, Ni and Cu metal complexes; Color code: Blue- Co metal, Red –Cu metal and Green – Ni metal complexes.

CONCLUSION

A series of novel Co(II), Ni(II) and Cu(II) complexes with bidentate Schiff base ligand, 4-bromo-2-chloro-6-[(1Z)-N-(phenyl) ethanimido yl] phenol (BCEP) have been synthesized and characterized by powder X-ray diffraction technique. Powder X-ray diffraction graph shows that the synthesized metal complexes have been crystalline in nature and Co and Cu metal complex crystallizes in monoclinic system, whereas Ni metal complex crystallizes in triclinic system. The well-defined, sharp peaks in the XRD patterns signify the good crystalline and single phase nature of the pure.

ACKNOWLEDGEMENTS

Dr. V. M. Barot is thankful to the management and the principal of Smt. S. M. Panchal Science College, Talod, who provided all kinds of facilities during the research work. Dr. S. A. Gandhi is grateful to the Department of Physics, Sardar Patel University, for collecting powder diffraction data and CCDC Software ltd. for providing free academic software license (DASH software).

REFERENCES

[1] Szliszka E, Czuba Z P, Mazur B, Sedek L, Paradysz A and Krol W. (2010) Int J Mole Sci., 11(1), 1-13.

[2] Awasthi S K, Mishra N, Kumar B, Sharma M, Bhattacharya A, Mishra L C and Bhasin V K. (2009), Medicinal Chem Res., 2009, 18(6), 407-420.

[3] Okunrobo L O, Usifoh C O and Uwaya J O (2006), Acta Poloniae Pharmaceutica – Drug Research, 63, 195-199.

[4] Wu Jiu H, Wang Xi H, Yi, Yang H and Lee Kuo H. (2003) Bioorg Med Chem Lett., 13(10), 1813-1815.

[5] Tan N D and Dao T T. (2011), Pharmacology Pharmacy, 2(4), 282-288.

[6] Sivakumar P M, Cometa S, Alderighi M, Veluchamy P, Doble M and Federica C. (2012) Carbohydrate Polymers,87(1), 353-360.

[7] Hasan A, Rasheed L and Malik A. (2007), Asian J Chem., 19(2), 937-948.

[8] Zandi K, Teoh, Boon-T, Sam Sing-S, Wong Pooi-F, Mustafa M R and AbuBakar S. (2011), J Med Plants Res., 5(23), 5534-5539.

[9] Kaushik S, Kumar N and Drabu S (2010) Pharma Research, 3(1), 257-262.

[10] Satyanarayana, M, Tiwari P, Tripathi B K, Srivastava A K and Pratap R. (2004) Bioorg Med Chem., 12(5), 883-889.

[11] Patel U H and Gandhi S A. (2008) Indian J Pure Appl Phys., 2008, 49, 263-269.

[12] Patel U H, S A Gandhi, Barot V M and Patel M C. (2009) Acta Cryst., 2009, E68(10),o2926-2927.

[13] Patel U H, Gandhi S A, Barot V M and Patel M C. (2013) Crystal Structure Theory Applications, 2, 167-175.

[14] Roisnel T and Rodriguez-Carvajal J (2001) Analysis Mater Sci Forum, 378(1), 118-123.

[15] Boultif, A. and Loüer, D. (2004). J. Appl. Crystallogr. 37, 724–731.

[16] David, W. I. F., Shankland, K., van de Streek, J., Pidcock, E., Motherwell, W. D. S. & Cole, J. C. (2006). Journal of Applied Crystallography 39, 910-915.

Table-1 : X-ray powder diffraction data of all three metal complexes of Co, Ni and Cu; the significant peaks of 2θ, d-spacing, FWHM and corresponding hkl.

No.	2-theta (deg)	d (ang.)	FWHM (deg)	(h k l)
For the Co metal complex				
1	8.924(2)	9.901(2)	0.119(3)	(1 1 0)
2	11.231(5)	7.872(3)	0.171(5)	(2 0 -1)
3	12.374(4)	7.147(2)	0.070(3)	(1 1 1)
4	14.748(5)	6.001(2)	0.169(17)	(3 0 -1)
5	18.908(12)	4.689(3)	0.147(12)	(0 1 2)
6	20.61(4)	4.306(8)	0.17(4)	(2 2 -1)
7	21.226(14)	4.182(3)	0.213(19)	(2 1 2)
8	22.09(3)	4.022(5)	0.42(7)	(3 2 -1)
9	22.553(17)	3.939(3)	0.201(19)	(4 0 -2)
10	23.282(5)	3.8175(9)	0.190(5)	(2 2 -2)
11	23.685(11)	3.7534(17)	0.200(13)	(5 1 0)
12	24.451(5)	3.6376(8)	0.198(7)	(1 0 -3)
For the Ni metal complex				
1	6.35(5)	13.92(12)	1.7(3)	(0 1 0)
2	8.959(4)	9.862(4)	0.172(11)	(1 0 -3)
3	11.46(2)	7.714(14)	0.125(17)	(1 -1 1)
4	23.012(3)	3.8616(5)	0.038(7)	(2 -2 0)
For the Cu metal complex				
1	8.976(3)	9.844(3)	0.184(4)	(2 0 0)
2	11.315(5)	7.814(3)	0.232(4)	(1 0 -1)
3	18.12(3)	4.891(9)	0.25(3)	(4 0 0)
4	19.006(5)	4.6655(13)	0.208(8)	(1 3 0)
5	21.33(3)	4.163(5)	0.27(3)	(0 3 1)
6	22.210(18)	3.999(3)	0.19(2)	(4 1 1)
7	22.725(15)	3.910(2)	0.280(17)	(2 0 -2)
8	23.280(4)	3.8178(7)	0.243(4)	(2 3 1)
9	23.784(14)	3.738(2)	0.32(2)	(5 1 0)
10	24.506(7)	3.6296(10)	0.221(7)	(0 2 2)
11	26.359(7)	3.3784(9)	0.309(6)	(3 1 2)

PRAJÑĀ - **Journal of Pure and Applied Sciences Vol. 24 – 25 : 106 – 109 (2017)**
ISSN 0975 - 2595

CORRELATION STUDY BETWEEN STRUCTURE AND ANTIBACTERIAL ACTIVITY OF SUBSTITUTED 1, 3, 4-OXADIAZOLE COMPOUNDS

J. J. TRAVADI[1], K. D. LADVA[2], M. S. VADODARIA[2], A. H. BAPODARA[3] AND M. B. BUDDH[4]

[1]Kamani Sc. and Prataprai Arts College, Amreli, Gujarat, (India).

[2]Smt. M. & N. Virani Science College, Rajkot, Gujarat, (India).

[3]M. D. Science College, Porbandar, (India).

[4]Alembic Pharmaceuticals Ltd., Baroda, (India).

Corresponding email: j.travadi72@gmail.com

ABSTRACT

Correlation study between activity data of substituted 1, 3, 4-oxadiazole compounds and their structural property data set has been carried out with stepwise regression analysis (regression analysis estimates the relationships among variables through a statistical process). Repeated activity data has been eliminated wherever was possible, and finally it became possible to find out good correlation between activity data and physical descriptors depends on structure e.g. Heat of formation, Torsion energy, and LUMO[1], which is presented as QSAR equation Y =78.05 +1035.59*X_1 + 0.9949*X_2 + 297.7474*X_3.

Keywords: 1, 3, 4-oxadiazole compounds, QSAR studies, physical descriptors, antibacterial activity data, regression analysis.

INTRODUCTION

In current era mankind are struggling to fight against new challenges in form of stubborn diseases like cancer, aids, liver cirrhosis ect. To overcome such challenges obviously it is require for chemists, pharmacists and scientists to go through number of aggressive chemical processes. QSAR studies helps to design novel drugs with improved biological activities with diminishing side-effects. QSAR technique is very useful to correlate the activity data and structure of the compounds through their physical properties. From liable QSAR equation one can predict activity of designed compound to be synthesized. With the help of such type of study we can avoid unnecessary labour, waste of chemicals, time, etc. Thus, this field supports the research in the era of "GREEN CHEMISTRY".

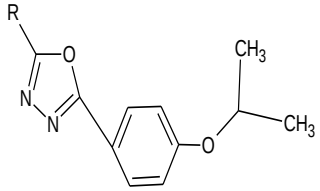

2-(4-ISOPROPOXYPHENYL)-5-(ARYL)-1,3,4-OXADIAZOLE
(**SERIES CODE:- JJTABLE 2)**

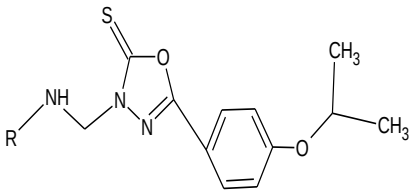

2-(4-ISOPROPOXYPHENYL)-3-N-(ARYL) AMINO METHYL-1,3,4-OXADIAZOLE-5(4H)-THIONE
(**SERIES CODE:- JJTABLE 3)**

MATERIALS AND METHODS

QSAR studies of some of the titled compounds have resulted in the identification of structural and physicochemical parameters (Torsion energy, Heat of formation, and LUMO) contributing to antimicrobial activity of substituted 1, 3, 4-oxadiazoles [2].

In order to establish Quantitative Structure-Activity Relationship (QSAR) the antibacterial activity data are taken as minimal bactericidal concentration (MBC) in µl at different dilution and were used as dependent variables by selection with attention that it should not to be repeated as much as possible.

Activity data were first correlated with different type of parameters such as steric parameters (i.e. Connolly Accessible Area, Connolly Molecular Area, Connolly Solvent-Excluded Volume), electronic parameters (i.e. HOMO, LUMO,) and

thermodynamic properties (i.e. Heat of Formation, Molar Refractivity, Torsion Energy, Partition Coefficient). Activity data and different type of parameters are presented in Table-1. All parameters were calculated from Chemdraw Ultra 3D (version 8.0). Statistical study including multi parameter regression analysis was carried out on Compaq Presario V3702 using KYplot (2.0) statistical software [3, 4].

RESULTS AND DISCUSSION

At primary stage, no significant relationship could have been established among activity data and physicochemical parameters. But later with regression analysis activity data and physicochemical parameters the relationship was showed. To improve the correlation between activity data and physicochemical parameters we led to minimize the activity data set.

On secondary stage of multivariate correlation analysis; some of the parameters (independent variables e.g. Connolly Solvent-Excluded Volume, Exact mass, Molar Refractivity) showed less correlation (r = -0.39 to -0.32) with E.coli activity data. Stepwise regression analysis of different combinations of these parameters were studied, which resulted in derivation of the following equation-1, with very good correlation (r^2 =0.86) of high statistical significance > 86 % (F=30.76). Which shows that physical parameters like torsion energy, heat of formation and LUMO are in good statistically agreement with biological activity against E.coli bacteria; (Equation 1). "Table-2" and "comparative graph of measured and predicted activity data" also support the statistical relationship between physical parameters and activity data against E.coli bacteria.

The calculated activities for the compounds by equation (1) were in good agreement.

$$Y = 78.05 + 1035.59*X_1 + 0.9949*X_2 + 297.7474*X_3 \quad \text{---- ----} \rightarrow \quad 1)$$

Where; n = 07, r^2 = 0.86, F = 30.76

X_1= Torsion Energy, X_2 = Heat of Formation, X_3 = LUMO

The general tendency of correlation between Torsion Energy and Activity data is that as Torsion Energy increases the activity data of compound decreases and vice-versa. In general comparison to LUMO contribution, it has been observed that as contribution of LUMO decreases the activity of compounds decreases in oxadiazoles contain only alkyl substitution (JJTABLE2J to JJTABLE2C @ TABLE-3).

CONCLUSION

It has been observed that among the number of physical descriptors some of them possess fine correlation with activity data. It has been observed that compounds with appropriate substitutional group at proper posion, increases value of Heat of formation and LUMO and decreases the value of torsion energy of the compounds, possess good anti microbial activity against E.coli. e.g. meta nitrophenyl substituted 1, 3, 4-oxadiazole compounds (JJTABLE3G)[Table-3]. They also predicted very good extent of activity against E. coli (MTCC 442) species as compare to other compounds which have been substituted by pera methoxyphenyl and phenyl functional groups.

From experimental data given in Table-3, it has been observed that the compounds containing sulphur element showed comparatively good antibacterial activity. Apart from this, oxadiazoles containing both sulphur and alkyl substitution posses less torsion energy than that of oxadiazoles contain only alkyl substitution.

ACKNOWLEDGEMENTS

The authors are thankful to TRC, Bhatt for giving us valuable suggestions, especially to Dr. Mandhre and Dr. Tully.

REFERENCES

[1] Bhavsar Ajit, (2004-05), Ph.D. Thesis, Bhavnagar University, 132-145.
[2] Buddh, Mayur, B. (2010) Studies on some compounds of Therapeutic Interest. PhD thesis, Saurashtra University, Rajkot.
[3] Raghuvir, R., S., Pissurlenkar, Shah Anamik et all, (2008), European Journal of Medicinal Chemistry, 43, 2103-2115.
[4] Desai Avik, Shah Anamik et all, (2001), Bioorganic & Medicinal Chemistry, 9, 1993-1998.

PRAJÑĀ - **Journal of Pure and Applied Sciences Vol. 24 – 25 : 106 – 109 (2017)**
ISSN 0975 - 2595

Table–1 "Activity data and different type of parameters"

Sr. no.	SAMPLE SERIES CODE	E.COLI MTCC 442	TORSION ENERGY	HEAT OF FORMATION	LUMO	MIN. STERIC ENERGY	LogP	CM AREA	CSE VOLUME	EXACT MASS	PARTION COEFFICIENT	HOMO	MR (CLOGP)
1	JJTABLE2A	1000	0.3829	21.27	-1.28	15.84	3.67	313.39	265.55	310.13	3.6	-8.9	8.6
2	JJTABLE2B	500	0.332	36.9	-1.18	14.77	3.799	284.34	239.92	280.121	3.55	-8.87	8.047
3	JJTABLE2C	1000	0.2291	-135.68	-1.805	8.53	NA	319.87	269.188	325.106	3.34	-9.094	8.66
4	JJTABLE2J	250	0.0288	-52.61	-0.227	12.76	3.2	294.777	255.14	290.11	2.31	-8.75	8.02
5	JJTABLE3A	250	0.0414	122.51	-1.05	9.59	4.63	360.15	327.69	371.13	4.9	-8.94	10.57
6	JJTABLE3D	500	0.169	145.95	-1.04	9.96	5.73	366.498	333.54	369.15	5.75	-8.885	10.88
7	JJTABLE3G	250	0.02	228.73	-1.22	7.19	NA	352.88	322.45	389.105	5.19	-9.12	10.56
8	r =		0.797448	-0.5791	-0.676	.3021	-0.1004	-0.2602	-0.3931	-0.3212	-0.2658	-.2293	-0.38434

Table-2 : Comparative data activity set (measured and predicted)

Table-2			
Compound number	Compound code	Measured activity	Predicted activity
1	JJTABLE2J	250	227.657
2	JJTABLE3G	250	234.45
3	JJTABLE3A	250	311.673
4	JJTABLE3D	500	417.516
5	JJTABLE2B	500	736.496
6	JJTABLE2A	1000	834.533
7	JJTABLE2C	1000	987.7257

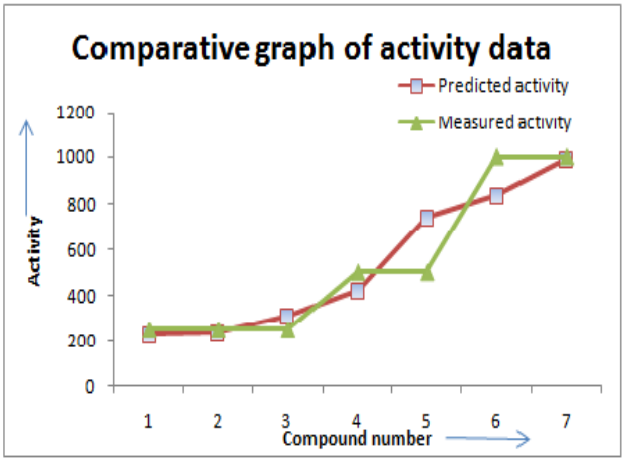

Table-3 : General tendency of correlation between Activity data and physical parameters.

Sample series Code	Predicted activity against E.coli	E.coli MTCC 442	Torsion Energy	Heat of formation	LUMO	Substitutional group R=
JJTABLE2J	227.657	250	0.0288	-52.61	-0.2265	C_4H_7S-
JJTABLE3G	234.450	250	0.0200	228.73	-1.22	3-NO_2-C_6H_4-
JJTABLE3A	311.673	250	0.0414	122.51	-1.05	4-OCH_3-
JJTABLE3D	417.516	500	0.169	145.95	-1.04	4-$(CH_3)_2$-
JJTABLE2B	736.496	500	0.332	36.90	-1.18	-C_6H_5
JJTABLE2A	834.533	1000	0.3829	21.27	-1.28	4-OCH_3-
JJTABLE2C	987.7257	1000	0.229	-135.68	-1.805	3-NO_2-C_6H_4-

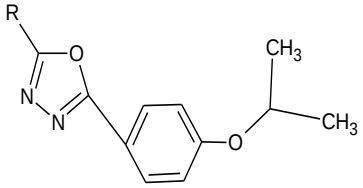

2-(4-ISOPROPOXYPHENYL)-5-(ARYL)-1,3,4-OXADIAZOLE
(**SERIES CODE:- JJTABLE 2)**

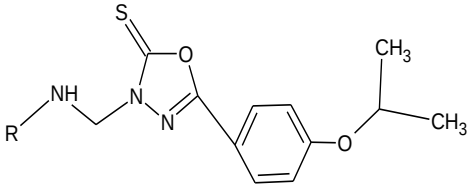

2-(4-ISOPROPOXYPHENYL)-3-N-(ARYL) AMINO METHYL-1,3,4-OXADIAZOLE-5(4H)-THIONE
(**SERIES CODE:- JJTABLE 3)**

PRAJÑĀ - **Journal of Pure and Applied Sciences Vol. 24 – 25 : 110 – 116 (2017)**
ISSN 0975 - 2595

SYNTHESIS OF SYMMETRICAL AND UNSYMMETRICAL 3,3-DI(INDOLYL)INDOLIN-2-ONES VIA FRIEDEL–CRAFTS SUBSTITUTION REACTION USING CELLULOSE SUPPORTED ACIDIC IONIC LIQUID

SHAILESH P. SATASIA, PIYUSH N. KALARIA, BEENA K. VAGHASIYA, JEMIN R. AVALANI AND DIPAK K. RAVAL

Department of Chemistry, Sardar Patel University, Vallabh Vidyanagar- 388 120, Gujarat, India

*Corresponding author. Tel.: +91-02692-226856 - Ext. - 211; Fax: +91-02692 236475.

E-mail: shailesh_satasia@yahoo.com, dipanalka@yahoo.com

ABSTRACT

A novel and highly efficient rapid protocol has been developed for the synthesis of 3,3-di(indolyl)indolin-2-ones viaFriedel–Crafts substitution reaction. C-C bond was formedby the reaction of indoles with isatins using catalytic amount of Cell-IL at room temperature in short reaction time in high yields. The generality of the method has been demonstrated by screening a series of isatin electrophiles as well as indole derivatives.

Keywords: Friedel–Crafts substitution, 3,3-di(indolyl)indolin-2-ones, C-C coupling, Heterogeneous catalyst, Solid acid catalyst

INTRODUCTION

The importance of indoles and their derivatives is well known by synthetic as well as biological chemists.[1] Since its discovery in 1866,[2] more than 80,000 papers related to indole chemistry have been published[3], Indoles have been widely used in pharmaceuticals, fragrances, agrochemicals, pigments and dyes, and material science.[4] Therefore, indole chemistry enjoys a mainstay of organic synthesis and notable interest is observed in the recent past.[3]

On the other hand, di(indolyl)indolin-2-ones are of significant importance due to their wide range of biological activities like anticancer activity[5],anticonvulsant, and antimicrobial activity[6]. 3-Arylidineindoline-2-one analogues, containing an indolinones scaffold exhibited potential HDAC inhibitory activity.[7]Indolinone hybrids also showed micromolar activity against lung cancer cells by partial depletion of intracellular Ca^{2+} stores and phosphorylation in growth inhibition assay.[8]

(Figure 1) depicts the importance of these derivatives. Inspired by these two biologically significant structures such as indole and indolinone, we envisioned that incorporation of an indole moiety into an indolinones scaffold would create a new skeleton of pharmaceutical interest.

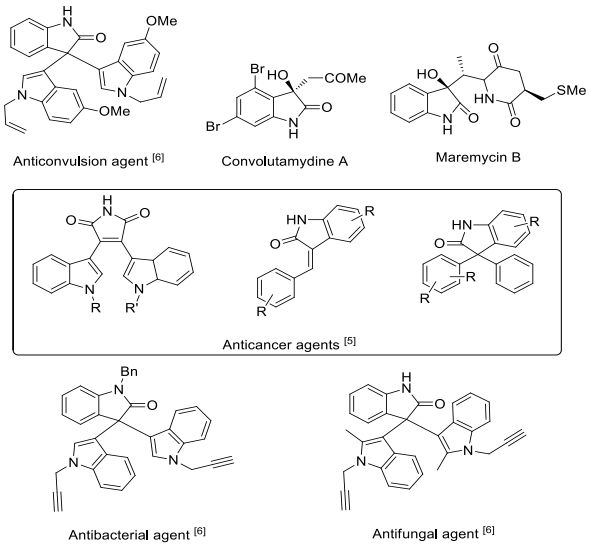

Figure 1. Some example of natural products and biologically active substances containing indole and indolinone motifs.

Friedel−Crafts reaction is one of the key reactions for carbon−carbon bond construction and has been widely used to generate important classes of building blocks.[9-11]several approaches for the formation of C-C bond via Friedel–Crafts reaction are reported in literature.[12-14] However, the reported methods often have some drawbacks like harsh reaction conditions and more catalyst loading. With the increased environmental and economic awareness, the development of greener and sustainable methods for this key transformation has emerged in recent years.[15, 16]Various synthetic methods for

the preparation of 3,3-di(indolyl)indolinones have been reported in the literature.[17-24]

Regarding scope of the reaction, almost all the reported protocols for the synthesis of 3,3-di(indolyl)indolinones, cited above, lacked the exploration of reaction in terms of yield and reaction time. Further, all of these methods suffer from at least single drawback from amongst strongly acidic or basic conditions, employing toxic reagents, costly and complex catalysts or reagents, harsh reaction conditions, tedious workup and moderate yields. Thus literature survey arose to the need to develop a protocol, which offers better results under milder reaction conditions with shorter reaction time and high yield.

In conjunction with our ongoing research, we are particularly interested in the development of biological active different heterocyclic scaffolds using green procedure,[25-36]we herein report a new simple and eco-friendly method to prepare 3,3-diindolyl oxyindolesderivatives.

EXPERIMENTAL

Materials and instrumentation

All reactions were performed using commercially available reagents. They were used without further purification.Cellulose supported ionic liquid (Cell-IL) was prepared as per our reported method.[34]The solvents used were of analytical grade. All reactions were monitored by thin-layer chromatography (TLC) on aluminium plates coated with silica gel 60 F254, 0.25 mm thickness (Merck). Detection of the components was made by exposure to iodine vapors or UV light. Melting points were taken in melting point apparatus µThermoCal10 (Analab Scientific Pvt. Ltd, India) and are uncorrected. The IR spectra were recorded in KBr on Perkin-Elmer Spectrum GX FT-IR Spectrophotometer (Perkin-Elmer, USA) and only the characteristic peaks are reported in cm^{-1}. Mass spectra were recorded on Shimadzu LCMS 2010 spectrometer (Shimadzu, Tokyo, Japan) purchased under PURSE program of DST at Sardar Patel University, Vallabh Vidyanagar. The synthesized compounds were identified by ^{1}H and ^{13}C NMR spectra recorded in DMSO-d_6 as a solvent on a BrukerAvance 400 MHz spectrometer (Bruker Scientific Corporation Ltd., Switzerland) using the residual solvent signal as an internal standard at 400 MHz and 100 MHz respectively.. Chemical shifts are reported in parts per million (ppm).

General procedure for the synthesis of 3,3-di(indolyl)indolin-2-one derivatives.

A mixture of isatins 1a-e (1 mmol), indoles 2a–d (2 mmol), and 5 mL of ethanol was stirred at room temperature in the presence of 20 mg of Cell-IL (Scheme 6.11) until the dissolution of the starting materials. The reaction progress was monitored by thin-layer chromatography (TLC). After completion of the reaction, the reaction mixture was treated with ethanol to recover the insoluble catalyst by filtration. The filtrate was then concentrated under vacuum and the desired product was obtained. The structures of the products were confirmed by ^{1}H NMR, Mass spectrometry, IR . The filtered catalyst was dried under vacuum for 3 h and was reused with fresh charge of the solvent and reactants for subsequent runs under the same reaction conditions to observe its recyclability as the efficient catalyst.

Spectral data:

***3,3-Bis(2-methyl-1H-indol-3-yl)indolin-2-one* (3a).**

Yield: 94%, mp>300 ˚C, IR (KBr, *ν*max, cm^{-1}): 3402, 3297, 1735, 1608, 1117 cm^{-1}; ^{1}H NMR (400 MHz, DMSO-d_6): δ 1.95 (s, 3H, CH_3), 2.08 (s, 3H, CH_3), 6.47 (d, J=8.4 Hz, 1H, Ar–H), 6.64 (t, 2H, Ar–H), 6.72 (d, J=8.0 Hz, 1H, Ar–H), 6.85-6.97 (m, 4H, Ar–H of indole), 7.06-7.24 (m, 4H, Ar–H of indole),10.52 (1H, s, amidic N–H), 10.84 (2H, s, N–H); ESI-MS(m/z): 392.4 (M+1).

3,3-Di(5-bromo-1H-indol-3-yl)indolin-2-one (3b).

Yield: 91%, mp>300 ˚C, IR (KBr, *ν*max, cm^{-1}):3389, 3310, 1714, 1624, 1085, 885cm^{-1}; ^{1}H NMR (400 MHz, DMSO-d_6): δ6.50 (s, 2H, Ar–H), 6.65-6.75 (m, 6H, Ar–H of indole), 6.93-6.97 (m, 4H, Ar–H), 10.91 (s, 2H, N–H), 11.28 (s, 1H, amidic N–H); ESI-MS (m/z): 522.1 (M+1).

5-Chloro-3,3-di(5-bromo-1H-indol-3-yl)indolin-2-one (3c).

Yield: 92%, mp>300 ˚C, IR (KBr, *ν*max, cm^{-1}):3411, 3289, 1721, 1602, 1118, 865cm^{-1}; ^{1}H NMR (400 MHz, DMSO-d_6): δ6.44-6.59 (m,

6H, Ar–H of indole), 6.72 (s, 2H, Ar–H), 7.07-7.16 (m, 3H, Ar–H), 10.98 (s, 2H, NH), 11.21 (s, 1H, amidic N–H); ESI-MS (m/z): 556.4 (M+1).

5-Nitro-3,3-di(5-bromo-1H-indol-3-yl)indolin-2-one (3d).

Yield: 85%, mp>300 ˚C, IR (KBr, *v*max, cm^{-1}):3424, 3294, 1733, 1619, 1109, 841cm^{-1}; ^{1}H NMR (400 MHz, DMSO-d_6): δ6.58 (s, 2H, Ar–H), 6.74-6.89 (m, 6H, Ar–H of indole), 7.13-7.27 (m, 3H, Ar–H), 11.11 (s, 2H, N–H), 11.38 (s, 1H, amidic N–H); ESI-MS (m/z): 567.3 (M+1).

5-Bromo-3,3-di(5-bromo-1H-indol-3-yl)indolin-2-one (3e).

Yield: 92%, mp>300 ˚C, IR (KBr, *v*max, cm^{-1}):3415, 3310, 1728, 1635, 1123, 877cm^{-1}; ^{1}H NMR (400 MHz, DMSO-d_6): δ6.47 (s, 2H, Ar–H), 6.54 -6.77 (m, 6H, Ar–H of indole), 6.89-7.12 (m, 3H, Ar–H), 10.90 (s, 2H, N–H), 11.18 (s, 1H, amidic N–H); ESI-MS (m/z): 601.0 (M+1).

5-Chloro-3,3-di(2-methyl-1H-indol-3-yl)indolin-2-one (3f).

Yield: 86%, mp= 292-293˚C, IR (KBr, *v*max, cm^{-1}):3389, 3326, 1698, 1614, 1142, 856cm^{-1}; ^{1}H NMR (400 MHz, DMSO-d_6): δ1.87 (s, 3H, CH3), 2.13 (s, 3H, CH3), 6.71-6.96 (m, 8H, Ar–H of indole), 7.05-7.09 (m, 2H, Ar–H), 7.62 (s, 1H, Ar–H), 11.09 (s, 2H, N–H), 11.22 (s, 1H, amidic N–H); ESI-MS (m/z): 426.8 (M+1).

5-Bromo-3,3-di(2-methyl-1H-indol-3-yl)indolin-2-one (3g).

Yield: 88%, mp= 289-291˚C, IR (KBr, *v*max, cm^{-1}):3416, 3308, 1725, 1634, 1108, 794cm^{-1}; ^{1}H NMR (400 MHz, DMSO-d_6): δ1.82 (s, 3H, CH3), 2.04 (s, 3H, CH3), 6.56-6.69 (m, 8H, Ar–H of indole), 7.11-7.16 (m, 2H, Ar–H), 7.50 (s, 1H, Ar–H),11.08 (s, 2H, N–H), 11.28 (s, 1H, amidic N–H); ESI-MS (m/z): 470.2(M+1).

***5-Nitro-3,3-di(2-methyl-1H-indol-3-yl)indolin-2-one* (3h).**

Yield: 91%, mp>300 ˚C, IR (KBr, *v*max, cm^{-1}): 3402, 3317, 1724, 1618, 1111, 795 cm^{-1}; ^{1}H NMR (400 MHz, DMSO-d_6): δ 1.96 (s, 3H, CH_3), 2.07 (s, 3H, CH_3), 6.50 (s, 1H, Ar–H), 6.65-6.75 (m, 8H, Ar–H of indole), 6.93-6.97 (m, 2H, Ar–H), 11.03 (s, 2H, N–H), 11.33 (s, 1H, amidic N–H); Anal. calcd for $C_{26}H_{20}N_4O_3$: C, 71.55; H, 4.62; N, 12.84; O, 11.00; found: C, 71.55; H, 4.57; N, 12.68; O, 11.21.

5-Nitro-3,3-di(1-methyl-indol-3-yl)indolin-2-one (3i).

Yield: 89%, mp= mp>300 ˚C, IR (KBr, *v*max, cm^{-1}):3414, 3327, 1708, 1623, 1102, 821cm^{-1}; ^{1}H NMR (400 MHz, DMSO-d_6): δ3.77 (s, 6H, 2CH3), 6.71-6.89 (m, 6H, Ar–H), 7.06 (s, 1H, Ar–H), 7.28-7.32 (m, 2H, Ar–H), 7.39-7.49 (m, 4H, Ar–H), 10.12 (s, 1H, amidic N–H); ESI-MS (m/z): 437.3(M+1).

5-Nitro-3,3-di(7-aza-1H-indol-3-yl)indolin-2-one (3j).

Yield: 84%, mp= 281-282˚C, IR (KBr, *v*max, cm^{-1}):3409, 3293, 1722, 1625, 1131, 886cm^{-1}; ^{1}H NMR (400 MHz, DMSO-d_6): δ6.44 (s, 1H, Ar–H), 6.61-6.79 (m, 6H, Ar–H of indole), 6.88-6.94 (m, 2H, Ar–H), 7.39-7.48 (m, 2H, Ar–H), 11.09 (s, 2H, N–H), 11.24 (s, 1H, amidic N–H); ESI-MS (m/z): 411.4 (M+1).

5-Chloro-3,3-di(1-methyl-indol-3-yl)indolin-2-one (3k).

Yield: 87%, mp= 292-293˚C, IR (KBr, *v*max, cm^{-1}):3407, 3313, 1717, 1608, 1121, 845cm^{-1}; ^{1}H NMR (400 MHz, DMSO-d_6): δ3.67 (s, 6H, 2CH3), 6.81-6.94 (m, 6H, Ar–H), 7.19 (s, 1H, Ar–H), 7.32-7.38 (m, 2H, Ar–H), 7.47-7.59 (m, 4H, Ar–H), 8.97 (s, 1H, amidic N–H); ESI-MS (m/z): 426.7(M+1).

***5-Fluoro-3,3-di(1-methyl-indol-3-yl)indolin-2-one* (3l).**

Yield: 92%, mp>300 ˚C, IR (KBr, *v*max, cm^{-1}): 3421, 3292, 1741, 1618, 1090, 789 cm^{-1}; ^{1}H NMR (400 MHz, DMSO-d_6): δ 3.73 (s, 6H, $2CH_3$), 6.86-6.99 (m, 6H, Ar–H), 7.13 (s, 1H, Ar–H), 7.20-7.23 (m, 2H, Ar–H), 7.28-7.37 (m, 4H, Ar–H), 8.60 (s, 1H, amidic N–H); Anal. calcd for $C_{26}H_{20}FN_3O$: C, 76.27; H, 4.92; F, 4.64; N, 10.26; O, 3.91; found: C, 76.27; H, 4.81; F, 4.62; N, 10.36; O, 4.08.

RESULTS & DISCUSSION

Cellulose supported ionic liquid was prepared and characterized as per our reported method[34] and was used as the catalyst for synthesis of 3,3-di(indolyl)indolin-2-one derivatives. In the exploratory study of our newly proposed Friedel–Crafts process for the preparation of 3,3-di(indolyl)indolin-2-one derivatives, we carried

out first experiment by reacting simple isatin (**1a**) with 2-methyl indole (**2a**) to understand the importance of prepared catalyst to afford 3a as the product.

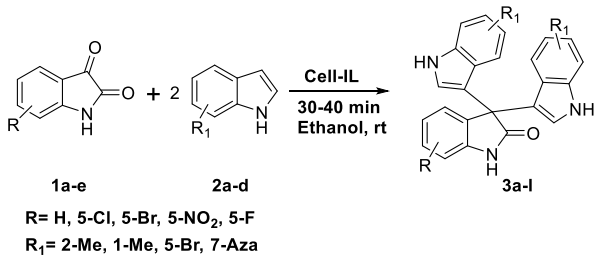

Scheme 1. Synthesis of 3,3 di(indolyl)indol-in-2-ones

The effectiveness of the reaction was affected by the amount of catalyst. The model reaction was attempted without any catalyst (Table 1, entry 1), which afforded the target compound 3a in very poor yield. From the performed sets of reactions, it was found that 20 mg of Cell-IL was the optimum amount of catalyst leading to 94% yield of 3a in ethanol at room temperature (Table 1, entry 5) in 30 min. Encouraged by these promising results, we then probed other catalyst for their catalytic activity towards the synthesis of 3,3-di(indolyl)indolin-2-one derivatives. Some other catalysts *viz.*, I_2, ceric ammonium nitrate (CAN), Amberlyst-15, HCl, *p*-TSA, $FeCl_3.6H_2O$, and Dowex50WX4 were found to promote the reaction with poor yield along with the impurities even after longer reaction time (Table 1, entries 9–14).It became evident that the catalysts played a vital role in the success of the reaction in terms of reaction time and yields of 3,3-di(indolyl)indolin-2-one derivatives.

Table 1. Optimization of reaction conditions[a] for the synthesis of 3a.[a]

Entry	Catalyst	Amout (mg)	Time (min) [b]	Yield (%)[c]
1	-	-	115	24
2	Cell-IL	5	85	54
3	Cell-IL	10	65	70
4	Cell-IL	15	45	81
5	Cell-IL	20	30	94
6	Cell-IL	25	40	92
7	Cell-IL	30	40	92
8	Iodine	20	75	84
9	CAN	20	85	70
10	Amberlyst-15	20	70	49
11	HCl	20	105	35
12	*p*-TSA	20	75	32
13	$FeCl_3.6H_2O$	20	70	21
14	Dowex50WX4	20	95	41

[a] Isatin (1 mmol) and 2-methylindole (2 mmol).
[b]All reactions were run in ethanol at rt till completion as indicated by TLC.
[c]Isolated yield.

Selection of an appropriate solvent for Friedel–Crafts reaction is very crucial. Among the solvents probed, ethanol was found to be the best choice for the synthesis of 3,3-di(indolyl)indolin-2-one derivatives (Table 2, entry 3).

Table 2.Solvent study on the synthesis of 3a[a].

Entry	Solvent	Time (min)[b]	Yield (%)[c]
1	-	85	56
2	Water	50	61
3	**Ethanol**	**30**	**94**
4	THF	65	35
5	Chloroform	90	59
6	DCM	80	21
7	Methanol	75	74
8	DMF	65	68

[a] Isatin (1 mmol) and 2-methylindole (2 mmol) and Cell-IL (20 mg).
[b]All reactions were run in ethanol at rt till completion as indicated by TLC.
[c] Isolated yield.

The best results were obtained with 1:2 mmol ratios of isatins and indoles in the presence of 20 mg Cell-IL at room temperature. Both the yield and reaction time for the reaction were found to be solvent and catalyst dependent. In this instance, high yield (94%) was achieved in short reaction time using Cell-IL as the catalyst (Table 1, entry 5). It was noteworthy that when I_2 was employed, 84% yield was obtained but the reaction took longer time for completion (Table 1, entry 8).

With the optimized conditions in hand, we determined the scope of the reaction with a variety of isatins (**1a-e**) and indoles (**2a-d**) (Scheme 1). Several indoles and isatin derivatives, having electron donating and electron withdrawing substituents, underwent the same reaction efficiently using Cell-IL as the catalyst. The results are listed in Table 3.

Table 3.Synthesis of 3,3-di(indolyl)indolin -2-one derivatives employing Cell-IL as the catalyst[a].

Entry	Isatins	Indoles	Products	Time (min.)[b]	Yield (%)[c]
1	H	2-CH_3	3a	30	94
2	H	5-Br	3b	30	91
3	5-Cl	5-Br	3c	35	92
4	5-NO_2	5-Br	3d	35	85
5	5-Br	5-Br	3e	35	92
6	5-Cl	2-CH_3	3f	30	86
7	5-Br	2-CH_3	3g	35	88
8	5-NO_2	2-CH_3	3h	30	91
9	5-NO_2	1-CH_3	3i	30	89
10	5-NO_2	7-aza	3j	40	84
11	5-Cl	1-CH_3	3k	30	87
12	5-F	1-CH_3	3l	30	92

[a] Isatin (1 mmol) and 2-methylindole (2 mmol) and Cell-IL (20 mg).
[b]All reactions were run in ethanol at rt till completion as indicated by TLC.
[c] Isolated yield.

However, when 3-methyl indole was used, no reaction occured under the same conditions even after long reaction time.The yield was observed to be relatively low when 7-aza indole**2d** was used (**3j**), which may be due to the low reactivity of the aza group.

Plausible reaction mechanism:

A plausible mechanistic elucidation to explain the formation of the observed 3,3-di(indolyl)indolin-2-ones might reasonably assume a Friedel−Crafts reaction path that implies an initial activation of carbonyl group of isatin by Cell-IL. After that nucleophilic addition of the indole onto the ketonic carbonyl group of isatin to yield the corresponding 3-(indol-3-yl)-3-hydroxyindolin-2-one (**I**). Instant dehydration of this adduct gives the intermediate (**Ia**), which subsequently undergoes 1,4-nucleophilic addition of the second indole molecule to provide the final product 3,3-di(indol-3-yl)indolin-2-ones (Scheme 2).

Scheme 2. Plausible mechanism for the 3,3-di(indolyl)indolin-2-one.

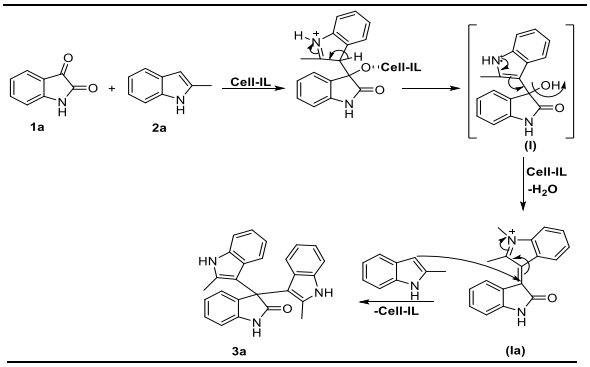

The reaction was feasible without the need of metal catalyst for formation of C-C bond. All the prepared compounds were obtained in pure form after recrystallization from hot ethanol.From the leaching test of the catalyst, it was found that no homogeneous catalyst was incorporated in the product.

Recyclability of the catalyst

The recovery and reuse of the catalyst was also investigated. After the completion of reaction w, the mixture was diluted with hot ethanol and Cell-IL was removed by simple filtration. The recovered catalyst was reused for the next cycle of the same reaction.(Table 4) presents the results of the efficient recycling of the catalyst. It is seen that the Cell-IL had been reused for 5 times without any significant loss in its activity.

Table 4.Reusability study

No. of runs	Fresh	1	2	3	4	5
% Yield	94	94	93	92	91	91

CONCLUSIONS

We have reported synthesis of 3,3-di(indolyl)indolin-2-ones via Friedel–Crafts substitution reaction involving C-C bond formation using Cell-IL as the catalyst. Easy procedure associated with the high yield of products, recyclability of the catalyst, and short reaction times at room temperature rendered the method as highly viable compared to existing procedures. The efficient, convenient and novel method offered here could be of broad interest for synthetic chemists.

ACKNOWLEDGEMENTS

University Grants Commission, New Delhi, INDIA awarded Research Fellowship for Science Meritorious Students (RFSMS) to SPS and PNK. The authors also thank the Head, Department of Chemistry, Sardar Patel University, Vallabh Vidyanagar-388 120, INDIA for providing research facilities. The assistance in form of elemental analysis on concessional rates by SICART, Vallabh Vidyanagar-388 120, INDIA is also gratefully acknowledged.

REFERENCES:

[1] Sundberg, R. J.; Katritzky, A. R.; Meth-Cohn, O.; Rees, C. S. *Indoles*; Elsevier Science, 1996.

[2] Baeyer, A. (1866): Ueber die Reduction aromatischerVerbindungenmittelstZinkstaub. *Justus LiebigsAnnalen der Chemie*, *140*: 295-296.

[3] Bandini, M.; Eichholzer, A. (2009): Catalytic Functionalization of Indoles in a New Dimension. *AngewandteChemie International Edition*, *48*: 9608-9644.

[4] Sundberg, R. *The Chemistry of Indoles*; Elsevier Science, 2012; Vol. Academic Press: New York.

[5] Kamal, A.; Srikanth, Y. V. V.; Khan, M. N. A.; Shaik, T. B.; Ashraf, M. (2010): Synthesis of 3,3-diindolyl oxyindoles efficiently catalysed by FeCl3 and their in vitro evaluation for anticancer activity. *Bioorganic & Medicinal Chemistry Letters*, *20*: 5229-5231.

[6] Praveen, C.; Ayyanar, A.; Perumal, P. T. (2011): Practical synthesis, anticonvulsant, and antimicrobial activity of N-allyl and N-propargyldi(indolyl)indolin-2-ones. *Bioorganic & Medicinal Chemistry Letters*, *21*: 4072-4077.

[7] Huber, K.; Schemies, J. r.; Uciechowska, U.; Wagner, J. M.; Rumpf, T.; Lewrick, F.; Süss, R.; Sippl, W.; Jung, M.; Bracher, F. (2009): Novel 3-Arylideneindolin-2-ones as Inhibitors of NAD+-Dependent Histone Deacetylases (Sirtuins). *Journal of Medicinal Chemistry*, *53*: 1383-1386.

[8] Natarajan, A.; Guo, Y.; Harbinski, F.; Fan, Y.-H.; Chen, H.; Luus, L.; Diercks, J.; Aktas, H.; Chorev, M.; Halperin, J. A. (2004): Novel Arylsulfoanilide−Oxindole Hybrid as an Anticancer Agent That Inhibits Translation Initiation. *Journal of Medicinal Chemistry*, *47*: 4979-4982.

[9] Friedel, C.; Crafts, J. (1877): Organic chemistry. *Journal of the Chemical Society*, *32*: 725-791.

[10] Mertins, K.; Iovel, I.; Kischel, J.; Zapf, A.; Beller, M. (2005): Transition-Metal-Catalyzed Benzylation of Arenes and Heteroarenes. *AngewandteChemie International Edition*, *44*: 238-242.

[11] Nicolaou, K. C.; Bulger, P. G.; Sarlah, D. (2005): Palladium-Catalyzed Cross-Coupling Reactions in Total Synthesis. *AngewandteChemie International Edition*, *44*: 4442-4489.

[12] Fürstner, A.; Voigtländer, D.; Schrader, W.; Giebel, D.; Reetz, M. T. (2001): A "Hard/Soft" Mismatch Enables Catalytic Friedel−Crafts Acylations. *Organic Letters*, *3*: 417-420.

[13] Gmouh, S.; Yang, H.; Vaultier, M. (2003): Activation of Bismuth(III) Derivatives in Ionic Liquids: Novel and Recyclable Catalytic Systems for Friedel−Crafts Acylation of Aromatic Compounds. *Organic Letters*, *5*: 2219-2222.

[14] Song, C. E.; Shim, W. H.; Roh, E. J.; Choi, J. H. (2000): Scandium() triflateimmobilised in ionic liquids: a novel and recyclable catalytic system for Friedel-Crafts alkylation of aromatic compounds with alkenes. *Chemical Communications*, 1695-1696.

[15] Huo, C.; Xu, X.; An, J.; Jia, X.; Wang, X.; Wang, C. (2012): Approach to Construct Polysubstituted 1,2-Dihydronaphtho[2,1-b]furans and Their Aerobic Oxidative Aromatization. *The Journal of Organic Chemistry*, *77*: 8310-8316.

[16] Huo, C.; Xu, X.; Jia, X.; Wang, X.; An, J.; Sun, C. (2012): Friedel–Crafts alkylation between chalcone epoxides and heteroarenes induced by triarylaminium salt. *Tetrahedron*, *68*: 190-196.

[17] Azizian, J.; Mohammadi, A. A.; Karimi, N.; Mohammadizadeh, M. R.; Karimi, A. R. (2006): Silica sulfuric acid a novel and heterogeneous catalyst for the synthesis of some new oxindole derivatives. *Catalysis Communications*, *7*: 752-755.

[18] Nikpassand, M.; Mamaghani, M.; Tabatabaeian, K.; Samimi, H. A. (2010): An Efficient and Clean Synthesis of Symmetrical and Unsymmetrical 3,3-Di(indolyl)Indolin-2-ones Using KSF. *Synthetic Communications*, *40*: 3552-3560.

[19] Paira, P.; Hazra, A.; Kumar, S.; Paira, R.; Sahu, K. B.; Naskar, S.; saha, P.; Mondal, S.; Maity, A.; Banerjee, S.; Mondal, N. B. (2009): Efficient synthesis of 3,3-diheteroaromatic oxindole analogues and their in vitro evaluation for spermicidal potential.

Bioorganic & Medicinal Chemistry Letters, *19*: 4786-4789.

[20] Praveen, C.; Wilson Sagayaraj, Y.; Perumal, P. T. (2009): Gold(I)-catalyzed sequential cycloisomerization/bis-addition of o-ethynylanilines: an efficient access to bis(indolyl)methanes and di(indolyl)indolin-2-ones. *Tetrahedron Letters*, *50*: 644-647.

[21] Rad-Moghadam, K.; Sharifi-Kiasaraie, M.; Taheri-Amlashi, H. (2010): Synthesis of symmetrical and unsymmetrical 3,3-di(indolyl)indolin-2-ones under controlled catalysis of ionic liquids. *Tetrahedron*, *66*: 2316-2321.

[22] Subba Reddy, B. V.; Rajeswari, N.; Sarangapani, M.; Prashanthi, Y.; Ganji, R. J.; Addlagatta, A. (2012): Iodine-catalyzed condensation of isatin with indoles: A facile synthesis of di(indolyl)indolin-2-ones and evaluation of their cytotoxicity. *Bioorganic & Medicinal Chemistry Letters*, *22*: 2460-2463.

[23] Wang, S.-Y.; Ji, S.-J. (2006): Facile synthesis of 3,3-di(heteroaryl)indolin-2-one derivatives catalyzed by ceric ammonium nitrate (CAN) under ultrasound irradiation. *Tetrahedron*, *62*: 1527-1535.

[24] Yadav, J. S.; SubbaReddy, B. V.; Gayathri, K. U.; Meraj, S.; Prasad, A. R. (2006): Bismuth(III) Triflate Catalyzed Condensation of Isatin with Indoles and Pyrroles-: A Facile Synthesis of 3,3-Diindolyl- and 3,3-Dipyrrolyl Oxindoles. *Synthesis*, *2006*: 4121-4123.

[25] Kalaria, P. N.; Makawana, J. A.; Satasia, S. P.; Raval, D. K.; Zhu, H.-L. (2014): Design, synthesis and molecular docking of novel bipyrazolylthiazolone scaffold as a new class of antibacterial agents. *MedChemComm*, *5*: 1555-1562.

[26] Kalaria, P. N.; Satasia, S. P.; Avalani, J. R.; Raval, D. K. (2014): Ultrasound-assisted one-pot four-component synthesis of novel 2-amino-3-cyanopyridine derivatives bearing 5-imidazopyrazole scaffold and their biological broadcast. *European journal of medicinal chemistry*, *83*: 655-664.

[27] Kalaria, P. N.; Satasia, S. P.; Raval, D. K. (2014): Synthesis, characterization and pharmacological screening of some novel 5-imidazopyrazole incorporated polyhydroquinoline derivatives. *European journal of medicinal chemistry*, *78*: 207-216.

[28] Kalaria, P. N.; Satasia, S. P.; Raval, D. K. (2014): Synthesis, characterization and biological screening of novel 5-imidazopyrazole incorporated fused pyran motifs under microwave irradiation. *New Journal of Chemistry*, *38*: 1512-1521.

[29] 29. Kalaria, P. N.; Satasia, S. P.; Raval, D. K. (2014): Synthesis, identification and in vitro biological evaluation of some novel 5-imidazopyrazole incorporated pyrazoline and isoxazoline derivatives. *New Journal of Chemistry*, *38*: 2902-2910.

[30] Kalaria, P. N.; Satasia, S. P.; Raval, D. K. (2014): L-Proline promoted green and regioselective synthesis of a novel pyrazole based trifluoromethylated fused thiazolopyran scaffold and its biological evaluation. *RSC Advances*, *4*: 32353-32362.

[31] Purohit, V. B.; Karad, S. C.; Patel, K. H.; Raval, D. K. (2014): Cu (N-heterocyclic carbene) chloride: an efficient catalyst for multicomponent click reaction for the synthesis of 1, 2, 3-triazoles in water at room temperature. *RSC Advances*, *4*: 46002-46007.

[32] Purohit, V. B.; Karad, S. C.; Patel, K. H.; Raval, D. K. (2015): Palladium N-heterocyclic carbene catalyzed regioselective C–H halogenation of 1-aryl-3-methyl-1 H-pyrazol-5 (4 H)-ones using N-halosuccinimides (NXS). *Catalysis Science & Technology*, *5*: 3113-3118.

[33] Satasia, S. P.; Kalaria, P. N.; Avalani, J. R.; Raval, D. K. (2014): An efficient approach for the synthesis of spirooxindole derivatives catalyzed by novel sulfated choline based heteropolyanion at room temperature. *Tetrahedron*, *70*: 5763-5767.

[34] Satasia, S. P.; Kalaria, P. N.; Raval, D. K. (2013): Acidic ionic liquid immobilized on cellulose: an efficient and recyclable heterogeneous catalyst for the solvent-free synthesis of hydroxylatedtrisubstituted pyridines. *RSC Advances*, *3*: 3184-3188.

[35] Satasia, S. P.; Kalaria, P. N.; Raval, D. K. (2014): Catalytic regioselective synthesis of pyrazole based pyrido [2, 3-d] pyrimidine-diones and their biological evaluation. *Organic and Biomolecular Chemistry*, *12*: 1751-1758.

[36] Satasia, S. P.; Kalaria, P. N.; Raval, D. K. (2014): Heteropolyanion-based sulfated ionic liquid catalyzed formamides synthesis by grindstone chemistry. *Journal of Molecular Catalysis A: Chemical*, *391*: 41-47.

PRAJÑĀ - **Journal of Pure and Applied Sciences Vol. 24 – 25 : 117 – 120 (2017)**
ISSN 0975 - 2595

ALIPHATIC-AROMATIC POLYESTERS DERIVED FROM ISOPHTHALOYL CHLORIDE, ETHYLENE GLYCOL AND HEXYLENE GLYCOL

YOGESHWAR CHAMKURE AND RAKESH SHARMA

Applied Chemistry Department, Faculty of Technology and Engineering, The Maharaja Sayajirao University of Baroda, Vadodara-390001, Gujarat, India. Email: raksharmain@yahoo.com

ABSTRACT

In the family of thermoplastic polyesters, polyethylene terephthalate(PET) is well known but polyethylene isophthalate(PEI) not explored much. In present work, we were synthesized the aliphatic-aromatic polyesters from monomeric compositions of IPC, EG and HG using phase-transfer catalyzed interfacial polycondensation technique. The synthesized polyesters were well-characterized through FTIR, ^{1}H-NMR, TGA, DSC and GPC techniques. The introduction of HG favours the solubility and loosens the stiffness of polyester because of the presence of branched methyl group. No significant difference exits among the thermal stabilities of these polyesters. Such polyesters with aforementioned properties are suitable for applications where rigidness of PET not require.

Keywords: Polyesters, polyethylene isophthalate, hexyelene glycol, thermal properties.

INTRODUCTION

Poly(ethylene isophthalate) (PEI) is a relatively unexplored polyester, although its isomer, poly(ethylene terephthalate) (PET), has been researched, developed, and utilized hugely. PEI is a long, high-molecular-weight polyester chain, with a repeat unit ($C_{10}H_8O_4$) containing backbone phenyl rings with carboxyl groups attached in the meta 1,3 positions. PEI has not been used in industry, although the conformational characteristics of its phenyl rings would suggest potential uses in applications where PET would not suffice [1, 2]. In PET, the phenyl rings with carboxyl groups attached in the parallel 1,4 positions. Such colinear attachment of ethylene glycol diester to the phenyl rings in PET allows for flipping of the rings. Even nonlinear attachment to the naphthyl rings in Poly(ethylene 2,6 naphthalate) PEN, as compare to the PET chain appears to be less flexible. Because of the noncolinear attachment of the phenyl rings in PEI as meta position, the phenyl rings of PEI may not be flipped. Hence PEI has a lower gas permeability and possibly substituted the PET in applications where this is a factor [2]. Copolymerization resulting from the mixture of aromatic and aliphatic units is well known approach aimed at modifying the polyester structure and thermal properties. It has resulted variety of new materials with more or less success and their properties evaluated with reference to the parent homopolymer [3-5]. PEI and its copolyesters are generally difficult to process because of their high melting temprature due to rigid structure. To the best of our knowledge, no one synthesized and studied the PEI copolyester in which hexylene glycol used as monomer. In this work, we have synthesized the poly(ethylene isophthalate), poly(hexylene isophthalate) and copolyester, poly(ethylene-co-hexylene isophthalate), with the objective of less rigid structure using versatile interfacial polycondensation technique for better applications.

SYNTHESIS OF POLYESTERS

The isophthaloyl chloride (Aldrich, USA, recrystallized with n-hexane), ethylene glycol (SD-Fine, India) and hexylene glycol (SD-Fine, India) monomers were purchased for polyester synthesis. SD-Fine chemicals of benzalkonium chloride (BKC), dichloro methane and sodium hydroxide were procured. The polyethylene isophthalate (PEI), polyhexylene isophthalate (PHI) and copolyester, poly(ethyelene-co-hexylene) isophthalates (PEHI) using 50:50 diol ratio of EG and HG, were synthesized through the interfacial polycondensation technique using as phase transfer catalyst[6](Scheme.1). In a three-necked round bottomed flask (500 mL) equipped with a nitrogen inlet tube, a dropping funnel, and a thermometer; the EG (2.13 gms, 0.0344 mol) dissolved in NaOH solution (0.1 N, 75 mL) was placed and stirred for 15 min at RT. To this mixture, BKC (2 %w/v, 5mL) was added dropwise with stirring. After 30 min, the IPC (7.0 gms, 0.0344 mol) dissolved in DCM (25 mL) was added dropwise to the reaction mixture and vigourously stirred (1500 rpm) for 3 h at RT.

PRAJÑĀ - Journal of Pure and Applied Sciences Vol. 24 – 25 : 117 – 120 (2017)
ISSN 0975 - 2595

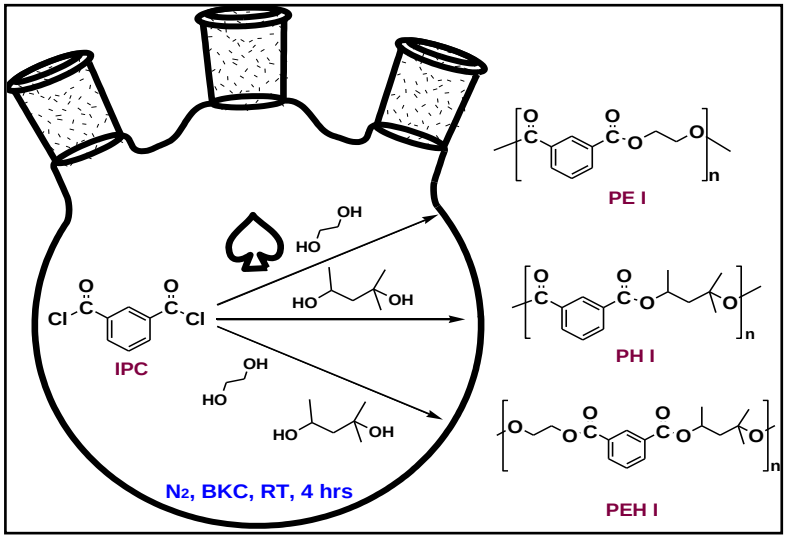

Scheme.1: Synthesis of PEI, PHI and PEHI

Table.1: Monomer compositions and characteristics of synthesized polyesters

Polyesters	EG	HG	IPC	T_i [a]	T_{50} [b]	T_{max} [c]	T_m [d]	η_{inh} [e]	Mw [f] (10^3 g/mol)	Mn [g] (10^3 g/mol)	PDI [h]
	Mol %										
PEI	100	00	100	219	296	476	302	0.060	-	-	-
PHI	00	100	100	170	274	358	288	0.031	3.42	3.02	1.13
PEHI	75	25	100	173	278	442	280	0.042	3.08	3.02	1.01

[a] initial decomposition temperature, [b] 50% weight loss, [c] maximum decomposition temperature, [d] melting temperature, [e]inherent viscosity, [f] weight average molecular weight, [g] number average molecular weight, [h] polydispersity index

The resultant content was poured into water; the precipitated polymer, PEI, is then filtered, washed with water and dried under reduced pressure at 40°C for 24 h. The similar procedure was followed for the synthesis of other two polyesters. Spectral characterizations of synthesized polyesters were recorded using FTIR (Shimadzu, 8400) and ^{1}H NMR (Bruker, 300MHz). The number average molecular weight (Mn), weight average molecular weight (Mw), and polydispersity index (PDI) of polyesters were determined using GPC (Perkin-Elmer) analysis. Thermal studies have been carried out with TGA (Shimadzu, TG50) and DSC (Shimadzu, 200F3) techniques. Physico-chemical behaviour of polyesters was discussed with solubility and viscosity studies.

RESULTS AND DISCUSSION

The white coloured crystalline powder forms of synthesized PEI, PHI and copolyester, PEHI, have shown low molecular weight compound (Mw = ~ 3 x 10^3 g/mol) with PDI of ~1.1 using GPC. The absorption bands inbetween 1782-1684 cm^{-1} (C=0 stretching) and 1303-1068 cm^{-1} (-C-O-C- stretching) in the IR spectrums of PEI, PHI and PEHI (Figure.1a) were indicated the presence of ester linkages [7]. ^{1}H NMR spectrum of PEHI was carried out in DMSO (Figure.1b). The signals of aromatic protons of the isophthalate ring were located at 8.48 ppm, 8.15 ppm, 7.65 ppm while aliphatic protons of methylene have appeared at 4.81-4.70 ppm. The signal at 1.73 ppm, 1.32 ppm, 1.10 ppm, 1.20 may be attributed to methyl protons of pentane moiety in the polyester chain. The resonance signals of methylene protons are observed at 1.91 ppm [2]. Both the techniques were confirmed the formation of copolyester, PEHI.

TGA curves of polyesters (Figure.1c) were thermally stable upto 169°-220°C with multistage degradation patterns. The initial decomposition (T_i) of PEI at 220°C, PHI at 170°C and PEHI around 173°C indicates that

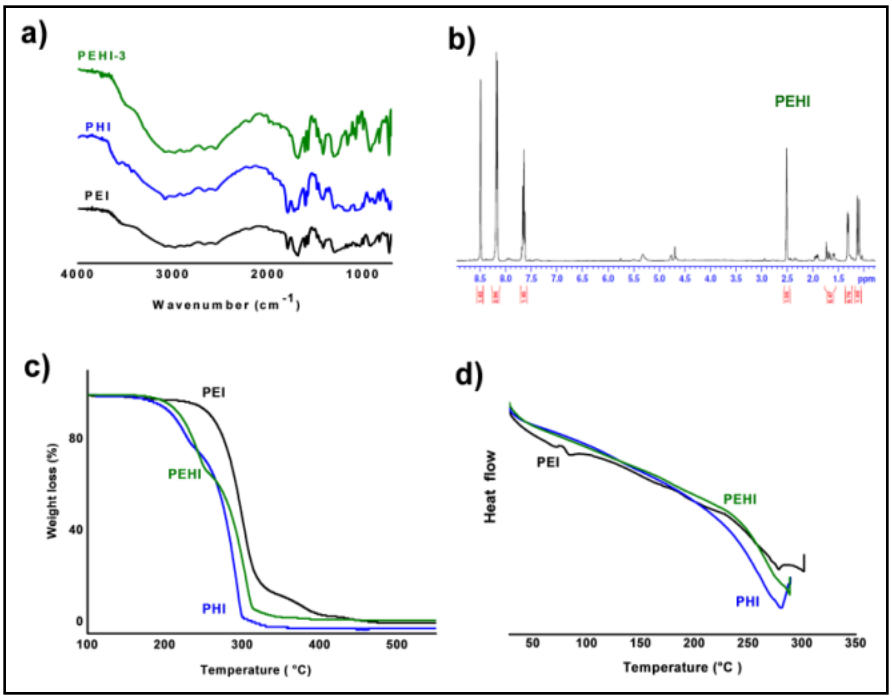

Figure.1: a) FTIR spectra, b) ^{1}HNMR spectra of PEHI, c) TGA curves and d) DSC thermograms of synthesized PEI, PHI and PEHI

hexylene moiety decreases the resonance in the polymer chain. The maximum thermal degradation (T_{max}) of PEI has started from 470°C and PHI from 360°C. But copolyester, PEHI, shows the T_{max} from 445°C. It was clearly indicated the stability of PEHI better than PHI [8]. From the DSC thermogram (Figure.1d), it can be concluded that melting temperature(T_m) of polyesters, PHI and PEHI, containing methyl side chain was less than PEI (not having methyl side chain). Results have proved that the rigidity of the polyester molecule reduces in the presence of HG.

Synthesised PHI and PEHI were easily soluble in aprotic polar solvents like THF, DMSO, DMF and insoluble in chlorinated solvents like DCM, chloroform as well as in water and HCs of toluene type solvents[9, 10]. But PEI has not been solubilized in the used solvents due to its rigid aromatic nature. Solubility studies were clearly proved that the introduction of methyl side chain in the parent polyester chain increases the solubility parameters. The decrease in inherent viscosity of HG based polyesters than PEI also confirmed the less rigidity in the molecule.

CONCLUSION

The aliphatic-aromatic polyesters, PEI, PHI and PEHI were successfully synthesized using phase -transfer catalyzed interfacial polycondensation technique and well-characterized through FTIR, ^{1}H-NMR, TGA, DSC and GPC techniques. Addition of HG with EG in the copolyester PEHI has shown better solubility and decreases the stiffness of polyester. Not much compromised in thermal stabilities of the polyesters was also fruitful for its applications. Copolyesters with flexi properties are better proccessable and applicable where PET not found better. Such flexible polyesters consumption has increased substantially in fibers and molding resins due to the strong demand for textile applications, as well as in food packaging and bottle markets.

ACKNOWLEDGEMENTS

The authors are gratefully thankful to Prof. R.C. Tandel, Head of Applied Chemistry Department, Faculty of Technology and Engineering, The Maharaja Sayajirao University of Baroda, Vadodara for providing the neccesary facilities.

REFERENCES

[1] Tonelli, A. E. (2002) : Conformational characteristics of poly(ethylene phthalate)s. *J. Poly. Sci. B: Poly. Phy.*, **40**: 1254-1260.

[2] Kotek, R., Pang, K., Schmidt, B. and Tonelli, A. (2004) : Synthesis and gas barrier characterization of poly(ethylene isophthalate). *J. Poly. Sci. B : Poly. Phys.*, **42**: 4247-4254.

[3] Namkajorn, M., Petchsuk, A., Opaprakasit, M. and Opaprakasit, P. (2010) : Synthesis and characterizations of degradable aliphatic-aromatic copolyesters from lactic acid, dimethyl terephthalate and diol: Effects of diol type and monomer feed ratio. *Exp. Poly. Letters.*, **4(7)**: 415-422.

[4] Hoppens, N.C., Hudnall, T.W., Foster, A. and Booth, C.J. (2004) : Aliphatic-aromatic copolyesters derived from 2,2,4,4-tetramethyl-1,3-cyclobutane diol. *J. Poly. Sci. A : Poly. Chem.*, **42**: 3473-3478.

[5] Li, W. D. and Ding, E. Y. (2007) : Preparation and characterization of a series of diol di-stearates as phase change heat storage materials. *Mater. Letters*, **61**: 4325-4328.

[6] Wang, D.C., Wang, C.Y., Chiu, W.Y. and Chen, L.W. (1997) : Synthesis of polyarylate through interfacial polycondensadtion by use of glycolyzed products of poly(ethylene terephthalate) glycolysis with bisphenol A. *J. Poly. Res.*, **4(1)**: 9-16.

[7] Wang, C. and Nakamura, S. (1995) : Synthesis of reactive copolyesters derived from isophthaloyl chloride, bisphenol A, and aliphatic diols with additional reactive groups. J. *Poly. Sci. A: Poly. Chem.*, **33**: 2027-2031.

[8] Aly, K. I. (1998) : New polymer syntheses VIII. Synthesis, characterization and morphology of new unsaturated copolyesters based on dibenzylidenecycycloalkanones. *Polymer Intl.*, **47**: 483-490.

[9] Murugavel, S.C., Swaminathan, C.S. and Kannan, P. (1997) : Synthesis and characterization of photocrosslinkable poly(benzylidene phosphoramide ester)s. *J. Appl. Poly. Sci.*, **38**: 5179-5183.

[10] Murugavel, S.C., Kaliyappan, T., Swaminathan, C.S. and Kannan, P. (1997) : Synthesis and spectral, thermal, and photocrosslinking studies of poly(benzylidene phosphoramide ester)s. *J. Appl. Poly. Sci.*, **65**: 2151-2157.

PRAJÑĀ - **Journal of Pure and Applied Sciences Vol. 24 – 25 : 121 – 129 (2017)**
ISSN 0975 - 2595

STUDIES ON ESTERIFICATION OF SUGARCANE BAGASSE (SCB)

JITENDRA K. PARMAR*[1] AND DIPAK K. RAVAL[2]

[1]Government Science College, Idar
[2]Department of Chemistry, Sardar Patel University, Vallabh Vidyanagar-388 120.
Email: aanal.virat@gmail.com

ABSTRACT

The esterification of cellulose has acquired great importance due to the wide applicability of the products for various useful purposes. Esterification is a well known reactions by which polysaccharide can easily be transformed into the modified form. Sugarcane bagasse (SCB) powder was activated by alkali treatment prior to modification. The phthalate, maleate and succinate derivatives of SCB were synthesized by employing respective acid anhydride as the esterifying agent and acetic acid as the solvent. Pyridine was used as the catalyst for preparation of the ester derivatives. The effects of reaction influencing factors like concentration of acid anhydride, amount of pyridine, liquid:solid ratio and reaction period were studied. The products were characterized by determination of ester, IR-Spectroscopy and by thermogravimetry.

Keywords: Esterification, Sugarcane Bagasse (SCB), Phthalate, Maleate, Succinate.

INTRODUCTION

In recent years, there observed an increasing trend towards more efficient utilization of agro-industrial residues such as sugarcane bagasse (generally known as "bagasse"), sugar beet pulp, and coffee pulp. These lingo-cellulosic materials are abundant and renewable, and they are promising to be used as alternatives to fossil resources [1]. Nowadays chemically modified SCB is used to remove water pollutants as its adsorption capacity of metal ions from aqueous solution is excellent [2,3].

Because of the increasing need for high performance biocompatible polymers, new synthetic paths for the defined chemical modification of the polyglucan cellulose were investigated[4]. Cerqueira A. D. et al. [5] reported membrane from cellulose acetate using poly (ethylene glycol) as additive. They used SCB as a cellulosic source for the study. Xie W. et al. [6] reported the chemical modification of corn starch by using ionic liquid as the catalyst. Succinic anhydride or acetic anhydride was employed as an esterifying agent and reaction was carried out using 1-butyl-3-methylimidazolium chloride ([bmim]Cl) as the reaction medium.

Acetylation of SCB was reported using N-bromosuccinimde (NBS) as a catalyst and the resultant product was used for the production of oil sorption-active materials [7,8]. Acetylation of sugarcane bagasse hemicelluloses was also reported under mild reaction conditions by using NBS as the catalyst [9]. Cellulose and cellulignin extracted from SCB was used for the fabrication of composites reinforced with polypropylene and effect of acetylation was also studied on mechanical and thermal properties of the fabricated composites [10]. H. M. Shaikh et al. have fractionated SCB to cellulose, hemicellulose and lignin by a proprietary steam explosion process, followed by downstream purifications. They demonstrated that the residual hemicellulose need not be considered as an impurity; rather it can be used in acetylated form as a plasticizer as well as a biodegradable additive for cellulose acetates from non-wood origin [11]. SCB cellulosic phthalate was prepared using 1-butyl-3-methylinidazolium chloride ionic liquid as an ionic liquid as reaction medium [12]. Cyanoethylation of Psyllium [13], incorporation of casein in urea-formaldehyde and melamine-formaldehyde resins[14,15,16] are reported earlier from our laboratory. Recently we have reported acetylation of Sugarcane Bagasse[17]. Ferreira, B.C.S., et al. has recently reported a solvent-free procedure involving esterification of sugarcane bagasse with Meldrum's acid[18].

From the literature survey, it reveals that very little work is reported on esterification of SCB powder in its native form. We have successfully attempted various SCB esters i.e. acetate, phthalate, maleate and succinate by using SCB powder in its native form in order to get valuable products by following simple protocol. The fractionation step of SCB into cellulose, hemicelluloses and lignin was intentionally circumvented to make the derivatives in the

cost-effective manner. The SCB powder was thus directly employed without any extraction process in order to search for the user friendly process for esterification.

EXPERIMENTAL

SCB was procured from local market. Procured bagasse was washed thoroughly to remove traces of sugar and then dried in sunlight. It was cut into small pieces and was again dried in oven at 60°C for 24 hours. It was then powdered and used for the chemical modification purpose.

Activation of SCB powder

SCB powder was carefully mixed with 10% aqueous sodium hydroxide solution by controlling the temperature of the reaction flask at 15°C. The reaction mixture was stirred for 1.5 hours at 15°C then neutralized with 10% aqueous acetic acid solution. The powder was then filtered and washed with water until the filtrate became neutral. Finally it was washed with methanol and dried in oven at 60°C for three hours. This dried material was used for further modification.

Preparation of SCB phthalate

2.5 g activated SCB powder was mixed with 3.7 – 10.4 g phthalic anhydride (25 to 70 mmol) and 1- 5 mL pyridine (12.38 to 61.90 mmol) in 10 mL acetic acid. The reaction mass was thoroughly mixed and the homogeneous paste thus obtained was heated at 120°C for different time intervals (2 to 10 hours) in an oil bath. After the completion of reaction, the reaction mixture was cooled to room temperature and was discharged in 200 mL of distilled water. The mixture was then acidified with dilute hydrochloric acid to remove pyridine. This solution was subjected to high speed agitation for the precipitation of product. The solvent mixture was decanted after the product settled down. The whole procedure of precipitation was repeated until the washings became acid free. The solid product was then filtered and dried in oven at 60°C. It was powdered to approximately uniform particle size (100 mesh) through woven wire mesh sieves according to technical requirement ISO 3310-1.

Preparation of SCB maleate and succinate

The maleate and succinate derivatives of SCB were prepared by employing respective acid anhydride as the esterifying agent and acetic acid as the solvent. The synthetic procedure for the esterification by these anhydride was similar to that described above for preparation of SCB phthalate.

Determination of Extent of esterifying group

In the current study, the extent of esterification was determined by evaluation of percentage of esterifying group rather than evaluating degree of substitution. Evaluation is based upon saponification of ester with a measured excess of alcoholic sodium hydroxide solution of known concentration and then back titration of excess sodium hydroxide with standard hydrochloric acid using phenolphthalein indicator [19]. The calculation formula employed for the calculation of percentage of esterifying group of different esters is as follows:

$$\%\ Esterifying\ group = \frac{(BR - SR) \times N_{HCl} \times MW}{W}$$

Where, BR is the volume of hydrochloric acid required for blank determination, SR is the volume of hydrochloric acid required for sample determination, N_{HCl} is the normality of hydrochloric acid solution, MW is the molecular weight of esterfying group (14.9 mol for phthalyl group, 9.9 mol for maleyl group and 10.1 mol succinyl group) and W is the weight of sample (in gram).

RESULTS AND DISCUSSION

Various set of products obtained upon esterification were characterized by determination of Extent of esterifying group, thermogravimetry and infra-red (IR) spectroscopy. The experimental data comprising of the effects of reaction influencing factors are given in Table 1 to 6.

Effect of amount of esterifying agent

Tables 1 to 3 show the dependency of extent of esterification on the amount of esterifying agents in the esterification of SCB. Tables 1-3 represent the effect for phthalate, maleate and succinate derivatives respectively.

In case of succinates, the extent of esterification was found to increase with increase in esterifying agents. While in that of maleates and phthalates, it was found to decrease with increase in amount of esterifying agent. In case of succinates, the maximum esterification was observed upto 62.80% when amount of succinic anhydride was increased from 15 mmol to 60

mmol. With further increase in succinic anhydride from 60 mmol to 75 mmol, 7.76%

Table 1: Effect of amount of phthalic anhydride on formation of SCB Phthalate

Sr. No.	Sample Code	Amount of phthalic anhydride		% Phthaloyl group
		g	mmol	
1	SCBPHPA-25	3.7	25	73.99%
2	SCBPHPA-40	5.9	40	80.63%
3	SCBPHPA-55	8.1	55	63.83%
4	SCBPHPA-70	10.4	70	56.95%

[*SCB: 2.0 g; Pyridine: 2 mL; Acetic acid: 25 mL; Reaction Time: 2 hrs; Reaction Temperature: 120°C*]

decrease was observed in esterification. For phthalates and maleates, the maximum percentage esterification was found upto 80.63% and 41.28% when amount of respective anhydride was increased from 25–40 mmol and 15.29–45.89 mmol respectively. Further increase in amount of respective anhydrides from 40–70 mmol and 45.89–76.48 mmol resulted in makeable decrease in percentage of esterification from 80.63% to 56.95% for phthalation and 41.28% to 34.64% for maleation. Any increase in the percentage esterification with increasing the anhydride group is obvious in the sense that esterification, an equilibrium process, can be shifted more towards the ester formation by using an excess of reagent. The enhanced availability of the anhydride molecules in the immediate environment of the SCB molecules, which are kept in the fixed concentration throughout the series, may be considered responsible for the increments. All the three esters attained a maximum level for extent of esterification within the concentration range of anhydrides under question. The leveling-off was observed at 80.63%, 41.28% and 62.80% respectively for phthalate, maleate and succinate. This is evident from Table 1 to Table 3. About 1.67 and 7.76 times increase in maleic anhydride and succinic anhydride (i.e. from 45.89 to 76.48 mmol and 60 to 75 mmol respectively) affects the percent esterification value to an extent of only 6.64% and 7.76%. The saturation in the degree of reaction may be ascribed to the reversibility of the reaction which is not driven only in the forward direction due to the formation of water in the product mixture. The dominance of the reverse reaction, acid catalyzed hydrolysis of ester, may be considered responsible for the abnormal development observed for phthalates and maleates beyond 40 mmol and 45.89 mmol of corresponding anhydrides respectively (Tables 1-3).

Table 2: Effect of amount of maleic anhydride on formation of SCB Maleate

Sr. No.	Sample Code	Amount of maleic anhydride		% Maleic group
		g	mmol	
1	SCBMAMA-1.5	1.5	15.29	37.77%
2	SCBMAMA-3.0	3.0	30.59	37.11%
3	SCBMAMA-4.5	4.5	45.89	41.28%
4	SCBMAMA-6.0	6.0	61.19	35.95%
5	SCBMAMA-7.5	7.5	76.48	34.64%

[*SCB: 2.0 g; Pyridine: 2 mL; Acetic acid: 25 mL; Reaction Time: 4 hrs; Reaction Temperature: 120°C*]

Table 3: Effect of amount of succinic anhydride on on formation of SCB Succinate

Sr. No.	Sample Code	Amount of succinic anhydride		% Succinoyl group
		g	mmol	
1	SCBSASA-15	1.5	15	31.12%
2	SCBSASA-30	3.0	30	37.91%
3	SCBSASA-45	4.5	45	58.32%
4	SCBSASA-60	6.0	60	62.80%
5	SCBSASA-75	7.5	75	55.04%

[*SCB: 2.0 g; Pyridine: 2 mL; Acetic acid: 25 mL; Reaction Time: 4 hrs; Reaction Temperature: 120°C*]

Effect of amount of Pyridine concentration

The effect of the concentration of pyridine as a catalyst on percentage esterification of various esters is depicted in Tables 4 to 6 respectively for phthalate, maleate and succinate. The retarding effect of pyridine was observed in phthalate and maleate esters. A fivefold increase in pyridine concentration brought about ~1.3 times decrease in esterification values in case of maleate. While 2.5 times increase in pyridine concentration brought about ~1.5 times decrease in that of phthalate. A decrease in the amount of anhydride actually available for the reaction enhances the difference between the moles of anhydride taken and used-up for the purpose. This results into lowering ratio of moles of

anhydride bound to the substrate to the moles of anhydride initially taken into the reaction mixture.

The above results may be viewed as enhanced intermolecular interaction between pyridine and anhydride molecules upon increasing pyridine concentration. The acylpyridinium cation is in equilibrium with the pyridine to anhydride complex ratio. More the concentration of the pyridine more will be the complex formation and more will be the active concentration of acylpyridinium cation.

Table 4: Effect of amount of pyridine on formation of SCB Phthalate

Sr. No.	Sample Code	Amount of pyridine		Phthalic anhydride: pyridine mole ratio	% Phthaloyl group
		mL	mmol		
1	SCBPHPy-1	1	12.38	3.23	71.49%
2	SCBPHPy-2	2	24.76	1.62	80.63%
3	SCBPHPy-3	3	37.14	1.08	74.48%
4	SCBPHPy-4	4	49.52	0.81	61.94%
5	SCBPHPy-5	5	61.90	0.65	52.17%

[*SCB: 2.0 g; Amount of phthalic anhydride: 5.9 g (40 mmol); Acetic acid: 25 mL; Reaction Time: 2 hrs; Reaction Temperature: 120°C*]

However, in phthalic anhydride and maleic anhydride, the presence of π-bond in conjugation with partial positive charge on carbonyl carbon of the cation may be considered responsible for the decreased reactivity towards the esterification. The higher electron density of the π-cloud will be attracted towards the carbonyl carbon, and thereby neutralizing the positive charge on it in part.

In maleic anhydride, the effect is observed to be more pronounced. This may be due to the additional repelling force exerted by carboxylate anion on the π-cloud which results into more shifting of π-electrons towards carbonyl dipole. The retarding effect may also be viewed as the consumption of acylpyridinium ions by the increased number of pyridine molecules in the medium to form similar ions through acyl shift. Thus the setting up of an equilibrium process, between pyridine and acylpyridinium ion, lower the chances for availability of such active cations for the desired purpose.

The succinate esters (Table 6) are observed to be increased in the extent of esterification value with increase in pyridine within the concentration range studied.

With increase in pyridine concentration from 12.38 mmol to 61.90 mmol, the value of percent esterification increases from 58.85% to 72.29%. i.e. with 5 times increase in the concentration of pyridine, the increase in percent esterification value of about ~1.2 times is observed.

Effect of liquid:solid ratio

Table 7, 8 and 9 depict the effect of liquid:solid

Table 5: Effect of amount of pyridine on formation of SCB Maleate

Sr. No.	Sample Code	Amount of pyridine		Maleic anhydride: pyridine mole ratio	% Maleic group
		mL	mmol		
1	SCBMAPy-1	1	12.38	3.71	45.59%
2	SCBMAPy-2	2	24.76	1.85	41.28%
3	SCBMAPy-3	3	37.14	1.24	37.51%
4	SCBMAPy-4	4	49.52	0.93	36.17%
5	SCBMAPy-5	5	61.90	0.74	35.12%

[*SCB: 2.0 g; Amount of maleic anhydride: 4.5 g (45.89 mmol); Acetic acid: 25 mL; Reaction Time: 4 hrs; Reaction Temperature: 120°C*]

Table 6: Effect of amount of pyridine on formation of SCB Succinate

Sr. No.	Sample Code	Amount of pyridine		Succinic Anhydride :pyridine mole ratio	% Succinoyl group
		mL	mmol		
1	SCBSAPy-1	1	12.38	4.85	58.85%
2	SCBSAPy-2	2	24.76	2.42	62.80%
3	SCBSAPy-3	3	37.14	1.62	66.19%
4	SCBSAPy-4	4	49.52	1.21	66.87%
5	SCBSAPy-5	5	61.90	0.97	72.29%

[*SCB: 2.0 g; Amount of succinic anhydride: 6.0 g (60 mmol); Acetic acid: 25 mL; Reaction Time: 4 hrs; Reaction Temperature: 120°C*]

ratio on the extent of phthalate, maleate and succinate formation respectively. The results for phthalate ester formation as furnished in Table 7 shows an initial increase followed by a rapid decrease in the extent of ester formation values with increase in the liquid:solid ratio. A maximum value of 80.63% is achieved at the ratio of 3.42. Then after nearly ~1.4 times increase in the liquid content decreases the percent values to 44.69 %. i.e. 1.8 times lower percent esterification is observed. In case of

succinates, a similar trend is observed. A maximum value of 72.29% is found at the ratio of 3.75. Further increase in liquid content to about ~1.5 times, ~3.4 times decrease in percent esterification is observed. This trend could be explained on the ground of the magnitude of the association of the reagents with cellulose molecules and their collision probability. At low values of the liquid:solid ratio, these parameters are more pronounced. An increase in the liquid content of the reaction mass decreases the chances of collision between reagent molecules and cellulose molecules. However, lower extent of esterification obtained at extreme lower ratios in each case may be due to the trapping of the reagent molecules within the cellulose matrix below the optimum level of the reaction medium required for the maximum collisions between the reagent and substrate molecules. The optimum level of liquid:solid ratio were found out to be 3.42, 6.31 and 3.75 respectively for phthalate, maleate and succinate series.

Table 7: Effect of liquid:solid ratio on formation of SCB Phthalate

Sr. No.	Sample Code	Amount of acetic acid		Liquid: solid ratio	% Phthaloyl group
		mL	mmol		
1	SCBPHAC-20	20	338.98	2.78	69.63%
2	SCBPHAC-25	25	423.73	3.42	80.63%
3	SCBPHAC-30	30	508.47	4.05	63.22%
4	SCBPHAC-35	35	593.22	4.68	44.69%

[*SCB: 2.0 g; Amount of phthalic anhydride: 5.9 g (40 mmol); Pyiridine: 2 mL; Reaction Time: 2 hrs; Reaction Temperature: 120°C*]

Table 9 represents the similar result for the formation of succinate derivatives. The astonishing behavior is marked for the maleate formation as depicted in Table 8. It shows that with increase in amount of acetic acid from 338.98 mmol to 677.96 mmol in the reaction matrix, the extent of ester formation was also slowly found to increase within the range studied respectively for phthalate, maleate and succinate derivatives.

Tables 10-12 show the effect of reaction time on extent of esterification respectively for phthalate, maleate and succinate derivatives. The extent of values of percent esterification were found to increase with prolonging the reaction period from 2 to 10 hours for phthalylation and

Table 8: Effect of liquid:solid ratio on formation of SCB Maleate

Sr. No.	Sample Code	Amount of acetic acid		Liquid: solid ratio	% Maleic group
		mL	mmol		
1	SCBMAAC-20	20	338.98	3.23	43.90%
2	SCBMAAC-25	25	423.73	4.00	45.59%
3	SCBMAAC-30	30	508.47	4.77	53.47%
4	SCBMAAC-35	35	593.22	5.54	59.69%
5	SCBMAAC-40	40	677.96	6.31	64.51%

[*SCB: 2.0 g; Amount of maleic anhydride: 4.5 g (45.89 mmol); Pyridine: 1 mL; Reaction Time: 4 hrs; Reaction Temperature: 120°C*]

Table 9: Effect of liquid:solid ratio on formation of SCB Succinate

Sr. No.	Sample Code	Amount of acetic acid		Liquid: solid ratio	% Succinoyl group
		mL	mmol		
1	SCBSAAC-20	20	338.98	3.13	55.29%
2	SCBSAAC-25	25	423.73	3.75	72.29%
3	SCBSAAC-30	30	508.47	4.38	24.44%
4	SCBSAAC-35	35	593.22	5.00	22.36%
5	SCBSAAC-40	40	677.96	5.63	21.50%

[*SCB: 2.0 g; Amount of succinic anhydride: 6.0 g (60 mmol); Pyridine: 5 mL; Reaction Time: 4 hrs; Reaction Temperature: 120°C*]

succinylation while 2 to 8 hours for maleation. In case of maleate and phthalate derivatives, the extent of esterification was found to decrease up to ~1.5 and ~1.7 times with increasing the reaction time from 4 to 8 hours for maleate and 4 to 10 hours for succinates. While in case of phthalate, with increase in reaction time from 2 to 10 hours, it was found to decrease in extent of esterification in the linear pattern from 80.63% to 45.02%.

Table 10: Effect of Reaction Time on formation of SCB Phthalate

Sr. No.	Sample Code	Reaction Time (hrs)	% Phthaloyl group
1	SCBPHRT-2	2	80.63%
2	SCBPHRT-4	4	68.62%
3	SCBPHRT-6	6	55.23%
4	SCBPHRT-8	8	49.74%
5	SCBPHRT-10	10	45.02%

[*SCB: 2.0 g; Amount of phthalic anhydride: 5.9 g (40 mmol); Pyiridine: 2 mL; Acetic acid: 25 mL; Reaction Temperature: 120°C*]

It can be concluded, from the time variation study, that a maximum level of esterification of SCB was reached by continuing the reaction for

Table 11: Effect of Reaction Time on formation of SCB Maleate

Sr. No.	Sample Code	Reaction Time (hrs)	% Maleic group
1	SCBMART-2	2	39.44%
2	SCBMART-4	4	64.51%
3	SCBMART-6	6	58.20%
4	SCBMART-7	7	49.08%
5	SCBMART-8	8	43.44%

[*SCB: 2.0 g; Amount of maleic anhydride: 4.5 g (45.89 mmol); Acetic acid: 40 mL; Pyridine: 1 mL; Reaction Temperature: 120°C*]

Table 12: Effect of Reaction Time on formation of SCB Succinate

Sr. No.	Sample Code	Reaction Time (hrs)	% Succinoyl group
1	SCBSART-2	2	36.19%
2	SCBSART-4	4	72.29%
3	SCBSART-6	6	47.18%
4	SCBSART-8	8	44.46%
5	SCBSART-10	10	41.91%

[*SCB: 2.0 g; Amount of succinic anhydride: 6.0 g (60 mmol); Acetic acid: 25 mL; Pyridine: 5 mL; Reaction Temperature: 120°C*]

the optimum time period under the set of reaction condition studied. After acquiring the optimum extent of esterification, the cellulose molecule did not undergo further electrophilic displacement with the acylpyridinium complex. Thus the leveling-off in the esterification value may be viewed as the establishment of equilibrium between the products and the reactants under the chosen set of reaction conditions. The maximum values achieved for the percent esterification after the optimum time duration of the reaction were 80.63%, 64.51% and 72.29% respectively for phthalate, maleate and succinate. The optimum time duration of the reaction was found to be 2 hours, 4 hours and 4 hours respectively for phthalate, maleate and succinate derivatives.

CHARACTERIZATION BY INFRA-RED (IR) SPECTROSCOPY

The spectral data of unmodified SCB and its derivatives are shown in the Table 13. The spectra were recorded on "PerkinElmer USA Spectrum GX" spectrophotometer using KBr pellets. The most striking evidence for the presence of >C=O group [20] shows the band at 1750 – 1735 cm-1. A new band was observed in each derivative at this region of IR spectrum. It was observed at 1722, 1735 & 1734 respectively for phthalate, maleate and succinate derivatives. Table 13 represents IR characteristics vibrations for unmodified SCB, SCB phthalate, SCB maleate and SCB succinate respectively. The band observed in the range of 1605–1638 cm-1 corresponds to the bending mode of the absorbed water [21,22,23,24] and is found in all the cases. The O–H bending vibration of the hydroxyl in plane deformation is characterized by the band at about 1380 cm-1. A series of peaks in all the spectra over the range 3750–3000 cm-1 may be considered as a broad band due to –OH absorption. In all the spectra, the band observed at about 1160 cm-1 may be assigned to the C–O–C asymmetrical stretching in the glucopyranose ring of cellulose [23]. The band observed at around 1050 cm-1 may be due to C–O stretching in C–O–C linkages. The sharp band at 897 cm-1 is originated from the β-glucosidic linkages between the sugar units [21].

Table 13: Main features observed from IR studies for the prepared esters of SCB

Unmodified SCB cm^{-1}	SCB Phthalate cm^{-1}	SCB Maleate cm^{-1}	SCB Succinate cm^{-1}
3425	3428	3424	3428
2920	2900	2924	2922
---	---	---	1784
---	1722	1735	1734
1638	1609	1631	1605
---	---	1401	1420
1377	1375	1377	1372
1163	1163	1165	1163
1060	1061	1057	1056
897	894	898	917

The strong and broad band extending from 1200-950 cm^{-1} consisting of several close bands which are typical of all cellulosic fibers has been found to change to a relatively transparent region and having only a few individual weaker bands [25].

CHARACTERIZATION BY THERMO-GRAVIMETRIC ANALYSIS (TGA)

Thermal behavior of prepared ester derivatives of SCB with different substitutions was studied.

PerkinElmer model Pyris 1 Thermo-gravimetric analyzer was employed to study the thermal behavior of prepared derivatives of SCB. The thermobalance consists of furnace, sample holder, glass enclosure and recording balance mechanism. The samples were powdered to the same average mesh size and dried carefully in vacuum desiccator. 10 mg of exact weight of sample was taken for each Thermo Gravimetric Analysis (TGA). Tables 14 to 16 show thermal behavior of prepared derivatives.

Table 14: Thermal parameters of SCB phthalate.

Sample code	Unmodified	SCBPH Py-5	SCBPH PA-55	SCBPH PA-40
% Substitution	-	52.17	63.83	80.63
Ti °C	162	210	213	219
T_{10} °C	223	253	255	261
T_{50} °C	298	328	327	329
T_{max} °C	303	322	321	327
IPDT °C	441.52	574.84	593.06	584.91
E kJmol^{-1}	65.67	34.76	39.28	49.13
% Char	19.83	29.2	20.74	22.86

Ti, initial decomposition temperature, was found to increase from 162°C (for native SCB) to 219°C, 178°C and 228°C respectively for phthalate, maleate and succinate i.e. the values of Ti was found to increase with the maximum possible substitution of esterifying group. The observed increase in the thermal stability may be due to the reduced reactivity of the hydroxyl group by its esterification [26].

T_{10} values observed for the derivatives were found to increase as compared to native SCB. This indicates that modification retards the rate of thermal degradation up to first 10% weight loss. T_{50} values for the prepared derivatives were found to be improved. T_{max} values observed for the different derivatives were found to increase as compared to the native SCB. IPDT values have been greatly influenced by modification of bagasses. For the prepared derivatives, it was observed almost 50°C to 150°C higher as compared to native SCB (i.e. 441°C). Activation energy values were found to decrease for all the derivatives covered under the thermal study as compared to native SCB.

Table 15: Thermal parameters of SCB maleate

Sample code	Unmodi-fied	SCBMA MA-7.5	SCBMA AC-30	SCBMA AC-40
% Substi-tution	-	34.64	53.47	64.51
Ti °C	162	178.32	172.13	164.33
T_{10} °C	222.89	237.79	238.89	235.07
T_{50} °C	297.93	334.58	334.62	319.05
T_{max} °C	303.18	312	321	311
IPDT °C	441.52	579.43	570.51	558.78
E kJmol^{-1}	65.67	34.33	31.38	28.19
% Char	19.9	15.8	31.7	12.76

Table 16: Thermal parameters of SCB succinate.

Sample code	Unmodi-fied	SCBSA AC-30	SCBSA SA-45	SCBSA Py-4
% Substitution	-	24.44	58.32	66.87
Ti °C	162	221.31	224.39	227.55
T_{10} °C	222.89	264.92	269.89	257.93
T_{50} °C	297.93	334.41	406.02	363.18
T_{max} °C	303.18	329	333	330
IPDT °C	441.52	590.8	581.51	561.82
E kJmol^{-1}	65.67	45.36	32.49	27.82
% Char	19.9	29.38	38.57	36.11

CONCLUSION

Treatment of Sugarcane Bagasse with alkali leads to remove lignin. This modification provided a very good method for esterification. Further, all the esterification processes were studied by varying amount of esterifying agents, pyridine concentration, liquid to solid ratio in reaction mixture and reaction time. By this, optimum reaction condition was found out which may help for further study in all aspect of science. Further, the cost and time is also reduced by direct use of Sugarcane Bagasse for the modification. So far as the industrial processes are concerned, we have just initiated a small step for modification of Sugarcane Bagasse without any need of extraction process.

AKNOWLEDGEMENTS

The authors are thankful to University Grants Commission, Government of India, New Delhi for the UGC-CEAP Research Fellowship to Jitendra Parmar.

REFERENCES

[1] Rowell, R. M., Keany, F. M. (1991) Fiberboards made from acetylated bagasse fiber. *Wood Fiber Sci.*, **23:** 15-22.

[2] Salwa, A. A., El-Roudi, A. M. and Alaa A. A. S. (2015) Removal of Mn(II) from Ground Water by Solid Wastes of Sugar Industry. Journal of Environmental Science and Technology, 8: 338-351.

[3] Gurgel, L. V. A., et al (2012) Application of succinylated sugarcane bagasse as adsorbent to remove methylene blue and gentian violet from aqueous solutions e Kinetic and equilibrium studies. Dyes and Pigments, 92: 967-974.

[4] Liebert, T. F. and Heinze T. (2005) Tailored Cellulose Esters: Synthesis and Structure Determination. Biomacromolecules, 6: 333-340.

[5] Cerqueira, A. D., Filho, R. G., De Assuncao, R. M. N., Da Silva, M. C., Toledo, C. L., Zeni, M., Mello, K. and Duarte, J. (2008) Characterization of cellulose triacetate membranes, produced from sugarcane bagasse, using PEG 600 as additive; Polym. Bull. 60: 397-404.

[6] Xie, W., Shao, L. and Liu, Y. (2010) Synthesis of starch esters in ionic liquids. J. Appl. Polym. Sci. 116: 218-24.

[7] Sun, X.F, Sun, R.C, Sun, J.X. (2004) Acetylation of sugarcane bagasse using NBS as a catalyst under mild reaction conditions for the production of oil sorption-active materials. Bioresource Technology, 95: 343–350.

[8] Sun, X.F, Sun, R.C, Sun, J.X. (2003) A convenient acetylation of sugarcane bagasse using NBS as a catalyst for the preparation of oil sorption-active materials. Journal of Materials Science, 38: 3915-3923.

[9] Sun, X.F, Sun, R.C, Zhao, L and Sun, J.X. (2004) Acetylation of sugarcane bagasse hemicelluloses under mild reaction conditions by using NBS as a catalyst. J Appl Polym Sci, 92: 53–61.

[10] Luz, S. M., Del Tio, J., Rocha, G. J. M., Gonçalves, A.R. and Del'Arco Jr., A. P. (2008) Cellulose and cellulignin from sugarcane bagasse reinforced polypropylene composites: Effect of acetylation on mechanical and thermal properties. Composites Part A: Applied Science and Manufacturing, 39: 1362-1369.

[11] Shaikh, H. M., Pandare, K. V., Nair, G. and Varma, A. J. (2009) Utilization of sugarcane bagasse cellulose for producing cellulose acetates: Novel use of residual hemicellulose as plasticizer. Carbohydrate Polymers, 76: 23–29.

[12] Liu, C. F., Sun, R. C., Zhang, A. P. and Ren, J. L. (2007) Preparation of sugarcane bagasse cellulosic phthalate using an ionic liquid as reaction medium. Carbohydrate Polymers, 68: 17–25.

[13] Raval, D. K., Parmar, J. K., Patel, J. P. and Prajapati, M. R. (2009) Studies on cyanoethylation of Plantago Ovata Seed Husks(Psyllium). PRAJNA-Jour. Pure & Appl. Sci., 17: 094-098.

[14] Raval, D. K., Narola, B. N. and Patel, A. J. (2005) Preparation, Characterization and composites form low formaldehyde emission urea-formaldehyde-casein copolymer J Appl Polym Sci, 98: 531.

[15] Raval, D. K., Patel, A. J. and Narola, B. N. (2005) Synthesis, Characterization & composites from resorcinol-urea-formaldehyde-casein resin Iran Polym J, 14: 775.

[16] Raval, D. K., Patel, A. J. and Narola, B. N. (2006) A study on composites from casein modified melamine-formaldehyde resin Polym Plast Technol Eng, 45: 293.

[17] Vyas, S.K., Parmar, J.K. and Raval, D.K. (2010) A study on composites from phenol-formaldehyde -casein resin, J.Appl.Polym.Sci., 115:2838–2846.

[18] Raval, D. K., and Parmar, J. K. (2016) A study on acetylation of Sugarcane Bagasse(SCB), International Journal of Scientific Development and Research (IJSDR), 1: 209-217.

[19] Ferreira, B. C. S., Teodoro, F. S., Mageste, A. B., Gil, L. F., Freitas, R. P. and Gurgel, L. V. A. (2015) Application of a new carboxylate-functionalized sugarcane bagassefor adsorptive removal of crystal violet from aqueous solution:Kinetic, equilibrium and thermodynamic studies. Ind. Crops Prod., 65: 521-534.

[20] Critchfield F. E. (1963) "International Series of Monographs on Analytical Chemistry", vol 8, Pergamon Press, p.141.

[21] Ehrhardt, A., Bui, H. M., Duelli, H. and Bechtold, T. (2010) NaOH/urea aqueous solutions improving properties of regenerated-cellulosic fabrics. J. Appl. Polym. Sci., 115: 2865-2874.

[22] Sun, X. F., Sun, R. C. and Sun, J. X. (2003) A convenient acetylation of sugarcane bagasse using NBS as a catalyst for the preparation of oil sorption-active materials; J. Mater. Sci., 38: 3915-3923.

[23] Liu, C. F., Sun, R. C., Zhang, A. P. and Ren, J. L. (2007) Preparation of sugarcane bagasse cellulosic phthalate using an ionic liquid as reaction medium. Carbohydr. Polym., 68: 17–25.

[24] Mulinari, D. R., Voorwald, H. J. C., Cioffi, M. O. H., da Silva, M. L. C. P. and Luz, S. M.

(2009) Preparation and properties of HDPE/sugarcane bagasse cellulose composites obtained for thermokinetic mixer. Carbohydr. Polym., 75: 317-321.

[25] Sun, R. C., Sun, X. F. and Tomkinson, J. (2004a) Hemicelluloses and their derivatives; ACS Symposium Series 864: 2–22.

[26] Kruger, L. M. and Rutenberg, M. W. (1967) "Starch Chemistry and Technology", vol. 2, Academic Press, New York, p.369.

[27] Desai, D. H., Patel, C. K. and Patel, R. D. (1976) Thermal Properties of Amylose and Its Derivatives. Part I; Starch 28: 377-381.

PRAJÑĀ - **Journal of Pure and Applied Sciences Vol. 24 – 25 : 130 – 140 (2017)**
ISSN 0975 - 2595

IMIDAZO[1,5-*a*]PYRIDINE BASED Ru(III) COMPLEXES AS BIOLOGICAL ACTIVE AGENT

DARSHANA N. KANTHECHA AND MOHAN N. PATEL*

*Department of Chemistry, Sardar Patel University, Vallabh Vidyanagar-388120, Gujarat, India

Corresponding Author tel.: +91 2692 226856

Email: jeenen@gmail.com

ABSTRACT

A series of imidazo[1,5-a]pyridine based Ru(III) complexes of type $[Ru(L^{1-5})_2Cl_2]PF_6$ has been synthesized and characterized by elemental analysis, conductance measurements, electronic spectroscopy and mass spectroscopy (MS). The interactions of the complexes with Herring Sperm (HS) DNA have been carried out by absorption titration and viscosity measurement. The studies suggest the intercalative mode of binding and also confirmed theoretically using a molecular docking study. The in vitro cytotoxicity of the complexes has been examined with a brine shrimp bioassay using Artemia cyst. In vivo cytotoxicity against S. pombe cells at a cellular level has been carried out for the synthesized compounds. Results indicate that the metal complexes show better activity against S. pombe cells compared to the ligands. The complexes have been screened for their antibacterial activity against two Gram$^{(+ve)}$ and three Gram$^{(-ve)}$ microorganisms. DNA extraction was carried out from S. pombe cells to study the DNA cleavage by agarose gel electrophoresis. Smearing of DNA in agarose gel suggests that complexes exhibit toxicity at the cellular level and break the DNA from nucleus to express their toxic effect.

Keywords: Ru(III) complexes, Imidazole, S. Pombe, Molecular modeling, Genotoxicity

INTRODUCTION

The chemistry of metallonuclease is a remarkable discovery for anticancer treatment. Therefore, metal based chemotherapeutic agents have received attention in the treatment of various types cancers or inflammatory disease. After the successful clinical use of anticancer agent cis-platin, a various platinum based chemotherapeutic agents, such as carboplatin, oxalinoplatin are also available in the market. Transition metal complexes including both platinum and non-platinum (Au, Cu, Os, Pd, Ru, Rh and Ir) with a larger variety of ligands utilized for the design and development of metal based drug. The alteration in the structure of ligand occurs when metal bind to the ligand and also changes the orientation of the complex, affects the mode of interaction, and binding stability of DNA and cytotoxicity. In order to understand the mechanisms of DNA binding and to design a bioactive agents, the study of various complexes having altered structural characteristics of intercalating ligands has been carried out. In this context, interactions of metal complexes with DNA are an interesting subject in relation to design the effective anticancer drugs [5,6]. Platinum based drugs exhibit side effects, severe toxicity, selectivity and resistance to living cells. The disadvantages of platinum based drugs have forced researcher and to expand the scope of non-platinum metallodrugs[7,8]. Ruthenium complexes are attractive alternates to platinum complexes because of their rich synthetic chemistry, variable oxidation states and photochemical activity towards DNA under physiological conditions [9,10]. DNA binding studies show that ruthenium(III) complexes can bind to DNA with different binding fashion such as intercalative binding, covalent binding, electrostatic binding and groove binding and to exhibit effective nuclease activities[11,12]. Ruthenium based drugs, such as imidazole based NAMI-A3 and indazolium based KP1019 are effective against lung metastasis and colon carcinomas respectively[4,13]. Further, investigation of biological active agents has been carried out on Ru(II) and Ru(III) complexes with N, N donor hetero moiety based ligands. It inspire us to design, biological activity ruthenium(III) complexes with imidazo[1,2-a]pyridine and evaluating biological properties such as DNA

binding, DNA cleavage, antibacterial and cytotoxicity.

EXPERIMENTAL SECTION

Chemicals and materials

All analytical grade chemicals and solvents were used as commercially received. Metal salt of $RuCl_3 \cdot XH_2O$ was purchased from Chemport (Mumbai, India). 2,2-Dipyridylketone, 2-benzoyl pyridine, benzaldehyde, 4-methyl benzaldehyde, 4-bromo benzaldehyde, 4-chloro benzaldehyde, 4-methoxy benzaldehyde, HS-DNA, KPF_6 and edta were purchased from Sigma Aldrich Chemical Co. (India). Agarose, Luria Broth (LB), ethidium bromide (EtBr), Tris–acetyl–edta (TAE) and bromophenol blue were purchased from Himedia (India). Culture for antibacterial activity *Bacillus subtilis (B. Subtilis-7193*), *Staphylococcus aureus (S. Aureus-3160), Pseudomonas aeruginosa (P. Aeruginosa-1688), Escherichia coli (E. Coli-433)* and *Serratia marcescens (S. Marcescens-7103)* were purchased from the Institute of Microbial Technology (Chandigarh, India). *S. Pombe* Var. Paul Linder 3360 was obtained from IMTECH, Chandigarh.

Physical measurements

Elemental analysis of C, H, and N were performed with a model EuroVector EA3000 (for ligands) and Perkin-Elmer 240 (for complex) elemental analyzer. The LC-MS spectra were recorded using Thermo scientific mass spectrophotometer (USA). Bruker Avance spectrophotometer was recorded ^{1}H NMR (400 MHz) and ^{13}C NMR (100 MHz) using an appropriate solvent in which compound properly dissolve. Melting points were determined in open capillaries on hermocal10 melting point apparatus (Analab Scientific Pvt. Ltd, India). The Gouy's method used for magnetic measurement of metal complexes taking mercury tetrathiocyanatocobaltate(II) as the calibrant (χ_g=16. 44 x 10^{-6} cgs units at 20 °C), citizen balance. UV-160A UV-Vis spectrophotometer, Shimadzu, Kyoto (Japan), was used for electronic spectra of metal complexes in the range of 200-800 nm using quarts cell having path length 1 cm. Ubbelohde viscometer in viscosity bath having a controllable temperature (25.0 ± 0.5^{0}C) were used for the study of hydrodynamic chain length. Antibacterial study was carried out by means of laminar air flow cabinet Toshiba, Delhi (India). Alphadigidoc^{tm} RT. Version V.4.0.0 PC– Image software, CA (USA) used for the Photo quantization of the DNA cleavage activity.

General method for synthesis of ligands and complexes

Synthesis of imidazo[1,2-a]pyridine derivatives were carried out by taking a mixture of pyridylketone (5 mmol), substituted benzaldehyde (5 mmol), and NH_4OAC (15 mmol) in 15 mL of glacial acetic acid in a 100 mL round bottom flask equipped with a condenser. The reaction mixture was heated at 80-120 °C under N_2 gas for 6-8 h. Upon checking TLC in interval of 1 h, when all the reactants were consumed and spot of product appears the reaction mixture was cooled to room temperature and then kept the solution under temp 15-20 °C to slow evaporation overnight. The resulting yellow residue was filtered and purified using column chromatography on silica gel by ethyl acetate: hexane (2:8) system as a mobile phase.

The methanolic solution of $RuCl_3 \cdot XH_2O$ was heated to reflux for 10 min to activate metal. Then dropwise a methanolic solution of ligand was added and the reaction mixture was heated to reflux overnight. Impurity was removed by filtering the hot solution. Then a saturated solution of KPF_6, was added. The solution was kept at 5-10 °C overnight. The obtained precipitate was washed with water and ether.

The proposed reaction mechanism for the general synthesis of imidazo[1,2-a]pyridine and their ruthenium(III) complexes are shown in scheme 1 and 2.

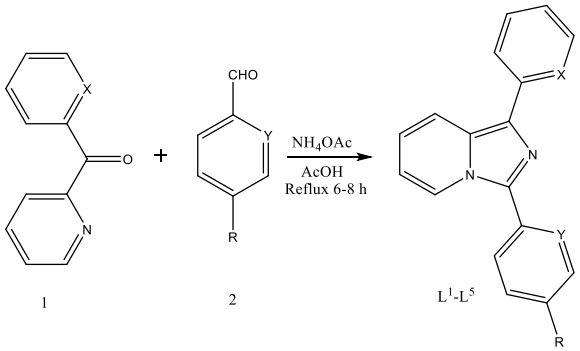

Scheme 1. General synthesis of the imidazo[1,2-a]pyridine ligands.

Ligand	1	2	3	4	5
X	CH	N	N	N	N
Y	N	CH	CH	CH	CH
R_1	H-	H-	CH_3-	Cl-	Br-

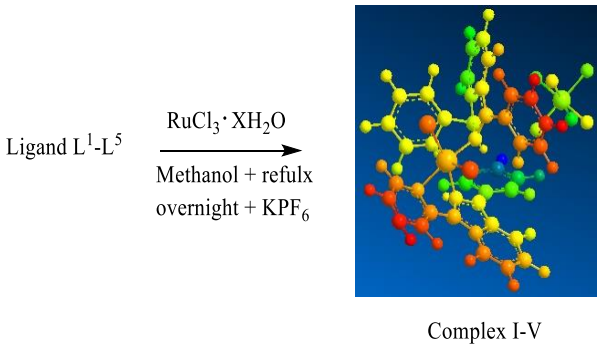

Scheme 2. General synthesis of the imidazo[1,2-a]pyridine based Ru(III) complexes.

1. 1-phenyl-3-(pyridin-2-yl)imidazo[1,5-a]pyridine (L^1)

Synthesized using 2-benzoyl pyridine with pyridine carboxaldehyde as per given procedure. Colour: yellow, Yield: 58%, mol. wt.: 271.32 g/mol, m.p.:124.3°C, Anal. Calc. (%) For $C_{18}H_{13}N_3$: C, 79.68; H, 4.83; N, 15.49 Found (%): C, 79.85; H, 4.72; N, 15.25. ^{1}H NMR (400 MHz, DMSO-d_6) δ/ppm: 6.793(1H, m), 6.963(1H, m), 7.236(1H, m), 7.351(1H, t, 7.6 Hz), 7.518(2H, t, 7.6 Hz), 7.823(1H, m), 7.930(1H, d, 9.2 Hz), 7.993(2H,dd, 0.8, 7.2 Hz), 8.510(1H, d, 8.0 Hz), 8.677(1H, dd, 0.8, 4.0 Hz), 10.057(1H, d, 7.6 Hz), ^{13}C NMR (100 MHz, DMSO-d_6) δ/ppm: 113.67(CH), 118.37(CH), 120.97(CH), 121.63(CH), 122.26(CH), 126.39(CH), 126.71(CH), 127.00(CH), 128.76(CH), 129.05(C_{qat}), 129.33(C_{qat}), 135.03(C_{qat}), 136.55(CH), 148.12(CH), 149.57(C_{qat}), 151.50(C_{qat}). Mass (m/z): 272

2. 3-phenyl-1-(pyridin-2-yl)imidazo[1,5-a]pyridine (L^2)

Synthesized using 2,2'-dipyridylketone with benzaldehyde as given procedure. Colour: yellow, Yield: 82%, mol. wt.: 271.32 g/mol, m.p.:108°C, Anal. Calc. (%) For $C_{18}H_{13}N_3$: C, 79.68; H, 4.83; N, 15.49 Found (%): C, 79.86; H, 4.74; N, 15.26. ^{1}H NMR (400 MHz, DMSO-d_6) δ/ppm: 6.668(1H, t, 6.4 Hz), 6.944(1H, dd, 2.8, 6.4 Hz), 7.120(1H, m), 7.486(1H, d, 7.6 Hz), 7.574(2H, t, 8.0 Hz), 7.741(1H, m), 7.868(2H, d, 7.2 Hz), 8.279(2H, d, 8.4 Hz), 8.658(1H, d, 5.2 Hz), 8.736(1H, d, 8.8 Hz). ^{13}C NMR (100 MHz, DMSO-d_6) δ/ppm: 113.91(CH), 119.96(CH), 120.45(CH), 121.02(CH), 121.62(CH), 121.89(CH), 128.41(CH), 128.94(CH), 129.05(CH), 130.17(C_{qat}), 130.23(C_{qat}), 130.65(CH), 136.27(CH), 138.06(C_{qat}), 149.01(CH), 155.09(C_{qat}). Mass (m/z): 272

3. 1-(pyridin-2-yl)-3-(p-tolyl)imidazo[1,5-a]pyridine (L^3)

Synthesized using 2,2'-dipyridylketone with p-tolylbenzaldehyde as given procedure. Colour: yellow, Yield: 79%, mol. wt.: 285.35 g/mol, m.p.:154.7°C, Anal. Calc. (%) For $C_{19}H_{15}N_3$: C, 79.98; H, 5.30; N, 14.73 Found (%): C, 80.08; H, 5.19; N, 14.73. ^{1}H NMR (400 MHz, DMSO-d_6) δ/ppm: 2.472(3H, s), 6.654(1H, t, 6.4 Hz), 6.930 (1H, dd, 2.8, 6.4 Hz), 7.113(1H, m), 7.378(2H, d, 8.0 Hz), 7.741(3H, m), 8.260(2H, t, 7.2 Hz), 8.650(1H, d, 4.8 Hz), 8.711(1H, d, 9.2 Hz). 13C NMR (100 MHz, DMSO-d6) δ/ppm: 21.43(CH_3), 113.74(CH), 119.94(CH), 120.36(CH), 120.86(CH), 121.68(CH), 121.82(CH), 127.27(Cqat), 128.32(CH), 129.72(CH), 130.09(Cqat), 130.57(Cqat), 136.20(CH), 138.26(Cqat), 138.95(Cqat), 148.98(CH), 155.15(Cqat). Mass (m/z): 286

4. 3-(4-chlorophenyl)-1-(pyridin-2-yl)imidazo[1,5-a]pyridine *(L^4)*

Synthesized using 2,2'-dipyridylketone with p-chlorobenzaldehyde as given procedure. Colour: yellow, Yield: 89%, mol. wt.: 305.77 g/mol, m.p.:165.01°C, Anal. Calc. (%) For $C_{18}H_{12}ClN_3$: C, 70.71; H, 3.96; N, 13.74 Found (%): C, 70.71; H, 3.63; N, 13.74. ^{1}H NMR (400 MHz, DMSO-d_6) δ/ppm: 6.709(1H, t, 6.0 Hz), 6.967(1H, dd, 3.6, 6.4 Hz), 7.131(1H, dd, 2.0, 4.4 Hz), 7.551(2H, d, 8.8 Hz), 7.748(1H, m), 7.825(2H, d, 8.4 Hz), 7.242(2H, t, 7.2 Hz), 8.657(1H, d, 4.0 Hz), 8.744(1H, d, 9.2 Hz). ^{13}C NMR (100 MHz, DMSO-d_6) δ/ppm: 114.28(CH), 116.99(C_{qat}), 119.96(CH), 120.63(CH), 121.13(CH), 121.39(CH), 122.04(CH), 122.72(C_{qat}), 128.73(C_{qat}), 129.33(CH), 129.57(CH), 134.87(C_{qat}), 136.41(CH), 136.80(C_{qat}), 149.16(CH), 154.92(C_{qat}). Mass (m/z): 306

5. *3-(4-bromophenyl)-1-(pyridin-2-yl)imidazo[1,5-a]pyridine (L^5)*

Synthesized using 2,2'-dipyridylketone with p-bromobenzaldehyde as given procedure. Colour: yellow, Yield: 85%, mol. wt.: 350.22 g/mol, m.p.:172.03°C, Anal. Calc. (%) For $C_{18}H_{12}BrN_3$: C, 61.73; H, 3.45; N, 12.00 Found (%): C, 61.62; H, 3.33; N, 11.55. ^{1}H NMR (400 MHz, DMSO-d_6) δ/ppm: 6.708(1H, t, 6.0 Hz), 6.966(1H, m), 7.133(1H, m), 7.718(2H, m), 7.751(1H, t, 2.4 Hz), 7.771(1H, d, 1.6 Hz), 8.248(2H, m), 8.655(1H, m), 8.730(1H, t, 0.8 Hz). ^{13}C NMR (100 MHz, DMSO-d_6) δ/ppm: 114.30(CH), 119.95(CH) 120.60(CH), 121.12(CH), 122.02(CH), 122.92(C_{qat}), 129.13(C_{qat}), 129.81(CH), 130.44(C_{qat}), 132.18(CH), 136.29(CH), 136.97(CH), 139.58(C_{qat}), 144.19(C_{qat}), 149.04(CH), 154.89(C_{qat}). Mass (m/z): 350

I. $Ru(L^1{}_2Cl_2)PF_6$

Colour: brown, Yield: 89%, mol. wt.: 859.58 g/mol, m.p.: >300 °C, Anal. Calc. (%) For $C_{36}H_{26}Cl_2F_6N_6PRu$: C, 50.30; H, 3.05; N, 9.78 Found (%): C, 50.24; H, 3.02; N, 9.81. Mass (m/z): 714

II. $Ru(L^2{}_2Cl_2)PF_6$

Colour: brown, Yield: 92%, mol. wt.: 859.58 g/mol, m.p.: >300 °C, Anal. Calc. (%) For $C_{36}H_{26}Cl_2F_6N_6PRu$: C, 50.30; H, 3.05; N, 9.78 Found (%): C, 50.24; H, 3.01; N, 9.81. Mass (m/z): 714

III. $Ru(L^3{}_2Cl_2)PF_6$

Colour: brown, Yield: 93%, mol. wt.: 887.63 g/mol, m.p.: >300 °C, Anal. Calc. (%) For $C_{38}H_{30}Cl_2F_6N_6PRu$: C, 51.42; H, 3.41; N, 9.47 Found (%): C, 51.54; H, 3.35; N, 9.38. Mass (m/z): 742

IV. $Ru(L^4{}_2Cl_2)PF_6$

Colour: brown, Yield: 90%, mol. wt.: 928.46 g/mol, m.p.: >300 °C, Anal. Calc. (%) $C_{36}H_{24}Cl_4F_6N_6PRu$: C, 46.57; H, 2.61; N, 9.05 Found (%): C, 46.60; H, 2.67; N, 9.09. Mass (m/z): 783

V. $Ru(L^5{}_2Cl_2)PF_6$

Colour: brown, Yield: 91%, mol. wt.: 1017.37 g/mol, m.p.: >300 °C, Anal. Calc. (%) For $C_{36}H_{24}Br_2Cl_2F_6N_6PRu$: C, 42.50; H, 2.38; N, 8.26 Found (%): C, 42.47; H, 2.42; N, 8.30. Mass (m/z): 872

BIOLOGICAL SCREENING OF SYNTHESIZED COMPOUNDS

UV–Vis absorbance titration

Binding mode and interaction strength of DNA with metal complexes have been examined effectively by electronic absorption spectra (UV–Vis absorbance titration) using Herring Sperm DNA (HS-DNA)[14].

Viscosity measurement

An Ubbelohde viscometer was used to measure the flow time of HS-DNA in phosphate buffer (pH 7.2) with a digital stopwatch and each compound were carried out three times to calculate average flow time[15].

Molecular docking study

Interaction between DNA and complexes at the molecular level were studied by advanced computational typical technique like molecular docking. The rigid molecular docking study was executed using HEX 8.0 software to conclude the orientation of the complexes binding to DNA. The structure of the DNA of sequence (5'-d(CGCGAATTCGCG)-3')$_2$ (PDB id: 1BNA, a familiar sequence used in oligodeoxynucleotide study) obtained from the Protein Data Bank (http://www.rcsb.org/pdb)[16].

Cytotoxicity

For the determination of *in vitro* cytotoxicity of compounds, brine shrimp (Artemia cysts) lethality bioassay method given by Meyer et al. [17] accomplished with brine shrimp nauplii in artificial seawater. After treatment counted the number of viability of nauplii (observing several seconds if nauplii did not exhibit any internal or external movement considered nauplii dead). Data were analyzed by the log concentration of sample vs percentage mortality of nauplii that gives LC_{50} values.

Cellular level cytotoxicity assay

Eukaryotic *Schizosaccharomyces pombe cells* were an important organism for the study of the effects of the metal complexes at the cellular level (cytotoxicity) to the DNA damage. Percentage viability were counted in triplicate where the number of dead cells and number of live cells were counted in three microscopic fields (microscope (40X)) and calculated the average percentage of live cells [18].

Antibacterial activity

All of the newly synthesized compounds were screened for their antibacterial activity using *Staphylococcus aureus, Bacillus subtilis, Serratia marcescens, Pseudomonas aeruginosa and Escherichia coli* micro-organisms. The broth dilution technique was used to determine the bactericidal effect by minimum inhibitory concentration (MIC) in terms of μM. MIC, lowest concentration that prevents the microbial growth. Antibacterial activity carried out according to reported method[19].

DNA cleavage study

Effect of compounds on the integrity of *S. pombe* cell's DNA was studied by agarose gel electrophoresis. The *S. pombe* cells were grown and treated by same manner in the cellular level cytotoxicity assay. The image was captured by a CCD camera and the Alpha Digi Doc system was used for analyzing gel[20].

RESULTS AND DISCUSSION

Magnetic moments, electronic spectra and conductance measurements

Magnetic moments measurement of Ru(III) complexes was carried out at room temperature. The obtained μ_{eff} values are in the range of 1.78–1.93 BM, which corresponds to a single unpaired electron in low-spin t_{2g}^5 configuration in an octahedral environment and confirms the +3 oxidation state of ruthenium complexes. The electronic spectra of Ru(III) complexes in DMSO showed three bands in the region 285–670 nm. Ru(III) complexes have relatively high oxidation properties, and the d–d transition band appeared at 645–670 nm. The spectral data in the UV region (below 400 nm) are designated as π–π* [350–380 nm] and n–π* [285–305 nm] transitions of non-bonding electrons present on the nitrogen of the imidazol group in Ru(III) complexes. The pattern of the electronic spectra of all the Ru(III) complexes indicate the presence of an octahedral environment around the ruthenium(III) metal ion. The molar conductivities values of the Ru(III)

complexes are in the range of 39-70 $cm^2\ \Omega^{-1}\ mol^{-1}$ at room temperature, representing electrolytic nature and one counter ion existing outside the coordination sphere of Ru(III) complexes. So, we conclude that all Ru(III) complexes exhibit ionic in nature.

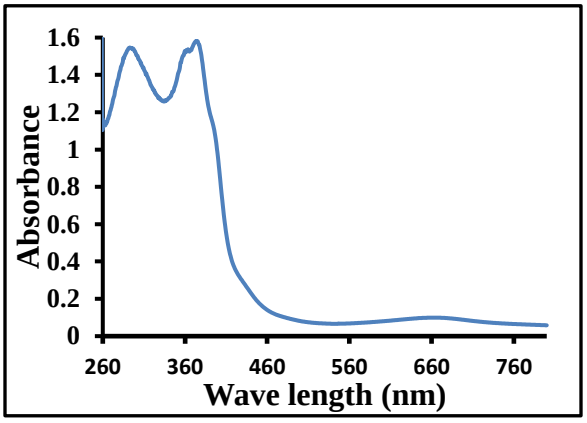

Figure 1. UV- Absorption spectra of representative complex-I in DMSO

Binding behaviour of complex with HS DNA

To examine the binding mode of metal complexes with DNA electronic absorption titration technique has been used in phosphate buffer solution (pH 7.2). Strong stacking interaction among chromophore of complex and DNA base pair results in hypochromic shift and red shift (bathochromic shift) in absorption spectra which generally indicate that intercalation binding[5,21]. An absorption titration graph for complex-II is represented in Figure 2. elucidate hypochromism with bathochromic shift with increasing in DNA concentration indicates intercalation mode of binding. The K_b value is determine from the ratio of the slope to intercept from the plot of [DNA]/(ε_a - ε_f) versus [DNA] and values for ligands and complexes are shown in figure 3.

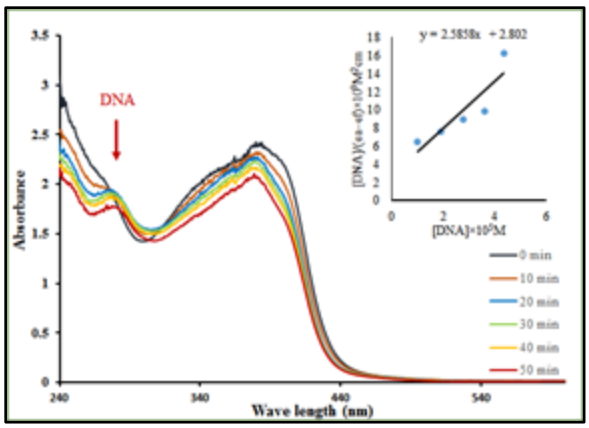

Figure 2. Absorption spectra of complex-**I** with increasing concentration of HS–DNA after incubation 10 min of each addition at 37 °C in phosphate buffer (pH 7.2) Inset: Plots of [DNA]/($\mathcal{E}_a$–$\mathcal{E}_f$) versus [DNA] for the titration of DNA with compounds.

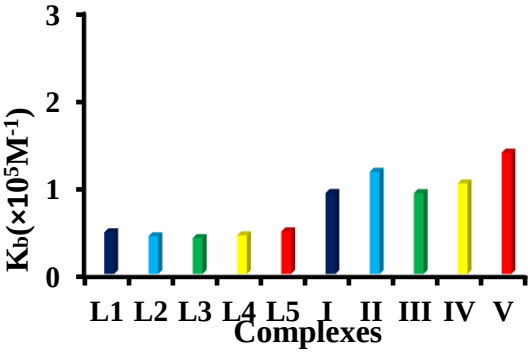

Figure 3. Plot of *Kb* values of synthesized ligands and complexes in L mol−1 using HS-DNA. Error bars represent the standard deviation of three replicates

Hydrodynamic volume measurement

The intrinsic viscosity depending on the mode of interaction with increasing concentration of complexes. Increasing in viscosity explain as separation of base pair occur when complex Insert in DNA base pair. Which leads to the DNA helix lengthens and proposed that the intercalation type of binding present [5][20]. Plot of relative specific viscosity $(\eta/\eta_0)^{1/3}$ versus [complex]/[DNA] (Figure 4) shows increasing in viscosity of the DNA with the addition of complexes. Which suggests that the intercalation binding mode of complexes with HS-DNA that cumulative observed in electronic absorption spectra.

Orientation of docked structure

The molecular docking study was accomplished to determine the orientation of the Ru(III) complexes with DNA and its binding affinity using HEX 8.0 software.

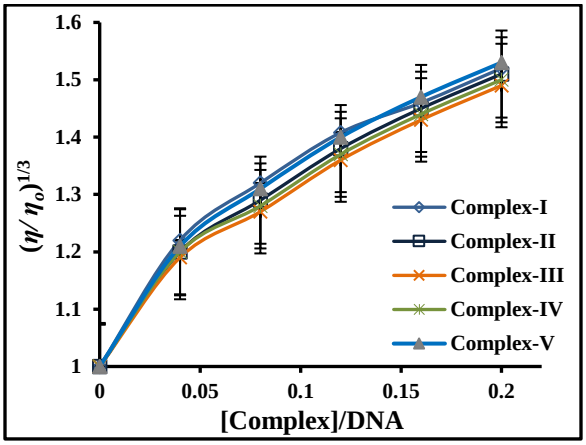

Figure 4. Effect on relative viscosity of HS DNA under the influence of increasing amount of complexes at 37±0.1 °C in phosphate buffer (pH 7.2) with standard deviation.

The resulting binding energies of docked ligands L^1-L^5 and complexes I-V are measurable as kJ mol^{-1} and values of energy are represent in Table 1. The results indicate the docked structure of complex (Figure 5) fit well into the intercalative mode of the targeted DNA and A–T rich region stabilized by van der Waal's interaction and hydrophobic contacts [19]. The docking study shows preferential intercalation binding when complexes interact with DNA. The more negative values of docked energy, the more effective binding between DNA and target molecules. Result arising from molecular docking promote binding similar to that of viscosity and spectroscopic absorption titration.

Docking energy			
Ligand	kJ\mol	Complex	kJ\mol
L1	-232.8	I	-289.98
L2	-225.9	II	-303.17
L3	-233.7	III	-309.57
L4	-241.9	IV	-306.54
L5	-240.8	V	-310.10

Table 1. Docked energy values of ligands and complexes in kJ/mol

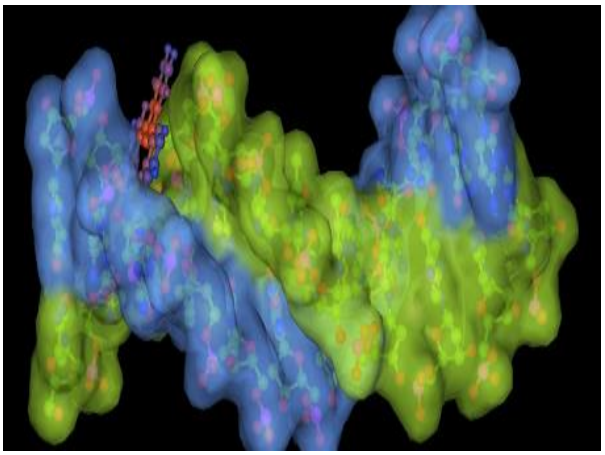

(a)

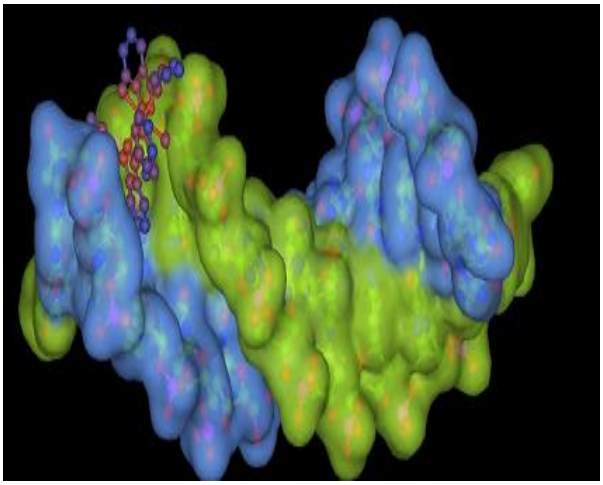

(b)

Figure 5. Docked structure of (a) Ligand-1 and (b) complex-I with the HS-DNA duplex of sequence $(5'\text{-d(CGCGAATTCGCG)-}3')_2$

Brine shrimp lethality bioassay

Simple and cheap methodology employed for the cytotoxicity study was brine shrimp (Artemia cysts) lethality bioassay[22]. The LC_{50} values obtained from the log concentration of sample vs. percentage mortality of nauplii. The comparative result of toxicity is represent in Figure 6 (LC_{50} = 5.63 – 27.82). The data suggest that tested compounds have strong ability to interact with the biological model system. The complexes show more toxicity than corresponding ligands. It is strongly supported that *in vitro* cytotoxicity study against brine shrimp assay is useful for the further study and preparation of effective medicine against various diseases. The order of

toxicity of compounds is V>IV>III>I>II>L^5>L^4>L^3>L^1>L^2. The result shows that the electron withdrawing group increases the toxicity of compounds.

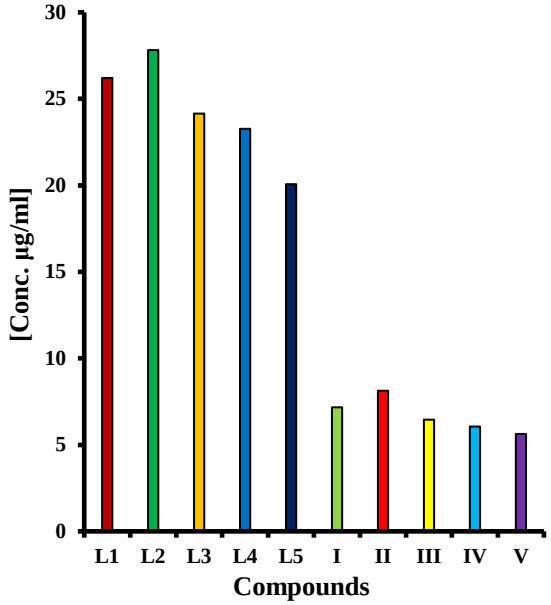

Figure 6. Cytotoxicity of synthesized ligand and complexes by brine shrimp assay.

In vivo cytotoxicity

Cytotoxicity data represented graphically in Figure 7, which shows % viability of cells treated by complexes and their ligand after 17 h treatment. From the results, it is observed that the % viability of ligands is higher than complexes, in another word toxicity of complexes is higher than their corresponding ligands.

Antibacterial activity

Antibacterial activity of the synthesized compound has been carried out against two Gram(+ve) (B. *subtilis and S. aureus)* and three Gram(–ve) *(P. aeruginosa, E. coli and S. marcescens)* bacteria.

Increasing in antibacterial activity may be considered in the light of an Overtone's concept [19] and chelation theory [23]. The result of *in vitro* antibacterial activity values of the ligands and corresponding complexes indicates that the metal complexes show relatively higher activity against bacteria. The MIC values for ligands and complexes are in the range of 230-320 µM and 75-120 µM, respectively (Figure 8). The complexes are comparatively more potent than ligands against all bacteria and they more effective on *S. aureus, B. subtilis and E. coli.*

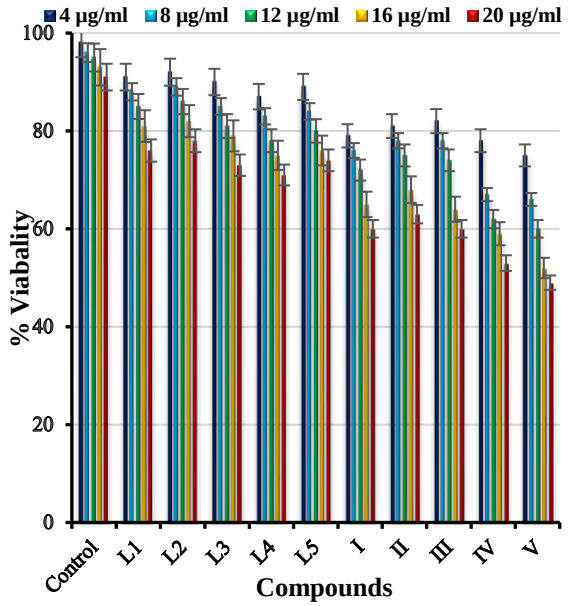

Figure 7. *S. pombe* cell viability represents as a percentage with a standard deviation of three independent experiments of synthesized compounds.

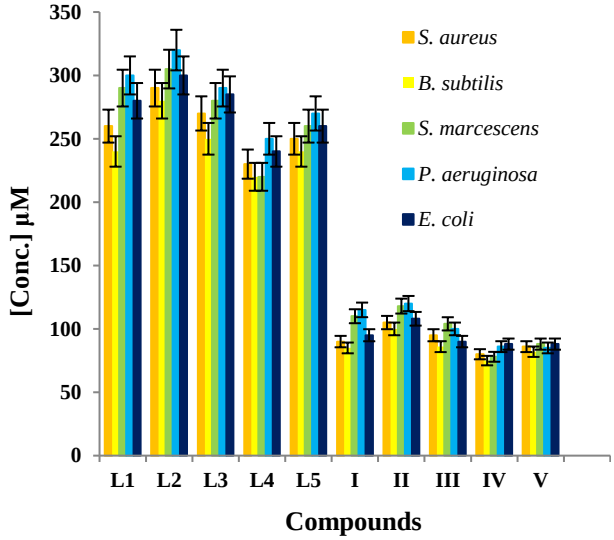

Figure 8. Minimum inhibition concentration (MIC) values of synthesized compounds given in µM.

Effect of compound on integrity of S. pombe cell's DNA

Agarose gel electrophoresis used for the study of DNA cleavage. The DNA extraction was carried out from *S. pombe* cells as reported method[20]. All the treated compound were incubated in TE buffer (pH 8) at a final volume of 10 μgL^{-1} for 24 h at 37 °C. Effects of compound on the integrity of DNA in agarose gel are shown in Figure 9. Smearing of DNA in complexes suggests that the damage occurs due to the toxic nature of the compound. Whereas control cell DNA and complex salt treated DNA appeared in intact band indicate that non-toxic or less toxicity compared to complexes. So, the result of complexes expresses their toxic effect at the cellular level and break the DNA from the nucleus.

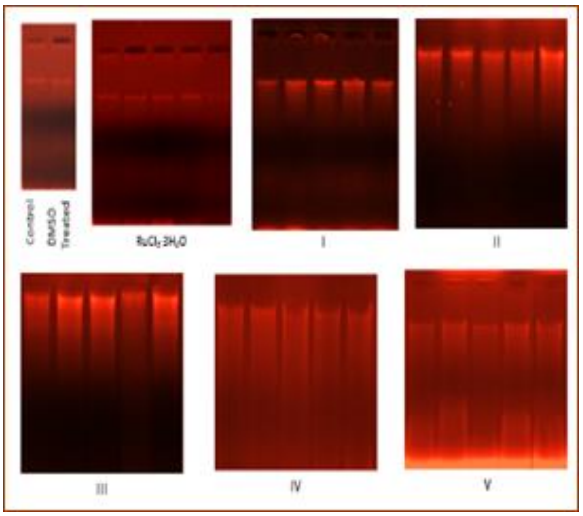

Fig. 9. Photogenic view of cleavage of *S. pombe* DNA (1 μgL^{-1}) with series of compounds using 1% agarose gel containing 0.5 (μgL^{-1}) EtBr.

CONCLUSION

The present study describes the synthesis of imidazo[1,5-a]pyridine based Ru(III) complexes of type $[Ru(L^{1-5})_2Cl_2]PF_6$ and characterized by elemental analysis, conductance measurements, electronic spectra, infrared (FT-IR) spectroscopy and mass spectroscopy. The characterization confirms the +3 oxidation of ruthenium complexes. The DNA interaction study shows the intercalation type of binding, which confirms through spectroscopic titration, viscosity measurements and molecular docking study. The result of antibacterial activity shows that complexes exhibit higher antibacterial activity than corresponding ligand. *In vitro* and *in vivo* cytotoxicity against brine shrimp and *S. pombe* indicate that toxicity increases when ligand coordinates to metal ion due to, alteration of structure of complexes. The DNA cleavage study of complexes shows the integrity of complexes with DNA and breaking of DNA from nuclease suggest that the toxic effect of the complexes at the cellular level. From all the results, we conclude that the synthesized Ru(III) complexes are biologically active and further study of the complexes may be leads to the alternate for anticancer drugs.

ACKNOWLEDGEMENTS

The authors are thankful to the Head, Department of Chemistry, Sardar Patel University, Vallabh Vidyanagar, Gujarat, India, for providing necessary research facilities, DST-PURSE, Sardar Patel University, Vallabh Vidyanagar for mass spectral analysis, SAIF and CIL, Punjab University for the ESI-MS and elemental analysis and U.G.C. New Delhi for providing financial assistance of UGC-BSR grant No. C/2013/BSR/Chemistry/1573.

REFERENCES

[1] Thangavel, S., Paulpandi, M., Friedrich, H. B., Murugan, K., Kalva, S. and Skelton, A. A. (2016): Synthesis, characterization, antiproliferative and molecular docking study of new half sandwich Ir(III), Rh(III) and Ru(II) complexes. *J. Inorg. Biochem.,* **159**: 50-61.

[2] Miao, T.-F., Li, S., Chen, Q., Wang, N.-L. and Zheng, K.-C. (2013): Probing DNA photocleavage efficiencies of Ru(II) polypyridyl complexes: Theoretical calculation of redox potentials. *Inorganica Chimica Acta*, **407**: 37-40.

[3] Mohanraj, M., Ayyannan, G., Raja, G. and Jayabalakrishnan, C. (2016): Synthesis, spectral characterization, DNA interaction, radical scavenging and cytotoxicity studies of ruthenium(II) hydrazone complexes. *Journal of Photochemistry and Photobiology B: Biology*, **158**: 164-173.

[4] Scintilla, S., Brustolin, L., Gambalunga, A., Chiara, F., Trevisan, A., Nardon, C. and Fregona, D. (2017): Ru(III) anticancer agents with aromatic and non-aromatic dithiocarbamates asligands: Loading into nanocarriers and preliminary biological studies. *J. Inorg. Biochem.,* **166**: 76.

[5] Deepika, N., Devi, C. S., Kumar, Y. P., Reddy, K. L., Reddy, P. V., Kumar, D. A., Surya, S. S. and Satyanarayana, S. (2016): DNA-binding, cytotoxicity, cellular uptake, apoptosis and photocleavage studies of Ru(II) complexes. *Journal of Photochemistry and Photobiology B: Biology*, **160**: 142-153.

[6] Kumar, A., Kumar, A., Gupta, R. K., Paitandi, R. P., Singh, K. B., Trigun, S. K., Hundal, M. S. and Pandey, D. S. (2016): Cationic Ru(II), Rh(III) and Ir(III) complexes containing cyclic π-perimeter and 2-aminophenyl benzimidazole ligands: Synthesis, molecular structure, DNA and protein binding, cytotoxicity and anticancer activity. *Journal of Organometallic Chemistry*, **801**: 68-79.

[7] Tan, C., Liu, J., Li, H., Zheng, W., Shi, S., Chen, L. and Ji, L. (2008): Differences in structure, physiological stability, electrochemistry, cytotoxicity, DNA and protein binding properties between two Ru(III) complexes. *J. Inorg. Biochem.,* **102**: 347-358.

[8] Matos, C. P., Valente, A., Marques, F., Adão, P., Paula Robalo, M., de Almeida, R. F. M., Pessoa, J. C., Santos, I., Helena Garcia, M. and Tomaz, A. I. (2013): New polydentate Ru(III)-Salan complexes: Synthesis, characterization, anti-tumour activity and interaction with human serum proteins. *Inorganica Chimica Acta*, **394**: 616-626.

[9] Abdel Aziz, A. A. and Elbadawy, H. A. (2014): Spectral, electrochemical, thermal, DNA binding ability, antioxidant and antibacterial studies of novel Ru(III) Schiff base complexes. *Spectrochimica Acta Part A: Molecular and Biomolecular Spectroscopy*, **124**: 404-415.

[10] Venkat Reddy, P., Rajender Reddy, M., Avudoddi, S., Praveen Kumar, Y., Nagamani, C., Deepika, N., Nagasuryaprasad, K., Satyanarayana Singh, S. and Satyanarayana, S. (2015): Design, synthesis, DNA-binding affinity, cytotoxicity, apoptosis, and cell cycle arrest of Ru(II) polypyridyl complexes. *Anal. Biochem.,* **485**: 49-58.

[11] Liu, X.-W., Shen, Y.-M., Li, Z.-X., Zhong, X., Chen, Y.-D. and Zhang, S.-B. (2015): Study on DNA binding behavior and light switch effect of new coumarin-derived Ru(II) complexes. *Spectrochimica Acta Part A: Molecular and Biomolecular Spectroscopy*, **149**: 150-156.

[12] Zeng, L., Xiao, Y., Liu, J. and Tan, L. (2012): Synthesis, characterization, DNA-binding and cytotoxic properties of Ru(II) complexes: [Ru(MeIm)4L]2+ (MeIm=1-methylimidazole, L=phen, ip and pip). *Journal of Molecular Structure*, **1019**: 183-190.

[13] Thota, S., Vallala, S., Yerra, R. and Barreiro, E. J. (2015): Design, synthesis, characterization, cytotoxic and structure activity relationships of novel Ru(II) complexes. *Chinese Chemical Letters*, **26**: 721-726.

[14] Chitrapriya, N., Sathiya Kamatchi, T., Zeller, M., Lee, H. and Natarajan, K. (2011): Synthesis, spectroscopic, crystal structure and DNA binding of Ru(II) complexes with 2-hydroxy-benzoic acid [1-(4-hydroxy-6-methyl-2-oxo-2H-pyran-3-yl)-ethylidene]-hydrazide. *Spectrochimica Acta Part A: Molecular and Biomolecular Spectroscopy*, **81**: 128-134.

[15] Cohen, G. and Eisenberg, H. (1969): Viscosity and sedimentation study of sonicated DNA–proflavine complexes. *Biopolymers*, **8**: 45-55.

[16] Gajera, S. B., Mehta, J. V., Kanthecha, D. N., Patel, R. R. and Patel, M. N. (2017): Novel cytotoxic oxovanadium(IV) complexes: Influence of pyrazole-incorporated heterocyclic scaffolds on their biological response. *Applied Organometallic Chemistry*: e3767-n/a.

[17] Meyer, B. N., Ferrigni, N. R., Putnam, J. E., Jacobsen, L. B., Nichols, D. E. and McLaughlin, J. L. (1982): Brine Shrimp: A Convenient General Bioassay for Active Plant Constituents. *Planta Med*, **45**: 31-34.

[18] Mehta, J. V., Gajera, S. B. and Patel, M. N. (2016): Biological applications of pyrazoline-based half-sandwich ruthenium(III) coordination compounds. *Journal of Biomolecular Structure and Dynamics*: 1-9.

[19] Mehta, J. V., Gajera, S. B., Thakor, P., Thakkar, V. R. and Patel, M. N. (2015): Synthesis of 1,3,5-trisubstituted pyrazoline derivatives and their applications. *RSC Advances*, **5**: 85350-85362.

[20] Thakkar, P. B. P. a. V. (2013): Cell Proliferation and DNA Damage Study by SCGE in Fission Yeast Exposed to Curcumin and 5-fluorouracil. *Asian Journal of Cell Biology*, **8**: 22-32.
[21] H Khan, N.-u., Pandya, N., Kureshy, R., Abdi, S., Agrawal, S., Bajaj, H., Pandya, J. and Gupte, A. (2009) *Synthesis, characterization, DNA binding and cleavage studies of chiral Ru(II) salen complexes*.
[22] Thakor, K. P., Lunagariya, M. V., Karia, P. S. and Patel, M. N. (2017): Evolution of palladium(II) complexes as DNA intercalator and artificial metallonuclease. *Monatshefte für Chemie - Chemical Monthly*.
[23] Tweedy, B. (1964): Plant extracts with metal ions as potential antimicrobial agents. *Phytopathology,* **55**: 910-914.

PRAJÑĀ - **Journal of Pure and Applied Sciences Vol. 24 – 25 : 141 – 146 (2017)**
ISSN 0975 - 2595

ADVANCED OXIDATION PROCESSES FOR COD REDUCTION

MAYANK VITHALANI, MAYUR KASODARIYA, MEHUL AMRUTIYA AND SURESH C. PANCHANI*

Department of Chemical Engineering, G H Patel College of Engineering & Technology,

VallabhVidynagar, Gujarat (INDIA) E-mail : sureshpanchani@gcet.ac.in

ABSTRACT

Most of the synthetic dyes are non-biodegradable and are toxic to the microorganisms. The effluent containing dyes is difficult to treat by conventional biological processes. These dyes can be easily treated if the conventional treatment methods are incorporated with the advanced oxidation processes (AOPs). AOPs can break the complex structure of dyes making them more amicable to bio-degradation. This paper deals with different AOPs like hydrogen peroxide, sonolysis and their combination like sono-chemical process for remediation of dye wastewater effluent and comparison of treatment efficiencies. It is observed that the efficiencies of various options were found to be dependent on characteristics of the wastewater to be treated. The paper also discusses the important parameters to scale-up AOPs on large scale for better efficiency in actual practice.

Keywords-Effluent; Dyes; Advanced Oxidation Processes (AOPs); Revamp

INTRODUCTION

The dye wastewater is characterized by high content of dyestuff, salts, high chemical oxygen demand (COD) derived from additives, suspended solid (SS) and fluctuating pH. Conventional processes to treat wastewater from dyes and textile industries includes chemical precipitation with alum or ferrous sulphate which suffers from drawbacks such as generation of a large volume of sludge, the contamination of chemical substances in the treated wastewater, etc. Moreover these processes are inefficient towards completely oxidizing dyestuffs and organic compounds of complex structure. To overcome these problems advanced oxidation processes (AOPs) have been developed to generate hydroxyl free radicals by different techniques. AOPs include hydrogen peroxide (H_2O_2), Ozone (O_3) and UV irradiation, which have proved to be much efficient in effluent treatment processes [1] [2].

The most efficient and feasible process which reduces the COD by maximum percent is selected for revamping of Effluent Treatment Plant of a particular chemical industry. The design related to modification of installed vessel would be done for large scale application of one of the AOPs in accordance with plant capacity.

The aim of AOP is the generation of free hydroxyl radical (OH●), a highly reactive, non-selective oxidizing agent, which can destroy even the recalcitrant pollutants. The generation of hydroxyl radical is highly accelerated by combining ozone (O_3), hydrogen peroxide (H_2O_2), titanium dioxide (TiO_2), heterogeneous photo-catalysis, UV radiation or high electron beam radiation. Various types of AOPs include Ozone/H_2O_2, Ozone/UV/H_2O_2, Ozone/TiO_2/H_2O_2, Ozone/TiO_2/Electron beam irradiation, H_2O_2/UV, H_2O_2/Fe^{+2}, H_2O_2/UV/Fe^{+2}, Ozone/UV [3,9]. In this paper Fenton's method, ultrasonication & sonochemical processes are discussed.

METHODOLOGY & MATERIALS

1. FENTON'S METHOD

The Fenton's process generates great amount of $HO^{\bullet}$ radicals with powerful oxidizing potential which has a very short life, but is reactive and attack dyes by either abstracting a hydrogen atom or adding itself to double bonds The Fenton process can be defined as the oxidation of

organic compounds in an aqueous solution. Initially an increase in colour removal was observed with the increase in amount of ferrous sulphate for all concentrations of green cationic dyes. The fact that the rate of decolourization increases with an increase in the concentration of ferrous ions was shown in the study performed by [4] on green cationic dyes in textile wastewater. The pH of the solution, amount of ferrous ions, and concentration of H_2O_2, initial concentration of the pollutant and presence of other ions considerably affects the Fenton's process [5]. Fenton's reagent can be electro-produced with abundant and cheap feedstock: oxygen saturated wastewater and solar energy [6].

Procedure for Fenton's method:
First of all the pH of Effluent was measured and then the pH was adjusted to 3 by adding concentrated H_2SO_4. 600 mL of effluent sample was taken in a 1 Litre beaker. Fenton's reagent was prepared by adding 3gm of $FeSO_4.7H_2O$ in 30 ml of 30% Hydrogen Peroxide. Prepared Fenton's reagent was added to the beaker containing effluent sample. The beaker was then set on a magnetic stirrer at room temperature. After regular intervals of 30 min, 50ml sample from the beaker was collected for 30, 60, 90 minutes mixing time. In each sample 2-3 drops of H_2SO_4 was added to prevent further reaction. The samples were kept in incubators and COD was measured [7, 10].

2. SONOCHEMICAL METHOD

When ultrasound was applied to effluent, water undergoes thermal dissociation to hydrogen and OH radicals. OH radical is highly reactive and can oxidise almost all contaminants in water. This primary oxidation is the reason for the degradation of contaminants in water [8,14]. Sonochemical reactions are normally characterised by the simultaneous occurrence of pyrolysis and radical reactions, especially at high solute concentrations. Phenols, chloro-phenols, nitrophenols, parathion, etc. are among a few regularly observed contaminants in industrial effluent. They are known to get degraded by the cavitation phenomenon. Degradation pathway is likely to change with the change in the intensity of ultrasound, concentration of the contaminant in water, etc. An unanticipated advantage is that sonication also kills some microorganisms and hence disinfects water [8, 11].

Procedure for sonochemical treatment :
The same procedure was repeated for effluent treatment as described under Fenton's Method but it was carried out under the ultrasonic cleaner at 20Hz fixed frequency for the cycle of 144/36 (on/off) seconds [7, 10].

Fig.1: Various Ultrasonic Experimental Data [12, 13] for comparison

Contaminants degraded	Concentration		Ultra sound concentration		
		Frequency (KHZ)	Iron typ[e and dosage	Power (w)	Reactor (ml)
Dye reactive Brillient Red	10-100mgL^{-1}	20	Fe^{+2}:1-5 µm	150	150
2,4 dinitro phenol	20 mgL^{-1}	20	Fe^{+2} 60 mgL^{-1}	200-800	75
1,4 dioxane	100 mgL^{-1}	20	Fe^{+2}or Fe^{0} 0.5 mgL^{-1}	300	-
Dinitrotoluenes and 2,4,6 tri nitrotoluene	DOC 150 mgL^{-1}	20	-	52-227W cm^{-2}	300
Pentacholrophenol	15 mgL^{-1}	25	FeO@Fe_2O_3 core –shell neneowires:100mg	100	150
P-Nitro phenol	0.5 and 1.0 %	25	$FeSO_4$:H_2O_2=1:5,1:7.5 and 1:10	1000	500
2,4-D and DNOC	2,4-D(1mM) DNOC(0.5mM)	28 and 460	Fe^{+3}: 0.1mM	20-80	250
Azo dye acid orange -7	1000 mgL^{-1}	40	Fe^{0}/GAC:12g/2.3g	100	250
Pentachlorophenol	37.5µm	40	Fe^{0}:2gL^{-1}	600	75
Azo dye Acid Black-I	0.041-0.162mm	40	Fe^{+2}:0.01-0.05Mm	20-50	100
Chlorobenzene	100 mgL^{-1}	200	Fe^{+2}:0.45mM Fe^{+2}:0.90mM	200	150
Methylene Blue	3.0µm	200-1063	Fe^{+3}:1x10^{-3}-1x10^{-2} M	35	300
Anthraquinonic dye,C.IAcid Blue25	10-50 mgL^{-1}	22.5 and 1,700	Fe^{+2} :10^{-3}M	14	100

OBSERVATIONS & RESULTS

Fenton's Method

Table 1 and 2 respectively depict the COD and % COD reduction at different time intervals for Fenton's method employing 1:10 ($FeSO_4$: H_2O_2) and 1:5 ($FeSO_4$: H_2O_2) reagent at 3 pH.

Table.1: COD by Fenton's method (1:10) At pH =3, Dosage = 1:10 ($FeSO_4$: H_2O_2)

Time (min)	COD	% COD reduction
0	2300	-
30	1940	15.61
60	1761	23.43
90	1517	34.03
120	1344	41.56
150	1136	50.6
180	960	58.26

Table.2: COD by Fenton's method (1:5**)**

- At pH =3
- Dosage = 1:5 ($FeSO_4$: H_2O_2)

Time (min)	COD	% COD reduction
0	2300	-
30	2041	11.25
60	1845	19.91
90	1628	29.2
120	1458	36.6
150	1235	46.8
180	1053	54.21

Sono-Chemical Method

Table 3 and 4 respectively represent the result in terms of COD and % COD reduction at different time intervals for Fenton's method employing 1:10 ($FeSO_4$: H_2O_2) and 1:5 ($FeSO_4$: H_2O_2) reagent at 3 pH under sonication at fixed 20Hz.

In each case COD is found to decrease and % COD reduction increases with time interval starting from 30 min to 180 min. 1:10:: $FeSO_4$: H_2O_2 is observed to be more efficient than 1:5::$FeSO_4$: H_2O_2 with and without sonication. A maximum of 74% reduction in COD was achieved by sonochemical method.

Table.3: COD by sonochemical method

- At pH =3
- Dosage = 1:10 ($FeSO_4$: H_2O_2)

Time (min)	COD	For ratio 1:10
0	2300	-
30	1794	21.97
60	1608	30.08
90	1365	40.62
120	1125	51.08
150	798	65.23
180	596	74.08

Table.4: COD by sonochemical method

- At pH =3
- Dosage = 1:5 ($FeSO_4$: H_2O_2)

Time (min)	COD	For ratio 1:5
0	2300	-
30	1806	18.33
60	1689	26.56
90	1450	36.3
120	1263	45.08
150	935	59.34
180	714	68.95

CONCLUSION

Comparision of Fenton's and sono-chemical process for different ratio of $FeSO_4$:H_2O_2 employed for the treatment of dye effluent is presented below in the bar diagram (Fig 2) and Table 5.

Fig 2: Overall % COD reduction

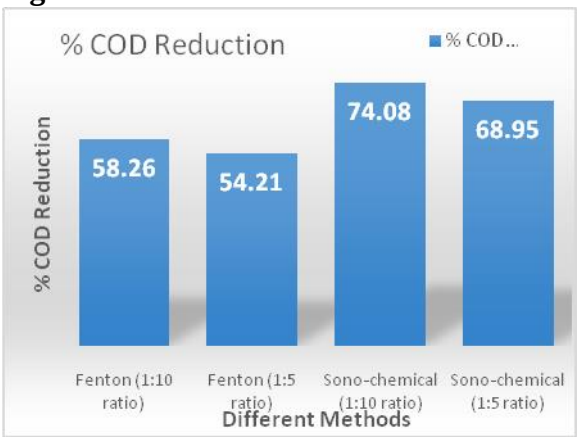

Table 5: Comparative Result

Methods	Fe^{2+}:H_2O_2 Ratio	COD	% COD Reduction
Initial sample	-	2300	-
Fenton	1:10	960	58.26
Fenton	1:5	1053	54.21
Sono-Chemical	1:10	596	74.08
Sono-Chemical	1:5	714	68.95

From the result, it is concluded that it is better to opt for sono-chemical process in the ETP plant with 20Hz frequency and 1:10 Fenton ratio. Approach for designing ETP should address following issues.

1. Quantity of wastewater generated
2. Characterization of wastewater
3. Inlet feed water quality
4. Wastewater treatability and treatment option
5. Mode of disposal of treated effluent
6. Disposal of sludge
7. Recycle/reuse of treated water
8. Modular process, scalable and flexible

Modifications Suggested

1. Feed : H_2O_2 ratio = 20 : 1 (30% H_2O_2)
2. $FeSO_4$:H_2O_2 ratio = 1:10
3. Frequency for Sonicator – 20 kHz
4. Vessel agitator should be connected along with Sonicator stirrer
5. Maintain pH between 2–3.
6. Reactor of 20000 kg requires 10 L (for usage of 50% concentration H_2SO_4) and 4 L (for usage of 98% concentration H_2SO_4).
7. Sound proof walls for reactor are recommended if high frequency sonicator is economically not feasible.

REFERENCES

1. S. Lidia, J. Claudia and N.K. Santosh, "A comparative study on oxidation of disperse dyes by electrochemical process, ozone, hypochlorite and fenton reagent," Water Research, vol. 35, 2001, pp. 2129–2136.
2. L. Stanislaw, S. Monika and Z. Renata, "Biodegradation, decolourisation and detoxification of textile wastewater enhanced by advanced oxidation processes," Journal of Biotechnology, vol. 89, 2001 pp. 175-184.
3. Zhou H. and Smith D.W., Advanced technologies in water and wastewater treatment, Journal Environmental Engineering Science, 1, 2002, 247-264.
4. C.S. Rodrigues, L.M. Madeira and R.A. Boaventura,"Treatment of textile effluent by chemical (Fenton's Reagent) and biological (sequencing batch reactor) oxidation," Journal of Hazardous Materials, vol. 172, 2009, pp. 1551–1559.
5. A.S. Stasinakis, "Use of selected advanced oxidation processes (AOPs) for wastewater treatment – A Mini Review," Global NEST Journal, Vol 10, No 3, 2008, pp 376-385.
6. S. Figueroa, L. Vázquez' and A. A.-Gallegos, "Decolorizing textile wastewater with Fenton's reagent electrogenerated with a solar photovoltaic cell" Science Direct, 2008.
7. Andrew D. Eaton, Lenore S. Clesceri, Arnold E.Greenberg, M. A. H. Franson*Standard methods for the examination of water and wastewater* – American Public Health Association,1995.
8. Amol A Kulkarni, Mugdha Deshpande and A B Pandit Techniques of Wastewater Treatment , Future Technologies Resonance December 2000 Pg.no: 64-74
9. Advanced Oxidation Processes for Treatment of Textile and Dye Wastewater: A Review Shashank Singh Kalra, Satyam Mohan, Alok Sinha and Gurdeep Singh International Conference on Environmental Science and Development IPCBEE vol.4 (2011).
10. GeorgeTchobanoglous, Franklin L. Burton, Metcalf & Eddy, H. David Stensel*Wastewater Engineering: Treatment and Reuse* – McGraw-Hill,2003.
11. Akram M, Chowdury A and Chakrabarti S, "Removal of Rhodamine B Dye from wastewater by ultrasound – assisted Fenton Process: A Process

Comparison between Bath and Probe type Sonicators", Environmental Science: An Indian Journal (2016).

12. Zahra Rahmani, Majid Kermani, Mira Gholami, Ahmad JonidiJafiri, and Niya Mohammad Mahmoodi "Effectiveness of photochemical and sonochemical processes in degradation of basic violet 16 dye from aqueous solution", Iranian Jounal of Environmental Health Science & Engineering,2012;9(1):14.
13. Juan Carlos Colmenares, Gregory Chatel*Sonochemistry: From Basic Principles to Innovative Applications*, Springer Top CurrChem(Z) (2016) pp.121-125.
14. Raji R. Nair, Reshma Patel "Treatment of Dye Wastewater by Sonolysis Process", International Journal of Research in Modern Engineering and Emerging Technology, Vol. 2, Issue: 1, April-May : 2014
15. Ma YS. Short Review: Current Trends and Future Challenges in the application of Sono-Fenton oxidation for wastewater treatment. Sustain Environ Res.2012;22(5):271-8.

PRAJÑĀ - **Journal of Pure and Applied Sciences Vol. 24 – 25 : 147 – 152 (2017)**
ISSN 0975 - 2595

2, 4-DIHYDROXY-5-BROMO HEXAPHENONE OXIME (DHBHPO) AS AN AMPEROMETRIC REAGENT FOR ANALYSIS OF COPPER(II) AND NICKEL(II)

PRATESH J SHAH[1]*, NITINKUMAR B PATEL [1]

[1]Shree Jayendrapuri Arts & Science College, Bharuch.(Gujarat)
Affiliated to Veer Narmad South Gujarat University, Surat-395007-Surat, INDIA
E-mail: pratesh.shah@gmail.com

ABSTRACT

DHBHPO has been used as an analytical reagent for amperometric determination of copper and nickel. Cu(II) and Ni(II) forms colored complex with the reagent at pH 5.0 and 8.5 respectively. After studying the polarographic behavior of the metal ions and the reagent at dropping mercury electrode (DME), applied potential were fixed at – 0.4 v (Vs SCE) for copper(II) and - 1.5v (Vs SCE) for Nickel(II). The method was applied for the determination of copper and nickel in german silver alloy. Newly synthesized reagent was characterized using analytical techniques such as IR spectra, NMR and elemental analysis.

Key words: Amperometric determination, DHBHPO, Applied potential, Dropping mercury electrode (DME), Secondary calomel electrode (SCE), Supporting electrolyte.

INTRODUCTION

The formation of coordination compounds by organic reagents with metal ions has been extensively used in analytical chemistry. Most of the selective reagents employed have hydroxyl groups. o-hydroxy ketoximes (1-8) , oximes (9-10) has been used for gravimetric and spectrophotometric determination of several metal ions. A very few analytical reagents have been employed for the polarographic determinations. The amperometric method of determining the end point is an extension of polarographic analysis. Gallacetophenone phenylhydrazone(11) was used for amperometric determination of Bismuth. o-hydroxyacetophenone oxime (12,13) , 2,5-Dihydroxy acetophenone oxime (14) were used as an amperometric reagent for Cu(II), Ni(II) and Pd(II). 2-Hydroxy-1-acetophenone oxime(15) and 1-hydroxy-2-acetophenone oxime (16) have been successfully employed for the determination of copper and nickel in binary solution. In the present work, we synthesized a new reagent with a view to extend the use of o-hydroxy ketoximes for the amperometric determination of metal ions at DME. DHBHPO performed successfully for the simultaneous determination of copper and nickel in alloy.

METHODOLOGY

Analytical grade chemicals and doubly distilled water was used. Stock solution of copper(II) and nickel(II) were prepared freshly by dissolving copper sulphate and nickel sulphate, respectively. Solution of other ions was prepared from their salts in distilled water. Sodium acetate (0.5M) and acetic acid (0.5M) buffer of pH 5.0 acted as supporting electrolyte for estimation of copper(II) while ammonium chloride (0.5M) and ammonia (0.5M) buffer of pH 8.5 acted as supporting electrolyte for estimation of nickel(II). A 0.2% aqueous solution of gelatin was prepared freshly before use. Purified nitrogen gas was employed for deaeration. All the titrations were performed at DME Vs SCE using a systronic manual polarograph model no 1632 with inbuilt digital micro ameter. A systronic digital pH meter 335 was use to adjust pH. Perkin-Elmer 2400 Elemental Analyser, Bruker Avance II 400 NMR spectrometer and Simadzu FT-IR spectrophotometer were used to characterize the reagent.

Synthesis of the Reagent [DHBHPO]

DHBHPO was synthesized according to the method of H.Nogami (17), reaction between Resocinol (0.05M), Hexanoic acid (0.05M) and anhydrous zinc chloride gave 2,4 dihydroxyhexaphenone (DHHP) liquid ketone having density of 1.23 gm/mL. Bromination of above ketone (0.01 M) with bromine in acetic acid (0.01M) results in the formation of 2,4-dihydroxy-5-bromohexaphenone (DHBHP). The product was treated with sodium bisulphite to remove excess bromine. White solid separated, was recrystallized from ethanol. M.P. 121° C. This bromo ketone derivative (2 gm) further refluxed with $NH_2OH.HCl$ (4 gm) in presence of sodium acetate (6 gm) for 4 hours forming the above reagent. Reagent was recrystallized after charcoal treatment from aqueous ethanol, M. P 148° C. A 0.02 M reagent solution was prepared in 95% ethanol just before used. Reagent is soluble in DMSO, DMF, $CDCl_3$ and absolute alcohol. It is insoluble in water, chloroform and carbon tetrachloride.

CHARACTERIZATION OF REAGENT :

Elemental analysis: Elemental analysis of the reagent shows that the percent elements found are in agreement with its molecular formula. The results are represented in Table 1.

FT-IR spectral studies: The IR spectrum of all reagents were taken by preparing pallet with KBr. The IR spectrum of DHBHPO shows strong band at 3475 cm^{-1} which may be assigned to O-H stretching due to Phenolic -OH group and at 3363 cm^{-1} due to -OH moiety of =N-OH group. Strong bands at 2854-2956 cm^{-1},1591 cm^{-1} , 1465 cm^{-1} and 1492 cm^{-1} may be assigned to aliphatic C-H stretching, aromatic C=C stretching , N-O stretching and C=N stretching respectively.

^{1}H and ^{13}C NMR spectral studies of 2, 4-dihydroxy-5- bromo hexaphenone oxime DHBHPO:

The ^{1}H NMR and ^{13}C NMR study for DHBHPO was carried out using $CDCl_3$ as solvent and TMS as reference. Assignment of signals to different protons and carbons are given in Table-2 and 3.

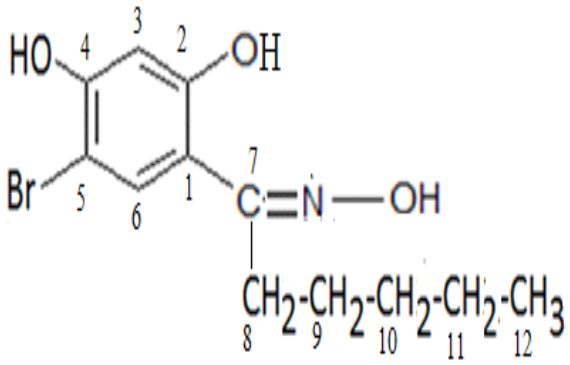

[2, 4-Dihydroxy-5-bromo hexaphenone oxime (DHBHPO)]

OBSERVATION

Determination of Cu(II) and Ni(II)

The polarographic behavior of DHBHPO, copper(II) and nickel (II) at DME was studied to arrive at the suitable voltage to be fixed for the amperometric determinations. 25 mL of acetate buffer (pH.5.0), 5 mL 0.02M reagent, 1.5 mL of 0.2% gelatin and 10 mL of alcohol were taken in titration cell and finally diluted to 50 mL. The solution was deoxygenated by bubbling nitrogen gas for 15 minutes. The drop time of the DME was adjusted to 3-4 seconds and the polarogram of the reagent was recorded. Experiment was repeated to record reagent polarogram at pH 8.5 using ammonia buffer. Similar procedure was followed to record polarogram for metal ions. 5 mL (0.01M) respective metal ion solution was used in place of reagent solution. Half wave potential was found to be -0.118V (Vs SCE) at pH 5.0 for Cu(II) (Figure 1) and -1.05V (Vs SCE) at pH 8.5 for Ni(II) (Figure 2). Half wave potential for the reagent DHBHPO was determined for both the pH and found -1.3V (Vs SCE) at pH 5.0 and -2.3V (Vs SCE) at pH 8.5. The titration were carried out by fixing the applied voltage -0.4V (Vs SCE) and -1.5V (Vs SCE) for Cu(II) and Ni(II) respectively.

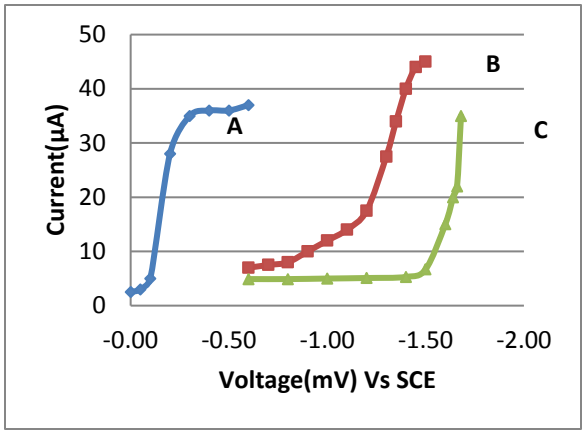

Figure 1: Polarograms of (A) Copper(II); (B) DHBHPO; (C) Supporting electrolyte (pH = 5.0, acetate buffer)

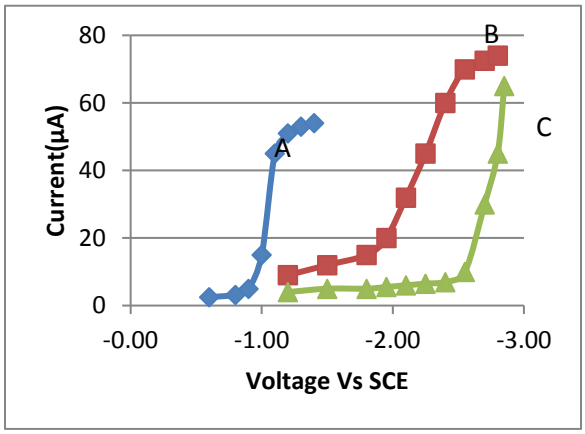

Figure 2: Polarograms of (A) Nickel(II) ; (B) DHBHPO; (C) Supporting electrolyte (pH = 8.5, ammonia buffer)

An aliquot of standard copper(II) solution (0.01 M, 0.6354 mg/mL) was transferred into the titration cell and above contents were added keeping the volume at 50 mL and pH 5.0. The voltage was fixed at -0.4V (Vs SCE) and the solution titrated against standard oxime solution (0.02 M). After the addition of the reagent from micro burette, nitrogen gas was passed into the solution to ensure through mixing and then corresponding current reading were noted. The current readings were corrected for dilution by the titrant was recorded as a function of the volume of the titrant. Dilution correction was made with the help of equation $i_{corr} = i_{obs}$ (V+v)/V, where i_{corr} is the corrected current, i_{obs} is the observed current, V is the volume of the solution taken initially and v is the volume of titrant added. Null point was obtained graphically taking i_{corr} along y-axis Vs volume of titrant added along x-axis. An 'L' shaped curve was obtained. The procedure was repeated with known but different aliquots.

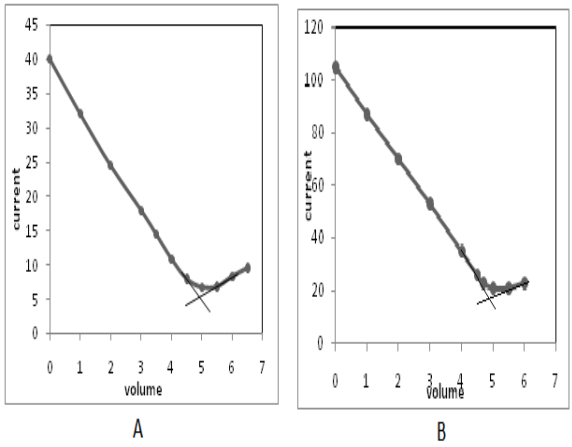

Figure 3: Amperometric titrations of (A) Cu(II) and (B) Ni(II) with DHBHPO

Similarly Nickel(II) solution (0.01M, 0.5869 mg/mL) was titrated at pH 8.5 and applied voltage -1.05V (Vs SCE). Results were calculated for the amount of copper and nickel from the graph (Figure 3: A and B). 1:2 (M:L) ratio found is in agreement with the ratio being established by the gravimetric procedure. The results of the determinations are given in Table 4.

Determination in presence of foreign ions

Study of interference of foreign ions in amperometric determination of copper(II) and nicke(II),was carried out.The interference due to foreign ions such as Iron(III), aluminum(III), arsenic(III), zinc(II), calcium(II) and lead(II) were studied as they are usually associated in ores, slags and alloys. Except Iron(III), the other metals did not interfered into the amperometric determination of copper(II) (3.177 mg copper), when they are present up to 25-30 fold excess. Interference due to Iron(III) was overcome by masking it with sodium fluoride. Iron(III), aluminium(III) and chromium(III) did not affect the current readings in the determination of nickel(II) (1.467 mg nickel), although they were precipitated as hydroxides. Palladium(II), zinc(II) and manganese(II) gave no precipitates with the reagent at 8.5 pH and hence did not interfered even when present 40-50 fold excess.

Trace amount of cobalt(II) (10 ppm) interfered in the determination.

Determination of Cu(II) and Ni(II) in german silver alloy

Copper(II) and nickel(II), have been accurately determined in german silver alloy at respective pH value. Percentage obtained agrees with the reported values within the experimental error.

The standard sample of german silver alloy, weighing 0.2860 gram was dissolved in nitric acid **(**1:1) by heating on sand bath. The excess acid was removed and mass dissolved in doubly distilled water and diluted to 250 mL. A 5 mL aliquot of the stock solution was pipette out into the polarographic cell. To this, ammonium chloride solution (20 mL,0.5 M), 1.5 mL (0.2%) gelatin solution was added and pH adjusted to 5.0 with hydrochloric acid. Addition of ammonium chloride was preferred to an acetate buffer to maintain above pH in order to avoid addition of large amount of ammonium hydroxide required to raise the pH to 8.5 in subsequent nickel(II) determination. The amount of copper(II) was estimated by adopting the general procedure described earlier. The titration was continued until the current readings remained constant-equivalent point for copper obtained. Titration was stopped after addition of only a few increments of the reagent beyond equivalence point. Then the cell voltage was raised to -1.4 V (Vs SCE) and the pH of the solution was raised to 8.5 with ammonia buffer. Titration was continued until the equivalence point for nickel(II) is obtained. Results are shown in Table 5.

Weight of alloy: 0.2860 gm in 250 mL stock solution.

5 mL stock solution contains 5.720 mg german silver

For the set of three determination of German Silver alloy, the average %age found was 50.17% Cu(II) and 24.83% Ni(II). Standard deviation was 0.0125 % and 0.04 % for Cu(II) and Ni(II), respectively.

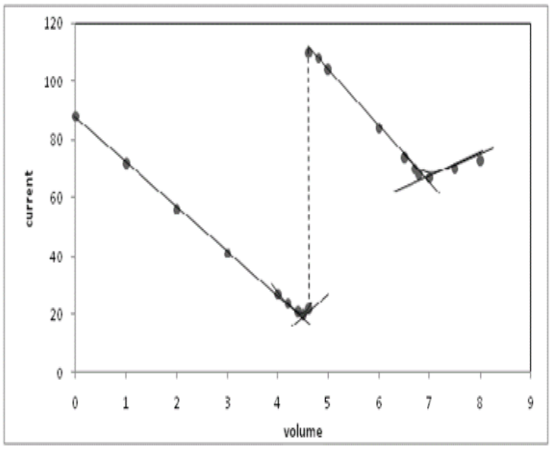

Figure 4: Simultaneous determination of copper(II) and nickel(II) from german silver alloy.

RESULTS AND DISCUSSION

The present amperometric method for simultaneous determination of Cu(II) and Ni(II) from german silver alloy, was found to be accurate and specific. The developed method is rapid and completes a single run in relatively short time.

CONCLUSION

The method enables rapid quantification and simultaneous analysis of both the metal from alloy without any interference of foreign ions. Therefore it can be concluded that the reported method could find practical application as rapid method for simultaneous determination of Cu(II) and Ni(II) ions in alloys and other mixture.

ACKNOWLEDGEMENT

The authors are very thankful to the Head (chemistry department) and Principal, Shree J. P. Arts and Science College, Bharuch for providing facilities to perform the practical work.

REFERENCES

[1] A.werner-Z. Anorg. Chem., **1893,** 3, 270

[2] Desai K.K. & Naik H.B., 2-Hydroxy-4-ethoxypropiophenone oxime as a gravimetric Reagent for Cu(II), Ni(II) & Pd(II), Indian J. Chem., **1986,** 25A, 297.

[3] Patel N. B. & Desai K. K., 2-Hydroxy-5-Nitropropiophenone oxime as an analytical reagent: Studies on Ni(II) and Pd(II) chelates., Asian J. Chem., **2003,**15, 751

[4] Shingadia S. K. & Desai K.K., 2-Hydroxy-5-methylbenzophenone oxime (HMBO) as an

Analytical Reagent for Gravimetric Determination of Cu(II), E.J. Chem., **2007,**4(1), 97
[5] Shingadia S .K. & Desai K.K., 2-Hydroxy-5-methylbenzophenone oxime (HMBO) as an Analytical Reagent for Molybdenum (VI),Oriental J. Chem., **2006,** 22(3), 703
[6] Patel V. M. & Patel N. B., 2,4-Dihydroxy-5-Bromo-α-phenylacetophenone oxime as an analytical Reagent: Studies on Ni(II) chelate, Acta Ciencia Indica, **2008,** Vol. XXXIV C, No. 3, 427.
[7] Patel N.B. and Parekh N. H., Spectroscopic determination of Co(II) with 2,4-Dihydroxy-5-Bromo[2'methyl] Propiophenone oxime ,International Journal of Chem Tech Research., **2013,** 5(2),307-311
[8] Shah Pratesh J, Patel N.B., 2, 4-Dihydroxy-5-Bromo Hexaphenone Oxime (DHBHPO) as a Gravimetric and Spectrophotometric Reagent: Studies on Mo (VI) chelate and its application, J.Applicable. Chem, 2017, 6(4):620-627.
[9] Ninan S., Varadarajan A., Jadhav, S. B. Kulkarni, A. J. & Malve S.P., Camphor-3-thioxo-2-oxime as analytical reagent for extractive spectrophotometric determination and separation of lead., Spectrochimica Acta, Part A, **1999,** 55, 825
[10] K.Wierma Lawrance F.Cott eter, Glyoximes a reagent for the gravimetric determination of bismuth, Analytical Chemica Acta,968,40,291.
[11] D.Venkatraman Reddy, A.Varada Reddy, Amperometric determination of Bismuth using Galacetophenone Phynylhydrzone , E-Journal of Chemistry, **2010,**7(4),1290-1295.
[12] S.N.Poddar and K.Ray, J.Ind.Chem.Soc., **1969**, 46,296.
[13] S.N.Poddar and K.Ray,Indian J.Appl.Chem.,**1970**,33,225.
[14] B O Gupta, and U.W.Malik, Mikrochim Acta., **1969**, 3,634.
[15] Hussain R.C, 2-Hydroxy -1-acetophenone oxime as titrimetric reagent (Ph.D.Thesis) S.V.University, Tirupati, **1978**.
[16] H.Nogami, J.Pharm Soc., Japan, **1945**,61, 46.

Table-1: Elemental Analysis of the reagent

Reagent	% Found (Calculated)		
	Carbon	Hydrogen	Nitrogen
DHBHPO	47.73 % (47.68%)	5.25 % (5.30%)	4.52 % (4.63%)

Table-2: ^{1}H-NMR

Reagent	**Alkyl group**	**Phenolic(-OH)**	**Oximino(-OH)**	**Aromatic Proton**
DHBHPO	1.6475-0.800 ppm (multiplate)	12.9469 ppm (singlet)	6.0504 ppm (singlet)	7.9667-7.1911 ppm (multiplate)

Table-3: ^{13}C-NMR

Assignment	**C1**	**C2**	**C3**	**C4**	**C5**	**C6**	**C7**	**C8**	**C9**	**C10**	**C11**	**C12**
Chemical shift(δ) in ppm	112.83	150.96	98.60	155.61	99.71	129.65	161.80	31.80	26.37	24.67	22.36	13.94

Table-4: Amperometric determination of copper(II) and nickel(II) with DHBHPO

Metal Ion	Taken (mg)	Found (mg)	Difference (mg)	Error (%)
Copper	3.177	3.165	- 0.012	- 0.38
	4.759	4.779	0.02	0.42
	6.354	6.367	0.013	0.21
Nickel	1.467	1.456	-0.012	-0.82
	2.935	2.917	-0.018	-0.61
	4.402	4.419	0.017	0.39

Table- 5: Simultaneous determination of Copper (II) and Nickel(II) in German Silver.

METAL	FOUND mg	% FOUND	% REPORTED	% ERROR
Copper	2.87	50.17	50.06	0.22
Nickel	1.42	24.83	25.0	-0.68

PRAJÑĀ - **Journal of Pure and Applied Sciences Vol. 24 – 25 : 153 – 158 (2017)**
ISSN 0975 - 2595

PROXIMATE AND PHYTO-CHEMICAL ANALYSIS OF DEHYDRATED FOUR DIFFERENT VARIETIES OF CAPSICUM (*Capsicum annuam L.*)

SURABHI MANDLOI AND BIJAL AMIN*

[1,2]Smt. Kamlaben P. Patel College of Home Science,Laboratory of Food Biotechnology,
Anand People's Medicare Society,Near Sardar Baug, S. P. University, Anand, Gujarat – 388001
Email: bijalpatel85@gmail.com

ABSTRACT

Bell pepper, also known as sweet pepper or a pepper and capsicum, is a cultivar group of the species Capsicum annuum. Cultivars of the plant produce fruits in different colors, including red, yellow, orange, green, chocolate/brown, vanilla/white, and purple. Bell peppers are sometimes grouped with less pungent pepper varieties as "sweet peppers". Bell peppers are sensitive to an abundance of moisture and excessive temperatures. Bell peppers can be dehydrated and stored in order to increase their availability. The main aim of this research is to determine the proximate principles and phytochemical properties of dried bell pepper samples, in samples of bell pepper with four different colours. Green capsicum was found to be rich with total phenol; Red capsicum was rich with ascorbic acid and β-Carotene. Yellow capsicum was rich with fat and phosphorous and also showed higher amounts of moisture. Purple capsicum was rich with flavonoid, calcium and protein content. Thus, capsicum, though not given any special importance in the diet, is a nutritive fruit and one should consume it in order to gain essential nutrients.

Key words:- Proximate, Phytochemical analysis, β-Carotene, Capsicum annuum L.

INTRODUCTION

Bell peppers (*Capsicum annuum L.*) are part of the Solanaceae family and have been cultivated for thousands of years, beginning in South and Central America before being brought back to Europe from North America by Christopher Columbus. They are grown throughout the world, but mainly in China, Mexico, and in the United States. While green, red, and yellow bell peppers are the most common ones. Other varieties such as orange, purple, brown, and black are also grown.

In the *Capsicum annuum L.* species there are many different varieties from the wild chili to the sweet consumer types. Among all the cultivars the spice paprika and the sweet fresh consumer varieties gained distinguished importance. Cultivars of the fresh consumer pepper produce are cultivated in different colors, size and shape. The produce of the pepper plant is a puffed berry which is hollow inside. The shape of the fruit can be round, flattened round, puffed prism, peaked, and crumpled inside or long thin. The color of the pepper fruit also can vary greatly: green, yellow, red, orange, purple, white and the pale or transition of the previously mentioned colors. The size of the produce varies from 1 cm to 25 cm. Bell peppers have a delightful, slightly watery crunch. Green and purple peppers have a slightly bitter flavour, while the red, orange and yellow are sweeter and almost fruity.

Capsicum was introduced in to India by the Portuguese during the 16th century. India has emerged today as the foremost producer and exporter of capsicum contributing to almost one fourth of the world production. Different species are cultivated in several countries of the world [1]. India is the largest producer of capsicum in the world contributing 25 % of the total world production. Beside India other producers and exporters of capsicums are China, Pakistan, Morocco, Mexico and Turkey. Indian chillies are exported mainly to Sri Lanka, USA, Canada, UK, Saudi Arabia, Singapore, Malaysia, Nepal, Mexico and Germany.

Export and local market both demand high quality sorted fruits and vegetables, which long preserves its fresh condition in the market. Additionally, there is an increased demand for fruits and vegetables that are beneficial for a healthy

life style as well as rich in ingredients that positively influence the prevention of any health malfunction.

Capsicum is an important aspect of the diet and is widely consumed in almost every part of Nigeria. They are also frequently used both chopped and raw in salads, or cooked in stir-fries or other mixed dishes. They can be sliced into strips and fried, roasted whole or in pieces, or chopped and incorporated into salsas or other sauces [2].

Dried foods are more concentrated than fresh foods with low moisture contents and can be stored at ambient temperatures for longer periods. Due to a considerable decrease in the water activity of the material, dried foods have reduced microbiological activity with minimized physical and chemical changes [3,4]. Peppers, similar to other vegetables, are perishable resulting in high losses due to storage problems and marketing. An alternative to the consumption of fresh vegetables is their dried form, which allows their use during the off-season. However, food products are sensitive to drying temperatures and methods that can induce degradation (e.g., oxidation, loss of color, shrinkage or loss of texture) and change the nutritional and functional properties of the products [5].

Capsicum can be preserved by drying, pickling or freezing. Dried peppers may be reconstituted whole, or processed into flakes, or powders. Pickled or marinated peppers are frequently added to sandwich or salads. Frozen peppers are used in stews, soups and salads. Extracts can be made and incorporated into hot sauces. It is widely enjoyed and is essential for African and Ivorian dishes [6] .

Capsicum has many primary and secondary uses, it protects against arthritis, appetite, asthma, bleeding, blood pressure (high/low), chills circulatory disorders, colds, depression, diabetes, heart problems, kidney problems, lung disorder, nausea, ulcers, wound bleeding, blood impurities, jaundice, skin disorder, burns , fever etc. All the four colored peppers exhibit significant abilities in preventing the oxidation of cholesterol or docosahexaenoic acid (DHA).

Capsicum is known to be a medicinal plant [7]. It is a powerful local stimulant, with no narcotic effect, largely used in hot climate as a condiment and most useful in atony of the intestine and stomach. It is antiseptic and therefore a most valuable agent as a gargle in ordinary sore throat or in diphtheria. The antiseptic properties in capsicum makes it effective in fighting food poisoning, couple with good supply of probiotics, yeasts and fungal infection problems like ring worm, shingle, athletes foot etc can be easily eliminated. It is also used as an antibacterial, antifungal, anti-aging and antioxidant agent.

The present investigation was undertaken to analyze the proximate nutrient and phytochemical content in four varieties of dried powder of sweet pepper (*Capsicum annuum L*) .

MATERIALS AND METHODS

Samples of four different colored (Red, Green, Yellow and Purple) sweet peppers *C.annuum* variety were obtained from the local market of Anand, Gujarat, India. The fruit samples were thoroughly washed,sliced with stainless kitchen knife, dried in moisture extraction oven at 65^0 C for about 48 hrs and milled. The dried pepper powders were packed in airtight glass containers and stored at 25 ± 1^0 C in the dark. Twenty grams (20g) of the flour of each variety was weighed, homogenized with 100 ml distilled water and centrifuged. The supernatant was used for determination of total phenol and flavonoid content.

Biochemical and Phytochemical analysis

Moisture, protein and ash content of the dry pepper flour were determined according to AOAC [8]. Calcium was determined by the method of Clark and Collip [9]. Phosphorus was estimated by the method of Fiske and Subbarao [10]. Vitamin-C was estimated by the method of Sadashivam S et al., [11]. β- Carotene estimation was done by the method of Plummer [12]. Total phenol estimation was carried out by the method of Malik and

Singh [13]. Flavonoid was estimated by the method of Lamalson and Carnet [14].

Statistical analysis

All the assays were carried out in triplicate. The results are expressed as mean values and standard error (SE) of the mean. The differences were analyzed using one-way analysis of variance (ANOVA) followed by Duncan tests. For all analyses, p-values <0.05 were considered statistically significant. Data was analyzed using SPSS version 16 program.

RESULTS AND DISCUSSION

Mean value of moisture content was found to be 10.00 gm% in yellow capsicum, which was the highest. Moisture content in green, red and purple capsicum were 4.00 gm%, 8.00 gm% and 7.33 gm%, respectively **(Fig:1)**, which showed no significant differences between the four varities of capsicum in moisture content. Fat content was 2.27 gm% in yellow capsicum which was the highest. Fat content in green, red and purple capsicum were 0.43, 0.47 and 0.93 respectively **(Fig:1)**. Green and red samples showed no significant differences where as yellow and purple showed highly significant differences ($p \leq 0.01$).

Protein content was 2.54 gm% in purple capsicum which was the highest. Protein content in green, red and yellow capsicum was found to be 1.74, 1.77 and 1.49gm% respectively **(Fig:1)**. No significant difference was seen between green and red capsicum, where as yellow and purple capsicum were found to be significantly different ($p \leq 0.01$). Ash content was found to be 10.00 gm% in red capsicum, which was the highest. Yellow and green capsicum showed an ash content of 6.00 gm% and 5.00 gm% respectively which was less than for red capsicum. Purple capsicum gave the least ash content of 2.00 gm % **(Fig:1)**. Red capsicum was highly significant ($p \leq 0.01$) when compared to the other three varieties of capsicum, whereas green, yellow and purple capsicum did not show any significant differences. Ash content of pepper is known to contain significant quantities of P, Ca and K salts that are valuable to humans [15].

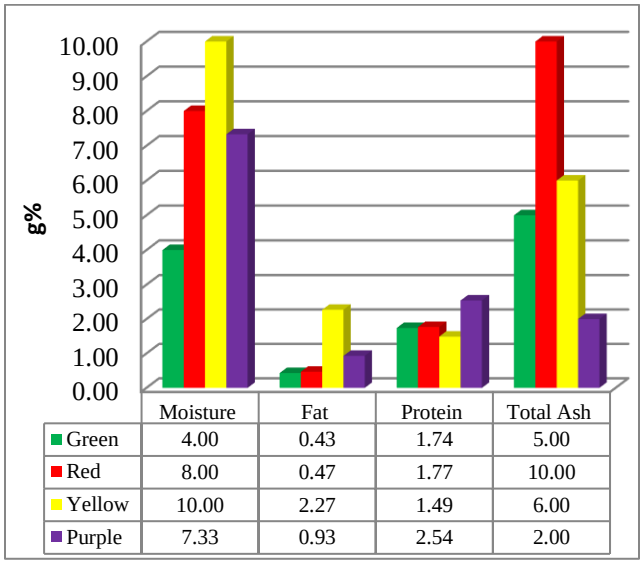

	Moisture	Fat	Protein	Total Ash
Green	4.00	0.43	1.74	5.00
Red	8.00	0.47	1.77	10.00
Yellow	10.00	2.27	1.49	6.00
Purple	7.33	0.93	2.54	2.00

Fig:1 Moisture, fat, protein, and total ash content from different varieties of dehydrated capsicum.

Mean value of calcium content was 44.41 mg% in purple capsicum, which was higher than the other three varieties of capsicum. Red and yellow capsicum showed calcium content of 25.11 mg% and 29.25 mg% respectively, which was less than purple capsicum. Green capsicum gave the least calcium content of 24.26 mg% **(Fig:2)**. Thus, purple capsicum showed a higher significant difference ($p \leq 0.01$) than green, red and yellow capsicum. There was no significant difference observed between green, red and yellow capsicum. Calcium is a major mineral used in the mineralization of bones and shells,. Its main function is in muscle contraction and it can bind to several different calcium modulated proteins. Calcium is known to stabilize cell membrane and thus may prevent physiological disorders attributed to calcium deficiency [16].

Mean value of phosphorus content was 21.67 mg% in yellow capsicum which was higher than the others. Green and red capsicum showed phosphorus content of

20.83 mg% and 18.33 mg% respectively, which was less than yellow capsicum. Purple capsicum had the least phosphorus content of 5.00 mg% **(Fig:2)**. Phosphorus content of purple capsicum showed a higher significant difference ($p \leq 0.01$), where green, red and yellow capsicum showed no significant differences.

Phosphorus is the main ingredient for the structural formation of bones by combining with calcium and forms calcium phosphate. Phospholipids are the main structural components of all cellular membranes. Nearly every cellular process that uses energy obtains it in the forms of ATP. ATP is also important for phosphorylation, a key regulatory event in cells.

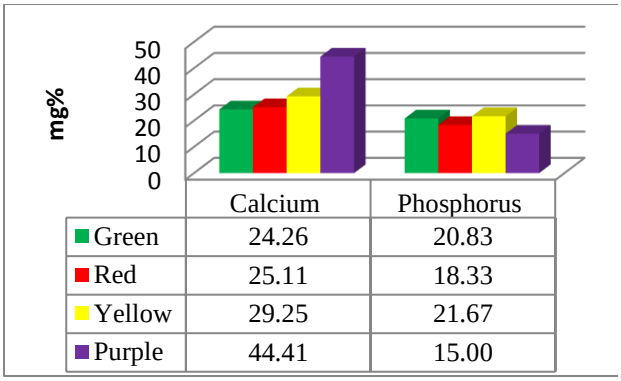

	Calcium	Phosphorus
Green	24.26	20.83
Red	25.11	18.33
Yellow	29.25	21.67
Purple	44.41	15.00

Fig:2 Calcium and phosphorus content from four different varieties of dehydrated capsicum.

Ascorbic acid (vitamin-C) content was 169.67 mg% in red capsicum, which was the highest. Yellow capsicum showed an ascorbic acid content of 143 mg% which was less than red capsicum. Green capsicum revealed 76.33 mg% ascorbic acid content which was less than yellow capsicum. Purple capsicum gave the least ascorbic acid content of 4.00 mg%. **(Fig:3)**, which showed a highly significant difference ($p \leq 0.01$) between all the four varieties of capsicum in ascorbic acid content.

The levels of vitamin C are very variable and may be affected by maturity, genotype and processing. This vitamin acts as a protector of pigments preserving them from chemical and biochemical oxidation [17]. Vitamin-C is hypothesized to prevent cancer by inhibiting the formation of N-nitroso compounds in the stomach and also by stimulating the immune system [2].

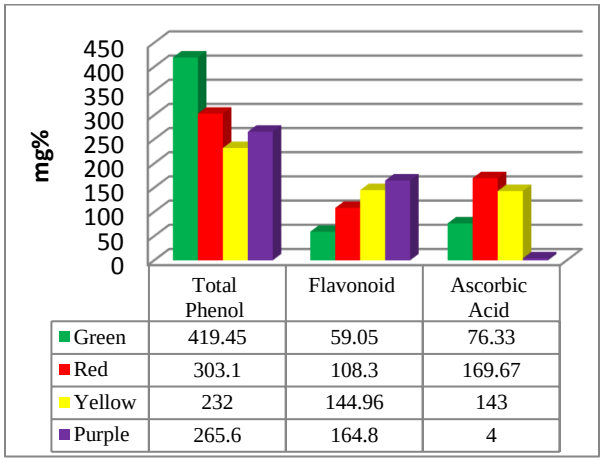

	Total Phenol	Flavonoid	Ascorbic Acid
Green	419.45	59.05	76.33
Red	303.1	108.3	169.67
Yellow	232	144.96	143
Purple	265.6	164.8	4

Fig: 3 Total phenol, flavonoids, ascorbic acid content from four different varieties of dehydrated capsicum

β-carotene content was 4320.10 µg% in red capsicum, which was the highest. Yellow capsicum showed a β-carotene content of 2172.31 µg% which was less than red capsicum. Green capsicum revealed 412.44 µg% β-carotene content which was less than red and yellow capsicum. Purple capsicum gave the least β-carotene content of 412.44 µg% **(Fig:4)**. Thus red capsicum showed a highly significant difference ($p \leq 0.01$) from the other three varieteies of capsicum. Green and purple capsicum showed no significant differences between each other.

The color of mature pepper fruit is determined by the composition of carotenoids. The fruit colour of red pepper is genetically determined by three loci, y, c_1, and c_2. [18]. β-carotene (Vitamin A) is an all important anti-oxidant and part of today's healthy lifestyle. [2].

Phenolic content was highest in green capsicum which was found to be 419.45 mg%. Red capsicum showed a total phenol content of 303.10 mg% which was less than green capsicum. Purple capsicum revealed 265.60 mg% phenol content.

Yellow capsicum gave the least phenol content of 232.00 mg% **(Fig:4)**. There was a highly significant difference ($p \leq 0.01$) between all the four varieties of capsicum. Phenolic compound rich foods contain antioxidant activity which plays a vital role in the human body system. Phytochemicals, including phenolics and flavonoids are suggested to be major bioactive compounds contributing to the health benefits of fruits and vegetables. [19].

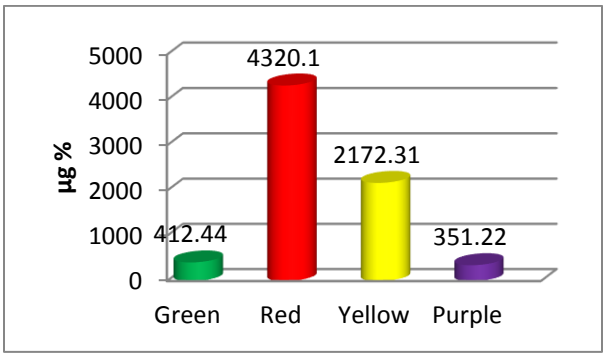

Fig: 4 β-carotene content from four different varieties of dehydrated capsicum.

Flavonoid content was highest in purple capsicum (164.80 mg%). Red and yellow capsicum showed flavonoid contents of 108.30 mg% and 144.96 mg% respectively. Green capsicum gave the least flavonoid content of 59.05 mg% **(Fig:4)**. There was a highly significant difference ($p \leq 0.01$) between all the four capsicum types. Flavonoids refer to a class of secondary metabolites . They are most commonly known for their antioxidant activity. However it is also known that they reduce the risk for the development of chronic diseases, such as cardiovascular disease and cancer [19].

CONCLUSION

According to the above analysis the moisture and fat contents were high in yellow capsicum as compared to the other three varieties of capsicum. Moisture content in purple capsicum was slightly lower than red capsicum and the fat content in green capsicum was slightly lower than red capsicum. Protein content was found to be fairly good in all four varieties of capsicum, but purple capsicum showed the highest amount of protein. Ash content was high in red capsicum as compared to the other three varieties, ash content in the green was slightly lower than in yellow capsicum. Phosphorus content was found to be fairly good in all four varieties of capsicum, but yellow capsicum showed the highest amount of phosphorus. Purple capsicum was found to be high in calcium content as compared to the other three varieties of capsicum. Ascorbic acid and β-carotene content was found to be higher in red capsicum as compared to the other three varieties of capsicum. Purple capsicum was found to be low in ascorbic acid and β-carotene content. Total phenol content in green capsicum was found to be high as compared to the other three varieties of capsicum, while yellow capsicum was found to be slightly lower than purple capsicum in phenol content. Purple capsicum was found to be higher in flavonoid content as compared to the other three varieties of capsicum. Purple capsicum showed higher levels of protein, calcium and flavanoid contents while red capsicum was richer in ash, ascorbic acid and β-carotene. Green capsicum was higher in total phenol content. Thus consumption of all the four varieties can enable many health benefits to control various diseases condition such as asthma, blood pressure, diabetes, heart problems, kidney problems, blood clotting, cancer, high blood cholesterol etc.

REFERENCES

[1] Maiti,R.K., (2007). Research advances in capsicum-pepper (Capsicum annum L.) and other species.Agrohouse, pp-243.

[2] Famurewa, J.A.V., Olvwamukomi,M.O., and Adenuga, A.L., (2006). Dehydration of osmosised Red Bell pepper (Capsicum annum L.).Journal of Food Technology,4(4); pp249-252.

[3] Araujo, E.A.F., Ribeiro, S.C.A., Azoubel, P.M., Murr, F.E.X., (2004). Drying kinetics of nectarine (Prunus persica) with and without shrinkage. In: Proceedings of the

14th International Drying Symposium, Sẵo Paulo, Brazil, C: pp. 2189-2194.

[4] Vega-Gálvez ,A., Uribe, E., Lemus-Mondaca, R., Miranda,M., (2007). Hot- air-drying characteristics of Aloe vera (Aloe barbadensis Miller) and influence of temperature on kinetic parameters. LWT– Food Sci. Tech., 40: 1698–1707.

[5] Attanasio, G., Cianquanta, L., Matteo, M.D., (2004). Effect of drying temperature on physico- chemical properties of dried and rehydrated chestnuts (Castanea sativa). Food Chem., 88: 583–590.

[6] Teirrible, J. N (1983). Plantes Alimentaires et Legumes locaux de cote d'Ivoire. L'elevation de la temperature affects la survice et la croissace des microorganisms selon leur nature. Food science nutrition, 28:1-30.

[7] Chenu, J and A. Ake, (1987). Plantes medicinales Tropicales et Ivoiriennes. Tome V. Edition Dareni Edition. Cote d'Ivoire, pp:166.

[8] AOAC (Association of Official Analytical Chemists). (1998). *Official Methods of Analysis* (16th edn, N°1-2). Association of Official Analytical Chemists: Washington D.C.

[9] Clark, F. P. and Collip, J. B. (1925), Determination of calcium by titrimetric method. *Journal Biol. Chem.*, 63: 461-464.

[10] Fiske C. H. and Subbrow Y. (1925), Colorimetric determination of phosphorus, *Journal Biol. Chem.*, 66:

[11] Sadasivam, S. and Manickam, A. (1997) Vitamins. In: Biochemical methods, Eds. Sadasivam, S. and Manickam, A. New Age International (P) Limited, New Delhi, 2nd Edition, 185-186.

[12] Plummer D.T. (1971). An introduction of practical Biochemistry, Tata McGraw-Hill, New Delhi.pp-228.

[13] Malik E.P., Singh M.B.(1980) "Plant Enzymology and Hittoenzymology" (1st Edn). Kalyani Publishers: New Delhi;pp-286.

[14] Lamaison, J.L.C. and A. Carnet. (1990). Teneurs en principaux flavonoids des fleurs de Crataegeus monogyna Jacq et de Crataegeus laevigata (Poiret D. C) function de la vegetation. Pharm. Acta. Helv. 65: 315-320.

[15] Bakker,N.P., Ul'chenko,N.T., and Glushenkona,A.I., (2001). Physiochemical Properties and Composition of Lipids Capsicum annuum seeds. Chemical of Natural compounds. Vol . 37.,pp-131-133.

[16] Max C. Saure. (2005). Calcium translocation to freshy fruit;its mechanism and endogenous control.Science Horticulture Vol-105,65-89.

[17] Hallmann. E., and Rembiakowska.E., (2008). The content of selected antioxidant compounds in bell pepper varieties from organic and conventional cultivation before and after freezing process. 16th IFOAM Organic World congress, Modena, Italy, June 16-20.

[18] J. Huh, B. C. Kang, S. Kim, B. D. Kim (2001). A candidate gene approach Identified phytoene synthase as the locus for mature fruit color in red pepper (capsicum spp.) TAG Theoretical and Applied Genetics. Volume 102, pp- 524-530.

[19] Shela, Gorinstein, Yonge-Seo Park, Jacek Namiesnik (2009). A comparative study of phenolic compounds and antioxidant and antiproliferative activities in frequently consumed raw vegetable .Food Res Technology ,228:903-911.

PRAJÑĀ - **Journal of Pure and Applied Sciences Vol. 24 – 25 : 159 – 163 (2017)**
ISSN 0975 - 2595

POSTURES ADOPTED AND PERCEPTION OF MUSCULOSKELETAL PAIN OF WORKERS AT JEWELLERY MAKING WORKSHOPS IN GUJARAT

PILOJPARA C AND DALAL P*

[1,2]Family Resource Management, P.G.Department of Home Science, Sardar Patel University,
Vallabh Vidyanagar, Gujarat. Email : paulomidalal@gmail.com

ABSTRACT

Background: Workers engaged in jewellery manufacturing are exposed to various occupational risk factors that lead to the development of musculoskeletal disorders. Objectives: *To study the postures adopted by workers engaged in jewellery making activity. *To assess the musculoskeletal disorders of respondents engaged in jewellery making activity. Methodology: Field survey was conducted on 80 respondents selected purposively from Rajkot (40) and Ahmedabad city (40). Results: Data revealed that respondents spend 10 - 12 hours per day in jewellery making activity and in poor posture. Majority of respondents revealed the symptoms of pain at neck, shoulder, arm, back and knee. Conclusion: The tasks carried out were in awkward postures for long durations with repetitive and forceful motions which led to the development of musculoskeletal pain among these workers.

Keywords: Jewellery making, Working Posture, RULA, Musculoskeletal Disorders.

INTRODUCTION

Jewellery making is one of the world's oldest manufacturing operations and has always involved some hazardous processes **[1].** Jewellery manufacturing activities involves precision design, setting the tiny metals and stones which require high visual attention and mental concentration and are often near - point task **[2].**

Preventing workers from occupational diseases, creating a healthy and reliable work environment are one of the most important issues in these days. If the working conditions are accustomed properly for the physical and mental working of someone, physical working is going to support the health and raise the performance. Otherwise, occupational diseases will appear and the performance of the employee is going to decrease **[3].** As mentioned above, jewellery manufacturing activity involves various precision designs such as setting the metal as well as the stones, polishing and filing. At every stage of manufacturing, checking the quality of the product is very important. As any rework increases the labor cost and material cost, workers need to pay high attention towards the quality of the product **[1].**

Jewellery making process is sedentary in nature and requires prolonged sitting occupying the same posture. There are various studies available, which report that risk factors are present for developing the MSDs, (Musculoskeletal Disorders) at the workplace of jewellery manufacturing **[4].**

The present study focuses on the problem of jewellery makers 'occupational health hazards'.

The purpose of the present study is to find out the health related issues among jewellery makers during work, with special reference to musculoskeletal disorders. The findings of the study will provide: Data for researchers and jewelers' for formulating future strategies improve posture and prevent musculoskeletal disorders of the workers engaged in the organized and unorganized sectors of jewellery making. 2. The study can provide useful data for manufacturers of equipment to design ergonomically sound tools for jewellery making workers to reduce their postural load and repetitive movements.

OBJECTIVES

*To study the postures adopted by workers engaged in jewellery making activity.

*To assess the musculoskeletal disorders of respondents engaged in jewellery - making activity.

METHODOLOGY

The research methodology adopted for conducting the present study was based on ergonomic problems during jewellery making.

The present study was conducted in one phase i.e. field survey. For the field survey, a sample consisting of 80 workers of Gujarat state engaged in jewellery making activity were

randomly selected from the cities of Rajkot (40) and Ahmedabad (40). Respondents who perform these activities almost daily were selected purposively.

Data was collected through interview schedule cum observation method. The background information and specific information about the activity was sought from the respondents by personal interview method. The postures adopted by them were noted down by observation method.

Background information covered the socio-demographic characteristics of the selected respondents (age, educational qualification, working time, break time and work experience at the current job). Specific information included their job profile and postures adopted while performing jewellery making activity and musculoskeletal problems faced by them.

A low cost tool was used to examine musculoskeletal disorders among the respondents. This was Rapid Upper Limb Assessment (RULA) developed by McAtamney and Corlett (2004) which focuses mainly on upper limb disorders and Body Mapping technique (perceived exertion). For RULA only 40 subjects could be included in the study based on willingness and time constraints.

According to the symptoms and type of pain, relevant musculoskeletal disorders were identified. Responses of the subjects were noted on a record sheet which contained the symptoms of musculoskeletal disorders associated with this activity using personal interview method and perceived exertion (P.E.) chart.

Mean scores were calculated. Frequencies and percentages were also calculated for analysis of data regarding musculoskeletal disorders.

RESULTS AND DISCUSSION

Age: Age is a very important variable in an occupational study as it affects the working capacity of an individual. Out of the total workers selected for the present study, maximum number of the respondents i.e. **53%** belonged to the age group of 18-32 years while **40%** belonged to the age group of 33-47 years. These results show that the people who are occupied with this job were the young population. **Education:** When we look at the educational background of the workers, 45**%** of them had studied up to higher education and **26%** up to primary school and their equivalents. This situation shows that the great majority of the workers had moved towards this occupation after higher education. **Work and Break Duration:** Data also shows the working hours the workers engaged in jewellery making. Fifty nine per cent **(59 %)** of the workers worked more than 11hour, forty one per cent **(41%)** of them worked for upto 10 hours. Maximum **93%** of break duration taken by the workers was of three hours whereas seven **(07%)** per cent of the workers took a break of less than or equal to two hours.

Table-1: Socio – personal profile of the selected respondents (N = 80)

Personal details	Group	Number	Percentage (%)
Age (years)	18-32	42	53
	33-47	32	40
	48 & above	06	07
	Total	**80**	**100**
Average age ≥ 32.78			
Education	Primary	21	26
	Secondary	07	09
	Higher Secondary	36	45
	Graduation	13	17
Total		**80**	**100**
Working time (in hrs.)	5-10	33	41
	11 & above	47	59
Total		**80**	**100**
Break time (in hrs.)	1-2	74	93
	2 & Above	06	07
Total		**80**	**100**

Table-2: Work experience of the respondents (N=80)

Years	Number	Percentage (%)
2 - 5 years	18	23
6 - 10 years	9	11
11 - 15 years	22	27
16 - 20 years	13	16
21 - 25 years	8	10
Above 25 years	10	13
Total	80	100

Table 2 gives the work experience of the respondents. When the respondents were asked about their experiences in performing the activity **27%** of them reported that they had been performing this activity since 11 to 15 years, sixteen **(16%)** per cent had more than fifteen years of experience and only **13%** of them had more than 25 years of experience in performing the activities of jewellery making.

(N=80)

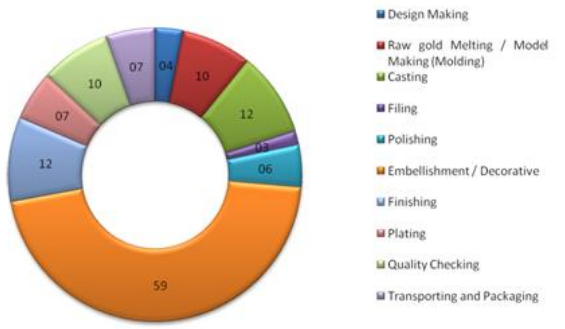

Note: Multiple responses.

Figure-1 Gold Jewellery Making Respondents (Job profile)

Plate-1 Working postures adopted by the jewellery makers at work (n=40)

Figure 1 shows that maximum (**59%)** of the respondents were engaged in 'Embellishment/Decorative' Gold jewellery. Twelve per cent **(12%)** and ten per cent **(10%)** of the respondents were engaged in 'Casting' & 'Finishing' and 'Raw gold melting' / 'Model Making (Molding)' respectively. In 'Quality Checking' activity ten per cent **(10%)** of the respondents were involved. Only three per cent **(03%)** of the respondents were engaged in for 'Filing' in Gold jewellery making.

Table-3: Assignment of RULA scores according to position of body part

RULA Score	Action	Number of respondents	Percentage (%)
1-2 =	Acceptable posture	00	00
3-4 =	Further investigation, change may be needed	33	82
5-6 =	Further investigation, change soon	06	15
7+	Investigate and implement change	01	03
Total		40	100

Percentage of workers under RULA level

Photographs of selected workers performing their work at the jewellery making workshop is shown in Plate 1. Critical analysis of the photographs was carried out and RULA score was calculated. The results of the posture analysis using RULA are shown in Table 3. About 82 % of the workers are at low risk level and change may be needed whereas 15% workers were found at medium risk a level which needs to be investigated further and changed soon. Around three percent (03%) of the workers were working investigate and implement change area.

These results reveal that all categories of the risk levels exist in the job postures of jewellery making workers. Further investigation with an immediate change was recommended to most of these workers. The table also shows that none of the workers were in the negligible risk level i.e. acceptable posture.

Details of the working position adopted by the respondents while performing activities related to jewellery making can be observed from Table 4.

Table-4: Type of working position during sitting and standing at work.

Position	Number	Percentage (%)
	Sitting	**(N=80)**
I. With proper backrest *(Blue print designing, CAD designing, Wax designing, Diamond assortment, Quality checking, Entry in stock, Packaging, Embellishment / decorative)*	75	94
Without proper backrest	05	06
II. Without proper backrest *(Master casting model, Rubber Diamond assortment, Wax setting ,Casting, Polishing, Plating, Filling, Embellishment / decorative, Finishing)*	76	95
With proper backrest	04	05
III. On stool *(Polishing, Plating)*	19	24
IV. On table *(Finishing)*	09	11
V. On mattress *(Diamond assortment , Embellishment / decorative)*	71	89
VI. Any other *(Blue print designing, CAD designing, design making)*	06	07
Standing (n = 25)		
VII. One leg supporting *(Casting)*	01	04
VIII. Even standing *(Casting, Finishing)*	21	84
IX. Uneven standing *(Casting)*	03	12

Note: Multiple Responses, Multiple tasks.

About **94%** of the sitting respondents position during these activities were 'with proper backrest', whereas **95%** also sat 'without proper backrest' based on the activity performed. Singh (2007) reported that a formal sitting position is undesirable to hold for a very long period because it increases the load on musculature supporting the head and it produces muscular pain in the neck and small portion of the back. The table also depicts that **89%** of the respondents' sit on 'mattresses' provided by the employers. Twenty four per cent and eleven per cent sat on 'stool' and 'table' respectively. Only seven per cent **(07%)** of them used a 'chair' for their work activity.

Amongst the workers who performed the activity of jewellery making in standing position, it was found that 84% of the respondents used the 'even standing' position which is a balanced position whereas 12 per cent of them carried out the task in 'uneven standing' position. According to Saha (1990) poor or faulty body position may lead to permanent body damage besides increasing the cost of work. **(N=80)**

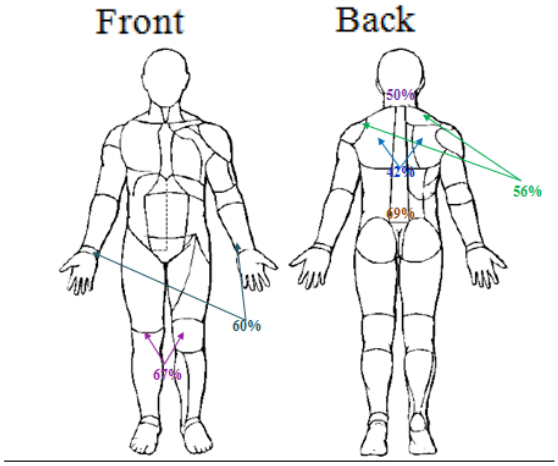

Figure 2 Survey locations of Musculoskeletal Disorder symptoms (Perceived Exertion)

Note: Multiple responses.

Figure 2 shows the location of musculoskeletal disorder symptoms as felt by the workers. Regarding the musculoskeletal disorders perceived by jewellery makers in different body parts, maximum pain was found to be **69% as** low back pain while **42%** respondents' complained about upper back pain. Fifty six per cent **(56%)** and fifty per cent **(50%)** indicated pain in the Neck and Shoulder, respectively. Sixty seven per cent **(67%)** and **60%** respondents' complained about Knee pain and arm pain, respectively. It can be seen that low back pain, knee and arm pain were reported by a high percentage of workers.

CONCLUSION

Evaluation of body posture was carried out in jewelry making workshops by RULA and Perceived exertion tools. Very low percentage of workers was under high risk of musculoskeletal disorders as determined from RULA risk level.

Workers engaged in jewellery making activity need to adopt awkward postures due to long

durations of their work. They perform the activity with repetitive and forceful motions. Prolonged sitting at different body positions was also noted by the investigators. This led to the development of musculoskeletal pains among these workers. In contrast RULA score did not indicate poor posture in majority of the workers. These pains, if ignored at an early stage can lead to musculoskeletal disorders later on.

The present of musculoskeletal pain indicates that there is a need for ergonomic intervention among the jewellery - making workers.

REFERENCES

[1]Jewellery Manufacturing Pollution Prevention Recommendations (2002), Retrieved from Fact Sheet *Website:* https://www.dtsc.ca.gov/HazardousWaste/Jewelry/upload/HWM_FS_Jewelry_P2_Recommendations.pdf

[2]De, A., Dhara U., Virkara T., Altekara C., Mishraa W., Parmara V., Mutakekara M., Iqbala R., and Chandrab A. M., (2012), "A study of subjective visual disturbances in jewellery manufacturing", National Institute of Industrial Engineering (NITIE), Mumbai, Department of Physiology, University of Calcutta, Kolkata. Retrieved from *Website:* https://pdfs.semanticscholar.org/20c0/721d2c1a05544d5a1fa884c073e578547750.pdf

[3] GÜZEL D., (2013), "An investigation of working conditions, occupational diseases and ergonomics in Jet (OLTU) stone dressing Erzurum", Institute of Interdisciplinary Business Research 413 5(5) Retrieved from *Website:* http://journal-archieves35.webs.com/413-421.pdf

[4]Salve U. (2015), "Prevalence of Musculoskeletal Disorder among the workers arranged in jewellery manufacturing", Indian Journal of Occupational environment and Medicine, 19(1):44-55, Retrieved from *Website:* https://www.ncbi.nlm.nih.gov/pmc/articles/PMC4446938/

[5] Mc Atamney, L. & Corlett, E.N. (2004) Rapid Upper Limb Assessment (RULA) In Stanton, N.et al. (eds.) Handbook of human Factors and Ergonomics Methods, pp.7

[6] Saha P N (1978) Aerobic capacity of steel workers in India. Ergonomics 21(12):1021-25 Cited from. Gupta, R., (2012), "Musculoskeletal Disorders among female workers engaged in papad rolling activity", Asian Journal of Home Science 2012 7(2): 275-281 Retrived from website: http://krishikosh.egranth.ac.in/bitstream/1/58100 16103/1/PAU-Gupta%2C%20Ritu.pdf

[7] Singh S. (2007) Ergonomic interventions for health and productivity. Himanshu Publications,New Delhi. Cited from Gupta, R., (2012), "Musculoskeletal Disorders among female workers engaged in papad rolling activity", 7(2): 275-281. Retrived from website: http://krishikosh.egranth.ac.in/bitstream/1/58100 16103/1/PAU-Gupta%2C%20Ritu.pdf

PRAJÑĀ - **Journal of Pure and Applied Sciences Vol. 24 – 25 : 164 – 173 (2017)**
ISSN 0975 - 2595

PREVALENCE OF RISK FACTORS OF CARDIOVASCULAR DISEASE AMONG THE ADULT FEMALE POPULATION OF ANAND CITY (GUJARAT)

AMI BRAHMBHATT[1], DP RAYKUNDALIYA[2,] NEETA DAVE[1], REMA SUBHASH[1], PATEL V.H. [1] AND VIRAJ ROGHELIA[1] *.

[1]*P.G. Department of Home Science, Sardar Patel University, Vallabh Vidyanagar, Gujarat, India.*
[2]*P.G. Department of Statistics, Sardar Patel University, Vallabh Vidyanagar, Gujarat, India.*
Email : virajshalin@gmail.com

ABSTRACT

The prevalence of risk factors of cardiovascular disease is increasing globally. The objective of this study was to determine the prevalence rate of risk factors of CVD and its association with the socio-economic, lifestyle and genetic factors among the adult female population of Anand. A survey was conducted among a total of 1072 female subjects (18 years and above) using a pretested questionnaire and their background information, medical history and dietary habits were collected. Anthropometric parameters, blood pressure and lipid profile of the subjects were studied using standard methods. The prevalence rate of risk factors of CVD among the adult female population of Anand was found to be as follows: systolic blood pressure - 46.6%, diastolic blood pressure - 37.7%, overweight - 30.6%, obesity - 1.3%, type I diabetes - 1.5%, type II diabetes- 4.5%, low HDL-c - 63.5%, high triglyceride level- 6.5% , high LDL-c 6.7% and hypercholesterolemia- 8.4%. Among all the variables, age was strongly associated with systolic blood pressure, diastolic blood pressure, cholesterol and HDL-c. The other socioeconomic factors like occupation, religion, level of education, type of exercise, sleeping pattern and consumption of outside food were significantly ($p<0.05$) related with systolic as well as diastolic blood pressure. Level of education and occupation showed a significant impact on total cholesterol, triglycerides and LDL-c. Type of diet also had an impact on the total cholesterol and LDL-c. The present study concludes that even though the prevalence rate of CVD is lower, the risk factors are more prevalent in the studied female subjects of Anand.

Key Words: Cardiovascular disease prevalence, risk factors, adult female population , Anand city

INTRODUCTION

Cardiovascular disease is one of the causes of death in developing countries of the world [1]. In 1920, about 28% of deaths were contributed to CVD which was estimated to increase up to 34% by 2020 [3]. Cardiovascular Disease (CVD) refers to conditions and diseases of heart and blood vessels, including coronary heart disease (CHD), heart attack, stroke, high blood pressure, congestive heart failure (CHF) and congenital heart disease. These diseases can be interrelated and usually have similar risk factors [4,5]. Various risk factors leading to CVD are divided into lifestyle factors, biophysical parameters, lipid profile and other co morbidities. Use of tobacco, smoking, alcohol consumption, type of exercise, body mass index, hypertension, hypercholestremia, hypertriglyceridemia, diabetes are risk factors of CVD [6]. CVD has shown higher mortality rates among the lower socio-economic groups and those with a lower level of education [7]. [Gu et al (2005)] have reported that 34.2 % and 33.2% of Chinese men had more than one or two different risk factors of CVD respectively while 35.1% and 24.0% of Chinese women were suffering from at least one and two different risk factors of CVD, respectively. Among the adult Nigerian population, a significant number of modifiable CVD risk factors were present in the rural and urban migrants. Central obesity, hypercholestremia, hypertension and hypertriglyceridemia were prevalent in more than 20% of the population. Low levels of HDL and obesity were prevalent in less than 20% of the population while the prevalence of prediabetes and diabetes was below 10% in the general population [1]. Another study in Chennai (India) reported 12.1% of diabetes prevalence in the population [2]. Therefore, the present study was planned to determine the prevalence rate of risk factors of cardiovascular disease among the female population of Anand city, Gujarat.

METHODOLOGY

Subject selection

The study was carried out during the period of December-2012 to April-2013 for finding the

prevalence rate of risk factors of CVD in adult females of Anand city. Census list of Anand city of the year 2011 was procured from the Anand Municipality Office. From a total of 14 wards, 6 wards were randomly chosen. From each of these wards, 6 blocks were randomly selected by using Microsoft excel. Nearly 1072 females above 18 years of age were selected as study subjects. Written consent was taken from all the enrolled subjects.

Data collection

Background information like age, occupation, religion, level of education, type of family, average family income and information on medical history such as obesity, diabetes, family history, illness frequency, medication, type of surgery done, presence of signs and symptoms pertaining to CVD were collected using a pretested questionnaire.

Anthropometric measurements

Height, weight, waist circumference and hip circumference were measured using standard tools and methods. BMI and waist to hip ratio was calculated using the formula given below.

$$\text{BMI} = \frac{\text{Weight(kg)}}{\text{Height(m2)}}$$

$$\text{WHR} = \frac{waistcircumference}{hipcircumference}$$

Blood pressure was also measured using a sphygmomanometer by a registered physician. The cut off values of various categories of BMI, waist to hip ratio and blood pressure are mentioned in Tables 1, 2 and 3, respectively.

Table 1 : Categories of BMI:

Presumptive diagnosis	Cut off points of BMI kg/m^2
Under weight	<18.50
Normal	18.50-24.99
Preobese	25.00-29.99
Obese class I	30.00-34.99
Obese class II	35.00-39.99
Obese class III	≥40.00

Source: The Asian Pacific Criteria (WHO 2004) [9]

Table 2: Standard Values for Waist:Hip ratio

	Acceptable		Unacceptable		
	Excellent	**Good**	**Average**	**High**	**Extreme**
Male	< 0.85	0.85 - 0.90	0.90 - 0.95	0.95 - 1.00	> 1.00
Female	< 0.75	0.75 - 0.80	0.80 - 0.85	0.85 - 0.90	> 0.90

Source : The Asian Pacific Criteria (WHO 2004) [9]

Table 3 The classification of blood pressure

Category	Systolic B.P. (mmHg)	Diastolic B.P. mmHg)
Hypotension	<90	<60
Desirable	90-119	60-79
Pre hypertension	120-139	or 80-89
Stage 1 hypertension	140-159	or 90-99
Stage 2 hypertension	160-179	or 100-109
Hypertensive crisis	≥180	or ≥110

Source: AHA, (2011) [10]

Blood collection and Bio-chemical estimation

Fasting blood was collected by a trained laboratory technician (Devasya Laboratory, Vallabh Vidyanagar) serum was separated and analyzed for lipid profile which included total cholesterol, triglyceride and HDL-c cholesterol using COBAS INTEGRA 400 PLUS, while VLDL, LDL and TC:HDL ratio were obtained by calculation using the values of total cholesterol, triglyceride and HDL-c using the formula below:

VLDL = Triglyceride / 5
LDL = Total Cholesterol–(HDL+VLDL)
TC: HDL = Total Cholesterol/HDL

The reference ranges [11] for the lipid profile is shown in **table 4**.

Statistical analysis

Analysis such as univariate, bivariate, ANOVA and regression was conducted by SPSS version 15.0. Variables included for the analysis were age, family income, level of education, occupation, religion, type of diet, type of exercise, BMI, total cholesterol, triglycerides, HDL-c, LDL-c and TC/HDL.

Table: 4 Reference Range for Lipid Profile

Lipid Profile	Range	Diagnosis
Total Cholesterol (mg/dl)	below 200mg/dl	Normal
	200-239mg/dl	Borderline
	≥239mg/dl	High
Triglycerides (mg/dl)	Below 150mg/dl	Normal
	150-199mg/dl	Borderline
	199-499mg/dl	High
	≥499mg/dl	Very High
HDL (mg/dl)	<40 mg/dl	Best
	40-59mg/dl(M)	Better
	≥59mg/dl	Poor
LDL (mg/dl)	100-129mg/dl	Ideal
	129-159mg/dl	Borderline
	159-189mg/dl	High
	≥189mg/dl	Very High

Source: Mayoclinic, (2012) [12]

RESULTS AND DISCUSSION

In the female population studied, majority of the subjects belonged to 18-30 years. More than 50% of the population fell in the age category of 40 years and above as shown in **Table 5**. The mean age of the respondents was found to be 42 years.

Table 5 depicts the distribution of the female subjects according to their BMI categories namely underweight, normal, preobese, obese class I, class II, and class III. Around 36.9 % of females were normal, 30.6% of females were preobese and had chances of obesity. Only 1.3% of subjects belonged to the category of class III obesity which would further increase the risk of CVD and Diabetes. As per Ahmad et al. (2006), the number of obese and non-obese persons in Lahore (Pakistan), were 162 (27.93%) and 418 (72.07%) respectively [13].

Majority of females in the present were in systolic pre hypertension (46.6 %) and diastolic prehypertension (37.7%) categories. About 2.6% and 2.5% subjects were found to be in systolic and diastolic hypertensive crisis respectively. Among the symptoms related to CVD, it was noticed that maximum subjects (16.3 %) were suffering from hypertension. An African (Gabon) study reported a high prevalence of 53.7% of hypertension among females aged between 50-60 years [14]. The prevalence of hypertension in Nigeria was 3.4% in the study population from which 0.89% were females [15].

Majority of the subjects (93.8%) responded that they were not suffering from any kind of chronic diseases. However, about

Table 5: Distribution of the female subjects as per various risk factors of CVD

	Category	%	
Age	18-30	31.5	
	30-40	13.8	
	40-50	19.9	
	50-60	18.8	
	60-70	13.7	
	70 and above	2.3	
BMI (Kg/m^2)	Under Weight	12.9	
	Normal	36.9	
	Pre Obese	30.6	
	Obese Class I	14.7	
	Obese Class II	3.6	
Systolic Blood pressure	Hypotension	0.0	
	Normal	24.5	
	Pre Hypertension	46.6	
	HT-Stage 1	19.2	
	HT- Stage 2	7.0	
	Hypertensive crisis	2.6	
Diastolic Blood pressure	Hypotension	0.3	
	Normal	25.5	
	Pre Hypertension	37.7	
	HT-Stage 1	25.9	
	HT- Stage 2	8.1	
	Hypertensive crisis	2.5	
Medical History	No chronic disease	93.8	
	Type I DM	1.5	
	Type II DM	4.5	
	CVD	0.2	
Symptoms experienced by the subjects	Chest Pain	Yes	8.1
		No	91.9
	Shortness of breath	Yes	5.7
		No	94.3
	Hypertension	Yes	16.3
		No	83.7
	Hypotension	Yes	9.2
		No	90.8
	Dizziness	Yes	2.3
		No	97.7
	Headache	Yes	12.9
		No	87.1

1.5% and 4.5% females were suffering from type I diabetes mellitus and type II diabetes mellitus, respectively. About 0.2% subjects were suffering from CVD. Zafar et al (2011) have reported that among 798 females in Punjab, 12.31% were suffering from diabetes mellitus [16]. As per Edgar et al. (2012), CVD prevalence rates were in Gabon (Africa) 14.7% and 11.5% for rural and urban men respectively and 14.9% and 8.9% for rural and urban women respectively [14].

Pertaining to the symptoms experienced related to CVD, about 12.9%, 9.2% and 8.1% of subjects have experienced headache, hypotension and chest pain, respectively. Very few female subjects have experienced dizziness and shortness of breath as shown in Table 5.

Table 6 depicts the data on lipid profile of the subjects studied. About 68.9% of the females showed normal cholesterol levels, while 31.1% of the female subjects showed cholesterol levels beyond the normal level. About 73.7% showed normal levels of triglyceride whereas 19.6% of the females showed borderline triglyceride levels, also 6.5% and 0.2% of female subjects showed high and very high levels of triglyceride, respectively. Pertaining to HDL-c levels of the subjects, majority of the subjects (63.5%) showed poor HDL levels which could increase the risk of CVD. It was also noticed that majority of the subjects (70.3%) showed ideal LDL levels (below 100-129mg/dl). Moreover, about 8.8% of the female subjects showed higher levels of LDL-c.

A study conducted in Vallabh Vidyanagar showed that the prevalence of major CVD risk factors were systolic blood pressure (32.1%), diastolic blood pressure (22.7%), overweight (30.23%), obesity (6.9%), diabetes (14.7%), low HDL-c (58.9%), high triglyceride level (15.6%), high LDL-c (7.4%), hypercholesterolemia (5.7%) [6]. Table -7 and 8 shows the association of the various socio-economic factors and lifestyle factors with systolic blood pressure and diastolic blood pressure, respectively. Among the socio-economic factors age, occupation and level of education showed a significant ($p < 0.01$) association with systolic blood pressure (Table-7). Systolic hypertension was more prevalent in the subjects belonging to 50-60 years (17.3%) followed by the subjects of 18-30 years (17.1%) and 40-50 years of age

Table 6: Serum Lipid profile of the female subjects

Lipid Profile	%
Total Cholesterol	
Normal	68.9
Borderline	22.7
High	8.4
Triglycerides	
Normal	73.7
Borderline	19.6
High	6.5
Very High	0.2
HDL	
Poor	63.5
Better	20.3
Best	16.2
LDL	
Ideal	70.3
Borderline	20.9
High	6.7
Very high	2.1

(17.1%). A study by Lloyd-jones et al (2010) in America stated that the subjects with favorable levels of risk factors in middle age can survive and have a better quality of life 25 years later. As risk factors related to CVD can begin decades before the disease is detected, it is important to take preventive measures as early in life as possible [17].

Pertaining to occupation, systolic hypertension was found to be more prevalent (28.0%) in the subjects busy with other kind of work such as baby sitting or vendors, while, the least number of housewives (0.3%) had systolic hypertension. As far as level of education is concerned, higher percentage of the subjects with elementary education (24.6%) had systolic hypertension.

Sleeping pattern and outside food consumption pattern of the subjects also showed a positive and significant ($p<0.01$) relation with systolic blood pressure (Table 7). However, type of diet and meal timings did not show any significant association with systolic blood pressure.

The subjects who were doing meditation (0.3%) and playing badminton

(0.7%) had normal systolic blood pressure. Whelton et al. (2008) reported that regular aerobic exercise could decrease systolic blood pressure by 3.8 mm Hg (95% CI 2.7 to 5.0 mm Hg, p <0.001) in sedentary adults [18]. Aerobic exercise showed a positive effect in overweight children in an 8-week period. They were more fit, had higher HDL-cholesterol levels, and better endothelial function [19].

Table 8 represents that the socio-economic risk factors like age, occupation, and level of education which showed a significant (p<0.01) association with diastolic blood pressure. Diastolic hypertension was more prevalent in the subjects belonging to 50-60 years (17.3%) followed by the subjects of 40-50 years of age (16.7%). in the subjects doing other kind of work (28.1%) such as baby sitting or vendors. While, the least percentage (0.3%) of diastolic hypertension was seen in housewives. Sleeping pattern of the subjects and frequency of consuming outside food also showed a positive and significant (p<0.01) relation with diastolic blood pressure. Maximum hypertensive respondents (25.4%) consumed outside food only occasionally.

Looking at the type of exercise, cycling (0.7%), dancing (0.0%), yoga (4.7%), meditation (0.4%) and stretches (0.1%) showed a significant (P<0.05) relation with diastolic blood pressure (Table-8). As per Whelton et al. (2008), regular aerobic exercise could decrease diastolic blood pressure by 2.6 mm Hg (95% CI 1.8 to 3.4 mm Hg, p < 0.001) in sedentary adults [18].

Pertaining to occupation, diastolic hypertension was found to be more prevalent
ANOVA was done to study the impact of level of education, occupation, family income, type of exercise and type of diet on systolic and diastolic blood pressure. The data in Table- 9 revealed that level of education, occupation, family income and type of exercise had a significant (p<0.05) impact on systolic blood pressure. Observing the level of education, the subjects with elementary education showed the highest systolic blood pressure levels (132.55 mmHg). As far as occupation is concerned, housewives showed the highest systolic blood pressure (133.40 mmHg) among all the occupational categories and the lowest value of systolic blood pressure was observed in subjects involved in other activities like maid servants, baby sitting and vendors (119.49mmHg).

Table: 7 Association of various socio-economic factors and life style factors with systolic blood pressure

Variable		Percentage (%)		χ^2
		Normal	Hypertension	
Age(years)	18-30	14.4%	17.1%	142.74*
	30-40	4.1%	9.7%	
	40-50	2.7%	17.1%	
	50-60	1.6%	17.3%	
	60-70	1.4%	12.3%	
	70 and above	0.3%	2.1%	
	Total	24.5%	75.5%	
Occupation	Professional	2.8%	13.2%	21.478*
	Private			
	Government			
	Business	1.8%	16.4%	
	Retired	2.1%	23.7%	
	Housewife	0.0%	0.3%	
	Laborer	0.4%	2.5%	
	Farmers	0.4%	1.0%	
	Others	7.5%	28.0%	
	Total	14.9%	85.1%	
Level of education	Elementary	4.7%	24.6%	66.64*
	High School	4.5%	17.8%	
	Diploma	2.3%	1.6%	
	Graduate	9.8%	18.7%	
	Post graduate	2.2%	6.4%	
	PhD	0.2%	0.2%	
	Total	24.6%	75.4%	
Sleeping pattern	Peaceful	19.9%	53.3%	10.615*
	Disturbed	4.7%	22.1%	
Outside food	Never	1.9%	6.2%	46.83*
	Once in a week	3.2%	10.2%	
	Once in 15 days	6.6%	7.0%	
	Once in a month	4.5%	9.9%	
	Twice in a month	0.6%	2.2%	
	Occasionally	8.0%	25.4%	
	Rarely	2.2%	11.9%	
	Total	27.2%	72.8%	
Type of Exercise	Badminton	0.3%	0.1%	5.523*
	Meditation	0.7%	0.6%	6.107*

* Indicates significance (P<0.05)

Table: 8 Association of various socio-economic factors and life style factors with diastolic blood Pressure

Variable		Percentage (%)		χ^2
		Normal	Hypertension	
Age (years)	18-30	15.6%	15.9%	157.6*
	30-40	3.3%	10.5%	
	40-50	3.1%	16.7%	
	50-60	1.6%	17.3%	
	60-70	1.6%	12.1%	
	70 and above	0.6%	1.8%	
	Total	25.7%	74.3%	
Occupation	Professional	2.9%	13.0%	20.372*
	Private			
	Government			
	Business	1.3%	16.9%	
	Retired	2.6%	23.2%	
	Housewife	0.0%	0.3%	
	Laborer	0.5%	2.4%	
	Farmers	0.3%	1.1%	
	Others	7.4%	28.1%	
	Total	15.0%	85.0%	
Sleeping patte	Peaceful	21.1%	52.1%	14.117*
	Disturbed	4.7%	22.1%	
Outside food	Never	1.9%	6.2%	46.83*
	Once in a week	3.2%	10.2%	
	Once in 15 days	6.6%	7.0%	
	Once in a month	4.5%	9.9%	
	Twice in a month	0.8%	2.2%	
	Occasionally	8.0%	25.4%	
	Rarely	2.2%	11.9%	
	Total	27.2%	72.8%	
Type of Exercise	Cycling	0.7%	0.7%	4.365*
	Dancing	0.3%	0.0%	9.018*
	Yoga	3.5%	4.7%	14.567*
	Meditation	0.8%	0.4%	13.016*
	Stretches	0.3%	0.1%	5.095*

* Indicates significance (P<0.05)

Table: 9 Influence of socio-economic and life style factors on systolic blood pressure of female respondents

Variable	Category	Systolic Blood Pressure (mmHg)	Homogeneity of Variance	F Value
Level of Education	Elementary	132.55 ± 17.591	5.255	19.808*
	High school	130.98 ± 19.974		
	Diploma	116.14 ± 16.642		
	Graduate	123.65 ± 16.305		
	Post graduate	125.18 ± 15.311		
	PhD	127.50 ± 23.629		
Occupation	Professional	125.54 ± 18.542	12.234	24.019*
	Business	129.67 ± 13.904		
	Retired	132.22 ± 19.316		
	House wife	133.40 ± 19.582		
	Laborer	123.88 ± 18.132		
	Others	119.49 ± 12.870		
Family Income (Rs)	Up to 10,000	130.9 ± 19.701	2.732	2.761*
	10,000–20,000	128.1 ± 18.947		
	25,000–50,000	126.6 ± 15.001		
	50,000 and more	127.4 ± 129.1		
Type of Exercise	Sedentary	127.5 ± 17.127	2.637	4.559*
	Light	133.6 ± 22.177		
	Heavy	123.2 ± 14.736		

* Statistically significant (P<0.05)
Values in column 3 are Mean±**SD**

Regarding family income, the highest systolic blood pressure was observed in the subjects having monthly income of Rs. 10,000/- (130.9 mmHg) and the lowest was found in the subjects having monthly income of Rs. 25,000-50,000/- (126.6 mmHg). It may be attributed to the fact that people with higher income may be on medication if they have been diagnosed with blood pressure while, in the lower income strata, subjects may not have been diagnosed for high blood pressure. As

per Oguoma et al. (2015), more than 80% of the global burden of CVD could occur in low and middle-income countries [1]. Pertaining to the type of exercise, the highest systolic blood pressure was seen in the subjects involved in light exercise (133.6 mmHg) while the lowest systolic blood pressure was observed in the subjects occupied with heavy exercise (123.2 mmHg).

Table 10 depicts that among the socioeconomic factors, level of education and occupation showed a significant (P<0.05) impact on diastolic blood pressure. Looking at the level of education, subjects with elementary education showed the highest (87.59 mmHg) diastolic blood pressure levels. Pertaining to occupation, housewives showed the highest diastolic blood pressure (86.34 mmHg) and the respondents involved in other activities such as baby-sitting and vendors showed the lowest value of diastolic blood pressure (77.62 mmHg).

Table: 10 Influence of socio-economic factors on diastolic blood pressure of female respondents

Variable	Category	Diastolic Blood Pressure (mmHg)	Homogeneity of Variance	F Value
Level of Education	Elementary	87.59 ± 46.661	0.691	4.034*
	High school	83.76 ± 10.281		
	Diploma	72.38 ± 12.362		
	Graduate	79.81 ± 9.613		
	Post graduate	83.13 ± 8.800		
	PhD	77.50 ± 17.078		
Occupation	Professional	80.00 ± 8.971	0.304	4.343*
	Business	85.67 ± 12.558		
	Retired	81.67 ± 9.707		
	Housewife	86.34 ± 32.415		
	Laborer	81.00 ± 10.066		
	Others	77.62 ± 9.877		

* Indicates significance (P<0.05). Values in column 3 are Mean±SD

The impact of socio economic factors was also evaluated on other risk factors of CVD namely serum total cholesterol, serum triglyceride, high density lipo-protein, low density lipo-protein and very low density lipo-protein. The data showed that the level of education and occupation had a significant (P<0.05) impact on serum total cholesterol (Table-11), triglycerides (Table-12) and LDL-c levels (Table-13) whereas the type of diet showed a significant relationship with cholesterol and LDL-C-c but not with the triglyceride levels.

Table: 11 Influence of socio-economic and life style factors on serum total cholesterol levels of female respondents

Variable	Category	Total cholesterol (mg/dl)	Homogeneity of Variance	F Value
Level of Education	Elementary	191.4427 ± 35.23061	3.138*	8.604*
	High school	188.7211 ± 35.61410		
	Diploma	166.6405 ± 22.09571		
	Graduate	181.6097 ± 32.95217		
	Post graduate	174.4292 ± 29.81455		
	PhD	203.4050 ± 36.88825		
Occupation	Professional	184.7179 ± 31.76571	17.984*	26.489*
	Business	183.7550 ± 33.18529		
	Retired	209.3411 ± 44.24798		
	Housewife	192. 9394 ± 35.21438		
	Laborer	176.0225 ± 29.25768		
	Others	167.3527 ± 22.13247		
Type of Diet	Vegetarian	184.9639 ± 33.82357	3.927*	4.297*
	Ovo vegetarian	179.5448 ± 27.63574		
	Non vegetarian	191.7008 ± 37.34346		

* Indicates significance (P<0.05). Values in column 3 are Mean±SD

The type of diet had an impact on cholesterol and LDL-c levels. The subjects who were non-vegetarians in habit showed the highest cholesterol levels (191.70mg/dl) and the ovo-vegetarian respondents showed the lowest cholesterol values (179.54mg/dl) as expressed in Table-11. Similarly, the data in Table-13 also depicts that the non vegetarian subjects showed the highest values of LDL-C (121.58mg/dl) and ovo-vegetarians showed the least value of LDL-c (108.55mg/dl).

According to Table-11, the highest cholesterol levels were observed in the subjects who were highly qualified (Ph.D)

(203.40 mg/dl) and the lowest values of cholesterol was found in the subjects with diploma (166.64mg/dl). A similar trend was observed for serum triglyceride levels (Table-12) and LDL-c levels (Table-13) pertaining to the level of education of the subjects.

In the occupation category, the highest and lowest values of serum cholesterol was noticed for the retired respondents (209.34 mg/dl) and subjects busy in doing other kinds of work (167.35 mg/dl), respectively. A similar pattern was noticed for LDL-c with regard to occupation of the subjects (Table-13). However, for triglyceride levels, the highest and the lowest levels of triglycerides were noted for subjects doing business (131.05mg/dl) and laborers (96.10 mg/dl), respectively (Table-12).

Table: 12 Influence of socio-economic factors on serum triglyceride levels of female respondents

Variable	Category	Triglycerides (mg/dl)	Homogeneity of Variance	F Value
Level of Education	Elementary	120.8190 ± 56.13822	2.8	4.907*
	High school	127.6503 ± 77.16312		
	Diploma	91.7119 ± 34.79145		
	Graduate	114.3178 ± 52.14037		
	Post graduate	104.6873 ± 45.64284		
	PhD	149.4675 ± 82.21562		
Occupation	Professional	120.9828 ± 66.14789	1.611	8.371*
	Business	131.0525 ± 56.54683		
	Retired	120.5678 ± 59.50000		
	Housewife	126.4933 ± 63.76309		
	Laborer	96.1006 ± 42.89551		
	Others	100.0726 ± 43.06867		

* Indicates significance (P<0.05)
Values in column 3 are Mean±SD

The risk of developing CVD increases exponentially as LDL-C levels rise. It is also reported that the subjects with a controlled LDL-C cholesterol level below the recommended guidelines, if the HDL level is lower than the recommended level, the risk of developing CVD increases [20].

Table: 13 Influence of socio-economic and life style factors on serum LDL-C levels of female respondents

Variable	Category	LDL-c (mg/dl)	Homogeneity of Variance	F Value
Level of Education	Elementary	120.54 ± 29.654	3.588	6.67*
	High school	116.26 ± 29.760		
	Diploma	103.46 ± 16.387		
	Graduate	111.33 ± 28.606		
	Post graduate	106.08 ± 26.913		
	PhD	129.70 ± 29.224		
Occupation	Professional	116.91 ± 26.768	15.25	21.997*
	Business	112.98 ± 31.094		
	Retired	137.82 ± 36.404		
	Housewife	120.10 ± 29.692		
	Laborer	114.53 ± 27.202		
	Others	100.62 ± 19.836		
Type of Diet	Vegetarian	113.87 ± 28.580	2.174	7.554*
	Ovo vegetarian	108.55 ± 24.160		
	Non vegetarian	121.58 ± 31.105		

* Indicates significance (P<0.05)
Values in column 3 are Mean±SD

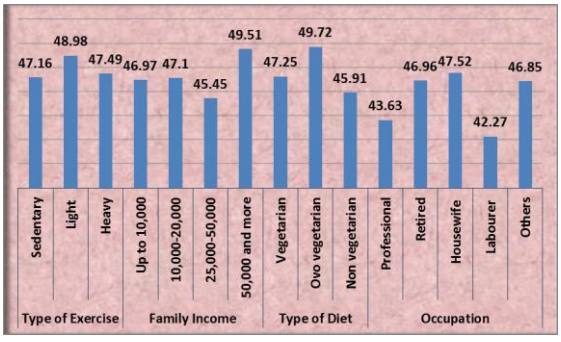

Figure 1: Influence of socio-economic factors and life style on HDL-c of female respondents

Figure 1 depicts the influence of socio-economic and life style factors on serum HDL- C levels of the female subjects. However, none of the socio-economic factors have shown a significant impact on the HDL-c levels.

In the regression analysis, the relationship between the dependent variables such as systolic blood pressure, diastolic blood pressure, total cholesterol, serum triglycerides, HDL-c, TC: HDL-c and independent variables such as age, occupation, level of education type of family income, BMI were studied.

According to this age and BMI showed a positive and significant ($P<0.05$) relationship with systolic blood pressure (R^2=0.208, F=139.015*, P-0.000). Similarly, age and BMI also showed a significant ($P<0.05$) relationship with HDL-c (R^2-0.065, F-16.425, P-0.000).

Equation-1: **Systolic Blood Pressure** = **100.867+0.462*Age+0.343*BMI**
Equation-2: **HDL = 52.575-0.394*BMI+0.107*Age**

As per equation 3, BMI showed a positive and significant ($P<0.05$) relation with diastolic blood pressure (R^2=0.022, F=23.911, P-0.000) and serum triglyceride (R^2-0.035, F-17.152, P-0.000).

Equation-3: **Diastolic Blood Pressure** = **73.385+0.241*BMI**
Equation-4: **Serum Triglyceride =57.235+0.842*BMI**

Age of the subjects showed a positive and significant ($P<0.05$) relationship with total cholesterol ($R^{2=}$0.164, F=206.959, P-0.007).

Equation-5: **Total cholesterol = 150.500+0.842*Age**

CONCLUSION

In the female population studied, the prevalence of selected risk factors of CVD namely obesity, systolic and diastolic prehypertension, poor HDL-c levels were high. Age, occupation, sleeping pattern, type of exercise and frequency of outside food consumption showed a significant association with systolic and diastolic blood pressure. Level of education, occupation and type of diet showed a significant impact on cholesterol and LDL-c levels of the female subjects. Along with socioeconomic factors, a significant relatioship of age and BMI with the lipid profile could be helpful to plan preventive strategies for reducing the risk factors related to cardiovascular disease

ACKNOWLEDGMENT

The authors are grateful to UGC-SAP-DRS-I for conceding financial assistance for the present research.

REFERENCES

[1] Victor, M.O., Ezekiel, U. N., Timothy, C.S., Kester, A., Wharentomah, D., Innocent, C. O., & Ross, S.R. (2015): Prevalence of cardiovascular disease risk factors among a Nigerian adult population: relationship with income level and accessibility to CVD risks screening, BMC Public Health. **15**:397.

[2] Ramachandran, A., Snehalatha, C., Kapur, A., Vijay, V., Mohan, V., Das, A. K., Rao, P. V., Yajnik, C. S., Prasanna Kumar, K. M., & Jyotsna, D. Nair. (2001): High prevalence of diabetes and impaired glucose tolerance in India: National Urban Diabetes Survey. Diabetologia, **44**(9): 1094–1101.

[3] Levenson, J. W., Skerret, P. J., & Gaziano, J.M. (2002): Reducing the Global burden of cardiovascular disease: the role of risk factors. Preventive cardiology, **5**(4):188-199.

[4] Gupta, R., Joshi, P., & Mohan, V. (2008): Epidemiology and causation of coronary heart disease and stroke in India. Heart, **94** :16-26.

[5] Thom (2006): c.f. Krause's Food & Nutrition Therapy, International Edition, Roshan Ketab medical publisher, **12** edition,614-629.

[6] Hinal, P., et al, Raykundaliya , D. P., Neeta, R. D., Rema S., V. H. Patel. (2014): Prevalence of risk factors for cardiovascular disease among the adult male population of Vallabh Vidyanagar, Gujarat, India. Research And Reviews: Journal of medical and health sciences, **3**(3).

[7] Eloi, D., Aurélie, F., & Yolande, E. (2012): Cardiovascular disease and psycho-social factors at work. Journal: Archieves of Cardiovascular Disease, **105**(1):33-39.

[8] Gu, D., Gupta, A., Muntner, P., Hu, S., Duan, X., Chen, J., Reynolds, R.F., Whelton, P.K., & He, J. (2005): Prevalence of cardiovascular disease risk factor clustering among the adult population of china, results from the international collaborative study of cardiovascular disease in Asia (interasia). Circulation, **112**(5): 658-665.

[9] World Health Organization (2004): The Atlas of Heart Disease and Stroke. 2004. c.f. www.who.org.

[10] American Heart Association. "Understanding blood pressure readings". (2011): c.f. http://www.americanheart.org/statitics2011/pdf

[11] Friedewald, W.T., Levy, R.I., & Fredrickson, D.S. (1972): Estimation of the concentration of low-density lipoprotein cholesterol in plasma, without use of the preparative ultracentrifuge. Clinical Chemistry, **18**(6): 499-502.

[12] Mayo Clinic. Mayo Foundation for Medical Education and Research (MFMER), (2012): c.f. www. MayoClinic.com.

[13] Ahmad, Z. and Pervaiz, M.K. (2006): Risk factors and diabetes mellitus: Statistical study of adults in Lahore, Pakistan. Journal of Statistics, Lahore Pakistan, **13**(1): 46-66.

[14] Edgar, B. N., Victor, A, Philomene, K., Roger, M., Jean, E., Ecke, N.,Carine, N., Marc, L., Pierre-Mari,e P., & Philippe, L. (2012): Prevalence of cardiovascular disease in Gabon: A population study, Archives of Cardiovascular disease. **105**(2):77-83.

[15] Kenneth, E. O., Valentine, U. O., Eze, K. N., & Kevin, E. P. (2009): Body Mass Index and Blood Pressure Pattern of Students in a Nigerian University. International Journal of Health Research; **2:** 177-182.

[16] Zafar, J., Fiaz, B., Nasim, A., Uzma, R., Rizwan, B., Saima, H., Ayesha, W., Fardah, Y., & Madeeha, N. U. (2011): Prevalence and risk factors for diabetes mellitus in a selected urban population of a city in Punjab. Journal of Pakistan Medical Association, **61**(1): 40-47.

[17] Lloyd-Jones, D.M., Hong, Y., Labarthe, D. (2010): Defining and setting national goals for cardiovascular health promotion and disease reduction: the American Heart Association's strategic impact goal through 2020 and beyond. circulation, journal of the American Heart Association , **121**: 586-613.

[18] Whelton, W., Harris S., Dariush, M., Eric, R., Penny. K. E, Lawrence, L. R., Lawrence, J. A., Marguerite, M. E., Mary, B. E., & Frank, S. (2008): Omega-6 fatty acids and risk for cardiovascular disease. Circulation, **119**: 902-907.

[19] Kelly, Must, A. (2008): The diet and 15-year death rate in the seven countries study. American Journal of Epidemiology, **124**: 903–915.

[20] Grundy (2004): c.f. Krause's Food & Nutrition Therapy, International Edition, Roshan Ketab medical publisher, **12** edition, 836-840.

PRAJÑĀ - **Journal of Pure and Applied Sciences Vol. 24 – 25 : 174 – 181 (2017)**
ISSN 0975 - 2595

EVALUATION OF ALPHA AMYLASE, ALPHA GLUCOSIDASE AND PROTEIN GLYCATION INHIBITORY ACTIVITIES OF DIFFERENT ELEMENTS OF MANGO (*Mangiferaindica*)

ANU MISHRA AND V.H. PATEL*
Laboratory of Foods and Nutrition, P.G.Department of Home Science, Sardar Patel University, Vallabh Vidyanagar- 388001, Gujarat, India. Email: patelvh2004@yahoo.co.in

ABSTRACT

The current study was conducted to analyse in vitro alpha amylase, alpha glucosidase and protein glycation inhibitory activities of different elements of mango (pulp, peel and leaves). The results represent that total phenolic content (TPC), flavonoids and total antioxidant capacity (TAC) by FRAP, DPPH-RSA and ABTS-RSA exhibited marked variation ranging from 1360.40 to 3394.46 mg GAE/100 gm, 420.55 to 2331.06 mg RE/100gm, 772.90 to 7303.25 mg TE/100gm, 300.76 to 4375.98 mg TE/100gm and 267.44 to 481.95 mg TE/100gm, respectively. The inhibitory effect of alpha-amylase and alpha-glucosidase assay ranged from 5.97% to 40.26% and 12.78 % to 73.42% among all the elements of mango, respectively. Mango pulp exhibited significantly ($p<0.05$) elevated inhibitory effect on AGE's formation in the BSA glycation system among all the elements of mango. Hence mango pulp may be used for controlling blood glucose level and in the prevention of the development of secondary complications in type 2 diabetes.

Keywords: mango elements, alpha amylase, alpha glucosidase, antioxidant, anti-glycation.

INTRODUCTION

Diabetes mellitus (DM) is a vital persistent disease caused by the improper balance of glucose homeostasis. The disease is characterized by hyperglycemia, hyperlipidemia and inadequacy of secretion or action of endogenous insulin. Increasing evidence in variedreported studies suggests that there is a substantial decrease in innate antioxidant status in diabetic patients while the simultaneous increase of oxidative stress plays a major role in the pathogenesis [1]. Free radicals are formed disproportionately in diabetes by glucose oxidation, glycation of proteins (albumin), and the subsequent oxidative degradation of glycated proteins. These lead to impairment of cellular organelles and enzymes, increased lipid peroxidation, β-cell dysfunction, impaired glucose tolerance and development of insulin resistance [2].The aftermath of the formation of advanced glycation end products (AGEs) in the pathogenesis of secondary diabetic complications are very life-threatening and have long lasting pernicious effects on multiple functional systems in the body like excretory system, nervous system, endothelial dysfunction, etc. [3,4]. Therefore there is a surge of demand for compounds with antioxidant and anti-glycation activities as they may offer therapeutic potential in delaying, controlling or preventing the onset of diabetic complications [5].

Diabetes is multifactorial in origin and one therapeutic approach to treat diabetes is to retard the absorption of glucose via inhibition of enzymes, such as alpha- amylase and glucosidase. Hydrolysis of dietary carbohydrates such as starch by alpha-amylase and intestinal alphaglucosidases is the major source of glucose in the blood. Inhibiting of these intestinal enzymes retards the elevation of blood sugar following a carbohydrate meal. So this has been a dietary supplement target for reducing the postprandial glucose load in the body [6].Medicinal plants are reported to be a good source of potent, safe and affordable alpha-glucosidase and amylase inhibitors and enhancers of glucose uptake and recently it is seen that there is a high demand for the same in treating diabetes [7,8].

Mango (*Mangifera indica*), also called "the king of fruits", is one of the most popular fruits in tropical regions [9]. This fruit is available plenty in season and it is a good and cheap source for the exploration of the development of nutraceuticals for diabetes [5]. It is considered as a good source of dietary compounds, such as ascorbic acid, phenolic compounds and carotenoids, which are beneficial to health due to their antioxidant capacity [9]. But no detailed studies are available on the effects of mango fruit pulp, peel and leaves on various targets relevant to diabetes to explore the antidiabetic properties of this edible fruit except for afew reported studies [10, 11].Current therapeutics for type 2

diabetes is often associated with undesirable side effects. Type 2 diabetes is mainly due to insulin resistance induced complications, the scope for the development of therapeutics is plenty [5].

Hence, the present investigation was designed to evaluate the carbohydrate digesting intestinal enzyme inhibition(alpha-amylase, alpha glucosidase) and antiglycation potential of mango fruit elements (pulp, peel and leaves).

MATERIALS AND METHODS

Chemicals: DPPH (2,2- Diphenyl-l-picrylhydrazyl) (D 9132), Trolox (6-Hydroxy-2,5,7,8- tetra methylchromane-2-carboxylic acid) (238813), Gallic acid (G 7384), Rutin hydrate (R 5143), TPTZ (2,4,6-Tris (2-pyridyl)-s-triazine) (T 1253), ABTS (2,2-Azino-bis (3-ethyl benzothiazoline-6-sulfonic acid) diammonium salt) (A 1888), PPA (porcine pancreatic α-amylase type VI-B) (A 3176), Acarbose (A 8980), pNPG (4-p-nitrophenyl-α-D-glucopyranoside) (N 1377), α-glucosidase (Type I from baker's yeast) (G 5003),NBT (Nitro blue tetrozolium) (N 5514), Girard's T stock (G 900) and Sodium formate (71539)were purchased from Sigma Aldrich Company (St. Louis, MO,USA). Soluble starch (1949150) was purchased from SRL Pvt. Ltd, Mumbai, India. All other chemicals procured were from local manufacturer and were of AR grade.

Plant Materials and Extraction: Elements of'*desi'* mango (pulp, peel and leaves) were procured from Anand Agricultural University, Anand. All the elements of mango were further identified and authenticated by the Department of Horticulture, Anand Agricultural University, Anand, Gujarat. The harvested mango elements were thoroughly washed underrunning tap water and air-dried until constant weight was obtained. Subsequently, the dried samples were ground (PHILIPS mixer grinder, India) and sieved to fine powder and then stored in a cool dry place prior to extraction. From this fine powder, duplicate extracts of each elements of mango was made using 80% methanol (pH 2) and stored at - 20^0C for the determination of total phenols, total antioxidant capacity (TAC), alpha amylase inhibition, alpha glucosidase inhibition and anti-glycation activity.

Determination of Total Phenols:
Total phenolic content (TPC) of elements of mango was determined using Folin–Ciocalteu reagent [12] and the results were expressed as % of gallic acid equivalentsof dry weight.
Flavonoid content was determined using the aluminium chloride colorimetric technique [13] and the results were expressed as % of rutin equivalents of dry weight.

Determination of Total Antioxidant Capacity:
Ferric Reducing Antioxidant Power Assay (FRAP): FRAP was assayed by Benzie and Strain (1996) [14] as a measure of antioxidant power and the results were determined as % of trolox equivalents of dry weight.
Free radical scavenging activity ability by the use of stable DPPH radical: The Antioxidant activity was determined by Brand Willams et al., 1995 [15] as the ability of methanolic extracts of these elements of mango to scavenge 2,2-Diphenyl-1-picrylhydrazyl (DPPH) radical. The results were demonstrated as % of trolox equivalents on dry weight basis.

Free radical scavenging activity ability by the use of stable ABTS radical: The free radical-scavenging activity was determined by ABTS radical cation decolorization assay described by Re et al., 1999 [16]. The results were expressed as % of trolox equivalents on dry weight basis.

Alpha-amylase Inhibition capacity:
***Alpha-amylase Inhibition by colorimetric assay*:**Alpha-Amylase activity was assessed using the slightly modified starch-iodine colour change method [17]. Briefly, 300 μl of alpha-amylase solution from porcine origin was added to 1 ml soluble starch solution and100 μlof sodium acetate buffer (0.1 M, pH 7.2).The reaction mixture was incubated for 37◦C for 1 h. Then, 100 μl from the reaction mixture was discharged into 3ml of distilled water and 100 µL of iodine solution. After mixing, the absorbance of the starch-iodine solution was measured at 565nm using a sprectophotometer (Systronics,166 India ltd.).For assessing the potential inhibitory activity of graded concentrations of elements of mango extracts (400–16000 μg/mL) 100-400 μL extract was preincubated with 300 μL enzyme solution at 37◦C for 30 min. Acarbose

solution was used as a positive control. The assay was then conducted as described above. Only starch (no enzyme), only enzyme (no starch) and substrate (enzyme and starch both) were carried out under similar assay conditions.The results were expressed as % inhibition of enzyme activity and calculated according to the following equation:
% Inhibition of Alpha-amylase enzyme activity = $(A_{ex}-A_e) / (A_s - A_e)*100$, where A_{ex} is the absorbance of extract, A_e is the absorbance of the enzyme and A_s is the absorbance of the starch.

***Alpha-amylase Inhibition by disc assay*:**The inhibitory capacity of elements of mango (pulp, peel and leaves) methanolic extracts against a-amylase by the bore method was evaluated according to the methods described by Roberta et al., 2004 [18].

Alpha-glucosidase Inhibition capacity:
The alpha-glucosidase inhibitory activity was modified and determined using the substrate p-nitrophenyl- α-D-glucopyranoside (pNPG), which could be hydrolyzed by alpha-glucosidase to release the product p-nitrophenol, and then monitored by a yellow colour development at 405 nm [19].The alpha-glucosidase inhibitory activity was expressed as percentage inhibition,
Inhibition % = $(A_{control}– A_{sample}) A_{control} \times 100\%$.

Measurement of antiglycation potential of plant extracts
In vitro glycation of BSA: Albumin glycation was performed according to the method of Tupe et al., 2013 [20]with some modifications. Glycated samples were prepared by incubating 10 ml of BSA (20 mg/ml), 5 ml of glucose (500 mM) in 10 ml of potassium phosphate buffer (0.2 M, pH 7.4 containing 0.02 % sodium azide) along with methanolicextracts of elements of mango (1 ml) and incubated at 37 °C for 30 days. Positive control (BSA+ AG + glucose) and control (BSA + glucose–plant extract) was maintained under similar conditions and all the incubations were performed in duplicates. Before incubation, all the solutions were placed in sterile plastic-capped vials to maintain sterility and strict asepsis was maintained during the entire process. After the incubation period, it was ensured that all the samples were free of microbiological contamination. The antiglycation potential of methanolic extracts of elements of mango was determined every week by estimation of three parameters from the glycation reaction mixture, i.e.–i) Nitro blue tetrazolium reductive assay, ii) Formation of alpha-dicarbonyl compounds and iii) AGEs.

Nitro blue tetrazolium reductive assay: Nitroblue tetrazolium (NBT) assay was modified and used to determine the level offructosamines (an amadori product) [21].

Formation of alpha-dicarbonyl compounds: The determination of alpha-dicarbonyl compounds was slightly altered and performed using the Girard-T assay [22]. Briefly, 200µL of the incubated solution was mixed with 100µL of deionized water, 100 µL of Girard-T reagent (500 mMin 20 mM sodium phosphate buffer), and 1.7ml of500 mM sodium formate (pH 2.9) in a test tube and incubated at ambient temperature (37 °C) for 1 h. The absorbance of thesolution at 290 nm using UV visible spectrophotometer (Shimadzu Inc., Kyoto, Japan) was then determined.

AGEs fluorescence measurement:The formation of total advanced glycation end products (AGEs)were assessed by determining the production of these fluorescent products of glycated albumin samples, positive control and control at excitation and emission wavelengths of 370 and 440 nm (slit = 10 nm) respectively on Hitachi F-7000 fluorescence spectrophotometer [20]. The results were expressed aspercent inhibition as calculated by the formula:$\%Inhibition=[(F_0–F_1)/F_0]\times100$, where F_0 is the fluorescence of the positive control and F_1 is the fluorescence of the glycated albumin samples co- incubated with methanolic extracts of elements of mango [20].

Statistical analysis: All the experimental results are expressed as mean ± standard deviation (SD) of four measurements of each sample. The results were also subjected to Analysis of Variance (ANOVA), while the significance of mean differences was determined by Duncan's post hoc test considering $p\leq0.05$ as the significant level of difference. Pearson's correlation coefficients (r) were also calculated to establish relationships among the data obtained. All the

statistical calculations were done using SPSS version 20.

RESULTS AND DISCUSSION

The total phenol, flavonoid content and FRAP, DPPH, ABTS free radical scavenging activity of the elements of mango i.e. pulp, peel and leaves are presented in **Table 1**.

The total phenol content of pulp, peel and leaves of mango was found to be 1360.40, 1953.27 and 3394.46 mg/100gm respectively. Previous studies reported lower total phenol in pulp (2.01mg/g) [23], peel (83.0 mg/g) [24] and leaves (30.73g/100gm) [25] than the present study. The flavonoid content of the element of mango was found to be highest in mango leaves 2331.06 mg RE/100 gm than the other elements of mango. Various researchers showed lower values of flavonoids for the elements of mango i.e. (151 µg QE/g) in pulp [26], (24.95 mg/g) in peel [23] and 37.57g QE/ 100gm in leaves [25] than the present findings. Radical scavenging activity by FRAP exhibited 772.90, 1066.01 and 7303 mg TE/100 gm in the pulp, peel and leaves of the mango.

The earlier reported studies were found to have decreased radical scavenging activity by FRAP in pulp (118.66-211.27 µg/ml) [27] and in peel (5.56mg/g) [24] than the present study. Hence, our results showed that mango leaves had significantly the highest ($p \leq 0.05$) total phenol, flavonoid and FRAPcontent than the other elements of mango in the present study andsimilar consistent results were found in the previous study also [27]. The antioxidant activity of phenolics is due to the reactivity of phenol moiety (OH group on aromatic ring). They have the ability to scavenge free radicals via hydrogen donation or electron donation [30]. Other radical scavenging activities of the present study by DPPH showed the highest activity in mango peel 4375 mg TE/100gm and in ABTS it was found to be high in mango pulp 481.95 mg TE/100 gm.The present study had the highest DPPH activity among all the elements of mango than values reported by various researchers [23, 25, 26]. The total antioxidant activity of these elements of mango have been reported to be modulated by the level of maturity, cultivar type, agronomic practices, climatic conditions, ripeness at harvest, and the postharvest storage conditions of the fruit [28].

The enzymatic inhibitory effects of elements of mango methanolic extracts on alpha amylase and alpha glucosidase activity are depicted in **Table 2**.

Diet containing high content of alpha-amylase and alpha-glucosidase inhibitors is one of the key target areas to control postprandial glucose levels. These intestinal enzyme inhibitors decrease the rate of glucose absorption through delayed carbohydrate digestion and prolong digestion time. As synthetic inhibitors exhibit side effects, inhibitors from plant sources offer an attractive therapeutic approach [24].

Table 1: Total Phenol, Flavonoid, FRAP, DPPH and ABTS of the elements of mango.

ELEMENTS OF MANGO	TOTAL PHENOL (mg GAE/100 gm)	FLAVONOIDS (mg RE/100 gm)	FRAP (mg TE/100 gm)	DPPH (mg TE/100 gm)	ABTS (mg TE/100 gm)
Pulp	1360.40±154.29^{a}	420.55±19.66^{a}	772.90±19.28^{a}	1468.75±107.17^{b}	481.95±20.88^{c}
Peel	1953.27±154.20^{b}	445.28±44.50^{a}	1066.01±28.49^{a}	4375.98±71.71^{c}	267.44±10.08^{a}
Leaves	3394.46±46.46^{c}	2331.06±7.41^{b}	7303.25±675.15^{b}	300.76±49.05^{a}	396.79±16.18^{b}
F-Value	264.02*	5952.53*	357.25*	2776.64*	175.16*

Values are mean of ± S.D. of four observations. Mean value of different superscripts within a column are significantly different from each other ($p \leq 0.05$). GAE-Gallic acid equivalent, RE-Rutin equivalent, TE-Trolox equivalent.

Therefore, *in vitro* antidiabetic property of the methanolic extract was examined by determining the inhibition of alpha- amylase and alpha-glucosidase activities by different elements of mango. The percentage inhibition of alpha amylase enzyme was found to be 40.26% in pulp, 7.06% in peel and 5.97% in leaves respectively. The percentage inhibition of alpha glucosidase enzyme was found to be the highest in pulp 73.42%, lower in peel 28.66% and the lowest in leaves 12.78% respectively. Mango pulp showed significantly ($p<0.05$) the highest inhibition among both alpha amylase and alpha glucosidase *in vitro* enzymatic activity in **Table 2**. Methanolic extracts of the elements

of mango showed alpha amylase IC 50 value of 11.65 mg/ml in pulp, 109.30 mg/ml in peel and 71.83 mg /ml in leaves respectively. The alpha glucosidase IC 50 value of 54.15 µg/ml in pulp, 381.11 µg/ml in peel and 1552.47 µg/ml in leaves.These IC50 values obtained in the present study, for both alpha amylase and alpha glucosidase inhibition with all the elements of mango extract are much lower than some of the reported values [24, 29]. The highest alpha amylase and alpha glucosidase inhibition value for mango pulp found in the present study may be possibly due to the presence of mangiferin and other phenols, flavonoids and carotenoids like gallic, eallagic, protocatecuic acids, quercitin, rutin and ß-carotene as reported by Ajila et al., 2010 [31].
The anti-amylase activity (%) by disc assay as depicted in **Plate 1** was found to be 100% in all the elements of mango (pulp, peel and leaves) at 24mg concentration where all the methanolic extracts have completely inhibited alpha amylase and have shown no clear zone compared to acarbose (alpha- amylase inhibitor) which has shown 12.46% inhibition at 120 µgconcentration.

The early stage glycation products by NBT assay i.e. amadori products were found to be inhibited by different elements of mango

extracts ranging from 35 to 45 %, where mango pulp exhibited maximum inhibition **(Figure 2)**, while the protein alpha dicarbony

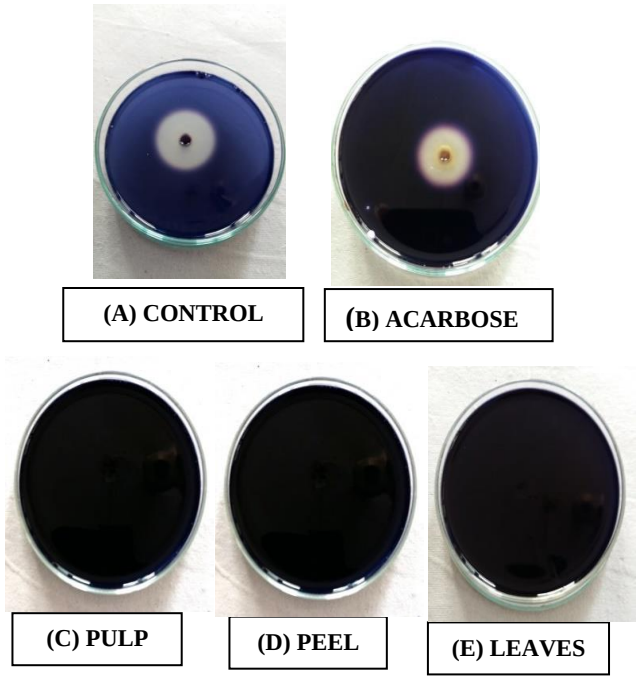

Plate 1: Alpha amylase inhibition by Disc Assay. The clear zone around the centre disc in (A) represents the area where starch has been degraded by a-amylase activity. (B) The clear zone around the centre disc represents area where starch has been degraded by Acarbose (120 µg) (C) Mango pulp, (D) Mango peel and (E) Mango leaves at 24 mgconcentration have inhibited amylase completely and show no clear zone.

Table 2: Elements of the Mango extracts with inhibitory effects on alpha amylase and alpha glucosidase activity

ELEMENTS OF MANGO	% alpha amylase inhibition	IC50 mg/ml alpha amylase inhibition	% alpha glucosidase inhibition	IC 50 µg/ml alpha glucosidase inhibition
Pulp	40.26±4.83^{b}	11.65	73.42±8.85^{b}	54.15
Peel	7.06±4.37^{a}	109.30	28.66±3.43^{a}	381.11
Leaves	5.97±1.72^{a}	71.83	12.78±3.00^{a}	1552.47
F-Value	4.83*		14.21*	

Values are mean of ± S.D. of four observations. Mean value of different superscripts within a column are significantly different from each other ($p \leq 0.05$)

compounds by Girad T assay, i.e. secondary stage markers was found to be inhibited upto 21–34 % and among the three elements in mango pulp extract it was maximally reduced. Fluorescence analysis of the later stage of glycation moieties-namely advanced glycationend products (AGEs) is also shown in Figure 2, suggested that all the elements of mango can inhibit these in the range of47 to 75 %. The values obtained in the present study, for AGE's inhibition with all the elements of mango extract are much lower than the reported values carried out by varied researchers [26].

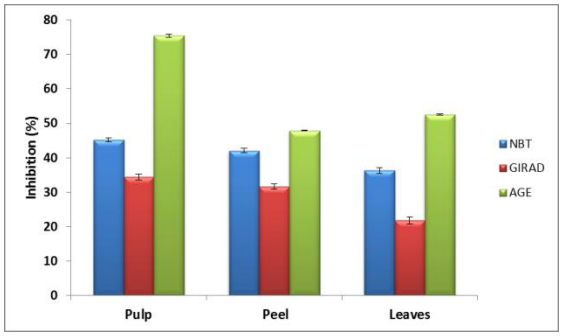

Figure 2: The effect of elements of mango methanolic extract on albumin glycation modification in terms of NBT assay, GIRAD T Assay and AGE's inhibition activity of pulp, peel and leaves of mango extract

Pearson's Correlation Coefficient (r) of various parameters was studied.The total phenolic content had a strong positive correlation with the flavonoid content (r =0.954, p≤0.01) and FRAP (r =0.955, p≤0.01). Total phenol content also had a negative and significant correlation with alpha glucosidase inhibition (r =-0.700, p≤0.05) and AGE's inhibition (r =-0.600, p≤0.05). The flavonoid content of all the elements of mango had a potent positive correlation withFRAP (r =0.993, p≤0.01) and a strong negative correlation with DPPH RSA (r =-0.713, p≤0.05). Flavonoid content also showed a negative and significant correlation with alpha glucosidase inhibition (r = - 0.622, p≤0.05).

Mangiferin and its derivatives i.e. phenolic acids, alkaloids, flavonoids, gallic acid, eallagic acid, rutin and other bioactive components are present in all the elements of mango. The most prominent one is the phenolic compoundmangiferin. Maniferin is being a potent phenolic compound maximally present in all the different elements of mango in varying amounts depending upon its different genotypes. It contains four (OH) groups at different positions and acts as a potential inhibitor for oxidants, glycation, alpha amylase and alpha glucosidase [32]. In the present study the total phenol and flavonoid content showed a negative relation with alpha amylase inhibition, alpha glucosidase inhibition and anti glycation activities. These results suggested that the high alpha amylase inhibition, alpha glucosidase inhibition and anti glycation activities of the different elements of mango could be due to non-phenolic bioactive compounds.

The obtained results are noteworthy not only because the phenolic and flavonoid of the extracts showed a positive relationship with the antioxidant activity, but not with the alpha amylaseinhibition assay, alpha glucosidase inhibition assay and antiglycation property.Many published studies have suggested that the phenolic and flavonoid compounds in plant extracts are responsible for the alpha amylase inhibition assay, alpha glucosidase inhibition assay and antiglycation property [26].

CONCLUSION

The results of the present study revealed that the pulp of mango had a better ability to ameliorate diabetes. It might also reduce secondary complications of diabetes as it also showed better antiglycation activity compared to the other two elements of mango. Hence, mango pulp could be used as a potential nutraceutical for diabetes.

ACKNOWLEDGMENT

The first author is thankful to the UGC- Meritorious BSR (Sanction no. 4-1/2006(BSR)/7-408/2012(BSR)), Government of India, New Delhi, for the award of a Senior Research Fellowship.

REFERENCES

[1] Puthucheary, S. D., & Nathan, S. A. (2008): Comparison of serum F2 isoprostane levels in diabetic patients and diabetic patients infected with Burkholderia pseudomallei. Singapore medical journal, **49(2):** 117.

[2] Wright, E., Scism-Bacon, J. L., & Glass, L. C. (2006): Oxidative stress in type 2 diabetes: the role of fasting and postprandial glycaemia. International journal of clinical practice, **60(3):** 308-314.

[3] Elosta, A., Ghous, T., & Ahmed, N. (2012): Natural products as anti-glycation agents: possible therapeutic potential for diabetic complications. Current diabetes reviews, **8(2):** 92-108.

[4] Schalkwijk, C. G., & Stehouwer, C. D. (2005): Vascular complications in diabetes

mellitus: the role of endothelial dysfunction. Clinical science, **109(2):** 143-159.

[5] Prathapan, A., Krishna, M. S., Nisha, V. M., Sundaresan, A., & Raghu, K. G. (2012): Polyphenol rich fruit pulp of Aegle marmelos (L.) Correa exhibits nutraceutical properties to down regulate diabetic complications—An in vitro study. Food research international, **48(2):** 690-695.

[6] Tamrakar, A. K., Jaiswala, N., Yadav, P. P., Maurya, R., & Srivastava, A. K. (2011): Pongamol from Pongamia pinnata stimulates glucose uptake by increasing surface GLUT4 level in skeletal muscle cells. Molecular and Cellular Endocrinology, **339:** 98–104.

[7] Bhat, M., Zinjarde, S. S., Bhargava, S. Y., Kumar, A. R., & Joshi, B. N. (2011): Antidiabetic Indian plants: A good source of potent amylase inhibitors. Evidence Based Complementary and Alternative Medicine, http://dx.doi.org/10.1093/ecam/nen040.

[8] Cheng, F. C., Shen, S. C., & Wu, J. S. (2009): Effect of guava (Psidium guajava L.) leaf extract on glucose uptake in rat hepatocytes. Journal of Food Science, **74:** 132–138.

[9] Abbasi, A. M., Guo, X., Fu, X., Zhou, L., Chen, Y., Zhu, Y., ... & Liu, R. H. (2015): Comparative assessment of phenolic content and in vitro antioxidant capacity in the pulp and peel of mango cultivars. International journal of molecular sciences, **16(6):** 13507-13527.

[10] Kaewnarin, K., Niamsup, H., Shank, L., & Rakariyatham, N. (2014): Antioxidant and antiglycation activities of some edible and medicinal plants. Chiang Mai J. Sci, **41(1):** 105-116.

[11] Gondi, M., & Rao, U. P. (2015): Ethanol extract of mango (Mangifera indica L.) peel inhibits α-amylase and α-glucosidase activities, and ameliorates diabetes related biochemical parameters in streptozotocin (STZ)-induced diabetic rats. Journal of food science and technology, **52(12):** 7883-7893.

[12] Singleton, V.L. & Rossi, J.A., Jr. (1965): Colorimetry of total phenolics with phosphomolybdic phosphotungstic acid reagents. American journal of Enology and Viticulture **16 (3):** 144-158.

[13] Zhishen Jia, Mengcheng Tang, Jianming Wu. (1999): The determination of flavonoid contents in mulberry and their scavenging effects on superoxide radicals. Journal of food Chemistry, **64**: 555-559.

[14] Benzie I and Strain J (1996): Ferric Radical Antioxidant Power Assay; Direct measures of total antioxidant activity of biological fluid and modified variation for simultaneous measurements of total antioxidant power and ascorbic acid concentration; Method in enzymology, **15**: 27.

[15] Brand-Williams, W., Cuvelier, M. E., & Berset, C. L. W. T. (1995): Use of a free radical method to evaluate antioxidant activity. LWT-Food science and Technology, **28(1):** 25-30.

[16] Re, R., Pellegrini, N., Proteggente, A., Pannala, A., Yang, M., & Rice-Evans, C. (1999): Antioxidant activity applying an improved ABTS radical cation decolorization assay. Free radical biology and medicine, **26(9):** 1231-1237.

[17] Picot, C., Subratty, A. H., & Mahomoodally, M. F. (2014): Inhibitory potential of five traditionally used native antidiabetic medicinal plants on α-amylase, α-glucosidase, glucose entrapment, and amylolysis kinetics in vitro. Advances in pharmacological sciences

[18] Correia, R. T., Mccue, P., Vattem, D. A., MAGALHÃES, M., Macedo, G. R., & Shetty, K. (2004): Amylase and Helicobacter pylori inhibition by phenolic extracts of pineapple wastes bioprocessed by Rhizopus oligosporus. Journal of food biochemistry, **28(5):** 419-434.

[19] Wang, T., Li, X., Zhou, B., Li, H., Zeng, J., & Gao, W. (2015): Anti-diabetic activity in type 2 diabetic mice and α-glucosidase inhibitory, antioxidant and anti-inflammatory potential of chemically profiled pear peel and pulp extracts (Pyrus spp.). Journal of Functional foods, **13**: 276-288.

[20] Tupe, R. S., Sankhe, N. M., Shaikh, S. A., Phatak, D. V., Parikh, J. U., Khaire, A. A., & Kemse, N. G. (2015): Aqueous extract of some indigenous medicinal plants inhibits glycation at multiple stages and protects erythrocytes from oxidative damage–an in vitro study. Journal of food science and technology, **52(4)**: 1911-1923.

[21] Baker, J. R., Metcalf, P. A., Johnson, R., Newman, D., & Rietz, P. (1985): Use of protein-based standards in automated colorimetric determinations of fructosamine in serum. Clinical chemistry, **31(9)**: 1550-1554.

[22] Wang, S. H., Chang, J. C., Pokkaew, R., Lee, J. F., & Chiou, R. Y. Y. (2011): Modified fast procedure for the detection and screening of antiglycative phytochemicals. Journal of agricultural and food chemistry, **59(13):** 6906-6912.

[23] Madalageri Deepa, Bharati P. C., Orsat V., Raghavan V. and Kage Udaykumar.(2015): Antioxidant Activity in Pulp and Peel of Three Mango Varieties. Journal of Horticultural Sciences, **10(2):** http://www.sphindia.org/index.php/jhs/article/view/14.

[24] Gondi Mahendranath & Rao Prasada U. J. S. (2015): Ethanol extract of mango (Mangifera indica L.) peel inhibits α-amylase and α-glucosidase activities, and ameliorates diabetes related biochemical parameters in streptozotocin (STZ)-induced diabetic rats. Journal of Food Science Technology, **52(12)**: 7883–7893.

[25] Fidrianny Irda, Rahmiyani Ira and Wirasutisna Ruslan Komar. (2013): Antioxidant Capacities From Various Leaves Extracts Of Four Varieties Mangoes Using DPPH, ABTS Assays And Correlation With Total Phenolic, Flavonoid, Carotenoid. International Journal of Pharmacy and Pharmaceutical Sciences, **5 (4):**189-194.

[26] Kaewnarin Khwanta, Niamsup Hataichanoke, Shank Lalida and Rakariyatham Nuansri. (2014): Antioxidant and Antiglycation Activities of Some Edible and Medicinal Plants. Chiang Mai Journal of Science, **41(1)**: 105-116.

[27] Kuganesan A., Thiripuranathar G., Navaratne A. N. and Paranagama P. A. (2017): Antioxidant and Anti-Inflammatory Activities of Peels, Pulps and Seed Kernels of Three Common Mango (Mangifera Indical L.) Varieties in Sri Lanka. International Journal of Pharmaceutical Sciences and Research, **8(1)**: 70-78.

[28] Nixwell, M. F., Johanna, M.,& Ngezimana, W. (2013): Effects of sulphur preservative on phytochemical and antioxidant capacity of peels of mango cultivars (Mangifera indica L.) produced in South Africa. African Journal of Biotechnology, **12 (41):** 6007.

[29] Bhuvaneshwari J, Salma Khanam, and Kshama Devi. (2014): In-vitro Enzyme Inhibition Studies for Antidiabetic Activity of Mature and Tender Leaves of Mangifera indica var. Totapuri. Research and Reviews: Journal of Microbiology and Biotechnology, **3 (3):** 36-41.

[30] Shahidi, F., & Wanasundara, P. K. J. P. D. (1992): Phenolic antioxidants.Critical Reviews in Food Science and Nutrition, **32**: 67–103.

[31] Ajila CM, Jaganmohan Rao L, Prasada Rao UJS. (2010): Characterization of bioactive compounds from raw and ripe Mangifera indica L. peel extracts. Journal of Food and Chemical Toxicology, **48:**3406–3411.

[32] Martin Masibo and Qian He. (2008): Major Mango Polyphenols and Their Potential Significance to Human Health. Comprehensive review in Food Science and Food Safety,**7**: 309-317.

PRAJÑĀ - **Journal of Pure and Applied Sciences Vol. 24 – 25 : 182 – 189 (2017)**
ISSN 0975 - 2595

IN VITRO ANTI-INFLAMMATORY, ANTIOXIDANT CAPACITY AND TOTAL PHENOLIC CONTENTS IN METHANOLIC EXTRACT FROM VEGETABLES

HINAL PATEL AND V.H.PATEL*

Laboratory of Foods and Nutrition, P. G. Department of Home Science, Sardar Patel University, Vallabh Vidyanagar-388120, Gujarat, India. Email: patelvh2004@yahoo.co.in

ABSTRACT

Anti-inflammatory and antioxidant activities are extensively used to screen chemopreventive foods. Four well-known vegetables bitter gourd, bottle gourd, drumstick leaves and ginger were assessed in this study. Total phenolics and flavonoid were estimated. The total antioxidant capacity was evaluated using FRAP; based on the scavenging ability of the cation radical DPPH RSA ABTS RSA and ORAC. Moreover, anti-inflammatory activity was determined based on the protein denaturation inhibition assay. The highest total phenolics and flavonoid content was observed in methanolic extract of drumstick leaves among four selected vegetables. Antioxidant capacity by FRAP was found to be highest in ginger, whereas scavenging activity by DPPH RSA and ABTS RSA was found to be high in drumstick leaves. The anti-inflammatory activity could be ranked based on the IC50 of the vegetables, as bitter gourd > ginger > bottle gourd > drumstick leaves. Additionally, a significant correlation existed between total phenolic content and antioxidant activity. This profound protective effect of vegetables may explain its extensive use in daily life and possible health benefits.

Key Words: In vitro anti-inflammation, protein denaturation, ORAC, Vegetables

INTRODUCTION

According to the World Health Organization, 46% of the global disease burden and 59% of global mortality are due to chronic diseases [1]. Inflammation has recently emerged as an important aspect of the pathophysiology of major chronic diseases of industrialized societies. Elevated plasma levels of inflammatory markers are risk factors, including obesity [2,3], insulin resistance, type 2 diabetes mellitus [4-6], metabolic syndrome [7] and many types of cardiovascular diseases [8,9].

Extensive research during the past two decades has revealed the mechanism by which continued oxidative stress can lead to chronic inflammation [10]. Inflammation is one of the manifestations of oxidative stress and the pathways that generate the mediators of inflammation, such as adhesion molecules and interleukins, are all induced by oxidative stress. Inflammation and oxidative stress are postulated to impair beta-cell function and exacerbate insulin resistance in type 2 diabetes [11] and often coexist in atherosclerosis and cardiovascular disease [12].

Anti-inflammatory agents, including nonsteroidal anti-inflammatory drugs (NSAID) are widely used in treating these disorders. However, many of them have dose-dependent side effects and none of them are suitable for primary prevention, which significantly limit their use. The World Health Organization (WHO) has estimated that 80% of the earth's inhabitants rely on traditional medicine for their primary health care needs and most of this therapy involves the use of plant extracts and their active components [13]. Epidemiological and experimental studies reveal a negative correlation between the consumption of diets rich in fruits and vegetables and the risks for chronic diseases [14-18]. These physiological functions of fruits and vegetables may be partly attributed by their abundance of phenolics including flavonoids and anthocyanins, and carotenoids [19-22]. Traditionally, deep colored fruits, vegetables or foods are recognized as more healthy to human body, especially in the oriental countries. There has been a growing interest in pigment components of fruits and vegetables, which may promote human health or lower the risk for disease [23]. Fruits and vegetables have had conferred the status of functional foods [24], they seem to be capable of delivering health benefits besides fulfilling physiological needs. Habitual consumption of fruits and vegetables confers significant benefits to human health [25]. *In vitro* studies as well as epidemiological data strongly suggest that foods containing phytochemicals with antioxidation and anti-inflammatory potential have strong protective effects against major disease risks including cancer and cardiovascular diseases [26-33]. In the present

study, the anti-inflammatory and anti-oxidant activity of different vegetables was evaluated by using a widely accepted model system.

MATERIALS AND METHODS

Vegetables and Sample Extraction: Plant parts of the four vegetables namely bitter gourd (*Momordica charantia*), bottle gourd (*Lagenaria siceraria*), ginger (*Zingiber officinale*) and drumstick leaves (*Moringa oleifera*) were purchased from the local market of Anand. About 2.0 g of plant material was extracted in 50 ml of acidified methanol at room temperature. The whole extracts were filtered, and used for further assays.

Determination of total phenolic and flavonoid content: Total phenolic content of extract was determined using Folin-Ciocalteu method [34]. Gallic acid was taken as standard and results were expressed as mg of GA equivalent per 100 g of sample. Flavonoid content was estimated using aluminium chloride colorimetric method using rutin as a standard [35] and the absorbance was read at 510 nm. Results were expressed as mg of rutin equivalent per 100 g of sample.

Ferric reducing antioxidant power assay (FRAP): The measure of FRAP of the methanolic extract was carried out by the method given by Benzie and Strain [36]. Results were expressed as mg Trolox Equivalent Antioxidant Capacity per 100 g of sample.

Scavenging effect on DPPH Radicals: The scavenging effects of methanolic extract from vegetables on DPPH were measured according to the method of Brand-Williams [37]. The extract was added to the methanolic solution of 2,2-Diphenyl-1-picryl-hydrazyl (DPPH) and absorbance was recorded at 517 nm. Results were expressed in terms of mg of Trolox Equivalent Antioxidant Capacity per 100 g of sample.

Scavenging effect on ABTS Radicals: The scavenging effects of methanolic extracts on ABTS were estimated using the modified method of Re et al [38]. Percentage inhibition was calculated and the results were expressed in terms of TEAC per 100 g of sample.

Oxygen radical absorbance capacity (ORAC): The ORAC assay is based upon the inhibition of the peroxyl-radical-induced oxidation initiated by thermal decomposition of azo compounds. Modified method of Ou et al [39] was used for the estimation. The final values were calculated using the area under the curve and results were expressed as trolox equivalents in micromole per gm.

***In vitro* anti-inflammatory effects on protein denaturation inhibition assay:** Protein denaturation inhibition assay was done by the reported protocol with minor modifications [40]. The methanolic extracts with different concentration were treated with bovine albumin; turbidity was measured spectophotometrically at 660 nm. Diclofenac sodium was taken as standard and percent inhibition of protein denaturation was calculated.

Statistical Analysis: Each experiment was performed in duplicate and expressed as mean±SD. Statistical analyses were performed using SPSS 20. Analyses of variance were performed using ANOVA. Significant difference (p<0.05) between the means were determined using Duncan's test. Pearson's correlation was calculated to study the relationship. Results were also subjected to multivariate data analysis by means of principal component analysis using SPSS 20.

RESULTS AND DISCUSSION

Fruits and vegetables are rich sources of antioxidants such as vitamin C, tocopherol, phenolics and β-carotene which contribute to their antioxidant or free radical or scavenging effects. Amongst these, phenolics serve as powerful antioxidants by virtue of the hydrogen-donating properties of their phenolic hydroxyl groups, as well as by donating electrons to stop free radical chain reactions emerging from oxidative stress [41].

Phenolic compounds are important contributors to functional quality and have an important role to play in counteracting reactive oxygen species (ROS) and thereby minimizing molecular damage [42]. Total phenolic content was found to vary significantly (p<0.05)

among vegetables and ranged from 52.41 to 372.82 mg GAE/100g depicting almost seven-fold variations (Figure 1). The hierarchy was bottle gourd<bitter gourd<ginger<drumstick leaves. The role of phenolics as natural antioxidants has attracted considerable interest due to their pharmacological functions. Increased consumption of phenolic compounds has been associated with the reduced risk of cardiovascular diseases and certain cancers [43-45]. Budrat [46] found 4.99 mg GAE/ gm of total phenolics content in bitter gourd by soxhlet extraction method. Le et al [47] found that aquous extract of drumstick leaves contains higher total phenolics content (105.04 mg gallic acid equivalents (GAE)/g), total flavonoids content (31.28 mg quercetin equivalents (QE)/g) and showed better antioxidant activity (85.77%).

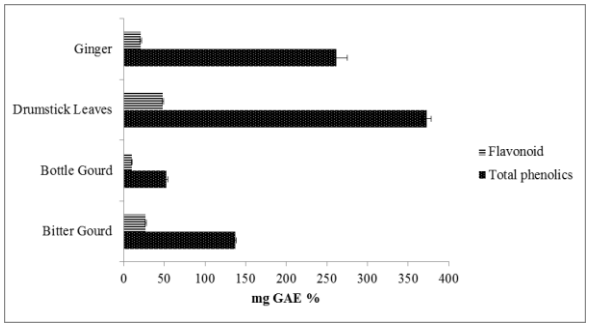

Values are mean ± SD; n=4. Total phenolics content in mg gallic acid equivalent per 100 g; Flavonoid content in mg rutin equivalent per 100 g.

Figure 1: Total phenolics and Flavonoid content of the methanolic extract of vegetables.

The content of flavonoids also varied significantly (p<0.05) and ranged between 10.02 to 48.56 mg RT/ 100g (Figure 1). The content in increasing order was: bottle gourd<ginger<bitter gourd< drumstick leaves. Flavonoids have been reported to have beneficial health effects including anti-inflammatory, inhibition of platelet aggregation and inhibition of mast cell histamine release [47].

Table 1 shows the antioxidant capacity of the vegetables. Results showed that bottle gourd had the lowest antioxidant capacity measured by four different methods compared to other vegetables. Ginger had the highest ferric reducing antioxidant capacity compared to other vegetables. Drumstick leaves showed the highest scavenging activity on DPPH and ABTS among the studied vegetables. The hierarchy for ORAC was: bottle gourd<ginger<bitter gourd<drumstick leaves. Data obtained by Sreelatha [48] suggested that the extracts of drumstick leaves both mature and tender have potent antioxidant activity against free radicals. Water, aqueous methanol, and aqueous ethanol extracts of freeze-dried leaves of *Moringa oleifera* were examined for radical scavenging capacities and antioxidant activities by Siddhuraju [49]. They concluded that both methanol (80%) and ethanol (70%) were found to be the best solvents for the extraction of antioxidant compounds from drumstick leaves.

A correlation was observed between total phenolic content and flavonoid (r = 0.855), FRAP (r = 0.764), DPPH RSA (r = 0.997), ABTS RSA (r = 0.991) and ORAC (r = 0.593) in the selected vegetables. The results revealed that flavonoid content in the selected vegetables significantly (p<0.05) correlated with DPPH RSA (r = 0.879), ABTS RSA (r = 0.828) and ORAC (r = 0.807) (Table 2).

Table 1: Total Antioxidant Capacity by FRAP, DPPH RSA, ABTS RSA and ORAC of selected vegetables

	FRAP	DPPH RSA	ABTS RSA	ORAC
	(mg TE/100gm)			(micromole/gm)
Bitter Gourd	173.66±10.47^{b}	454.17±37.80^{b}	249.26±26.09^{b}	54.45±7.23^{c}
Bottle Gourd	65.89±10.76^{a}	173.33±7.22^{a}	39.20±3.22^{a}	28.54±5.86^{a}
Drumstick Leaves	764.31±33.39^{c}	1236.00±25.99^{d}	896.19±79.31^{d}	55.76±1.84^{c}
Ginger	1216.12±41.47^{d}	838.68±32.37^{c}	624.92±15.55^{c}	40.49±0.25^{b}
F-Value	1508.36*	1068.48*	323.90*	29.39*

Values are mean ± SD; n=4. Different alphabets within column are significantly different (p≤0.05) from each other. ORAC, oxygen radical absorbance capacity; FRAP, ferric reducing antioxidant power assay; DPPH RSA, DPPH radical scavenging activity; ABTS RSA, ABTS radical scavenging activity; TE, trolox equivalent.

Table 2: Correlation between total phenolics, flavonoid and total antioxidant capacity of methanolic extracts of selected vegetables

	TP	Flavonoid	FRAP	DPPH RSA	ABTS RSA
Flavonoid	0.855**				
FRAP	0.764**	0.336			
DPPH RSA	0.997**	0.869**	0.743**		
ABTS RSA	0.991**	0.828**	0.787**	0.986**	
ORAC	0.593*	0.807**	0.166	0.604*	0.558*

**Correlation is significant at the 0.01 level (2-tailed). *Correlation is significant at the 0.05 level (2-tailed). TP, total phenolics; FRAP, ferric reducing antioxidant power assay; DPPH RSA, DPPH radical scavenging activity; ABTS RSA, ABTS radical scavenging activity.

However, FRAP content in the selected vegetables did not significantly correlate with flavonoid (r = 0.336) and ORAC (r =0.166) respectively. FRAP, ORAC and ABTS do not measure the same antioxidant phenomenon [50]. For example, FRAP is sensitive to single electron transfers while ORAC, to hydrogen atom transfer. The ABTS radical is thought to be sensitive to both single electron and hydrogen atom transfer. In effect, these three methods operate on different reaction mechanisms, accounting for the observation that they are not correlated with each other.

The percent inhibition and IC_{50} value of protein denaturation for vegetables were analyzed graphically and presented in figure 2 and table 3. The ability to inhibit protein denaturation by vegetables was displayed in the order of bitter gourd>ginger>bottle gourd>drumstick leaves. The lowest IC 50 value was observed for bitter gourd suggested the highest anti-inflammatory activity. Studies on different models revealed the same results as found in this study [51-53]. Juice of bottle gourd showed anti-inflamamtory activity against acute inflammatory models of paw edema [54,55]. Sulaiman [56] had evaluated *Moringa oleifera* aqueous extract for anti-inflammatory activity and they concluded that the aqueous extract of drumstick leaves exhibited significant anti-inflammatory activity in a dose dependent manner.

Principal component analysis is a variable reduction procedure and to develop a smaller number of artificial variables that will account for most of the variance in the observed variables. PCA was performed on the significant factor loading values, higher than or equal to 0.7 were used to identify the most important variables and attributes in each dimension, or principal components (PCs). First two PCs explained approximately 95.82% of total data variability, called PC1 (51.84%) and PC2 (43.98%) (Figure 3). In general, antioxidant capacity measured by FRAP, DPPH RSA and ABTS RSA located in the right hand of the component plot between attribute vectors indicate higher predictable capacity.

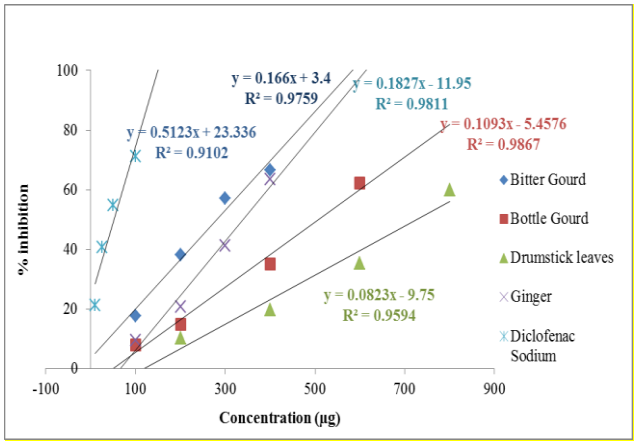

Figure 2: Anti-inflammatory activity of vegetables by protein denaturation inhibition assay

Table 3: Anti-inflammatory activity (% inhibition and IC_{50} value) of selected vegetables

Extracts	Concentration (µg)	% inhibition	IC_{50} (µg/ml)
Bitter Gourd	400	66.6	280.72
Bottle Gourd	400	35.1	507.31
Drumstick Leaves	400	19.8	726.00
Ginger	400	63.5	340.38
Diclofenac sodium	50	54.91	50.06

Values are mean ± SD; n=4.

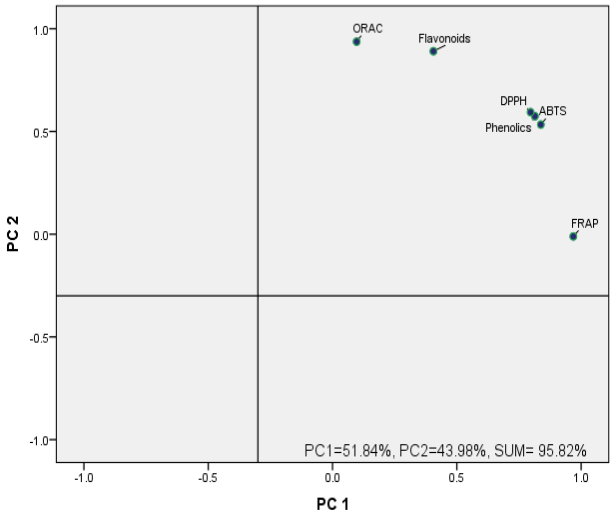

Figure 3: Principal component analysis (PCA) scatterplot obtained from the total phenolics, flavonoid and total antioxidant capacity by FRAP DPPH RSA, ABTS RSA and ORAC

CONCLUSION

In conclusion, this study found wide diversity in the phenolic, flavonoid content and antioxidant capacities in the selected vegetables. The methanolic extracts of vegetables exhibited anti-inflammatory activity which may possibly be due to the presence of phenolic compounds. The findings of the present study suggested that the extracts from several vegetables were found to possess strong antioxidant activity and scavenging effects on free radicals, that would have great importance as therapeutic agents in preventing or slowing the process of reactive oxygen species and associated oxidative stress related degenerative diseases. Hence it is recommended that the consumption of vegetables should be increased in the diet of human beings.

ACKNOWLEDGEMENT

This research work was supported by the Department of Science and Technology (DST)-INSPIRE fellowship (IF130975), New Delhi awarded to the first author.

REFERENCE

[1] Bengmark, S. (2006) : Impact of nutrition on ageing and disease. Current Opinion in Clinical *Nutrition & Metabolic Care*, **9(1):** 2-7.

[2] Ramos, E. J., Xu, Y., Romanova, I., Middleton, F., Chen, C., Quinn, R., ... & Meguid, M. M. (2003): Is obesity an inflammatory disease?. *Surgery*, **134(2):** 329-335.

[3] Williams, K.J., & Tabas,I. (2002): Atherosclerosis and inflammation. Science, **297(5581):** 521-522.

[4] Paresh, D., Ahmad, A., Ajay,C., Priya, M., & Rajesh, G. (2005): Metabolic syndrome:A comprehensive perspective based on interactions between obesity, diabetes, and inflammation. *Circulation*, **111:** 1448-1454.

[5] Hanada, T., & Yoshimura, A. (2002): Regulation of cytokine signaling and inflammation. *Cytokine & growth factor reviews*, **13(4):** 413-421.

[6] Makarov, S.S. (2000): NF- κB as a therapeutic target in chronic inflammation:recent advances. *Molecular medicine today*, **6(11):** 441-448.

[7] Panagiotakos, D.B., Pitsavos, C., Yannakoulia, M., Chrysohoou, C., & Stefanadis, C. (2005): The implication of obesity and central fat on markers of chronic inflammation: the ATTICA study. *Atherosclerosis*, **183(2):** 308–315.

[8] Theuma, P., Fonseca, VA. (2003): Inflammation and emerging risk factors in diabetes mellitus and atherosclerosis. *Current diabetes reports*, **3(3):** 248–254.

[9] Strzelecka, M., Bzowska, M., Koziel, J., Szuba, B., Dubiel, O., Heinrich, M., & Bereta, J. (2005): Anti-inflammatory effects of extracts from some traditional Mediterranean diet plants. *Journal of Physiology and Pharmacology.* Supplement, **56(1):** 139-156.

[10] Evans, J.L., Goldfine, I.D., Maddux, B.A., & Grodsky, G.M. (2002): Oxidative stress amd stress activated signalling pathways: a unigying hypothesis of type-2 diabetes, *Endocrine Reviews*, **23(5):** 599-622.

[11] Wellen, K.E. & Hotamisligil, G.S. (2005): Inflammation, stress, and diabetes. *Journal of Clinical Investigation*, **115(5)**: 1111-1119.

[12] Strocker, R. & Keaney, J.F. (2004): Role of oxidative modifications in atherosclerosis. *Physiological Reviews*, **84(4):** 1381-1478.

[13] Krishnaiah, D., Sarbatly, R., & Nithyanandam, R. (2011): A review of the antioxidant potential of medicinal plant

species. *Food and bioproducts processing*, ***89*(3):** 217-233.

[14] Chen, C. C., Liu, L. K., Hsu, J. D., Huang, H. P., Yang, M. Y., & Wang, C. J. (2005): Mulberry extract inhibits the development of atherosclerosis in cholesterol-fed rabbits. *Food chemistry*, ***91*(4)**: 601-607.

[15] Middleton, E., Kandaswami, C., & Theoharides, T. C. (2000): The effects of plant flavonoids on mammalian cells: implications for inflammation, heart disease, and cancer. *Pharmacological reviews*, ***52*(4)**: 673-751.

[16] Prior, R. L. (2003): Fruits and vegetables in the prevention of cellular oxidative damage. *The American journal of clinical nutrition*, ***78*(3):** 570S-578S.

[17] Saleem, A., Husheem, M., Härkönen, P., & Pihlaja, K. (2002): Inhibition of cancer cell growth by crude extract and the phenolics of Terminalia chebula retz. fruit. *Journal of Ethnopharmacology*, ***81*(3):** 327-336.

[18] Zhang, Y., Vareed, S. K., & Nair, M. G. (2005): Human tumor cell growth inhibition by nontoxic anthocyanidins, the pigments in fruits and vegetables. *Life sciences*, ***76*(13)**: 1465-1472.

[19] Cieslik, E., Gręda, A., & Adamus, W. (2006): Contents of polyphenols in fruit and vegetables. *Food chemistry*, ***94*(1)**: 135-142.

[20] Qian, J. Y., Liu, D., & Huang, A. G. (2004): The efficiency of flavonoids in polar extracts of Lycium chinense Mill fruits as free radical scavenger. *Food Chemistry*, ***87*(2)**: 283-288.

[21] Sass-Kiss, A., Kiss, J., Milotay, P., Kerek, M. M., & Toth-Markus, M. (2005): Differences in anthocyanin and carotenoid content of fruits and vegetables. *Food Research International*, ***38*(8)**: 1023-1029.

[22] Trappey, A., Bawadi, H. A., Bansode, R. R., & Losso, J. N. (2005): Anthocyanin profile of mayhaw (Cretaegus opaca). *Food Chemistry*, ***91*(4)**: 665-671.

[23] Lin, J. Y., & Tang, C. Y. (2007): Determination of total phenolic and flavonoid contents in selected fruits and vegetables, as well as their stimulatory effects on mouse splenocyte proliferation. *Food chemistry*, ***101*(1):** 140-147.

[24] Hasler, C. M. (1998): Functional foods: their role in disease prevention and health promotion. *Food technology-champaign then chicago-*, ***52***: 63-147.

[25] Steinmetz, K. A., & Potter, J. D. (1996). Vegetables, fruit, and cancer prevention: a review. *Journal of the American Dietetic Association*, ***96*(10)**: 1027-1039.

[26] Steinberg, D. (1991): Antioxidants and atherosclerosis. A current assessment. *Circulation*, ***84***: 1420-1425.

[27] Block, G., Patterson, B., & Subar, A. (1992): Fruit, vegetables, and cancer prevention: a review of the epidemiological evidence. *Nutrition and cancer*, ***18*(1)**: 1-29.

[28] Ames, B. N., Shigenaga, M. K., & Hagen, T. M. (1993): Oxidants, antioxidants, and the degenerative diseases of aging. *Proceedings of the National Academy of Sciences*, ***90*(17)**: 7915-7922.

[29] Hertog, M. G., Feskens, E. J., Kromhout, D., Hollman, P. C. H., & Katan, M. B. (1993): Dietary antioxidant flavonoids and risk of coronary heart disease: the Zutphen Elderly Study. *The Lancet*, ***342*(8878)**: 1007-1011.

[30] Byers, T., & Guerrero, N. (1995): Epidemiologic evidence for vitamin C and vitamin E in cancer prevention. *The American journal of clinical nutrition*, ***62*(6)**: 1385S-1392S.

[31] Knekt, P., Järvinen, R., Seppänen, R., Heliövaara, M., Teppo, L., Pukkala, E., & Aromaa, A. (1997). Dietary flavonoids and the risk of lung cancer and other malignant neoplasms. *American journal of epidemiology*, ***146*(3)**: 223-230.

[32] Elliott, J. G. (1999): Application of antioxidant vitamins in foods and beverages: Developing nutraceuticals for the new millenium. *Food Technology*, ***53*(2)**: 46-48.

[33] Kaur, C., & Kapoor, H. C. (2001). Antioxidants in fruits and vegetables–the millennium's health. *International journal of food science & technology*, ***36*(7)**: 703-725.

[34] Singleton, V. L., Orthofer, R., & Lamuela-Raventós, R. M. (1999): [14] Analysis of total phenols and other oxidation substrates and antioxidants by means of folin-ciocalteu reagent. *Methods in enzymology*, ***299:*** 152-178.

[35] Zhishen, J., Mengcheng, T., & Jianming, W. (1999): The determination of flavonoid contents in mulberry and their scavenging

effects on superoxide radicals. *Food chemistry*, ***64*(4)**: 555-559.

[36] Benzie, I. F., & Strain, J. J. (1999): [2] Ferric reducing/antioxidant power assay: Direct measure of total antioxidant activity of biological fluids and modified version for simultaneous measurement of total antioxidant power and ascorbic acid concentration. *Methods in enzymology*, ***299****:* 15-27.

[37] Brand-Williams, W., Cuvelier, M. E., & Berset, C. L. W. T. (1995): Use of a free radical method to evaluate antioxidant activity. *LWT-Food science and Technology*, ***28*(1)**: 25-30.

[38] Re, R., Pellegrini, N., Proteggente, A., Pannala, A., Yang, M., & Rice-Evans, C. (1999): Antioxidant activity applying an improved ABTS radical cation decolorization assay. *Free radical biology and medicine*, ***26*(9)**: 1231-1237.

[39] Ou, B., Hampsch-Woodill, M., & Prior, R. L. (2001): Development and validation of an improved oxygen radical absorbance capacity assay using fluorescein as the fluorescent probe. *Journal of agricultural and food chemistry*, ***49*(10)**: 4619-4626.

[40] Mizushima, Y., & Kobayashi, M. (1968): Interaction of anti-inflammatory drugs with serum proteins, especially with some biologically active proteins. *Journal of Pharmacy and Pharmacology*, ***20*(3)**: 169-173.

[41] John, J. A., & Shahidi, F. (2010): Phenolic compounds and antioxidant activity of Brazil nut (Bertholletia excelsa). *Journal of Functional Foods*, ***2*(3)**: 196-209.

[42] Koley, T. K., Kaur, C., Nagal, S., Walia, S., & Jaggi, S. (2011): Antioxidant activity and phenolic content in genotypes of Indian jujube (Zizyphus mauritiana Lamk.). *Arabian Journal of Chemistry*.

[43] Liu, R. H. (2004): Potential synergy of phytochemicals in cancer prevention: mechanism of action. *The Journal of nutrition*, ***134*(12)**: 3479S-3485S.

[44] Liu, R. H. (2007): Whole grain phytochemicals and health. *Journal of Cereal Science*, ***46*(3)**: 207-219.

[45] Dykes, L., & Rooney, L. W. (2007): Phenolic compounds in cereal grains and their health benefits. *Cereal foods world*, ***52*(3)**: 105-111.

[46] Budrat, P., & Shotipruk, A. (2008): Extraction of phenolic compounds from fruits of bitter melon (Momordica charantia) with subcritical water extraction and antioxidant activities of these extracts. *Chiang Mai J Sci*, ***13***: 123-130.

[47] Le Marchand, L. (2002): Cancer preventive effects of flavonoids—a review. *Biomedicine & pharmacotherapy*, ***56*(6)**: 296-301.

[48] Sreelatha, S., & Padma, P. R. (2009): Antioxidant activity and total phenolic content of Moringa oleifera leaves in two stages of maturity. *Plant foods for human nutrition*, ***64*(4)**: 303.

[49] Siddhuraju, P., & Becker, K. (2003): Antioxidant properties of various solvent extracts of total phenolic constituents from three different agroclimatic origins of drumstick tree (*moringa oleifera* lam.) leaves. *J. Agric. Food Chem*, ***51****:* 2144-2155.

[50] Huang, D., Ou, B., & Prior, R. L. (2005): The chemistry behind antioxidant capacity assays. *Journal of Agricultural and Food Chemistry*, **53**: 1841–1856.

[51] Umukoro, S., & Ashorobi, R. B. (2006): Evaluation of anti-inflammatory and membrane stabilizing property of aqueous leaf extract of Momordica charantia in rats. *African Journal of Biomedical Research*, ***9*(2)**: 119-124.

[52] Lin, W. C., & Lin, J. Y. (2010): Five bitter compounds display different anti-inflammatory effects through modulating cytokine secretion using mouse primary splenocytes in vitro. *Journal of agricultural and food chemistry*, ***59*(1)**: 184-192.

[53] Kobori, M., Nakayama, H., Fukushima, K., Ohnishi-Kameyama, M., Ono, H., Fukushima, T., ... & Deguchi, T. (2008): Bitter gourd suppresses lipopolysaccharide-induced inflammatory responses. *Journal of agricultural and food chemistry*, ***56*(11)**: 4004-4011.

[54] Milind, P., & Kaur, S. (2011): Is bottle gourd a natural guard. *Int Res J Pharm*, *2*(6): 13-17.

[55] Ghule, B. V., Ghante, M. H., Upaganlawar, A. B., & Yeole, P. G. (2006): Analgesic and anti-inflammatory activities of Lagenaria siceraria Stand. fruit juice extract in rats and mice. *Pharmacognosy magazine*, ***2*(8)**: 232.

[56] Sulaiman, M. R., Zakaria, Z. A., Bujarimin, A. S., Somchit, M. N., Israf, D. A., & Moin, S. (2008): Evaluation of Moringa oleifera aqueous extract for antinociceptive and anti-inflammatory activities in animal models. *Pharmaceutical biology*, ***46*(12)**: 838-845.

PRAJÑĀ - **Journal of Pure and Applied Sciences Vol. 24 – 25 : 190 – 194 (2017)**
ISSN 0975 - 2595

USE OF DPPH RSA TEST TO EVALUATE THE LIPID OXIDATION IN COTTON SEED OIL DURING FRYING OF FOOD PRODUCT- BESAN SEV

V.H.PATEL*

P. G. Department of Home Science, Sardar Patel University, Vallabh Vidyanagar-388120, Gujarat, India
Email: patelvh2004@yahoo.co.in

ABSTRACT

This research was carried out to study the possibility of using 2,2-diphenyl-1-picrylhydrazyl radical (DPPH RSA) test to measure the lipid oxidation events during frying. To full-fill this objective, besan sev was fried in cotton seed oil continuously for 10 hours at 180 ºC and the oil sample was collected at 2.0 hour interval. These oil samples were measured for their Peroxide value (PV), p-anisidine value (P-AV), totox value, thiobarbituric acid (TBA) test and DPPH RSA. The results showed that the decrease of the DPPH RSA was well correlated with the increase of the PV for cotton seed oil heated at 180°C (R^2 = 0.882). The DPPH RSA was negatively correlated with P-AV (R^2 = 0.869), totox value (R^2 = 0.872) and TBA test (R^2 = 0.926). From the results, it is concluded that the monitoring DPPH RSA absorbance in cotton seed oil could be useful indicator/test for measuring lipid oxidation in cotton seed oil during frying of high moisture food.

Keywords: DPPH RSA, lipid oxidation, cotton seed oil and frying

INTRODUCTION

Frying is the most popular and accepted method of cooking at home as well as at industrial level. It improves the overall sensory score of the food by increasing the flavor, crispiness and taste; moreover it also extends the self-life of food products by decreasing the moisture content during frying. During frying, oil is subjected to various chemical changes like hydrolysis, oxidation and polymerization that result in quality deterioration with respect to sensory quality and nutritive value [1]. In addition, frying also produced some unwanted compounds affecting human health. These unwanted compounds are probably nonvolatile and are produced due to oxidation and polymerization of unsaturated fatty acid [2,3].

As frying method decreases the quality of oil in respect of both food quality and human health, evaluation at lipid oxidation is very important.

At present several methods of evaluation of lipid oxidation in oil are in use. These methods are PV, Acid value, P-AV, totox value, iodine value, TBA test, conjugated dines and trines. Of all these

methods, peroxide value measures the primary oxidized product namely hydroperoxides whereas, P-AV and TBA test measures the secondary oxidation products-aldehydes. The peroxide value, P-AV and TBA test are most in use to measure lipid oxidation in oils as well as in food products.

The DPPH RSA is a test which is used to measure the total antioxidant capacity of foods of pure antioxidant compounds [4]. Recently, this method is used for the evaluation of lipid oxidation and antioxidant effectiveness of free radical scavengers in oils [5]. Yeo et al, [6] and Van et al, [7] also used DPPH radical method to measure lipid oxidation in thermally-oxidized oil.

The utilization of cotton seed oil in human consumption received attention in our country in meeting the shortage of edible oil [8]. Cotton seed oil is most popular cooking oil in the Gujarat state at house hold level as well as industrial level considering its cost compared to ground nut oil. In India, potato chips, besan sev in different sizes and taste are the two most fried food products gain industrial importance. Considering above the objective of the present study was to test the DPPH RSA as a simple test for evaluation of lipid oxidation in cotton seed oil used for frying of besan sev.

MATERIALS AND METHODS

Sample preparation and treatment: 3.0 kg of gram flour or besan (Uttam brand) was purchased from the local market of vallabh Vidyanagar-Gujarat. It was sieved in big steel plate and to this 1650 ml water and containing 90.0 gm of salt was added and made fine soft dough. The hand machine for sev making was

filled with the dough. At the same time 10.0 kg of cottonseed oil was filled up in thermostat control fryer and was switched on to raise the temperature at 180 ºC. Once temperature obtained at 180 ºC, frying of besan sev was started. One batch of besan sev was fried for 6 minutes. A total 10 batches were fried at every one hour and frying was carried out up to 10 hours. During frying, at every two hours, oil samples were collected, cooled and were stored at -20 ºC till the analysis.

Determination of DPPH RSA: The DPPH RSA was determined by the method given by Brand et al, [4]. As oil does not dissolve completely in methanol, butanol was used instead.

Physicochemical analysis: Duplicate determinations of the peroxide value [9], *p*-anisidine value [10], Thiobarbituric acid value [11] of oil samples were done. Totox value was calculated using the standard formula.

Statistical analysis: The results from the assays of oxidized sample were analyzed statistically by analysis of variance (ANOVA) using Duncan's multiple range test and Pearson's correlation using SPSS 20 software program. A p value <0.05 was considered as significant.

RESULTS AND DISCUSSION

Peroxide value is conventionally used as a measure of oxidative deterioration of oil, fat and fatty foods. It is usually presented in milli equivalent of oxygen per kg of fat [9]. It measures the peroxides formed during oxidation of fat. Peroxides are important intermediates of oxidative reactions in oils and fats because they decompose under the influence of transition metals, irradiation and elevated temperature to form free radicals. The classical method for quantification of hydroperoxides thus formed is the determination of PV. The results for DPPH RSA and PV of cotton seed oil heated at 180°C are shown in figure 1. The mean peroxide value of cotton seed oil increased significantly ($p<0.05$) in response to different frying times. It was increased about three times at the end of 10 h of frying period.

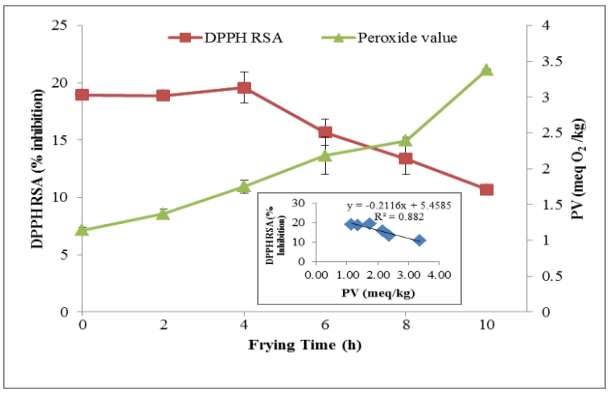

Figure 1: The PV and DPPH RSA of cotton seed oil heated at 180 °C during frying of besan sev. The relationship between PV and DPPH RSA is inserted.

Similar types of results are reported by various researchers. The increase in PV suggested that free radicals are accepted by PUFA present in cotton seed oil and lead to formation of hydroperoxide. The relationship between PV and DPPH RSA is shown in figure 1. The figure demonstrated that the DPPH RSA decreased at around the same time as primary oxidation products were formed. A reduction of DPPH RSA with the regression equation of $Y= -0.2116x+ 5.4585$ ($R^2 = 0.882$) with the PV. The PV was increased constantly till the 8h of frying time and was increased sharply between 8 to 10 h of frying. The similar types of results were reported in soybean oil at 110 °C by Van et al, [7]. The reduction in DPPH RSA could be due to the loss in naturally occurring antioxidants like phenolic compounds and α-tocopherol present in cotton seed oil. Andrikopoulos et al, [12] reported that the retention of α and (β + γ) - tocopherols was decrease as the frying period increased in virgin olive oil. They reported the complete loss of (β + γ) - tocopherols after sixth frying of potato chips in sunflower oil. They also reported the deterioration of phenolic compounds during the frying. Tannic acid, oleuropein and hydroxytyrosol-elenolic acid dialdeydic form showed remarkable resistance in all frying sessions in both frying methods (deep frying and pan frying), while hydroxytyrosol and hydroxytyrosol-elenolic acid were eliminated faster.

When hydroperoxides break down, they produce volatile alhehydes like hexanal, leaving behind a non-volatile portion of the fatty acid that remains as a part of the

glyceride molecule. This non-volatile reaction product can be measured by reaction with anisidine. High anisidine values are an indication that a fat has been oxidized even when TBA and other aldehydes tests give low results because volatile aldehydes, may incidentally or intentionally be removed during processing. Anisidine value is defined as 100 times the absorbance (at 350 mm) of a solution resulting from reaction of 1 g of fat in 100 ml of solvent.

The mean values of P-AV of cotton seed oil at varying frying time interval and its relation with DPPH RSA is shown in figure 2, The P-AV was 33.95 of fresh oil and was increased significantly ($p<0.05$) about approximately 4 times at the end of 10 h of frying time. The increased P-AV during frying was reported by Lee et al, [13] in palm oil and soybean oil. The DPPH RSA value decreased at the same time when secondary oxidized products were formed. A reduction of DPPH RSA was seen with the regression equation of $Y= -8.6215x+ 212.91$ with $R^2= 0.869$. There was a sharp increase in P-AV after two hours of frying and there after increase steadily till the 10 h of frying period. The DPPH RSA was reduced sharply after four hours of frying. These results revealed that the cotton seed oil contain enough antioxidants which can neutralized the free radicals produced in response of frying of high moisture food that is besan sev in oil up to four hour of frying.

Hydroperoxides are only transitory intermediates and decompose into various carbonyl and other compounds. Although a properly conducted peroxide value determination is a good guide to fat quality, oxidized oil can be reprocessed to give a deceptively low peroxide value. In such cases, the presence of secondary products plus lower level of antioxidant present will enable further rapid oxidation to occur. For this reason it is preferable not to rely solely upon peroxide values as an index of oil quality, but undertake an anisidine test in addition, such as "Totox" determination is very useful in the detection of oxidation of lipid. An expression termed the totox or oxidation value (OV), which is equivalent to 2x peroxide value + anisidine value, has been suggested for the assessment of oxidation in oils.

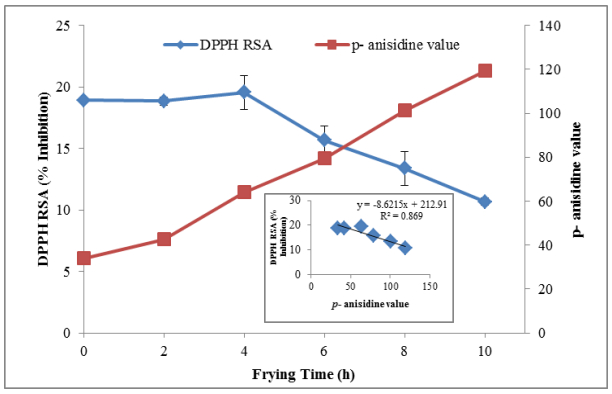

Figure 2: The P-AV and DPPH RSA of cotton seed oil heated at 180 °C during frying of besan sev.

The mean values of totox value of cotton seed oil at varying frying time interval and its relation with DPPH RSA is shown in figure 3, the totox value of fresh oil was 36.24 and it increased significantly to 126.16 after 10 hours of frying. The relationship between DPPH RSA and totox value is expressed in figure 3. This relation suggested the increase of totox value and decrease in DPPH RSA after 4 h of frying of besan sev in cotton seed oil at 180 ˚C. Van et al, [7] reported that the anti radical power of oil with intermediate frying decreased significantly ($p<0.05$) slower than oil that was heated alone. They explained their results by the fact that during frying water in the form of steam was released from the product. The contact of steam with oil induced hydrolysis, when a steam blanket covered the oil, so that the oxygen supply was limited [14].

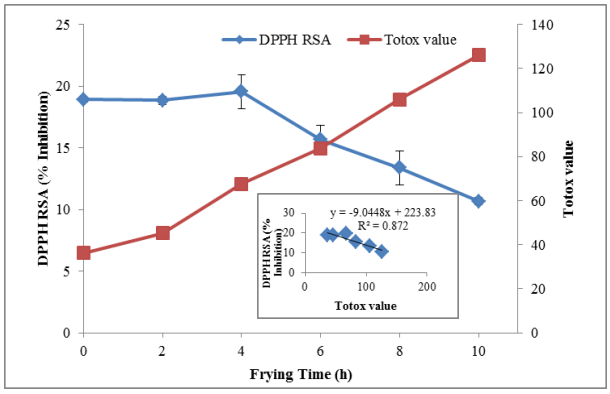

Figure 3: The totox value and DPPH RSA of cotton seed oil heated at 180 °C during frying of besan sev.

There are two stages of oil oxidation, i.e. the first phase is the formation of hydroperoxides and the second one is the decomposition of hydroperoxides to produce

secondary oxidation products, which could react with TBA reagent to produce colored compounds that absorb usually at 530 nm.

The mean values of TBA of cotton seed oil at varying frying time interval and its relation with DPPHRSA is shown in figure 4, The TBA was 3.00 µg/gm of oil of fresh oil and was increased significantly ($p<0.05$) about approximately three times at the end of 10 h of frying time. Regression between DPPH RSA and TBA showed positive relationship (R^2= 0.926).

Table 1: Pearson's correlation between PV, P-AV, totox value, TBA and DPPH RSA of cotton seed oil heated at 180 °C

	Peroxide value	*p*- anisidine value	totox value	TBA
***p*- anisidine value**	0.973**			
totox value	0.975**	1.000**		
TBA	0.974**	0.990**	0.990**	
DPPH RSA	-0.938**	-0.932**	-0.934**	-0.962**

**. Correlation is significant at the 0.01 level (2-tailed).

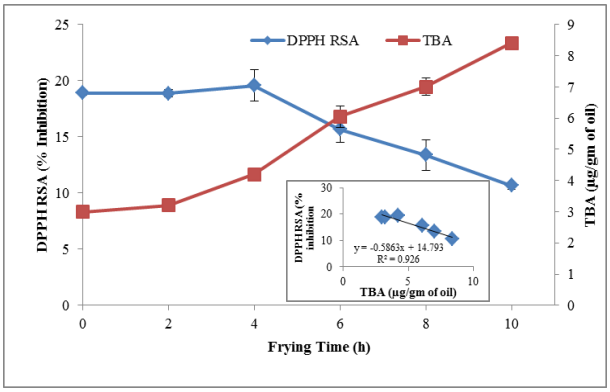

Figure 4: The TBA and DPPH RSA of cotton seed oil heated at 180 °C during frying of besan sev.

In this study the correlation between various conventional methods (PV, P-AV, totox, TBA and DPPH RSA) was studied and results obtain are presented in table 1. DPPH RSA correlated negatively with PV (R^2 = -0.938, $p< 0.01$), P-AV (R^2 = -0.932, $p< 0.01$), totox value (R^2 = -0.934, $p< 0.01$) and TBA (R^2 = -0.962, $p< 0.01$). Sikwese and Duodu [15] reported that sunflower oil with crude phenolic extract (CPE) had lower peroxide values compared to control oils.

They also reported that sunflower oil with tertiary butyl hydroquinone (TBHQ) had lower peroxide value.

These results suggested that the DPPH RSA has shown a strong relation with all four conventional methods commonly used for evaluation of oxidation status in fat or oil exposed to heat alone or during frying of various foods, hence from these results it is recommended that the DPPH RSA could also be used as one of the methods of measuring lipid oxidation in oil or fat or high fat containing foods. It is also a simple and less time consuming method.

ACKNOWLEDGMENT:

Author is thankful to the University Grant Commission, New Delhi, for financial support under Major Research Project (F.31-277/2005(SR); Date:5/4/2006).

REFERENCES

[1] Man, Y. C., Liu, J. L., Jamilah, B., & Rahman, R. A. (1999): Quality changes of refined-bleached-deodorized (rbd) palm olein, soybean oil and their blends during deep-fat frying. *Journal of Food Lipids*, ***6*(3):** 181-193.

[2] Abdulkarim, S. M., Long, K., Lai, O. M., Muhammad, S. K. S., & Ghazali, H. M. (2007): Frying quality and stability of high-oleic Moringa oleifera seed oil in comparison with other vegetable oils. *Food Chemistry*, ***105*(4)**: 1382-1389.

[3] Aladedunye, F., & Przybylski, R. (2013): Frying stability of high oleic sunflower oils as affected by composition of tocopherol isomers and linoleic acid content. *Food chemistry*, ***141*(3):** 2373-2378.

[4] Brand-Williams, W., Cuvelier, M. E., & Berset, C. L. W. T. (1995): Use of a free radical method to evaluate antioxidant activity. *LWT-Food science and Technology*, ***28*(1)**: 25-30.

[5] Lee, J., Chung, H., Chang, P. S., & Lee, J. (2007): Development of a method predicting the oxidative stability of edible oils using 2, 2-diphenyl-1-picrylhydrazyl (DPPH). *Food chemistry*, ***103*(2)**: 662-669.

[6] Yeo, J., Jeong, M. K., & Lee, J. (2010): Application of DPPH absorbance method to monitor the degree of oxidation in thermally-oxidized oil model system with antioxidants. *Food Science and Biotechnology*, ***19*(1)**: 253-256.

[7] Van Loon, W. A., Linssen, J. P., Legger, A., & Voragen, A. G. (2006): Anti-radical power gives insight into early lipid oxidation events during frying. *Journal of the Science of Food and Agriculture*, ***86*(10):** 1446-1451.

[8] Mehta, B. V. (2006): Overview of the Indian oilseed sector and demand of edible Oils. *Exchange Traded Commodities Outlook*.

[9] AOAC (2000): Peroxide value of oils and fats 965.33.12. Official methods of analysis of AOAC international (17th ed.). USA: Maryland.

[10] AOCS. (1998): Official methods and recommended practices of the American Oil Chemists' Society. Method Cd 18-90. Champaign, IL: AOCS.

[11] Tarladgis, B. G., Watts, B.M., Younathan, M.T., and Dugan, L.R. (1960): A distillation method for the quantitative determination of malonaldehyde in ransid foods. *Journal of the American oil chemists Society* **37**:1.

[12] Andrikopoulos, N. K., Dedoussis, G. V., Falirea, A., Kalogeropoulos, N., & Hatzinikola, H. S. (2002): Deterioration of natural antioxidant species of vegetable edible oils during the domestic deep-frying and pan-frying of potatoes. *International journal of food sciences and nutrition*, ***53*(4):** 351-363.

[13] Lee, J., Kim, M., & Choe, E. (2004): Effects of carrot powder in dough on the lipid oxidation and carotene content of fried dough during storage in the dark. *Journal of food science*, ***69*(5):** 69-81.

[14] Saguy, I. S., & Dana, D. (2003): Integrated approach to deep fat frying: engineering, nutrition, health and consumer aspects. *Journal of food engineering*, ***56*(2):** 143-152.

[15] Sikwese, F. E., & Duodu, K. G. (2007): Antioxidant effect of a crude phenolic extract from sorghum bran in sunflower oil in the presence of ferric ions. *Food chemistry*, ***104*(1):** 324-331.

PRAJÑĀ - **Journal of Pure and Applied Sciences Vol. 24 – 25 : 195 – 201 (2017)**
ISSN 0975 - 2595

DESIGN AND DEVELOPMENT OF LABORATORY BASED MODEL OF REWORK SYSTEM FOR BGA SEMICONDUCTOR DEVICES

SHAHERA S.PATEL

Department of Electronics, Sardar Patel University, V.V.Nagar – 388 120 Email: swamibhavin@gmail.com

ABSTRACT

With the evolvement of new technology in semiconductor science, most of the sophisticated instruments contains compact multilayer printed circuit boards with large number of small size components and integrated circuits. These integrated circuits are mounted on the PCB by Ball Grid Array (BGA) technique. This paper contains new design approach for the development of a system for making and removing contacts of BGA semiconductor chips on PCBs by using ferromagnetic balls. The developed system includes Top heater coil with fan assembly and special regulated power supply, Bottom Infrared Heaters, Temperature sensor attached with Temperature controller, relays and supporting mechanical assembly with Rack and Pinion arrangement for top heater movement. The design and development approach of BGA rework system is having high density, good conduction and low induction leads. The development stages of different sections for BGA system are discussed.

Key Words : Solder, Infrared Heater, Ball Grid Array(BGA), Thermocouple, Controller.

INTRODUCTION

In recent years, with the technological advancement in electronics science and engineering have resulted in development of more compact sophisticated Gadgets/Instruments and components having reduced size. Since there is an extensive requirement for compact packages, density of surface mount components and other interconnecting joints, the solder attachment techniques and methods must also modify and continue to evolve.

In last decade, most electronic instruments used PCB 's in which components were based on Surface Mount Technology (SMT) and Pin Grid Array (PGA) Technology. The advancement in soldering technology and related processes are discussed.[1-7]

The most recent era now a days uses instruments having multilayer printed circuit boards which contains large number of components like Integrated Circuits (ICs) based on Ball Grid Array (BGA) techniques for Improved performance.

The assembling of integrated circuits are very important for the function of any devices. To get the density requirement for many SMT components, the Ball Grid Array (BGA) technique have been evolved with reliability. In the BGA technology instead of pins, for the contacts it uses metal balls which are soldered on to the surface of the printed circuit board.BGA can provide more interconnection pins that can be put on a DIP (dual in line or PGA)Package. In PGA technique, instead of using perimeter all bottom surface of the devices can be used. The leads are shorter which gives better performance for high speed device applications.

The BGA technique known as BGA Rework station/system is used for the repair or refinishing i.e. solder/desolder operation of BGA semiconductor chips/devices in an electronic printed circuit board (PCB).[8]

In the present era of computer and mobile technology and their tremendous use in routine day to day life, there are more possibilities for the failure / damage of these devices. In particular there are more chances for the damage of Integrated circuits - Surface mount device package(SMD). In order to repair these kind of electronic instruments/gadgets, replacement of the SMDs can be done more easily & conveniently compared to other methods by means of BGA rework method.

The main aim of BGA rework system is to produce high-quality, high density effective Soldering. With the use of BGA rework streamline operation can be carried out which gives improvement in the success rate of soldering and also reduces the overall Soldering costs.

OBJECTIVE OF THE DEVELOPMENT OF BGA SYSTEM :

For numerous SMT components, to meet the required density, conventional SMAA soldering techniques i.e. BGA have been challenged with reasonable reliability, automatic processing and difficulties associated with its inspection.

Technology of mass processing is not effectively and easily applicable for repairing or replacement of single device. Therefore, it is necessary to change the faulty/damaged components using special manual methods by experts using proper equipment. In particular various area array packages such as BGA devices require appropriate tools and expertise.

A rework system is a system to do all type of work. The word rework is used for the mounting and demounting of BGA ICs on an electronic printed circuit board. (PCB).

Many hardware Users have been involved in handling scientific sophisticated research instruments, computer maintenance, repair of medical equipment, communications equipment maintenance, video game maintenance, training teaching, and in variety of such other fields.

BGA rework system existing in the market are very costly. In this context, it is of high demand to develop such type of BGA rework system for the technical persons who are involved in repairing of such kind of the electronic instruments/gadgets.

Since very few companies are involved in developing the BGA Rework Station, the main aim and objective of this work was to design and develop Ball Grid Array rework system where for BGA integrated circuits temperature profile is calibrated to assemble and disassemble it from various circuit boards having different sizes.

With this view, It was initiated and attempt was made to design and develop low cost, profile based, more reliable laboratory based model of BGA rework system which is having high density, good conductor and low inductance leads.

The developed model includes Infrared Heaters, Heater coil with fan assembly and special regulated power supply, temperature controller, contactors, relays and supporting mechanical assembly with Rack and Pinion arrangement for the Heater movement.

THE MAIN OBJECTIVES ARE

(i) Design and Development of BGA rework system for technical persons involved in repairing of sophisticated Instruments/Gadgets in which mostly BGA Integrated circuits are used.

(ii) To focus on awareness about the latest technological development i.e. GRID technology among students of electronics science, physics and electrical engineering discipline.

(iii)To impart hands on Practical / Project training at chip level for assembling and disassembling SMD based components in multilayer PCB's which is now a days widely used in computers, laptops and other sophisticated instruments to generate technical manpower /Hardware technician

TECHNOLOGICAL BACKGROUD AND ADVANCEMENT :

(i) Early days, Integrated circuits used were of

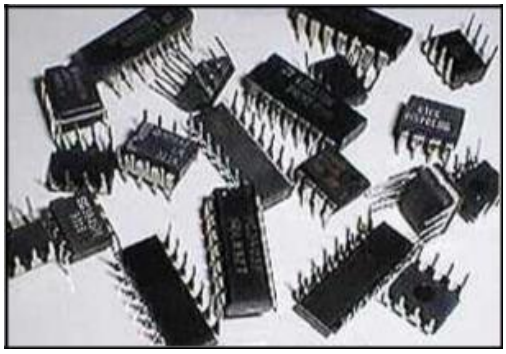

DIP or Metal can packages having,

- Increased Size of IC's.
- Wide and Thick pin connection.
- More space & More complexity in PCB.
- Big size and weight of Instruments.

Ex: Big Computers – occupied more space.

Demand for Miniaturization

(ii) Surface Mount Devices (SMD) :

(a) Pin Grid Array (PGA) :

Less Pin Thickness, More pin allocation in small size IC's

(b) Ball Grid Array (BGA) :

1. Less distance between IC and PCB. Therefore low thermal resistance between IC package & PCB. Soldering of IC through metal Balls (Leaded and Lead free)
2. Avoids overheating of PCB
3. High Density, Good conduction which leads to the better performance for high speed devices.

EXPERIMENTAL AND DISCUSSION :

DETAIL DESCRIPTION OF INSTRUMENTATION AND HARDWARE DEVELOPED FOR BGA REWORK SYSTEM

This is an advanced new design approach for the development of low cost BGA rework system.

This developed BGA rework system gives joining of SM components easier than normal bench top techniques. It also makes mounting of IC's perfectly. The advantage of this system is it minimizes thermal stresses due to difference in temperature during rework and mounting.

BGA Rework system is composed of Heater Assembly which consist of Top Heater and Bottom Infrared Heaters. The function of Top Heater is to blows hot air directly on the BGA IC. This ensures that the IC gets enough heat so that the required melting point is achieved thus the IC soldered/desoldered well. The Bottom IR Heaters are connected in series

which covers more heating surface at the bottom. This is required to pre heat the Printed Circuit Board uniformly so that it can not crack because of differential temperature.

BGA Rework Station also uses PCB Table with cooling Fan and Locking handle seat / Temperature controller which controls the upper and lower heater assembly.

Fig 1 Shows the develop BGA system with its parts name indicated.

Fig.1 : Developed BGA rework system
(Top) Upper Heater

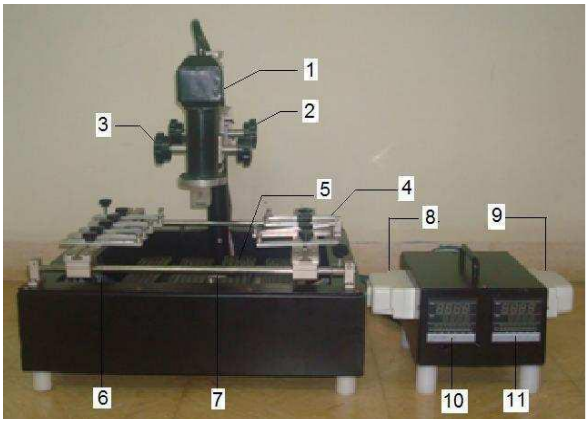

1. X-axis Regulator
2. Y-axis Lifting Regulator
3. PCB Table and locking handle seat
4. Cooling Fan
5. Bottom Infrared Heater (Pre-Heater)
6. Temperature Sensor

7. Main RCB switch

8. MCB switch for Heaters

9. Upper Profile based Temperature Controller

10. Bottom Profile based Temperature Controller

DETAIL DESIGN, ARRANGEMENT AND ASSEMBLY OF INDIVIDUAL PART :

1. **(Top) Upper Heater Assembly :** The function of Top Heater is to blow Hot air to the SMD IC for Soldering, Disoldering and Reballing purpose

Fig.2 Development of Top Heater Assembly

2 and 3. X-axis and Y-axis Lifting Regulator :

This is used to move the Top heater in X,Y and Z direction to adjust the Printed circuit board to obtained best position for hot air to blow.

Fig.3 Development of Rack and Pinion Arrangement

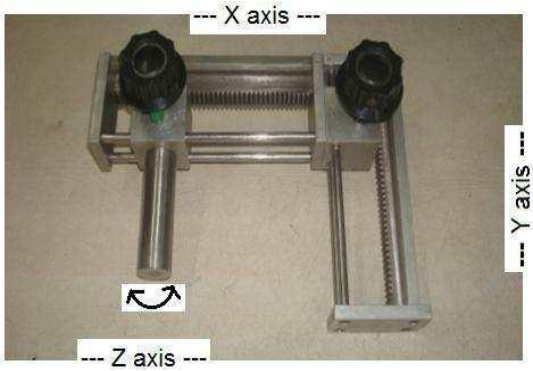

4. PCB Table and locking handle seat :

This is used to hold the Printed circuit board from which IC is to be replaced or reballing is to be carried out.

Fig.4 PCB table and Locking handle seat

5. Cooling Fan : (fig. 5)

It is used to cool the bottom Infrared Heater. Rating of the Fan is 12V DC, 0.60A.

Fig.5 Cooling Fan

6. Bottom Infrared Heater (Pre-Heater) : (fig.6)

This is used to produce uniform temperature to the Printed Circuit Board. Total five IR heaters are used.

3 IR heaters used with capacity : 600W and
2 IR heaters used with capacity : 300W

IR Heater having Ceramic coating.

Fig.6 Bottom Infrared Heater

7. Temperature sensors used with Top and Bottom IR Heater :

This is used to sense the heat produced by the Top and Bottom IR Heater. Sensors used Chromel – Alumel (Cr- Al) K-type temperature sensor. Range of the maximum temperature measurement used is about 350^0C

Fig.7 Temperature Sensor

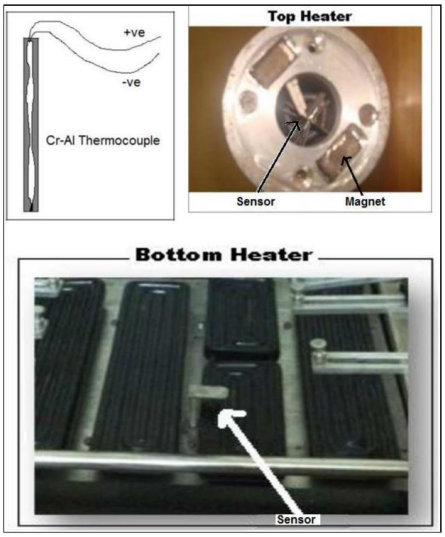

8,9,10,11. Profile based Temperature controller (PFY 700) along with Main RCB Switch and MCB Switch for Heaters :

This is used to control the profile based temperature of Top and Bottom IR Heater. It is having Solid State Relay based output. 16 steps of Temperature Profile can be controlled. Here the calibration of Temperature measurement profile was carried out to get proper melting of solder balls.

Technical Specification of Model PFY 700 :

Input Supply voltage : AC 230V

Frequency : 50 HZ

Power consumption : Approx : 3 VA

Accuracy : 0.2 % FS ± 1digit

Sample time : 250ms

Thermo Couple : K type

Facility : Output 1 and Output 2 :

For heating and cooling control use.

Fig.8 Profile based Temperature Controller with MCB and RCB switches

ACCESSORIES USED :

(i) **IC Stencils and Solder Balls** :

IC Stencils and Solder Balls of Different sizes are shown in Fig.9. Depending on the sizes of BGA IC and number of pins used proper selection of stencils can be done.

Fig.9 IC Stencils and Solder Balls of Different sizes

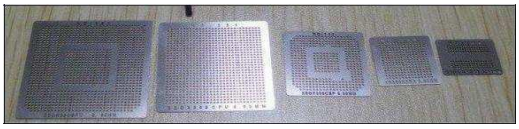

BALL SPECIFICATIONS :

- **Ball Diameter** (mm)
- 0.76mm
- 0.635mm
- 0.50mm
- 0.45mm
- 0.406mm
- 0.35mm
- 0.30mm
- 0.25mm
- 0.20mm
- 0.15mm
- 0.10mm

(ii) **Ultrasonic Cleaner :**

It is used to clean the PCB and Stencils. Also, the function of ultrasonic cleaner is to remove the stencil from the Printed Circuit Board after Re balling operation. This is done because suitably vibrating the sensor probe .

Fig.10 Ultrasonic Cleaner

COMPLETE SCHEMATIC DIAGRAM OF BGA REWORK SYSTEM :

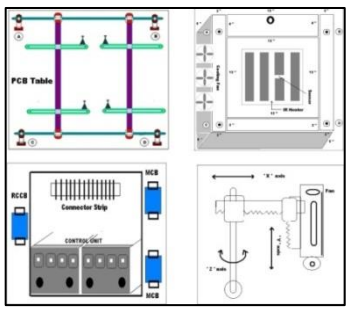

OPERATING PROCEDURE :

Once the faulty IC is detected it is required to replace/ reball the IC with the help of BGA system which includes the following steps.

1. Fill the Faulty IC with BGA flux.
2. Place BGA IC in PCB Table and locking handle seat of BGA rework system. Heat the IC up to 230^0C to 260^0C by Top Heater and give 200^0C temperature by Bottom IR Heater (Take due care while placing PCB)
3. Remove IC from the Printed circuit board. Clean it properly with NC Thinner and Flux
4. Clean the IC and their appropriate Stencils with NC Thinner.
5. Paste flux on both IC and Stencil.
6. Spread the solder ball on both the components.
7. Again follow the step 2 to heat both the IC and Stencil.
8. To separate the stencil form the IC both the arrangement are to be dipped in the tray filled with NC Thinner proper vibration is given by Ultrasonic Cleaner to the thinner solution.
9. In this way the BGA IC is reballed .
10. The PCB with reballed IC is used to test for its proper functioning.

PARAMETERS OF BGA :

(i) Upper Heating IR : 600W
(ii) Bottom Heating IR : 2400W
(iii) Total Power Consumption of the instrument 3000W

CONCLUSION :

Laboratory based model of rework system for BGA semiconductor devices is designed and developed. This is a new design approach in

which Infrared heaters are used. These are used because it has special feature of local heating and good penetration power which avoids damage and overheating of nearby components. The developed system is reliable, simple and easy to operate. The reballing work with this system is done effectively and efficiently. It provides accurate and precise temperature control which is the demand of recent advance IC packages. The temperature profile for the system is calibrated.

ACKNOWLEDGEMENT :

Author is grateful to S. P. University for sanctioning Research Project under SEED money grant.

REFERENCES :

[1] Rahn, Armin,(1993) The Basics of Soldering (Newyork, John willy &Sons,Inc,)
[2] Manko, Howard H, (1995) Soldering Hand book for Printed Circuits and Surface Mounting Technology (New York : Van Nostrand Reinhold,)
[3] Pecht, Michael G, (1993) Soldering processes and Equipment (New York : John Whiley & Sons,Inc)

[4] www.epemag.wimborne.co.uk
[5] www.ifixit.com

[6] Patel S.S.(2014), Advancement in soldering technology. Main issues and its perspectives-Part-I, IJRITCC, Vol.2 Issue 9: page no.2883-2886
[7] Patel S.S.(2014), Advancement in soldering technology. Main issues and its perspectives-Part-II, IJRITCC, Vol.2 Issue 10: page no.3307-3310
[8] Patel S.S.(2014), Advancement in soldering technology. Main issues and its perspectives-Part-III, IJRITCC, Vol.2 Issue 11: page no.3784-3787

PRAJÑĀ - **Journal of Pure and Applied Sciences Vol. 24 – 25 : 202 – 208 (2017)**
ISSN 0975 - 2595

EXPERT SYSTEM FOR SELECTION OF RESEARCH AREA IN ACADEMIA

HARDIK B. PANDIT AND DIPTI B. SHAH

G H Patel Post Graduate Department of Computer Science, Sardar Patel University
Vallabh Vidyanagar, Gujarat, India. Email : dbshah66@yahoo.com

ABSTRACT

Research is an essential component in the career of academician. As per informal discussion with students looking to pursue academic research, it is found that selection of research area and research topic is one of the most difficult phases. Moreover, many research supervisors also find it difficult to suggest appropriate research area or topic to the students. The process of finalizing area of research as well as topic of research is very confusing and time consuming activity. To simplify the task of supervisors and research seekers, an expert system is developed which assists the user to finalize the research area and topic in the field of computer science and application. This paper focuses on the expert system for assistance in analysis of the user responses to the questionnaire asked by the system, to suggest the most suitable research area to the user. The expert system is implemented as a component of a decision support system being developed for selection of research topic and prevention of plagiarism.

Keywords: Expert System, Knowledge Base, Inference Engine, Forward Chaining, Decision Support System

INTRODUCTION

An expert system is a computer based system which emulates the ability of decision-making of a human expert. [2]
An expert system is divided into two disjoint components: (i) inference engine and (ii) knowledge base. The knowledge base represents facts and rules. The inference engine applies the rules to the facts which are known to produce new facts. [3]
This paper explains the research work done to design and implement an expert system to assist in decision making for selecting an appropriate research area. The system provides a user interface, which is a questionnaire containing 20 questions. There are three categories of questions: (i) to know attitude and aptitude of student towards various types of researches (ii) to know the area of interest of student (iii) to know the interest of student in inter disciplinary research. Based on responses given by student, the inference engine generates output. The output is the suggestions to the student in textual format. The student may decide area of research based on this output or can reappear in the questionnaire for more clarification.

SCOPE OF THE SYSTEM

The expert system for assistance in selection of research area in academia is a component of a model of decision support system for research topic selection and prevention of plagiarism. [1] The parent system is for assistance in making choice of research topic for research in academia. The model of parent system is based on the combination of the approaches of decision support system and web mining to finalize the most suitable area of research for the student.
The model of parent system and place of this expert system in the model is as shown in figure 1. [1]

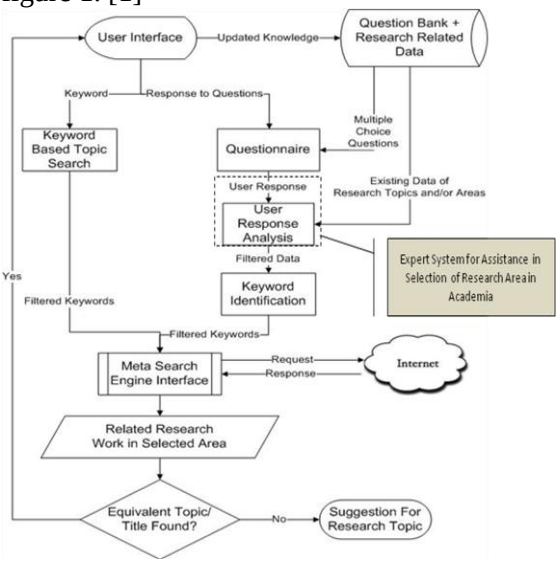

Figure 1: Relationship between the expert system and its parent system

The dotted rectangle highlights the component of the model which is implemented as an expert system for assistance in selection of research area in academia.
Thus, the developed expert system is a subsystem, whose output, in textual format, is consumed by the parent system to generate the final output which is the suggested research topic.

LITERATURE REVIEW

There is an ample of work done on expert systems in various fields, but if one has to consider the expert systems in the area of selection of research topics in academia, much work is not found.

Li Yu, Jie Yang, Dong Yang, and Xiaoping Yang have described a research topic decision support system to help a user to quickly find suitable research topic based on iteratively paper recommendation .[1]

A framework and model of a Decision Support System (DSS) is presented by Iyigün, M. Güven, as a tool to help choose projects using complex criteria such as risk, cost, decision hierarchies, and budget objectives. [1]

A research work is carried out and hosted in Purdue University, Indiana in the field of selection of research topic in the area of computer science. Name of the tool is "A CS Research Topic Generator" or "How To pick A Worthy Topic In 10 Seconds". [1]

The study is also done of websites of the of Massachusetts Institute of Technology, University of Buffalo, and University of Illinois Urbana-Champaign for guidelines of research topic selection. [1]

In nutshell, after conducting review of literature thoroughly it is found that there are many systems which guide the students for selection of research topic, but none of these systems provide an expert system for decision making in selecting a research area and research topic.

SCOPE OF RESEARCH

Academic research faces many challenges. One of the prominent challenges is the first step of research, that is, selection of the area of research. Many students who are desperate to conduct research face trouble in deciding the area of research. Especially, in the field of computer science where industry is giving tough competition, finding area of research is really a confusing job.

Same challenge is faced by supervisors. They are expected to guide the student in the selection of area of research. If the supervisor is not aware of attitude and aptitude of a student towards various areas of computer science, it is really very difficult to suggest the suitable choice for the candidate.

Thus, there is a need of a system which can assist the students to decide the area of research that is suitable to his/her personality.

MODEL OF THE SYSTEM

The system consists of two components, (i) user interface and (ii) user response analysis as shown in figure 2.

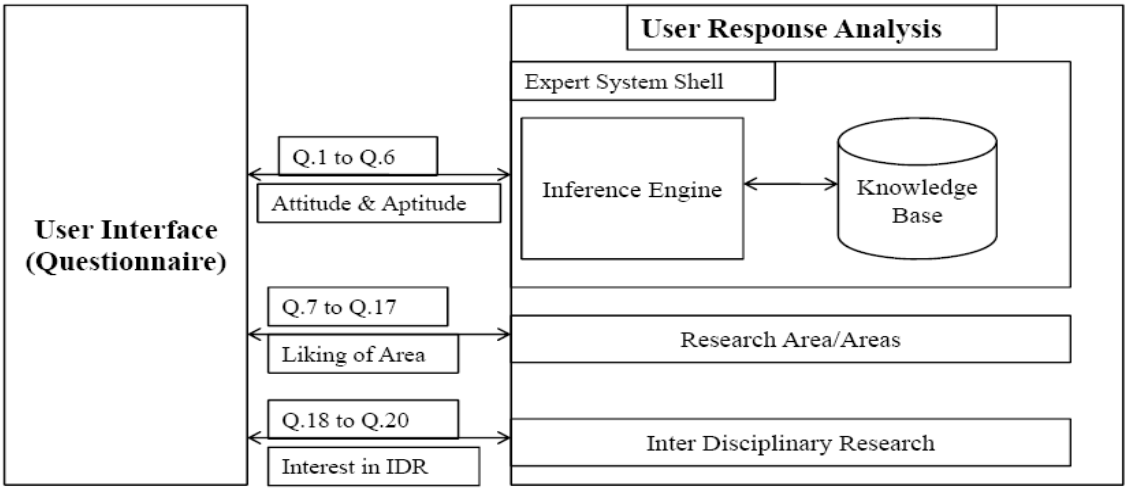

Figure 2: Model of the Expert System for Selection of Research Area in Academia

5.1 User Interface:

The user interface collects input from the user. The user interface has a questionnaire consisting of 20 multiple choice questions. Among these questions, first six questions fetch information about attitude and aptitude of the student towards the research areas mentioned in the knowledge base. Questions 7 to 17 asks student about his/her willingness to work with the various areas of research at certain level. That is, if he/she is interested to work with the particular area of research or not. If yes, then whether it is the area of research in which student wants to work or he/she wants to use applications of that research area. Questions 18 to 20 collect the information about the willingness of the student to work with inter disciplinary research areas. The structure of questions and multiples choices for the same are based on knowledgebase. The knowledgebase is created after conducting personal interviews and discussions with the eminent professors of the reputed universities of Gujarat like The M. S. University of Baroda, Saurashtra University, Sardar Patel University, and Uka Tarsadia Univesity. The questionnaire based on knowledge base is shown in Table 1.

Table 1: Structure of Questionnaire based on the Knowledgebase

Questionnaire Based on Knowledge Base					
Q. No.	Question	Option A	Option B	Option C	Option D
1	Which was your favourite type of subjects during your post graduation study?	Analysis and Design of Algorithms/Protocols for various Processes	Low Level Programming/ Design of Compilers/API	Theoretical Computer Science/Software Engineering	Window/Web Application Development
2	Which type of research work would you like to carry?	Development of a system which is directly applicable to solve a problem	Development of a model/conceptual idea which can be used to solve a problem	Comparative study of existing models/systems to find most suitable one to solve a problem	Development of a system which could be a sub-system of existing system
3	How good are you at programming skills?	Poor	Average	Good	Excellent
4	How good are you at designing new algorithms?	Poor	Average	Good	Excellent
5	How good are you at analysis of existing system?	Poor	Average	Good	Excellent
6	Which method of learning do you like the most to understand any concept/topic?	Reading Books	Online Tutorials	Reading Journals	Reading Magazines
7	Up to which depth would you like to work on Digital Image Processing and Analysis?	Would not like to work on	May use applications of it	Would like to work in depth	Would like to know about this area
8	Up to which depth would	Would not like	May use	Would like to	Would like to

	you like to work on Artificial Intelligence and Machine Learning?	to work on	applications of it	work in depth	know about this area
9	Up to which depth would you like to work on Compilers/Interpreters/Assemblers?	Would not like to work on	May use applications of it	Would like to work in depth	Would like to know about this area
10	Up to which depth would you like to work on Software Engineering/Process Design/Process Model Design/SDLC Phases?	Would not like to work on	May use applications of it	Would like to work in depth	Would like to know about this area
11	Up to which depth would you like to work on RDBMS/Big Data/Data Warehousing/Data Mining/Data Analytics ?	Would not like to work on	May use applications of it	Would like to work in depth	Would like to know about this area
12	Up to which depth would you like to work on Web Searching Techniques/Search Engine Optimization/Web Crawlers/Optimized Searching?	Would not like to work on	May use applications of it	Would like to work in depth	Would like to know about this area
13	Up to which depth would you like to work on Voice Processing/Natural Language Processing/Text to Voice/Voice to Text?	Would not like to work on	May use applications of it	Would like to work in depth	Would like to know about this area
14	Up to which depth would you like to work on Cloud Computing/Fog Computing/Internet of Things?	Would not like to work on	May use applications of it	Would like to work in depth	Would like to know about this area
15	Up to which depth would you like to work on Embedded Systems/System Software/Assembly Programming/Operating System Design/Process Design?	Would not like to work on	May use applications of it	Would like to work in depth	Would like to know about this area
16	Up to which depth would you like to work on Network Design/Routing Algorithms/Network Protocols/Networking Models?	Would not like to work on	May use applications of it	Would like to work in depth	Would like to know about this area
17	Up to which depth would you like to work on Decision Support	Would not like to work on	May use applications of it	Would like to work in depth	Would like to know about this area

	Systems/Management Information Systems/Business Process Analysis?				
18	Up to which depth would you like to work with other Electronic/Electrical/Mechanical devices?	Would not like to work on	May use applications of it	Would like to work in depth	Would like to know about this area
19	Up to which depth would you like to work on Applications of Computers in other fields as Agriculture/Food Processing/Production/Commerce/Arts/Music/Archaeology/Areas other than Science?	Would not like to work on	May use applications of it	Would like to work in depth	Would like to know about this area
20	Up to which extent would you like to work with experts from other disciplines?	Would not like to work with	Would like to take a little help	Would like to work	Would like to use outsourcing service from experts

5.2 User Response Analysis

The key sub component of user response analysis is inference engine. The inference engine works in a forward chaining mode. It collects facts in terms of user input and generates the output. The model of inference engine is shown in figure 3.

User's Answer for Question 1	Test Condition and System's Output
A	Test Condition: 1A AND 2A AND 4C OR 4D AND 5C OR 5D AND 6A OR 6D System's Output: Development of a new model of a system OR conceptual idea which can be used to solve a problem (Strongly Recommended)
B	Test Condition: 1B AND 3C OR 3D AND 6B OR 6D AND 18C System's Output: Machine Level Programming OR Design of Compilers OR Robotics OR API development (Strongly Recommended)
C	Test Condition: 1C AND 5C OR 5D AND 6A OR 6C System's Output: Theoretical Computer Science OR basic concepts of Software Engineering (Strongly Recommended)
D	Test Condition:

	1D AND 2B OR 2D AND 3C OR 3D AND 5C OR 5D AND 6B OR 6D System's Output: Window OR Web based Application Development in suitable areas (Strongly Recommended)
	Test Condition: (Default Case) If none of the above condition matches System's Output: System does not recommend anything strongly but suggests as per choice of Q.1- A,B,C, OR D and the decision is based on answers of questions 7 to 20

Figure 3: Model of Inference Engine

The output generated by inference engine will guide the student towards his/her aptitude regarding respective subject. For example, if the student has selected option 1- B which is low level programming or development of system software, but he/she has not selected 3-C or 3-D which means he/she is not having good programming skills, the system will not suggest him to carry research in the area of intensive programming. The decision will be based on his choices for questions 7 to 20, and student can think for other three options for question 1 in the area of his choice.

From question number 7 to 17, as shown in table 1, the user can select his favourite area of research. There are four possibilities student can go for; (i) If student selects first option for any of the questions, then that option is discarded from the list of areas for suggestions. (ii) If student is strongly interested in the area, then that area is added in the list of suitable areas of research and the output is merged with the results of inference engine. (iii) If student wants to use just an application of that area or (iv) want to know about that area then that area of research is added as keyword in the final result, to search for.

Questions from 18 to 20 fetch the willingness of the students to work on interdisciplinary area of research.

The output of these components are merged to generate combined output to be sent to user interface, where student can read the analysis performed by the system. Furthermore, the same output will be processed by "Keyword Identification" module of the parent system as shown in figure 1, to identify keywords from the text generated.

RESULTS

The model shown in figure 2 is implemented in C#.NET. The system has generated output as expected and mentioned in section 5 of this paper. Figure 4 demonstrates the result obtained by the system. One can observe both, (i) structure of questionnaire by looking at question and its multiple choices and (ii) the analysis of the responses of student to these questions.

Figure 4: Output Generated by the Expert System for Selection of Research Area in Academia

CONCLUSION

Selection of research area and research topic is very crucial activity for a student opting for academic research. To assist the student in this intellectual task, a model of decision support system for selection of research topic is proposed. The expert system for assistance in selection of research area in academia is a component of the above mentioned decision support system. The working model of this expert system is explained and the results are presented. The analysis generated by the expert system is easy to understand for the student. Furthermore, the keywords can also be identified for further processing. Thus, the newly designed expert system is usable.

REFERENCES

[1]. Hardik Pandit, Dipti Shah, "A Model of Decision Support System for Research Topic Selection and Plagiarism Prevention", The International Journal Of Engineering And Science (IJES), Volume 6, Issue 1, January 2017, ISSN (e): 2319 – 1813 ISSN (p): 2319 – 1805, Pages: 40-42

[2]. Jackson and Peter (1998), Introduction To Expert Systems (3rd edition), Addison Wesley, ISBN 978-0-201-87686-4

[3]. Rich and Knight, Artificial Intelligence, Tata McGraw Hill Publishing Co. Ltd., 21st Indian Reprint, 2001

[4]. https://en.wikipedia.org/wiki/Expert_systems

PRAJÑĀ - **Journal of Pure and Applied Sciences Vol. 24 – 25 : 209 – 218 (2017)**
ISSN 0975 - 2595

BENHANCING FOG COMPUTING WITH USERS PROFILE AND TAXONOMY OF EXPERIENCE

PRITI SRINIVAS SAJJA
GH Patel PG Department of Computer Science & Technology, Sardar Patel University, Vallabh Vidyanagar-388120
Email: priti@pritisajja.info

ABSTRACT

Modern information and communication facilities have opened up new dimensions in handling day to day transactions as well as spectacular activities. With the help of web platform, problem solving and decision making have become very effective. The Web has enabled use of remote resource such as hardware and software efficiently with the help of cloud computing paradigm; which has its own limitations. To overcome limitations of the cloud computing, fogging is introduced in this paper. This paper discusses fog computing, work done in the area, and proposes a generic framework for hybrid fuzzy fog computing. The architecture works in conjunction of users' profile and user experience defined with the help of fuzzy logic. To evaluate the proposed architecture, an experiment of the customized web content filtering is discussed with necessary technical details. The experiment also utilizes the artificial neural network. Technical details of the underlying neural network such as structure, training data set, etc. are also provided in this paper. At the end, the paper concludes with advantages, applications and possible future enhancements..

***Keywords: Fog Computing, Users Profile, Fuzzy Logic, Neural Network, Web Filtering*.**

INTRODUCTION TO FOG COMPUTING AND STATE OF THE ART

Cloud computing has become buzz word in modern scenario as it provides facilities in various aspects such as platform, processes and infrastructure to many computing applications in order to store, use, and manage voluminous data/processes on network. However, in spite of benefits like readily available software, data and infrastructure, cost-effectiveness, portability and mobility, etc. there are issues too. The major issues with cloud computing is losing control on ones data, security, customization, reliability, and lack of standard problems. People would not like to transport their data on some unknown computing resources. Further, cloud computing needs networking infrastructure as bandwidth, which is poor sometimes. Above this, Internet and network latency also increase intensity of the issues.

When it comes to Internet of Things (IoT) and Internet of Everything (IoE), and many other personal applications based on domestic devices; they need data &other computing functionalities at the edge, not on the far cloud. Instead of centralized repository of various facilities, there is a need of decentralized computing as per the customized requirements of that edge. To facilitate this, technique of edge computing is suggested. As said, cloud may be logically far, but 'fog' is near earth, and hence the word fog computing/edge computing has evolved. Since such edge computing operates on end of the network, preferably at client's side, it eliminates need of establishing the full-fledged and dedicated channels for cloud. The term 'fog' is introduced by CISCO while suggesting new model of wireless computing. As per their view, "fog computing extends the cloud computing paradigm to the devices and applications, that do not conceptually fit into the paradigm" [1].

Figure 1 shows an architecture of the fog computing.

As stated, fog is comparatively nearer to the local devices and performs computing with less latency and quick response utilizing less bandwidth. Following are the major advantages of fogging.

Security and privacy: As the data are kept at the edge, not on the far cloud, security and privacy is better.

Efficiency: Since the fog node is at the edge, data can be efficiently communicated.

Decentralized communication: Instead of keeping all the data at the centralized server, the edge possesses the important data.

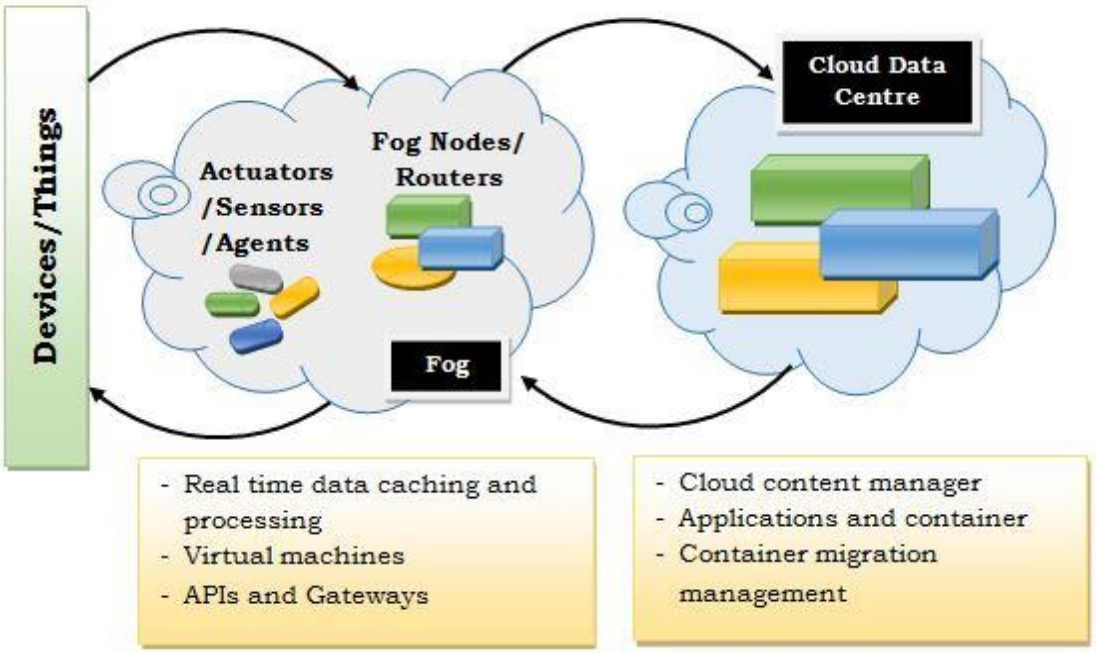

Figure 1: Fog Computing Architecture

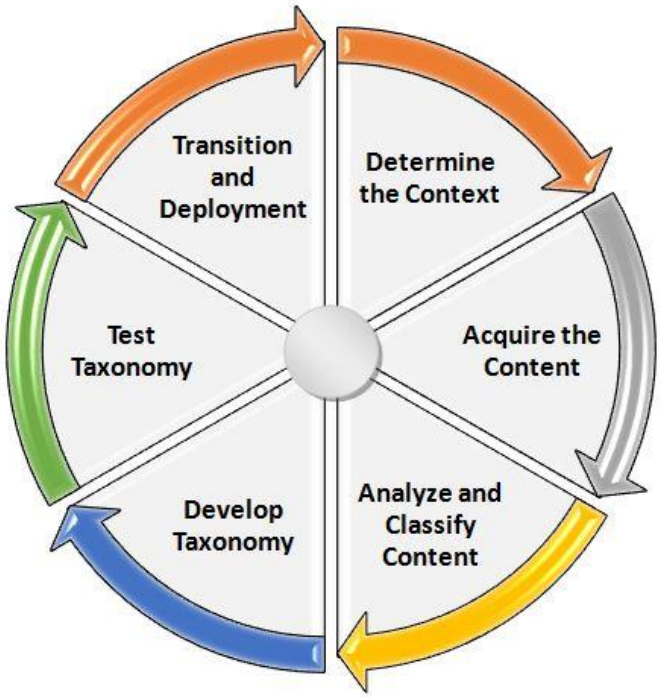

Figure 2: Lifecycle of Taxonomy

Modular approach: In between the client and server, there is an extra layer introduced, as an extension of the local network, which gives the advantages of structured approach.

Customized computing: Fog computing infrastructure allows development of customized systems for user.

Dependency: As per the OpenFog Consortium[1], fog computing is least dependent on protocol or radio systems, instead it is conceptual and resides at systems level.

Following are the some major areas, where fog computing is beneficial.

Opportunities in Pure Computer Science and Engineering

- Web filtering and content mining
- Mobile applications related to distributed intelligence
- Semantic web
- Monitoring and intrusion detention at end devices such as gate sensors, mobiles, etc.

Applied domains

- News summarization
- Health awareness and informatics
- Smart cities applications such as Smart traffic lights
- Self-maintaining transport and connected cars
- Tourism
- Crowd monitoring, etc.

Attracted from the advantages and versatility of the fog computing, many researchers have contributed; majority of them have chosen area of IoT/IoE and distributed intelligence as discussed by Flavio Bonomi and Rodolfo Milito [2]. Theoretical models and issues related to fogging are discussed by many researchers [3], [4], [5], [6], [7], and [8]. Fogging is also used for smart cities and vehicle monitoring applications by Xueshi Hou et al., [9]. Similar application for IoT is demonstrated by Antonio Brogi [10]. Further, the fog computing has become first choice for researcher working for 5G systems [11]. Modern scenario of the fog computing is surveyed by Ivan Stojmenovic & Sheng Wen [12] and Janakiram MSV [13].

Other approaches/techniques related with the fog computing are also been in practice. To name a few, "cloudlet: data centre in a box" and micro-data centre. Cloudlet was introduced at Carnegie Mellon University [14]. Similarly, Microsoft[2] also suggested use of micro data centre (modular data centre).

TAXONOMY, ITS APPLICATIONS AND STATE OF THE ART

Taxonomy is defined as systematic documentations of various classes of entities (things or concepts) under domain of consideration. For example, all biological species or organisms can be defined and documented in systematic way. Similarly for numbers also, there exist various taxonomies. In the domains such as economics, education, medical science, military and defense, taxonomies are used. Many of us have used the ACM Computing Classification System (CCS), which is classification system for various computer related subjects by Association for Computing Machinery (ACM).ACM has implemented the classification system in 1964, and now using the latest version[3] of it.

Taxonomy of experience is a field which is less traversed, when it comes to the generic classification. Application/domain specific taxonomy about experience of entities are generally developed and used. Long back in the year 1983, a canonical model of the emotional experience was proposed by Eleanor Daly et al., [15]. Taxonomy of prospection (envisioning future in closed domain] is also proposed by Karl Szpunar et al., [16]. Latest work includes modeling of taxonomy of news items [17].

Typical life cycle of taxonomy encompasses variety of phases, namely context and content determination, content acquisition, analysis and classification of the content, developing & testing taxonomy, and deployment. These phases are denoted in Figure 2.

[1] *https://www.openfogconsortium.org*

[2] *https://www.microsoft.com*

[3] http://www.acm.org/about/class/

To generate taxonomy of experiences of users related to webpages, following major aspects have been considered. This information can be collected from a well-organized survey on the target audience and formal documentation of experience of users can be done to generate sophisticated taxonomy of experience. Each entity is encoded and concern code is reoffered in user's profile.

- Topic and context
- Nature of content (reliable, efficient, timely, and useful)
- Type of content (research, teaching, general, advertisement, entertainment, personal, news, etc.)
- Sub-content
- Relevance of the content
- Length of content
- Format and interface (multi media) and copy editing, readability
- Level (as per user) and problem solving capacity
- Connection to social media and similar facilities, internal and external links, and comments
- Interests

The taxonomy may incorporate fuzzy words on need, as some of the features, may be vague and uncertain. Such fuzzy words are incorporated with help of fuzzy logic; which is a multi-valued logic invented by Lotfi Zadeh [18].

USE OF TAXONOMY OF EXPERIENCE FOR FOG COMPUTING

In this paper, a personalized taxonomy of experience of users for an entity or concept in a given domain is designed and utilized for further computing processes in order to make it more effective. The basic objective to encode experience of the users is to present useful information to the users in highly customized manner without giving unnecessary details. The taxonomy of experience of users encompasses various aspects such as domain and sub-domain information, description, usability, resources, cost, other users, issues, outcomes, risk involved, etc. These fields are generic in nature. Besides these fields, one also needs to encode domain specific experience. For example, if health awareness and monitoring is required, field like disease, symptoms, remedies, history of treatment, etc. are to be added. Some of the fields in general as well as domain specific categories are again vague and difficult to be measured in standard predefined units. To document such information fuzzy logic help is taken. With this, not only vagueness and uncertainty are managed, but also increases ease of operation. Here machine tries to identify meaning of the linguistic parameters, and hence enables machine learning. Later, based on the field experts' opinion and domain heuristics, classification of the collected experience information is done to generate taxonomy; which is partly domain dependent.

Once repository of the taxonomy of the experience about the target users in a domain is designed, it is ready to be encompassed with the fog computing framework. Along with repository of taxonomy, use of users profile repository is suggested. Basic idea behind such repository is to provide customized output as per users need. Along with the code of the taxonomy of the experience from the repository, a profile of users containing personal information, business information, web log/history, interests, priorities, habits, and preferences, health related information such as diagnosis, treatment history, etc. is also used. The users profile repository is generally stored at the client machine to save time and make the process more secure by hiding the users' personal information. The proposed framework of the fog computing in conjunction with the fuzzy user profile and taxonomy of experience is illustrated in Figure 3.

The fog computing framework takes the users query and validates it after necessary preprocessing such as correction of spellings and stop words deletions. Such preprocessing makes the query well formatted. The query then passes through the frequently visited pages (history - FVP) to check similarities. If similar result is readily available, instead of sending the request to cloud, the ready result is submitted to the user. Here the query may use fuzzy linguistic words, which are application specific and dependent on domain selected. The fuzzy user profile is also unique for every user and contains sufficient information by which the system knows the user. The fuzzy profile also consists

of experience of users about entities of domain. Since it is challenging to store description of experience, which is machine readable, here the experiences about the events and concepts (called entities) are encoded as per repository of taxonomy. This is a kind of database normalization, achieved by generating dedicated taxonomy of experience, encode them and the code is used in user profile.

Second layer plays key role in understanding the fuzzy linguistic words used in the query with help of fuzzy membership functions after separating them by tokenizer. Further, the user profiles as well as the taxonomy are encoded in XML format, so as to make them machine readable. For that, we need metadata and Document Type Definitions (DTD).Activities related to decision making and problem solving are supported by fuzzy rules and inference engine[19]. The decision taken can be converted into crisp output and send to the application specific utility to the layer 3.

The fog computing framework demonstrated in Figure 3 is generic in nature and can be applied to any domain suitable for edge computing. One needs to define the domain specific applications, fuzzy membership function and rules, meta data and bag of words (synonyms). To demonstrate the working of the above mentioned generic framework, an application of web content filtering is selected and discussed in detail in the following section. The user profile and taxonomy of experience related to the domain are also defined and discussed.

EXPERIMENTING THE PROPOSED FRAMEWORK IN THE PERSONALIZED CONTENT FILTERING

Web has become a giant repository of everything. Earlier, the web was read only; great people used to contribute to the Web and many reads from it. Later the Web has become 'read-write' and people can write to and read from the Web. With the innovations of modern, secure, and platform independent languages such as java, it has become easy to execute some functions of Web; hence the Web has become 'read-write-execute'. So now, the Web has become repository of everything by everybody for everybody! Most of the users surf Web for content (content mining in a way); however, the web log mining, and web structure mining also in practice. For customized web content filtering, the system must know its users and presents the customized content, specific to users need [19]; [20].Further, for every user the output of the filtering must be unique and tailor made. In Figure 5 the proposed approach of the fog computing framework for effective and personalized content filtering is illustrated.

As stated, the system must 'know' its users. For that the user profile is created, which contains information on various aspects such as:

- Information specific to users such as age, gender, job type and location
- Users job and activities
- Users education information
- Family and social information (optional)
- Users history of surfing
- Users interests and hobbies
- Personal preferences
- Sequence of experience codes

It is to be noted that values of some of the fields are fuzzy in nature, and need to be represented with fuzzy linguistic variable.
The profile is encoded as shown in Figure 4.

The example illustrated in Figure 4 shows user's interest is in the field of "Research" with "High" value. This high value is fuzzy and can be encoded with help of fuzzy membership functions as shown in Figure 4.Once the user profile is encoded and necessary fuzzy membership functions are defined along with taxonomy of experience encoding, next step is to finalize the application logic. Here to meet the objective of customized web content filtering, an Artificial Neural Network (ANN) is used. Query given by users is first checked with the client local memories for frequently visited pages and history, if no match is found, the keyword of the query will be separated and given different weights by refereeing fuzzy rule base and bag of words. The normalized input vector is generated and sent to the underlying ANN. Since there are no generalized rules available for the domain, with large amount of the sample data only the web page filtering can be done. The ANN must be trained with good quality of valid vectors with the back propagation algorithm in supervised manner. The fuzzy variables are used

directly in rules, which have structure as shown in Table 1[21].

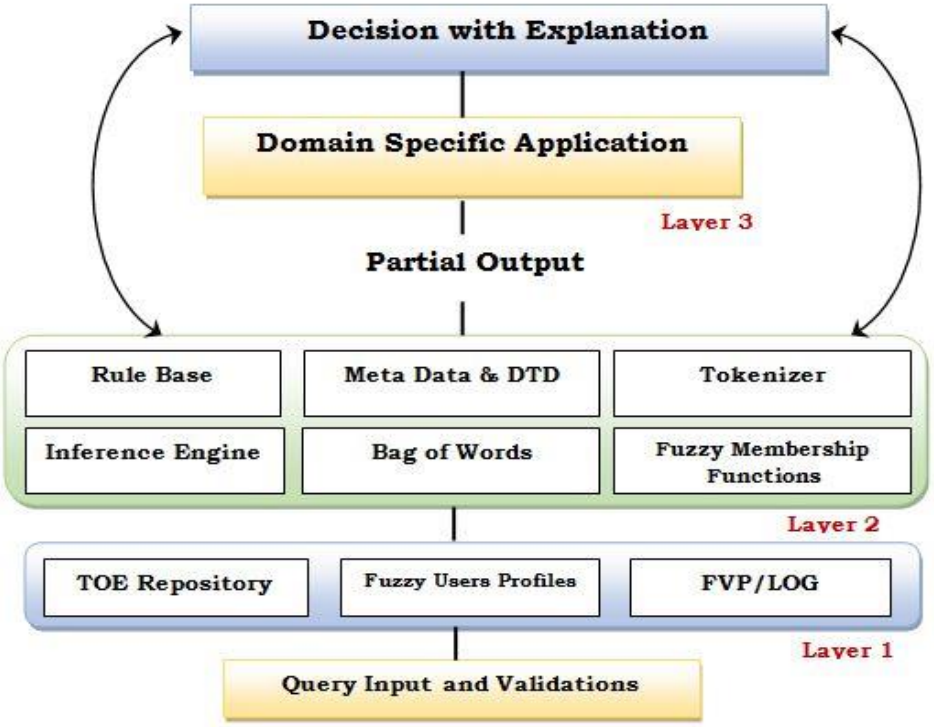

Figure 3: Proposed Fog Computing Framework with Taxonomy of Experience and Fuzzy Users Profile Repositories

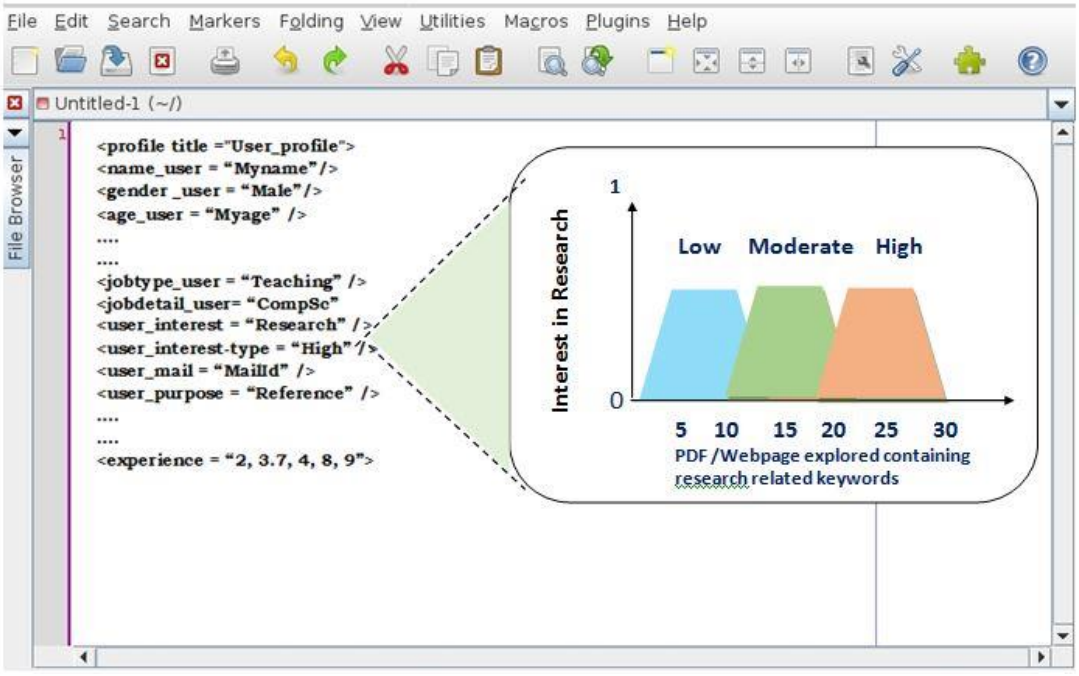

Figure 4: Fuzzy User Profile and Sample Membership Function

The fuzzy rule schema can be referred as IN Table 2.

Table 1: Fuzzy Rule Structure

```
<xs : schema id="Fuzzy_Rule" elementFormDefault= "qualified" xmlns :xs="http://www.w3.org /2001/XMLSchema">
<xs:complexType name = "Fuzzy_Rule">
<xs : sequence>
   <xs : element name ="rule "
        <xs:element name="antecedent" type="xs:string"
                <xs:element name="variable" type="xs:string"/>
                <xs:element name="value " type="xs:string"/>
                <xs:element name="acc_modifier" type="xs:string"/>
                ……../>
        <xs:element name="consequent " type="xs:string"
                <xs:element name="generally" type="xs:string"/>
                <xs:element name="specifically" type="xs:string"/>
                ……../>
   />
</ xs : sequence>
</ xs : complexType>
</ xs : element>
</ xs : schema>
```

Table 2: Fuzzy Rule Schema

```
"<xs:schema id="Sample" elementFormDefault="qualified" xmlns :xs="http://www.w3.org/2001/XMLSchema">
<xs:includeschemaLocation = "Fuzzy.xsd"/>"
```

The neural network classifies the web content by features and query provided into three categories in this application. The categories are recommendable, presentable, and rejected. Based on the users choice/level the web content/pages can be presented to the users. Optionally, with the help of fuzzy layers of the framework, the justification of the decision taken is also provided. The overall framework with application is illustrated as in Figure 5.

To prepare training data set, data are collected from various users about the choice of the suitable webpage and its placement into three pre-defined classes namely, recommendable, presentable, and rejected. Once users provide sample data, about query, webpage and its class (where the user thinks the webpage should belongs to); noise will be cleared from the data, synonyms of the keywords are found. The keywords are further given weights depending of their importance or frequency of occurrence. Locations of the keywords are also considered; for example, if the keyword is in title of the page, the weight is higher. Let the frequencies are f_1, f_2, f_3,…,f_n for the respective keywords q_1,q_2,q_3,…,q_n. Following vector of normalized values will be considered as input to the ANN.

Training data set 1

{ (F), (Q), (D) }

The above training data contains the values of frequencies (F) f_1,f_2,f_3,…,f_n and (Q) q_1,q_2,q_3,…,q_n. This is generalized equation; actual training data set contains real domain specific values and sufficient number of vectors to make base ANN learn from the data. (D) denotes category, here in the experiment, three categories are chosen. Category d1 stands for "Recommendable", d2 for "Presentable", and d3 for "Rejected".

Examples of some actual training data set used are as follows.

{ (1,2,0,1,2,1…), ("Xbook", "video", "age", "game", "birthday", "like", …), 0, 0, 1}

Here first two subsets represent input data and last three values represent sample output category. Further, "Xbook:" is name of site which is not permitted (eg. Visiting social networking sites during office time on office client/machine) and to be rejected.

As the web pages are to be classified in three categories, for preferable category, the output digit is 1, for other it is zero. In the above mentioned training data, the webpage is to be filtered out (rejected) and would not be presented to the user.

Here is another set of sample data.

{ (3,2,1,0,1,1…), ("SPU", "Semester", "Examinations", "Result", "Festival", "Course", …), 1, 0, 0}

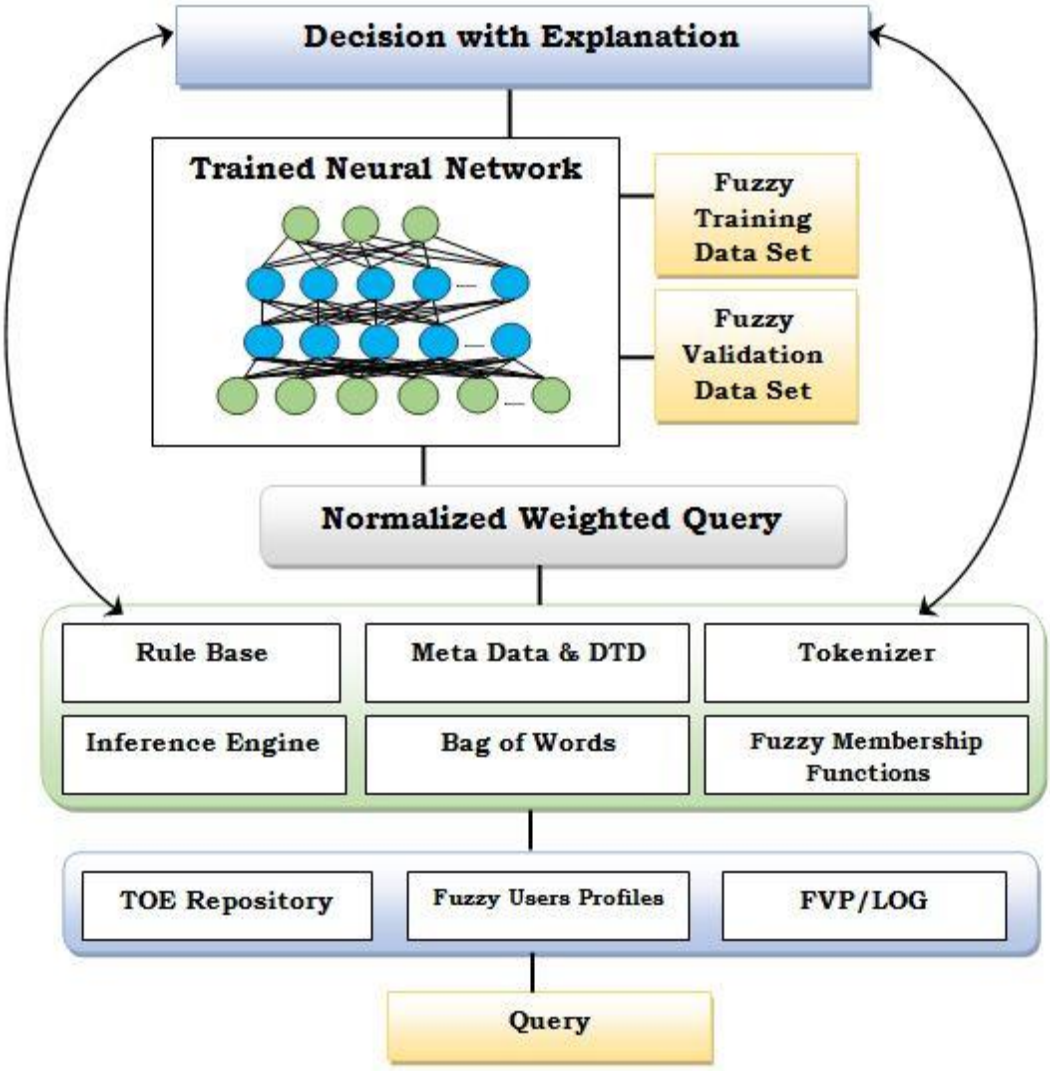

Figure 5: Personalized Web Content Filtering from Web through Fog Computing Framework

While training, the ANN considers each set of training data one by one and learns how to classify webpages into recommendable, presentable, and rejected categories. First the ANN takes only input data and calculates what it "thinks"! Later its output is compared with the actual output provided within sample data. It goes back, adjusts its weights of connections and reprocess in forward direction. After many such forward and backward passes, the ANN is able to categorize only one webpage. Such multiple and good quality training data sets are needed for completely and thoroughly trained ANN. Training data sets may vary as per the application. The base neural network is shown in Figure 6.

Later, when actual values are extracted by the fog node or at the client machine, the underlying ANN has only input. As per its training, the ANN provides correct output, classifies the webpage and presents only recommendable webpages. The experiment of webpage filtering

will be helpful in many aspects. Such system can be used in institutes to identify web content which is malicious and prohibited. It has got domestic applications also, in order to block some unwanted sites, as per the parents/authorities need; automatically the web content will be put into rejected category and not shown to the users.

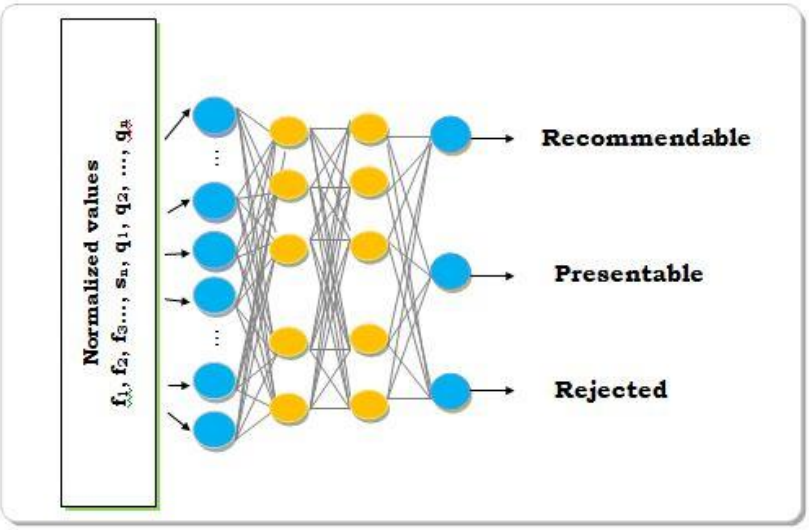

Figure 6: Underlying Artificial Neural Network

CONCLUSION

The architecture proposed is generic in nature and can be used for any applications. For demonstration, web content filtering is taken into consideration. Other example applications, which can be benefited with the proposed architecture, are as follows.

- Health care,
- Smart cities,
- IoT based systems,
- Customized data and Web mining,
- Mobile fogging,
- Vehicle and object tracking,
- etc.

At the edge of clients network/devices when cloud computing is to be used, one can go for such light weight cloud computing via fog. Open source software and forums such as fog project[4] and OpenFog are also available to guide developers.

In future, one can work on distributed intelligence systems for fog computing, in order to make fogging efficient and cost-effective. Fog computing research can also involve research in 5G systems, fog software agents, generic fog architecture, particularly layer dealing with abstraction, embedded systems within network devices, big data visualization in customized way, and applied IoT and IoE research in various domains. Further, the type 2 fuzzy logic can also be considered. Commercialization of the fog architecture and patenting can also be done.

[4] *https://fogproject.org/*

REFERENCES

[1] M. Abdelshkour, "IoT, from Cloud to Fog Computing," 18 September 2017. [Online]. Available: http://blogs.cisco.com/perspectives/iot-from-cloud-to-fog-computing. [Accessed 18 September 2017].

[2] B. Flavio and M. Rodolfo, "Fog Computing and its Role in the Internet of Things," in *Proceedings of the MCC workshop on Mobile Cloud Computing*, 2012.

[3] S. Sarkar and S. Misra, "Theoretical Modelling of Fog Computing: A Green Computing

Paradigm to Support IoT Applications," *IET Networks*, vol. 5, no. 2, p. 23–29, 2016.

[4] P. Lopez, A. Montresor, D. Epema, A. Datta, T. Higashino, A. Iamnitchi, M. Barcellos, P. Felber and E. Riviere, "Edge-Centric Computing: Vision and Challenges," *ACM SIGCOMM Computer Communication Review*, vol. 45, no. 5, pp. 37-42, 2015.

[5] M. Vaquero and R. Luis, "Finding Your Way in the Fog: Towards a Comprehensive Definition of Fog Computing," HP Laboratories Technical Report, 2014.

[6] J. Numhauser and J. Mesa, "XMPP Distributed Topology as a Potential Solution for Fog Computing," in *MESH 2013: The Sixth International Conference on Advances in Mesh Networks*, Spain, 2013.

[7] T. Perry, "What Comes After the Cloud? How About the Fog?," 08 February 2013. [Online]. Available: https://spectrum.ieee.org/tech-talk/computing/networks/what-comes-after-the-cloud-how-about-the-fog. [Accessed 13 October 2017].

[8] W. Shi, J. Cao, Q. Zhang, Y. Li and L. Xu, "Edge Computing: Vision and Challenges," *IEEE Internet of Things Journal*, vol. 3, no. 5, p. 637–646, October 2016.

[9] X. Hou, Y. Li, M. Chen, D. Wu, D. Jin and S. Chen, "Vehicular Fog Computing: A Viewpoint of Vehicles as the Infrastructures," *IEEE Transactions on Vehicular Technology*, vol. 65, no. 6, p. 3860–3873, June 2016.

[10] B. Antonio and F. Stefano, "QoS-Aware Deployment of IoT Applications Through the Fog," *IEEE Internet of Things Journal*, vol. 1, no. 1, p. 99, 2017.

[11] S. Kitanov and T. Janevski, "State of the Art: Fog Computing for 5G Networks," in *Telecommunications Forum (TELFOR), 2016 24th*, 2016.

[12] I. Stojmenovic and S. Wen, "The fog Computing Paradigm: Scenarios and Security Issues," in *Federated Conference on Computer Science and Information Systems (FedCSIS)*, 2014.

[13] M. Janakiram, "Is Fog Computing the Next Big Thing in the Internet of Things," 18 April 2016. [Online]. Available: https://www.janakiram.com/posts/blog/is-fog-computing-the-next-big-thing-in-internet-of-things. [Accessed 5 October 2017].

[14] M. Satyanarayanan, P. Bahl, R. Caceres and N. Davies, "The Case for VM-Based Cloudlets in Mobile Computing," *IEEE Pervasive Computing*, vol. 8, no. 4, 2009.

[15] E. Daly, W. Lancee and J. Polivy, "A Canonical Model for the Taxonomy of Emotional Experience," *Journal of Personality and Social Psychology*, vol. 45, no. 2, pp. 443-457, 1983.

[16] K. Szpunar, R. Spreng and D. Schacter, "A Taxonomy of Prospection: Introducing an Organizational Framework for Future-oriented Cognition," in *Proceedings of the National Academy of Sciences of the United States of America*, 2014.

[17] W. Wang, "Understanding User Experience of News Applications by Taxonomy of Experience," in *Behaviour & Information Technology*, Taylor & Francis, 2017, pp. 1-11.

[18] L. A. Zadeh, "Fuzzy Sets," *Information and Control*, pp. 338-358, 1965.

[19] P. S. Sajja, "Intelligent Web Content Filtering Through Neuro-Fuzzy Approach," *International Journal of Data Mining and Emerging Technologies*, vol. 3, no. 1, pp. 33-39, 2013.

[20] P. S. Sajja and R. A. Akerkar, Intelligent Technologies for Web Applications, Boka Raton, FL, USA: CRC Press (Taylor & Francis Group), 2012.

[21] P. S. Sajja, "Knowledge Representation Using Fuzzy XML Rules in Web Based Expert System for Medical Diagnosis," in *Fuzzy Expert Systems for Disease Diagnosis*, Hershey, PA, USA, IGI Global Book Publishing,, 2014, pp. 138-167.

PRAJÑĀ - **Journal of Pure and Applied Sciences Vol. 24 – 25 : 219 – 222 (2017)**
ISSN 0975 - 2595

CYBER SECURITY: ATTACKS AND ITS COUNTERMEASURES

PRASHANT P. PITTALIA

Department Of Computer Science, Sardar Patel University, Vallabh Vidyanagar-388120, Gujarat, India
E-mail:prashantppittalia@yahoo.com

ABSTRACT

The Internet is growing rapidly. It has given rise to new opportunity in every field like – business, financial institution, education, health, sports, entertainment, government, defense, power sector, etc. It has removed the geographical boundaries between the users and allowed the Internet users to access the information or resources from any place by sitting only on the single place. The biggest drawbacks of the Internet is cyber crime, which is an illegal activity performed by the users using the Internet. Cyber crime involves breakdown of the privacy of a system, damages files and folders, involves unethical hacking of the credential information, identifies the loopholes in the website and misuses for malicious task. In today era, most of the cyber crimes are committed by the people who have knowledge of a technology. To remove such malicious activities, it is necessary to understand their activities and apply the proper prevention strategies. Organizations or persons who use the Internet have a lack of responsibilities of online resources and allow the cyber attacker to breach the security. This paper provides a current scenario of cybercrime and proper prevention steps.

Keywords: Cyber crime, hacking, port scanning, ransomware, firewall

INTRODUCTION

In today's IT environment, the Internet and computer network is very important and useful part of daily work. The people are doing most of their work like selling, purchasing, payment of goods, storing their important contents, sharing their useful and secret information. Today internet is become a part of human lives. The growing fastest world of internet is known as cyber world. Today cyber security is most important in the Internet world.

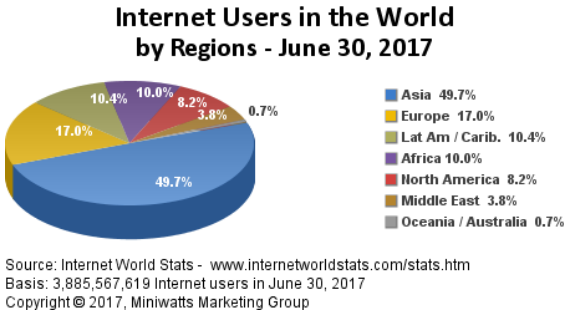

Fig: 1. Internet Users in the world by Regions – June 30, 3017 [1]

Asia is the continent having 49.7% of the Internet users in the world. It shows that most of the users on Internet are from Asia. It shows that more number of users spare their time on Internet for doing their online activities like social media, online transactions, surfing the net and transfer different types of files.

CYBER ATTACKS

Attackers are typically trying to attack or manipulate one or more networks to achieve their objective. The Internet was designed for utility and robustness. Cyber criminals use internet and computer technology to hack user's personal computers, laptops, mobile phone's data, and credential details from social media, business websites, national secrets etc. Criminals who perform these illegal activities through the internet are called – Hackers. The majority of cyber crimes are as follow.

Phishing

In this type of crime hackers provides a link which redirects to the fake website which is looks and feel like same as the legitimate one. Users are move to that fake sites and gives his/her credential information, which steal by the attacker and misuse or sell to the others. In such attacks the URL are similar to the original websites only few characters are changed or the name should be as it is but the domain name should be change. Most of phishing attacks are done by sending an email to the people and provide their credential information. [3]

Malicious Code

It is a code that damages a computer or system. It could not be identified by the antivirus software. Virus, worms, Trojan horse, java attack applets, ActiveX control are the various types of code which may be attached with the application or attachment to harmful the system or computer. Attackers identify the weakness of the operating systems or the application by testing various new malicious codes on such software and then such tested malicious code is spread across Internet.

Defacement

Website defacement means changes the content of a website by attacker by cracking the security of a website owner. Such type of attacker targets some government agencies of other countries and shows their strength by identifying weaknesses in their website.

Spam

It is the use of electronic messaging systems to send unwanted messages, especially advertising, as well as sending messages repeatedly on the same website.

Network Scanning

It is used to identify the network of an organization by knowing the IP addresses in the network, operating systems and applications running on the system, port numbers used to access the particular application. Also it identifies which port numbers are live and what applications are running on it and find out the weaknesses of it to perform the malicious task. Standard operating systems and software having predefined services running on predefined port numbers. Also it has pre-configured the some default usernames and passwords, which leads to easy task of the attacker to scan such port numbers using such data. [5]

Hacking:

In Internet world most dangerous cyber crime is hacking. Hacking simply refers to the breaking into the computer system and steals valuable information from the system without any permission. Hacking is done by hackers who run the client or server program and able to spoof the data.

Fake Certificates and Certificate Authorities

On internet trustworthy websites are identify by seeing the HTTPS (Secure Hyper Text Transfer Protocol) at the address bar in the web browser. The CA (Certificate Authority) verify the identity of a requester and if it is valid than issue a signed certificate which mention the purpose of the website and validity of the certificate. Every browser comes with a copy of CA's signatures so that when user tries to access the website it is trustworthy or not is easily identify. If CA's of signed certificate on a website is not trusted by a web browser, it will warn the users about it.

Attackers target these trusted CAs and try to get fake certificate IDs signed by the CA to make them as original. Then when a victim connects to the website a legitimate certificate send bypassing the inbuilt security and web browser could not provide warning to the users.

Identity theft:

In identity theft, the attacker use someone else identity to misuse and on behalf of actual user it fraud with others. In such attack it theft money or getting benefits by pretending to someone else. Without permission use someone else electronic signature, unique identification features like password is known as identity theft.

CYBERSPACE & CYBERCRIME

With rapid growth of the Internet also increase incidents of online attacks. In 2017, ransomware attacks like "WannaCry" and "Petya" spreading around the world and demanding for bit coins. According to analysts with IT-security software firm G Data, in 2017 the number of new malware specimen is more than 7.4 million.

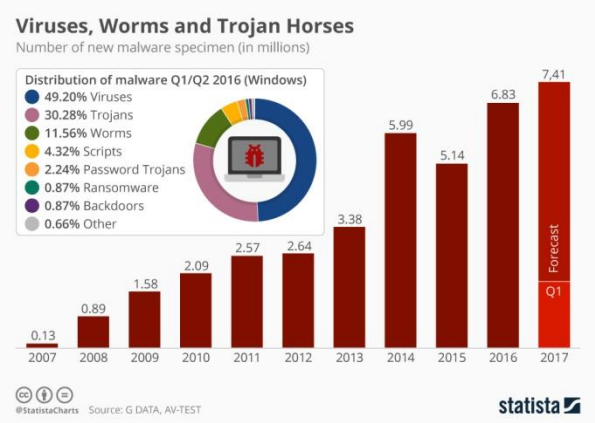

Fig: 2. Number of new malware specimen (in millions) and the share of windows-based malware (in percent) [2]

CYBER SECURITY: PREVENTION STEPS

Today the cybercrime is the major threat for the development of any state or country. Cyber criminals wants to get money, destroy the systems, or harassment someone. It is necessary to implement the cyber crime prevention techniques in very well manner. It is needed to awareness internet users about the cyber threats and how to secure their credential information. Internet users should be aware about the security tools to reduce the risk of cyber crime. The following steps are important to prevent the system against the malicious activity on a system.

Use Strong Passwords:

Use the different password and username combinations for various accounts and instead of write it down on paper keep it in your mind.

Make Social Media Account Safe:

Be sure to keep your social networking profiles (Face book, Twitter, YouTube, etc.) private. Be sure to check your security settings. Think twice before making someone as a member of your group and careful of what information you post online and whom you allow to access it.

Secure your Mobile Devices:

Mobile devices are also vulnerable to malicious software, such as computer viruses and cyber attackers. Always download applications from trusted sources. It is also important to update operating system time-to-time. Install standard anti-virus and firewalls. Also set the pattern matching or biometric authentication, otherwise, anyone can access all your personal information, if you misplace it or even set it down for a few moments. Someone could install malicious software that uses your GPS and track about your movement. Do not hurry to download the apps or games on your device. Before download check the permissions that should be demands by the application.

Protect your data:

Credential information like (financial records, credit card and debit card details, tax related information) should be stored with strong cryptographic algorithms that supports authentication, confidentiality and integrity of the data.

Keep your device with latest patches and updates:

Every operating systems and applications are releasing the new version with latest updated information to more secure their software. Regularly update your device with patches when they become available. It helps to block attackers from being able to take advantage of software vulnerabilities that they could otherwise use to crack your system.

Install security software:

Security software essentials like firewall and antivirus programs. Firewall controls who can communicate with your computer system online & what information is allowed to access. It continuous watches all the data attempting to flow in and out of your computer on the Internet, allowing communications that it knows are safe and blocking “bad” traffic such as attacks from ever reaching your computer. It checks your

current connections and according to it allows only those packets which belong to those connections to and from your computers. Proper configuration of firewall on a system is very essential to protect from outsider attacks. [4]

Choose the right person for help:

If you are victim of any type of cyber attacks do not be hesitate, If you come across illegal online content, or if you suspect a cybercrime, identity theft or a commercial scam, just like any other crime report this to your nearest police station.

CONCLUSION

Today's Internet websites are mostly utilized for the sales, marketing of products, services of an organization, financial institutions, government projects & social networking etc. It can be used for knowledge, research, online transactions, fun and maintain relationship with people. There is a vast amount of credential information stored on various websites, and the lack of proper security makes these applications an ideal sandbox for attackers. Such websites can place an individual or a company in a compromising position or at serious risk. Peoples needs to understand what is secret and what to share online and to whom, otherwise it will harmful for the user or organization.

REFERENCES

[1] Internet world stats:http://www.internetworldstats.com / stats.htm

[2] Statista - The portal for statistics: https://www.statista.com/chart/10045/new-malware-specimen-and-share-of-windows-based-malware/

[3]Computer Hope: https://www.computerhope.com/jargon/c/compcrim.htm

[4]Digital care solutions: https://www.digitalcare.org/cybercrime-prevention-tips/

[5] Cyber Security Understanding Cyber Crimes, Computer Forensics and Legal Perspectives by Nina Godbole and Sunit Belpure, Publication Wiley

PRAJÑĀ - **Journal of Pure and Applied Sciences Vol. 24 – 25 : 223 – 232 (2017)**
ISSN 0975 - 2595

SYNERGISTIC EFFECT OF Ni-Zn BASED CATALYSTS ON THE GROWTH OF CARBON NANOMATERIALS

JIGNESH VALAND, SHIV PATEL, ANJALI VANPARIYA AND RASMIKA PATEL*
Department of Materials Science, Sardar Patel University,
Vallabh Vidyanagar-388120, Gujarat. Email: rasmi29@yahoo.com

ABSTRACT

Carbon nanomaterials were prepared by the chemical vapour deposition (CVD). CVD is an accepted method for production of carbon nanotubes/fibers due to its relative simplicity of operation, process control, energy efficiency, versatility in the use of raw materials, high yield and product purity. The principle of CVD is the decomposition of various hydrocarbons over metal supported catalyst. Nickel and Zinc based mono and bimetallic catalysts were prepared by wet impregnation method. Catalysts were used for the preparation of nanocarbon by CVD method to investigate their synergistic effect. Prepared carbon nanomaterials were characterized by Scanning Electron Microscopy (SEM), X-ray Diffraction (XRD), Raman Spectroscopy, Thermal Analysis and Transmission Electron Microscopy (TEM). Diameter of the prepared carbon nanotubes/fibers were observed in the range 40-120 nm under TEM microscopy. Carbon deposition and average growth rate were found maximum for Ni-Zn based silica supported bimetallic catalyst under CVD method.

Keywords: Nanomaterials, Bimetallic catalysts, CVD, SEM, Raman spectroscopy

INTRODUCTION

In the field of materials science, structure-property-application relationship is an important aspect. Many materials are known for their very unique properties and structural relationship. One of the most versatile materials is carbon and it is interesting to know the relation between its versatility and allotropes. Carbon exists in several allotropes like diamond, graphite and fullerenes [1]. As the structures of allotropes vary, they also have different physical and chemical properties. Research in the field of carbon science is increasing on alarming rate since the discovery of Fullerene in 1985 [2]. Among all carbon materials, carbon nanomaterials attracted much attention from scientific community since last few decades. There are many types of carbon nanomaterials like carbon nanotubes (CNTs), carbon nanofibers (CNFs), carbon nanospheres, graphene etc. Oberlin et al. [3] reported the Chemical Vapour Deposition (CVD) growth of carbon nanofibers (CNFs) by benzene decomposition. In 1991, Iijima reported formation of multiwalled carbon nanotubes (MWNTs) [4]. Two years later singlewalled carbon nanotubes (SWNTs) were synthesized by Iijima and Ichihashi [5] and Bethune et al. [6] with the help of metal catalyst particles. Carbon nanotubes (CNTs) and various types of carbon nanofibers (CNFs) have also drawn increasing attention due to their special properties and potential applications [4,7-9]. The Catalytic Chemical Vapor Deposition (CCVD) method is one of the most powerful techniques for synthesis of CNTs and CNFs, although carbon nanomaterials can be synthesized using various methods including arc discharge and laser vaporization [10]. The morphology and quality of the prepared nanocarbon depends on factors such as (i) selection of catalyst and carbon source, (ii) reduction temperature of the catalyst, (iii) reaction temperature and (iv) nature of catalyst support etc. [11].

The most widely used carbon sources are acetylene, methane, ethylene, ethanol, benzene, xylene and toluene. Due to the thermodynamic properties and chemical structures of the organic molecules, the hydrocarbon intermediates generated on catalyst surface have a significant effect on the morphology of final products [11]. Selection of appropriate catalyst is a major factor for synthesis of carbon nanomaterials through chemical vapour deposition method. For preparation of catalysts, researchers have used various precious metals as well as transition metals on different supports. It is known that Fe, Co and Ni nanoparticles provide centers for carbon nucleation and act as active sites for the decomposition of carbon species [11]. Transition metals, which are widely used as catalyst for growth of carbon nanomaterials, have vacancies in the d-electron orbital and with increasing d-electron vacancies they show increasing affinity

for carbon. Metals without any vacancy in d-shells like Zn or Cu has little affinity for carbon [12-14]. It is interesting to investigate behavior of metals like Zn and Cu with other active metals like Fe, Ni for the growth of carbon nanomaterials. In addition of monometallic catalysts, researchers have identified the role of more than one metal i.e. multimetallic catalyst systems for the growth of carbon nanomaterials. Carbon nanotubes were synthesized using Co-Mn, Fe-Co, Fe-Ni, Co-Mo, Fe-Mo, Ni-Co and these catalysts have been found to improve the CNTs growth [15-18].

It was found that supporting a metal or a mixture of metals on different oxides (MgO, SiO_2, Al_2O_3), zeolites, clay would result in enhancement of catalytic activity and ultimately it affects the formation of carbon nanomaterials [19-23]. It is obvious that the optimum interaction between metal and support has a positive effect on the growth of carbon nanostructures. The interactions between a metal and support can be either physical or chemical. Vander Wal et al. [24] reported that, physical interaction between metal and support can be responsible for the size distribution of metal particles.

Catalysts preparation can be done by introduction of metal precursors onto a suitable support and this can be accomplished by several, established methods. Common methods include: (i) impregnation, which involves deposition of a metal precursor onto a support, typically from an aqueous solution (ii) co-precipitation, in which the support and metal precursor are simultaneously precipitated from solution, (iii) ion-exchange, as commonly used for the preparation of zeolite supported catalysts (iv) sol-gel method and (v) physical deposition [25,26]. Each method has its own advantages and disadvantages. Due to simplicity, impregnation is generally used for the preparation of catalysts. Two different modes of impregnation are known and well implemented: wet impregnation and incipient wet impregnation. In wet impregnation, the support material is brought into contact with a solution containing metal precursors. By evaporation of the solvent followed by calcination, the metal is impregnated into the support. In general, the wet impregnation results in the metal being dispersed inside the pore as well as on the surface of supports.

The role of mono (nickel)/bimetallic (nickel with zinc) system and catalyst support for the growth of carbon nanomaterials is in the center of the present investigation. It is very interesting to check the behaviour of zinc in absence and presence of nickel for nanomaterials growth. For this purpose, different catalysts, supported on both silica (SiO_2) and alumina (γ- Al_2O_3), were prepared using wet-impregnation method. CVD method was used to prepare carbon nanomaterials. Various characterization techniques have been used to investigate nanomaterials properties and their relation with catalytic activity.

EXPERIMENTAL

Preparation of mono and bimetallic catalysts

Metal salts of nickel and zinc were used as metal precursors for the preparation of catalysts which were responsible for the growth of nanomaterials. Better dispersion of metal particles and small particle size are the major challenges for the preparation of suitable catalysts. Supported catalysts are more active catalysts; therefore silica and alumina were used as support to disperse the metal particles. Resultant metal particles on the support surface are the active sites for the growth of carbon nanomaterials. To get better dispersion, wet-impregnation method has been applied to synthesize mono and bimetallic catalysts. $Ni(NO_3)_2 \cdot 6H_2O$ solution and $ZnSO_4 \cdot 7H_2O$ solution were added to SiO_2/γ-Al_2O_3 slurry (made in distilled water) as a support. The mixture was stirred for 3 hours at room temperature and heated to 90°C for 1-2 hours under stirring (until all the water in the mixture evaporated). Then the paste was dried in an oven for 12 hours at temperature of 90°C. The resulting powder was calcined at 550°C for 3 hours. Monometallic catalysts were prepared by same manner, but each metal salt was impregnated separately on SiO_2 support. For monometallic and bimetallic catalysts comparison study, three silica supported catalysts were prepared ($10NiSiO_2$, $5ZnSiO_2$, $10Ni5ZnSiO_2$) and for support comparison, bimetallic catalysts on silica and alumina ($10Ni5ZnSiO_2$, $10Ni5ZnAl_2O_3$) were prepared.

Catalysts code, compositions and other details are presented in Table-1.

CVD set-up

The experimental setup used for the preparation of the carbon nanofibers/tubes is schematically shown in Figure 1. The reactor is made up of 930 mm long quartz tube of 32 mm inner diameter with provisions of inlet of reactants and outlet of spent vapor. The reactor was placed in a tubular electrical furnace. The catalyst was kept in sample holder present in heating zone of the horizontal quartz reactor.

The experimental set-up shown in figure was first flushed with nitrogen gas. The temperature of the heating zone was controlled by programmable temperature controller. Carbonaceous source used for production of carbon nanomaterials was xylene and it was injected using syringe pump. After deposition of carbon under optimized reaction conditions, the vapor/gas was allowed to go out through the gas bubbler to exhaust.

Synthesis of carbon nanomaterials

Quartz boat containing appropriate amount of metal oxide catalyst was kept into reactor. N_2 gas was passed through the quartz reactor and simultaneously the temperature increased up to 500˚C at the rate of around 2.4˚C/min. At the reduction temperature of 500˚C, subsequently N_2 was replaced by H_2 with the flow rate of 20 ml/min for 20 minutes to reduce metal oxides and hence it get transformed into active metal particles which can act as a nucleation site for the growth of nanocarbons. Further, temperature was increased at the rate of 2˚C/min to 800˚C in N_2 atmosphere only. At 800˚C, reaction was carried out in presence of N_2 (150 ml/min) and H_2 mixture. Simultaneously, carbon source xylene (analytical grade) was injected at the rate of 0.5 ml/min for 30 min of duration. Due to high temperature in the reactor, xylene was vaporized and decomposed on catalyst. After 30 minutes, H_2 flow was stopped and temperature decreased gradually. Samples were collected after the decreasing of temperature up to room temperature. Carbon deposition and Average growth rate can be calculated using following equations,

$$\text{Carbon Deposition \%} = \frac{Mtotal - Mcatalyst}{Mcatalyst} \times 100$$

$$\text{Average growth rate} = \frac{Mtotal - Mcatalyst}{Total\ growth\ time}$$

Reaction conditions used in the present study are the suitable conditions which were established well during previous experiments and reported elsewhere [27].

Nanomaterials characterization

Nanomaterials produced by CVD method were characterized by different sophisticated techniques. Samples were observed under Scanning Electron Microscope (SEM) Hitachi S-3000N to ascertain formation of nano size elongated structures (fibers or tubes). Transmission Electron Microscopic observation was done using Philips (TEM), Tecnai-20. Thermo Gravimetric Analysis (TGA) of carbon materials was carried out up to 800˚C on Mettler Thermal Analysis system TA 4000 with TG50 for getting information about amount of catalyst present in the product and also to study oxidation behaviour of carbon nanomaterials. The phases present in the resultant materials were detected using powder X-ray Diffraction (XRD) conducted on a Philips, X-pert MPD. Raman Spectroscopy of carbon samples were performed by Renishaw inVia Raman Microscope.

RESULTS AND DISCUSSION

Nanocarbon deposition

Catalyst preparation for the growth of carbon nanomaterials is crucial. Appropriate choice of metal or combination of different metals can lead the growth rate, but at the same time selection of support can also play a vital role. For the better growth, better dispersion of metal particles on the support is required and optimum metal-support interaction (MSI) improves the catalytic activity. Generally, wet-impregnation method provides the fine and better dispersion of the particles on the suitable support. In this study, two different systems (i) mono and bimetallic metals on same support i.e. SiO_2 and (ii) γ-Al_2O_3 and SiO_2 supports with bimetallic system have been used to investigate the behaviour of different supports. All the catalysts were prepared using wet-impregnation method as discussed in experimental procedure. All reaction conditions were exactly similar as discussed in experimental section. Nanocarbon

was prepared at 800˚C temperature, showed black soot like appearance by naked eye. After the reactions, results in the form of carbon deposition and average growth rate are complied in Table-2.

Role of mono and bimetallic catalysts on silica

To investigate the role of each metal on the growth of carbon nanomaterials and synergistic effect of metals, three different catalysts of Ni, Zn, Ni:Zn on SiO_2 support (Table-1 and 2) were used. First, monometallic catalyst of 10 wt.% Ni on SiO_2 was used for chemical vapor deposition process and it showed 50.62% of carbon deposition. To check the activity of only Zinc, monometallic sample of 5 wt. % Zn on silica was used for CVD under similar conditions and it showed very less amount of carbon deposition i.e. 4.96%. Zinc has no d-vacancies in their electron configuration so it exhibits a negligible affinity for carbon [12-14]. To find out the specific role of Zn with Ni, silica supported bimetallic catalyst with 10 wt.% Ni and 5 wt.% Zn was placed in CVD chamber under the similar reaction conditions, and 104.96% of carbon deposition was found (Figure 2). It is revealed that zinc is acting as a promoter with nickel as main metal for the growth of carbon nanomaterials. In the case of bimetallic catalyst (Ni:Zn), more carbon deposition occurred due to Zn might be helping Ni for better dispersion than monometallic (only Ni) on silica and as a result carbon deposition rate is faster in bimetallic system. In addition, there may be possibility to prevent aggregation of catalyst particles in the case of Ni:Zn system. From this study, we can say that deposition of a carbon material and average growth rate over silica supported bimetallic catalyst are higher than monometallic due to synergistic effect of Ni:Zn particles i.e. $10Ni5ZnSiO_2 > 10NiSiO_2 > 5ZnSiO_2$ (Fig. 2).

Effect of support in bimetallic catalysts

Figure 3 shows relation between carbon deposition and type of support in the case of bimetallic catalysts i.e. $10Ni5ZnSiO_2$ and $10Ni5ZnAl_2O_3$. To find out the effect of support, Ni:Zn based silica and alumina supported catalysts were used for CVD reaction under similar conditions as applied in mono and bimetallic study, explained previously. Catalytic activity is the major concern for the growth of carbon nanomaterials, especially in CVD method. Dispersion of active metal particles, nature of support, metal-support interaction, catalytic activities are main characteristics and they are interrelated with each other. Silica and alumina are well known conventional supports, albeit their compatibility with different metals to get higher yield is still required further study. As seen in figure 3, the maximum carbon yield can be achieved in silica supported catalyst. Experimental results show that average growth rate of nanomaterials is also better on silica catalyst than alumina catalyst (Table-2). When the support is a metal oxide, oxidation/reduction reactions occur through the transfer of an oxygen atom from support to metal and vice versa. Acid/base interactions are depending on the Lewis acid and base characteristics of the materials. In the cases of metal oxides, surface anions act as Lewis base sites (electron pair donor) and cations as Lewis acid sites (electron pair acceptor) [24]. The nature of the catalysts depends on the interaction between metal and its support, therefore nature of catalysts is a key feature associated with the dispersion of the metal on its support. In the present study, there is a possibility of less active area of metal particles available on alumina and it resulted in smaller amount of carbon deposition occurred than on silica catalyst.

Nanocarbon characterizations

Scanning electron microscopy (SEM) and transmission electron microscopy (TEM)

Prepared samples were viewed under Scanning Electron Microscope (Hitachi S-3000N). Figure 4 displays SEM micrographs of carbon nanomaterials grown over metallic catalysts having lengths in the range of several micrometers. It also shows the morphology of the catalysts which provide nucleation sites for the growth of nanomaterials. Nanomaterials were grown by the diffusion of carbon through a metal catalyst and its subsequent precipitation as carbon products in various shapes. Growth of carbon in the shape of fibers/tubes can be seen in Ni containing mono and bimetallic catalysts ($10NiSiO_2$ and $10Ni5ZnSiO_2$, Fig. 4a and 4c). In case of $10ZnSiO_2$ and $10Ni5ZnAl_2O_3$, formations of carbon fibers are not observed. In these cases catalysts are surrounded by carbon aggregates. Maximum carbon materials

deposition can be clearly observed in $10Ni5ZnSiO_2$ bimetallic catalyst.

In Figure 5, it is observed that carbon deposited in the form of fibers on bimetallic sample ($10Ni5ZnSiO_2$) which was viewed under Transmission Electron Microscope. The long carbon fibrous nanostructures were observed under TEM analysis (Figure 5). The produced fibers/tubes show similar and unusual morphology throughout the sample. The resultant fibers/tubes have dimension between 40 nm to 120 nm. As seen in the images, it is revealed that elongated structures of about 100 nm dimensions and entangled with each other.

X-ray diffraction (XRD)

XRD is used in order to ascertain the quality and crystalline nature carbon materials. From the XRD pattern of carbon deposited on silica supported catalyst (Figure 6), the characteristic peaks for carbon can be seen at 2θ positions of 26.22˚and 44.50˚, which are attributed to (002) and (101) reflections respectively ((JCPDS card No. 75-1621). Peaks at 44.50˚and 51.90˚(2θ) corresponds to Ni are also presented in diffractogram (JCPDS card No. 65-0380). Carbon deposited on nickel catalysts is also confirmed by XRD results.

Thermo gravimetric analysis (TGA)

TGA of carbon materials was carried out using Mettler Thermal Analysis system TA 4000 with TG50 for getting information about amount of catalyst present in the product and also to study oxidation behaviour of carbon nanotubes. TGA of carbon materials was carried out in presence of air with heating rate 15 ˚C /min up to 800˚C.

Figure 7 shows TGA graph of carbon nanomaterials obtained from xylene on $10Ni5ZnSiO_2$. Nanocarbon prepared on Ni:Zn based catalyst at 800˚C exhibits higher oxidation initiation temperature (560˚C), thereby indicating that this carbon material have good thermal stability. It is known that crystalline carbon exhibits oxidation at higher temperatures than amorphous carbon. Single step weight loss is indication of one type of carbon form present in the material i.e. carbon nanomaterials.

Raman spectroscopy

Raman spectroscopy is commonly used to characterize nanomaterials. It reflects different characteristic spectra for sp^3, sp^2, and sp carbons, as well as for disordered sp^2. The Raman spectrum was taken using a 514 nm Argon Laser excitation wavelength. The first order Raman spectrum is composed of two main peaks, at 1350 cm^{-1} and 1580 cm^{-1}, which are assigned as the disorder (D band) and graphite band (G band), respectively [28]. Figure 8 shows Raman spectra results of carbon prepared on mono and bimetallic catalysts. It attributes the presence of D-band and G-band. The calculated ratio of the integrated intensity of the D and G peaks, $R_I = I_D/I_G$, characterizes the disorder in the carbon nanomaterials. R_I=0.66 is for $10NiSiO_2$, R_I=0.73 for $5ZnSiO_2$, R_I=0.89 for $10Ni5ZnSiO_2$ and R_I=0.81 for $10Ni5ZnAl_2O_3$. Therefore, it can be predicted from the calculation that fibrous carbon deposited on nickel supported silica is more crystalline in nature than the other catalyst systems.

CONCLUSIONS

Carbon nanomaterials were grown by CVD method using Ni and Zn based monometallic and bimetallic catalysts. The morphology and growth were found to be dependent on the type of catalyst and combination of metals as well as support system (silica and alumina). SEM and TEM micrographs showed that Ni and Ni-Zn based silica catalysts were suitable to grow carbon tubes/fibers among all four catalysts systems, where as fiber formation was not observed in case of Zn-based monometallic silica catalyst. Furthermore, the combination of Zinc and Nickel makes a significant difference in catalyst activity and responsible to finalize the shape of carbon deposition. The growth of carbon products were observed higher in silica supported bimetallic catalyst ($10Ni5ZnSiO_2$) than the monometallic catalyst systems. The presence of Zn and Ni on silica support have influenced structure, carbon deposition and average growth rate of carbon materials, whilst the catalyst prepared with Zn and Ni on alumina support resulted in lower carbon deposition than silica bimetallic catalyst. No fiber formation was observed on alumina catalyst. In the present investigation, silica supported catalysts were found better than alumina supported catalyst in terms of catalytic activity and formation of carbon nanomaterials.

ACKNOWLEDGEMENT

We are thankful to SICART, Vallabh Vidyanagar for providing instrumental facility and sample analysis.

REFERENCES

[1] Radushkevich, L.V. and Lukyanovich, V.M. (1952) : The structure of carbon forming in thermal decomposition of carbon monoxide on an iron catalyst. *Russian Journal of Physical Chemistry*, **26:** 88-95.

[2] Kroto, H.W., Health, J.R., O'Brien, S.C., Curl, R.F. and Smally, R.E. (1985) : C60 Buckminsterfullerene. *Nature*, **318:** 162-163.

[3] Oberlin, A., Endo, M. and Koyama, T. (1976) : Filamentous growth of carbon through benzene decomposition. *Journal of Crystal Growth*, **32:** 335-349.

[4] Iijima, S. (1991) : Helical microtubules of graphitic carbon. *Nature*, **354:** 56-58.

[5] Ijima, S. and Ichihashi, T. (1993) : Single-Shell carbon nanotubes of 1-nm diameter. *Nature*, **363:** 603-605.

[6] Bethune, D.S., Kiang, C.H., De Vries, M.S., Gorman, G., Savoy, R., Vazquez, J. and Beyers, R. (1993) : Cobalt-catalysed growth of carbon nanotubes with single-atomic-layer walls. *Nature*, **363:** 605-607.

[7] Ihara, S. and Itoh, S. (1995) : Helically coiled and toroidal cage forms of graphitic carbon. *Carbon*, **33:** 931-939.

[8] Nishimura, K., Kim, Y.A., Matsushita, T., Hayashi, T. and Endo, M. (2000) : Structural characterization of boron-doped submicron vapor-grown carbon fibers and their anode performance. *Journal of Materials Research*, **15:** 1303-1313.

[9] Manocha, L.M., Valand, J., Patel, N., Warrier, A., and Manocha, S. (2006) : Nanocomposites for structural applications. *Indian Journal of Pure & Applied Physics*, **44:** 135-142.

[10] Suda, Y., Takikawa, H. and Tanoue, H. (2011) Syntheses and electronic applications of helical carbon nanofibers. INTECH: Rijeka, Croatia, pp. 37-70.

[11] Xiaosi, Q., Chuan, Q., Wei, Z., Chaktong, A., Xiaojuan, Y. and Youwei, D. (2010) : Large-Scale synthesis of carbon nanomaterials by catalytic chemical vapor deposition: a review of the effects of synthesis parameters and magnetic properties. *Materials*, **3:** 4142-4174.

[12] Hoch, M. (1998) : Phase stability of carbon in FCC and BCC metals. *Calphad*, **12:** 83-88.

[13] Yazyev, O.V. and Pasquarello, A. (2008) : Effect of metal elements in catalytic growth of carbon nanotubes. *Physical Review Letters*, **100:** 156102.

[14] Yang, R., Goethel, P., Schwartz, J. and Lund, C. (1990) : Solubility and diffusivity of carbon in metals. *Journal* of *Catalysis*, **122:** 206-210.

[15] Yang, W., Feng, Y-Y., Jiang, C-F. and Chu, W. (2014) : Synthesis of multi-walled carbon nanotubes using CoMnMgO catalysts through catalytic chemical vapor deposition. *Chinese Physics B*, **23:** 128201-1-128201-5.

[16] Hao, L., Yong, Z., Ruying, Li., Xueliang, S. and Hakima, A-R. (2011) : Effects of bimetallic catalysts on synthesis of nitrogen-doped carbon nanotubes as nanoscale energetic materials. *Particuology*, **9:** 465-470.

[17] Sepideh, S.M., Karim, Z. and Mahmood, G. (2016) : Role of growth temperature in CVD synthesis of Carbon nanotubes from Ni-Co bimetallic catalysts. *International Journal of Nano Dimension*, **7:** 240-246.

[18] Arabshahi, Z. S., Pasha, A. M. and Shahi, F. (2017) : Growth of CNTs over Fe–Co/Nanometric TiO_2 catalyst by CVD: The effects of catalyst composition and growth temperature. *International Journal* of *Nanoscience and Nano technology*, **13:** 1-9.

[19] Abdulkareem, A.S., Suleiman, B., Abdulazeez, A.T., Kariim, I., Abubakre, O.K. and Afolabi, A.S. (2016) : Synthesis and characterization of carbon nanotubes on Fe/Al_2O_3 composite catalyst by chemical vapor deposition method, *In Proceedings of the World Congress on Engineering and Computer Science Vol II,* USA, pp. 601-606.

[20] Inoue, M., Asai, K., Nagayasu, Y., Takane, K., Iwamoto, S., Yagasaki, E. and Ishii, K.I. (2008) : Formation of multi-walled carbon nanotubes by Ni-catalyzed decomposition of methane at 600-750˚C. *Diamond Related Materials*, **17:** 1471-1475.

[21] Yu, G.J., Gong, J.L., Zhu, D.Z., He, S.X., Cao, J.Q. and Zhu, Z.Y. (2006) : Efficient synthesis of carbon nanotubes over rare earth zeolites by thermal chemical vapor deposition at low temperature. *Diamond Related Materials*, **15:** 1261-1265.

[22] Tang, T., Chen, X.C., Meng, X.Y., Chen, H. and Ding, Y.P. (2005) : Synthesis of multiwalled carbon nanotubes by catalytic combustion of polypropylene. *Angewandte Chemie International Edition*, **44:** 1517-1520.

[23] Kim, H.S., Kim, B., Lee, B., Chung, H., Lee, C.J., Yoon, H. G. and Kim, W. (2009) : Synthesis of aligned few-walled carbon nanotubes on conductive substrates. *The Journal of Physical Chemistry C*, **113:** 17983-17988.

[24] Vander Wal, R.L., Ticich, T.M. and Curtis, V.E. (2001) : Substrate–support interactions in metal-

catalyzed carbon nanofiber growth. *Carbon*, **39:** 2277-2289.

[25] Dupuis, A.C. (2005) : The catalyst in the CCVD of carbon nanotubes - a review. *Progress in Materials Science*, **50:** 929-961.

[26] Schwarz, J. A., Contescu, C. and Contescu, A. (1995) : Methods for preparation of catalytic materials. *Chemical Reviews*, **95:** 477-510.

[27] Manocha, L.M., Valand, J. and Manocha, S. (2005) : Role of metal catalyst and substrate site for the growth of carbon nanomaterials. *Carbon Letters*, **6:** 79-85.

[28] Dresselhaus, M.S., Dresselhaus, G., Saito, R. and Jorio, A. (2005) : Raman spectroscopy of carbon nanotubes. *Physics Reports*, **409:** 47-99.

Table-1 : Catalysts code and conditions used for the preparation of catalysts

Catalyst Code	Ni loading wt. (%)	Zn loading wt. (%)	RPM (Stirring)	Resultant mass of prepared catalysts (gm)	Calcination temperature (℃)
$10NiSiO_2$	10	-	300	4.14	550
$5ZnSiO_2$	-	5	300	4.89	550
$10Ni5ZnSiO_2$	10	5	300	5.11	550
$10Ni5ZnAl_2O_3$	10	5	300	4.75	550

Table-2 : Weight percentage of deposited carbon and average growth rate of prepared carbon

Catalyst code	Metal present	Support	Reaction temperature (℃)	Carbon deposition (%)	Average growth rate (mg/min)
$10NiSiO_2$	Only Ni	SiO_2	800	50.62	0.27
$5ZnSiO_2$	Only Zn	SiO_2	800	4.96	0.02
$10Ni5ZnSiO_2$	Ni and Zn	SiO_2	800	104.96	0.56
$10Ni5ZnAl_2O_3$	Ni and Zn	Al_2O_3	800	40.37	0.21

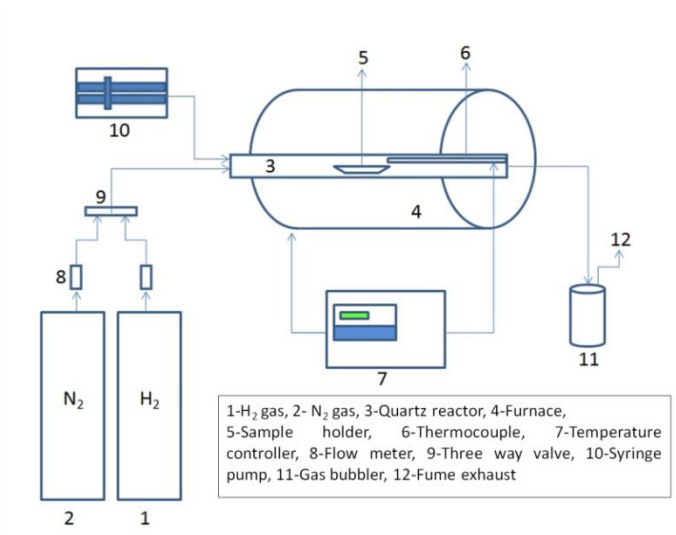

Figure 1 : Schematic diagram of CVD set-up

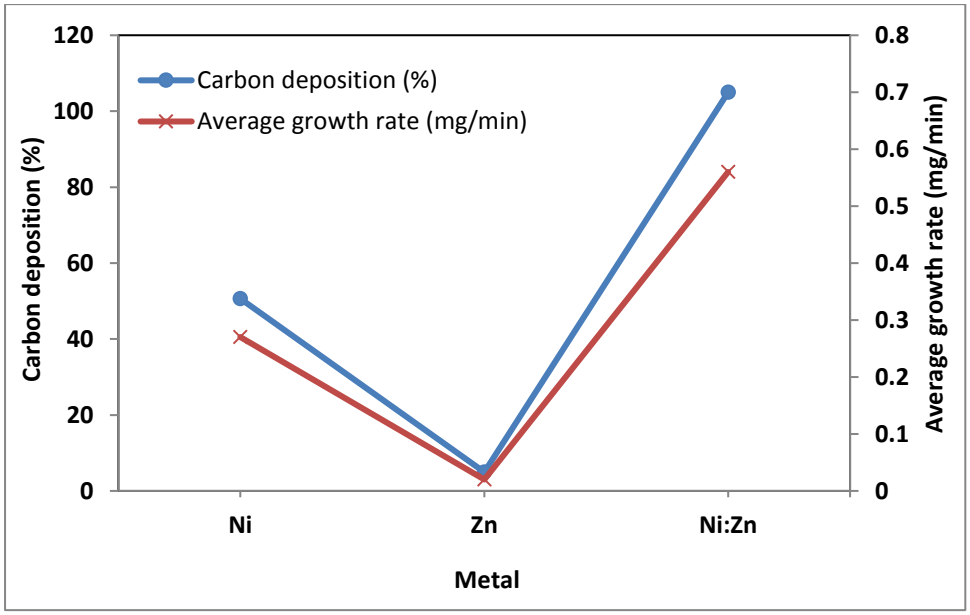

Figure 2 : Effect of metal on carbon deposition

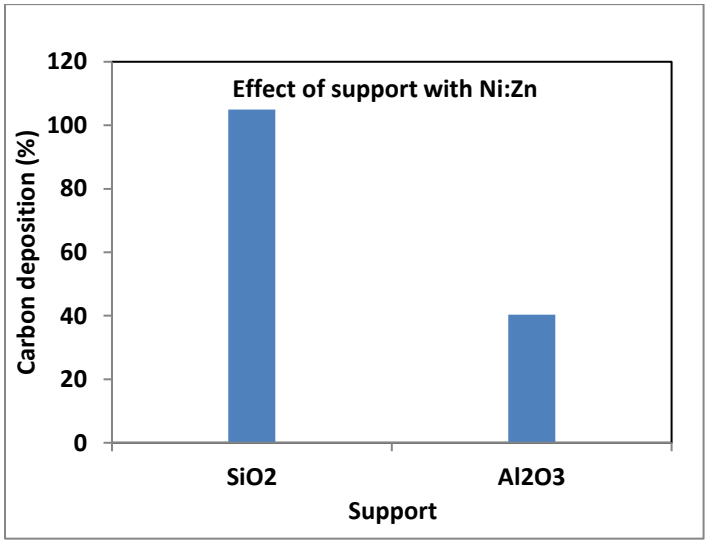

Figure 3 : Effect of support on carbon deposition

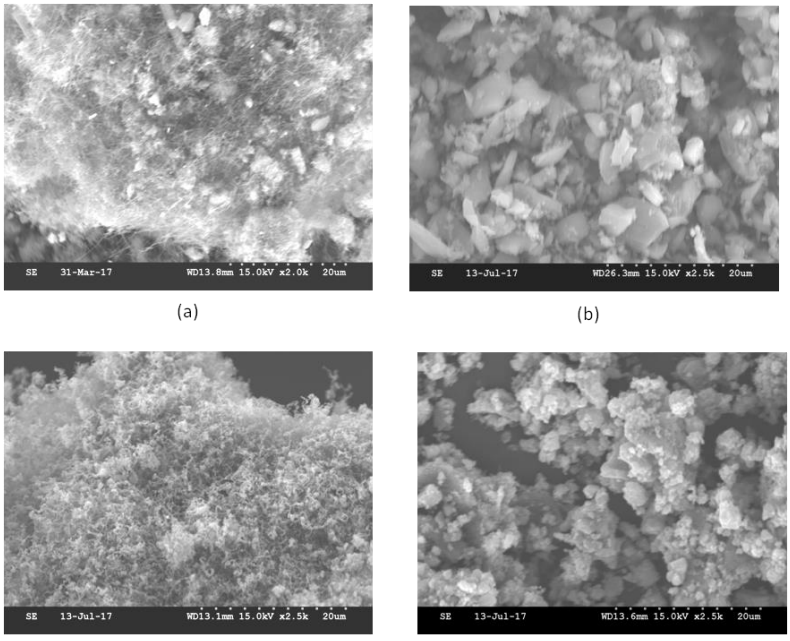

Figure 4 : SEM images of (a) $10NiSiO_2$ (b) $5ZnSiO_2$ (c) $10Ni5ZnSiO_2$ (d) $10Ni5ZnAl_2O_3$

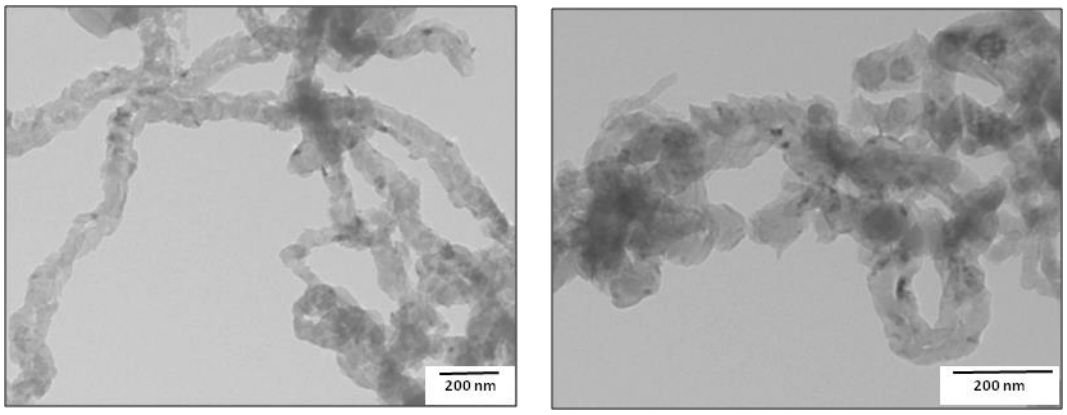

Figure 5 : TEM images of $10Ni5ZnSiO_2$

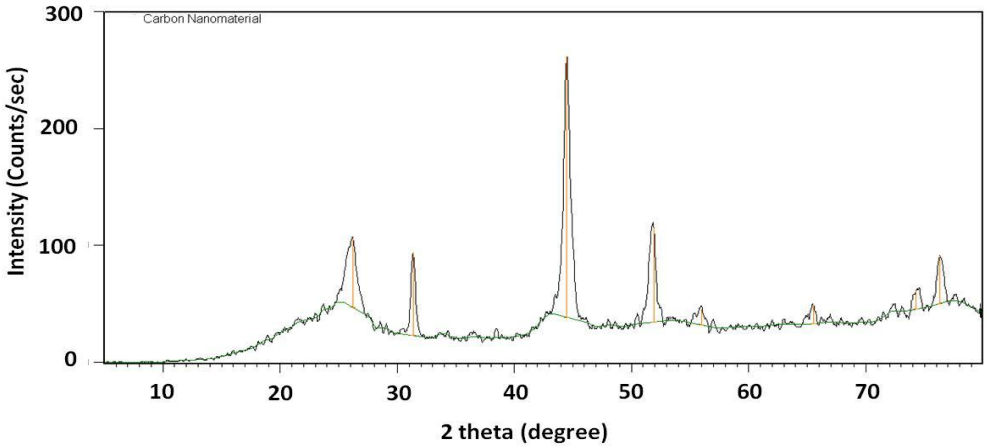

Figure 6 : X-ray diffractogram of carbon on silica supported catalyst

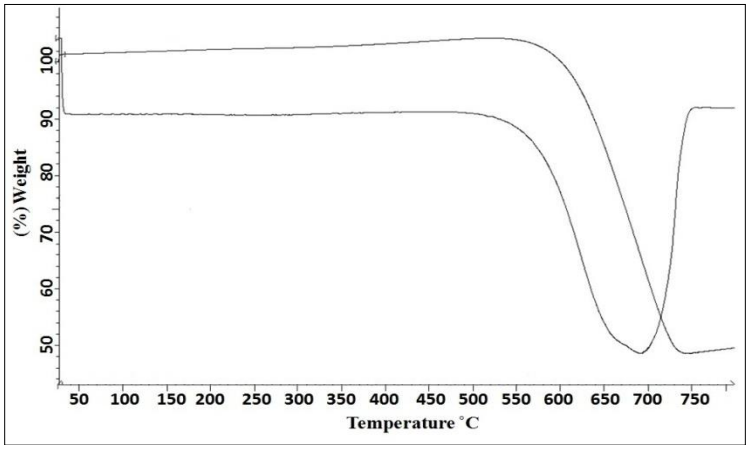

Figure 7 : TGA of $10Ni5ZnSiO_2$

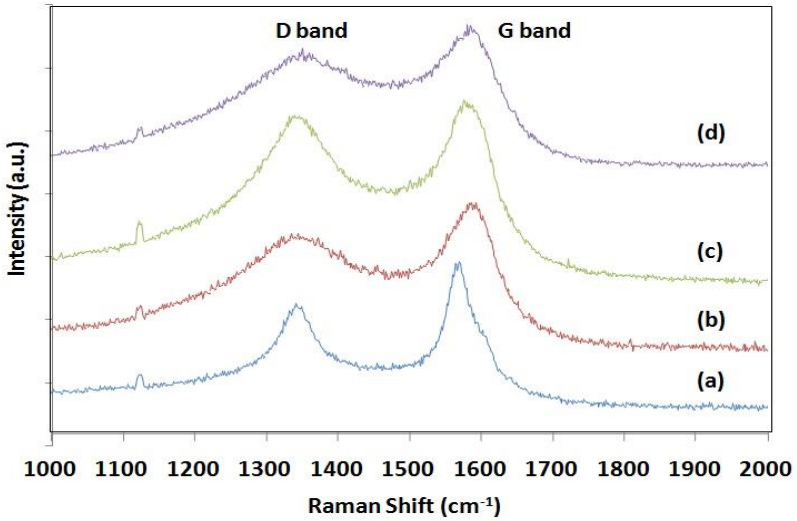

Figure 8 : Raman spectroscopy of (a) $10NiSiO_2$ (b) $5ZnSiO_2$ (c) $10Ni5ZnSiO_2$ (d) $10Ni5ZnAl_2O_3$

Instructions for preparation of manuscripts:

1. The paper should be submit into template format of the PRAJÑÃ.
2. The paper should be written in English and typed with double spacing.
3. The title of the paper and the name(s) of the author(s) be in the capital letters. The name of the institution be given in small letters below the name(s) of the author(s).
4. The 'Abstract of the paper, in not more than 150 words, should be provided on a separate page along with 4-6 keywords.
5. The heading, e.g. INTRODUCTION, should be written in capital letters and sub heading e.g. Chemical reagents and materials, should be written in sentence case.
6. Displayed formulae, mathematical equations and expressions should be numbered serially. Table should be with a title in addition to a serial number for it.
7. Photographs/Figures should be original with good contrast so as to be in a form suitable for direct reproduction scanning.
8. Footnotes are not normally allowed, except to identify the author for correspondence.
9. All figures must be numbered serially as they appear in the text, and their legends/captions should necessarily be provided.
10. References should be numbered in brackets [ ] in the order of appearance in the text. All the references in the bibliographic list must correspond to in-text references and vice versa. Abbreviated periodical titles should follow standard subject Abstracts. Names which are not listed by any standard subject indexing organizations should be spelled out in full.
11. All references should be clear and follow the examples below:

Periodical articles

[2] Sadqui, M., Fushman, D. and Munoz, V. (2006) Atom-by-atom analysis of global downhill protein folding. *Nature***, 442: 317-321.**

Books

[16] Stebbins, G. L. (1974) *Flowering plants: Evolution above the species level*, Amold Press, London, pp. 1-399.

Chapters from a book

[19] Schafer, H. and Muyzer, G. (2001) Denaturing gradient gel electrophoresis in marine microbial ecology, In *Methods in Microbiology* (Ed. Paul, J. H.), Academic Press, London, Vol. 30, pp. 425-468.

Thesis or other diplomas

[21] Nayak, S. (2004) *The visionary studies on the lichen genus Lecanora sensu lato in India.* Ph. D. Thesis, Dr. R. M. L. Ayadh University, Faizabad, India.

Conference proceedings

[4] Mohapatra, G. C. (1981) Environment and culture of early man in the valley of river Chenab and Ravi, western sub- Himalayas. In *Proceeding X Congress of IUPPS,* Mexico, pp. 90-123.

Online documentation

[9] Koning, R. E. (1994) Home Page for Ross Koning. Retrieved 26-6-2009 from *Plant Physiology Information Website:* http://plantphys.info/index.html

Note: - Manuscripts prepared faithfully in accordance with the instructions will accelerate their processing towards publication; otherwise it would be delayed in view of their expected re-submission.

For and on behalf of Editorial
Dr. M. N. Patel
Department of Chemistry
Sardar Patel University
Vallabh Vidyanagar, Gujarat-388 120
spu.prajna@gmail.com
jeenen@gmail.com
Website:www.spuvvn.edu

NOTE: This information may kindly be circulated among your colleagues.